

Chamber studies and modeling of secondary organic aerosol formation

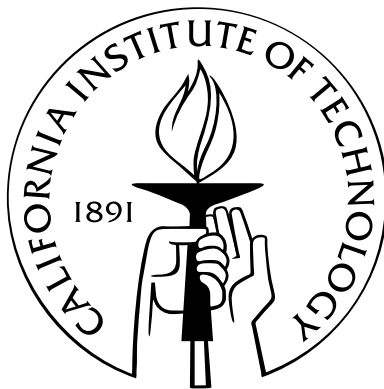
Thesis by

Arthur W. H. Chan

In Partial Fulfillment of the Requirements

for the Degree of

Doctor of Philosophy



California Institute of Technology

Pasadena, California

2010

(Defended May 11, 2010)

© 2010

Arthur W. H. Chan

All Rights Reserved

Dedicated to Mum and Dad, who worry about everything so that I do not need to.

Acknowledgements

I owe a tremendous debt of gratitude to many people, without whom this work would not have been possible. They all made my last five years at Caltech the most memorable and most enjoyable time of my life.

First and foremost, I would like to express the deepest gratitude to my main advisor, John Seinfeld. John has been the greatest advisor a graduate student can ask for. What I appreciate most is the trust and respect he has shown me, while at the same time his availability for guidance and advice. In my first few months of research, he gave me a small modeling project to get me started. He let me struggle with the nitty gritty details of programming and optimization in MATLAB, but insisted that I meet with him almost every other day, making sure that I understood the science and did not get lost in sea of code. This small project eventually became a major part of my work, and helped me conceptualize what is going on in our chamber experiments.

After I started lab work, John placed me under Sally's tutelage, and since then he has given me (and the rest of the roof lab) great research direction. In the beginning he would tell us what project to work on, and I was always amazed at how he is frequently one step ahead of everyone else in the field. His forward "big-picture" thinking makes our work very relevant, and I have been very fortunate to participate in these projects. John has also been very receptive to our ideas, and whenever we have ideas for projects, he is always willing to discuss them in our "what is next on our list" meetings. And during the experiments, he seldom checks in on us which has allowed us to work rather independently. When we bring him results, he is always very excited and listens to what we have to say, dropping whatever he is working on. (We often impersonate his "Oh!" when we tell him we have results.) Whatever the results, he has always trusted us in designing and performing

our experiments with care and thought, and is always willing to accept our findings, even when they go against his initial hypothesis. John has also offered a lot of advice on my career, and helped me figure out what I want to do after I graduate. I am very lucky to work under such an enthusiastic and patient mentor, for a supportive and trusting advisor, and with a thoughtful and dedicated scientist. I am not surprised that so many of his students have gone on to greater achievements in the field.

Most graduate students are lucky to have one advisor care about their research. I have been extremely fortunate to have Rick Flagan as my co-advisor, and Paul Wennberg as my unofficial third advisor. Rick cares not only about our work, but also our safety and our personal lives. He has made sure that our experiments run smoothly and efficiently. I have also gone to him numerous times to ask for advice on instrumentation and, more recently, designs of our new chambers in Robinson. Each time he has offered many excellent ideas that I would never have thought of. Sometimes he would show me a random piece of old equipment tucked away in our “museum” (storage room) that solved my problems. Rick has also been a great friend, and I have always been comfortable talking with him on a more personal level. He has never turned us down when we ask to host a group party at his place, even when he was on crutches. We have had so much fun playing croquet at his nice house in San Marino.

My thesis work would not have been possible without collaboration with Paul Wennberg’s group. I am fortunate to be one of the first roof labbers to use his group’s gas-phase mass spectrometry techniques to study chemistry of aerosol formation. More importantly, I have been able to work with a brilliant scientist who never stops asking questions. When sometimes I was too task-oriented and just wanted to give up and move on, he insisted that I look at the problem in more detail, and looking back I am glad I listened to him, because it has ensured the quality of my work. He is one of the smartest people I have met: whenever we see something interesting in an experiment, he can instantaneously take that observation and think a few steps ahead of what further experiments we can do, and what the implications are. I have also learned from Paul to be creative about experimental design, and in the last few projects, his advice on running experiments has helped reveal a lot of

information about the chemistry. I sincerely appreciate his interest in my work, and hopefully I have learned a thing or two from his insight into chemical mechanisms. I am sure that in the coming years, the Seinfeld/Flagan/Wennberg collaboration will be able to do a lot of great science, and answer many important questions. I would also like to thank my undergraduate research advisor at the University of Pennsylvania, Warren Seider, who has introduced me to scientific research, and has encouraged me to pursue my interests in environmental science at Caltech. I am truly grateful to him for paving the road for me to come to Caltech and work with such great people here.

I would also like to thank my two biggest mentors in lab, Jesse Kroll and Sally Ng, from whom I learned everything I needed to know about anything, ranging from RO₂ chemistry and aerosol science to Swagelok fittings and chemical syntheses. I had the great opportunity to work with Jesse Kroll on my first project, and overlapped with him at Caltech for a few months. He has introduced to me a dynamic framework to think about organic aerosols. From working with him closely on one of his papers and one of my own, I have learned how to write an interesting paper and to present it coherently and logically. His interest in online videos almost parallels his interest in science, both of which made the roof lab a source of great science and great fun. Among all the people whom I have worked with, Sally is the one who has taught me the most. She has shown me how to run the roof lab chambers, and that is the least important lesson I have learned from her. Her relentless scientific pursuit (always insisting every piece of instrument be run to get the most data) and borderline superstitious attitude have been the most impressive to me. She has also been the most passionate about science, and would always come to lab in the morning with new ideas and questions she thought of overnight. Always cheerful, never down, she has the most positive attitude about everything and everyone, which is infectious upon people around her. She has taught me the importance of returning borrowed items just as they were before they were borrowed, singing during chemical syntheses, and asking for help when it is needed. Together, Jesse and Sally have done some great work during the years they were here, but more importantly, they have made the roof lab the best community one can work in.

Over my five years in the roof lab, I have worked most closely with Puneet Chhabra, Kathryn

(Beth) Kautzman, and Jason Surratt. Puneet and I have been working together every step along the way in our PhDs, from taking first year classes, to quals, starting in the roof lab, working in the roof lab, candidacy, conferences, meetings, and much more. I have enjoyed our scientific discussions and from them we have come up with many great ideas for chamber experiments and data analysis. Despite my constant bashing of the AMS, he has helped me a lot with understanding experimental results using data from his instrument. We have had so much fun in and outside of lab over the years, and I will always cherish playing baseball, jokes about NIL, jokes about anything, his man points, his face, tape measure wars, rotating the air filtration system, driving the NO_x box to Irvine, the racially insensitive Garden Cafe employee, and all the great memories we have shared over the years.

It has also been a great honor to work with Jason, whose knowledge of analytical chemistry has provided crucial information about chemical composition of aerosols. I have always appreciated his enthusiasm and his attention to detail. We have also had many long discussions about science and life in general, and I have learned a lot about organic and analytical chemistry from him. I would also like to express many thanks to him for always taking the graveyard shift of shutting down the experiments late at night or early in the morning. I wish him great success at the University of North Carolina, where I am sure he will go on to do great things.

I had the great pleasure of working with Beth, who has been great in giving me advice on matters ranging from GC/MS to fixing a pump to how I should plan my career. She is also extremely fun to work with, and together with Puneet, they have made the roof lab a fun place to be in. Beth, I wish you and Art a great and happy future on the East Coast.

I want to thank all the people in the roof lab, for sharing laughs and tears, cheers and sufferings, and a lot of wonderful memories. It has been a great pleasure to mentor Christine Loza and Lindsay Yee. They have been so motivated to learn new things and take on even the most menial tasks that I really did not have to spend any extra effort or time to be their mentor. Christine has been a great partner-in-crime in chemical synthesis and chamber operation. I will never forget how we struggled through our MPAN and methyl nitrite syntheses. I really appreciate her persistence and her positive

attitude that has helped me through my last projects. Lindsay's exceptional organizational skills have been invaluable to both current chamber operations and designing the new chamber facilities in Robinson. They have shown enough promise that I feel very comfortable leaving the roof lab in their hands. I am excited to see what they will accomplish in the next few years, especially with the new and improved chamber facilities in Robinson that they have worked so hard on. I would also like to thank Man Nin Chan for always being willing to do all the filter sampling and helping with everything else in the lab. He has also been very passionate about science and has given me many great research ideas, as crazy as they always seem. I am grateful to Varuntida (Tomtor) Varutbangkul and Andrew Metcalf for all their help on the DMA. It is always comforting to know if the DMA breaks, I can always go to one of them, either over email or in person, and the problems always get fixed. I am especially grateful to Andrew for being my roommate for the last four years. He has been, simply, the greatest roommate I have ever had, and I will never forget our great times together. I have also been fortunate to have collaborated with Melissa Galloway and Frank Keutsch from the University of Wisconsin.

All my other co-workers on the experimental side of the research group have been nothing short of amazing: Armin Sorooshian, Shane Murphy, Harmony Gates, Adam Olsen, Tracey Rissman, Xerxes Lopez-Yglesias, Andreas Kürten, Andy Downard, Mandy Grantz, Jill Craven, Scott Hersey, Jason Gamba, Tristan Day, Ruoyu Zhang, James House, and Ann Miguel. They have all been extremely friendly and helpful, and I would like to thank them for letting me borrow parts and supplies, discussing research, troubleshooting problems, and chatting about life outside of research. I would also like to express appreciation to all the modelers in the group: Havala Pye, Wei-Ting (Anne) Chen, Chinghang (Candy) Tong, Daven Henze, Amir Hakami, Phillip Stier, Zach Lebo, Yi-Chun (Jean) Chen, Andreas (Andi) Zuend, and Joseph (Joey) Ensberg. I would especially like to thank Havala for being a great office mate. I will dearly miss the great time we had in Spalding 119, and our scientific discussions. I have also had the distinct pleasure of working closely with members the Wennberg group: Alan Kwan, Nathan Eddingsaas, Fabien Paulot, John Crounse, Jason St. Clair, and Melinda Beaver. Everyone, modeler or experimentalist, Seinfeld or Flaganite or Wennberger,

has been a helpful and supportive colleague, and a great friend. I will always remember our daily one-hour lunches outside Chandler, trying to fit everyone around a small table, and all the random conversations we had. I will miss that very much.

I would also like to thank a number of people on the Caltech staff for all their assistance and support. Nathan Dalleska has been tremendously helpful with the GC instruments and lab-related matters. Yvette Grant has provided a great deal of administrative support. I appreciate her help the most when I need to get my chemical orders to arrive on time, and she gets it done with the world's biggest smile. I have always been amazed at how good the research support at Caltech is. Every person on the Caltech staff is very friendly, highly capable, and always willing to help: Rick Gerhart (glassblower), Rick Germond (central warehouse), Gabriel and Luis (transportation), Moses and Cory (central stockroom), Mike Vondrus (machinist), and Suresh Guptha (systems administrator).

Lastly I would like to thank all my friends I have made here at Caltech, including my chemical engineering class (with whom I suffered first year classes and quals), friends with whom I had numerous cookouts and hiking and camping trips (Kathleen, Claire, Yvonne, "chemistry" Eric, "physics" Erik, Anna, Diana, Mary), friends from the Caltech Y (Shankar, Mayank, Abhishek, Michelle, Nicole, Athena, and Greg), friends from HKSA, and all others. I have grown as much professionally as I have personally, and you have all made the last five years at Caltech the greatest time of my life. I would like to thank Christine Romano for being such an important part of my life. Most importantly, I would like to thank my family, including my parents, Alex and Peggie Chan, my sister Annette and my grandparents. Thanks for believing in me all these years. Your love and support has meant so much to me. Dad, please stop trying to send me cash.

Abstract

Secondary organic aerosol (SOA), formed from atmospheric oxidation of gas-phase hydrocarbons, comprise a large fraction of ambient particulate matter. Significant uncertainties exist in identifying the sources and mechanisms responsible for SOA formation, making it difficult to understand its impact on global climate and local air quality. Laboratory chambers have been a valuable tool to study underlying chemical mechanisms of SOA formation and to quantify SOA formation from select hydrocarbons in a controlled environment. However, a good understanding of the chemical processes involved is required to be able to extrapolate data acquired from smog chamber studies. This thesis presents results from experimental investigation of SOA formation from atmospherically important compounds, and model simulations of kinetic mechanisms involved in SOA formation.

The distinguishing mechanism of SOA formation is the partitioning of semivolatile hydrocarbon oxidation products between the gas and aerosol phases. While SOA formation is typically described in terms of partitioning only, the rate of formation and ultimate yield of SOA can also depend on the kinetics of both gas- and aerosol-phase processes. Here a general equilibrium/kinetic model of SOA formation is presented to provide a framework for evaluating the extent to which the controlling mechanisms of SOA formation can be inferred from laboratory chamber data.

Current atmospheric models systematically underpredict SOA formation, suggesting that in current models, 1) significant SOA precursors could be missing and 2) SOA forming processes could be misrepresented. Aerosol formation from oxidation of 2-methyl-3-buten-2-ol (MBO) and polycyclic aromatic hydrocarbons (PAHs), two important classes of compounds previously assumed to be an insignificant SOA source, is studied. Upon photooxidation, MBO produces glyoxal (an important SOA intermediate), but the yields are too low to be atmospherically important. Photooxidation of

napthalene and other 2-ring PAHs leads to substantial amounts of aerosol, and can account for a large fraction of SOA formed from oxidation of diesel exhaust and other primary emissions.

Isoprene is a significant source of atmospheric organic aerosol; however, the oxidation pathways that lead to SOA have remained elusive. Under remote low- NO_x conditions, epoxydiols are formed from gas-phase photooxidation of isoprene, and are found to undergo reactive uptake to lead to low-volatility compounds, such as C_5 -methylnitrols and organosulfates observed in ambient particulate matter. Under urban high- NO_x conditions, methacrolein, an important C_4 aldehyde formed from isoprene oxidation, is found to form SOA via reaction with NO_2 to form peroxy methacryloyl nitrate, which subsequently forms low-volatility oligoester products. As a result of radical chemistry of aldehydes, SOA formation from isoprene depends critically on the NO_2/NO ratio, and the implications on ambient aerosol formation are discussed.

Contents

Acknowledgements	iv
Abstract	x
1 Introduction	1
2 Reactions of semivolatile organics and their effects on secondary organic aerosol formation	5
2.1 Abstract	6
2.2 Introduction	6
2.3 Experimental	8
2.4 Results and Discussion	9
2.5 Model Description	12
2.6 Model Predictions	13
2.7 Implications	16
3 Kinetic modeling of secondary organic aerosol formation: effects of particle- and gas-phase reactions of semivolatile products	28
3.1 Abstract	29
3.2 Introduction	29
3.3 Model Description	32
3.4 General Model Behavior	33
3.4.1 Odum model	33

3.4.2	Case (a): First-generation product only with aerosol-phase reaction	33
3.4.3	Case (b): First-generation product with unimolecular aerosol-phase reaction and with gas-phase conversion to a volatile second-generation product	34
3.4.4	Case (c): First- and second-generation semivolatile products with no aerosol- phase reaction	35
3.4.5	Case (d): Volatile first-generation product and semivolatile second-generation product	36
3.5	Effect of Kinetic Conditions on SOA Growth	37
3.5.1	Molecularity of aerosol-phase reaction and experimental timescales	37
3.5.2	Rate of hydrocarbon oxidation	38
3.5.3	Extent of reaction	39
3.5.4	Effect of particle-phase reaction vs. further gas-phase reaction	40
3.6	Application to SOA-forming Systems	41
3.6.1	Fitting experimental data to the kinetic model	41
3.6.2	α -Pinene ozonolysis	42
3.6.3	Isoprene photooxidation under low-NO _x conditions	42
3.6.4	<i>m</i> -Xylene photooxidation under low-NO _x conditions	43
3.7	Implications	43
4	Photooxidation of 2-methyl-3-buten-2-ol (MBO) as a potential source of sec- ondary organic aerosol	64
4.1	Abstract	65
4.2	Introduction	65
4.3	Experimental Section	67
4.4	Results	69
4.4.1	MBO photooxidation	69
4.4.2	Secondary organic aerosol formation	70
4.5	Discussion	70

4.5.1	Gas-phase mechanism of MBO photooxidation	70
4.5.2	SOA formation: High NO _x	71
4.5.3	SOA formation: Low NO _x	73
5	Secondary organic aerosol formation from photooxidation of naphthalene and alkylnaphthalenes: implications for oxidation of intermediate volatility organic compounds (IVOCs)	87
5.1	Abstract	88
5.2	Introduction	88
5.3	Experimental	90
5.4	Results	92
5.4.1	Concentrations of NO and NO ₂	92
5.4.2	Gas-phase composition	93
5.4.3	Aerosol formation	93
5.5	Aerosol Formation	94
5.5.1	Relative rates of oxidation steps	94
5.5.2	NO _x dependence of SOA growth	95
5.5.3	Aerosol formation and yields	96
5.6	Estimation of SOA Production from Light Aromatics, PAH, and Long-Chain <i>n</i> -Alkanes	97
5.6.1	Diesel exhaust	97
5.6.2	Wood burning	99
5.6.3	Other anthropogenic sources	100
5.7	Implications	100
6	Reactive intermediates revealed in secondary organic aerosol formation from isoprene	120
6.1	Abstract	121
6.2	Introduction	121

6.3	Results and Discussion	122
6.3.1	Isoprene SOA formation under low-NO _x conditions: Role of aerosol acidity	122
6.3.2	Identification of IEPOX as the intermediate responsible for acid-enhanced isoprene SOA	125
6.3.3	Mechanism of isoprene SOA formation under low-NO _x conditions	127
6.3.4	Isoprene SOA formation under high-NO _x conditions: Role of MPAN	128
6.3.5	Identification of MPAN as a key intermediate in formation of SOA from isoprene and MACR	130
6.4	Atmospheric Implications	132
6.5	Materials and Methods	133
6.5.1	Experimental details	133
6.5.2	Gas-phase measurements	134
6.5.3	Aerosol-phase measurements	134
6.5.4	Materials	134
6.6	Acknowledgments	135
6.7	Supporting Information	135
6.7.1	Experimental details of chamber operation	135
6.7.2	Procedures to confirm purity of MPAN	136
6.7.3	Details of the CIMS technique	136
6.7.4	Filter extraction and operation protocols for the GC/EI-MS technique	137
6.7.5	Materials	138
7	Role of aldehyde chemistry and NO_x concentrations in secondary organic aerosol formation	160
7.1	Abstract	161
7.2	Introduction	161
7.3	Experimental Section	163
7.3.1	Experimental protocols	163

7.3.2	Materials	164
7.3.3	Measurements	165
7.4	SOA Formation	167
7.4.1	Methacrolein	167
7.4.2	Acrolein and crotonaldehyde	169
7.4.3	Other aldehydes and methylbutenols (MBO)	169
7.5	Chemical Composition of SOA	170
7.5.1	Offline chemical analysis	170
7.5.2	Online AMS measurements	171
7.6	Effect of NO ₂ /NO Ratios on SOA Yield and Composition	172
7.7	Role of PAN in SOA Formation	174
7.7.1	Unsaturated aldehydes	174
7.7.2	Methylbutenols (MBO)	177
7.8	Conclusions	178
7.9	Supplementary Material: Negative Chemical Ionization Tandem Mass Spectrometry	182
8	Conclusions	216
A	Secondary organic aerosol formation from <i>m</i>-xylene, toluene, and benzene	220
B	Effect of NO_x level on secondary organic aerosol (SOA) formation from the photooxidation of terpenes	235
C	Organosulfate formation in biogenic secondary organic aerosol	252
D	Secondary organic aerosol (SOA) formation from reaction of isoprene with nitrate radicals (NO₃)	287
E	Glyoxal uptake on ammonium sulphate seed aerosol: reaction products and reversibility of uptake under dark and irradiated conditions	312

F	Modeling of secondary organic aerosol yields from laboratory chamber data	328
G	Chemical composition of gas- and aerosol-phase products from the photooxidation of naphthalene	341

List of Tables

4.1	Experimental conditions.	80
4.2	Experimental results.	81
5.1	Experimental conditions and results.	108
5.2	Effective SOA densities (g cm^{-3}), obtained in nucleation experiments.	109
5.3	SOA yield parameters.	110
5.4	Estimated SOA production from gas-phase oxidation of diesel exhaust	111
5.5	Estimated SOA production from gas-phase oxidation of emissions from fireplace burning of pine wood	112
6.1	High- NO_x MPAN SOA Constituents.	145
6.2	Summary of experimental conditions for low- NO_x experiments.	146
6.3	Summary of experimental conditions for high- NO_x experiments.	147
7.1	Hydrocarbons studied.	193
7.2	Experimental conditions and results.	194
7.3	SOA constituents detected by UPLC/(-)ESI-TOFMS and AMS in methacrolein experiments	195
7.4	SOA constituents detected by UPLC/(-)ESI-TOFMS and AMS in acrolein/high- NO_2 experiments	196
7.5	SOA constituents detected by UPLC/(-)ESI-TOFMS and AMS in crotonaldehyde/high- NO_2 experiments	197
7.6	SOA constituents detected by UPLC/(-)ESI-TOFMS in 2M2B/high- NO_2 experiments	198

7.7	SOA constituents detected by UPLC/(-)ESI-TOFMS in 2-pentenal/high-NO ₂ experi-	
	ments	199

List of Figures

2.1	“Growth curves” for photooxidation of <i>m</i> -xylene and toluene	24
2.2	Mechanisms for SOA formation from a single semivolatile species A	25
2.3	Predictions from the mechanism in Fig. 2.2d	26
2.4	Yield curves predicted from the kinetic model	27
3.1	Kinetic schemes for SOA formation.	51
3.2	Characteristic growth curve for the two-product Odum model	52
3.3	Characteristic growth curves for the formation of first-generation product with only aerosol-phase reaction	53
3.4	Characteristic growth curves for the formation of first-generation product with unimolecular aerosol-phase reaction and with gas-phase conversion to a volatile second-generation product	54
3.5	Characteristic growth curves for the formation of first- and second-generation semivolatile products with no aerosol-phase reaction	55
3.6	Simulated SOA yields of case (e) under typical chamber experiment conditions and atmospheric conditions	56
3.7	SOA yields in case (f) under typical chamber experiment conditions and atmospheric conditions	57
3.8	Effect of HC oxidation rate on SOA growth	58
3.9	Growth curves under different initial hydrocarbon concentrations	59
3.10	Growth curves for the overall kinetic model	60
3.11	Growth curves for SOA formation from α -pinene ozonolysis	61

3.12	SOA growth during isoprene photooxidation	62
3.13	SOA growth during <i>m</i> -xylene photooxidation	63
4.1	Time profiles of MBO (blue), glycolaldehyde (red), HMPR (green), and glyoxal (black) in (a) Experiment 4 (high-NO _x) and (b) Experiment 6 (low-NO _x).	82
4.2	AMS organic/sulfate ratio and DMA aerosol volume concentration during MBO low- NO _x photooxidation.	83
4.3	Mechanism of MBO photooxidation.	84
4.4	Yields of glycolaldehyde and HMPR from MBO photooxidation under high-NO _x con- ditions.	85
4.5	AMS spectra obtained during MBO photooxidation.	86
5.1	Structure of PAHs studied and OH rate constants	113
5.2	Reaction profile during a typical high-NO _x experiment	114
5.3	PTR-MS spectra under high- and low-NO _x conditions	115
5.4	Proposed compounds and structures for ion peaks observed by PTR-MS	116
5.5	Time-dependent SOA growth curves for all experiments	117
5.6	Simplified mechanisms for oxidation of naphthalene and 1-MN	118
5.7	SOA yield as a function of organic loading for naphthalene, 1-MN, and 2-MN under high-NO _x conditions	119
6.1	Comparison of important gas- and particle-phase products produced from isoprene under low-NO _x conditions	148
6.2	(-)-CIMS time traces	149
6.3	Mechanism for the enhancement of SOA formation from isoprene under low-NO _x con- ditions	150
6.4	UPLC/(-)-ESI-TOFMS BPCs	151
6.5	Possible chemical mechanism for the formation of isoprene SOA under high-NO _x con- ditions	152

6.6	GC/EI-MS mass spectra for isoprene low-NO _x SOA constituents formed in the highly acidified sulfate seed aerosol experiment	153
6.7	UPLC/(-)ESI-TOFMS mass spectra for isoprene low-NO _x SOA constituents	154
6.8	Particle-phase constituents formed from the dark reactive uptake of BEPOX	155
6.9	GC/MS EICs of m/z 248 and corresponding mass spectrum from 50 mg of BEPOX dissolved in 0.5 mL of 0.1 M H ₂ SO ₄ in water (green line) and a reactive uptake experiment of BEPOX	156
6.10	PILS/IC time traces of sulfate aerosol mass concentrations observed in experiments examining the reactive uptake of BEPOX	157
6.11	UPLC/(-)ESI-TOFMS EICs of organosulfates formed from the reactive uptake of BEPOX in the presence of highly acidified sulfate seed aerosol	158
6.12	UPLC/(-)ESI-TOFMS EICs associated with three major classes of oligoesters previously observed in isoprene high-NO _x SOA	159
7.1	Concentration profiles of gas-phase species during a typical methacrolein/high-NO experiment	200
7.2	Concentration profiles of gas-phase species during a typical methacrolein/high-NO ₂ experiment	201
7.3	Time-dependent SOA growth curves for methacrolein photooxidation	202
7.4	Time-dependent SOA growth curves for acrolein photooxidation	203
7.5	Time-dependent SOA growth curves for crotonaldehyde photooxidation	204
7.6	Comparisons of time-dependent SOA growth from photooxidation of aldehydes and alcohols	205
7.7	Absolute peak areas of all deprotonated ions detected by UPLC/(-)ESI-TOFMS in methacrolein/high-NO experiments	206
7.8	AMS V-mode organic spectra of SOA from high-NO ₂ photooxidation of isoprene and methacrolein	207

7.9	High-resolution W-mode AMS peaks of a number of the major fragment ions observed in methacrolein/high-NO ₂ experiments	208
7.10	Proposed mechanism to form aerosol-phase products from α, β -unsaturated aldehydes	209
7.11	SOA mass yields from isoprene photooxidation as a function of organic loading	210
7.12	Time trends of gas-phase CIMS m/z 311 and SOA growth during high-NO ₂ photooxidation of methacrolein and crotonaldehyde	211
7.13	UPLC/(-)ESI-TOFMS base peak ion chromatograms (BPCs) for high-NO ₂ photooxidation of unsaturated aldehydes	212
7.14	Rotational conformers of possible SOA intermediate in methacrolein and crotonaldehyde mechanism	213
7.15	Mechanism of MBO231 and MBO232 photooxidation under high-NO _x conditions . . .	214
7.16	Gas-phase ion signals of C ₄ -hydroxy-PAN and C ₅ -dihydroxynitrate from photooxidation of MBO231 and MBO232	215

Chapter 1

Introduction

Organic material is a major component of ambient aerosols (also termed particulate matter, PM), and can contribute up to 90% of total aerosol mass. Organic aerosol (OA) can be directly emitted (known as Primary Organic Aerosol, or POA) or formed from oxidation of gas-phase hydrocarbon precursors (known as Secondary Organic Aerosol, or SOA). It has been estimated that during smog episodes, up to 80% of the organic carbon can be secondary in nature. Establishing how SOA is formed from volatile organic compound (VOC) emissions is therefore key to understanding the effects of biogenic and anthropogenic sources on regional air quality and global climate.

Formation of SOA is a complex process, involving gas-phase oxidation chemistry, partitioning of oxidation products between the gas and particulate phases, and aerosol-phase chemistry. The ability to correctly describe and predict ambient SOA growth requires an accurate model of the mechanisms of SOA formation. Currently, SOA formation is described by an absorptive model with semivolatile partitioning products. The equilibrium volatility distributions of oxidation products, measured in laboratory chamber studies, are used in global and regional air quality models to empirically represent SOA yields for a number of parent VOCs. Recent laboratory work has demonstrated that SOA formation is more complex than the simple scheme of equilibrium semivolatile partitioning. Aerosol-phase reactions involving dissolved semivolatile compounds are now known to be important in SOA formation, evidence for which includes the presence of high molecular weight oligomers in SOA and increased SOA yields under acidic conditions. It has also been shown that for a number of hydrocarbons, low-volatility compounds are formed as a result of multiple gas-phase oxidation steps. Atmospheric models must therefore account for the reaction kinetics in SOA formation, as there could be a significant difference in kinetic conditions between chamber experiments and the atmosphere. In Chapters 2 and 3, an equilibrium/kinetic model to describe SOA formation is introduced as a framework to understand how reaction kinetics of semivolatile products in both the gas and aerosol phases affect extrapolation of laboratory chamber data to predict ambient SOA formation.

Recent work has also shown that current models substantially underpredict the amount of SOA in the atmosphere, often by an order of magnitude or more. The discrepancy between modeled and

observed SOA loading can be a result of missing sources of SOA-forming VOCs from the model or misrepresentation of such processes. There is evidence that further oxidation of primary organic aerosols (presumably nonvolatile) produces even more organic particulate matter, hinting that a large pool of hydrocarbons with the potential to form significant amounts of SOA could be missing from atmospheric models. Polycyclic aromatic hydrocarbons (PAHs) is an important class of organic compounds previously assumed to be nonvolatile and not considered to be important SOA precursors. In Chapter 5, aerosol formation from photooxidation of gas-phase naphthalene and other 2-ring PAHs is investigated and the potential contribution to urban SOA formation is discussed.

Levels of nitrogen oxides (NO and NO₂, collectively termed NO_x) have been found to be highly influential in SOA production for a variety of compounds. For example, isoprene, a C₅ conjugated diene and the most abundantly emitted nonmethane hydrocarbon, produces SOA at higher mass yields (mass of SOA formed per mass of hydrocarbon reacted) under low-NO_x conditions than under high-NO_x conditions. While the NO_x effect has been attributed to peroxy radical chemistry, the exact mechanism by which relative concentrations of HO₂, NO and NO₂ radicals affect isoprene SOA formation remains highly uncertain. In Chapter 6, the formation mechanisms of low-volatility compounds observed in isoprene SOA from both high- and low-NO_x photooxidation are elucidated and the reactive intermediates responsible for SOA formation are revealed. In particular, under high-NO_x conditions, peroxy methacryloyl nitrate (MPAN) is formed from reactions of acyl peroxy radical + NO₂, and produces SOA similar to those from isoprene. As a result, SOA formation can be highly sensitive to the NO₂ concentration, an effect of aldehyde chemistry that had previously not been recognized. Chapter 7 details a systematic study of the effect of the NO₂/NO ratio on SOA formation from methacrolein and two other α,β -unsaturated aldehydes, acrolein and crotonaldehyde. In addition, other structurally similar aldehydes and alcohols are studied to provide insight into the reaction mechanism and to establish the role of similar compounds as important SOA intermediates. 2-methyl-3-buten-2-ol (MBO), for example, is a C₅ unsaturated alcohol structurally similar to isoprene, is emitted in large quantities, and can be important for forest photochemistry. In Chapters 4 and 7, yields of potential SOA intermediates from MBO photooxidation, such as glyoxal and peroxy

acyl nitrates (PAN), are measured under high- NO_x conditions. In Chapter 4, SOA production from MBO photooxidation under low- NO_x conditions is also compared to that from isoprene photooxidation under similar conditions. The goal of these studies is to probe the potential role of MBO as a major source of ambient SOA.

To study the chemistry and quantify the yields of SOA formation, experiments were conducted in the Caltech dual 28-m³ Teflon chambers. The laboratory chambers provide a controlled environment to investigate systematically the effects of key variables, most notably NO_x concentrations. A suite of instruments were employed. The aerosol volume and mass concentrations were quantified by differential mobility analyzers (DMA). Parent gas-phase hydrocarbons were quantified by gas chromatography with flame ionization detector (GC/FID). Gas-phase composition was studied using chemical ionization mass spectrometry, a useful tool for detecting gas-phase oxidation products and SOA intermediates. Aerosol-phase composition was characterized by both online and offline mass spectrometry techniques. Knowledge of gas- and aerosol-phase products provide important clues to understanding the pathways leading to gas-to-particle conversion of hydrocarbon oxidation products.

Chapter 2

Reactions of semivolatile organics and their effects on secondary organic aerosol formation*

*Reproduced with permission from “Reactions of semivolatile organics and their effects on secondary organic aerosol formation” by Jesse H. Kroll, Arthur W. H. Chan, Nga L. Ng, Richard C. Flagan, and John H. Seinfeld, *Environmental Science and Technology*, 41 (10), 3545–3550, 2007. Copyright 2007 by the American Chemical Society.

2.1 Abstract

Secondary organic aerosol (SOA) constitutes a significant fraction of total atmospheric particulate loading, but there is evidence that SOA yields based on laboratory studies may underestimate atmospheric SOA. Here we present chamber data on SOA growth from the photooxidation of aromatic hydrocarbons, finding that SOA yields are systematically lower when inorganic seed particles are not initially present. This indicates that concentrations of semivolatile oxidation products are influenced by processes beyond gas-particle partitioning, such as chemical reactions and/or loss to chamber walls. Predictions of a kinetic model in which semivolatile compounds may undergo reactions in both the gas and particle phases in addition to partitioning are qualitatively consistent with the observed seed effect, as well as with a number of other recently observed features of SOA formation chemistry. The behavior arises from a kinetic competition between uptake to the particle phase and reactive loss of the semivolatile product. It is shown that when hydrocarbons react in the absence of preexisting organic aerosol, such loss processes may lead to measured SOA yields lower than would occur under atmospheric conditions. These results underscore the need to conduct studies of SOA formation in the presence of atmospherically relevant aerosol loadings.

2.2 Introduction

Secondary organic aerosol (SOA), formed in the atmospheric oxidation of gas-phase organic compounds and subsequent gas-particle partitioning of lower-volatility reaction products, is known to be a major contributor to the total tropospheric particulate burden (Kanakidou et al., 2005). As a result, our need for an accurate understanding of atmospheric aerosols and their effects requires that models of atmospheric chemistry include processes governing the formation and fate of SOA. Because the chemistry of SOA formation is so complex and uncertain, most descriptions of SOA formation (e.g., de Gouw et al., 2005; Heald et al., 2005; Volkamer et al., 2006) are semi-empirical, constrained by environmental chamber studies of SOA formation and growth.

The primary framework for including SOA formation in atmospheric chemistry models, and

relating the amount of aerosol generated in chambers with that in the troposphere, is the treatment of condensable species in SOA as semivolatile organics, present in appreciable amounts in both the gas and particle phases. Work by Pankow (1994a,b) and Odum et al. (1996) demonstrated that SOA yield Y (defined as $\Delta M/\Delta HC$, the amount of aerosol formed per hydrocarbon reacted) can be expressed in terms of the gas-particle partitioning of a collection of i semivolatile species:

$$Y = \frac{\Delta M}{\Delta HC} = M \sum_i \frac{\alpha_i K_{p,i}}{1 + MK_{p,i}} \quad (2.1)$$

in which α_i and $K_{p,i}$ are the stoichiometric coefficient and gas-particle partitioning coefficient of species i , respectively, and M is the mass concentration of absorbing (typically organic) aerosol present. Therefore, SOA formation is a function of not only the amount and volatility of the semivolatile compounds, but also the aerosol mass into which they can partition. This non-stoichiometric nature of aerosol yields is a known feature of SOA formation, and aerosol growth data have been shown to be well-represented by Eq. 2.1 (typically as “yield curves”, plots of Y vs. M) (Odum et al., 1996; Seinfeld and Pankow, 2003). This expression is also used to describe SOA formation in the atmosphere: α ’s and K_p ’s for a given hydrocarbon are those determined in chamber studies, and M is the ambient atmospheric organic aerosol mass loading, typically 1–20 $\mu\text{g}/\text{m}^3$. However, recent work suggests that this semi-empirical approach, in which SOA formation is estimated based on experimentally-determined aerosol yields, generally predicts SOA levels that are substantially lower (often by an order of magnitude or more) than measured values (de Gouw et al., 2005; Heald et al., 2005; Volkamer et al., 2006). Such discrepancies suggest that the reaction conditions of environmental chambers may promote less SOA growth than occurs in the atmosphere, though unidentified SOA precursors may also play a role.

In this work we examine a chemical system for which SOA yields are dependent on the timing of the onset of gas-particle partitioning. Specifically, it is shown that in the photooxidation of aromatic compounds, aerosol growth begins sooner, and hence aerosol yields are higher, in the presence of seed particles. Such an effect indicates that processes governing the amount of SOA formed are

more complex than the simple formation and condensation of semivolatile compounds. Additional reactions of semivolatile organics may occur in both the gas and particle phases, changing the concentration and/or volatility of the organics. We examine the kinetics and partitioning of a model semivolatile compound which may undergo reactions in the gas and particle phases, in order to better understand the effect of such reactions on SOA growth. It is also shown that in the absence of initial absorbing aerosol mass, SOA yields as measured in chambers may be significantly lower than in the real atmosphere.

2.3 Experimental

SOA formation from the photooxidation of aromatic hydrocarbons was measured, using experimental protocols described previously in detail (Cocker et al., 2001a; Keywood et al., 2004; Kroll et al., 2006). Briefly, ~ 3 ppm H_2O_2 (the OH precursor) and the aromatic (71–72 ppb *m*-xylene or 87–91 ppb toluene, Aldrich) are added to a 28 m³ Teflon chamber; for some experiments NO and/or ammonium sulfate seed are also added. For “NO_x” experiments, initial NO and NO₂ levels are 85 ± 4 ppb and 6 ± 4 ppb, respectively (otherwise NO_x levels are < 1 ppb), and for seeded experiments, seed number concentrations are $21,000 \pm 4,000$ particles/cm³ (otherwise concentrations are $< 5/\text{cm}^3$). Reaction begins when the blacklights surrounding the chamber are turned on; hydrocarbon concentration is monitored by gas chromatography-flame ionization detection, and aerosol volume by a differential mobility analyzer. Particle volume is corrected for losses of particles to the walls (Keywood et al., 2004). Temperature and relative humidity are the same in all experiments (initial values of 23–25 °C and 4–7%, respectively). A total of eight experiments, systematically varying aromatic hydrocarbon (toluene vs. *m*-xylene), ammonium sulfate seed (“seeded” vs. “nonseeded”) and NO_x level (“NO_x” vs. “NO_x-free”), were conducted.

2.4 Results and Discussion

Shown in Fig. 2.1 is SOA growth from all four pairs of seeded/nonseeded experiments. Data are presented as “growth curves”, plots of aerosol growth vs. hydrocarbon reacted. As hydrocarbon measurements are made with much lower frequency than those of particle volume, the HC values shown are obtained by interpolation of GC measurements, fitting the data to a double-exponential decay (which reproduces measured hydrocarbon concentrations well, $R^2 > 0.95$). Only the growth near the beginning of the experiments (including the atmospherically relevant range of M) is shown; beyond this, the shapes of the curves do not change substantially, remaining slightly curved until all hydrocarbon is consumed ($\Delta HC = HC(0)$). Aerosol yields are generally higher than previously reported for aromatic photooxidation (Odum et al., 1997), likely a result of the lower NO_x levels employed in this work (Song et al., 2005; Johnson et al., 2004).

We focus on the systematic differences between aerosol growth in the seeded and nonseeded cases; the effects of the other parameters varied (hydrocarbon structure and NO_x level) are beyond the scope of this work and will be discussed in a forthcoming paper. The presence of seed is expected to have a negligible effect on hydrocarbon oxidation, and indeed the observed decays of the hydrocarbon (from reaction with OH) are the same in seeded and nonseeded experiments. However, in all cases the aerosol growth exhibits a marked dependence on whether seed particles are present. In all seeded experiments, SOA growth is observed to begin essentially immediately, whereas in all nonseeded experiments, there is a substantial “induction period”, a period of time during which the parent hydrocarbon reacts away but no aerosol is formed. The amount of hydrocarbon reacted during this period in the non-seeded cases ranges from $20 \mu\text{g}/\text{m}^3$ (~ 5 ppb) for the toluene/ NO_x -free experiment to $120 \mu\text{g}/\text{m}^3$ (~ 27 ppb) for the *m*-xylene/ NO_x experiment. Once SOA growth begins, its rate is the same as in the seeded experiments, leading to roughly fixed differences in ΔM at a given value of ΔHC , and hence differences in SOA yields. Such differences persist throughout the experiments, but are most pronounced at lower (atmospherically relevant) aerosol loadings: for example, in the *m*-xylene/ NO_x experiments, at $M = 5 \mu\text{g}/\text{m}^3$ SOA yield in the seeded case is almost twice that of the nonseeded case (assuming unit density). We note that such a difference between yields in

seeded and nonseeded experiments was not observed in an earlier study of high- NO_x photooxidation of *m*-xylene from our laboratory (Cocker et al., 2001b); in that study there were few data at low ($< 25 \text{ } \mu\text{g}/\text{m}^3$) aerosol loadings, the condition at which this effect is most pronounced, as well as higher scatter in the yield results than we currently observe (Keywood et al., 2004) and possibly differing chemistry due to higher NO_x levels.

The observed effect of seed on SOA growth implies differences in effective gas-particle partitioning coefficients (Kroll and Seinfeld, 2005): partitioning into the particle phase is stronger in the seeded experiments than in the nonseeded ones. This difference cannot be explained by the simple model of SOA formation described in the Introduction (and shown in Fig. 2.2a): the semivolatile species initially formed are the same regardless of the presence of seed, and the solid seed particles cannot promote absorptive partitioning. Instead, the distribution of reaction products must be affected by additional processes, leading to enhancements in lower-volatility compounds in the presence of seed particles, and/or decreases in their absence.

The former possibility is consistent with recent work suggesting that particle-phase reactions, forming high-MW, low-volatility products, are important processes in SOA formation. The formation of such compounds, including oligomers (Tobias and Ziemann, 2000; Tolocka et al., 2004; Kalberer et al., 2004; Iinuma et al., 2004; Gao et al., 2004a,b; Surratt et al., 2006) and organosulfates (Liggio et al., 2005; Liggio and Li, 2006; Surratt et al., 2007), is accompanied by the depletion of the semivolatile reactants in the particle phase; the resulting shift in the gas-particle equilibrium leads to more SOA formation than would be inferred on the basis of physical partitioning alone (Johnson et al., 2004; Jang et al., 2002). Many such products are thermally stable (e.g., Tobias and Ziemann (2000); Surratt et al. (2006); Liggio et al. (2005); Liggio and Li (2006); Surratt et al. (2007)), suggesting their formation is irreversible, with no reversion to reactants over the timescales studied (though experimental studies of the reversibility of SOA formation are largely lacking at present). The irreversible formation of nonvolatile species in SOA suggests the reaction scheme shown in Fig. 2.2b, in which the semivolatile species (A_p) reacts further in the condensed phase to form a purely particle-phase species (B_p). The promotion of such reactions by ammonium sulfate particles

may account for the differences in SOA growth illustrated in Fig. 2.1.

Alternately, such differences could result from reactions of semivolatile species forming products other than SOA. Such processes serve to lower the concentration of the gas-phase species, thereby reducing the amount that partitions into the aerosol phase. Shown in Fig. 2.2c is such a mechanism, in which the gas-phase semivolatile organic (A_g) reacts to form X, a generic non-particle-phase product. This may be a volatile species present only in the gas phase, formed by bond-breaking oxidation or photolysis reactions; or it may represent organics lost to the chamber walls. Such losses of semivolatile species have received little study in terms of their role in SOA formation, but certainly occur in many cases. For example, it has been shown that photolysis of organic aerosol components forms relatively volatile organics (Presto et al., 2005; Gomez et al., 2006; Park et al., 2006), which lead to reductions in SOA mass. Similarly, glyoxal, formed in the oxidation of aromatics, is known to efficiently partition into the particle phase (Liggio et al., 2005; Hastings et al., 2005; Kroll et al., 2005), but it is also known to react with OH, photolyze, and be taken up onto surfaces; all these processes are expected to compete with gas-particle partitioning and hence reduce SOA growth.

Thus additional reactions of semivolatile organics, such as those shown in Figs. 2.2b and 2.2c, may qualitatively explain differences in SOA yields between seeded and nonseeded photooxidation experiments (Fig. 2.1). However, neither scheme represents a reasonable mechanism by which all semivolatile compounds will react: in one case (Fig. 2.2b) all the organic is incorporated into the gas phase, so growth does not depend on gas-particle partitioning, and in the other (Fig. 2.2c), at long reaction times no SOA is formed at all. Instead, most SOA-forming reactions involve a spectrum of semivolatile products, which likely exhibit varying chemistries, including reactions in both phases. The generalized mechanism shown in Fig. 2.2d, in which the semivolatile species A can react by both pathways in Figs. 2.2b and 2.2c, serves as a useful model system for investigating the role of the reactions of semivolatile organics in SOA growth, and may even roughly approximate the behavior of a more complex mixture. In this scheme, SOA yields are dependent not only on the volatility of the product A, but also on the rates of these additional reactions. In the following sections, we illustrate the possible role of such chemistry on aerosol growth. The dependence of SOA

growth on the presence of seed particles is predicted, due largely to the delayed onset of gas-particle partitioning in the nonseeded case.

2.5 Model Description

The mechanism shown in Fig. 2.2d is considered for only a single semivolatile species; we emphasize this is not intended to be a detailed mechanism of SOA formation, but rather a model system for studying the role of additional chemical reactions on gas-particle partitioning. All steps in the mechanism are represented as unimolecular processes, with rate constants k_{HC} , k_g , and k_p for the reactions $HC \rightarrow A_g$, $A_g \rightarrow X$, and $A_p \rightarrow B_p$, respectively. For simplicity, specific reaction conditions such as oxidant level are omitted, and all reactions are assumed to be irreversible over the timescale of the simulation; the effects of specific reaction conditions and reversible processes are beyond the scope of this work, but are worth further study. Gas-particle partitioning is treated as in Bowman et al. (1997), with the net rate of uptake of a species by physical partitioning given by J , its flux to the particle surface:

$$J = \frac{N_p 2\pi D_p \lambda \bar{c} ([A_g] - [A_g]_{eq})}{1 + \frac{8\lambda}{\alpha_c D_p}} \quad (2.2)$$

in which N_p is the particle number density, D_p the diameter of the particle, λ the mean free path of air (65 nm), \bar{c} the mean molecular speed of the species, α_c the accommodation coefficient, and $[A_g]$ and $[A_g]_{eq}$ the bulk and near-surface (equilibrium) mass concentrations of the gas-phase species, respectively. $[A_g]_{eq}$ is calculated by absorptive partitioning (Pankow, 1994a):

$$[A_g]_{eq} = \frac{[A_p]}{K_p M} = \frac{[A_p]}{K_p ([A_p] + [B_p] + M(0))} \quad (2.3)$$

in which $M(0)$ is the mass concentration of preexisting organic aerosol. For simulations of reactions carried out in the absence of organic aerosol (i.e., chamber experiments), initial absorbing aerosol mass loading $M(0)$ is set to a very small but nonzero value (0.1 ng/m³). The kinetics of gas-particle partitioning (Eq. 2) require values for D_p and N_p ; to simplify the modeling, three assumptions

are made: (1) particle number concentration is fixed at $2 \times 10^4/\text{cm}^3$, (2) the aerosol population is monodisperse, and (3) the organic aerosol has unit density. Relaxation of any of these assumptions is expected to have a minimal effect on model results.

For the simulations discussed here, the parent hydrocarbon reacts with rate $k_{HC} = 0.015 \text{ min}^{-1}$, forming A with a stoichiometric yield of 0.2, reasonable values for an SOA-forming reaction. Rates of the reactions of species A are chosen to be comparable to hydrocarbon oxidation, with $k_p = k_{HC}$ and $k_g = 0.3k_{HC}$; if the reactions were substantially slower, their effects would not be observed in the timescale of chamber experiments. The semivolatile compound A is assigned a K_p of $0.1 \text{ } \mu\text{g}^{-1} \text{ m}^3$ (for a saturation vapor pressure of $10 \text{ } \mu\text{g}/\text{m}^3$), of 200 m/s (corresponding to a MW of $\sim 150 \text{ g/mol}$), and α_c of 0.02 (as determined for glyoxal (Schweitzer et al., 1998)). For most simulations, only the initial conditions ($HC(0)$, $M(0)$, and seed volume) are varied.

2.6 Model Predictions

Figure 2.3a shows concentrations as a function of time after reaction initiation, for conditions typical of seeded chamber experiments: initial hydrocarbon concentration is relatively high ($HC(0) = 91 \text{ } \mu\text{g}/\text{m}^3$), and the preexisting aerosol seed is ammonium sulfate ($20 \text{ } \mu\text{g}/\text{m}^3$), with negligible initial organic mass ($M(0) = 0.1 \text{ ng}/\text{m}^3$).

Following reaction initiation, there is an induction period, a result of the absence of absorbing aerosol into which the semivolatile organic may partition. Thus the semivolatile species increases in concentration in the gas phase, during which time some fraction reacts away to form X. Only when A_g approaches its saturation vapor pressure does partitioning begin and SOA mass is formed. After ~ 12 hours all the hydrocarbon is reacted away, A has fully reacted to form X or B_p , and aerosol formation is completed, with $\Delta M = 10 \text{ } \mu\text{g}/\text{m}^3$. Thus the SOA mass yield is 11% at an organic aerosol loading of $10 \text{ } \mu\text{g}/\text{m}^3$.

SOA yields over a range of aerosol mass loadings are generally determined by varying the amount of hydrocarbon reacted, which leads to differences in M . Calculated yields over a range of M 's are presented in Fig. 2.4 (curve a). The curve of yield vs. M (over the atmospherically relevant range of

M 's) has the qualitative shape of a typical “yield curve”, consistent with the simple partitioning of a single semivolatile compound (Fig. 2.2a). Thus SOA growth is governed by semivolatile partitioning, even though nonvolatile species are also formed. This yield curve (and the others in Fig. 2.4) may be fit to the single-product partitioning expression (Eq. 2.1), to obtain effective partitioning parameters; however, these do not match those used in the model, as SOA growth is also strongly influenced by reaction rates (k_p and k_g).

The effects on SOA yields of the values of these reaction rates are illustrated by the dashed curves in Fig. 2.4. The upper curve is the case in which k_p , the particle-phase reaction rate constant, is increased by 50%; this is consistent with laboratory measurements of enhanced SOA yields in the presence of acidic seed particles, presumably by acid-catalyzed reactions (Tolocka et al., 2004; Iinuma et al., 2004; Gao et al., 2004a,b; Jang et al., 2002). The lower curve shows the effect of increasing k_g , the rate constant for reaction in the gas phase, by 25%, leading to decreased aerosol yields. This is consistent with laboratory evidence that photolysis of semivolatile compounds leads to the formation of relatively volatile products (Presto et al., 2005; Gomez et al., 2006; Park et al., 2006). In the case where such gas-phase reactions dominate ($k_g > k_p$) and the condensable product is reasonably nonvolatile (high K_p), SOA mass can actually decrease via this volatilization mechanism; such behavior has been observed recently in SOA formation from isoprene oxidation under NO_x -free conditions (Kroll et al., 2006). These gas phase reactions reduce SOA growth by reducing the concentration of the semivolatile species in the gas phase; similarly, an increase in the rate of formation of the semivolatile species, which increases its gas-phase concentration, will increase the SOA yield. The role of hydrocarbon oxidation rate on SOA formation from aromatic photooxidation will be explored in forthcoming work.

Shown in Fig. 2.3b is the reaction profile for the “nonseeded” case, with conditions the same as those in Fig. 2.3a, only without any ammonium sulfate seed present. Nucleation dynamics are not explicitly included in this model, as very small particles ($D_p < 5$ nm), composed of the trace preexisting organic mass (0.1 ng/m^3), are assumed to be present. The hydrocarbon oxidation (and hence formation of the semivolatile species) is the same as in the “seeded” case, but because of the

much lower particle surface area, there is a mass transfer limitation to gas-particle partitioning. Thus A accumulates in the gas phase, even exceeding its saturation vapor pressure, and partitioning (SOA formation) does not occur until later in the reaction. Such an increase in the induction period was predicted by Bowman et al. (1997), but in that work the semivolatile organic underwent partitioning only (as in Fig. 2.2a), so only the rate of SOA growth was affected. However, in the present case, the reaction $A_g \rightarrow X$ competes with partitioning, so that longer induction periods lead to more depletion of the semivolatile compound, and less SOA is formed.

As shown in Fig. 2.4 (curve b), yields in the nonseeded case are consistently lower than those in the seeded case, over a range of values of M . Thus, this mechanism is qualitatively consistent with the seed effect observed in aromatic photooxidation (Fig. 2.1). Fitting the SOA growth data to this kinetic model is beyond the scope of this work, but simple comparisons are possible; for example, the fact that in the seeded case no induction period is observed, even though one is predicted, suggests that aromatic oxidation products are less volatile (higher K_p) than simulated in the model. The modeled differences between the seeded and nonseeded cases in Fig. 2.4 are relatively modest, but would be larger under conditions of more aerosol formation during the induction period (higher K_p , higher k_p , etc.), or a longer induction period (higher saturation ratio S prior to aerosol growth).

Therefore reactions of semivolatile compounds may have a large influence on SOA yields, and their importance is governed in part by the timing of the onset of gas-particle partitioning. In the seeded case (Fig. 2.3a) this induction period is a result of the initial lack of organic aerosol mass into which the semivolatile organics may partition; in the unseeded case (Fig. 2.3b), it is longer due to the mass-transfer limitation arising from the initially small aerosol surface area. However, in the atmosphere, organic aerosol is generally present, so such effects are not expected. Shown in Fig. 2.3c is a simulation using more realistic tropospheric conditions: a small amount of hydrocarbon ($HC(0) = 1 \text{ } \mu\text{g}/\text{m}^3$) reacted in the presence of background organic aerosol ($M(0) = 10 \text{ } \mu\text{g}/\text{m}^3$). These initial conditions are different than those of chamber experiments (Fig. 2.3a,b), in which large amounts of hydrocarbon are reacted with no organic aerosol present; however all other parameters are left unchanged. Because absorbing aerosol is already present, there is no induction period and

gas-particle partitioning of the semivolatile species begins immediately. As a result, a smaller fraction of A reacts to form X in the early stages of the reaction. Final aerosol growth (ΔM) is $0.14 \mu\text{g}/\text{m}^3$, for SOA yield of 14% at an organic mass loading of $10.1 \mu\text{g}/\text{m}^3$; this yield is significantly higher than that of the “seeded” case (Fig. 2.3a) at nearly the same value of M .

Aerosol yields over a range of organic aerosol loadings are shown in Fig. 2.4, curve c. Unlike for chamber studies (curves a–b), M is varied by changing not $HC(0)$ (which is fixed at $1 \mu\text{g}/\text{m}^3$), but instead the preexisting organic aerosol loading $M(0)$. Over the range of M ’s shown, SOA yields in the atmospheric case are significantly higher than those in the chamber case, owing to differences in initial partitioning conditions. Such differences in yields are significant (at $M = 5 \mu\text{g}/\text{m}^3$, yield in the “atmosphere” case is about twice that in the “unseeded” case), and are comparable to those from changing reaction conditions (dashed curves).

2.7 Implications

We have presented experimental data showing that SOA yields from the photooxidation of aromatic hydrocarbons are enhanced when ammonium sulfate is present. Such an effect is inconsistent with a mechanism of SOA formation that involves only the formation and partitioning of semivolatile species (Fig. 2.2a). Instead, there must be additional processes (chemical reactions and/or surface losses) that affect the concentrations of semivolatile organics; the effect on SOA yields of such reactions, particularly those occurring in the gas phase, have so far received little attention. We propose as a model system the mechanism shown in Fig. 2.2d, in which a semivolatile species may undergo reactions in both the gas phase (reducing its concentration and hence reducing SOA formation) and the particle phase (promoting SOA formation). The kinetics of this mechanism indicate this seed effect arises from loss of the semivolatile compound during the induction period, which is longer in the nonseeded experiment as a result of mass-transfer limitations. The additional reactions of semivolatile species may also account for a number of other recent experimental observations, such as nonvolatile species in SOA, increased SOA yields with acidic seed, and photochemical loss of SOA mass. An important implication of these reactions is that SOA yields may be quite dependent on

detailed reaction conditions. In particular, in laboratory studies of SOA formation, an induction period prior to gas-particle partitioning, during which time gas-phase semivolatile species may be depleted by chemical reaction or wall loss, may lead to lower SOA formation than occurs under atmospheric conditions. Such an effect may contribute to the discrepancies between modeled and measured SOA in the atmosphere (de Gouw et al., 2005; Heald et al., 2005; Volkamer et al., 2006).

Our results suggest that chamber experiments need to be carried out as much as possible under atmospherically realistic conditions, in terms of not only chemistry (oxidant levels, NO_x levels, etc.) but also partitioning (preexisting aerosol). The aromatic photooxidation results presented here indicate that the presence of inorganic seed aerosol can be important for initiating gas-particle partitioning, as lack of aerosol surface area may inhibit uptake of organics; our modeling results suggest the presence of organic aerosol, which allows for immediate absorptive partitioning of organics, may be important as well. Running experiments under conditions similar to those of Fig. 2.3c is infeasible, but the presence of even a small amount of organic seed aerosol (a few $\mu\text{g}/\text{m}^3$) would eliminate the induction period, substantially reducing differences between “chamber” and “atmospheric” conditions. The loading of preexisting organic seed is a parameter that has not been explored in chamber experiments of SOA formation thus far, and certainly warrants future study.

This seed effect, and the effect of additional reactions of semivolatile species in general, is expected to be most important for reactions that form semivolatile compounds with relatively high vapor pressures (low K_p ’s), and hence which exhibit significant induction times. For reactions which occur relatively rapidly (high k_{HC}) and involve relatively low-volatility condensable compounds (high K_p ’s), SOA growth begins very early in the reaction. For these reactions, such as α -pinene ozonolysis (Ng et al., 2006; Presto and Donahue, 2006), the induction period is negligible, and gas-particle partitioning occurs throughout the experiment at atmospherically relevant levels.

The induction periods described here are a result of the buildup of semivolatile products in the gas phase prior to gas-particle partitioning; induction periods may arise from other effects as well. Examples include photooxidation reactions carried out under high- NO_x conditions, in which SOA formation does not begin until $[\text{NO}]$ falls to ppb levels (e.g., Kroll et al. 2006; Johnson et al. 2004),

and reactions involving multiple rate-limiting steps to SOA formation (Bowman et al., 1997; Ng et al., 2006). In both cases the delay is in the formation of the semivolatile species rather than in gas-particle partitioning, and so may occur under atmospheric conditions. The sources of (and relationships between) different induction periods need to be understood in order for chamber yield measurements to accurately represent atmospheric conditions.

We emphasize that the mechanism shown in Fig. 2.2d, while possibly valid for some semivolatile organics, is not intended as a general scheme describing the chemistry of all condensable compounds. Most SOA-forming reactions involve a very large number of semivolatiles, which may react via any number of mechanisms, including those shown in Fig. 2.2. This mechanism is instead used as a model system illustrating the potential influence of reactions of semivolatile species on SOA formation, and the resulting dependence of SOA yields on reaction and partitioning conditions. Such reactions are often not treated explicitly in models of SOA formation, but certainly occur for a wide range of compounds: most organics are susceptible to reaction with OH, and loss to chamber walls is a potential sink for species that are efficiently taken up to the aerosol phase. If these processes are fast on the timescale of chamber experiments, they may have a substantial impact on SOA growth, and on the relationship between chamber studies and real atmospheric conditions. Only by explicitly including such reactions in models of SOA formation, or by making SOA yield measurements under oxidative and partitioning conditions relevant to the atmosphere, can such effects be taken fully into account.

Acknowledgments

This research was funded by the U. S. Environmental Protection Agency Science to Achieve Results (STAR) Program grant number RD-83107501-0, managed by the EPA’s Office of Research and Development (ORD), National Center for Environmental Research (NCER), and by the U.S. Department of Energy Biological and Environmental Research Program DE-FG02-05ER63983; this work has not been subjected to the EPAs required peer and policy review and therefore does not necessarily reflect the views of the Agency and no official endorsement should be inferred.

Bibliography

- Bowman, F. M., Odum, J. R., Seinfeld, J. H., and Pandis, S. N.: Mathematical model for gas-particle partitioning of secondary organic aerosols, *Atmos. Environ.*, 31, 3921–3931, 1997.
- Cocker, D. R., Flagan, R. C., and Seinfeld, J. H.: State-of-the-art chamber facility for studying atmospheric aerosol chemistry, *Environ. Sci. Technol.*, 35, 2594–2601, 2001a.
- Cocker, D. R., Mader, B. T., Kalberer, M., Flagan, R. C., and Seinfeld, J. H.: The effect of water on gas-particle partitioning of secondary organic aerosol: II. *m*-xylene and 1,3,5-trimethylbenzene photooxidation systems, *Atmos. Environ.*, 35, 6073–6085, 2001b.
- de Gouw, J. A., Middlebrook, A. M., Warneke, C., Goldan, P. D., Kuster, W. C., Roberts, J. M., Fehsenfeld, F. C., Worsnop, D. R., Canagaratna, M. R., Pszenny, A. A. P., Keene, W. C., Marchewka, M., Bertman, S. B., and Bates, T. S.: Budget of organic carbon in a polluted atmosphere: Results from the New England Air Quality Study in 2002, *J. Geophys. Res.-Atmos.*, 110, D16305, doi:10.1029/2004JD005623, 2005.
- Gao, S., Keywood, M., Ng, N. L., Surratt, J., Varutbangkul, V., Bahreini, R., Flagan, R. C., and Seinfeld, J. H.: Low-molecular-weight and oligomeric components in secondary organic aerosol from the ozonolysis of cycloalkenes and α -pinene, *J. Phys. Chem. A*, 108, 10 147–10 164, 2004a.
- Gao, S., Ng, N. L., Keywood, M., Varutbangkul, V., Bahreini, R., Nenes, A., He, J. W., Yoo, K. Y., Beauchamp, J. L., Hodyss, R. P., Flagan, R. C., and Seinfeld, J. H.: Particle phase acidity and oligomer formation in secondary organic aerosol, *Environ. Sci. Technol.*, 38, 6582–6589, 2004b.
- Gomez, A. L., Park, J., Walser, M. L., Lin, A., and Nizkorodov, S. A.: UV photodissociation spectroscopy of oxidized undecylenic acid films, *J. Phys. Chem. A*, 110, 3584–3592, 2006.
- Hastings, W. P., Koehler, C. A., Bailey, E. L., and De Haan, D. O.: Secondary organic aerosol formation by glyoxal hydration and oligomer formation: Humidity effects and equilibrium shifts during analysis, *Environ. Sci. Technol.*, 39, 8728–8735, 2005.

- Heald, C. L., Jacob, D. J., Park, R. J., Russell, L. M., Huebert, B. J., Seinfeld, J. H., Liao, H., and Weber, R. J.: A large organic aerosol source in the free troposphere missing from current models, *Geophys. Res. Lett.*, 32, L18809, doi:10.1029/2005GL023831, 2005.
- Inuma, Y., Böge, O., Gnauk, T., and Herrmann, H.: Aerosol-chamber study of the α -pinene/ O_3 reaction: influence of particle acidity on aerosol yields and products, *Atmos. Environ.*, 38, 761–773, 2004.
- Jang, M. S., Czoschke, N. M., Lee, S., and Kamens, R. M.: Heterogeneous atmospheric aerosol production by acid-catalyzed particle-phase reactions, *Science*, 298, 814–817, 2002.
- Johnson, D., Jenkin, M. E., Wirtz, K., and Martin-Reviejo, M.: Simulating the formation of secondary organic aerosol from the photooxidation of toluene, *Environ Chem*, 1, 150–165, 2004.
- Kalberer, M., Paulsen, D., Sax, M., Steinbacher, M., Dommen, J., Prevot, A. S. H., Fisseha, R., Weingartner, E., Frankevich, V., Zenobi, R., and Baltensperger, U.: Identification of polymers as major components of atmospheric organic aerosols, *Science*, 303, 1659–1662, 2004.
- Kanakidou, M., Seinfeld, J. H., Pandis, S. N., Barnes, I., Dentener, F. J., Facchini, M. C., Van Dingenen, R., Ervens, B., Nenes, A., Nielsen, C. J., Swietlicki, E., Putaud, J. P., Balkanski, Y., Fuzzi, S., Horth, J., Moortgat, G. K., Winterhalter, R., Myhre, C. E. L., Tsigaridis, K., Vignati, E., Stephanou, E. G., and Wilson, J.: Organic aerosol and global climate modelling: a review, *Atmos. Chem. Phys.*, 5, 1053–1123, 2005.
- Keywood, M. D., Varutbangkul, V., Bahreini, R., Flagan, R. C., and Seinfeld, J. H.: Secondary organic aerosol formation from the ozonolysis of cycloalkenes and related compounds, *Environ. Sci. Technol.*, 38, 4157–4164, 2004.
- Kroll, J. H. and Seinfeld, J. H.: Representation of secondary organic aerosol laboratory chamber data for the interpretation of mechanisms of particle growth, *Environ. Sci. Technol.*, 39, 4159–4165, 2005.

- Kroll, J. H., Ng, N. L., Murphy, S. M., Varutbangkul, V., Flagan, R. C., and Seinfeld, J. H.: Chamber studies of secondary organic aerosol growth by reactive uptake of simple carbonyl compounds, *J. Geophys. Res.-Atmos.*, 110, D23207, doi:10.1029/2005JD006004, 2005.
- Kroll, J. H., Ng, N. L., Murphy, S. M., Flagan, R. C., and Seinfeld, J. H.: Secondary organic aerosol formation from isoprene photooxidation, *Environ. Sci. Technol.*, 40, 1869–1877, 2006.
- Liggio, J. and Li, S. M.: Organosulfate formation during the uptake of pinonaldehyde on acidic sulfate aerosols, *Geophys. Res. Lett.*, 33, L13808, doi:10.1029/2006GL026079, 2006.
- Liggio, J., Li, S. M., and McLaren, R.: Heterogeneous reactions of glyoxal on particulate matter: Identification of acetals and sulfate esters, *Environ. Sci. Technol.*, 39, 1532–1541, 2005.
- Ng, N. L., Kroll, J. H., Keywood, M. D., Bahreini, R., Varutbangkul, V., Flagan, R. C., Seinfeld, J. H., Lee, A., and Goldstein, A. H.: Contribution of first- versus second-generation products to secondary organic aerosols formed in the oxidation of biogenic hydrocarbons, *Environ. Sci. Technol.*, 40, 2283–2297, 2006.
- Odum, J. R., Hoffmann, T., Bowman, F., Collins, D., Flagan, R. C., and Seinfeld, J. H.: Gas/particle partitioning and secondary organic aerosol yields, *Environ. Sci. Technol.*, 30, 2580–2585, 1996.
- Odum, J. R., Jungkamp, T. P. W., Griffin, R. J., Forstner, H. J. L., Flagan, R. C., and Seinfeld, J. H.: Aromatics, reformulated gasoline, and atmospheric organic aerosol formation, *Environ. Sci. Technol.*, 31, 1890–1897, 1997.
- Pankow, J. F.: An absorption-model of gas-particle partitioning of organic-compounds in the atmosphere, *Atmos. Environ.*, 28, 185–188, 1994a.
- Pankow, J. F.: An absorption-model of the gas aerosol partitioning involved in the formation of secondary organic aerosol, *Atmos. Environ.*, 28, 189–193, 1994b.
- Park, J., Gomez, A. L., Walser, M. L., Lin, A., and Nizkorodov, S. A.: Ozonolysis and photolysis of alkene-terminated self-assembled monolayers on quartz nanoparticles: implications for photochemical aging of organic aerosol particles, *Phys Chem Chem Phys*, 8, 2506–2512, 2006.

- Presto, A. A. and Donahue, N. M.: Investigation of α -pinene plus ozone secondary organic aerosol formation at low total aerosol mass, *Environ. Sci. Technol.*, 40, 3536–3543, 2006.
- Presto, A. A., Hartz, K. E. H., and Donahue, N. M.: Secondary organic aerosol production from terpene ozonolysis. 1. Effect of UV radiation, *Environ. Sci. Technol.*, 39, 7036–7045, 2005.
- Schweitzer, F., Magi, L., Mirabel, P., and George, C.: Uptake rate measurements of methanesulfonic acid and glyoxal by aqueous droplets, *J. Phys. Chem. A*, 102, 593–600, 1998.
- Seinfeld, J. H. and Pankow, J. F.: Organic atmospheric particulate material, *Annu. Rev. Phys. Chem.*, 54, 121–140, 2003.
- Song, C., Na, K. S., and Cocker, D. R.: Impact of the hydrocarbon to NO_x ratio on secondary organic aerosol formation, *Environ. Sci. Technol.*, 39, 3143–3149, 2005.
- Surratt, J. D., Murphy, S. M., Kroll, J. H., Ng, N. L., Hildebrandt, L., Sorooshian, A., Szmigielski, R., Vermeylen, R., Maenhaut, W., Claeys, M., Flagan, R. C., and Seinfeld, J. H.: Chemical composition of secondary organic aerosol formed from the photooxidation of isoprene, *J. Phys. Chem. A*, 110, 9665–9690, 2006.
- Surratt, J. D., Kroll, J. H., Kleindienst, T. E., Edney, E. O., Claeys, M., Sorooshian, A., Ng, N. L., Offenberg, J. H., Lewandowski, M., Jaoui, M., Flagan, R. C., and Seinfeld, J. H.: Evidence for organosulfates in secondary organic aerosol, *Environ. Sci. Technol.*, 41, 517–527, 2007.
- Tobias, H. J. and Ziemann, P. J.: Thermal desorption mass spectrometric analysis of organic aerosol formed from reactions of 1-tetradecene and O_3 in the presence of alcohols and carboxylic acids, *Environ. Sci. Technol.*, 34, 2105–2115, 2000.
- Tolocka, M. P., Jang, M., Ginter, J. M., Cox, F. J., Kamens, R. M., and Johnston, M. V.: Formation of oligomers in secondary organic aerosol, *Environ. Sci. Technol.*, 38, 1428–1434, 2004.
- Volkamer, R., Jimenez, J. L., San Martini, F., Dzepina, K., Zhang, Q., Salcedo, D., Molina, L. T., Worsnop, D. R., and Molina, M. J.: Secondary organic aerosol formation from anthro-

pogenic air pollution: Rapid and higher than expected, *Geophys. Res. Lett.*, 33, L17811, doi: 10.1029/2006GL026899, 2006.

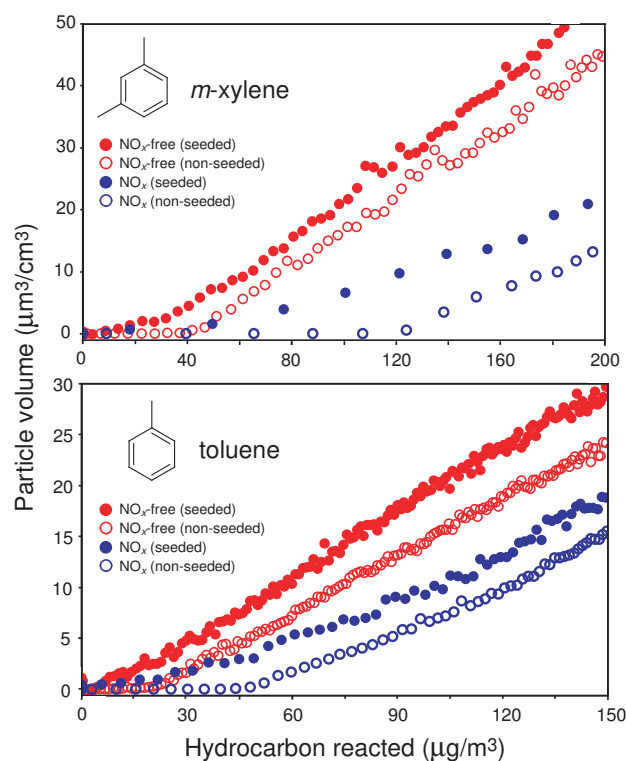


Figure 2.1: “Growth curves” for photooxidation of *m*-xylene and toluene. Each curve represents a single experiment; individual points are in 4 minute increments. Color denotes NO_x condition (red: NO_x -free, blue: ~ 90 ppb NO_x initially present) and symbol denotes seed (filled circles: ammonium sulfate seed present, open circles: no seed present). In all nonseeded experiments there is a substantial induction period, leading to lower SOA yields.

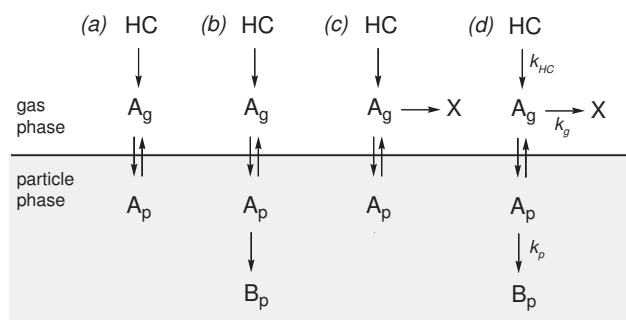


Figure 2.2: Mechanisms for SOA formation from a single semivolatile species A. (a) simple gas-particle partitioning, the standard model for SOA growth; (b) gas-particle partitioning followed by irreversible reaction to form nonvolatile product B_p ; (c) competition between gas-particle partitioning and irreversible loss of the gas-phase semivolatile compound; (d) both gas- and particle-phase reactions in addition to partitioning.

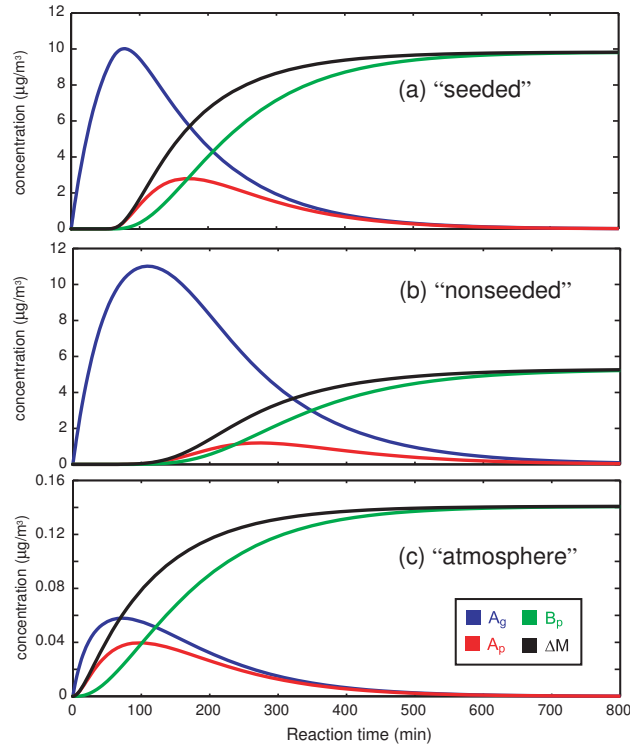


Figure 2.3: Predictions from the mechanism in Fig. 2.2d, showing the time-dependent mass concentrations of key species. In all cases $\alpha = 0.2$, $K_p = 0.1 \text{ m}^3 \mu\text{g}^{-1}$, $k_{HC} = k_p = 0.015 \text{ min}^{-1}$, and $k_g = 0.0045 \text{ min}^{-1}$. (a) Initial concentrations typical of chamber conditions: $HC(0) = 92 \mu\text{g/m}^3$, $M(0) = 0.1 \text{ ng/m}^3$, and $20 \mu\text{g/m}^3$ ammonium sulfate seed. (b) Same as (a), but with no ammonium sulfate present. (c) Initial concentrations more typical of atmospheric conditions: $HC(0) = 1 \mu\text{g/m}^3$ and $M(0) = 10 \mu\text{g/m}^3$.

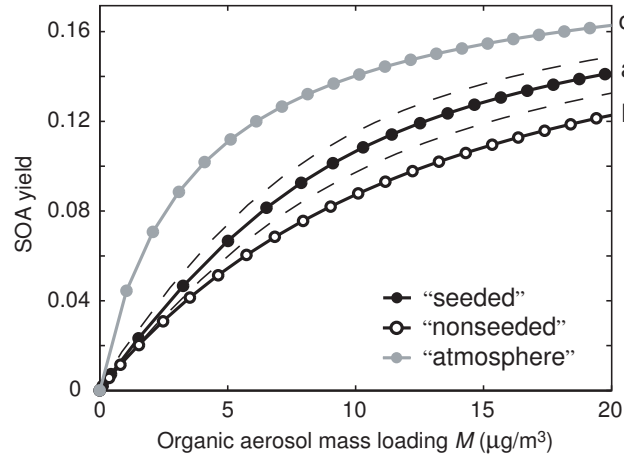


Figure 2.4: Yield curves predicted from the kinetic model. Curves a and b: “seeded” and “non-seeded” cases, in which model parameters are the same as those in Fig. 2.3a and 2.3b. M is varied by changing $HC(0)$, as is typically done in chamber studies (increments of $5 \mu\text{g}/\text{m}^3$). Dashed lines are the same as curve a but with k_p increased by 50% (upper curve) or k_g increased by 25% (lower curve). Curve c: “atmosphere” case, as in Fig. 2.3c. M is varied by changes to $M(0)$ (in increments of $1 \mu\text{g}/\text{m}^3$); $HC(0)$ is held at $1 \mu\text{g}/\text{m}^3$.

Chapter 3

Kinetic modeling of secondary organic aerosol formation: effects of particle- and gas-phase reactions of semivolatile products*

*Reproduced with permission from “Kinetic modeling of secondary organic aerosol formation: effects of particle- and gas-phase reactions of semivolatile products” by A. W. H. Chan, J. H. Kroll, N. L. Ng, John H. Seinfeld, *Atmospheric Chemistry and Physics*, 7 (15), 4135–4147, 2007. Copyright 2007 by Authors. This work is licensed under a Creative Commons License.

3.1 Abstract

The distinguishing mechanism of formation of secondary organic aerosol (SOA) is the partitioning of semivolatile hydrocarbon oxidation products between the gas and aerosol phases. While SOA formation is typically described in terms of partitioning only, the rate of formation and ultimate yield of SOA can also depend on the kinetics of both gas- and aerosol-phase processes. We present a general equilibrium/kinetic model of SOA formation that provides a framework for evaluating the extent to which the controlling mechanisms of SOA formation can be inferred from laboratory chamber data. With this model we examine the effect on SOA formation of gas-phase oxidation of first-generation products to either more or less volatile species, of particle-phase reaction (both first- and second-order kinetics), of the rate of parent hydrocarbon oxidation, and of the extent of reaction of the parent hydrocarbon. The effect of pre-existing organic aerosol mass on SOA yield, an issue of direct relevance to the translation of laboratory data to atmospheric applications, is examined. The importance of direct chemical measurements of gas- and particle-phase species is underscored in identifying SOA formation mechanisms.

3.2 Introduction

Particulate matter formed by condensation of oxidation products of volatile organic compounds (VOCs), termed secondary organic aerosol (SOA), can contribute a significant fraction of airborne particulate matter (Seinfeld and Pandis, 2006). Environmental chamber studies are the principal means by which the aerosol-forming potential of VOCs is established. SOA formation is a complex process, involving gas-phase oxidation chemistry, partitioning of oxidation products between the gas and particle phases, and aerosol-phase chemistry. While it is possible, in principle, to simulate SOA formation using explicit, detailed gas-phase chemical mechanisms coupled to gas-particle equilibrium (Johnson et al., 2006; Griffin et al., 2002a,b; Pun et al., 2002), those mechanisms currently used in regional and global atmospheric chemical transport models are generally semi-empirical, the parameters of which are derived from laboratory chamber studies. The cornerstone of SOA formation

is the generation of semivolatile oxidation products that undergo absorptive partitioning between the gas and particulate phases (Seinfeld and Pankow, 2003; Pankow, 1994a,b; Donahue et al., 2006). A consequence of the absorptive partitioning is that SOA formation depends not only on the amount and volatility of these oxidation products, but also on the amount and nature of the aerosol mass into which the compounds partition.

A widely-used semi-empirical mechanism for SOA formation is the Odum model (Odum et al., 1996, 1997), in which oxidation of the parent VOC leads to semivolatile first-generation products, and in which the SOA yield, Y , of a particular VOC, defined as the ratio of mass of SOA formed, ΔM_o , to the mass of hydrocarbon reacted, ΔHC , is given by

$$Y = \frac{\Delta M_o}{\Delta HC} = M_o \sum_{i=1}^n \frac{\alpha_i K_{p,i}}{1 + K_{p,i} M_o} \quad (3.1)$$

where α_i is the mass-based stoichiometric coefficient of semivolatile product i , $K_{p,i}$ is its gas-particle partitioning equilibrium constant, and M_o is the total mass concentration of the absorbing (aerosol) medium. Equation 3.1 has traditionally been used to describe the yield of SOA as a function of total organic aerosol loading, M_o , after the parent hydrocarbon has been entirely consumed. In a typical experimental study, a set of data of Y versus M_o , the characteristic “yield curve” for a particular VOC, is fitted to Eq. 3.1, by varying α_i and $K_{p,i}$ (typically $n=2$), in which each product has a different volatility (see “Odum Model” in Fig. 3.1), is sufficient in describing the experimental SOA yield for most VOCs. It is important to note that the model underlying Eq. 3.1 is an equilibrium rather than kinetic model in that it relates the mass of aerosol formed, ΔM_o , to ΔHC without regard to the rate at which the parent hydrocarbon is oxidized. This model has been used to empirically represent SOA yields for more than 50 different parent VOCs (see Seinfeld and Pankow (2003)).

Aerosol-phase reactions involving condensed semivolatile compounds are known to be important in SOA formation, evidence for which includes the presence of high molecular weight oligomers in SOA (Gao et al., 2004a,b; Tolocka et al., 2004; Kalberer et al., 2004) and increased SOA yields under acidic conditions (Gao et al., 2004a,b; Iinuma et al., 2004; Jang et al., 2002; Czoschke et al., 2003).

Kroll and Seinfeld (2005) showed that if a semivolatile product undergoes a reversible, unimolecular reaction with an equilibrium constant, K_{rxn} , in the aerosol phase, the corresponding gas-particle partitioning equilibrium constant K_p in the Odum model can be replaced by a total gas-particle partitioning equilibrium constant (K^*), which includes contribution from particle-phase processes. The thermal stability of some aerosol-phase reaction products, such as peroxyhemiacetals (Tobias and Ziemann, 2000), esters (Surratt et al., 2006; Liggio et al., 2005) and organosulfates (Liggio et al., 2005; Liggio and Li, 2006; Surratt et al., 2007), implies that aerosol-phase reactions forming these species may be irreversible, with products not reverting to reactants over timescales relevant to the atmosphere. It has also been shown that for a number of hydrocarbons, low-volatility compounds are formed as a result of multiple gas-phase oxidation steps. Examples for such compounds include terpenes with multiple double bonds (Ng et al., 2006), aromatic compounds (Ng et al., 2007), and long-chain alkanes (Lim and Ziemann, 2005).

As noted, the most important fundamental aspect of SOA formation is the equilibrium distribution of semivolatile oxidation products between the gas and particle phases. An essential question is – can one infer from experimental data the extent to which various kinetic processes, such as aerosol-phase reaction and gas-phase reaction of oxidation products, influences SOA formation? For example, it has been shown that the characteristic behavior of how the amount of SOA generated, ΔM_o , evolves as the parent hydrocarbon is consumed, ΔHC , the “time-dependent SOA growth curve” reflects both kinetic and equilibrium processes (Kroll and Seinfeld, 2005; Ng et al., 2006; Sato et al., 2004). The goal of the present work is to present a hierarchy of general models of SOA formation that include both equilibrium and kinetic processes. Given a set of experimental data, the models would allow one to evaluate the extent to which the observed SOA formation data are consistent with particular controlling mechanisms and thereby suggest avenues for more in-depth study.

3.3 Model Description

The set of kinetic models is given in Fig. 3.1. The overall kinetic model is shown, together with special cases, denoted (a)–(f). In each case, the parent hydrocarbon is oxidized to a first-generation product denoted A_1^g (with pseudo-first-order rate constant k_{HC} and mass stoichiometric coefficient α_1). The models are developed considering only one oxidation product; they can readily be extended to a spectrum of oxidation products (Donahue et al., 2006). If there is initial organic material present ($M_o(0) > 0$), and A_1 is semivolatile (as it is for all cases except case (d)), A_1^g immediately partitions into the particulate phase as A_1^p with a partitioning coefficient K_1 ; otherwise, A_1^g partitions only after it reaches its saturation concentration in the gas phase. Instantaneous partitioning equilibrium can be assumed, since the characteristic timescale for gas-particle transport is typically much faster than that for oxidation of the parent hydrocarbon (Bowman et al., 1997). Aerosol-phase reaction is represented by irreversible conversion of A_1^p to B_1^p . As noted, Kroll and Seinfeld (2005) have considered the case of reversible aerosol-phase reaction. The aerosol-phase reaction can also be represented as a bimolecular reaction; this is included in cases (e) and (f). The first-generation semivolatile product A_1^g can be further oxidized in the gas phase, represented by first-order reaction of A_1^g with a rate constant k_g to form a second-generation semivolatile product or a volatile product, A_2^g . A_2^g itself may then partition as A_2^p , which itself may also react irreversibly in the aerosol phase to form B_2^p .

The qualitative kinetic behavior of the general system depends on the magnitudes of the various rate constants relative to the intrinsic HC oxidation rate constant k_{HC} , as reflected by the ratios $\beta_g (=k_g/k_{HC})$, $\beta_{p1} (=k_{p1}/k_{HC})$, and $\beta_{p2} (=k_{p2}/k_{HC})$. In general, the quantities, k_{HC} and $M_o(0)$, are known. The most general form of the kinetic model admits a number of special cases, (a)–(f) depending on the relative values of the parameters.

3.4 General Model Behavior

The purpose of this subsection is to examine the qualitative nature of SOA formation as would be observed experimentally if the mechanism of SOA formation adheres to each of the cases in Fig. 3.1. This will allow us to assess the sensitivity of the dynamic SOA formation processes to the particular mechanism involved.

3.4.1 Odum model

Figure 3.2 shows the characteristic time-dependent growth curve of SOA (ΔM_o) versus HC reacted (ΔHC) for the Odum model (assuming two semivolatile products). At low ΔHC and $M_o(0)=0$, no aerosol forms until the condensable products exceed their saturation concentrations. Because this is strictly an equilibrium model, aerosol growth follows the same curve regardless of the initial HC concentration ($HC(0)$). Aerosol formation is governed only by the timescale of HC oxidation.

3.4.2 Case (a): First-generation product only with aerosol-phase reaction

Case (a) in Fig. 3.1 includes irreversible reaction of the first-generation semivolatile product in the aerosol phase. When particle-phase reaction is slow compared to HC oxidation ($\beta_{p1}=0.1$, see panel (a) of Fig. 3.3), only after most of the HC has been consumed does A_1^p react to form an appreciable amount of B_1^p , drawing the partitioning equilibrium toward the aerosol phase. This behavior is evidenced by significant growth (the vertical portion) after HC is essentially consumed. If the aerosol-phase reaction is irreversible, the semivolatile product is entirely converted to B_1^p , and the final SOA yield is simply $\Delta M_o = \alpha_1 \Delta HC$. This gives rise to two distinct regions in the growth curve: the first associated with the early gas-particle partitioning and the second associated with the slower aerosol-phase reaction. If the aerosol-phase reaction is fast relative to HC oxidation ($\beta_{p1}=10$, see panel (a) of Fig. 3.3), as soon as A_1^p is formed it is quickly converted to B_1^p . A_1^g continues to condense to maintain partitioning equilibrium, leading to rapid aerosol formation. A_1^g is eventually entirely depleted because its rate of loss through A_1^p exceeds the rate of supply from the HC oxidation. Again, if the aerosol-phase reaction is irreversible, all of oxidation product A_1

must eventually be converted to the nonvolatile aerosol-phase reaction product B_1^P , regardless of the value of β_{p1} . As a result, for this mechanism the final SOA yield is independent of the initial hydrocarbon concentration, and the yield curve ($\Delta M_o/\Delta HC$) is independent of the organic aerosol mass concentration.

The amount of initial organic material present, $M_o(0)$, also affects the shape of the growth curve, as shown in panel (b) of Fig. 3.3. As $M_o(0)$ increases, the partitioning equilibrium is shifted in favor of A_1^P . Initial SOA formation occurs earlier, so that at any particular value of ΔHC , the larger the value of $M_o(0)$, the greater the amount of aerosol formed. Once the initial hydrocarbon is consumed, the amount of SOA formed is the same regardless of $M_o(0)$, although the paths by which ΔM_o approach the final yield are quite different; this is an important observation relative to comparison of experimentally-determined SOA yields when the initial hydrocarbon is not entirely reacted.

3.4.3 Case (b): First-generation product with unimolecular aerosol-phase reaction and with gas-phase conversion to a volatile second-generation product

Case (b) has been considered in Kroll et al. (2007). Irreversible loss of gas-phase semivolatile product can occur either by chemical reaction (further oxidation) or physical processes (scavenging, wall loss). Aerosol formation depends on the competition between the formation of B_1^P and A_2^g . The final yield is governed not only by the partitioning between A_1^g and A_1^P , but also by the relative rates of gas-phase loss of first-generation product and aerosol-phase reaction. The SOA yield differs for different amounts of initial organic material present, despite the same total organic aerosol loading; consequently, the SOA yield could be underestimated in chamber experiments owing to the induction period associated with the absence of organic or inorganic seed particles (Kroll et al., 2007).

Figure 3.4 shows growth curves for kinetic model case (b). If the rate of the aerosol-phase reaction substantially exceeds that of the gas-phase loss ($\beta_{p1}=10$), the growth curve is similar to that in case (a), and most A_1^g condenses and forms B_1^P . As β_{p1} decreases, the final yield decreases, as more of

the oxidation product A_1 is ultimately converted to A_2^g . At $\beta_{p1}=0.1$, the aerosol-phase reaction is sufficiently slow that A_1^p repartitions to the gas phase and is lost to A_2^g , and, as a result, total SOA mass reaches a maximum and decreases. Case (b) also provides a possible representation for the “acid catalysis” effect when competing gas-phase reactions are present, in which acidity can increase the overall (“final”) SOA yield by catalyzing the rate of the aerosol-phase reaction.

Since SOA formation in case (b) depends on both the gas-particle partitioning equilibrium between A_1^g and A_1^p and the relative rates of gas-phase loss and aerosol-phase reaction, the initial amount of organic material affects the relative amounts of A_1^p and A_1^g , and thus the relative rates of gas-phase and aerosol-phase reactions. Kroll et al. (2007) showed that less gas-phase semivolatile oxidation product is lost irreversibly with the introduction of seed particles because the induction period for SOA growth is shorter, leading to higher SOA yields, despite constant total organic aerosol loading.

3.4.4 Case (c): First- and second-generation semivolatile products with no aerosol-phase reaction

Case (c) includes the contribution of semivolatile compounds formed from further gas-phase reaction of the first-generation product. If gas-phase conversion of A_1^g to A_2^g is relatively slow (e.g., $\beta_g=0.1$), the second-generation aerosol product A_2^p does not form in an appreciable amount until most of the HC has been consumed. As β_g increases, formation of A_2^p occurs earlier and in the limit of $\beta_g \gg 1$ approaches instantaneous partitioning. Panel (a) of Fig. 3.5 shows the dependence of ΔM_o on ΔHC for $\beta_g=0.1$, 1, and 10 (at $K_2/K_1=10$). At $\beta_g=0.1$, relatively little aerosol is formed until a significant amount of A_2^g forms, because the second-generation product is less volatile. Eventually all the aerosol ends up as A_2^p , and the ultimate yield is independent of the value of β_g . A vertical portion at the end of the growth curve indicates that most of the SOA is second-generation product formed after the parent HC is consumed. If $K_2 < K_1$, the first-generation product is less volatile. As the reaction proceeds, A_1^p evaporates and reacts to form the second-generation product, which is more volatile. As in case (b), the total mass of SOA can decrease over the course of the HC

oxidation (panel (b) of Fig. 3.5). Note that regardless of the values of K_1 and β_g , the final SOA yield is identical for the same $HC(0)$. This is because all the HC reacted must eventually be in the form of A_2^g or A_2^p , and hence the final SOA yield is determined only by the partitioning between A_2^g and A_2^p .

3.4.5 Case (d): Volatile first-generation product and semivolatile second-generation product

When the first-generation product A_1^g is completely volatile, SOA growth results only from the second-generation product ($K_1=0$), and the kinetics of this system admit an analytical solution which describes the time-dependent growth curve of the system:

$$\Delta M_o = \begin{cases} A_{2,eq}^p & \text{if } A_{2,eq}^p > 0 \\ 0 & \text{otherwise} \end{cases} \quad (3.2)$$

where

$$A_{2,eq}^p = \frac{\left[\frac{1}{K_2} - A_2 + M_o(0) \right] + \sqrt{\left[\frac{1}{K_2} - A_2 + M_o(0) \right]^2 + 4A_2M_o(0)}}{2}$$

$$A_2 = \begin{cases} \alpha_1 \Delta HC - \frac{\alpha_1 HC(0)}{\beta_g - 1} \left[\left(1 - \frac{\Delta HC}{HC(0)} \right) - \left(1 - \frac{\Delta HC}{HC(0)} \right)^{\beta_g} \right] & \text{if } \beta_g \neq 1 \\ \alpha_1 \Delta HC - \alpha_1 HC(0) \left(1 - \frac{\Delta HC}{HC(0)} \right) \ln \left(1 - \frac{\Delta HC}{HC(0)} \right) & \text{if } \beta_g = 1 \end{cases}$$

A_2 represents the sum of A_2^p and A_2^g , and $A_{2,eq}^p$ is the concentration of A_2^p if the gas- and particle-phases are in partitioning equilibrium. The analytical solution allows us to see more clearly the dependence of the SOA growth curve on the kinetic and equilibrium parameters: a lower $HC(0)$ requires a longer time to reach the same ΔHC , which gives a higher amount of A_2 (and hence, higher SOA growth) for the same ΔHC . The dependence of SOA growth on the extent of reaction, $\Delta HC/HC(0)$, will be discussed in more detail.

3.5 Effect of Kinetic Conditions on SOA Growth

3.5.1 Molecularity of aerosol-phase reaction and experimental timescales

Up to this point we have assumed for convenience that the aerosol-phase reaction, e.g., $A_1^P \rightarrow B_1^P$, is kinetically first-order. If aerosol-phase reactions are bimolecular, such as in the formation of oligomers in the aerosol phase ($A_1^P + A_1^P \rightarrow B_1^P$), the rate of the reaction is intrinsically second-order with respect to the aerosol-phase compound. We show in the Appendix that in this case the rate constant still has the units of inverse time. Thus the ratio of the aerosol-phase reaction rate constant to the HC oxidation rate constant (β_{p1}) is still a useful parameter for representing the relative rate of aerosol-phase reaction. Case (e) in Fig. 3.1 describes the case in which the first-generation semivolatile product undergoes only a second-order aerosol-phase reaction.

For the same set of parameters $\{k_{HC}, \beta_{p1}, K_1\}$, in the case of second-order reaction the aerosol-phase reaction rate in case (e) decreases significantly as the concentration of A_1^P approaches zero. As a result, the semivolatile compound A_1 may not be completely consumed within typical timescales of a chamber experiment, and the observed yield is lower than the theoretical yield of α_1 (Fig. 3.6). This effect is greater when $HC(0)$ is lower because the aerosol-phase reaction rate decreases nonlinearly with respect to concentration. Unlike case (a), the SOA yield is not constant; it decreases as M_o decreases. The system exhibits partitioning behavior similar to that seen in the Odum equilibrium model, but such behavior is not a direct result of the amount of the organic material present; rather, it occurs because of the slower aerosol-phase reaction at lower hydrocarbon concentrations.

Figure 3.6 also shows SOA yield curves from simulation of case (e) under typical ambient and chamber conditions. The ambient SOA yield (“atmosphere”) for this case, in which the aerosol-phase reaction is bimolecular, is lower than that measured in chamber experiments (“chamber”). This occurs because the rate of the bimolecular aerosol-phase reaction is proportional to both the total concentration of semivolatile compound in the system ($\mu\text{g}/\text{m}^3$ air) and x_A , the fraction of the condensed semivolatile compound in the organic phase ($\mu\text{g A}/\mu\text{g organics}$) (see Appendix). In a typical chamber experiment, the organic aerosol generally is entirely SOA, so the fraction of the

condensable species in the organic phase is high. In contrast, the absorbing aerosol in the atmosphere arises mainly from preexisting organic material, so SOA components will be substantially diluted. Hence, bimolecular aerosol-phase reactions may occur at a higher rate in chamber experiments, where relatively higher VOC concentrations are used (Kalberer et al., 2004; Paulsen et al., 2006). For the same set of parameters $\{k_{HC}, \beta_{p1}, K_1\}$, the rate of a first-order unimolecular aerosol-phase reaction is faster than that of a bimolecular aerosol-phase reaction. It is therefore likely that under atmospheric conditions, the SOA yield for case (a), in which the aerosol-phase reaction is unimolecular, is higher than that in case (e), where the aerosol-phase reaction is bimolecular.

Case (f) includes gas-phase loss of the first-generation semivolatile product, in addition to the bimolecular aerosol-phase reaction. Since there is a competition between gas-phase loss of A_1^g and aerosol-phase reaction of A_1^p , the final SOA yield depends directly on the relative rates of these reactions. The SOA yield for such a system would be lower in the atmosphere, where the fraction of A_1^p in the organic phase, x_A , is small and the bimolecular aerosol-phase reaction is slow (Fig. 3.7). Since the gas-phase loss is first-order, the SOA yield would be overestimated when applying chamber measurements to the atmosphere. On the other hand, for the same set of parameters $\{k_{HC}, \beta_{p1}, \beta_g, K_1\}$, aerosol growth in case (b), in which the aerosol-phase reaction is unimolecular, is higher than that in case (f), where the rate of the bimolecular aerosol-phase reaction becomes much slower as A_1^p is consumed and the fraction of A_1^p in the organic phase (x_A) approaches 0.

3.5.2 Rate of hydrocarbon oxidation

Ng et al. (2007) and Kroll et al. (2005) reported SOA yields from the photooxidation of *m*-xylene and isoprene, respectively, that were higher than previously measured (Odum et al., 1996; Pandis et al., 1991). In these experiments, HONO is used as an OH precursor, which rapidly photolyzes to produce substantially higher concentrations of OH radicals than are generally formed from HC/NO_x irradiations. While it is possible that this increases the rate of further gas-phase oxidation to produce less volatile compounds observable within chamber timescales, here we show that the rate of hydrocarbon oxidation can cause substantial differences in SOA yield even without further gas-

phase oxidation steps (in case (b)).

Figure 3.8 shows the growth curves for case (b) with increasing hydrocarbon oxidation rate k_{HC} . The rates of the other process k_g and k_{p1} are kept constant; this assumes they are independent of OH concentration. At higher k_{HC} , the total concentration of A_1 is higher at any given time. Owing to the nonlinear nature of absorptive partitioning, the gas-particle equilibrium is shifted in favor of the particle phase when more organic material is present (Pankow, 1994a,b). In other words, higher total concentrations of semivolatile compound A_1 leads to not only a higher absolute concentration of A_1^p , but also a larger ratio of A_1^p to A_1^g at any given time. This increases the rate of aerosol-phase reaction relative to the gas-phase loss, which increases SOA growth. Such a “rate effect” is the result of competition between gas-phase loss to nonreactive volatile compounds and aerosol-phase reaction which lowers the vapor pressure of semivolatile compounds. Therefore, there is a kinetic dependence of SOA growth on the rate of oxidation, and this highlights the need to carry out chamber experiments under atmospherically relevant rates of oxidation.

3.5.3 Extent of reaction

In the Odum model, it is assumed that the SOA yield at a particular ΔHC is independent of the extent of reaction, since SOA growth is governed only by the amount of semivolatile formed. As a result, the growth curves under different $HC(0)$ overlap. As shown in Fig. 3.9, when secondary reactions are present in the gas- or aerosol-phase (cases (a) and (c)), aerosol growth for different $HC(0)$ does not follow the same curve. The growth is higher for a lower $HC(0)$ at the same ΔHC , because it takes longer at lower $HC(0)$ than at higher $HC(0)$ to consume the same amount of hydrocarbon, ΔHC , allowing more time for the gas- or aerosol-phase reaction of the first-generation semivolatile product, producing a less volatile product. Such dependence of SOA growth on $HC(0)$ (higher growth for lower $HC(0)$ at the same ΔHC) is also shown in Eq. 3.2, for the special case where the first generation product is completely volatile (case (d)). This dependence of SOA growth on initial hydrocarbon concentration has been observed in some systems (Ng et al., 2006, 2007; Sato et al., 2004). As a result, when measuring SOA yield in the chamber, it is desirable to consume the

parent hydrocarbon to the fullest extent for the measurement to be atmospherically relevant.

3.5.4 Effect of particle-phase reaction vs. further gas-phase reaction

From the overall kinetic model, one may be able to infer the relative importance of kinetic processes in a particular system by studying the behavior of the SOA growth curve exhibited by that system. In the general model in Fig. 3.1, both irreversible aerosol-phase reaction and further gas-phase reaction leading to products with even lower volatility are considered (ignoring the aerosol-phase reaction of A_2^P). Figure 3.10 shows the growth curves of systems in which the further gas-phase reaction that leads to an essentially nonvolatile compound is dominant ($\beta_g=1$, $\beta_{p1}=0.01$) and another system in which the aerosol-phase reaction is more important than further gas-phase reaction ($\beta_g=0.01$, $\beta_{p1}=1$). If the initial amount of organic material, $M_o(0)$, is small (as illustrated in panel (a) of Fig. 3.10), most of the semivolatile compound A_1 stays in the gas phase as A_1^g . In the case in which the gas-phase reaction of A_1 is relatively fast, the semivolatile compound A_1 reacts to form A_2 , which is essentially nonvolatile, and the delay in SOA growth is therefore short. On the other hand, if the gas-phase reaction of A_1 is relatively slow, the SOA growth is small until there is sufficient partitioning to form A_1^P . There is a significant delay between formation of semivolatile A_1 in the gas phase and condensation and further reaction in the aerosol phase to form the nonvolatile B_1^P . Although the final yield is the same for these two cases (both final products B_1^P and A_2^P are assumed to be nonvolatile), the growth in the latter case occurs later than that in the former case. However, if there is a significant amount of background organic material (such that partitioning occurs quickly) or if the secondary reactions (gas- and aerosol-phase reactions of A_1) are sufficiently rate-limiting compared to the oxidation of the parent hydrocarbon, the difference between the two growth curves becomes smaller and they cannot easily be distinguished from each other, as illustrated in panels (b) and (c) of Fig. 3.10.

3.6 Application to SOA-forming Systems

3.6.1 Fitting experimental data to the kinetic model

To evaluate the extent to which it is possible to fit a unique set of kinetic and equilibrium parameters for the models in Fig. 3.1 to experimental data, the models were used to generate synthetic SOA growth data, which were then used as a basis for recovering the parameters used to generate the data via optimization. With the exception of case (d), in which SOA growth results only from condensation of one semivolatile compound, the “true” parameters could not be easily recovered and the minimized errors between simulated and modeled SOA growth do not necessarily represent the global minimum. In these cases, SOA growth results from either a first-generation product (A_1^P) or a product from further gas- or aerosol-phase reaction (B_1^P or A_2^P). Since the measured SOA growth represents the sum of all aerosol-phase products (ΔM_o), some of the parameters (such as K_1 and β_{p1}) are not independent and multiple sets of parameters can describe the same SOA growth curve. When the same test was performed using both measured SOA growth (total ΔM_o) and the concentration of a gas-phase product (e.g., A_1^g), the true parameters were recovered.

Even in the case in which sufficient gas-phase data are not available in order to estimate a unique set of parameters, kinetic modeling can be used to provide a theoretical framework for interpreting trends in SOA growth data from chamber experiments and gain insight into the mechanisms of SOA formation. From the qualitative nature of time-dependent growth curves, one can infer information about the kinetic mechanisms important to SOA growth and the relative rates of reaction, as shown in the following subsections.

3.6.2 α -Pinene ozonolysis

SOA growth data for α -pinene ozonolysis are shown in Fig. 3.11 (Ng et al., 2006). The growth curves from each experiment (with varying $HC(0)$) can be fitted to a single growth curve of two partitioning products, which is characteristic of a system that behaves like the equilibrium Odum model. Although aerosol-phase reactions exist in the α -pinene/ O_3 system (Gao et al., 2004a,b; Tolocka et al., 2004; Iinuma et al., 2004), the behavior in Fig. 3.11 suggests that any aerosol-phase reactions are essentially reversible for this system (Kroll and Seinfeld, 2005; Grieshop et al., 2007). Since the growth curves at different initial hydrocarbon concentrations overlap, the first step of hydrocarbon oxidation is rate-limiting (Ng et al., 2006), such that the extent of reaction has no effect on the yield at any given ΔHC . The data are consistent with an aerosol-phase equilibrium that is established quickly, and the values of the overall partitioning coefficients include the contribution from partitioning and aerosol-phase reaction equilibrium constants (Kroll and Seinfeld, 2005).

3.6.3 Isoprene photooxidation under low- NO_x conditions

In studies of isoprene photooxidation under low- NO_x conditions, photochemical loss of SOA mass after initial formation of SOA is observed (Kroll et al., 2006), indicative of loss of semivolatile compounds by photolysis or further oxidation reactions (Fig. 3.12). SOA formation likely occurs from condensation of hydroperoxides (Miyoshi et al., 1994; Kroll et al., 2006; Surratt et al., 2006), formed from reaction of RO_2 with HO_2 radicals, and the growth behavior exhibited in this system is likely due to a mechanism similar to case (b) of the kinetic model.

Figure 3.12 shows that the time-dependent SOA growth data are consistent with case (b) of the kinetic model. Fitting of the data shows that the gas-phase loss of semivolatile products is about one order of magnitude slower than formation of the semivolatile product ($k_g = k_{HC}\beta_g \approx 0.003 \text{ min}^{-1}$). The formation of products in the aerosol phase, evidenced by decrease in peroxide concentrations and increase in high-MW product concentrations over time (Kroll et al., 2006; Surratt et al., 2006), is even slower ($k_{p1} = k_{HC}\beta_{p1} \approx 0.0003 \text{ min}^{-1}$); the net result is that the condensed semivolatile compounds evaporate as gas-phase semivolatiles react and the total SOA mass decreases over time.

3.6.4 *m*-Xylene photooxidation under low-NO_x conditions

Figure 3.13 shows SOA growth during photooxidation of *m*-xylene under low-NO_x conditions (Ng et al., 2007). The divergence of the growth curves at different $HC(0)$ suggests that the mechanism contains multiple reaction steps to form SOA, and the oxidation of *m*-xylene is not entirely rate-determining. Similar divergence has been observed in the photooxidation of toluene (Ng et al., 2007; Sato et al., 2004). Measured SOA growth in each experiment is consistent with the general behavior of case (d), the parameters of which have been adjusted to fit the experimental growth curves, with values: $\alpha_1=0.383$, $\beta_g=6.45$, $K_2=7.01\text{ m}^3/\mu\text{g}$. Because of the low NO_x levels in these experiments, the two most likely first-generation products are organic peroxides formed from reaction of the bicyclic peroxy radical with HO₂, and dimethylphenols formed from reaction of the cyclohexadienyl radical with O₂ (Calvert et al., 2002). The relative magnitudes of rate constants derived from fitting of the data to case (d) ($\beta_g=6.45$) are in rough agreement with literature values for photooxidation of *m*-xylene and dimethylphenols ($k_{\text{OH}+m\text{-xylene}} = 2.31 \times 10^{-11}\text{ cm}^3/\text{molec}\cdot\text{s}$, $k_{\text{OH}+2,4\text{-dimethylphenol}} = 9.1 \times 10^{-11}\text{ cm}^3/\text{molec}\cdot\text{s}$, for a calculated β_g of 3.9) (MCM v 3.1, <http://mcm.leeds.ac.uk/MCM/>), but the mass yield of dimethylphenols from *m*-xylene photooxidation as predicted by the Master Chemical Mechanism v 3.1 is only 20%, suggesting that there are likely other channels that lead to SOA formation.

3.7 Implications

An idealized kinetic model is presented here that is a compact representation of different mechanisms of SOA formation, such as heterogeneous reaction, chemical loss of total SOA over time, and delayed SOA formation. The analysis reveals a number of important features of SOA formation that are not generally appreciated. When gas-phase formation of semivolatile compounds occurs via multiple steps, the kinetics of SOA growth may differ under different initial hydrocarbon concentrations, $HC(0)$, even with the same amount of hydrocarbon reacted, ΔHC . In addition, if the SOA formation mechanism involves a competition between irreversible gas-phase loss of semivolatile

products to volatile compounds and irreversible aerosol-phase reaction to form additional particle-phase products, the SOA yield depends on the amount of initial organic material, even at constant total organic aerosol loading. Also, the rate of hydrocarbon oxidation can affect the SOA yield. As a result, to predict the amount of SOA formed from hydrocarbon oxidation, one must measure SOA yield under atmospherically relevant kinetic and equilibrium conditions, such as extent of reaction, seed level, and rate of hydrocarbon oxidation.

Simulation of bimolecular reactions in the aerosol phase, such as oligomerization reactions, shows that these reactions can be kinetically unfavorable under atmospheric conditions, and the relative importance of these reactions could be overestimated in chamber experiments. The rate of such reactions is limited by the fraction of SOA formed from VOC oxidation in the organic phase; in ambient aerosols, this fraction is smaller than in typical chamber experiments. On the other hand, pseudo-unimolecular reactions, such as formation of organosulfates on seed aerosols containing large amounts of sulfate (Liggio et al., 2005; Liggio and Li, 2006; Surratt et al., 2007), could be relatively more important in contributing to total SOA growth. This observation again suggests that to correctly represent atmospheric SOA formation, chamber experiments should be conducted with an appropriate amount of seed such that preexisting organic material occupies a significant fraction of the final organic phase volume. Experiments exploring the effects of parameters such as seed composition and concentration on SOA yields will be useful in understanding the mechanisms of SOA growth relevant to the atmosphere.

In summary, the dominant feature of SOA formation is the gas-phase generation of semivolatile oxidation products that undergo equilibrium partitioning between the gas and particle phases. The rate at which SOA actually forms depends on the timescales of competing processes, such as multiple generations of gas-phase reactions and particle-phase reactions of semivolatile organics, which may occur over several generations; the ultimate amount of SOA that is produced can depend on the quantity of pre-existing aerosol. From the analysis presented here it is clear that, while different controlling mechanisms can lead to differing SOA growth behavior, it is not generally possible to infer the precise mechanism of SOA formation solely on the basis of the SOA growth data (ΔM_o

versus ΔHC). We note that the fits to the data do not necessarily indicate the accuracy of a given mechanism. For example, it may not be possible to deduce from growth data alone the relative split between products that undergo semivolatile partitioning versus further gas-phase reaction or whether two products are formed in series or in parallel. While kinetic models presented here show how reaction rates may have a profound influence on SOA formation from a given hydrocarbon, to distinguish between reaction mechanisms that lead to similar overall SOA growth behavior requires detailed chemical measurements of gas- and aerosol-phase species.

Appendix: Second-order aerosol-phase reaction involving semi-volatile products

The reaction rate per unit volume of condensed phase species A that undergoes self-reaction can be expressed as:

$$\frac{1}{V_o(t)} \frac{dN_A}{dt} = -2k \left(\frac{N_A}{V_o(t)} \right)^2 \quad (3.3)$$

where N_A is the number of moles of species A in the organic phase, $V_o(t)$ is the volume of the organic phase, and k is the second-order rate constant (m^3/mols). We can express this reaction rate per unit volume of air V (m^3) as:

$$\frac{d(N_A/V)}{dt} = -2k \left(\frac{N_A}{V} \right)^2 \left(\frac{V}{V_o(t)} \right) \quad (3.4)$$

Assuming that the mass density of the organic phase is constant, the reaction rate expressed in terms of the rate of change of the mass of A in the organic phase, m_A (μg), is:

$$\frac{1}{MW_A} \frac{d(m_A/V)}{dt} = \frac{2k\rho_o}{MW_A^2 M_o(t)} \left(\frac{m_A}{V} \right)^2 \quad (3.5)$$

where MW_A is the molecular weight of A ($\mu\text{g}/\text{mol}$), ρ_o is the mass density of the organic phase ($\mu\text{g}/\text{m}^3$ of the organic phase), and M_o is the total mass concentration of the organic phase ($\mu\text{g}/\text{m}^3$).

of air). Upon rearranging, the reaction rate can be expressed as:

$$r_A = \frac{dc_A}{dt} = - \left(\frac{2k\rho_o}{MW_A} \right) \frac{c_A^2}{M_o} = -k' \frac{c_A^2}{M_o} \quad (3.6)$$

where c_A is the mass concentration of A ($\mu\text{g}/\text{m}^3$ of air). The rate constant, $k' = \frac{2k\rho_o}{MW_A}$, has units of s^{-1} . Alternatively, the rate of the bimolecular aerosol-phase reaction is:

$$r_A = -k' c_A \left(\frac{c_A}{M_o} \right) = -k' c_A x_A \quad (3.7)$$

where x_A is the mass fraction of species A in the organic phase. The rate is therefore dependent on both the total concentration of A in the system ($\mu\text{g}/\text{m}^3$ of air) and the fraction of A in the organic phase ($\mu\text{g } A/\mu\text{g organics}$).

Acknowledgements

This research was funded by U.S. Department of Energy Biological and Environmental Research Program DE-FG02-05ER63983.

Bibliography

- Bowman, F. M., Odum, J. R., Seinfeld, J. H., and Pandis, S. N.: Mathematical model for gas-particle partitioning of secondary organic aerosols, *Atmos. Environ.*, 31, 3921–3931, 1997.
- Calvert, J. G., Atkinson, R., Becker, K. H., Kamens, R. M., Seinfeld, J. H., Wallington, T. J., and Yarwood, G.: The mechanisms of atmospheric oxidation of aromatic hydrocarbons, Oxford University Press, 2002.
- Czochke, N. M., Jang, M., and Kamens, R. M.: Effect of acidic seed on biogenic secondary organic aerosol growth, *Atmos. Environ.*, 37, 4287–4299, 2003.

- Donahue, N. M., Robinson, A. L., Stanier, C. O., and Pandis, S. N.: Coupled partitioning, dilution, and chemical aging of semivolatile organics, *Environ. Sci. Technol.*, 40, 2635–2643, 2006.
- Gao, S., Keywood, M., Ng, N. L., Surratt, J., Varutbangkul, V., Bahreini, R., Flagan, R. C., and Seinfeld, J. H.: Low-molecular-weight and oligomeric components in secondary organic aerosol from the ozonolysis of cycloalkenes and α -pinene, *J. Phys. Chem. A*, 108, 10 147–10 164, 2004a.
- Gao, S., Ng, N. L., Keywood, M., Varutbangkul, V., Bahreini, R., Nenes, A., He, J. W., Yoo, K. Y., Beauchamp, J. L., Hodyss, R. P., Flagan, R. C., and Seinfeld, J. H.: Particle phase acidity and oligomer formation in secondary organic aerosol, *Environ. Sci. Technol.*, 38, 6582–6589, 2004b.
- Grieshop, A. P., Donahue, N. M., and Robinson, A. L.: Is the gas-particle partitioning in alpha-pinene secondary organic aerosol reversible?, *Geophys. Res. Lett.*, 34, L14810, doi: 10.1029/2007GL029987, 2007.
- Griffin, R. J., Dabdub, D., and Seinfeld, J. H.: Secondary organic aerosol - 1. Atmospheric chemical mechanism for production of molecular constituents, *J. Geophys. Res.-Atmos.*, 107, 4332, doi: 10.1029/2001JD000541, 2002a.
- Griffin, R. J., Dabdub, D., Kleeman, M. J., Fraser, M. P., Cass, G. R., and Seinfeld, J. H.: Secondary organic aerosol - 3. Urban/regional scale model of size- and composition-resolved aerosols, *J. Geophys. Res.-Atmos.*, 107, 4334, doi:10.1029/2001JD000544, 2002b.
- Iinuma, Y., Boge, O., Gnauk, T., and Herrmann, H.: Aerosol-chamber study of the α -pinene/ O_3 reaction: influence of particle acidity on aerosol yields and products, *Atmos. Environ.*, 38, 761–773, 2004.
- Jang, M. S., Czoschke, N. M., Lee, S., and Kamens, R. M.: Heterogeneous atmospheric aerosol production by acid-catalyzed particle-phase reactions, *Science*, 298, 814–817, 2002.
- Johnson, D., Utembe, S. R., Jenkin, M. E., Derwent, R. G., Hayman, G. D., Alfarra, M. R., Coe, H., and McFiggans, G.: Simulating regional scale secondary organic aerosol formation during the TORCH 2003 campaign in the southern UK, *Atmos. Chem. Phys.*, 6, 403–418, 2006.

- Kalberer, M., Paulsen, D., Sax, M., Steinbacher, M., Dommen, J., Prevot, A. S. H., Fisseha, R., Weingartner, E., Frankevich, V., Zenobi, R., and Baltensperger, U.: Identification of polymers as major components of atmospheric organic aerosols, *Science*, 303, 1659–1662, 2004.
- Kroll, J. H. and Seinfeld, J. H.: Representation of secondary organic aerosol laboratory chamber data for the interpretation of mechanisms of particle growth, *Environ. Sci. Technol.*, 39, 4159–4165, 2005.
- Kroll, J. H., Ng, N. L., Murphy, S. M., Flagan, R. C., and Seinfeld, J. H.: Secondary organic aerosol formation from isoprene photooxidation under high-NO_x conditions, *Geophys. Res. Lett.*, 32, L18808, doi:10.1029/2005GL023637, 2005.
- Kroll, J. H., Ng, N. L., Murphy, S. M., Flagan, R. C., and Seinfeld, J. H.: Secondary organic aerosol formation from isoprene photooxidation, *Environ. Sci. Technol.*, 40, 1869–1877, 2006.
- Kroll, J. H., Chan, A. W. H., Ng, N. L., Flagan, R. C., and Seinfeld, J. H.: Reactions of semivolatile organics and their effects on secondary organic aerosol formation, *Environ. Sci. Technol.*, 41, 3545–3550, 2007.
- Liggio, J. and Li, S. M.: Organosulfate formation during the uptake of pinonaldehyde on acidic sulfate aerosols, *Geophys. Res. Lett.*, 33, L13808, doi:10.1029/2006GL026079, 2006.
- Liggio, J., Li, S. M., and McLaren, R.: Heterogeneous reactions of glyoxal on particulate matter: Identification of acetals and sulfate esters, *Environ. Sci. Technol.*, 39, 1532–1541, 2005.
- Lim, Y. B. and Ziemann, P. J.: Products and mechanism of secondary organic aerosol formation from reactions of n-alkanes with OH radicals in the presence of NO_x, *Environ. Sci. Technol.*, 39, 9229–9236, 2005.
- Miyoshi, A., Hatakeyama, S., and Washida, N.: OH radical-initiated photooxidation of isoprene – An estimate of global CO production, *J. Geophys. Res.-Atmos.*, 99, 18 779–18 787, 1994.
- Ng, N. L., Kroll, J. H., Keywood, M. D., Bahreini, R., Varutbangkul, V., Flagan, R. C., Seinfeld, J. H., Lee, A., and Goldstein, A. H.: Contribution of first- versus second-generation products

- to secondary organic aerosols formed in the oxidation of biogenic hydrocarbons, *Environ. Sci. Technol.*, 40, 2283–2297, 2006.
- Ng, N. L., Kroll, J. H., Chan, A. W. H., Chhabra, P. S., Flagan, R. C., and Seinfeld, J. H.: Secondary organic aerosol formation from *m*-xylene, toluene, and benzene, *Atmos. Chem. Phys.*, 7, 3909–3922, 2007.
- Odum, J. R., Hoffmann, T., Bowman, F., Collins, D., Flagan, R. C., and Seinfeld, J. H.: Gas/particle partitioning and secondary organic aerosol yields, *Environ. Sci. Technol.*, 30, 2580–2585, 1996.
- Odum, J. R., Jungkamp, T. P. W., Griffin, R. J., Flagan, R. C., and Seinfeld, J. H.: The atmospheric aerosol-forming potential of whole gasoline vapor, *Science*, 276, 96–99, 1997.
- Pandis, S. N., Paulson, S. E., Seinfeld, J. H., and Flagan, R. C.: Aerosol formation in the photooxidation of isoprene and β -pinene, *Atmos. Environ.*, 25, 997–1008, 1991.
- Pankow, J. F.: An absorption-model of gas-particle partitioning of organic-compounds in the atmosphere, *Atmos. Environ.*, 28, 185–188, 1994a.
- Pankow, J. F.: An absorption-model of the gas aerosol partitioning involved in the formation of secondary organic aerosol, *Atmos. Environ.*, 28, 189–193, 1994b.
- Paulsen, D., Weingartner, E., Alfarra, M. R., and Baltensperger, U.: Volatility measurements of photochemically and nebulizer-generated organic aerosol particles, *Journal of Aerosol Science*, 37, 1025–1051, 2006.
- Pun, B. K., Griffin, R. J., Seigneur, C., and Seinfeld, J. H.: Secondary organic aerosol - 2. Thermodynamic model for gas/particle partitioning of molecular constituents, *J. Geophys. Res.-Atmos.*, 107, 4333, doi:10.1029/2001JD000542, 2002.
- Sato, K., Klotz, B., Hatakeyama, S., Imamura, T., Washizu, Y., Matsumi, Y., and Washida, N.: Secondary organic aerosol formation during the photo-oxidation of toluene: Dependence on initial hydrocarbon concentration, *Bull. Chem. Soc. Jpn.*, 77, 667–671, 2004.

- Seinfeld, J. H. and Pandis, S. N.: Atmospheric chemistry and physics, John Wiley, 2006.
- Seinfeld, J. H. and Pankow, J. F.: Organic atmospheric particulate material, *Annu. Rev. Phys. Chem.*, 54, 121–140, 2003.
- Surratt, J. D., Murphy, S. M., Kroll, J. H., Ng, N. L., Hildebrandt, L., Sorooshian, A., Szmigielski, R., Vermeylen, R., Maenhaut, W., Claeys, M., Flagan, R. C., and Seinfeld, J. H.: Chemical composition of secondary organic aerosol formed from the photooxidation of isoprene, *J. Phys. Chem. A*, 110, 9665–9690, 2006.
- Surratt, J. D., Kroll, J. H., Kleindienst, T. E., Edney, E. O., Claeys, M., Sorooshian, A., Ng, N. L., Offenberg, J. H., Lewandowski, M., Jaoui, M., Flagan, R. C., and Seinfeld, J. H.: Evidence for organosulfates in secondary organic aerosol, *Environ. Sci. Technol.*, 41, 517–527, 2007.
- Tobias, H. J. and Ziemann, P. J.: Thermal desorption mass spectrometric analysis of organic aerosol formed from reactions of 1-tetradecene and O_3 in the presence of alcohols and carboxylic acids, *Environ. Sci. Technol.*, 34, 2105–2115, 2000.
- Tolocka, M. P., Jang, M., Ginter, J. M., Cox, F. J., Kamens, R. M., and Johnston, M. V.: Formation of oligomers in secondary organic aerosol, *Environ. Sci. Technol.*, 38, 1428–1434, 2004.

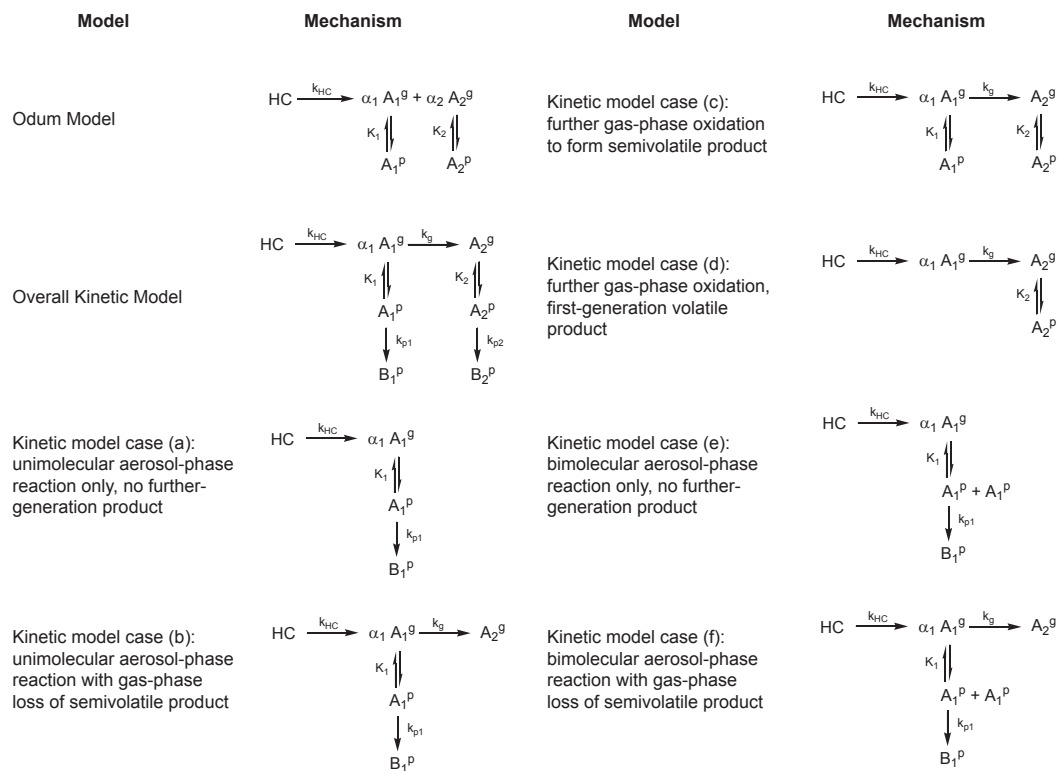


Figure 3.1: Kinetic schemes for SOA formation.

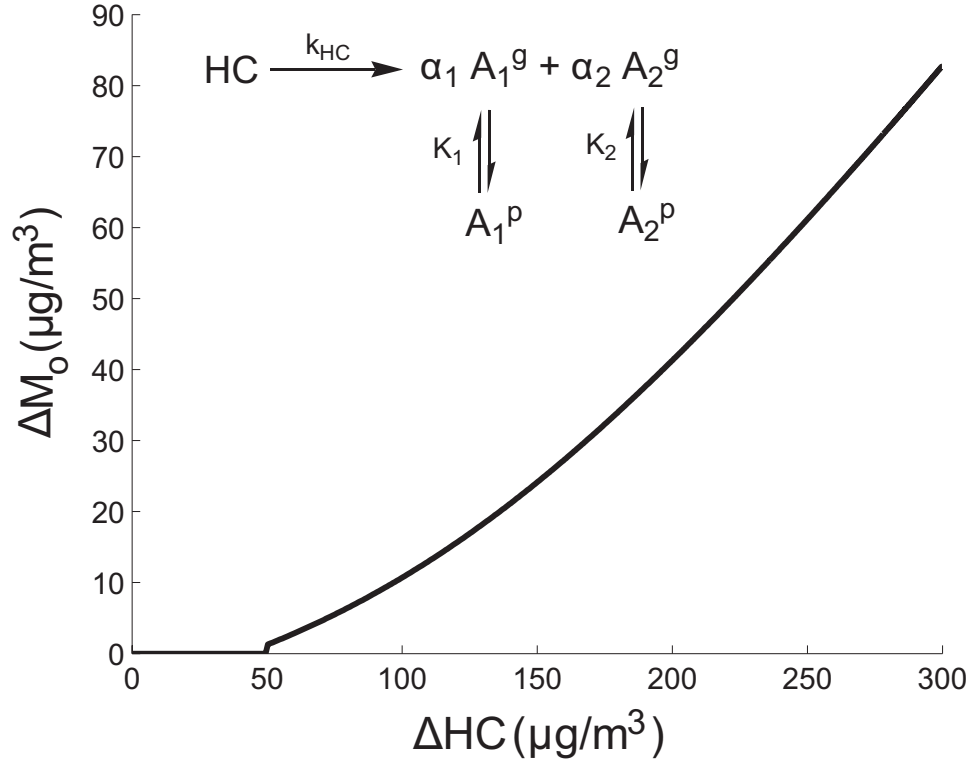
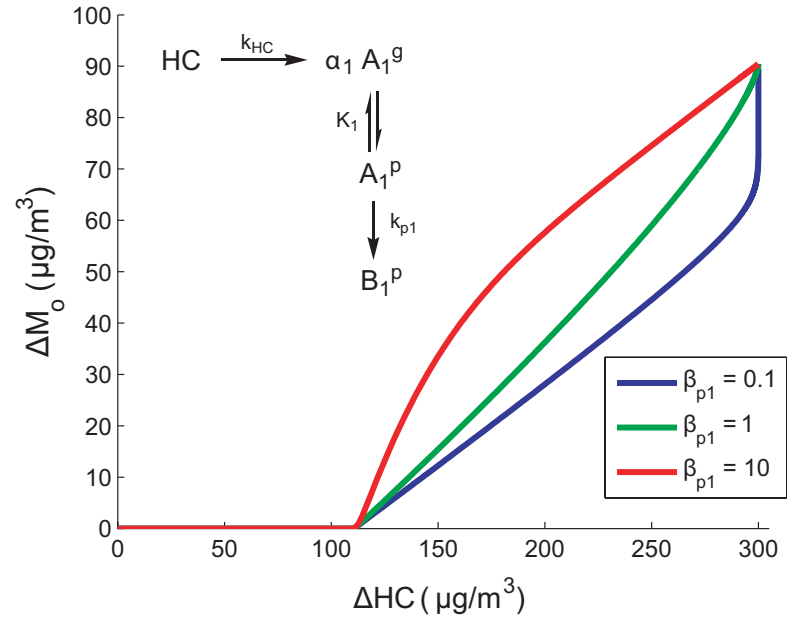


Figure 3.2: Characteristic growth curve (ΔM_o vs ΔHC) for the two-product Odum model (Eq. 3.1). ($HC(0)=300 \mu\text{g}/\text{m}^3$, $M_o(0)=0$, $\alpha_1=0.4$, $K_1=0.01 \text{ m}^3/\mu\text{g}$, $\alpha_2=0.1$, $K_2=0.2 \text{ m}^3/\mu\text{g}$) The discontinuity at $HC(0)=50 \mu\text{g}/\text{m}^3$ is a result of the instantaneous equilibria of two semivolatile products with different partitioning coefficients. When the less volatile product (product 2) saturates and begins to form aerosol, it provides an absorbing medium for the more volatile product (product 1) to condense instantaneously.

(a)



(b)

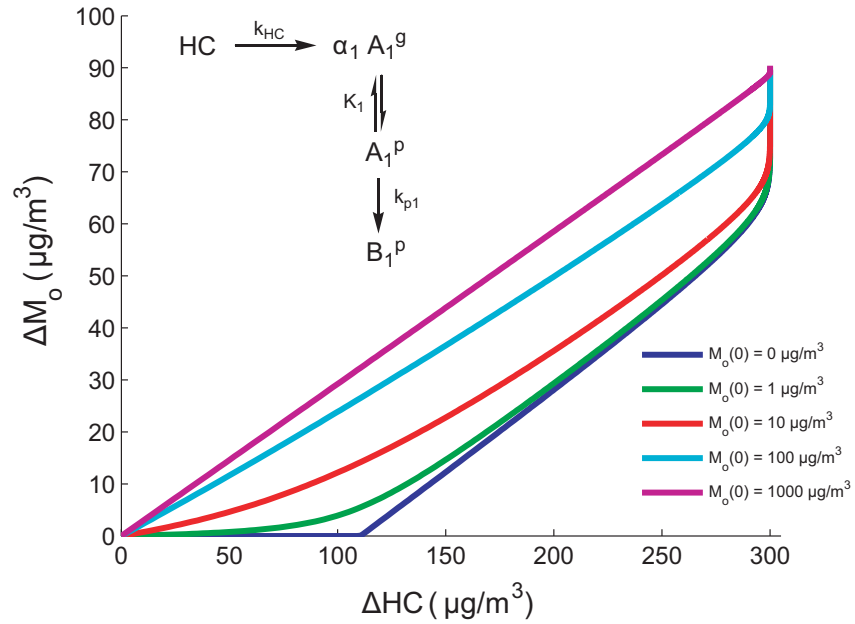


Figure 3.3: Characteristic growth curves for the formation of first-generation product with only aerosol-phase reaction (case (a)), with $\alpha_1=0.3$. Panel (a): Growth curves for a fast (red), medium (green), and slow (blue) aerosol phase reaction. Panel (b): Effect of changing initial amount of organic material $M_o(0)$ for $\beta_{p1}=0.1$.

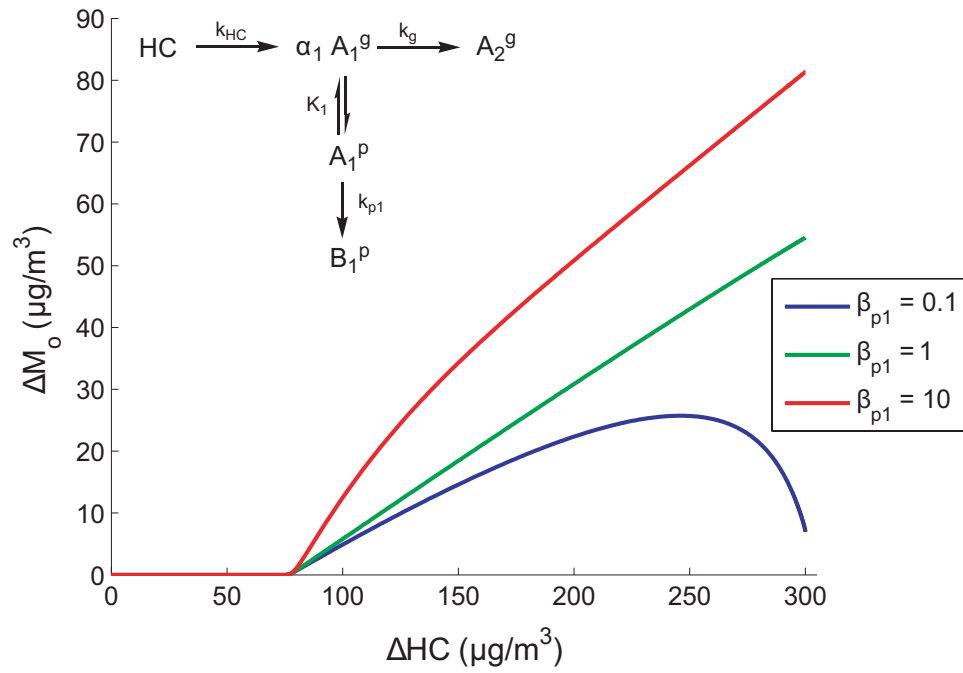


Figure 3.4: Characteristic growth curves for the formation of first-generation product with uni-molecular aerosol-phase reaction and with gas-phase conversion to a volatile second-generation product (case (b)). The curves shown here are for fast (red), medium (green) and slow (blue) aerosol-phase reactions and $\beta_g=1$, $\alpha_1=0.3$.

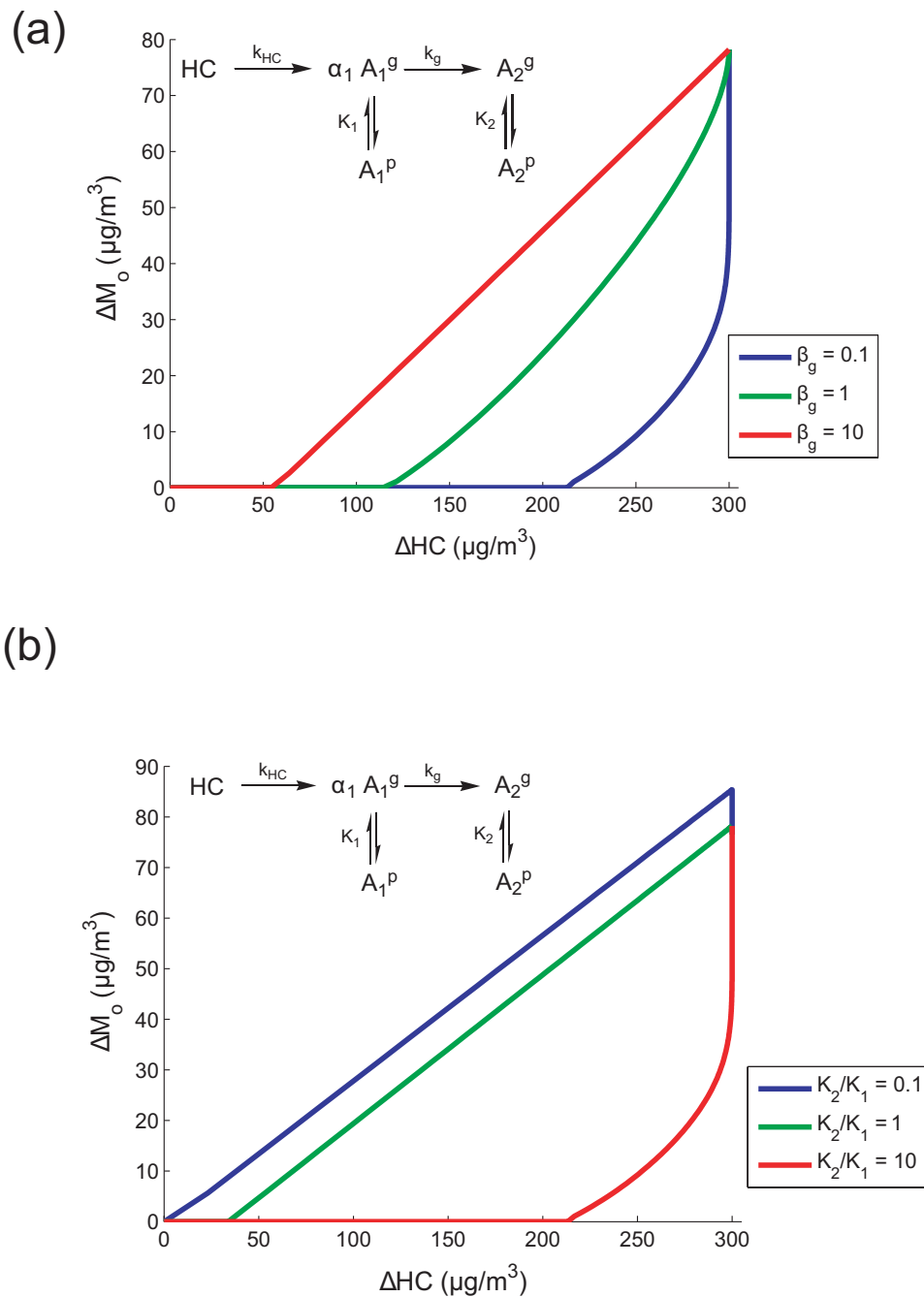


Figure 3.5: Characteristic growth curves for the formation of first- and second-generation semivolatile products with no aerosol-phase reaction (case (c)), with $\alpha_1=0.3$. Panel (a): Growth curves for slow, medium, and fast further oxidation of first-generation semivolatile compound ($K_1=0.01 \text{ m}^3/\mu\text{g}$, $K_2=0.1 \text{ m}^3/\mu\text{g}$). Panel (b): Growth curves of case (c) when $K_1 \gg K_2$, $K_1=K_2$, and $K_1 < K_2$ for $\beta_g=0.1$ and $K_2=0.1 \text{ m}^3/\mu\text{g}$. SOA growth for $K_1 \gg K_2$ (blue) decreases after all the HC has been reacted because the first-generation semivolatile product is further oxidized to a more volatile compound in a slow reaction step.

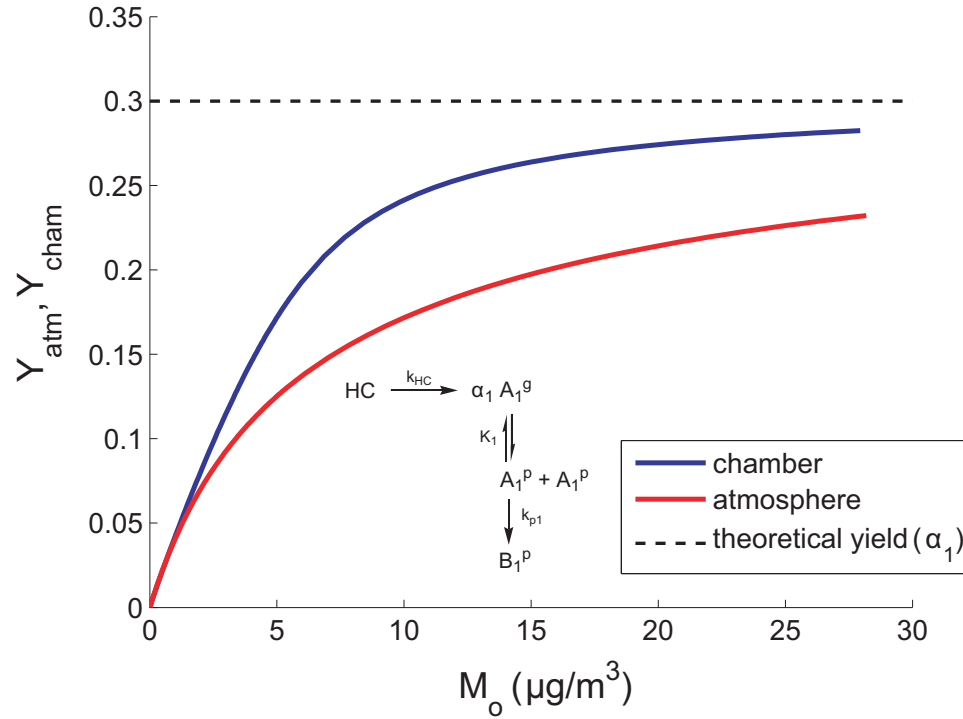


Figure 3.6: Simulated SOA yields of case (e) under typical chamber experiment conditions and atmospheric conditions. The values of the parameters are $\alpha_1=0.3$, $K_1=0.1 \text{ m}^3/\mu\text{g}$, $\beta_{p1}=1$. For the chamber simulations, no organic material is assumed to be initially present ($M_o(0)=0$) and a relatively large amount of hydrocarbon is reacted ($HC(0)=10$ to $100 \mu\text{g}/\text{m}^3$). The total simulation time for the “chamber” case is 1 day. For the “atmosphere” simulation, most of the aerosol loading is assumed to be from background organic material ($M_o(0)$ up to $28 \mu\text{g}/\text{m}^3$), and a relatively small amount of parent hydrocarbon is reacted ($HC(0)=1 \mu\text{g}/\text{m}^3$). Since the typical lifetime of SOA in the atmosphere is less than 1 week, we use 3 days as the total simulation time for the “atmosphere” case.

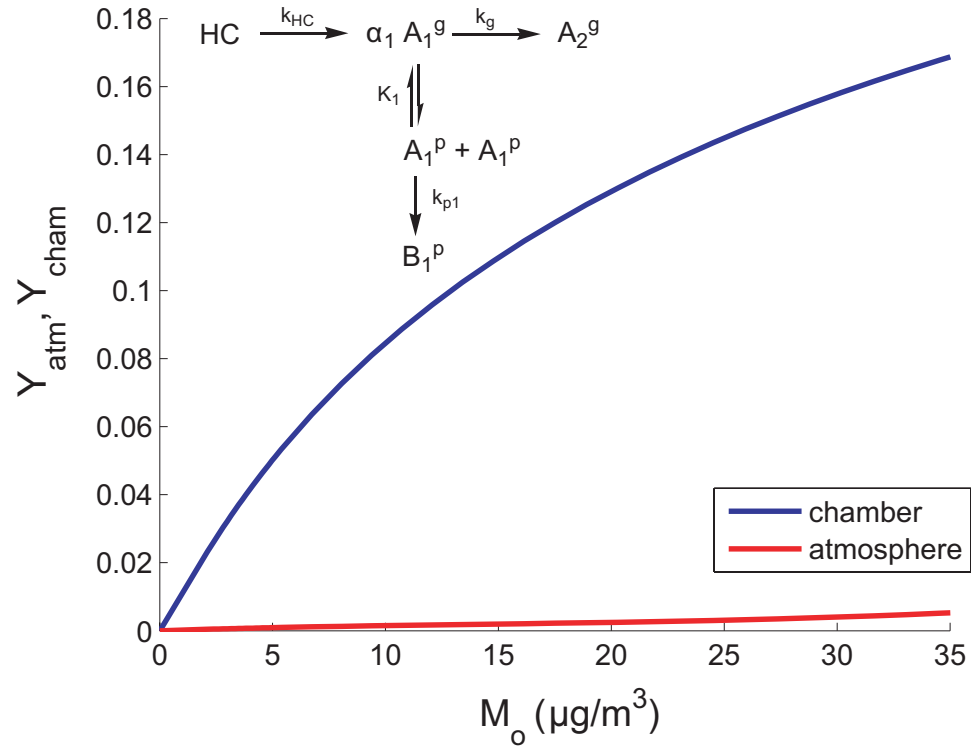


Figure 3.7: SOA yields in case (f) under typical chamber experiment conditions and atmospheric conditions. For the chamber simulations, $M_o(0)=0$, $HC(0)=200$ to $700 \mu\text{g}/\text{m}^3$. For the simulations of atmosphere, $M_o(0)$ up to $35 \mu\text{g}/\text{m}^3$, $HC(0)=1 \mu\text{g}/\text{m}^3$. The values for the kinetic parameters are $\alpha_1=0.3$, $K_1=0.1 \text{ m}^3/\mu\text{g}$. Shown here is the SOA yield for case (f) where the gas-phase loss rate and the aerosol-phase reaction rate are comparable ($\beta_g=1$, $\beta_{p1}=1$). The total simulation time is 1 day for the “chamber” case, and 3 days for the “atmosphere” case.

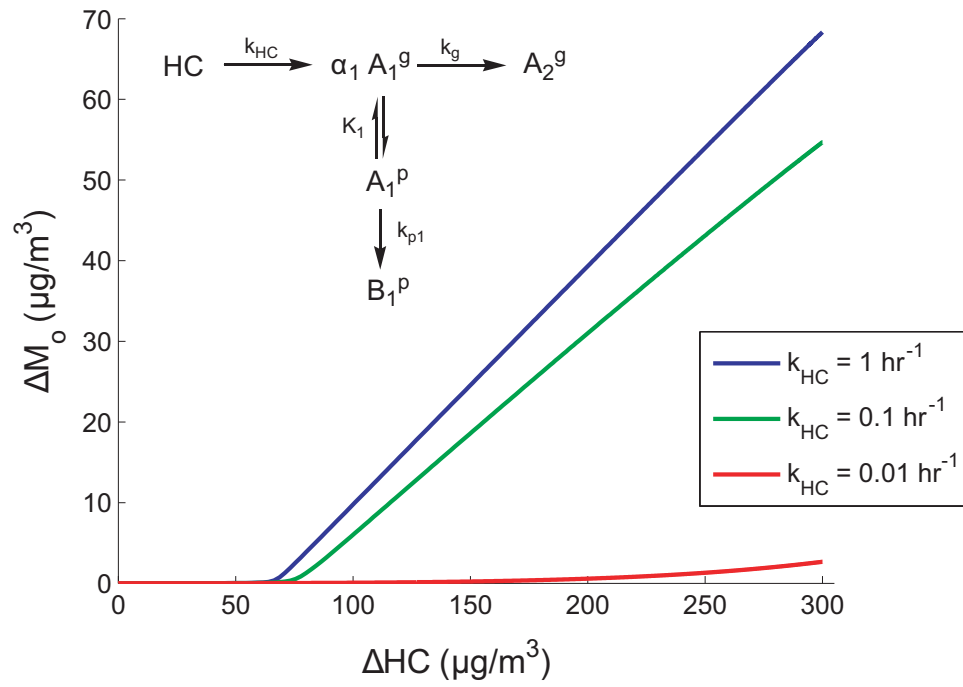


Figure 3.8: Effect of HC oxidation rate (k_{HC}) on SOA growth in case (b) with fast (blue), medium (green), and slow (red) hydrocarbon oxidation. $k_g=k_{p1}=1 \text{ hr}^{-1}$, $\alpha_1=0.3$, $K_1=0.05 \text{ m}^3/\mu\text{g}$, $M_o(0)=0.01 \mu\text{g}/\text{m}^3$.

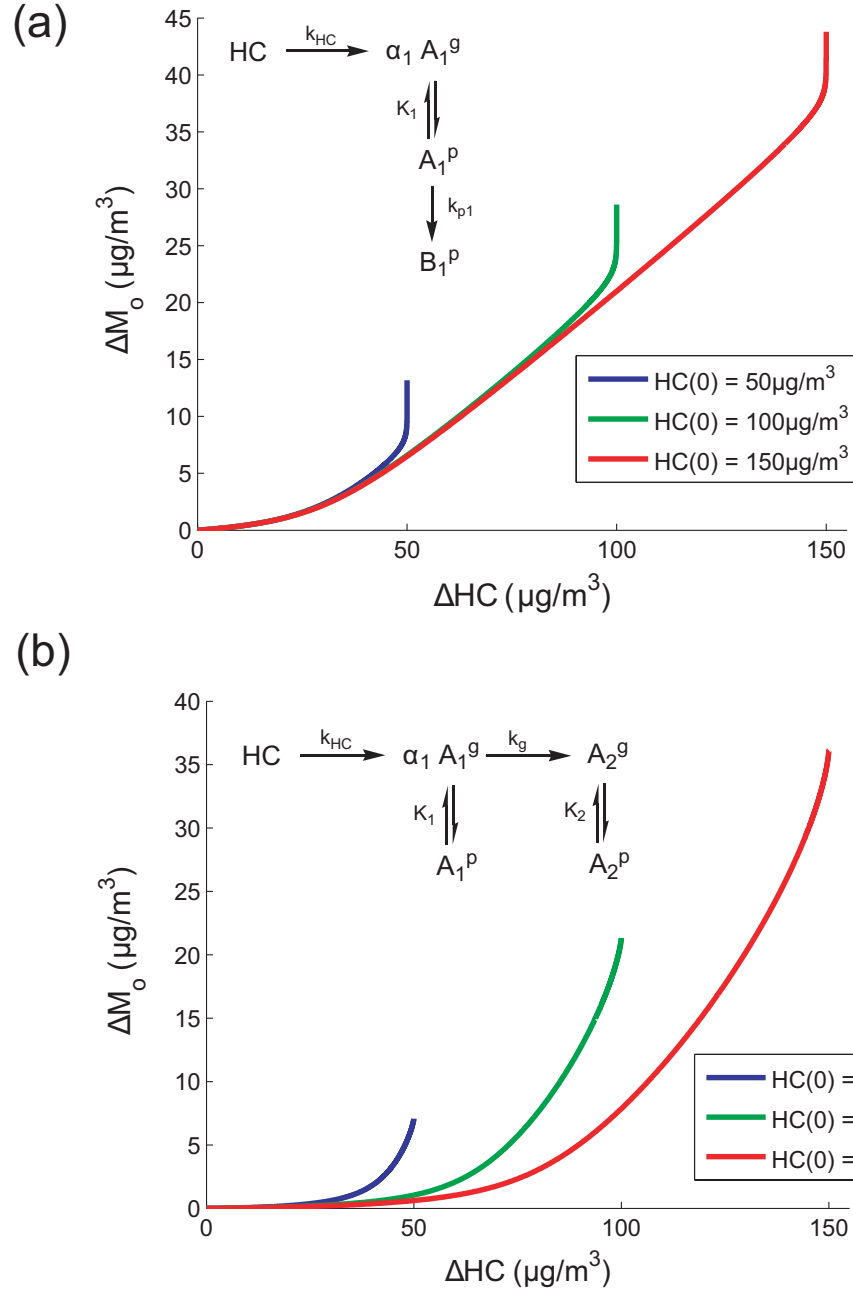


Figure 3.9: Growth curves under different initial hydrocarbon concentrations, $\text{HC}(0)$. Panel (a): Growth curves of case (a) with a relatively slow aerosol-phase reaction of semivolatile product ($\beta_{p1}=0.1$, $K_1=0.1 \text{ m}^3/\mu\text{g}$). Panel (b): Growth curves of case (c) with gas-phase reaction of semivolatile product to further generation semivolatile product ($K_1=0.01 \text{ m}^3/\mu\text{g}$, $K_2=0.1 \text{ m}^3/\mu\text{g}$, $\beta_g=0.1$). In both cases, $\alpha_1=0.3$, $M_o(0)=1 \mu\text{g}/\text{m}^3$.

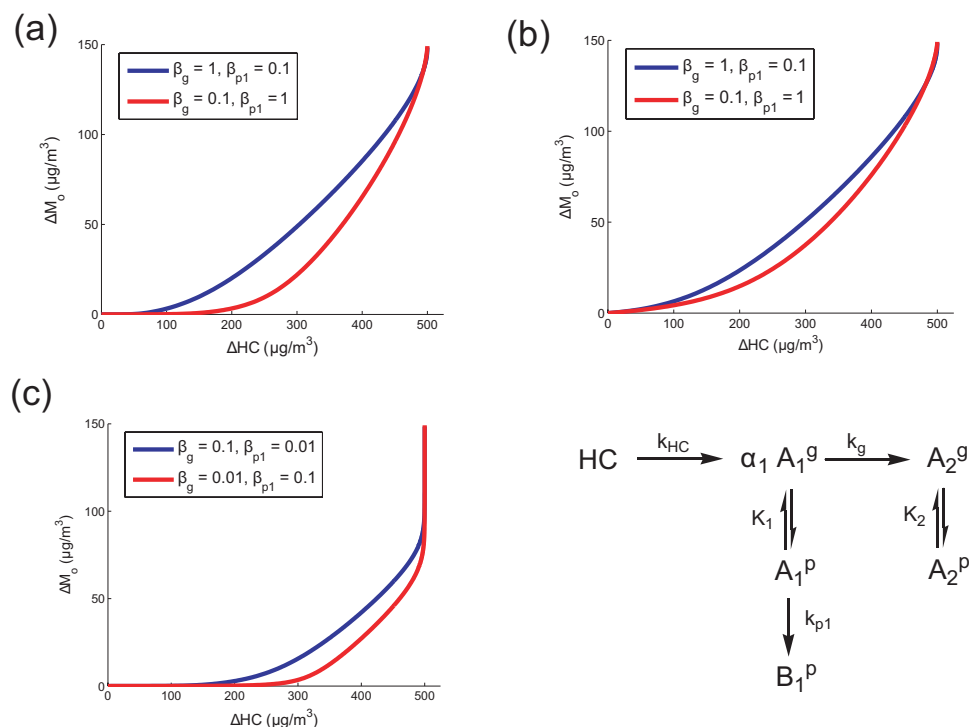


Figure 3.10: Growth curves for the overall kinetic model, including both gas-phase reaction to form low volatility products and aerosol-phase reaction (ignoring the aerosol-phase reaction of A_2^p). The blue curves represent cases in which the gas-phase reaction is faster than the aerosol-phase reaction ($\beta_g \gg \beta_{p1}$), and the red curves represent cases in which the aerosol-phase reaction is faster than the gas-phase reaction ($\beta_g < \beta_{p1}$). Panel (a): Growth curves of the overall kinetic model with a small amount of initial organic material ($M_o(0) = 0.1 \mu\text{g}/\text{m}^3$). Panel (b): Growth curves of the same model with a large amount of initial organic material ($M_o(0) = 10 \mu\text{g}/\text{m}^3$). Panel (c): Growth curves of the same model with the same amount of initial organic material as that depicted in panel (a) ($M_o(0) = 0.1 \mu\text{g}/\text{m}^3$), but the gas- and aerosol-phase reactions of A_1 are 10 times slower than in panel (a).

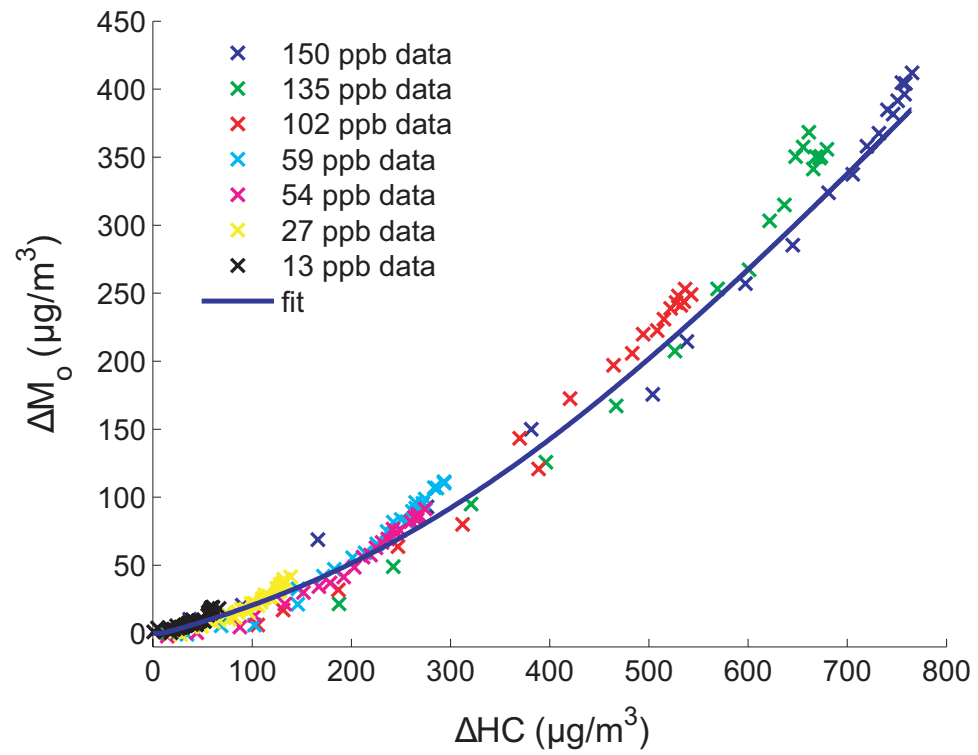


Figure 3.11: Growth curves for SOA formation from α -pinene ozonolysis at different $HC(0)$ (Ng et al., 2006). Data for different experiments adhere to the prediction of the Odum model (blue line). Values for the parameters of the fitted curve are $\alpha_1=0.19$, $K_1=0.52 \text{ m}^3/\mu\text{g}$, $\alpha_2=0.64$, $K_2=0.0025 \text{ m}^3/\mu\text{g}$.

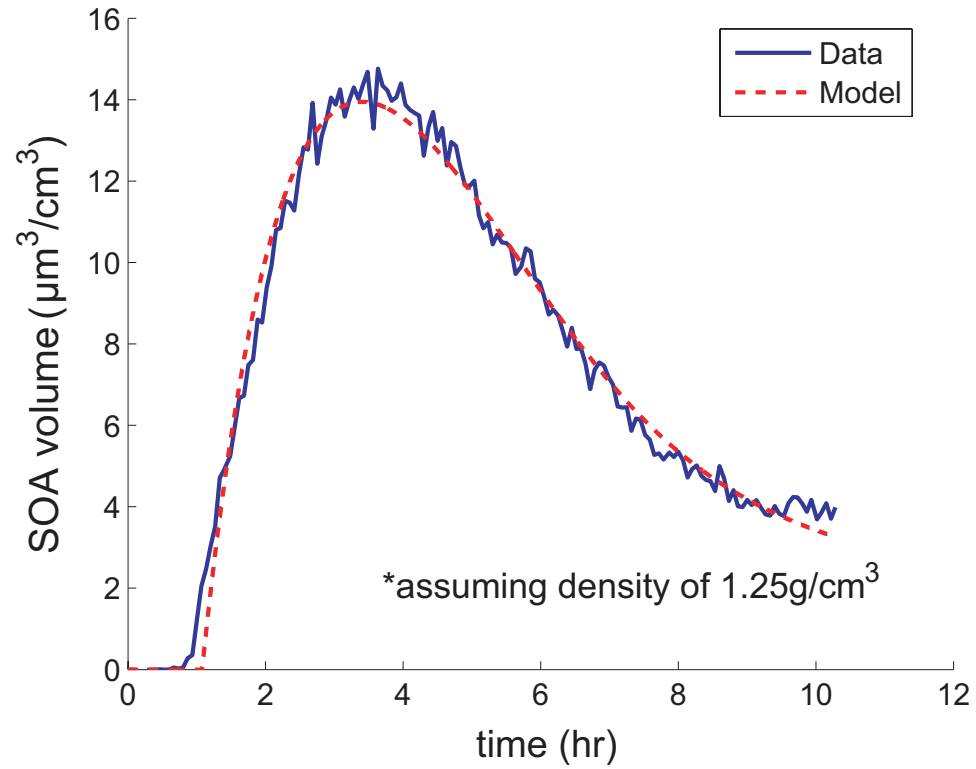


Figure 3.12: SOA growth data observed during isoprene photooxidation under low- NO_x conditions fit to case (b) of kinetic model. Values of the fitted parameters are $\alpha_1=0.30$, $K_1=0.033 \text{ m}^3/\mu\text{g}$, $\beta_g=0.24$, $\beta_{p1}=0.027$. The rate constant of isoprene oxidation, k_{HC} , was measured from the hydrocarbon decay to be 0.0114 min^{-1} . Data from Experiment 5, Fig. 2 of Kroll et al. (2006).

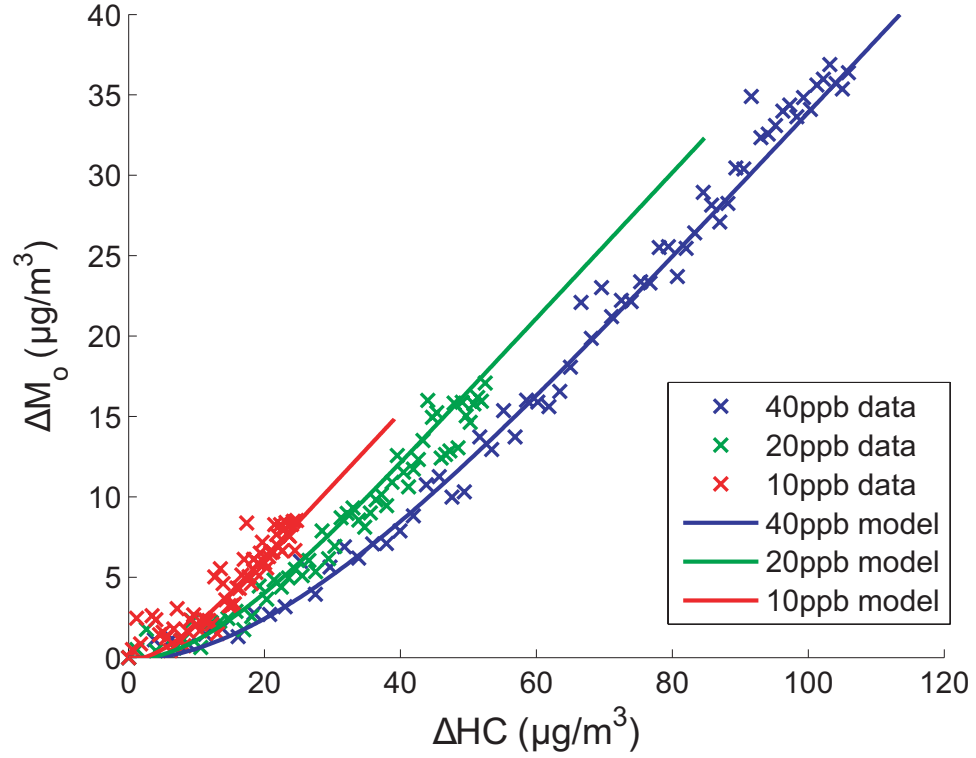


Figure 3.13: SOA growth data observed during *m*-xylene photooxidation under low-NO_x conditions (Ng et al., 2007) are consistent with case (d) of the kinetic model. The crosses represent SOA growth from each experiment, and the solid lines represent numerical solutions to case (d) of the kinetic model, with identical experimental conditions ($HC(0)$, $M_o(0)$, k_{HC}). The parameters in the model are adjusted to fit the experimental data: $\alpha_1=0.383$, $\beta_g=6.45$, $K_2=7.01 \text{ m}^3/\mu\text{g}$.

Chapter 4

Photooxidation of 2-methyl-3-buten-2-ol (MBO) as a potential source of secondary organic aerosol*

*Reproduced with permission from “Photooxidation of 2-Methyl-3-Buten-2-ol (MBO) as a Potential Source of Secondary Organic Aerosol” by Arthur W. H. Chan, Melissa M. Galloway, Alan J. Kwan, Puneet S. Chhabra, Frank N. Keutsch, Paul O. Wennberg, Richard C. Flagan, John H. Seinfeld, *Environmental Science and Technology*, 43 (13), 4647–4652, 2009. Copyright 2009 by the American Chemical Society.

4.1 Abstract

2-Methyl-3-buten-2-ol (MBO) is an important biogenic hydrocarbon emitted in large quantities by pine forests. Atmospheric photooxidation of MBO is known to lead to oxygenated compounds, such as glycolaldehyde, which is the precursor to glyoxal. Recent studies have shown that the reactive uptake of glyoxal onto aqueous particles can lead to formation of secondary organic aerosol (SOA). In this work, MBO photooxidation under high- and low-NO_x conditions was performed in dual laboratory chambers to quantify the yield of glyoxal and investigate the potential for SOA formation. The yields of glycolaldehyde and 2-hydroxy-2-methylpropanal (HMPR), fragmentation products of MBO photooxidation, were observed to be lower at lower NO_x concentrations. Overall, the glyoxal yield from MBO photooxidation was 25% under high-NO_x and 4% under low-NO_x conditions. In the presence of wet ammonium sulfate seed and under high-NO_x conditions, glyoxal uptake and SOA formation were not observed conclusively, due to relatively low (< 30 ppb) glyoxal concentrations. Slight aerosol formation was observed under low-NO_x and dry conditions, with aerosol mass yields on the order of 0.1%. The small amount of SOA was not related to glyoxal uptake, but is likely a result of reactions similar to those that generate isoprene SOA under low-NO_x conditions. The difference in aerosol yields between MBO and isoprene photooxidation under low-NO_x conditions is consistent with the difference in vapor pressures between triols (from MBO) and tetrols (from isoprene). Despite its structural similarity to isoprene, photooxidation of MBO is not expected to make a significant contribution to SOA formation.

4.2 Introduction

Large quantities of biogenic volatile organic compounds (BVOCs) are emitted into the atmosphere and have been linked to production of tropospheric ozone and formation of secondary organic aerosol (SOA) (Chameides et al., 1988; Kanakidou et al., 2005). While much of the study on the atmospheric chemistry of BVOCs has focused on isoprene and monoterpenes because of their abundant emissions (Guenther et al., 1995), it has been demonstrated that local photochemistry involving

oxygenated species, such as 2-methyl-3-buten-2-ol (MBO, $\text{CH}_3\text{-C(OH)(CH}_3\text{)-CH=CH}_2$), can be important (Spaulding et al., 2003). MBO, which is structurally similar to isoprene, is emitted in large quantities by a few specific species of pine (Goldan et al., 1993; Harley et al., 1998; Baker et al., 1999). Up to 6 ppb of MBO has been measured in pine forests (Spaulding et al., 2003); in some cases, local mixing ratios of MBO can exceed those of isoprene by a factor of 6 to 8 (Goldan et al., 1993). Estimates of global MBO and isoprene emissions are 9.6 and 430 Tg per year, respectively (Fu et al., 2008; Guenther et al., 2006). Although global emissions of MBO are small compared to those of isoprene, MBO can affect local production of ozone and HO_x radicals in forested areas (Steiner et al., 2007).

The principal atmospheric sink of MBO is reaction with OH radicals, the major products of which include acetone, glycolaldehyde, 2-hydroxy-2-methylpropanal (HMPR), and formaldehyde (Fantechi et al., 1998a; Ferronato et al., 1998; Alvarado et al., 1999; Reisen et al., 2003). Further reaction of glycolaldehyde leads to formation of glyoxal (Niki et al., 1987; Bacher et al., 2001; Magneron et al., 2005; Butkovskaya et al., 2006), which has also been shown to be reactively taken up onto aqueous particles and contribute to SOA growth (Liggio et al., 2005b; Kroll et al., 2005b; Volkamer et al., 2007; Carlton et al., 2007). Previous product studies have shown that photooxidation of MBO yields $\sim 60\%$ glycolaldehyde under high- NO_x conditions (Ferronato et al., 1998; Alvarado et al., 1999; Reisen et al., 2003; Carrasco et al., 2007). Under low- NO_x conditions, published glycolaldehyde yields vary between 28% and 79% (Fantechi et al., 1998a; Carrasco et al., 2007).

Slight aerosol formation has been observed from reactions of MBO with O_3 (Carrasco et al., 2007) and NO_3 (Noda and Ljungstrom, 2002), with aerosol yields (mass of SOA per mass of MBO reacted) less than 1%. In one study, photooxidation of MBO under high- NO_x conditions did not result in SOA formation (Carrasco et al., 2007). In each of these studies, inorganic seed particles were not present to promote condensation of semivolatile compounds, which might have led to underestimation of SOA formation as compared to ambient conditions (Kroll et al., 2007). Photooxidation of isoprene produces C_5 -tetrols, which are found in both field and chamber samples (Surratt et al., 2006; Claeys et al., 2004; Edney et al., 2005; Böge et al., 2006), and can react heterogeneously to form oligomers

(Surratt et al., 2006) or sulfate esters (Surratt et al., 2007). MBO is structurally similar to isoprene, but the extent to which MBO photooxidation leads to SOA growth is uncertain. Therefore, in addition to quantifying the yields of glycolaldehyde and glyoxal from MBO photooxidation under high- and low- NO_x conditions, another goal of this study is to evaluate the potential for SOA formation from photooxidation of MBO.

4.3 Experimental Section

Experiments were carried out in the Caltech indoor dual 28-m³ Teflon chambers, previously described in detail (Cocker et al., 2001; Keywood et al., 2004). A summary of the experimental conditions is given in Table 4.1. In Experiments 1 and 2, the rates of glyoxal photolysis and OH reaction were measured. Glyoxal was prepared using the method described in Kroll et al. (2005b). Cyclohexane (EMD, Omnisolv) was added to act as an OH scavenger during glyoxal photolysis (Experiment 1), or as a reference compound to determine the rate constant of the glyoxal-OH reaction (Experiment 2). In Experiment 2, photolysis of nitrous acid (HONO) was used as the OH precursor, prepared by adding 1 wt% aqueous NaNO_2 dropwise into 10 wt% sulfuric acid, and introduced into the chamber using an air stream. Photooxidation of MBO was carried out under high- and low- NO_x conditions. While MBO is typically not emitted in areas with high NO_x concentrations, a higher glyoxal yield is expected, making it easier to study glyoxal uptake on aerosol. In the high- NO_x experiments (Experiments 3–5), HONO was used as the OH precursor. A known volume of liquid MBO (Aldrich, 98%) was first injected into a glass bulb and vaporized into the chamber. HONO was then introduced as described in the previous section. The amount of HONO introduced was between 175 ppb and 310 ppb. Additional NO (Scott Marrin, Inc.) was added such that the total measured NO_x concentration was ~ 900 ppb. 10% of the available blacklights were used to irradiate the chambers and initiate photooxidation. For low- NO_x experiments (Experiments 6 and 7), H_2O_2 served as the OH precursor. Prior to injection of MBO, H_2O_2 was introduced by bubbling air through an aqueous H_2O_2 solution (Fluka). 50% of the blacklights were used owing to the relatively weak absorption of H_2O_2 with these blacklights. During irradiation, reactants (MBO and OH precursors)

were not added over the course of the experiment. In Experiments 5–7, seed particles were introduced into the chamber to act as a condensation substrate; this addition was achieved by atomization of a dilute (0.015 M – 0.03 M) aqueous ammonium sulfate solution using a constant rate atomizer. In Experiment 5, the chamber was humidified ($\text{RH} = 66\%$) by passing air through two large water bubblers in series, one of which was heated to $\sim 30^\circ\text{C}$.

Concentrations of MBO and cyclohexane were monitored using gas-chromatograph with flame ionization detector (GC-FID, Agilent 6890N). A custom modified Varian 1200 Chemical Ionization Mass Spectrometer (CIMS) was used to monitor the concentrations of various gas-phase species (Crounse et al., 2006). In brief, the reagent ion CF_3O^- clusters with protonated compounds, forming ions at m/z $\text{MW} + 85$ ($\text{HX} \cdot \text{CF}_3\text{O}^-$), or, with more acidic species, at m/z $\text{MW} + 19$ ($\text{HF} \cdot \text{X}^-$). As a calibration standard for glycolaldehyde (m/z 145), a dilute solution of glycolaldehyde dimer (Aldrich, $\geq 98\%$) in methanol was vaporized into a 60-L FEP Teflon bag. The sensitivities of the CIMS instrument to HMPR (m/z 173), dihydroxynitrate (fragments at m/z 184, 230, 250), and C_5 -triol (m/z 205) relative to glycolaldehyde are assumed to be equal to their relative rates of collision with the CF_3O^- ion (Paulot et al., 2008), and their dipole moments and polarizabilities were estimated with the B3LYP/6-31G(d) method. The uncertainty in this calculation is assumed to be 20%.

Gas-phase glyoxal was detected via Laser-Induced Phosphorescence (LIP) using the University of Wisconsin - Madison LIP Instrument (Huisman et al., 2008). This instrument utilizes a White-type multipass cell with gated photon counting. The technique is highly sensitive, permitting specific, direct, in situ measurement of glyoxal with a 1-min limit of detection of 12 pptv. For the high glyoxal concentrations typical of chamber studies, a 2 rather than 32 multi-pass configuration was used to ensure that photon counting rates stayed within the linear detector response range.

The aerosol size distribution, number concentration, and volume concentration were measured using a differential mobility analyzer (DMA, TSI 3081) coupled with a condensation nucleus counter (CPC, TSI 3760). The aerosol volume was corrected for wall loss by applying size-dependent coefficients determined from inert particle wall loss experiments (Keywood et al., 2004). An Aerodyne

High-Resolution Time-of-Flight Aerosol Mass Spectrometer (ToF-AMS) was used to obtain real-time aerosol mass spectra (DeCarlo et al., 2006). Temperature, relative humidity, O₃, NO, and NO_x were also continuously monitored.

4.4 Results

4.4.1 MBO photooxidation

Figure 4.1a shows the time evolution of MBO, glycolaldehyde, HMPR, and glyoxal in a typical high-NO_x photooxidation experiment. MBO decay was rapid in the first 2 h, but slowed after HONO was depleted. The reaction profile of MBO photooxidation under low-NO_x conditions is shown in Fig. 4.1b. The photolysis of H₂O₂ is much slower than that of HONO, resulting in a slower decay of MBO.

The molar yields of glycolaldehyde (α_{glyc}), HMPR (α_{HMPR}), dihydroxynitrate ($\alpha_{nitrate}$), and C₅-triol (α_{triol}) from MBO, and the molar yield of glyoxal from glycolaldehyde (α_{gly}) are summarized in Table 4.2. The observed product concentrations of glycolaldehyde and HMPR were corrected for further reaction with OH radicals. The glyoxal concentrations were corrected for photolysis and OH reaction. The photolysis rate constant of glyoxal was determined from Experiment 1 to be 0.034 h⁻¹ with 10% lights, and 0.17 h⁻¹ with 50% lights. The OH rate constant of glyoxal was measured in Experiment 2 to be 1.25×10^{-11} cm³ molec⁻¹ s⁻¹. In Experiment 7, because glycolaldehyde measurements were not available, α_{glyc} was instead estimated from glyoxal and MBO measurements, assuming a value of 0.26 for α_{gly} .

Experimental protocols were varied to confirm the yields. In Experiment 5, the lights were turned off after 10 min of irradiation. The concentrations of MBO and glycolaldehyde were allowed to stabilize before irradiation resumed. 56 ppb of MBO was consumed, forming 38 ppb of glycolaldehyde, 20 ppb of HMPR, and a negligible amount (0.6 ppb) of glyoxal. This implies a glycolaldehyde yield of 68% and an HMPR yield of 36%. In Experiment 4, after HONO was depleted, the concentrations of all species remained stable for > 1 h. More HONO was added, and glyoxal increased by 7 ppb.

Simultaneously, a decrease of 28 ppb of glycolaldehyde was observed. Combining this net decrease with a glycolaldehyde source of ~ 7 ppb from oxidation of the remaining MBO (11 ppb MBO reacted \times 68% glycolaldehyde yield) leads to an inferred total of 35 ppb glycolaldehyde reacted. α_{gly} is therefore determined to be 20%, not correcting for photochemical loss of glyoxal.

4.4.2 Secondary organic aerosol formation

A blank experiment was first performed under high- NO_x and humid conditions in the absence of MBO. The background level of organic growth observed by the AMS was found to be $0.1 \mu\text{g m}^{-3}$. The measured SOA volume concentration and organic mass concentration for each experiment are also listed in Table 4.2. There was no discernible change in aerosol volume in all high- NO_x experiments. In low- NO_x photooxidation of MBO, the amount of SOA growth reached a maximum after 3 h of irradiation and then decreased significantly. This loss of SOA was not a result of particle wall deposition, as the organic/sulfate ratio displayed a similar trend (see Fig. 4.2).

4.5 Discussion

4.5.1 Gas-phase mechanism of MBO photooxidation

Figure 4.3 shows the oxidation mechanism of MBO (Fantechi et al., 1998a; Ferronato et al., 1998; Alvarado et al., 1999; Reisen et al., 2003; Carrasco et al., 2007). Glycolaldehyde is a product of OH addition to the 4-position to form the peroxy radical, followed by formation of the alkoxy radical and decomposition. Under high- NO_x conditions, as MBO is oxidized, RO_2 and HO_2 radicals react rapidly with NO to produce NO_2 , which photolyzes to form O_3 . The concentration of O_3 increased to a maximum of 70 ppb after 6 h, at which point the rate of MBO ozonolysis became comparable to that of photooxidation (Fantechi et al., 1998b). The ozonolysis reaction, however, is not expected to be significant, as the decay of MBO after 6 h was less than 2 ppb h^{-1} . Under low- NO_x conditions, ozone formation was negligible.

The average yields of glycolaldehyde, HMPR, and dihydroxynitrate under high- NO_x conditions

determined from this study are in agreement with the literature (Ferronato et al., 1998; Alvarado et al., 1999; Reisen et al., 2003; Carrasco et al., 2007). In Fig. 4.4, the yields of glycolaldehyde and HMPR from different studies are shown as a function of the ratio of hydrocarbon to total NO ($\text{RONO} + \text{NO}$, $\text{R} = \text{H}$ in our case), which determines the relative rate of $\text{RO}_2 + \text{RO}_2$ to that of $\text{RO}_2 + \text{NO}$. Although the data are somewhat scattered, there appears to be a downward trend of glycolaldehyde and HMPR yields with increasing MBO:NO ratio. At high MBO:NO ratios, the self-reaction of RO_2 radicals can still form RO (which decomposes to form glycolaldehyde or HMPR), but a larger fraction of RO_2 forms the C_5 -triol and C_5 -dihydroxycarbonyl. As the MBO:NO ratio increases, $\text{RO}_2 + \text{RO}_2$ becomes increasingly important, favoring cross reactions to form C_5 -triol and C_5 -dihydroxycarbonyl over formation of glycolaldehyde and HMPR. The glycolaldehyde and HMPR yields are considerably lower under low- NO_x conditions (0.29 and 0.12 respectively) than under high- NO_x conditions (0.66 and 0.36 respectively). Fantechi et al. (1998a) also observed a glycolaldehyde yield of 0.28 under NO_x -free conditions, but Carrasco et al. (2007) reported a much higher yield of 0.79. The decreasing trend of glycolaldehyde yield with decreasing NO_x concentrations suggest a lower yield of glycolaldehyde under low- NO_x conditions is more likely.

The average glyoxal yield from glycolaldehyde obtained is 0.34 and is higher under high- NO_x conditions. Since there is no peroxy radical intermediate in the formation of glyoxal from glycolaldehyde, the branching ratio of the glyoxal-forming channel (and hence product yield of glyoxal) should not depend on NO_x conditions. However, the yields obtained here span a wide range of values, from 0.26 to 0.42. The glyoxal yield is higher than those previously obtained (Magneron et al., 2005; Butkovskaya et al., 2006). It is unclear if the loss processes (photolysis and OH reaction) of glyoxal were taken into account. Ignoring these processes, the glyoxal yield from the present study would be 0.20, which agrees with the value obtained by Magneron et al. (2005).

4.5.2 SOA formation: High NO_x

Relatively low SOA yields ($<0.2\%$) from MBO photooxidation under both high- and low- NO_x conditions were observed in this study. By comparison, the SOA yield of isoprene photooxidation is

0.2–3% under high-NO_x conditions (Kroll et al., 2005a) and 1–5% under low-NO_x conditions (Kroll et al., 2006). Under high-NO_x conditions, the major channel that leads to isoprene SOA formation is further oxidation of methacrolein to 2-methylglyceric acid, which can oligomerize (Surratt et al., 2006; Edney et al., 2005). The second oxidation step of MBO, which has only one double bond, is quite different from that of isoprene. Oxidation of HMPR, the analog of methacrolein in the MBO system, occurs via OH abstraction of the aldehydic hydrogen atom, producing stable volatile compounds, including acetone and formaldehyde (Carrasco et al., 2006).

It has been shown that glyoxal can serve as a monomer unit for higher-MW species, which have sufficiently low volatility to remain in the aerosol phase (Liggio et al., 2005b,a; Hastings et al., 2005). In Experiment 5, the chamber RH and seed aerosol were at levels sufficient for glyoxal hydration (Kroll et al., 2005b; Hastings et al., 2005), and 0.4 $\mu\text{g m}^{-3}$ of organic growth was observed by the AMS. Previous experiments have suggested that in the absence of irradiation, glyoxal uptake is likely reversible, with an effective Henry’s Law constant of $2.6 \times 10^{-7} \text{ M atm}^{-1}$ (Kroll et al., 2005b). Assuming an average gas-phase glyoxal concentration of 25 ppb and seed aerosol volume concentration of $68 \mu\text{m}^3 \text{ cm}^{-3}$ in Experiment 5, this corresponds to an organic growth of 0.4 $\mu\text{g m}^{-3}$. While the amount of observed organic growth is consistent with calculated uptake, the AMS mass spectra do not show peaks representative of glyoxal oligomers: m/z 77, 88, 105, 117 and 135 (see Fig. 4.5) (Liggio et al., 2005a). Instead, the spectra are consistent with those observed in the blank experiment, in which the chambers were irradiated under similar conditions (seed, NO_x, humidity) in the absence of MBO. In the blank experiment, since MBO was not introduced, the organic growth likely resulted from background contamination in the chambers. The concentrations of MBO in this work were chosen to match those in previous experiments of isoprene photooxidation, but as a result the gas-phase glyoxal concentration observed in Experiment 5 (< 30 ppb) was lower than those studies in which significant glyoxal uptake was observed (Kroll et al., 2005b; Volkamer et al., 2008), and the small amount of SOA formed was indistinguishable from that of the background in the chamber. In Kroll et al. (2005b), at a glyoxal concentration of 25 ppb and ammonium sulfate seed volume concentration of $78 \mu\text{m}^3 \text{ cm}^{-3}$, aerosol growth was below detection limit.

4.5.3 SOA formation: Low NO_x

Under low-NO_x conditions, the aerosol mass yields were on the order of 0.1%. No glyoxal uptake was expected due to the low RH in these experiments. The AMS spectrum obtained during the peak of organic growth is shown in Fig. 4.5. The relatively strong signals at m/z 43 (C₂H₃O⁺) and 59 (C₃H₇O⁺) and weak signal at m/z 44 (CO₂⁺) suggest that the condensed-phase organics are only partially oxidized. The identities of these fragments are confirmed by the exact mass under high-resolution mass spectrometry, and are clearly not related to glyoxal or its oligomers. The amount of SOA reaches a maximum and decreases, and the decrease in organic mass is more rapid than that in sulfate mass. The loss in organic mass does not correlate in time with the 5 °C temperature rise owing to blacklight irradiation, ruling out temperature effects. Similar photochemical loss has been observed in SOA from low-NO_x photooxidation of isoprene (Kroll et al., 2006), and was attributed to reactions of condensed-phase organic peroxides, leading to formation of higher volatility products (Surratt et al., 2006; Kroll et al., 2006). The similarity in the trend of MBO low-NO_x aerosol growth suggests that the loss mechanisms are likely similar.

Under low-NO_x conditions, formation of C₅-tetrols has been proposed to be the major pathway leading to isoprene SOA formation (Surratt et al., 2006; Claeys et al., 2004; Edney et al., 2005; Böge et al., 2006), with a maximum aerosol yield (at peak growth) of 2–10% (Kroll et al., 2006). In the MBO system, C₅-triol is formed from the RO₂+RO₂ reactions as a first-generation product, with an observed gas-phase molar yield of 0.12. With only 3 hydroxyl groups, the C₅-triol formed from MBO photooxidation is more volatile than the C₅-tetrol from isoprene photooxidation by a factor of ~170 (Pankow and Asher, 2008), which is consistent with the difference in aerosol yields between the two systems. Despite its structural similarity to isoprene, photooxidation of MBO is therefore not expected to make a significant contribution to ambient SOA formation, even in areas where MBO emissions are dominant.

Acknowledgements

This research was funded by the U.S. Department of Energy Biological and Environmental Research Program DE-FG02-05ER63983, the U.S. Environmental Protection Agency STAR grant RD-83374901 and the U.S. National Science Foundation grant ATM-0432377. This work was also supported by the Camille and Henry Dreyfus Foundation and development of the Madison-LIP instrument was supported by the National Science Foundation, Division of Atmospheric Sciences, Atmospheric Chemistry Program (grant 0724912), and the NDSEG-ARO. This publication has not been formally reviewed by the EPA. The views expressed in this document are solely those of the authors and the EPA does not endorse any products mentioned in this publication. The authors would like to thank Henrik Kjaergaard for density functional theory calculations of the dipole moments and polarizabilities of various gas-phase species.

Bibliography

- Alvarado, A., Tuazon, E. C., Aschmann, S. M., Arey, J., and Atkinson, R.: Products and mechanisms of the gas-phase reactions of OH radicals and O₃ with 2-methyl-3-buten-2-ol, *Atmos. Environ.*, 33, 2893–2905, 1999.
- Bacher, C., Tyndall, G. S., and Orlando, J. J.: The atmospheric chemistry of glycolaldehyde, *J Atmos Chem*, 39, 171–189, 2001.
- Baker, B., Guenther, A., Greenberg, J., Goldstein, A., and Fall, R.: Canopy fluxes of 2-methyl-3-buten-2-ol over a ponderosa pine forest by relaxed eddy accumulation: Field data and model comparison, *J. Geophys. Res.-Atmos.*, 104, 26 107–26 114, 1999.
- Böge, O., Miao, Y., Plewka, A., and Herrmann, H.: Formation of secondary organic particle phase compounds from isoprene gas-phase oxidation products: An aerosol chamber and field study, *Atmos. Environ.*, 40, 2501–2509, 2006.
- Butkovskaya, N. I., Pouvesle, N., Kukui, A., and Le Bra, G.: Mechanism of the OH-initiated

- oxidation of glycolaldehyde over the temperature range 233–296 K, *J. Phys. Chem. A*, 110, 13 492–13 499, 2006.
- Carlton, A. G., Turpin, B. J., Altieri, K. E., Seitzinger, S., Reff, A., Lim, H. J., and Ervens, B.: Atmospheric oxalic acid and SOA production from glyoxal: Results of aqueous photooxidation experiments, *Atmos. Environ.*, 41, 7588–7602, 2007.
- Carrasco, N., Doussin, J. F., Picquet-Varrault, B., and Carlier, P.: Tropospheric degradation of 2-hydroxy-2-methylpropanal, a photo-oxidation product of 2-methyl-3-buten-2-ol: Kinetic and mechanistic study of its photolysis and its reaction with OH radicals, *Atmos. Environ.*, 40, 2011–2019, 2006.
- Carrasco, N., Doussin, J. F., O'Connor, M., Wenger, J. C., Picquet-Varrault, B., Durand-Jolibois, R., and Carlier, P.: Simulation chamber studies of the atmospheric oxidation of 2-methyl-3-buten-2-ol: Reaction with hydroxyl radicals and ozone under a variety of conditions, *J. Atmos. Chem.*, 56, 33–55, 2007.
- Chameides, W. L., Lindsay, R. W., Richardson, J., and Kiang, C. S.: The role of biogenic hydrocarbons in urban photochemical smog - Atlanta as a Case-Study, *Science*, 241, 1473–1475, 1988.
- Claeys, M., Graham, B., Vas, G., Wang, W., Vermeylen, R., Pashynska, V., Cafmeyer, J., Guyon, P., Andreae, M. O., Artaxo, P., and Maenhaut, W.: Formation of secondary organic aerosols through photooxidation of isoprene, *Science*, 303, 1173–1176, 2004.
- Cocker, D. R., Flagan, R. C., and Seinfeld, J. H.: State-of-the-art chamber facility for studying atmospheric aerosol chemistry, *Environ. Sci. Technol.*, 35, 2594–2601, 2001.
- Crounse, J. D., McKinney, K. A., Kwan, A. J., and Wennberg, P. O.: Measurement of gas-phase hydroperoxides by chemical ionization mass spectrometry, *Anal. Chem.*, 78, 6726–6732, 2006.
- DeCarlo, P. F., Kimmel, J. R., Trimborn, A., Northway, M. J., Jayne, J. T., Aiken, A. C., Gonin, M.,

- Fuhrer, K., Horvath, T., Docherty, K. S., Worsnop, D. R., and Jimenez, J. L.: Field-deployable, high-resolution, time-of-flight aerosol mass spectrometer, *Anal. Chem.*, 78, 8281–8289, 2006.
- Edney, E. O., Kleindienst, T. E., Jaoui, M., Lewandowski, M., Offenberg, J. H., Wang, W., and Claeys, M.: Formation of 2-methyl tetrols and 2-methylglyceric acid in secondary organic aerosol from laboratory irradiated isoprene/ NO_x / SO_2 /air mixtures and their detection in ambient $\text{PM}_{2.5}$ samples collected in the eastern United States, *Atmos. Environ.*, 39, 5281–5289, 2005.
- Fantechi, G., Jensen, N. R., Hjorth, J., and Peeters, J.: Mechanistic studies of the atmospheric oxidation of methyl butenol by OH radicals, ozone and NO_3 radicals, *Atmos. Environ.*, 32, 3547–3556, 1998a.
- Fantechi, G., Jensen, N. R., Hjorth, J., and Peeters, J.: Determination of the rate constants for the gas-phase reactions of methyl butenol with OH radicals, ozone, NO_3 radicals, and Cl atoms, *Int. J. Chem. Kinet.*, 30, 589–594, 1998b.
- Ferronato, C., Orlando, J. J., and Tyndall, G. S.: Rate and mechanism of the reactions of OH and Cl with 2-methyl-3-buten-2-ol, *J. Geophys. Res.-Atmos.*, 103, 25 579–25 586, 1998.
- Fu, T. M., Jacob, D. J., Wittrock, F., Burrows, J. P., Vrekoussis, M., and Henze, D. K.: Global budgets of atmospheric glyoxal and methylglyoxal, and implications for formation of secondary organic aerosols, *J. Geophys. Res.-Atmos.*, 113, D15303, doi:10.1029/2007JD009505, 2008.
- Goldan, P. D., Kuster, W. C., Fehsenfeld, F. C., and Montzka, S. A.: The Observation of a C5 Alcohol Emission in a North-American Pine Forest, *Geophys. Res. Lett.*, 20, 1039–1042, 1993.
- Guenther, A., Hewitt, C. N., Erickson, D., Fall, R., Geron, C., Graedel, T., Harley, P., Klinger, L., Lerdau, M., McKay, W. A., Pierce, T., Scholes, B., Steinbrecher, R., Tallamraju, R., Taylor, J., and Zimmerman, P.: A global model of natural volatile organic compound emissions, *J. Geophys. Res.-Atmos.*, 100, 8873–8892, 1995.
- Guenther, A., Karl, T., Harley, P., Wiedinmyer, C., Palmer, P. I., and Geron, C.: Estimates of

- global terrestrial isoprene emissions using MEGAN (Model of Emissions of Gases and Aerosols from Nature), *Atmos. Chem. Phys.*, 6, 3181–3210, 2006.
- Harley, P., Fridd-Stroud, V., Greenberg, J., Guenther, A., and Vasconcellos, P.: Emission of 2-methyl-3-buten-2-ol by pines: A potentially large natural source of reactive carbon to the atmosphere, *J. Geophys. Res.-Atmos.*, 103, 25 479–25 486, 1998.
- Hastings, W. P., Koehler, C. A., Bailey, E. L., and De Haan, D. O.: Secondary organic aerosol formation by glyoxal hydration and oligomer formation: Humidity effects and equilibrium shifts during analysis, *Environ. Sci. Technol.*, 39, 8728–8735, 2005.
- Huisman, A. J., Hottle, J. R., Coens, K. L., DiGangi, J. P., Galloway, M. M., Kammrath, A., and Keutsch, F. N.: Laser-induced phosphorescence for the in situ detection of glyoxal at part per trillion mixing ratios, *Anal. Chem.*, 80, 5884–5891, 2008.
- Kanakidou, M., Seinfeld, J. H., Pandis, S. N., Barnes, I., Dentener, F. J., Facchini, M. C., Van Dingenen, R., Ervens, B., Nenes, A., Nielsen, C. J., Swietlicki, E., Putaud, J. P., Balkanski, Y., Fuzzi, S., Horth, J., Moortgat, G. K., Winterhalter, R., Myhre, C. E. L., Tsigaridis, K., Vignati, E., Stephanou, E. G., and Wilson, J.: Organic aerosol and global climate modelling: a review, *Atmos. Chem. Phys.*, 5, 1053–1123, 2005.
- Keywood, M. D., Varutbangkul, V., Bahreini, R., Flagan, R. C., and Seinfeld, J. H.: Secondary organic aerosol formation from the ozonolysis of cycloalkenes and related compounds, *Environ. Sci. Technol.*, 38, 4157–4164, 2004.
- Kroll, J. H., Ng, N. L., Murphy, S. M., Flagan, R. C., and Seinfeld, J. H.: Secondary organic aerosol formation from isoprene photooxidation under high-NO_x conditions, *Geophys. Res. Lett.*, 32, L18808, doi:10.1029/2005GL023637, 2005a.
- Kroll, J. H., Ng, N. L., Murphy, S. M., Varutbangkul, V., Flagan, R. C., and Seinfeld, J. H.: Chamber studies of secondary organic aerosol growth by reactive uptake of simple carbonyl compounds, *J. Geophys. Res.-Atmos.*, 110, D23207, doi:10.1029/2005JD006004, 2005b.

- Kroll, J. H., Ng, N. L., Murphy, S. M., Flagan, R. C., and Seinfeld, J. H.: Secondary organic aerosol formation from isoprene photooxidation, *Environ. Sci. Technol.*, 40, 1869–1877, 2006.
- Kroll, J. H., Chan, A. W. H., Ng, N. L., Flagan, R. C., and Seinfeld, J. H.: Reactions of semivolatile organics and their effects on secondary organic aerosol formation, *Environ. Sci. Technol.*, 41, 3545–3550, 2007.
- Liggio, J., Li, S. M., and McLaren, R.: Heterogeneous reactions of glyoxal on particulate matter: Identification of acetals and sulfate esters, *Environ. Sci. Technol.*, 39, 1532–1541, 2005a.
- Liggio, J., Li, S. M., and McLaren, R.: Reactive uptake of glyoxal by particulate matter, *J. Geophys. Res.-Atmos.*, 110, D10304, doi:10.1029/2004JD005113, 2005b.
- Magneron, I., Mellouki, A., Le Bras, G., Moortgat, G. K., Horowitz, A., and Wirtz, K.: Photolysis and OH-Initiated oxidation of glycolaldehyde under atmospheric conditions, *J. Phys. Chem. A*, 109, 4552–4561, 2005.
- Niki, H., Maker, P. D., Savage, C. M., and Hurley, M. D.: Fourier-transform infrared study of the kinetics and mechanisms for the Cl-atom-initiated and HO-radical-initiated oxidation of glycolaldehyde, *J. Phys. Chem.*, 91, 2174–2178, 1987.
- Noda, J. and Ljungstrom, E.: Aerosol formation in connection with NO_3 oxidation of unsaturated alcohols, *Atmos. Environ.*, 36, 521–525, 2002.
- Pankow, J. F. and Asher, W. E.: SIMPOL.1: a simple group contribution method for predicting vapor pressures and enthalpies of vaporization of multifunctional organic compounds, *Atmos. Chem. Phys.*, 8, 2773–2796, 2008.
- Paulot, F., D. Crounse, J., Kjaergaard, H. G., Kroll, J. H., Seinfeld, J. H., and Wennberg, P. O.: Isoprene photooxidation mechanism: resonance channels and implications for the production of nitrates and acids, *Atmos. Chem. Phys. Discuss.*, 8, 14 643–14 716, 2008.
- Reisen, F., Aschmann, S. M., Atkinson, R., and Arey, J.: Hydroxyaldehyde products from hydroxyl

- radical reactions of Z-3-hexen-1-ol and 2-methyl-3-buten-2-ol quantified by SPME and API-MS, *Environ. Sci. Technol.*, **37**, 4664–4671, 2003.
- Spaulding, R. S., Schade, G. W., Goldstein, A. H., and Charles, M. J.: Characterization of secondary atmospheric photooxidation products: Evidence for biogenic and anthropogenic sources, *J. Geophys. Res.-Atmos.*, **108**, 4247, doi:10.1029/2002JD002478, 2003.
- Steiner, A. L., Tonse, S., Cohen, R. C., Goldstein, A. H., and Harley, R. A.: Biogenic 2-methyl-3-buten-2-ol increases regional ozone and HO_x sources, *Geophys. Res. Lett.*, **34**, L15806, doi:10.1029/2007GL030802, 2007.
- Surratt, J. D., Murphy, S. M., Kroll, J. H., Ng, N. L., Hildebrandt, L., Sorooshian, A., Szmigielski, R., Vermeylen, R., Maenhaut, W., Claeys, M., Flagan, R. C., and Seinfeld, J. H.: Chemical composition of secondary organic aerosol formed from the photooxidation of isoprene, *J. Phys. Chem. A*, **110**, 9665–9690, 2006.
- Surratt, J. D., Kroll, J. H., Kleindienst, T. E., Edney, E. O., Claeys, M., Sorooshian, A., Ng, N. L., Offenberg, J. H., Lewandowski, M., Jaoui, M., Flagan, R. C., and Seinfeld, J. H.: Evidence for organosulfates in secondary organic aerosol, *Environ. Sci. Technol.*, **41**, 517–527, 2007.
- Volkamer, R., Martini, F. S., Molina, L. T., Salcedo, D., Jimenez, J. L., and Molina, M. J.: A missing sink for gas-phase glyoxal in Mexico City: Formation of secondary organic aerosol, *Geophys. Res. Lett.*, **34**, L19807, doi:10.1029/2007GL030752, 2007.
- Volkamer, R., Ziemann, P. J., and Molina, M. J.: Secondary organic aerosol formation from acetylene (C₂H₂): seed effect on SOA yields due to organic photochemistry in the aerosol aqueous phase, *Atmos. Chem. Phys. Discuss.*, **8**, 14 841–14 892, 2008.

Table 4.1: Experimental conditions.

#	Compound	Initial conc (ppb)	OH source	Lights	Initial NO (ppb)	Seed conc ^a ($\mu\text{m}^3\text{cm}^{-3}$)	T (K)	RH (%)
1	glyoxal	640	none	50%	<2	0	298	3
2	glyoxal	735	HONO	10%	283	0	294	5
3	MBO	288	HONO	10%	304	0	295	4
4	MBO	255	HONO	10%	422	13	295	4
5	MBO	239	HONO	10%	539	68	293	66
n/a	blank	—	HONO	10%	635	63	294	60
6	MBO	299	H ₂ O ₂	50%	<2	14	298	6
7	MBO	289	H ₂ O ₂	50%	<2	17	298	6

^a Ammonium sulfate seed

Table 4.2: Experimental results.

#	NO _x	α_{glyc}	α_{HMPR}	$\alpha_{nitrate}$	α_{triol}	α_{glyc}	ΔV_{org}	ΔM_{org}	Aerosol Mass Yield
3	High	0.64±0.02	0.35±0.07	0.10±0.04	0	0.33	0	0	—
4	High	0.70±0.02	0.41±0.08	0.11±0.04	0	0.26	< 0.5	<0.1	<0.001
5	High	0.65±0.02	0.34±0.07	0.08±0.04	0	0.29	< 0.5	0.4	<0.001
6	Low	0.26±0.05	0.12±0.02	0	0.12±0.04	0.26	1.5±1.0	0.6	0.0014
7	Low	0.32±0.06 ^c	n/a ^c	n/a ^c	n/a ^c	n/a ^c	1.0±1.0	0.9	0.001

^a As measured by DMA at the peak of organic growth

^b As measured by AMS at the peak of organic growth

^c CIMS measurements not available; α_{glyc} estimated from glyoxal and MBO measurements, assuming a value of 0.26 for α_{gly} .

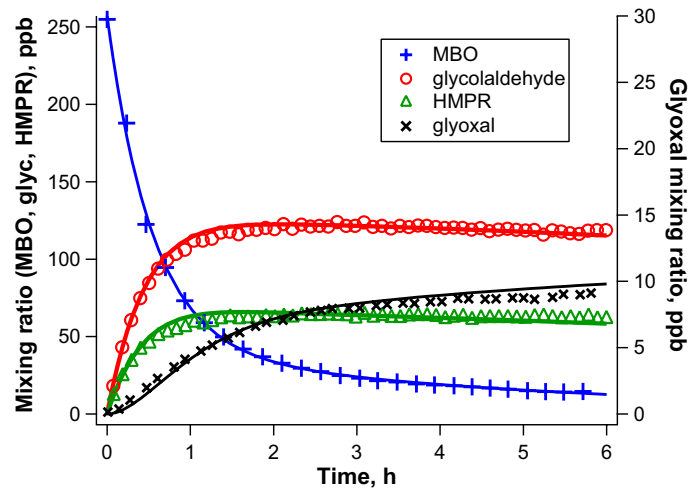
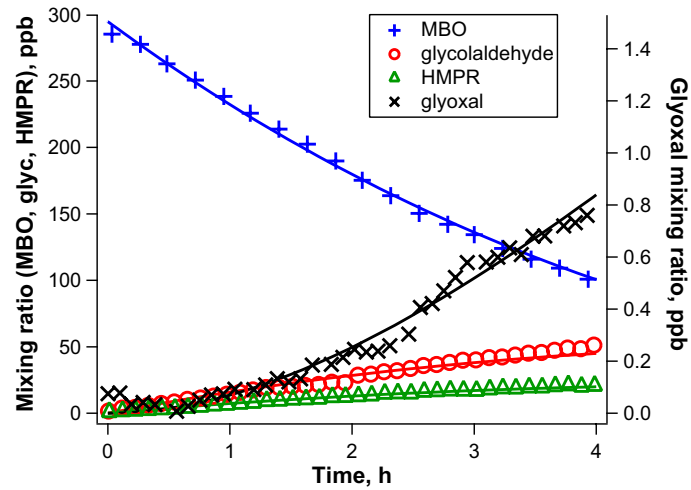
(a) High- NO_x (b) Low- NO_x 

Figure 4.1: Time profiles of MBO (blue), glycolaldehyde (red), HMPR (green), and glyoxal (black) in (a) Experiment 4 (high- NO_x) and (b) Experiment 6 (low- NO_x). Markers represent experimental data points, and lines represent best fits (see Table 4.2).

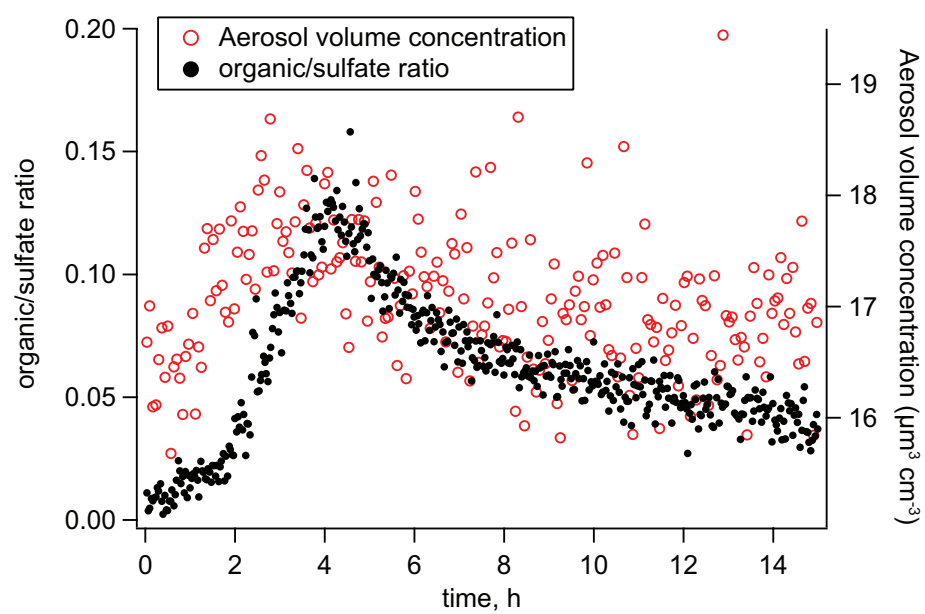


Figure 4.2: AMS organic/sulfate ratio and DMA aerosol volume concentration in Experiment 6. The volume concentration has been corrected for particle wall loss.

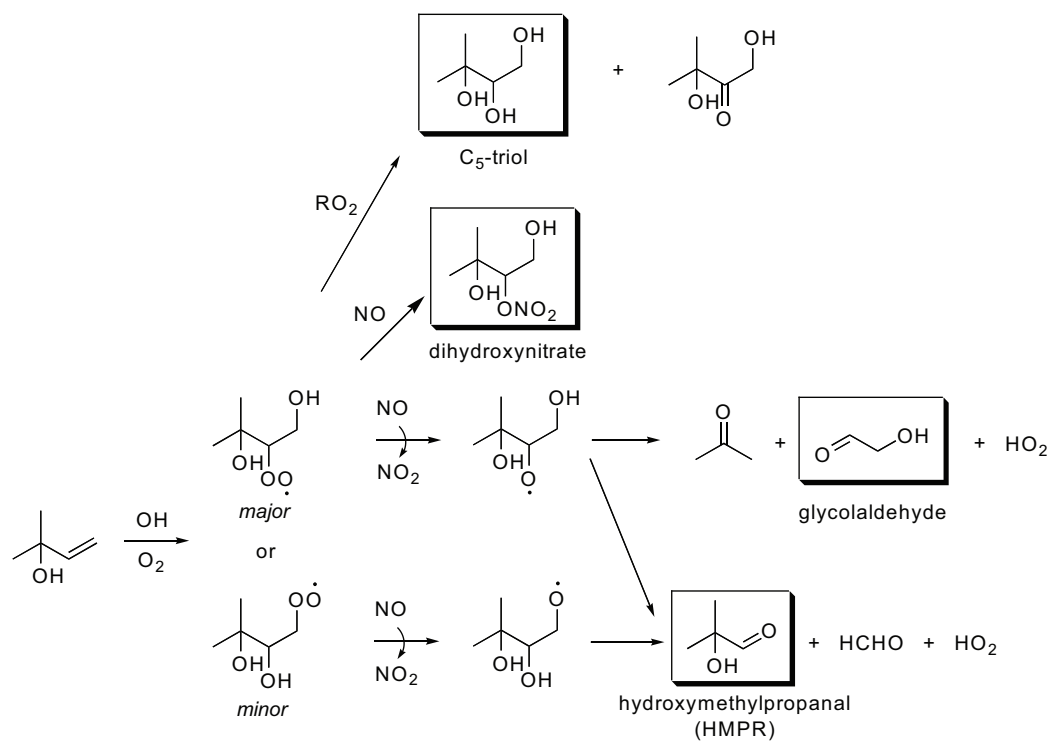


Figure 4.3: Mechanism of MBO photooxidation (Ferronato et al., 1998; Alvarado et al., 1999; Reisen et al., 2003; Carrasco et al., 2007). Structural isomers not shown.

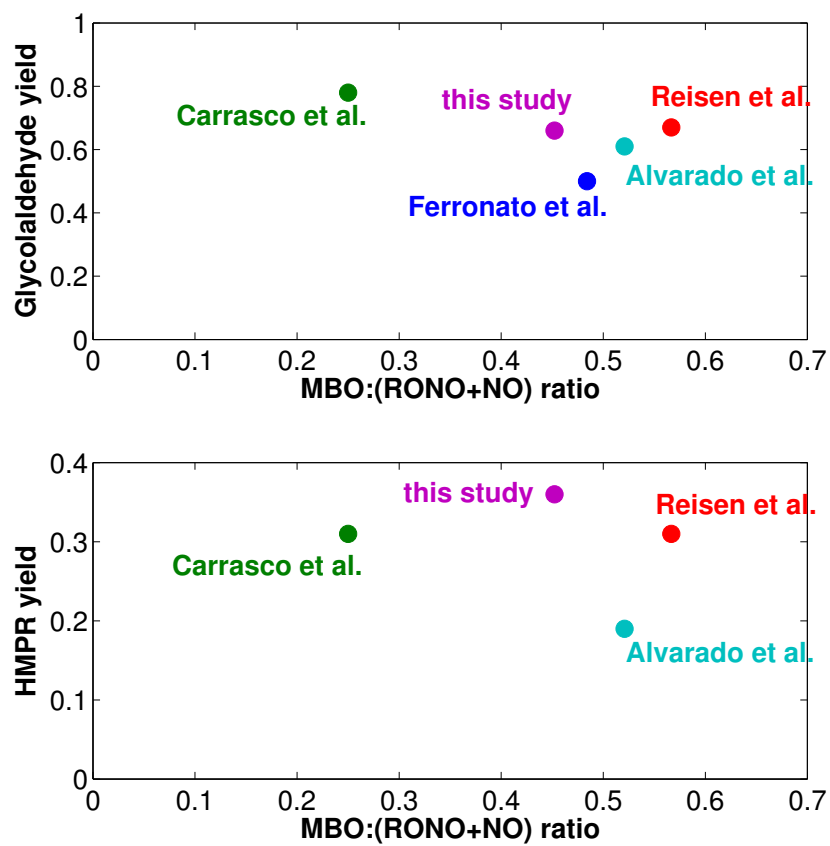


Figure 4.4: Yields of glycolaldehyde and HMPR from MBO photooxidation under high- NO_x conditions (Ferronato et al., 1998; Alvarado et al., 1999; Reisen et al., 2003; Carrasco et al., 2007).

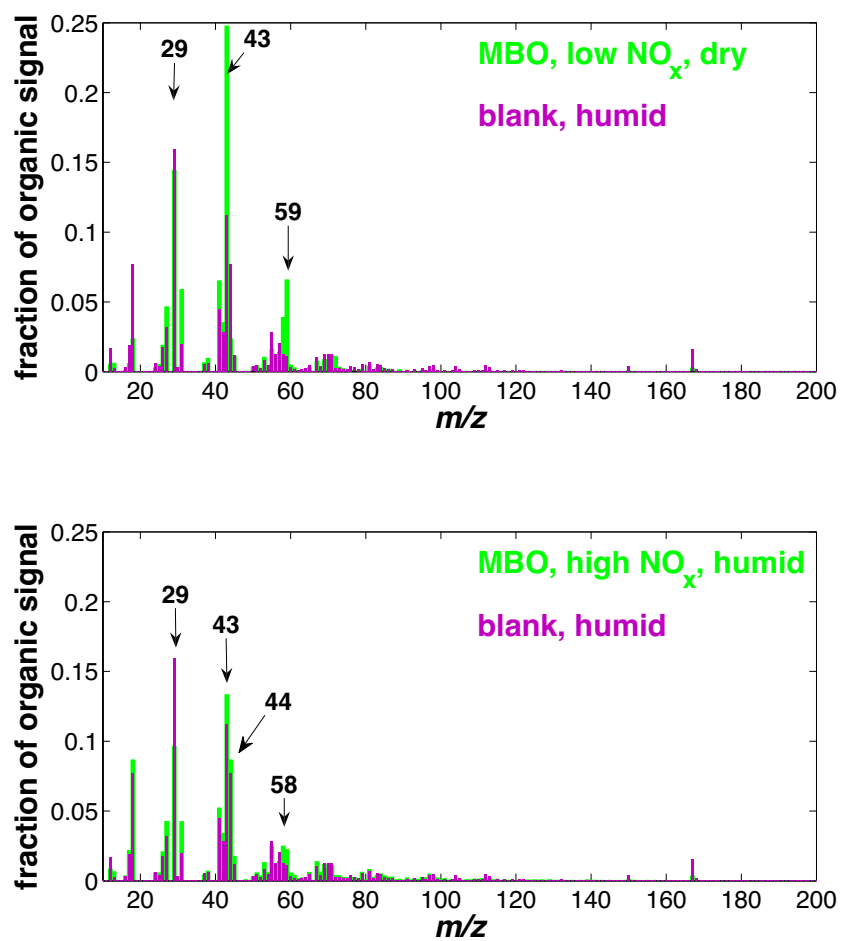


Figure 4.5: AMS spectra obtained in Experiments 5 and 6, compared to the spectrum obtained in the blank experiment.

Chapter 5

Secondary organic aerosol formation from photooxidation of naphthalene and alkylnaphthalenes: implications for oxidation of intermediate volatility organic compounds (IVOCs)*

*Reproduced with permission from “Secondary organic aerosol formation from photooxidation of naphthalene and alkylnaphthalenes: implications for oxidation of intermediate volatility organic compounds (IVOCs)” by A. W. H. Chan, K. E. Kautzman, P. S. Chhabra, J. D. Surratt, M. N. Chan, J. D. Crounse, A. Kürten, P. O. Wennberg, R. C. Flagan, and J. H. Seinfeld, *Atmospheric Chemistry and Physics*, 9 (9), 3049–3060, 2009. Copyright 2009 by Authors. This work is licensed under a Creative Commons License.

5.1 Abstract

Current atmospheric models do not include secondary organic aerosol (SOA) production from gas-phase reactions of polycyclic aromatic hydrocarbons (PAHs). Recent studies have shown that primary emissions undergo oxidation in the gas phase, leading to SOA formation. This opens the possibility that low-volatility gas-phase precursors are a potentially large source of SOA. In this work, SOA formation from gas-phase photooxidation of naphthalene, 1-methylnaphthalene (1-MN), 2-methylnaphthalene (2-MN), and 1,2-dimethylnaphthalene (1,2-DMN) is studied in the Caltech dual 28-m³ chambers. Under high-NO_x conditions and aerosol mass loadings between 10 and 40 µg m⁻³, the SOA yields (mass of SOA per mass of hydrocarbon reacted) ranged from 0.19 to 0.30 for naphthalene, 0.19 to 0.39 for 1-MN, 0.26 to 0.45 for 2-MN, and constant at 0.31 for 1,2-DMN. Under low-NO_x conditions, the SOA yields were measured to be 0.73, 0.68, and 0.58, for naphthalene, 1-MN, and 2-MN, respectively. The SOA was observed to be semivolatile under high-NO_x conditions and essentially nonvolatile under low-NO_x conditions, owing to the higher fraction of ring-retaining products formed under low-NO_x conditions. When applying these measured yields to estimate SOA formation from primary emissions of diesel engines and wood burning, PAHs are estimated to yield 3–5 times more SOA than light aromatic compounds over photooxidation timescales of less than 12 h. PAHs can also account for up to 54% of the total SOA from oxidation of diesel emissions, representing a potentially large source of urban SOA.

5.2 Introduction

Organic aerosol (OA) accounts for a large fraction of urban particulate matter (Seinfeld and Pankow, 2003; Zhang et al., 2007), and thus has important implications for health, climate, and visibility. OA has traditionally been classified into two categories: primary organic aerosol (POA), which is directly emitted as particulate matter, and secondary organic aerosol (SOA), which is formed from atmospheric oxidation of volatile organic compounds (VOCs). POA has been assumed to be nonvolatile and chemically inert in atmospheric models, and is emitted primarily from anthropogenic

sources, such as diesel and gasoline engines, wood burning and cooking operations (Schauer et al., 1996). On the other hand, SOA, formed from gas-phase oxidation of biogenic and anthropogenic volatile precursors, is an important source of OA both on global and local scales (Goldstein and Galbally, 2007; Docherty et al., 2008). Nonetheless, the amount of OA observed in urban sites is consistently higher than that for which volatile SOA precursors can account (de Gouw et al., 2005; Heald et al., 2005; Volkamer et al., 2006).

This POA/SOA classification has recently been called into question; during laboratory chamber photooxidation of diesel and biomass burning emissions, volatile SOA precursors, which consist primarily of light aromatic compounds such as benzene, toluene, and xylene, can account for only a small fraction of the SOA produced (Robinson et al., 2007; Grieshop et al., 2009a,b). Robinson et al. (2007) proposed that gas-phase reactions of low-volatility compounds likely contribute to a large fraction of the SOA formed, as oxidation of these low-volatility organic vapors produces aerosol that closely resembles OA observed in field measurements (Weitkamp et al., 2007; Sage et al., 2008; Grieshop et al., 2009a). While some of these compounds, including long chain *n*-alkanes, polycyclic aromatic hydrocarbons (PAHs), and large olefins, exist exclusively in the gas phase, they have lower volatilities than traditional SOA precursors and are typically ignored in current atmospheric models. These compounds, which have saturation concentrations between 10^3 and 10^6 $\mu\text{g m}^{-3}$, are termed intermediate volatility organic compounds (IVOCs) (Donahue et al., 2009).

PAHs have been identified as a major component in emissions from diesel engines and wood burning sources (Schauer et al., 1999a, 2001). While PAHs with fewer than 4 aromatic rings exist primarily in the gaseous phase, photooxidation of these compounds has been shown to yield high molecular weight (MW) oxygenated compounds (Sasaki et al., 1997; Bunce et al., 1997; Wang et al., 2007), which can partition into the particle phase and lead to significant SOA formation (Mihele et al., 2002). Moreover, nitronaphthalene, an oxidation product of naphthalene, and other nitro PAHs have been observed in urban particulate matter (Arey et al., 1989). The oxidation of PAHs in the gas phase will likely have significant impacts on both the quantity and the properties of SOA formed in urban atmospheres. In this study, we present results on SOA formation from gas-phase

photooxidation of naphthalene, 1-methylnaphthalene (1-MN), 2-methylnaphthalene (2-MN), and 1,2-dimethylnaphthalene (1,2-DMN). The SOA yields, the mass of SOA formed per mass of PAH reacted, are then used to evaluate the importance of PAHs as effective SOA precursors.

5.3 Experimental

Experiments were carried out in the Caltech dual 28-m³ Teflon chambers. Details of the facilities have been described previously (Cocker et al., 2001; Keywood et al., 2004). Before each experiment, the chambers were flushed with dried purified air for >24 h, until the particle number concentration was <100 cm⁻³ and the volume concentration was <0.1 $\mu\text{m}^3 \text{ cm}^{-3}$.

In most experiments, an inorganic seed aerosol was used to provide a surface for condensation of semivolatile oxidation products. Seed aerosol was generated by atomization of a 0.015 M aqueous ammonium sulfate solution. The aerosol size distribution, number and volume concentrations were measured with a differential mobility analyzer (DMA, TSI, 3081) coupled with a condensation nuclei counter (TSI, CNC-3760). The volume concentration was corrected for particle wall loss by applying size-dependent first-order loss coefficients, obtained in a separate seed-only experiment (Keywood et al., 2004).

After atomization of inorganic seed, the parent hydrocarbon was then injected into the chamber; the injection method varied depending on its phase under room temperature conditions. For naphthalene and 2-MN, the hydrocarbon was introduced into the chamber by flowing purified air through an FEP tube packed with the solid PAH at 1 L min⁻¹. For 1-MN and 1,2-DMN, a known volume of the liquid PAH was injected into a heated glass bulb, and the vapor was carried into the chamber with 5 L min⁻¹ of purified air. The parent hydrocarbons studied and their stated purities are as follows: naphthalene (Sigma-Aldrich, 99%), 1-methylnaphthalene (Fluka, $\geq 97\%$), 2-methylnaphthalene (Fluka, $\geq 95\%$), and 1,2-dimethylnaphthalene (Aldrich, 95%). The hydrocarbon was measured using a gas chromatograph with flame ionization detector (GC/FID, Agilent 6890N), equipped with an HP5 15 m \times 0.53 mm ID column \times 1 μm thickness column. The GC response was calibrated by dissolving a known mass of the parent PAH in dichloromethane, and vaporizing a small

volume of that solution into a 38L Teflon chamber.

For high- NO_x experiments (initial $[\text{NO}] > 300$ ppb), nitrous acid (HONO) was used as an OH precursor. Nitrous acid was prepared by adding 10 mL of 1 wt% aqueous NaNO_2 dropwise into 20 mL of 10 wt% sulfuric acid in a glass bulb. A stream of purified air was then passed through the bulb, sending HONO into the chamber. This process also forms NO and NO_2 as side products. The injection of HONO was stopped when $[\text{NO}_2]$ reached about 80 ppb in the chamber. Additional NO was added until total $[\text{NO}]$ was about 400 ppb. NO_2 was monitored by a gas chromatograph with luminol detector (University of California, Riverside, CA), in which NO_2 and PAN were separated by gas chromatograph and detected by chemiluminescence of reaction with luminol (Burkhardt et al., 1988). Reaction of HONO with luminol is unlikely, and thus would not interfere with the NO_2 signal. A commercial chemiluminescence NO/ NO_x analyzer (Horiba, APNA 360) was used to monitor NO and total NO_y . For low- NO_x experiments, hydrogen peroxide (H_2O_2) was used as an OH precursor. Prior to atomization of the ammonium sulfate seed, H_2O_2 was introduced by bubbling purified air through a 50% aqueous H_2O_2 solution for 2.5 h at 5 L min^{-1} .

After allowing for all concentrations to stabilize, irradiation was initiated. The temperature of the chamber reached 299 K, and the RH of the experiments was between 5 and 8%. Figure 5.1 lists the structures of the parent hydrocarbons and their OH reaction rate constants (k_{OH}). The experimental conditions prior to beginning of irradiation and the results are summarized in Table 5.1. Photooxidation of 1,2-DMN under low- NO_x conditions was not studied. Owing to its fast OH reaction rate, 1,2-DMN will likely be consumed near its ambient sources, where NO_x concentrations are likely to be high.

A proton transfer reaction mass spectrometer (PTR-MS), a custom modified Varian 1200 system, was used to monitor the concentrations of various gas-phase species. Details of the instrument are given in Ng et al. (2007a). In brief, positively charged water clusters, $(\text{H}_2\text{O})_n \cdot \text{H}^+$, react via proton transfer with the analyte, A , to form the positively charged ion, $A \cdot (\text{H}_2\text{O})_x \cdot \text{H}^+$, where $0 \leq x \leq n$. Species were predominantly observed at $m/z = M + 1$, where M is the molecular mass of the species. Hydrates, $A \cdot (\text{H}_2\text{O}) \cdot \text{H}^+$, were also observed for 2-formylcinnamaldehyde and phthalic anhydride.

Real-time aerosol mass spectra were obtained using an Aerodyne high-resolution time-of-flight aerosol mass spectrometer (HR-TOF-AMS) (DeCarlo et al., 2006). These data were also used to calculate the density of SOA by comparing the particle mass distribution obtained using the particle time-of-flight mode and the volume distribution obtained by the DMA in nucleation (seed-free) experiments (Bahreini et al., 2005).

5.4 Results

5.4.1 Concentrations of NO and NO₂

Figure 5.2 shows mixing ratios of NO and NO₂ in a typical high-NO_x experiment (6/16). Following the onset of irradiation, photolysis of HONO produces OH and NO. The level of NO remained above 400 ppb, and no ozone formation was observed. Also, owing to the high NO levels, the reaction of RO₂ radicals (produced in the OH oxidation) with NO likely dominated over that with HO₂ or RO₂ radicals.

Following the addition of OH to the aromatic ring, the aromatic-cyclohexadienyl radical can react with NO₂ to form nitronaphthalenes or with O₂ to form peroxy radicals (Atkinson et al., 1987; Nishino et al., 2008). The relative rates of these reactions depend on the concentration of NO₂, which remained between 50 and 100 ppb in all high-NO_x experiments, as measured by the GC/NO₂-PAN analyzer. This level is typical of urban polluted conditions, and suggests that the branching ratios in these experiments are relevant for regions where PAHs are commonly emitted. Nishino et al. (2008) reports that the reaction rates of OH-naphthalene adduct with NO₂ and O₂ are equal at [NO₂] \approx 60 ppb.

In the low-NO_x experiments, NO and NO₂ concentrations were below limits of detection (2 ppb). Ozone was formed at a rate of 2.5 ppb h⁻¹, likely due to reactions of NO_y contaminants on the chamber walls. Based on the low reaction rate constants of aromatic compounds with O₃, such reactions are not expected to be significant.

5.4.2 Gas-phase composition

The gas-phase photooxidation products of naphthalene have been identified in previous studies (Sasaki et al., 1997; Bunce et al., 1997; Wang et al., 2007; Nishino et al., 2009). Oxidation products identified in the current work by PTR-MS are consistent with those previously observed. Gas-phase mass spectra measured by PTR-MS during photooxidation of naphthalene under high- and low- NO_x and the proposed structures for the ions observed are shown in Figs. 5.3 and 5.4, respectively.

5.4.3 Aerosol formation

Figure 5.2 shows the mixing ratio of naphthalene and the mass concentration of SOA formed in the experiment on 6/16. Under high- NO_x conditions, owing to the efficient photolysis of HONO, the average OH concentrations are on the order of $1.5 \times 10^7 \text{ molec cm}^{-3}$, as estimated from the parent hydrocarbon decay. After 100 min of irradiation, HONO was depleted and, for naphthalene, further SOA formation was insignificant. Due to the relatively slow reaction rate of naphthalene with OH, only 85% of the initial naphthalene had been consumed before HONO was depleted. In one high- NO_x experiment with an initial naphthalene concentration of 17 ppb (6/20), 4 ppb remained after HONO was depleted. More HONO was added to consume the remaining naphthalene, resulting in further aerosol formation. For the other PAHs, less than 7% of the initial concentration remained unreacted. Under low- NO_x , a continuous supply of OH radicals was generated from the slow photolysis of H_2O_2 , and the parent hydrocarbon concentration was below detection limits at the end of the experiment. The average OH concentrations for these experiments were on the order of $3 \times 10^6 \text{ molec cm}^{-3}$.

The SOA mass concentrations and yields for all experiments are summarized in Table 5.1. To calculate the mass concentration of SOA, the volume concentration measured by the DMA was multiplied by its respective SOA density, obtained in separate nucleation experiments. Values for the densities are summarized in Table 5.2.

5.5 Aerosol Formation

5.5.1 Relative rates of oxidation steps

Figure 5.5 shows the time-dependent growth curves, mass concentration of SOA formed, ΔM_o , as a function of mass of hydrocarbon reacted, ΔHC , for all experiments. For naphthalene under both high- and low- NO_x conditions, the growth curves overlap; the lack of a vertical portion indicates that SOA formation likely results either from first-generation products, or from higher generation products that are formed rapidly (Ng et al., 2006; Chan et al., 2007). In the high- NO_x experiment in which a second HONO addition was conducted (6/20), SOA growth from the second injection of HONO was identical to that in another experiment with a higher initial hydrocarbon concentration. These observations suggest that the first oxidation step is rate-limiting, and the trend in aerosol growth for naphthalene can be represented by a single growth curve.

On the contrary, the growth curves for methylsubstituted naphthalenes display a vertical portion (hook) at higher ΔHC . In photooxidation of 1-MN and 2-MN under both high- and low- NO_x , and that of 1,2-DMN under high- NO_x , delayed aerosol growth was observed after a large fraction (>90%) of the parent PAH had been consumed. In addition, the degree of divergence for different growth curves is greater for 1,2-DMN, which has a larger number of methyl groups. While one cannot rule out the possibility of forming low-volatility compounds from photolysis of aromatic carbonyls and hydroperoxides, the delay in aerosol growth relative to the first oxidation step can also be explained by the relative rates of reaction. Figure 5.6 shows the oxidation mechanisms for naphthalene and 1-methylnaphthalene that lead to the major dicarbonyl product. As the aromatic ring becomes more substituted, the reaction rate of OH with the parent PAH increases (Phousongphouang and Arey, 2002). Further reaction of the dicarbonyl can occur by OH addition to the olefinic double bond, or by abstraction of aldehydic hydrogen atom. OH addition to the olefinic double bond is likely unaffected by substitution of methyl groups, and H-abstraction is slower for the methyl-substituted dicarbonyl product because of one fewer aldehyde group. As a result, the relative rate of the second step is slower for methyl-substituted naphthalenes, resulting in divergence of growth curves and

delayed SOA growth relative to the oxidation of the parent PAH. Since further oxidation of gas-phase intermediates will likely lead to even lower volatility products and more SOA formation, the observed yields measured in these experiments represent a lower limit for PAH oxidation in the atmosphere.

5.5.2 NO_x dependence of SOA growth

In this study, the SOA yields under high- and low-NO_x conditions are 25–45% and 55–75%, respectively, at a total organic aerosol loading, M_o , of $15\text{ }\mu\text{g m}^{-3}$. This is consistent with previous studies that have shown that SOA formation is less efficient under high-NO_x conditions (Kroll et al., 2006; Presto et al., 2005; Ng et al., 2007b), owing to formation of alkoxy radicals, followed by their decomposition. Large hydrocarbons, such as sesquiterpenes and long-chain alkanes, are exceptions to this behavior since isomerization of alkoxy radicals is more favorable (Ng et al., 2007a; Lim and Ziemann, 2005). Although the PAHs studied here also have relatively high MW, isomerization is not possible owing to the structure of the aromatic ring. As a result, fragmentation dominates under high-NO_x conditions, leading to compounds that are more volatile.

The higher volatility of high-NO_x SOA is evidenced by the dependence of SOA yields on M_o . Under high-NO_x, aerosol growth was not observed until $20\text{ }\mu\text{g m}^{-3}$ of the parent hydrocarbon had been reacted, indicating that gas-phase oxidation products are relatively volatile. Also, with the exception of 1,2-DMN, the final SOA yields increase with increasing M_o . This is characteristic of semivolatile partitioning, in which higher organic aerosol loading induces more partitioning into the aerosol phase. Under low-NO_x, aerosol growth was observed almost immediately, as products have a much lower saturation concentration. The SOA yields are more or less constant, suggesting the SOA formed under low-NO_x conditions is essentially nonvolatile in the range of M_o studied here.

The gas-phase PTR mass spectra obtained under high- and low-NO_x photooxidation of naphthalene are shown in Fig. 5.3. These spectra are taken at the same fraction of naphthalene reacted, and thus the extents of reaction are similar. Figure 5.4 summarizes the proposed compounds for the major ion peaks based on previous gas-phase mechanistic studies (Bunce et al., 1997; Sasaki et al.,

1997; Wang et al., 2007). Under high- NO_x , 2-formylcinnamaldehyde, phthalaldehyde, and phthalic anhydride represent the largest peaks in the mass spectrum. We refer to these compounds as “ring-opening” products. Formation of these ring-opening compounds is consistent with the formation of alkoxy radicals via $\text{RO}_2 + \text{NO}$ followed by decomposition of the alkoxy radicals. In a subsequent study, we will also show that phthalic acid, the hydrated form of phthalic anhydride, is the major product identified in the aerosol phase.

Under low- NO_x conditions, these ring-opening products are formed in the absence of NO, as $\text{RO}_2 + \text{RO}_2$ can also form alkoxy radicals, but the relative abundance is smaller than under high- NO_x conditions. Reaction of RO_2 with HO_2 radicals produces hydroperoxides, but owing to the lack of structural information from the PTR-MS, one cannot distinguish between the protonated hydroperoxide ($\text{C}_{10}\text{H}_{10}\text{O}_3 \cdot \text{H}^+$) and the water cluster of protonated 2-formylcinnamaldehyde ($\text{C}_{10}\text{H}_8\text{O}_2 \cdot \text{H}_2\text{O} \cdot \text{H}^+$). However, the relative abundance of other “ring-retaining” products, such as epoxides, naphthols, and quinones, is greater, likely because formation of the alkoxy radical is no longer dominant. Since these compounds and their oxidation products likely have a higher MW than ring-opening products, their volatilities are lower, resulting in the overall low volatility of SOA formed and essentially constant yields under low- NO_x conditions. It is also possible that the relatively lower concentrations of ring-opening products under low- NO_x are a result of longer UV exposure time. The OH concentrations are a factor of 5 lower under low- NO_x conditions. A longer irradiation time is needed to achieve the same fraction of naphthalene reacted, resulting in greater loss of 2-formylcinnamaldehyde by photolysis (Nishino et al., 2009).

5.5.3 Aerosol formation and yields

A widely-used semi-empirical model for SOA formation is based on the gas-particle equilibrium partitioning of semivolatile products (Odum et al., 1996, 1997), in which the SOA yield, Y , of a particular VOC, defined as the ratio of mass of SOA formed, ΔM_o , to the mass of hydrocarbon reacted, ΔHC , is given by

$$Y = \frac{\Delta M_o}{\Delta HC} = M_o \sum_{i=1}^n \frac{\alpha_i K_{p,i}}{1 + K_{p,i} M_o} \quad (5.1)$$

where α_i is the mass-based stoichiometric coefficient of semivolatile product i , $K_{p,i}$ is its gas-particle partitioning equilibrium constant, and M_o is the total mass concentration of the absorbing (aerosol) medium. In this study, since no organic aerosol seed was used, the total organic mass is equal to the mass of SOA formed ($M_o = \Delta M_o$). The final SOA yields for all experiments have been fitted to Eq. (5.1) for naphthalene, 1-MN and 2-MN photooxidation under high-NO_x conditions, shown in Fig. 5.7. For naphthalene, a two-product model was used; for 1-MN and 2-MN, one product is sufficient to describe the experimental data. For 1,2-DMN under high-NO_x, and all other PAHs under low NO_x, the SOA yields are constant. The fitting parameters are summarized in Table 5.3. The SOA yields for naphthalene and alkylnaphthalenes quantified in this study are on the order of 25–45% under high-NO_x conditions, which are about three times those for light aromatics under similar photooxidation conditions (Ng et al., 2007b).

5.6 Estimation of SOA Production from Light Aromatics, PAH, and Long-Chain n -Alkanes

Using the compounds studied here as surrogates for PAHs, we estimate the contribution of PAH photooxidation to urban SOA formation from different anthropogenic sources.

5.6.1 Diesel exhaust

Diesel exhaust is an important source of POA in the urban atmosphere (Schauer et al., 1996). As noted above, diesel exhaust, upon photooxidation, is also an SOA source (Robinson et al., 2007). The gas-phase component of diesel emissions consists primarily of light aromatics, PAHs, and long-chain n -alkanes (Schauer et al., 1999a). For compound i emitted in the gas phase, the amount of SOA formed from photooxidation of that compound, $\Delta M_{o,i}$, expressed in units of $\mu\text{g km}^{-1}$, over a time Δt , can be estimated by

$$\Delta M_{o,i} = [HC_i](1 - e^{-k_{\text{OH},i}[\text{OH}]\Delta t}) \times Y_i \quad (5.2)$$

where HC_i is the amount of gas-phase emission of compound i in $\mu\text{g km}^{-1}$, $k_{\text{OH},i}$ is its reaction rate constant with OH radicals, $[\text{OH}]$ is the concentration of OH radicals (taken to be $2 \times 10^6 \text{ molec cm}^{-3}$) and Y_i is its SOA yield. To obtain a specific value of Y_i , we assume a total organic aerosol loading of $15 \mu\text{g m}^{-3}$. Emissions of each compound (and hence the amount of SOA formed), measured in μg per km driven, are taken from Schauer et al. (1999a). OH reaction rate constants are taken from literature where available (Atkinson and Arey, 2003; Phoussongphouang and Arey, 2002), or estimated from structure activity relationships (Kwok and Atkinson, 1995) or extrapolated from similar compounds. The high- NO_x SOA yields measured here are used in this analysis. For purpose of comparison, we use the SOA yields for benzene, toluene, and *m*-xylene measured under similar photooxidation conditions (OH precursor, concentrations of NO_x and light intensity) (Ng et al., 2007b). SOA yields for *n*-alkanes were estimated based on modeling of gas-phase radical chemistry and gas-particle partitioning (Lim and Ziemann, 2005; Jordan et al., 2008).

Table 5.4 summarizes the contribution of each VOC identified to the total SOA formed from gas-phase photooxidation of these three classes of compounds. Although the gas-phase emissions are dominated by light aromatics, these compounds are estimated to account for only 14% of the SOA formed in the first 3 h of photooxidation. This estimate is consistent with laboratory results of photooxidation of diesel exhaust (Robinson et al., 2007), in which the “known” gas-phase precursors, consisting primarily of single-ring aromatics, account for at most 15% of the SOA formed. In addition to their relatively low SOA yields, the rate of oxidation of these compounds is slow, and hence only a small fraction is reacted over 3 h. On the contrary, although PAH emissions are a factor of 4 lower than those of light aromatics, their relatively fast reaction with OH radicals and high SOA yields lead to significant SOA production in the first 3 h, accounting for 4 times the amount formed from light aromatics. The contribution of PAH to SOA is still significant after 12 h of oxidation, at which point the SOA from PAH is about twice that from light aromatics.

To estimate the SOA production from diesel exhaust over longer timescales ($>12 \text{ h}$), we assume that the reaction time is sufficiently long that all of the hydrocarbon has been consumed by reaction with OH radicals (ignoring nighttime chemistry and deposition of gas-phase hydrocarbons). This

also allows for the air mass to be transported away from the sources, where the NO_x levels are lower and aromatic compounds are expected to produce SOA at higher mass yields (Henze et al., 2008; Ng et al., 2007b). To account for the difference in SOA formation from light aromatics between high- and low- NO_x pathways, we use the branching ratios calculated by Henze et al. (2008) for benzene, toluene, and *m*-xylene. Because naphthalene has a similar OH rate as *m*-xylene, we use the same branching ratio for naphthalene. For all other PAHs, we assume they all react under high- NO_x as a conservative estimate. For *n*-alkanes, since their low- NO_x yields are not known, they are not included in this part of the analysis. We caution readers that this is a zeroth order to compare SOA formation of light aromatics and PAHs over longer timescales. Multi-generation oxidation chemistry and aerosol aging will play an as yet undetermined role beyond the timescale over which these SOA yields were measured. Nonetheless, over very long timescales, the contribution of PAHs to overall SOA production is about half that of light aromatics (see Table 5.4).

Another important class of primary compounds is *n*-alkanes, which have been shown to have significant aerosol yields under high- NO_x conditions if the number of carbons is greater than 8 (Lim and Ziemann, 2005). In this calculation, SOA production from long-chain *n*-alkanes ranging from C_{12} to C_{20} is estimated to be higher than from light aromatics by a factor of 1.5 for the first 3 h. Only a small fraction of the compounds present in diesel emissions are speciated in Schauer et al. (1999a), but considering only these three classes of compounds, PAHs are estimated to account for up to 54% of the SOA formed in the first 12 h of diesel exhaust photooxidation, representing a potentially large source of atmospheric SOA.

5.6.2 Wood burning

Wood burning has also been shown to produce a significant amount of SOA that cannot be accounted for by known volatile precursors (Grieshop et al., 2009b). Gas-phase emissions of aromatic compounds from fireplace wood burning are detailed in Schauer et al. (2001), in which 90% of the emissions (by mass) were identified. The gas-phase composition of wood combustion emissions depends on temperature, type of fuel, and method of burning (open vs. fireplace), and quantifying

SOA from such sources can be difficult. Nonetheless, we repeat the previous analysis, and Table 5.5 summarizes the estimated SOA production from light aromatics and PAHs from fireplace burning of pine wood. Again, despite their relatively low emissions, the high SOA yields and rapid rate of oxidation of PAHs result in higher SOA formation over shorter timescales. The amount of SOA from PAHs is estimated to be more than 4 times that from light aromatics after 12 h of oxidation, suggesting a potentially large source of SOA from oxidation of wood burning emissions. Assuming the SOA yields do not change, PAHs contribute a comparable amount of SOA to light aromatics over very long timescales.

5.6.3 Other anthropogenic sources

For gasoline exhaust, the emissions of PAHs relative to light aromatics are low such that their contribution to SOA formation is likely insignificant (Schauer et al., 2002a). For other sources, such as meat and seed oil cooking, the emissions of light aromatics and PAHs are insignificant (Schauer et al., 1999b, 2002b). One class of compounds not addressed in this analysis is *n*-C₁₀-C₁₄ aldehydes, which are emitted in significant quantities from each of the sources considered here. To the authors' knowledge, SOA yields for these compounds have not been quantified and could potentially contribute to urban SOA formation.

We stress that the analysis presented here constitutes a first-order estimate of SOA production from PAHs. The calculations are based on emissions measured from single sources, rather than on overall emissions inventories. Future work will address the prediction of SOA formation based on atmospheric emissions inventories of gas-phase PAHs.

5.7 Implications

In this study, we have investigated the formation of SOA from gas-phase photooxidation of four 2-ring PAHs (naphthalene, 1-MN, 2-MN, and 1,2-DMN) under high- and low-NO_x conditions. Under high-NO_x and at organic aerosol loadings between 10 and 40 $\mu\text{g m}^{-3}$, SOA yields ranged from 0.19 to 0.30 for naphthalene, 0.19 to 0.39 for 1-MN, and 0.26 to 0.45 for 2-MN. The SOA products were

found to be semivolatile, consistent with the gas-phase products being dominated by ring-opening compounds. Under low-NO_x conditions, the SOA yield was found to be constant in the range of M_o studied, and was measured to be 0.73, 0.68, and 0.58, for naphthalene, 1-MN, and 2-MN, respectively. More ring-retaining products were found in the gas phase under low-NO_x conditions, contributing to the low volatility of the SOA and constant SOA yields. The SOA formed from high-NO_x photooxidation of 1,2-DMN was also nonvolatile under these loadings.

When applying these measured yields to a simple model of SOA formation from primary emissions, SOA from PAH oxidation is found to contribute a significant amount. Traditionally thought to be the most important anthropogenic SOA precursors, light aromatics are estimated to produce 3–5 times less SOA than from PAHs, based on the emissions inventories employed here. PAHs represent a potentially large source of urban SOA, accounting for up to 54% of SOA formed from diesel exhaust, and up to 80% of SOA from fireplace wood burning. Over longer timescales, PAHs are expected to contribute a nonnegligible amount of SOA. Long-chain *n*-alkanes are also expected to produce a smaller but significant fraction of SOA from diesel exhaust.

To properly account for SOA formation from anthropogenic sources, photooxidation of low-volatility precursors, such as PAH and *n*-alkanes, should be included in atmospheric SOA models, likely increasing the amount of predicted anthropogenic SOA significantly. Other IVOCs, such as aliphatic aldehydes and large olefins, could also be an important source of SOA, but further study is required to evaluate their potential to form SOA. In a forthcoming study, we will examine the mechanism of PAH oxidation and the composition of the SOA generated from the experiments reported here to assess the atmospheric relevance of these results.

Acknowledgements

This research was funded by the Office of Science (BER), US Department of Energy Grant No. DE-FG02-05ER63983, US Environmental Protection Agency STAR Research Assistance Agreement No. RD-83374901 and US National Science Foundation grant ATM-0432377. This publication has not been formally reviewed by the EPA. The views expressed in this document are solely those of

the authors and EPA does not endorse any products mentioned in this publication. The authors would like to thank D. R. Fitz for use of the GC/NO₂-PAN analyzer, L. D. Yee for assistance with running experiments, and C. E. Jordan for helpful discussion.

Bibliography

- Arey, J., Atkinson, R., Zielinska, B., and Mcelroy, P. A.: Diurnal concentrations of volatile polycyclic aromatic-hydrocarbons and nitroarenes during a photochemical air-pollution episode in Glendora, California, *Environ. Sci. Technol.*, **23**, 321–327, 1989.
- Atkinson, R. and Arey, J.: Atmospheric degradation of volatile organic compounds, *Chem. Rev.*, **103**, 4605–4638, 2003.
- Atkinson, R., Arey, J., Zielinska, B., and Aschmann, S. M.: Kinetics and products of the gas-phase reactions of OH radicals and N₂O₅ with naphthalene and biphenyl, *Environ. Sci. Technol.*, **21**, 1014–1022, 1987.
- Bahreini, R., Keywood, M. D., Ng, N. L., Varutbangkul, V., Gao, S., Flagan, R. C., Seinfeld, J. H., Worsnop, D. R., and Jimenez, J. L.: Measurements of secondary organic aerosol from oxidation of cycloalkenes, terpenes, and *m*-xylene using an Aerodyne aerosol mass spectrometer, *Environ. Sci. Technol.*, **39**, 5674–5688, 2005.
- Bunce, N. J., Liu, L., Zhu, J., and Lane, D. A.: Reaction of naphthalene and its derivatives with hydroxyl radicals in the gas phase, *Environ. Sci. Technol.*, **31**, 2252–2259, 1997.
- Burkhardt, M. R., Maniga, N. I., Stedman, D. H., and Paur, R. J.: Gas-chromatographic method for measuring nitrogen-dioxide and peroxyacetyl nitrate in air without compressed gas-cylinders, *Anal. Chem.*, **60**, 816–819, 1988.
- Chan, A. W. H., Kroll, J. H., Ng, N. L., and Seinfeld, J. H.: Kinetic modeling of secondary organic aerosol formation: effects of particle- and gas-phase reactions of semivolatile products, *Atmos. Chem. Phys.*, **7**, 4135–4147, <http://www.atmos-chem-phys.net/7/4135/2007/>, 2007.

- Cocker, D. R., Flagan, R. C., and Seinfeld, J. H.: State-of-the-art chamber facility for studying atmospheric aerosol chemistry, *Environ. Sci. Technol.*, 35, 2594–2601, 2001.
- de Gouw, J. A., Middlebrook, A. M., Warneke, C., Goldan, P. D., Kuster, W. C., Roberts, J. M., Fehsenfeld, F. C., Worsnop, D. R., Canagaratna, M. R., Pszenny, A. A. P., Keene, W. C., Marchewka, M., Bertman, S. B., and Bates, T. S.: Budget of organic carbon in a polluted atmosphere: Results from the New England Air Quality Study in 2002, *J. Geophys. Res.-Atmos.*, 110, D16305, doi:10.1029/2004JD005623, 2005.
- DeCarlo, P. F., Kimmel, J. R., Trimborn, A., Northway, M. J., Jayne, J. T., Aiken, A. C., Gonin, M., Fuhrer, K., Horvath, T., Docherty, K. S., Worsnop, D. R., and Jimenez, J. L.: Field-deployable, high-resolution, time-of-flight aerosol mass spectrometer, *Anal. Chem.*, 78, 8281–8289, 2006.
- Docherty, K. S., Stone, E. A., Ulbrich, I. M., DeCarlo, P. F., Snyder, D. C., Schauer, J. J., Peltier, R. E., Weber, R. J., Murphy, S. M., Seinfeld, J. H., Grover, B. D., Eatough, D. J., and Jimenez, J. L.: Apportionment of primary and secondary organic aerosols in southern California during the 2005 Study of Organic Aerosols in Riverside (SOAR-1), *Environ. Sci. Technol.*, 42, 7655–7662, 2008.
- Donahue, N. M., Robinson, A. L., and Pandis, S. N.: Atmospheric organic particulate matter: From smoke to secondary organic aerosol, *Atmos. Environ.*, 43, 94–106, 2009.
- Goldstein, A. H. and Galbally, I. E.: Known and unexplored organic constituents in the earth’s atmosphere, *Environ. Sci. Technol.*, 41, 1514–1521, 2007.
- Grieshop, A. P., Donahue, N. M., and Robinson, A. L.: Laboratory investigation of photochemical oxidation of organic aerosol from wood fires 2: analysis of aerosol mass spectrometer data, *Atmos. Chem. Phys.*, 9, 2227–2240, <http://www.atmos-chem-phys.net/9/2227/2009/>, 2009a.
- Grieshop, A. P., Logue, J. M., Donahue, N. M., and Robinson, A. L.: Laboratory investigation of photochemical oxidation of organic aerosol from wood fires 1: measurement and simu-

- lation of organic aerosol evolution, *Atmos. Chem. Phys.*, 9, 1263–1277, <http://www.atmos-chem-phys.net/9/1263/2009/>, 2009b.
- Heald, C. L., Jacob, D. J., Park, R. J., Russell, L. M., Huebert, B. J., Seinfeld, J. H., Liao, H., and Weber, R. J.: A large organic aerosol source in the free troposphere missing from current models, *Geophys. Res. Lett.*, 32, L18809, doi:doi:10.1029/2005GL023831, 2005.
- Henze, D. K., Seinfeld, J. H., Ng, N. L., Kroll, J. H., Fu, T.-M., Jacob, D. J., and Heald, C. L.: Global modeling of secondary organic aerosol formation from aromatic hydrocarbons: high- vs. low-yield pathways, *Atmos. Chem. Phys.*, 8, 2405–2420, 2008.
- Jordan, C. E., Ziemann, P. J., Griffin, R. J., Lim, Y. B., Atkinson, R., and Arey, J.: Modeling SOA formation from OH reactions with C₈–C₁₇ *n*-alkanes, *Atmos. Environ.*, 42, 8015–8026, 2008.
- Keywood, M. D., Varutbangkul, V., Bahreini, R., Flagan, R. C., and Seinfeld, J. H.: Secondary organic aerosol formation from the ozonolysis of cycloalkenes and related compounds, *Environ. Sci. Technol.*, 38, 4157–4164, 2004.
- Kroll, J. H., Ng, N. L., Murphy, S. M., Flagan, R. C., and Seinfeld, J. H.: Secondary organic aerosol formation from isoprene photooxidation, *Environ. Sci. Technol.*, 40, 1869–1877, 2006.
- Kwok, E. S. C. and Atkinson, R.: Estimation of hydroxyl radical reaction-rate constants for gas-phase organic-compounds using a structure-reactivity relationship – an update, *Atmos. Environ.*, 29, 1685–1695, 1995.
- Lim, Y. B. and Ziemann, P. J.: Products and mechanism of secondary organic aerosol formation from reactions of *n*-alkanes with OH radicals in the presence of NO_x, *Environ. Sci. Technol.*, 39, 9229–9236, 2005.
- Mihele, C. M., Wiebe, H. A., and Lane, D. A.: Particle formation and gas/particle partition measurements of the products of the naphthalene-OH radical reaction in a smog chamber, *Polycycl. Aromat. Comp.*, 22, 729–736, 2002.

- Ng, N. L., Kroll, J. H., Keywood, M. D., Bahreini, R., Varutbangkul, V., Flagan, R. C., Seinfeld, J. H., Lee, A., and Goldstein, A. H.: Contribution of first- versus second-generation products to secondary organic aerosols formed in the oxidation of biogenic hydrocarbons, *Environ. Sci. Technol.*, 40, 2283–2297, 2006.
- Ng, N. L., Chhabra, P. S., Chan, A. W. H., Surratt, J. D., Kroll, J. H., Kwan, A. J., McCabe, D. C., Wennberg, P. O., Sorooshian, A., Murphy, S. M., Dalleska, N. F., Flagan, R. C., and Seinfeld, J. H.: Effect of NO_x level on secondary organic aerosol (SOA) formation from the photooxidation of terpenes, *Atmos. Chem. Phys.*, 7, 5159–5174, <http://www.atmos-chem-phys.net/7/5159/2007/>, 2007a.
- Ng, N. L., Kroll, J. H., Chan, A. W. H., Chhabra, P. S., Flagan, R. C., and Seinfeld, J. H.: Secondary organic aerosol formation from *m*-xylene, toluene, and benzene, *Atmos. Chem. Phys.*, 7, 3909–3922, <http://www.atmos-chem-phys.net/7/3909/2007/>, 2007b.
- Nishino, N., Atkinson, R., and Arey, J.: Formation of nitro products from the gas-phase OH radical-initiated reactions of toluene, naphthalene, and biphenyl: effect of NO_2 concentration, *Environ. Sci. Technol.*, 42, 9203–9209, 2008.
- Nishino, N., Arey, J., and Atkinson, R.: Formation and reactions of 2-Formylcinnamaldehyde in the OH radical-initiated reaction of naphthalene, *Environ. Sci. Technol.*, 43, 1349–1353, 2009.
- Odum, J. R., Hoffmann, T., Bowman, F., Collins, D., Flagan, R. C., and Seinfeld, J. H.: Gas/particle partitioning and secondary organic aerosol yields, *Environ. Sci. Technol.*, 30, 2580–2585, 1996.
- Odum, J. R., Jungkamp, T. P. W., Griffin, R. J., Flagan, R. C., and Seinfeld, J. H.: The atmospheric aerosol-forming potential of whole gasoline vapor, *Science*, 276, 96–99, 1997.
- Phouongphouang, P. T. and Arey, J.: Rate constants for the gas-phase reactions of a series of alkylnaphthalenes with the OH radical, *Environ. Sci. Technol.*, 36, 1947–1952, 2002.
- Presto, A. A., Hartz, K. E. H., and Donahue, N. M.: Secondary organic aerosol production from terpene ozonolysis. 2. Effect of NO_x concentration, *Environ. Sci. Technol.*, 39, 7046–7054, 2005.

- Robinson, A. L., Donahue, N. M., Shrivastava, M. K., Weitkamp, E. A., Sage, A. M., Grieshop, A. P., Lane, T. E., Pierce, J. R., and Pandis, S. N.: Rethinking organic aerosols: Semivolatile emissions and photochemical aging, *Science*, 315, 1259–1262, 2007.
- Sage, A. M., Weitkamp, E. A., Robinson, A. L., and Donahue, N. M.: Evolving mass spectra of the oxidized component of organic aerosol: results from aerosol mass spectrometer analyses of aged diesel emissions, *Atmos. Chem. Phys.*, 8, 1139–1152, <http://www.atmos-chem-phys.net/8/1139/2008/>, 2008.
- Sasaki, J., Aschmann, S. M., Kwok, E. S. C., Atkinson, R., and Arey, J.: Products of the gas-phase OH and NO₃ radical-initiated reactions of naphthalene, *Environ. Sci. Technol.*, 31, 3173–3179, 1997.
- Schauer, J. J., Rogge, W. F., Hildemann, L. M., Mazurek, M. A., and Cass, G. R.: Source apportionment of airborne particulate matter using organic compounds as tracers, *Atmos. Environ.*, 30, 3837–3855, 1996.
- Schauer, J. J., Kleeman, M. J., Cass, G. R., and Simoneit, B. R. T.: Measurement of emissions from air pollution sources. 2. C₁ through C₃₀ organic compounds from medium duty diesel trucks, *Environ. Sci. Technol.*, 33, 1578–1587, 1999a.
- Schauer, J. J., Kleeman, M. J., Cass, G. R., and Simoneit, B. R. T.: Measurement of emissions from air pollution sources. 1. C₁ through C₂₉ organic compounds from meat charbroiling, *Environ. Sci. Technol.*, 33, 1566–1577, 1999b.
- Schauer, J. J., Kleeman, M. J., Cass, G. R., and Simoneit, B. R. T.: Measurement of emissions from air pollution sources. 3. C₁-C₂₉ organic compounds from fireplace combustion of wood, *Environ. Sci. Technol.*, 35, 1716–1728, 2001.
- Schauer, J. J., Kleeman, M. J., Cass, G. R., and Simoneit, B. R. T.: Measurement of emissions from air pollution sources. 5. C₁-C₃₂ organic compounds from gasoline-powered motor vehicles, *Environ. Sci. Technol.*, 36, 1169–1180, 2002a.

- Schauer, J. J., Kleeman, M. J., Cass, G. R., and Simoneit, B. R. T.: Measurement of emissions from air pollution sources. 4. C₁-C₂₇ organic compounds from cooking with seed oils, *Environ. Sci. Technol.*, 36, 567–575, 2002b.
- Seinfeld, J. H. and Pankow, J. F.: Organic atmospheric particulate material, *Annu. Rev. Phys. Chem.*, 54, 121–140, 2003.
- Volkamer, R., Jimenez, J. L., San Martini, F., Dzepina, K., Zhang, Q., Salcedo, D., Molina, L. T., Worsnop, D. R., and Molina, M. J.: Secondary organic aerosol formation from anthropogenic air pollution: Rapid and higher than expected, *Geophys. Res. Lett.*, 33, L17811, doi: 10.1029/2006GL026899, 2006.
- Wang, L., Atkinson, R., and Arey, J.: Dicarbonyl products of the OH radical-initiated reactions of naphthalene and the C₁- and C₂-alkylnaphthalenes, *Environ. Sci. Technol.*, 41, 2803–2810, 2007.
- Weitkamp, E. A., Sage, A. M., Pierce, J. R., Donahue, N. M., and Robinson, A. L.: Organic aerosol formation from photochemical oxidation of diesel exhaust in a smog chamber, *Environ. Sci. Technol.*, 41, 6969–6975, 2007.
- Zhang, Q., Jimenez, J. L., Canagaratna, M. R., Allan, J. D., Coe, H., Ulbrich, I., Alfarra, M. R., Takami, A., Middlebrook, A. M., Sun, Y. L., Dzepina, K., Dunlea, E., Docherty, K., DeCarlo, P. F., Salcedo, D., Onasch, T., Jayne, J. T., Miyoshi, T., Shimojo, A., Hatakeyama, S., Takegawa, N., Kondo, Y., Schneider, J., Drewnick, F., Borrmann, S., Weimer, S., Demerjian, K., Williams, P., Bower, K., Bahreini, R., Cottrell, L., Griffin, R. J., Rautiainen, J., Sun, J. Y., Zhang, Y. M., and Worsnop, D. R.: Ubiquity and dominance of oxygenated species in organic aerosols in anthropogenically-influenced Northern Hemisphere midlatitudes, *Geophys. Res. Lett.*, 34, doi: 10.1029/2007GL029979, 2007.

Table 5.1: Experimental conditions and results.

Date (2008)	Compound	$[HC]_0$, ppb	$[NO]_0$, ppb	$[NO_2]_0$, ppb	V_0^a , $\mu\text{m}^3 \text{cm}^{-3}$	ΔHC , $\mu\text{g m}^{-3}$	ΔM_o , $\mu\text{g m}^{-3}$	Yield
6/12	naphthalene	7.5	^b	^c	12.9	39.5 \pm 2.5	29.0 \pm 2.6	0.73 \pm 0.11
6/14	naphthalene	4.4	^b	^c	14.2	22.8 \pm 2.1	17.0 \pm 1.7	0.74 \pm 0.15
6/17	naphthalene	6.0	^b	^c	13.9	31.2 \pm 2.1	22.9 \pm 2.2	0.73 \pm 0.12
6/19	naphthalene	2.7	^b	^c	14.5	14.4 \pm 2.0	10.2 \pm 1.5	0.71 \pm 0.21
6/13	naphthalene	12.1	411	83	14.5	58.6 \pm 2.0	10.9 \pm 1.5	0.19 \pm 0.03
6/16	naphthalene	21.2	304	73	13.6	92.7 \pm 2.1	27.7 \pm 3.0	0.30 \pm 0.04
6/18	naphthalene	9.5	351	73	15.2	39.6 \pm 2.0	8.0 \pm 1.2	0.20 \pm 0.04
6/20	naphthalene	17.0	411	66	15.4	65.0 \pm 1.6	13.6 \pm 1.7	0.21 \pm 0.03
						83.9 \pm 2.1 ^f	22.8 \pm 2.2 ^f	0.27 \pm 0.03 ^f
7/16	2-MN	7.5	^b	^c	13.2	58.6 \pm 3.4	35.0 \pm 3.1	0.60 \pm 0.09
7/22	2-MN	4.4	^b	^c	14.6	31.5 \pm 3.0	18.6 \pm 1.8	0.59 \pm 0.11
7/24	2-MN	6.0	^b	^c	12.9	22.5 \pm 3.3	13.1 \pm 1.5	0.58 \pm 0.15
7/27	2-MN	2.7	^b	^c	13.3	43.3 \pm 3.0	24.6 \pm 2.1	0.57 \pm 0.09
7/21	2-MN	21.2	398	52	14.1	28.0 \pm 3.4	7.4 \pm 0.9	0.26 \pm 0.06
7/23	2-MN	9.5	376	51	14.2	47.3 \pm 3.5	18.8 \pm 1.9	0.40 \pm 0.07
7/25	2-MN	17.0	^d	55	12.9	70.7 \pm 3.4	31.6 \pm 2.6	0.45 \pm 0.06
7/29	2-MN	7.5	^d	61	13.4	60.0 \pm 3.6	24.3 \pm 2.2	0.40 \pm 0.06
8/2	1-MN	7.3	^b	^c	11.4	42.9 \pm 3.9	30.5 \pm 2.5	0.71 \pm 0.12
8/5	1-MN	9.9	^b	^c	13.1	57.4 \pm 3.4	37.6 \pm 3.0	0.66 \pm 0.09
8/8	1-MN	2.8	^b	^c	13.8	15.7 \pm 3.4	10.7 \pm 1.1	0.68 \pm 0.22
8/17	1-MN	5.9	^b	^c	14.0	35.2 \pm 3.6	24.0 \pm 2.4	0.68 \pm 0.14
8/4	1-MN	10.5	^d	77	13.6	51.8 \pm 3.0	16.5 \pm 1.6	0.32 \pm 0.05
8/7	1-MN	5.3	333	55	13.5	30.1 \pm 3.4	5.6 \pm 0.9	0.19 \pm 0.05
8/9	1-MN	14.6	388	62	14.7	79.6 \pm 3.6	30.9 \pm 2.6	0.39 \pm 0.05
8/11	1-MN	16.8	401	56	14.6	91.0 \pm 3.6	34.9 \pm 3.1	0.38 \pm 0.05
9/10	1,2-DMN	34.8	392	51	14.7	215.7 \pm 6.8	66.9 \pm 5.3	0.31 \pm 0.03
9/12	1,2-DMN	12.3	397	60	14.9	76.8 \pm 4.4	23.1 \pm 2.3	0.30 \pm 0.05
9/14	1,2-DMN	4.1	377	55	14.2	25.4 \pm 3.3	7.8 \pm 1.4	0.31 \pm 0.10

^a V_o : volume concentration of ammonium sulfate seed;

^b below detection limit of 2 ppb;

^c NO_2 concentration was not measured by gas-chromatograph in these experiments due to H_2O_2 interference with NO_2 signal, but inferred to be <2 ppb from NO/NO_x analyzer;

^d NO concentration not measured, but expected to be similar to that of other high- NO_x experiments;

^e Nucleation experiments not shown; with the exception of seed concentration, conditions were similar to those of experiments shown here;

^f After second addition of HONO.

Table 5.2: Effective SOA densities (g cm^{-3}), obtained in nucleation experiments.

	high-NO _x	low-NO _x
naphthalene	1.48	1.55
1-MN	1.4	1.43
2-MN	1.35	1.3
1,2-DMN	^a	—

^a Not measured; assumed to be 1.4.

Table 5.3: SOA yield parameters.

	α_1	$K_1, \text{ m}^3 \mu\text{g}^{-1}$	α_2	$K_2, \text{ m}^3 \mu\text{g}^{-1}$	Yield at $M_o=15 \mu\text{g m}^{-3}$
<i>high-NO_x</i>					
naphthalene	0.21	0.59	1.07	0.0037	0.26
1-MN	0.50	0.11	—	—	0.33
2-MN	0.55	0.13	—	—	0.38
1,2-DMN	0.31	^a	—	—	0.31
<i>low-NO_x</i>					
naphthalene	0.73	^a	—	—	0.73
1-MN	0.68	^a	—	—	0.68
2-MN	0.58	^a	—	—	0.58

^a Constant yield.

Table 5.4: Estimated SOA production from gas-phase oxidation of diesel exhaust (Schauer et al., 1999a).

	$[HC_i]$, $\mu\text{g km}^{-1}$	k_{OH} , $\text{cm}^3 \text{ molec}^{-1} \text{ s}^{-1}$	Y (high- NO_x)	$\Delta t=3 \text{ h}$ $\Delta M_{o,i}$, $\mu\text{g km}^{-1}$	$\Delta t=12 \text{ h}$ $\Delta M_{o,i}$, $\mu\text{g km}^{-1}$	Y (low- NO_x)	$\Delta t=\infty$ $\Delta M_{o,i}$, $\mu\text{g km}^{-1}$
<i>light aromatics</i>							
benzene	2740	1.22×10^{-12a}	0.19 ^f	14	53	0.37 ^f	778
toluene	3980	5.63×10^{-12a}	0.10 ^f	47	158	0.3 ^f	700
ethylbenzene	470	7.00×10^{-12a}	0.10 ^g	7	22	0.3 ^g	83
xylene	2330	1.36×10^{-11a}	0.06 ^h	35	96	0.36 ^h	321
<i>o</i> -xylene	830	2.31×10^{-11a}	0.06 ^h	19	43	0.36 ^h	114
<i>n</i> -propylbenzene	100	1.43×10^{-11a}	0.10 ^g	3	7	0.3 ^g	18
<i>p</i> -ethyltoluene	520	1.18×10^{-11a}	0.10 ^g	12	34	0.3 ^g	92
<i>m</i> -ethyltoluene	210	1.86×10^{-11a}	0.10 ^g	7	17	0.3 ^g	37
1,3,5-TMB	260	5.67×10^{-11a}	0.06 ^h	11	15	0.36 ^h	36
1,2,4-TMB	880	3.25×10^{-11a}	0.06 ^h	27	49	0.36 ^h	121
<i>Total</i>				182	496		2300
<i>PAHs</i>							
naphthalene	617	2.30×10^{-11a}	0.26	62	136	0.73	234
2-methylnaphthalene	611	4.86×10^{-11b}	0.38	152	231	^k	231
1-methylnaphthalene	378	4.09×10^{-11b}	0.33	73	120	^k	120
C2-naphthalenes	542	6.00×10^{-11c}	0.31	122	167	^k	167
C3-naphthalenes	240	8.00×10^{-11d}	0.31	61	74	^k	74
C4-naphthalenes	97.3	8.00×10^{-11d}	0.31	25	30	^k	30
other PAHs	886.7	8.00×10^{-11d}	0.31	226	275	^k	275
<i>Total</i>				721	1033		1131
<i>n-alkanes</i>							
dodecane	503	1.32×10^{-11a}	0.02 ⁱ	2	5		
tridecane	477	1.51×10^{-11a}	0.03 ⁱ	4	10		
tetradecane	629	1.79×10^{-11a}	0.05 ⁱ	10	23		
pentadecane	398	2.07×10^{-11a}	0.08 ⁱ	11	25		
hexadecane	711	2.32×10^{-11a}	0.12 ^j	34	75		
heptadecane	614	2.85×10^{-11e}	0.20 ⁱ	55	110		
octadecane	601	3.51×10^{-11e}	0.30 ^j	96	172		
nonadecane	411	4.32×10^{-11e}	0.42 ^j	105	168		
eicosane	271.8	5.31×10^{-11e}	0.56 ^j	104	151		
<i>Total</i>				420	740		

^aAtkinson and Arey (2003);^bPhousongphouang and Arey (2002);^cAverage of all dimethylnaphthalenes in Phousongphouang and Arey (2002);^dExtrapolated from dimethylnaphthalenes, assumed to be same for all other PAHs;^eEstimated from structure-reactivity relationships (Kwok and Atkinson, 1995);^fNg et al. (2007b);^gAssumed to be the same as toluene;^hAssumed to be the same as *m*-xylene;ⁱEstimated from modeling of gas-phase chemistry and gas/particle partitioning (Jordan et al., 2008);^jExtrapolated from smaller *n*-alkanes;^kAssume all reacted under high- NO_x .

Table 5.5: Estimated SOA production from gas-phase oxidation of emissions from fireplace burning of pine wood (Schauer et al., 2001)

	$[HC_i]$, mg kg ⁻¹	k_{OH} , cm ³ molec ⁻¹ s ⁻¹	Y (high-NO _x)	$\Delta t = 12h$ $\Delta M_{o,i}$, mg kg ⁻¹	Y (low-NO _x)	$\Delta t = \infty$ $\Delta M_{o,i}$, mg kg ⁻¹
<i>light aromatics</i>						
benzene	383	1.22×10^{-12}	0.19	7.5	0.37	108.8
toluene	158	5.63×10^{-12}	0.10	6.3	0.3	27.8
ethylbenzene	22.9	7.00×10^{-12}	0.10	1.1	0.3	4.0
xylene	60	1.36×10^{-11}	0.06	2.5	0.36	8.3
<i>o</i> -xylene	18.1	2.31×10^{-11}	0.06	0.9	0.36	2.5
<i>Total</i>				18.2		151.4
<i>PAHs</i>						
naphthalene	227	2.30×10^{-11}	0.26	50.0	0.73	86.0
2-methylnaphthalene	15	4.86×10^{-11}	0.38	5.7	–	5.7
1-methylnaphthalene	10.6	4.09×10^{-11}	0.33	3.4	–	3.4
C2-naphthalenes	13.8	6.00×10^{-11}	0.31	4.3	–	4.3
other PAHs	63.7	8.00×10^{-11}	0.31	19.7	–	19.7
<i>Total</i>				80.9		119.0

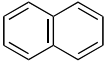
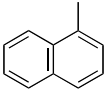
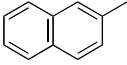
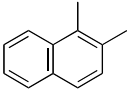
Compound	Structure	OH rate constant, $\text{cm}^3 \text{ molec}^{-1} \text{ s}^{-1}$
naphthalene		2.44×10^{-11}
1-methylnaphthalene (1-MN)		4.09×10^{-11}
2-methylnaphthalene (2-MN)		4.86×10^{-11}
1,2- dimethylnaphthalene (1,2-DMN)		5.96×10^{-11}

Figure 5.1: Structure of PAHs studied and OH rate constants (Phousongphouang and Arey, 2002).

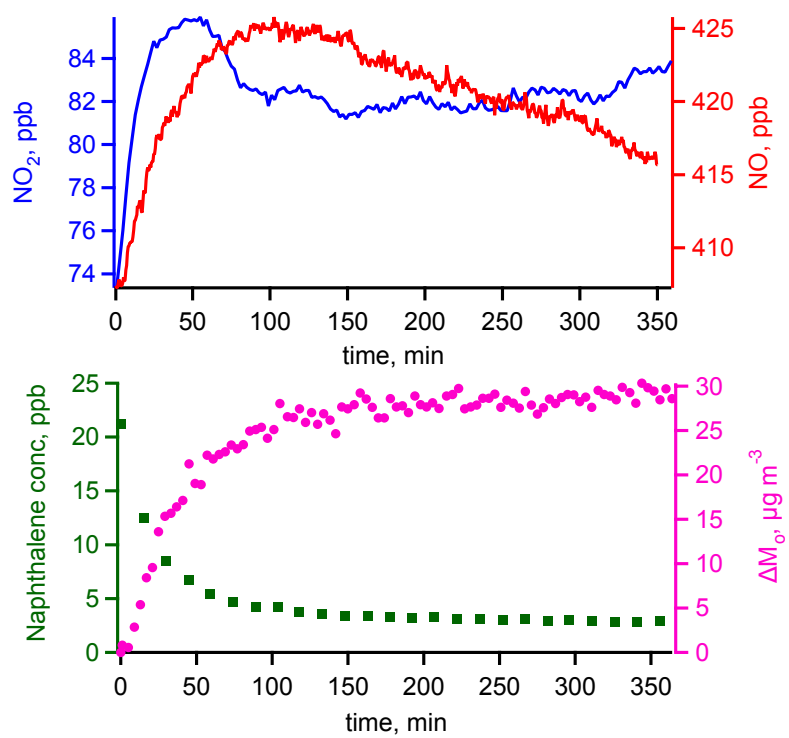


Figure 5.2: Reaction profile during a typical high- NO_x experiment. The mass concentration of SOA has been corrected for particle wall loss.

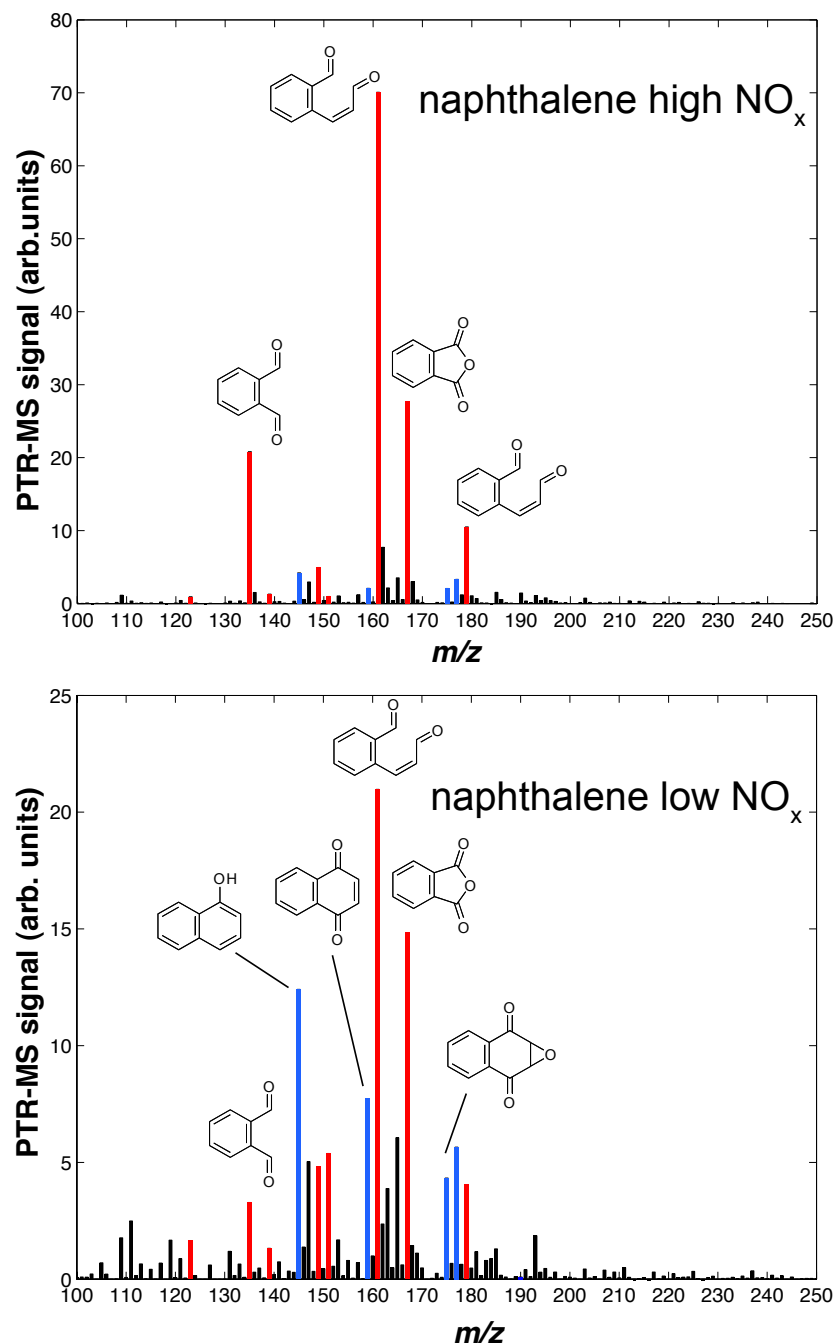
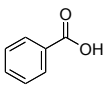
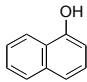
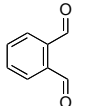
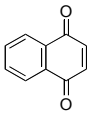
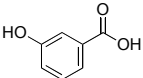
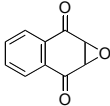
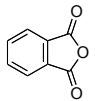
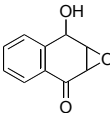
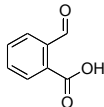
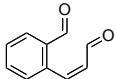
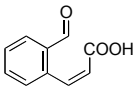


Figure 5.3: PTR-MS spectra under high- and low-NO_x conditions. The fractions of naphthalene reacted are 0.66 and 0.67, respectively. The red peaks indicate ions associated with ring-opening products, and the blue peaks indicate those associated with ring-retaining products. The proposed structures for these ion peaks are given in Fig. 5.4.

Name	Proposed Structure	PTR-MS <i>m/z</i> (+)	Name	Proposed Structure	PTR-MS <i>m/z</i> (+)
<u>Ring-opening products</u>			<u>Ring-retaining products</u>		
benzoic acid		123	naphthol		145
phthalaldehyde		135	1,4-naphthoquinone		159
hydroxybenzoic acid		139	2,3-epoxy-1,4-quinone		175
phthalic anhydride		149, 167	4-hydroxy-2,3-epoxy-carbonyl		177 ^a
formylbenzoic acid		151			
2-formyl-cinnamaldehyde		161, 179			
formylcinnamic acid		177 ^a			

^a 2 proposed isomers for *m/z* 177

Figure 5.4: Proposed compounds and structures for ion peaks observed by PTR-MS. The ring-opening gas-phase products are marked red and the gas-phase ring-retaining products are marked blue, to correspond to Fig. 5.3.

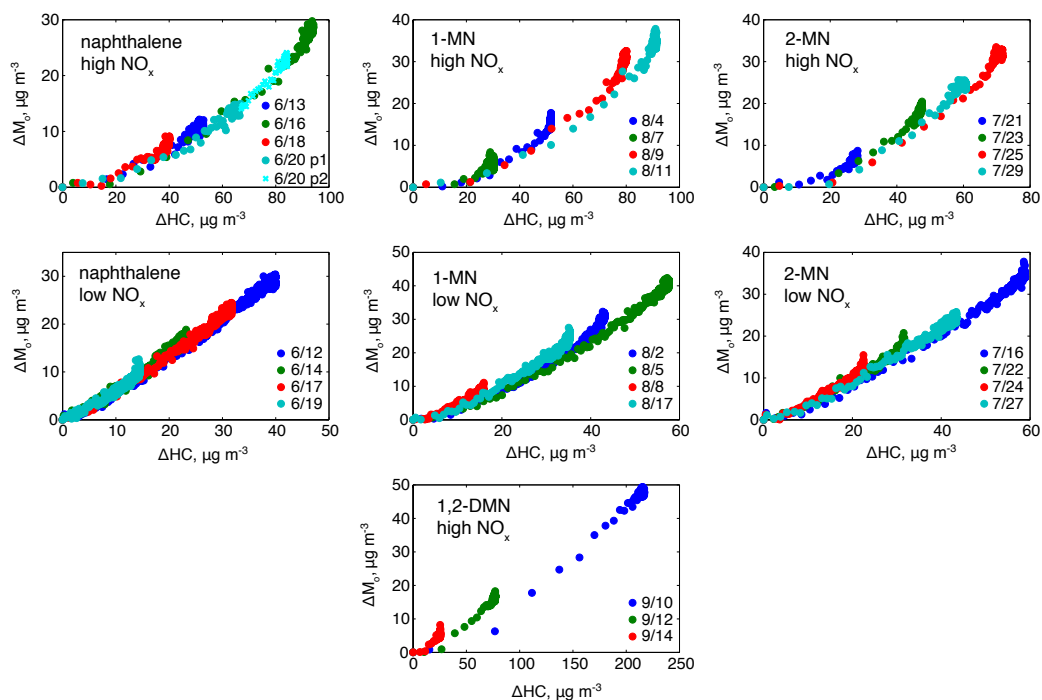


Figure 5.5: Time-dependent SOA growth curves for all experiments. In one naphthalene high- NO_x experiment (6/20), more HONO was added after the first injection was consumed. SOA growth before the second HONO addition is marked light blue and labelled “6/20 p1”, and the growth after the second addition is marked bright cyan and labelled “6/20 p2”.

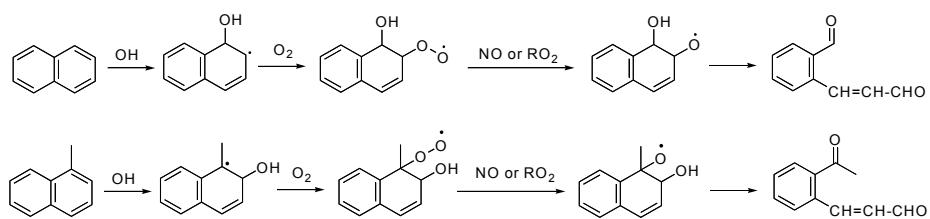


Figure 5.6: Simplified mechanisms for oxidation of naphthalene and 1-MN to form first-generation dicarbonyl fragmentation products (Wang et al., 2007).

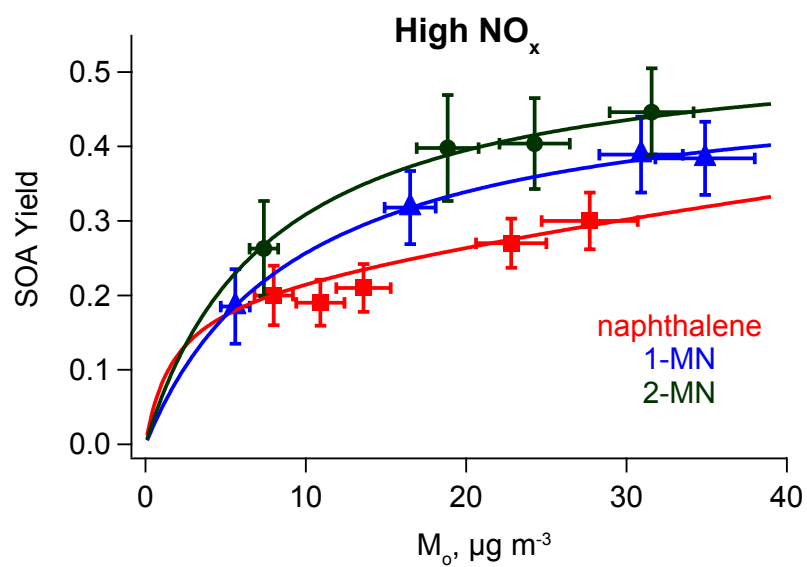


Figure 5.7: SOA yield as a function of organic loading for naphthalene, 1-MN, and 2-MN under high- NO_x conditions. The fitting parameters used are summarized in Table 5.3. Under low- NO_x conditions, the SOA yields are essentially constant.

Chapter 6

Reactive intermediates revealed in secondary organic aerosol formation from isoprene*

*Reproduced with permission from “Reactive Intermediates Revealed in Secondary Organic Aerosol Formation from Isoprene” by Jason D. Surratt, Arthur W. H. Chan, Nathan C. Eddingsaas, Man N. Chan, Christine L. Loza, Alan J. Kwan, Scott P. Hersey, Richard C. Flagan, Paul O. Wennberg and John H. Seinfeld, *Proceedings of the National Academy of Sciences of the United States of America*, 107, 6640–6645, 2010.. Copyright 2010 by the National Academy of Sciences.

6.1 Abstract

Isoprene is a significant source of atmospheric organic aerosol; however, the oxidation pathways that lead to secondary organic aerosol (SOA) have remained elusive. Here, we identify the role of two key reactive intermediates, epoxydiols of isoprene (IEPOX = β -IEPOX + δ -IEPOX) and methacryloylperoxynitrate (MPAN), that are formed during isoprene oxidation under low- and high-NO_x conditions, respectively. Isoprene low-NO_x SOA is enhanced in the presence of acidified sulfate seed aerosol (mass yield 28.6%) over that in the presence of neutral aerosol (mass yield 1.3%). Increased uptake of IEPOX by acid-catalyzed particle-phase reactions is shown to explain this enhancement. Under high-NO_x conditions, isoprene SOA formation occurs through oxidation of its second-generation product, MPAN. The similarity of the composition of SOA formed from the photooxidation of MPAN to that formed from isoprene and methacrolein (MACR) demonstrates the role of MPAN in the formation of isoprene high-NO_x SOA. Reactions of IEPOX and MPAN in the presence of anthropogenic pollutants (i.e., acidic aerosol produced from the oxidation of SO₂ and NO₂, respectively) could be a substantial source of “missing urban SOA” not included in current atmospheric models.

6.2 Introduction

Isoprene (2-methyl-1,3-butadiene, C₅H₈) is the most abundant non-methane hydrocarbon emitted into the Earth’s atmosphere, with emissions estimated to be 440–660 TgC yr^{−1} (Guenther et al., 2006). The atmospheric hydroxyl (OH) radical-initiated oxidation of isoprene, so-called photooxidation, plays a key role in establishing the balance of hydrogen oxide (HO_x = OH + HO₂) radicals in vegetated areas (Lelieveld et al., 2008; Paulot et al., 2009b) and influences urban ozone formation in populated areas blanketed with biogenic emissions (Chameides et al., 1988). Formation of low-volatility compounds during isoprene oxidation has been estimated to be the single largest source of atmospheric organic aerosol (i.e., SOA) (Claeys et al., 2004; Henze et al., 2008; Hallquist et al., 2009; Carlton et al., 2009).

The photooxidation of unsaturated volatile organic compounds (VOCs) proceeds through formation of a hydroxy peroxy (RO_2) radical, the fate of which depends on the concentration of nitrogen oxides ($\text{NO}_x = \text{NO} + \text{NO}_2$). Higher SOA yields from isoprene are observed under low- NO_x (or NO_x -free) conditions; in this regime, RO_2 radicals react primarily with HO_2 , a pathway that tends to produce lower-volatility oxidation products than that involving the reaction of RO_2 with NO (Kroll et al., 2006; Presto et al., 2005; Kroll and Seinfeld, 2008). Under high- NO_x conditions, RO_2 radicals react with NO to produce alkoxy (RO) radicals, or as a minor pathway, organic nitrates (RONO_2). For small VOCs ($\leq \text{C}_{10}$), like isoprene, these RO radicals generally fragment into smaller more volatile products, resulting in small amounts of SOA (Kroll et al., 2006; Presto et al., 2005; Kroll and Seinfeld, 2008). Despite the fact that SOA from isoprene has been extensively studied (Carlton et al., 2009), the chemical pathways to its formation under both low- and high- NO_x conditions have remained unclear. In this study we examine the mechanism of isoprene SOA formation in these two limiting regimes.

6.3 Results and Discussion

6.3.1 Isoprene SOA formation under low- NO_x conditions: Role of aerosol acidity

Formation of SOA from the photooxidation of isoprene under low- NO_x conditions is enhanced in the presence of acidified sulfate seed aerosol over that in the presence of neutral aerosol (Surratt et al., 2006); this is not observed under high- NO_x conditions since the aerosol phase is likely acidic enough due to the formation and presence of nitric acid (HNO_3) (Lim and Ziemann, 2009) and/or organic acids (Surratt et al., 2006). The effect of increasing aerosol acidity on both gas- and aerosol-phase composition provides a critical clue to the chemical mechanism of SOA formation from isoprene under low- NO_x conditions. Enhancement of isoprene SOA mass with increasing aerosol acidity observed in laboratory chamber studies (Surratt et al., 2006; Edney et al., 2005; Surratt et al., 2007b), including increased mass concentrations of the 2 methyltetrols (Edney et al., 2005; Surratt et al., 2007b),

organosulfates of isoprene (i.e., hydroxy sulfate esters) (Surratt et al., 2007b), and high-MW SOA constituents (Surratt et al., 2007b), has been explained by acid-catalyzed particle-phase reactions. Although a linear correlation between the SOA mass formed and measured aerosol acidity (i.e., $\text{nmol H}^+ \text{ m}^{-3}$) has been found under dry conditions ($\sim 30\%$ RH) (Surratt et al., 2007b), the actual acid-catalyzed particle-phase reactions responsible for these observed enhancements in isoprene SOA formation remain unclear, especially since previously proposed reactions, like that of organosulfate formation by alcohol sulfate esterification (Surratt et al., 2007a; Gómez-González et al., 2008; Surratt et al., 2008), appear to be kinetically unfavorable at atmospheric conditions (Minerath and Elrod, 2009).

Shown in Fig. 6.1A–F are the chemical ionization mass spectrometry (CIMS) (see Materials and Methods) time traces for selected ions corresponding to the important gas-phase products formed from the photooxidation of 49 and 40 ppb of isoprene in the presence of neutral and highly acidified sulfate seed aerosol, respectively. The SOA mass yields from isoprene were 1.3% and 28.6% for the neutral and highly acidified sulfate seed aerosol experiments, respectively. Under the conditions of these experiments, the RO_2 radicals formed react primarily with HO_2 . In addition to the formation of hydroxycarbonyls, methyl-butenediols, hydroxyhydroperoxides (ISOPOOH), MACR, and methyl vinyl ketone (MVK), all of which are first-generation gas-phase oxidation products (Fig. 6.1A–D), we also observed the formation of second-generation IEPOX, as indicated in Fig 6.1F (i.e., 9 ppb and 0.6 ppb of IEPOX were measured in the neutral and acidic cases, respectively). Although the 2-methyltetrols (Fig. 6.1E) can be produced from RO_2 radical-cross reactions, their formation through this route is of minor significance (~ 0.2 ppb) in these experiments owing to the dominant $\text{RO}_2 + \text{HO}_2$ pathway. The hydroxycarbonyls (~ 0.8 ppb) and methyl-butenediols (~ 0.8 ppb) are first-generation products also formed from RO_2 radical-cross reactions; however, part of the CIMS signal associated with the methyl-butenediols (Fig. 6.1B) arises from later-generation oxidation products with the elemental composition $\text{C}_4\text{H}_6\text{O}_3$, likely a C_4 -hydroxydicarbonyl and/or C_4 -acid. Hydroxynitrates of isoprene were also observed (< 0.1 ppb). Their formation results from background NO in the chamber. Thus a fraction of the MACR and MVK produced results from $\text{RO}_2 + \text{NO}$ reactions ($\sim 3\%$

of RO₂ radicals reacted with NO).

IEPOX (i.e., δ -IEPOX) was proposed to form from the photooxidation of isoprene under low-NO_x conditions in order to tentatively explain the formation of chemically characterized SOA constituents (Paulot et al., 2009b; Wang et al., 2005). Gas-phase IEPOX (β -IEPOX and δ -IEPOX) was recently shown to form in substantial yields (upwards of 75%) from the further oxidation of ISOPOOH (\sim 12 ppb measured in both the neutral and acidic cases in Fig. 6.1C) by OH under low-NO_x conditions (Paulot et al., 2009b). The substantial reduction of gas-phase IEPOX in the presence of highly acidified sulfate seed aerosol (Fig. 6.1F) confirms the role of IEPOX in the enhancement of isoprene SOA mass under lower-NO_x conditions at increased aerosol acidity.

Isoprene low-NO_x SOA was analyzed off line by gas chromatography/electron ionization-quadrupole mass spectrometry (GC/EI-MS) with prior trimethylsilylation and ultra performance liquid chromatography/electrospray ionization-time-of-flight mass spectrometry operated in the negative ion mode (UPLC/(-)ESI-TOFMS) (see Methods and Materials). Particle-phase IEPOX is characterized here for the first time. The GC/EI-MS mass spectra of the trimethylsilyl (TMS)-derivatives of IEPOX associated with the two chromatographic peaks in Fig. 6.1G are shown in Fig. 6.6. Extracted ion chromatograms (EICs) of selected ions corresponding to particle-phase IEPOX, as well as the previously characterized C₅-alkene triols (Wang et al., 2005), 2 methyltetrols (Claeys et al., 2004), hemiacetal dimers (Surratt et al., 2006), organosulfate derivatives of the 2 methyltetrols (Surratt et al., 2006; Gómez-González et al., 2008), and organosulfate derivatives of the hemiacetal dimers (Surratt et al., 2007a) are shown in Fig. 6.1G–L, respectively. Mass spectra in the present study for the previously characterized low-NO_x SOA constituents shown in Fig. 6.1H–L correspond to those collected in prior work (Claeys et al., 2004; Surratt et al., 2006, 2007a; Wang et al., 2005), and are shown in Fig. 6.6 and Fig. 6.7. The abundances of all low-NO_x SOA constituents shown in Fig. 6.1G–L are enhanced significantly in the presence of acidified sulfate seed aerosol. Using a suitable surrogate standard (i.e., meso-erythritol to quantify the 2-methyltetrols), we estimate that the mass concentrations of these compounds increased from 0.1 $\mu\text{g m}^{-3}$ for the neutral case to 5.1 $\mu\text{g m}^{-3}$ for the highly acidic case, corresponding to \sim 10 to 20%, respectively, of the total SOA mass

formed.

6.3.2 Identification of IEPOX as the intermediate responsible for acid-enhanced isoprene SOA

We hypothesize that particle-phase reactions of IEPOX play a significant role in the formation of the other major low-NO_x SOA constituents shown in Fig. 6.1H-L, as well as in the enhancement of total SOA mass. To test this hypothesis, we synthesized 2,3-epoxy-1,4-butanediol (BEPOX) (see Materials and Methods), which is the butadiene derivative of IEPOX, and conducted reactive uptake experiments in the presence of both neutral and highly acidified sulfate seed aerosol. BEPOX is used in these experiments instead of IEPOX, as precursors for IEPOX are not commercially available. In these dark and dry (<10% RH) experiments, no OH precursor (e.g., H₂O₂) or NO_x was present; thus, only reactive uptake of BEPOX onto seed aerosol occurred. Two variations of these reactive uptake experiments were carried out: (1) BEPOX was added first, followed by the injection of seed aerosol; or (2) seed aerosol was added first, followed by the injection of BEPOX. CIMS time traces corresponding to version (1) of the BEPOX reactive uptake experiments are shown in Fig. 6.2A. The only parameter varied was the acidity of the sulfate seed aerosol. BEPOX is rapidly removed from the gas phase within the first hour after the acidified sulfate seed aerosol is injected into the well-mixed chamber. Upon the injection of neutral sulfate seed aerosol, BEPOX disappears from wall loss only and not reactive uptake. Once the injection of gas-phase BEPOX ended (indicated at time zero in Fig. 6.2A), it decayed at similar rates before either the neutral or highly acidified sulfate seed aerosol was injected. The clear conclusion is that BEPOX loss to the highly acidic seed aerosol results from acid-catalyzed particle-phase reactions.

SOA formed in the acidified BEPOX reactive uptake experiments shown in Fig. 6.2A was collected for off-line chemical analyses by GC/EI-MS and UPLC/(-)ESI-TOFMS (Fig. 6.8). In addition to sharing similar retention times (RTs), the mass spectrum of the TMS-derivative of the particle-phase BEPOX (Fig. 6.8) corresponds exactly to that of the synthesized BEPOX standard (see Fig. 6.9). The major chromatographic peak observed in the EIC of m/z 248 (Fig. 6.8) is attributable

only to particle-phase BEPOX, whereas the two later-eluting minor peaks represent background contributions. The other major SOA constituents characterized from the reactive uptake of BEPOX are also exact analogues of isoprene SOA formed under low- NO_x conditions (i.e., differing by a mass of 14 Da, which corresponds to a CH_2 group); these include: C_4 -alkene triols, tetrols (i.e., threitol and erythritol), dimers, organosulfate derivatives of the tetrols, and organosulfate derivatives of the dimers (Fig. 6.8). Equivalent to the low- NO_x isoprene SOA (Fig. 6.1G–L), these BEPOX SOA constituents were significantly enhanced under increased seed aerosol acidity, consistent with the rapid removal of gas-phase BEPOX onto the highly acidified sulfate seed aerosol. The tetrols (i.e., threitol and erythritol) were quantified by GC/EI-MS and their summed mass was found to increase from 43 ng m^{-3} to $1.3 \text{ } \mu\text{g m}^{-3}$ from neutral to highly acidic conditions.

In version (2) of the BEPOX reactive uptake experiments, within the first hour after the addition of BEPOX, the sulfate aerosol mass concentration decayed more rapidly (by $\sim 58\%$ of its initial loading) in the highly acidic case than that which could be explained by wall loss alone, indicating depletion of the inorganic sulfate through chemical reaction with BEPOX (Fig. 6.10). A similar observation made in isoprene SOA formation (Surratt et al., 2006) is consistent with the reactive uptake of IEPOX forming organosulfates of isoprene. The SOA mass generated after the injection of gas-phase BEPOX increased from 0.9 to $15.8 \text{ } \mu\text{g m}^{-3}$ from neutral to acidified sulfate seed aerosol. Importantly, organosulfates of BEPOX (i.e., organosulfate derivatives of the tetrols and dimers, as well as higher order organosulfates shown in Fig. 6.11) were also characterized in these experiments (Fig. 6.8). We conclude from these observations that conversion of inorganic sulfate into organosulfates occurs by the acid-catalyzed ring opening of the epoxydiols followed by the subsequent nucleophilic addition of inorganic sulfate.

Reactive uptake onto acidified sulfate seed aerosol also occurs when BEPOX and IEPOX are formed from butadiene and isoprene photooxidation, respectively. 100 ppb of butadiene and 50 ppb of isoprene were initially irradiated in the absence of seed aerosol (Fig. 6.2B and 6.2C, respectively). Once sufficient gas-phase levels of both BEPOX and IEPOX formed, seed aerosol was injected. For the butadiene experiment (Fig. 6.2B), only highly acidified sulfate seed aerosol was injected. Because

hydroxyhydroperoxides and BEPOX, gas-phase oxidation products of butadiene, are isomers both detected by the CIMS technique at m/z 189, characteristic daughter ions produced from m/z 189 were used to differentiate between these two compounds. The daughter ions at m/z 63 and 169 are uniquely characteristic of the hydroxyhydroperoxide and BEPOX, respectively (Paulot et al., 2009b). Upon the injection of acidified sulfate seed aerosol, BEPOX was the only oxidation product rapidly removed from the gas-phase mixture (decayed by $\sim 75\%$ within the first hour after seed aerosol was injected). The SOA constituents from butadiene shown in Fig. 6.2B are precisely those shown in Fig. 6.8. In the case of isoprene photooxidation (Fig. 6.2C), as observed for the BEPOX reactive uptake and butadiene photooxidation (Fig. 6.2A and 6.2B, respectively), gas-phase IEPOX disappeared significantly only in the presence of acidified sulfate seed aerosol (Fig. 6.2C). Moreover, the constituents characterized in the SOA formed from the latter experiment are precisely those shown in Fig. 6.6G–L.

6.3.3 Mechanism of isoprene SOA formation under low- NO_x conditions

An updated chemical mechanism for SOA formation from isoprene under low- NO_x conditions is shown in Fig. 6.3. The gas-phase formation of IEPOX has been fully characterized by Paulot et al. (2009b). Here we have established that the reactive uptake of IEPOX occurs by the acid-catalyzed ring opening of this epoxydiol, followed by the subsequent addition of the following nucleophiles: (1) H_2O ; (2) inorganic sulfate; (3) a 2-methyltetrol already formed in the aerosol; and (4) a hydroxy sulfate ester already present in the aerosol. Unreacted particle-phase IEPOX observed in the isoprene SOA is likely a result of equilibrium gas-to-particle partitioning. Although the formation of 2-methyltetrols has been detected from the further oxidation of methyl-butenediols under conditions in which $\text{RO}_2 + \text{RO}_2$ reactions dominate (at large isoprene mixing ratios, i.e., 8–12 ppmC) (Kleindienst et al., 2009), the atmospheric formation of the 2-methyltetrols will occur primarily via the further reaction of IEPOX as shown in Fig. 6.3, since the HO_2 concentration exceeds that of all RO_2 radicals (Ren et al., 2003) and because rate coefficients of $\text{RO}_2 + \text{RO}_2$ reactions are usually smaller than those for $\text{RO}_2 + \text{HO}_2$ reactions (Atkinson et al., 2006). The organosulfates of isoprene are shown

conclusively to form from the reactive uptake of IEPOX, rather than by the previously proposed alcohol sulfate esterification mechanism (Surratt et al., 2008). This conclusion is consistent with recent work by Iinuma et al. (2009), who showed organosulfates of α - and β -pinene form through the reactive uptake of α - and β -pinene oxides, only in the presence of acidified sulfate seed aerosol. Additionally, recent work has shown that organosulfate formation is kinetically favorable only for epoxides and not for alcohols at atmospherically relevant conditions (Minerath and Elrod, 2009).

Although the C₅-alkene triols were observed in these experiments, their exact formation mechanism remains unclear. We cannot rule out the possibility that these compounds are produced from the trimethylsilylation step prior to GC/EI-MS analysis, as a TMS-derivative of the synthesized BE-POX standard was found to have a contribution from C₄-alkene triols. Preliminary results suggest that these compounds are more abundant than the tetrols under high RH conditions. Enhanced C₅-alkene triol concentrations have been observed when transitioning from the dry to wet seasons in the Amazon (Wang et al., 2005). Finally, the dimers previously observed in both laboratory-generated isoprene SOA and organic aerosol collected from the Amazon are likely not a result of hemiacetal formation (Surratt et al., 2006); rather these dimers are shown to form from polymerization of IEPOX by acid-catalyzed ring opening of IEPOX.

6.3.4 Isoprene SOA formation under high-NO_x conditions: Role of MPAN

The majority of the high-NO_x SOA yield from isoprene has previously been traced to the oxidation of a major (25% yield (Tuazon and Atkinson, 1990a)) first-generation oxidation product of isoprene, MACR (Kroll et al., 2006; Surratt et al., 2006). Providing further evidence of the role of MACR, the chemical composition of the SOA produced in the oxidation of MACR is similar to that found in studies of the oxidation of isoprene, especially 2-methylglyceric acid (2-MG), a C₄-dihydroxycarboxylic acid, which undergoes esterification to produce low-volatility oligoesters (Surratt et al., 2006; Szmigielski et al., 2007). Both 2-MG and its corresponding diester have been observed in ambient aerosol samples (Hallquist et al., 2009).

The preservation of the four-carbon backbone in the SOA produced, following the oxidation of

MACR, provides significant constraints on the gas-phase mechanism that yields the SOA precursor. Oxidation of MACR by OH proceeds both via addition to the double bond ($\sim 55\%$) and abstraction of the aldehydic hydrogen (45%) (Tuazon and Atkinson, 1990b; Orlando et al., 1999). Preservation of the carbon backbone generally precludes formation of RO radicals as they rapidly decompose to form hydroxyacetone (via OH addition) and methylvinyl radicals (via aldehydic abstraction) (Orlando et al., 1999). This suggests that, following abstraction of the aldehydic hydrogen by OH, formation of MPAN is likely key to SOA production. MPAN is formed from MACR with a maximum yield of $\sim 45\%$ (Tuazon and Atkinson, 1990b; Bertman and Roberts, 1991). Following addition of OH to the double bond, the only known gas-phase mechanism that prevents C-C fragmentation in the presence of NO_x is the channel leading to the formation of a hydroxynitrate (Hallquist et al., 2009; Tuazon and Atkinson, 1990b; Paulot et al., 2009a). Thus, to oxidize both the double bond and the aldehydic hydrogen, one route to C_4 preservation leads to the formation of the hydroxynitrate of MPAN. Alternatively, the addition of OH to MPAN might lead to the formation of bridged oxygen compounds if the alkyl radical (or subsequent RO_2 or RO radicals) rearrange unimolecularly and decompose by breaking off the weak peroxyxynitrate moiety forming peroxy or epoxy carbonyls.

To test the hypothesis that the formation of MPAN is key for SOA formation, MACR was oxidized by OH (formed via HONO photolysis) in the presence of a very high concentration of NO (>500 ppb). Under these conditions, the peroxyacyl radical formed following H abstraction (and addition of O_2) reacts primarily with NO to form formaldehyde, CO, and CO_2 rather than with NO_2 to form MPAN (Tuazon and Atkinson, 1990a; Bertman and Roberts, 1991). Although formation of hydroxynitrate was observed from the addition channel ($\sim 10\text{--}15\%$ of hydroxyacetone), little SOA was produced (mass yield $<2\%$). SOA yields (2.9% from 257 ppb MACR) were higher when 290 ppb of NO was added, and highest (5.1% from 285 ppb MACR) when 350 ppb of additional NO_2 (instead of NO) was injected. As shown in Fig. 6.12, the relative aerosol-phase concentrations of oligoesters are also enhanced under higher $[\text{NO}_2]/[\text{NO}]$ ratios, consistent with the trends observed in SOA yields from MACR photooxidation. The RTs and molecular formulas match those of the oligoester products formed in isoprene high- NO_x SOA. NO levels remained above 120 ppb during the

course of all the experiments, and thus $\text{RO}_2 + \text{HO}_2$ and $\text{RO}_2 + \text{RO}_2$ reactions are not competitive. HONO levels, as measured by CIMS, were within 15% among these experiments. The observed increase in SOA at higher NO_2 levels is also unlikely to be a result of condensation of nitric acid from $\text{OH} + \text{NO}_2$ reactions, as addition of gas-phase nitric acid did not lead to additional aerosol growth. The observed effect of $[\text{NO}_2]/[\text{NO}]$ ratio on oligoester formation and overall aerosol yields in MACR photooxidation suggests the importance of peroxyxynitrate formation via an $\text{RO}_2 + \text{NO}_2$ pathway. In the chamber, the lifetime of MPAN against thermal decomposition is about 100 min (Roberts and Bertman, 1992), and can be effectively much longer under higher $[\text{NO}_2]/[\text{NO}]$ ratios, as the peroxyacyl radicals formed following thermal decomposition react preferentially with NO_2 reforming MPAN.

6.3.5 Identification of MPAN as a key intermediate in formation of SOA from isoprene and MACR

To verify the hypothesis that the route to high- NO_x SOA formation from isoprene goes through MPAN, experiments were carried out with synthesized MPAN (see Materials and Methods). When MPAN was injected into the chamber in the presence solely of ammonium sulfate seed, SOA was not observed. Significant aerosol growth was observed only upon photooxidation of MPAN (with photolysis of HONO used as the OH source). Moreover, as shown in Fig. 6.4, the composition of SOA formed from MPAN oxidation was similar to that from high- NO_x photooxidation of MACR and isoprene. In particular, 2-MG and its corresponding oligoesters are identified in all three aerosol samples using both GC/EI-MS and UPLC/(-)ESI-TOFMS. Detailed chemical characterization of 2-MG and its corresponding oligoesters (Surratt et al., 2006; Szmigielski et al., 2007) and similar analysis of the current samples confirm the presence of these products in aerosol formed from MPAN oxidation (Fig. 6.4 and Table 6.1). Other aerosol components found in isoprene SOA, such as compounds with a C_5 -hydroxynitrate backbone, are not found in MACR or MPAN SOA, but their contribution to total aerosol mass is likely small, and their formation mechanisms have been tentatively established (Surratt et al., 2008). We confirmed that 2-MG and its corresponding oli-

goesters are formed as a result of MPAN oxidation and not an impurity (i.e., methacrylic acid) (see Supporting Information).

Additional experiments provide insight into the mechanism by which 2-MG is formed from the OH reaction of MPAN. Oxidation of 2-methyl-3-buten-2-ol (MBO), structurally similar to isoprene, but lacking the second double bond, leads to no aerosol formation. This suggests that formation of 2-MG requires OH reaction with the double bond of MPAN. OH addition to the MPAN double bond, followed by addition of O₂, leads to formation of an RO₂ radical; under the chamber conditions, reaction with NO is most likely, leading to formation of either an RO radical or a C₄-hydroxynitrate-PAN. Owing to the 2-position of the alkoxy group, this C₄-alkoxy radical is unlikely to undergo traditional H-atom transfer isomerization, and therefore decomposes rapidly to break the C₄-backbone. One possibility is that 2-MG is formed through the C₄-hydroxynitrate-PAN channel (see Fig. 6.5). Dommen et al. (2006) observed lower-volatility isoprene SOA (which is consistent with the formation of oligomers) to form under dry rather than humid conditions, which is consistent with a mechanism that involves decomposition of the C₄-hydroxynitrate-PAN into 2-MG and allows for subsequent esterification of 2-MG into the observed oligoesters. We do not, however, have conclusive chemical evidence to support the hypothesis that the C₄-hydroxynitrate-PAN is the main precursor to the isoprene high-NO_x SOA. Indeed, there is some evidence that this is not the route. A signal, comparable in magnitude to the hydroxynitrate of MACR (at m/z 234) and highly correlated to the time trace of SOA formation, is observed at m/z 311 – a mass consistent with the cluster of CF₃O[−] with the C₄-hydroxynitrate-PAN. Assuming the same CIMS response factor as glycolaldehyde, the signal at m/z 311 is consistent with all of the C₄-hydroxynitrate-PAN being accounted for in the gas phase (assuming the yield of the C₄-hydroxynitrate from MPAN is comparable to the yield of the hydroxynitrate from MACR), and as a result, this compound could not be the SOA precursor. Thus, it is possible that some unknown C₄-preserving chemical reaction is occurring when MPAN is oxidized by OH (e.g., similar to the formation of IEPOX under low-NO_x conditions, the OH-MPAN radical adduct intramolecularly rearranges into a highly-strained epoxide before O₂ adds).

The OH reaction rate constants of saturated peroxyacyl nitrates (PANs) are sufficiently small

($< 1 \times 10^{-13} \text{ cm}^3 \text{ molec}^{-1} \text{ s}^{-1}$) that the major sink for these compounds in the atmosphere is thermal decomposition to the peroxyacyl radical followed by reaction with NO and subsequent decomposition to CO_2 . By contrast, the OH reaction of MPAN is competitive with thermal decomposition (Orlando et al., 1999). Here we confirm that MPAN is the key intermediate in the isoprene and MACR systems in the formation of 2-MG and its corresponding low-volatility oligoesters in the aerosol phase. If a PAN-type compound is involved in the formation of aerosol-phase products, the aerosol yields should depend on the $[\text{NO}_2]/[\text{NO}]$ ratio, as this ratio determines whether the peroxyacyl radicals produced via thermal decomposition reform PANs or react with NO and decompose. With urban $[\text{NO}_2]/[\text{NO}]$ ratios typically around 7, SOA mass yields from isoprene and MACR previously measured at $[\text{NO}_2]/[\text{NO}]$ ratios around 1 could be underestimated (Carlton et al., 2009). Experimentally, such high $[\text{NO}_2]/[\text{NO}]$ ratios are not achieved using HONO as an OH source, as NO is produced from both the synthesis of HONO and photolysis of HONO with UV irradiation.

6.4 Atmospheric Implications

The importance of IEPOX and MPAN in forming isoprene SOA under low- and high- NO_x conditions, respectively, provides significant insights into heretofore-unidentified aerosol precursors. In the presence of anthropogenic pollutants, such as NO_2 and acidic aerosol produced from the oxidation of SO_2 , SOA mass yields from isoprene under high- and low- NO_x conditions, respectively, increase substantially. As isoprene is estimated to be the largest single contributor to global SOA, these results may help to resolve two existing dilemmas in atmospheric chemistry: (1) radiocarbon (^{14}C) data consistently indicate that well over half of the ambient SOA is of modern (biogenic) origin (7, 33)(Hallquist et al., 2009; Schichtel et al., 2008), whereas correlations between water-soluble organic carbon and anthropogenic tracers, such as CO, suggest that much of the SOA is actually of anthropogenic origin (Weber et al., 2007; de Gouw et al., 2005); and (2) comparisons between measured and predicted SOA based on known precursors suggest that there is a substantial amount of “missing urban SOA” not included in current models (de Gouw et al., 2005; Heald et al., 2005; Volkamer et al., 2006). Revising the chemistry of isoprene in regional and global SOA models could

lead to a decrease in this discrepancy; however, the measurement and parameterization of aerosol acidity requires additional work.

6.5 Materials and Methods

6.5.1 Experimental details

The experiments were carried out in the Caltech dual 28-m³ FEP Teflon chambers (Keywood et al., 2004). Seed aerosol is generated using a constant rate atomizer. Dilute solutions (concentrations of 0.06M or lower) of ammonium sulfate and magnesium sulfate with sulfuric acid are used for neutral and highly acidic seed aerosol, respectively. The particle number and volume concentrations are corrected for particle wall loss using size-dependent coefficients determined from loss of inert particles. Isoprene, MACR, or MBO is added to the chamber by vaporizing a known volume of the hydrocarbon in a glass bulb. In the reactive uptake experiments (see Table 6.2 and Supporting Information), BEPOX is injected into the chamber by vaporizing a small (~ 30 mg) amount of the solid at $\sim 60^\circ\text{C}$ in a small glass vial and introducing the vapor into the chamber in a stream of N_2 . The amount injected into the chamber is estimated by measuring the mass loss of BEPOX after injection. MPAN is injected in a similar manner in a -10°C ice-salt bath. At -10°C , dodecane has a negligible vapor pressure, and as a result, not expected to be introduced into the chambers. In low- NO_x photooxidation experiments (see Table 6.2 and Supporting Information), the photolysis of H_2O_2 is used to generate OH radicals. In order to prevent partitioning of H_2O_2 into the seed aerosol, all low- NO_x experiments were conducted under dry conditions ($<10\%$ RH). At the relatively high mixing ratios of H_2O_2 , significant HO_2 radical levels are produced by the $\text{OH} + \text{H}_2\text{O}_2$ reaction, which is favored at the slow chamber photolysis rate of H_2O_2 . In high- NO_x photooxidation experiments, the photolysis of nitrous acid (HONO) is used as the OH precursor (see Table 6.3 and Supporting Information).

6.5.2 Gas-phase measurements

The concentrations of isoprene, MACR, and MBO are monitored by a gas chromatograph equipped with a flame ionization detector (GC/FID, Agilent 6890N). NO/NO_x and O₃ are monitored by commercial chemiluminescence monitors (Horiba, APNA 360 and APOA 360, respectively). A custom-modified Varian 1200 CIMS was used to continuously monitor gas-phase species (see Paulot et al. (2009b) and Supporting Information).

6.5.3 Aerosol-phase measurements

Aerosol size distributions and volume concentrations are measured using a differential mobility analyzer (DMA, TSI 3081) with a condensation nuclei counter (CPC, TSI 3760). Aerosol samples are collected onto Teflon filters for off-line chemical characterization by both GC/EI-MS with prior trimethylsilylation and UPLC/ESI-TOFMS. Filter handling and extraction protocols in high purity methanol have been described previously for aerosol samples analyzed by the UPLC/(-)ESI-TOFMS technique (Surratt et al., 2008). Details of the sample preparation and operation protocols for the GC/EI-MS technique can be found in the Supporting Information. Selected SOA samples formed from the reactive uptake of BEPOX on either neutral or acidified sulfate seed aerosol were continuously sampled by a particle-into-liquid sampler (PILS) with subsequent offline analysis by ion chromatography (IC) (Sorooshian et al., 2006).

6.5.4 Materials

Isoprene (Aldrich, 99%), MACR (Aldrich, 95%), and MBO (Aldrich, 98%) are obtained from commercial sources. BEPOX is synthesized following the procedure derived by Skinner et al. (1958) (see Supporting Information). MPAN is synthesized from methacrylic anhydride (Aldrich, 94%) in dodecane (Sigma-Aldrich, 99+%, anhydrous) based on the method of Nouaime et al. (1998) with a few modifications (see Supporting Information). The purity of the product is confirmed by gas-phase FTIR spectroscopy (see Supporting Information).

6.6 Acknowledgments

This work was supported by the Office of Science (Biological and Environmental Research), U.S. Department of Energy grant DE-FG02-05ER63983, and U.S. Environmental Protection Agency (EPA) STAR agreement RD-833749. The CIMS instrument was purchased as part of a major research instrumentation grant from the National Science Foundation (ATM-0619783); assembly and testing was supported by the Davidow Discovery Fund. We thank Andreas Kürten for assembling the CIMS instrument and John D. Crounse for synthesizing and characterizing (with H-NMR) the BEPOX. The Waters UPLC-LCT Premier XT time-of-flight mass spectrometer was purchased in 2006 with a grant from the National Science Foundation, Chemistry Research Instrumentation and Facilities Program (CHE-0541745). N.C.E. was supported by the Camille and Henry Dreyfus Postdoctoral Program in Environmental Chemistry. This work has not been formally reviewed by the EPA. The views expressed in this document are solely those of the authors, and the EPA does not endorse any products or commercial services mentioned in this publication. We also thank Magda Claeys for useful discussions.

6.7 Supporting Information

6.7.1 Experimental details of chamber operation

6.7.1.1 Low-NO_x Experiments

280 μ L of 50% H₂O₂ solution (Aldrich) is injected into a glass bulb, vaporized in a 30°C water bath, and introduced into the chamber in an air stream, resulting in an estimated chamber concentration of 4 ppmv. 50% of the available blacklights are used to irradiate the chambers.

6.7.1.2 High-NO_x experiments

HONO is prepared by adding 1 wt% aqueous NaNO₂ dropwise into 10 wt% sulfuric acid, and introduced into the chamber using an air stream (Chan et al., 2009). NO or NO₂ are injected into the chambers from gas cylinders (Scott Marrin). 10% of the available blacklights are used to

irradiate the chambers.

6.7.2 Procedures to confirm purity of MPAN

The purity of the MPAN sample was quantified by comparison of gas-phase FTIR spectra with those published in other studies (see MPAN synthesis below). The major impurity, methacrylic acid, does not contribute to SOA. We oxidized methacrylic acid under the same conditions used in the MPAN study and SOA formation was not observed. At the NO levels (>10 ppb) in the photooxidation experiments, $\text{RO}_2 + \text{HO}_2$ and $\text{RO}_2 + \text{RO}_2$ reactions do not compete with $\text{RO}_2 + \text{NO}$ or $\text{RO}_2 + \text{NO}_2$ reactions, and aerosol-phase formation of 2-MG from isoprene cannot be attributed to gas-phase RO_2 radical-cross reactions of methacrylic acid.

6.7.3 Details of the CIMS technique

6.7.3.1 Operating conditions

The CIMS was operated in negative ion mode where CF_3O^- is used as the reagent ion, and in positive ion mode of proton transfer mass spectrometry (PTR-MS) (Crounse et al., 2006). In negative ion mode, CF_3O^- selectively clusters with compounds with high fluorine affinities to form a complex detected at $m/z = \text{MW}+85$, while highly acidic molecules will mainly form the transfer product detected at $m/z = \text{MW}+19$ (Crounse et al., 2006). To distinguish between hydroxyisoprene hydroperoxide and isoprene epoxydiols (both of which are both detected at m/z 203), an MS/MS technique was used (Paulot et al., 2009b). In the first quadrupole the parent ion is selected, and in the second quadrupole a small amount of N_2 is present to act as a collision partner producing collision-induced daughter ions, which are subsequently selected in the third quadrupole. Depending on the nature of the ion, different collision-induced daughter ions can be formed. Two daughter ions of particular interest are at m/z 63 and m/z 183. The daughter ion at m/z 63 is selective for the hydroperoxide group, while the isoprene epoxydiols fragment in sufficient yield at m/z 183. In PTR-MS mode, residual H_2O in N_2 is reacted with N_2^+ ions to form $\text{H}^+ \cdot (\text{H}_2\text{O})_n$ reagent ions.

6.7.3.2 Correction of the MS/MS daughter ion signal associated to IEPOX

ISPOOH and IEPOX are isomers, and as a result, are both detected at m/z 203. As noted above, using the MS/MS technique of the CIMS, these isomers can be separated from each other due to their production of different characteristic daughter ions. It has also been shown that IEPOX does not interfere with the daughter ion at m/z 63 associated to ISPOOH. IEPOX is known to fragment in good yield to m/z 183; however, ISPOOH also fragments to this ion to a lesser extent. In order to determine the extent that ISPOOH fragments to m/z 183 in the second quadrupole, a large number of the daughter ions from the parent ion at m/z 203 were analyzed and it was determined that only two compounds were present at this ion (i.e., ISPOOH and IEPOX). Next, the data from an experimental run where ISPOOH was only present in the gas phase was analyzed to determine the amount of the daughter ion at m/z 183 that was from ISPOOH. It was found that 20% of the daughter ion at m/z 183 was from ISPOOH and this amount was subtracted from all MS/MS spectra of m/z 183 so that only IEPOX was displayed. This corrected signal was also used to determine the concentration of IEPOX.

6.7.4 Filter extraction and operation protocols for the GC/EI-MS technique

Filter extractions for aerosol samples analyzed by the GC/EI-MS technique are similar to the UPLC/(-)ESI-TOFMS technique; however, following the removal of the methanol extraction solvent with ultra-high purity N_2 , the dried residue was trimethylsilylated by the addition of 100 mL of BSTFA + trimethylchlorosilane (99:1 (v/v), Supleco) and 50 mL of pyridine (Sigma-Aldrich, 98%, anhydrous), and the resultant mixture was heated for an hour at 70 °C. This latter step converted all isoprene SOA constituents containing carboxyl and hydroxyl functions into volatile trimethylsilyl (TMS) derivatives. GC/EI-MS analyses of the TMS derivatives were performed with a system comprised of a Hewlett Packard (HP) 5890 Series 2 Plus chromatograph, interfaced to a HP 5972 Series mass selective detector. A Restek RTX-5MS fused-silica capillary column (5% diphenyl, 95% dimethyl polysiloxane, 0.25 mm film thickness, 30 m x 0.25 mm i.d.) was used to separate the TMS

derivatives before MS detection. 1 mL aliquots of each sample were injected in the splitless mode onto the column by a HP 7673 Series GC injector and autosampler. Helium was used as the carrier gas at a flow rate of 0.8 mL min⁻¹. The 65.17 min temperature program of the GC was as follows: isothermal hold at 60 °C for 1 min, temperature ramp of 3 °C min⁻¹ up to 200 °C, isothermal hold at 200 °C for 2 min, temperature ramp of 20 °C min⁻¹ to 310 °C, and isothermal hold at 310 °C for 10 min. The MS scan was performed in the m/z 50–500 range. A solvent delay time of 7.5 min was employed. The ion source was operated at an electron energy of 70 eV. The temperatures of both the GC inlet and detector were at 250 °C.

6.7.5 Materials

6.7.5.1 BEPOX synthesis

In general, an aqueous solution of 2-butene-1,4-diol (Fluka, purum, $\geq 98.0\%$) is reacted with H₂O₂ catalyzed by tungstic acid, followed by removal of H₂O and other impurities. NMR of the final product reveals purity greater than 95% and the product is used as is.

6.7.5.2 MPAN synthesis

Methanesulfonic acid (Fluka, puriss., $\geq 99.0\%$) is used in place of sulfuric acid as suggested by Williams et al. (Williams et al., 2000) to improve the purity of the product. No column purification is carried out. Instead, the MPAN solution is purified by 20–25 successive washes with deionized water (Millipore, 18.2 M Ω · cm). Spectra of the MPAN sample showed strong peaks at 1065, 1297, 1740, 1807 cm⁻¹, which are associated with MPAN (Bertman and Roberts, 1991). No peaks associated with methacrylic anhydride and methacrylic acid are observed in spectra obtained from the MPAN sample.

Bibliography

- Atkinson, R., Baulch, D. L., Cox, R. A., Crowley, J. N., Hampson, R. F., Hynes, R. G., Jenkin, M. E., Rossi, M. J., and Troe, J.: Evaluated kinetic and photochemical data for atmospheric chemistry: Volume II - gas phase reactions of organic species, *Atmos. Chem. Phys.*, 6, 3625–4055, 2006.
- Bertman, S. B. and Roberts, J. M.: A PAN analog from isoprene photooxidation, *Geophys. Res. Lett.*, 18, 1461–1464, 1991.
- Carlton, A. G., Wiedinmyer, C., and Kroll, J. H.: A review of Secondary Organic Aerosol (SOA) formation from isoprene, *Atmos. Chem. Phys.*, 9, 4987–5005, 2009.
- Chameides, W. L., Lindsay, R. W., Richardson, J., and Kiang, C. S.: The role of biogenic hydrocarbons in urban photochemical smog - Atlanta as a case study, *Science*, 241, 1473–1475, 1988.
- Chan, A. W. H., Kautzman, K. E., Chhabra, P. S., Surratt, J. D., Chan, M. N., Crounse, J. D., Kurten, A., Wennberg, P. O., Flagan, R. C., and Seinfeld, J. H.: Secondary organic aerosol formation from photooxidation of naphthalene and alkylnaphthalenes: implications for oxidation of intermediate volatility organic compounds (IVOCs), *Atmos. Chem. Phys.*, 9, 3049–3060, 2009.
- Claeys, M., Graham, B., Vas, G., Wang, W., Vermeylen, R., Pashynska, V., Cafmeyer, J., Guyon, P., Andreae, M. O., Artaxo, P., and Maenhaut, W.: Formation of secondary organic aerosols through photooxidation of isoprene, *Science*, 303, 1173–1176, 2004.
- Crounse, J. D., McKinney, K. A., Kwan, A. J., and Wennberg, P. O.: Measurement of gas-phase hydroperoxides by chemical ionization mass spectrometry, *Anal. Chem.*, 78, 6726–6732, 2006.
- de Gouw, J. A., Middlebrook, A. M., Warneke, C., Goldan, P. D., Kuster, W. C., Roberts, J. M., Fehsenfeld, F. C., Worsnop, D. R., Canagaratna, M. R., Pszenny, A. A. P., Keene, W. C., Marchewka, M., Bertman, S. B., and Bates, T. S.: Budget of organic carbon in a polluted atmosphere: Results from the New England Air Quality Study in 2002, *J. Geophys. Res.-Atmos.*, 110, D16305, doi:10.1029/2004JD005623, 2005.

- Dommen, J., Metzger, A., Duplissy, J., Kalberer, M., Alfarra, M. R., Gascho, A., Weingartner, E., Prevot, A. S. H., Verheggen, B., and Baltensperger, U.: Laboratory observation of oligomers in the aerosol from isoprene/NO_x photooxidation, *Geophys. Res. Lett.*, **33**, L13805, doi:10.1029/2006GL026523, 2006.
- Edney, E. O., Kleindienst, T. E., Jaoui, M., Lewandowski, M., Offenberg, J. H., Wang, W., and Claeys, M.: Formation of 2-methyl tetrols and 2-methylglyceric acid in secondary organic aerosol from laboratory irradiated isoprene/NO_x/SO₂/air mixtures and their detection in ambient PM_{2.5} samples collected in the eastern United States, *Atmos. Environ.*, **39**, 5281–5289, 2005.
- Gómez-González, Y., Surratt, J. D., Cuyckens, F., Szmigielski, R., Vermeylen, R., Jaoui, M., Lewandowski, M., Offenberg, J. H., Kleindienst, T. E., Edney, E. O., Blockhuys, F., Van Alsenoy, C., Maenhaut, W., and Claeys, M.: Characterization of organosulfates from the photooxidation of isoprene and unsaturated fatty acids in ambient aerosol using liquid chromatography/(–) electrospray ionization mass spectrometry, *J Mass Spectrom.*, **43**, 371–382, 2008.
- Guenther, A., Karl, T., Harley, P., Wiedinmyer, C., Palmer, P. I., and Geron, C.: Estimates of global terrestrial isoprene emissions using MEGAN (Model of Emissions of Gases and Aerosols from Nature), *Atmos. Chem. Phys.*, **6**, 3181–3210, 2006.
- Hallquist, M., Wenger, J. C., Baltensperger, U., Rudich, Y., Simpson, D., Claeys, M., Dommen, J., Donahue, N. M., George, C., Goldstein, A. H., Hamilton, J. F., Herrmann, H., Hoffmann, T., Iinuma, Y., Jang, M., Jenkin, M. E., Jimenez, J. L., Kiendler-Scharr, A., Maenhaut, W., McFiggans, G., Mentel, T. F., Monod, A., Prevot, A. S. H., Seinfeld, J. H., Surratt, J. D., Szmigielski, R., and Wildt, J.: The formation, properties and impact of secondary organic aerosol: current and emerging issues, *Atmos. Chem. Phys.*, **9**, 5155–5236, 2009.
- Heald, C. L., Jacob, D. J., Park, R. J., Russell, L. M., Huebert, B. J., Seinfeld, J. H., Liao, H., and Weber, R. J.: A large organic aerosol source in the free troposphere missing from current models, *Geophys. Res. Lett.*, **32**, L18809, doi:10.1029/2005GL023831, 2005.

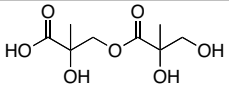
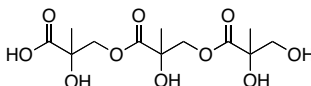
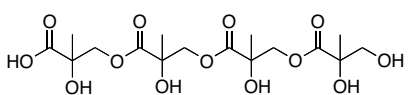
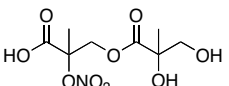
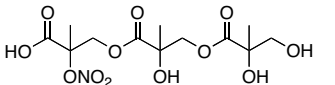
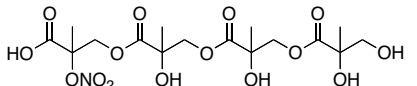
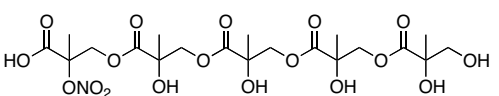
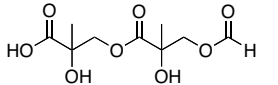
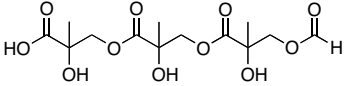
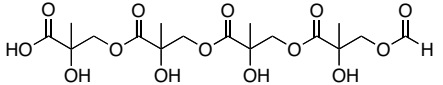
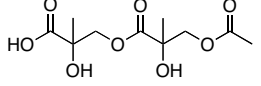
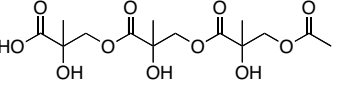
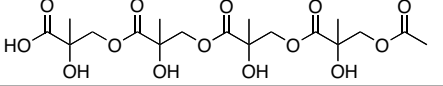
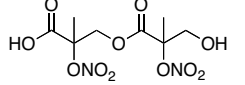
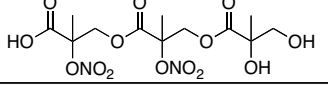
- Henze, D. K., Seinfeld, J. H., Ng, N. L., Kroll, J. H., Fu, T. M., Jacob, D. J., and Heald, C. L.: Global modeling of secondary organic aerosol formation from aromatic hydrocarbons: high- vs. low-yield pathways, *Atmos. Chem. Phys.*, 8, 2405–2420, 2008.
- Iinuma, Y., Boge, O., Kahnt, A., and Herrmann, H.: Laboratory chamber studies on the formation of organosulfates from reactive uptake of monoterpene oxides, *Phys Chem Chem Phys*, 11, 7985–7997, 2009.
- Keywood, M. D., Varutbangkul, V., Bahreini, R., Flagan, R. C., and Seinfeld, J. H.: Secondary organic aerosol formation from the ozonolysis of cycloalkenes and related compounds, *Environ. Sci. Technol.*, 38, 4157–4164, 2004.
- Kleindienst, T. E., Lewandowski, M., Offenberg, J. H., Jaoui, M., and Edney, E. O.: The formation of secondary organic aerosol from the isoprene plus OH reaction in the absence of NO_x , *Atmos. Chem. Phys.*, 9, 6541–6558, 2009.
- Kroll, J. H. and Seinfeld, J. H.: Chemistry of secondary organic aerosol: Formation and evolution of low-volatility organics in the atmosphere, *Atmos. Environ.*, 42, 3593–3624, 2008.
- Kroll, J. H., Ng, N. L., Murphy, S. M., Flagan, R. C., and Seinfeld, J. H.: Secondary organic aerosol formation from isoprene photooxidation, *Environ. Sci. Technol.*, 40, 1869–1877, 2006.
- Lelieveld, J., Butler, T. M., Crowley, J. N., Dillon, T. J., Fischer, H., Ganzeveld, L., Harder, H., Lawrence, M. G., Martinez, M., Taraborrelli, D., and Williams, J.: Atmospheric oxidation capacity sustained by a tropical forest, *Nature*, 452, 737–740, 2008.
- Lim, Y. B. and Ziemann, P. J.: Chemistry of secondary organic aerosol formation from OH radical-initiated reactions of linear, branched, and cyclic alkanes in the presence of NO_x , *Aerosol. Sci. Tech.*, 43, 604–619, 2009.
- Minerath, E. C. and Elrod, M. J.: Assessing the potential for diol and hydroxy sulfate ester formation from the reaction of epoxides in tropospheric aerosols, *Environ. Sci. Technol.*, 43, 1386–1392, 2009.

- Nouaime, G., Bertman, S. B., Seaver, C., Elyea, D., Huang, H., Shepson, P. B., Starn, T. K., Riemer, D. D., Zika, R. G., and Olszyna, K.: Sequential oxidation products from tropospheric isoprene chemistry: MACR and MPAN at a NO_x -rich forest environment in the southeastern United States, *J. Geophys. Res.-Atmos.*, 103, 22 463–22 471, 1998.
- Orlando, J. J., Tyndall, G. S., and Paulson, S. E.: Mechanism of the OH-initiated oxidation of methacrolein, *Geophys. Res. Lett.*, 26, 2191–2194, 1999.
- Paulot, F., Crounse, J. D., Kjaergaard, H. G., Kroll, J. H., Seinfeld, J. H., and Wennberg, P. O.: Isoprene photooxidation: new insights into the production of acids and organic nitrates, *Atmos. Chem. Phys.*, 9, 1479–1501, 2009a.
- Paulot, F., Crounse, J. D., Kjaergaard, H. G., Kurten, A., St Clair, J. M., Seinfeld, J. H., and Wennberg, P. O.: Unexpected epoxide formation in the gas-phase photooxidation of isoprene, *Science*, 325, 730–733, 2009b.
- Presto, A. A., Hartz, K. E. H., and Donahue, N. M.: Secondary organic aerosol production from terpene ozonolysis. 2. Effect of NO_x concentration, *Environ. Sci. Technol.*, 39, 7046–7054, 2005.
- Ren, X. R., Edwards, G. D., Cantrell, C. A., Leshner, R. L., Metcalf, A. R., Shirley, T., and Brune, W. H.: Intercomparison of peroxy radical measurements at a rural site using laser-induced fluorescence and Peroxy Radical Chemical Ionization Mass Spectrometer (PerCIMS) techniques, *J. Geophys. Res.-Atmos.*, 108, 4605, doi:10.1029/2003JD003644, 2003.
- Roberts, J. M. and Bertman, S. B.: The thermal decomposition of peroxyacetic nitric anhydride (PAN) and peroxyethacrylic nitric anhydride (MPAN), *Int. J. Chem. Kinet.*, 24, 297–307, 1992.
- Schichtel, B. A., Malm, W. C., Bench, G., Fallon, S., McDade, C. E., Chow, J. C., and Watson, J. G.: Fossil and contemporary fine particulate carbon fractions at 12 rural and urban sites in the United States, *J. Geophys. Res.-Atmos.*, 113, D02311, doi:10.1029/2007JD008605, 2008.
- Skinner, J., H., W. C., and G.J., C.: Production of epoxides, United States Patent Office, 2, 1958.

- Sorooshian, A., Brechtel, F. J., Ma, Y. L., Weber, R. J., Corless, A., Flagan, R. C., and Seinfeld, J. H.: Modeling and characterization of a particle-into-liquid sampler (PILS), *Aerosol. Sci. Tech.*, 40, 396–409, 2006.
- Surratt, J. D., Murphy, S. M., Kroll, J. H., Ng, N. L., Hildebrandt, L., Sorooshian, A., Szmigielski, R., Vermeylen, R., Maenhaut, W., Claeys, M., Flagan, R. C., and Seinfeld, J. H.: Chemical composition of secondary organic aerosol formed from the photooxidation of isoprene, *J. Phys. Chem. A*, 110, 9665–9690, 2006.
- Surratt, J. D., Kroll, J. H., Kleindienst, T. E., Edney, E. O., Claeys, M., Sorooshian, A., Ng, N. L., Offenberg, J. H., Lewandowski, M., Jaoui, M., Flagan, R. C., and Seinfeld, J. H.: Evidence for organosulfates in secondary organic aerosol, *Environ. Sci. Technol.*, 41, 517–527, 2007a.
- Surratt, J. D., Lewandowski, M., Offenberg, J. H., Jaoui, M., Kleindienst, T. E., Edney, E. O., and Seinfeld, J. H.: Effect of acidity on secondary organic aerosol formation from isoprene, *Environ. Sci. Technol.*, 41, 5363–5369, 2007b.
- Surratt, J. D., Gomez-Gonzalez, Y., Chan, A. W. H., Vermeylen, R., Shahgholi, M., Kleindienst, T. E., Edney, E. O., Offenberg, J. H., Lewandowski, M., Jaoui, M., Maenhaut, W., Claeys, M., Flagan, R. C., and Seinfeld, J. H.: Organosulfate formation in biogenic secondary organic aerosol, *J. Phys. Chem. A*, 112, 8345–8378, 2008.
- Szmigielski, R., Surratt, J. D., Vermeylen, R., Szmigielska, K., Kroll, J. H., Ng, N. L., Murphy, S. M., Sorooshian, A., Seinfeld, J. H., and Claeys, M.: Characterization of 2-methylglyceric acid oligomers in secondary organic aerosol formed from the photooxidation of isoprene using trimethylsilylation and gas chromatography/ion trap mass spectrometry, *J. Mass. Spectrom.*, 42, 101–116, 2007.
- Tuazon, E. C. and Atkinson, R.: A product study of the gas-phase reaction of isoprene with the OH Radical in the presence of NO_x , *Int. J. Chem. Kinet.*, 22, 1221–1236, 1990a.

- Tuazon, E. C. and Atkinson, R.: A product study of the gas-phase reaction of methacrolein with the OH Radical in the presence of NO_x, *Int. J. Chem. Kinet.*, 22, 591–602, 1990b.
- Volkamer, R., Jimenez, J. L., San Martini, F., Dzepina, K., Zhang, Q., Salcedo, D., Molina, L. T., Worsnop, D. R., and Molina, M. J.: Secondary organic aerosol formation from anthropogenic air pollution: Rapid and higher than expected, *Geophys. Res. Lett.*, 33, L17811, doi:10.1029/2006GL026899, 2006.
- Wang, W., Kourtchev, I., Graham, B., Cafmeyer, J., Maenhaut, W., and Claeys, M.: Characterization of oxygenated derivatives of isoprene related to 2-methyltetrols in Amazonian aerosols using trimethylsilylation and gas chromatography/ion trap mass spectrometry, *Rapid Commun. Mass. Sp.*, 19, 1343–1351, 2005.
- Weber, R. J., Sullivan, A. P., Peltier, R. E., Russell, A., Yan, B., Zheng, M., de Gouw, J., Warneke, C., Brock, C., Holloway, J. S., Atlas, E. L., and Edgerton, E.: A study of secondary organic aerosol formation in the anthropogenic-influenced southeastern United States, *J. Geophys. Res.-Atmos.*, 112, D13302, doi:10.1029/2007JD008408, 2007.
- Williams, J., Roberts, J. M., Bertman, S. B., Stroud, C. A., Fehsenfeld, F. C., Baumann, K., Buhr, M. P., Knapp, K., Murphy, P. C., Nowick, M., and Williams, E. J.: A method for the airborne measurement of PAN, PPN, and MPAN, *J. Geophys. Res.-Atmos.*, 105, 28 943–28 960, 2000.

Table 6.1: High-NO_x MPAN SOA Constituents.

Table S1. High-NO _x MPAN SOA Constituents						
	[M – H] [–] ion	UPLC/ESI- TOFMS Measured Mass	TOFMS Suggested Ion Formula	Error (mDa)	i-Fit	Structure ^a
Oligoester Series 1	221	221.0661	C ₈ H ₁₃ O ₇ [–]	1.6	0.3	
	323	323.0979	C ₁₂ H ₁₉ O ₁₀ [–]	0.1	22.6	
	425	425.1290	C ₁₆ H ₂₅ O ₁₃ [–]	-0.5	48.0	
Oligoester Series 2	266	266.0507	C ₈ H ₁₂ NO ₉ [–]	-0.5	32.8	
	368	368.0831	C ₁₂ H ₁₈ NO ₁₂ [–]	0.2	11.4	
	470	470.1149	C ₁₆ H ₂₄ NO ₁₅ [–]	0.3	56.3	
	572	572.1510	C ₂₀ H ₃₀ NO ₁₈ [–]	4.7	1.0	
Oligoester Series 3 ^b	249	249.0616	C ₉ H ₁₃ O ₈ [–]	0.6	2.7	
	351	351.0912	C ₁₃ H ₁₉ O ₁₁ [–]	-1.5	46.9	
	453	453.1248	C ₁₇ H ₂₅ O ₁₄ [–]	0.4	63.7	
Oligoester Series 4 ^c	263	263.0740	C ₁₀ H ₁₅ O ₈ [–]	-2.7	4.7	
	365	365.1061	C ₁₄ H ₂₁ O ₁₁ [–]	-2.3	54.9	
	467	467.1434	C ₁₈ H ₂₇ O ₁₄ [–]	3.3	23.7	
Oligoester Series 5	311	311.0333	C ₈ H ₁₁ N ₂ O ₁₁ [–]	-3.0	58.9	
	413	413.0664	C ₁₂ H ₁₇ N ₂ O ₁₄ [–]	-1.6	71.9	

^a For simplicity, only one isomer is shown.^b This oligoester series involves the esterification with formic acid.^c This oligoester series involves the esterification with acetic acid.

Table 6.2: Summary of experimental conditions for low-NO_x experiments.

HC ^{a,b}	[HC] ₀ (ppb)	OH precursor	Seed Aerosol ^c	Seed volume ($\mu\text{m}^3 \text{ cm}^{-3}$)	RH (%)	SOA volume ($\mu\text{m}^3 \text{ cm}^{-3}$) ^d	SOA mass ($\mu\text{g m}^{-3}$) ^e	injection order
BEPOX	9	none	neutral	^f	4	^f	^f	BEPOX then seed
isoprene	40	H ₂ O ₂	highly acidic	14.5	6	21.3	31.8	all reactants present at start
isoprene	49	H ₂ O ₂	neutral	16.5	12	1.1	1.7	all reactants present at start
BEPOX	7	none	highly acidic	^f	5	^f	^f	BEPOX then seed
3-butene-1,2-diol	100 ^g	none	highly acidic	^f	12	^f	^f	butenediol then seed
BEPOX	^f	none	neutral	9.7	7	0.4	0.9	seed then BEPOX
BEPOX	^f	none	highly acidic	17.9	9	10.2	15.8	seed then BEPOX
butadiene	100 ^g	H ₂ O ₂	highly acidic	^f	11	^f	^f	2.5 hours oxidation then seed

^a HC = hydrocarbon; BEPOX = 2,3-epoxy-1,4-butanediol^b Temperatures = 294-299 K.^c neutral = (NH₄)₂SO₄; highly acidic = MgSO₄ + H₂SO₄^d not corrected for wall loss^e corrected for wall loss, assuming density of 1.4^f not available owing to order of injection^g estimated based on amount injected

Table 6.3: Summary of experimental conditions for high-NO_x experiments.

HC ^{a,b}	[HC] ₀ (ppb)	OH precursor	additional NO _x	[NO] ₀ (ppb)	[NO ₂] ₀ (ppb)	[NO ₂] ₀ /[NO] ₀	RH (%)	seed (μm ³ cm ⁻³)	SOA volume (μm ³ cm ⁻³) ^c	SOA mass (μg m ⁻³) ^d
methacrolein	277	HONO	+NO	725	365	0.5	9	11.4	5.2	10.1
methacrolein	285	HONO	+NO ₂	296	692	2.3	9	12.3	12.8	24.5
methacrolein	257	HONO	+NO	527	407	0.8	9	12.1	8.5	14.4
MPAN ^e		HONO	none	177	260	1.5	9	7.6	66.4	118
MBO	218	H ₂ O ₂	+NO+NO ₂	198	177	0.9	10	11.1	<2	<2
methacrylic acid	100	HONO	none	313	461	1.5	9	12.3	<2	<2
isoprene	523	HONO	none	312	510	1.6	9	10.8	41.7	65.2

^a HC = hydrocarbon; MPAN = methacryloylperoxynitrate; MBO = 2-methyl-3-buten-2-ol

^b Temperatures = 295-296 K

^c not corrected for wall loss

^d corrected for wall loss, assuming density of 1.4

^e not measured

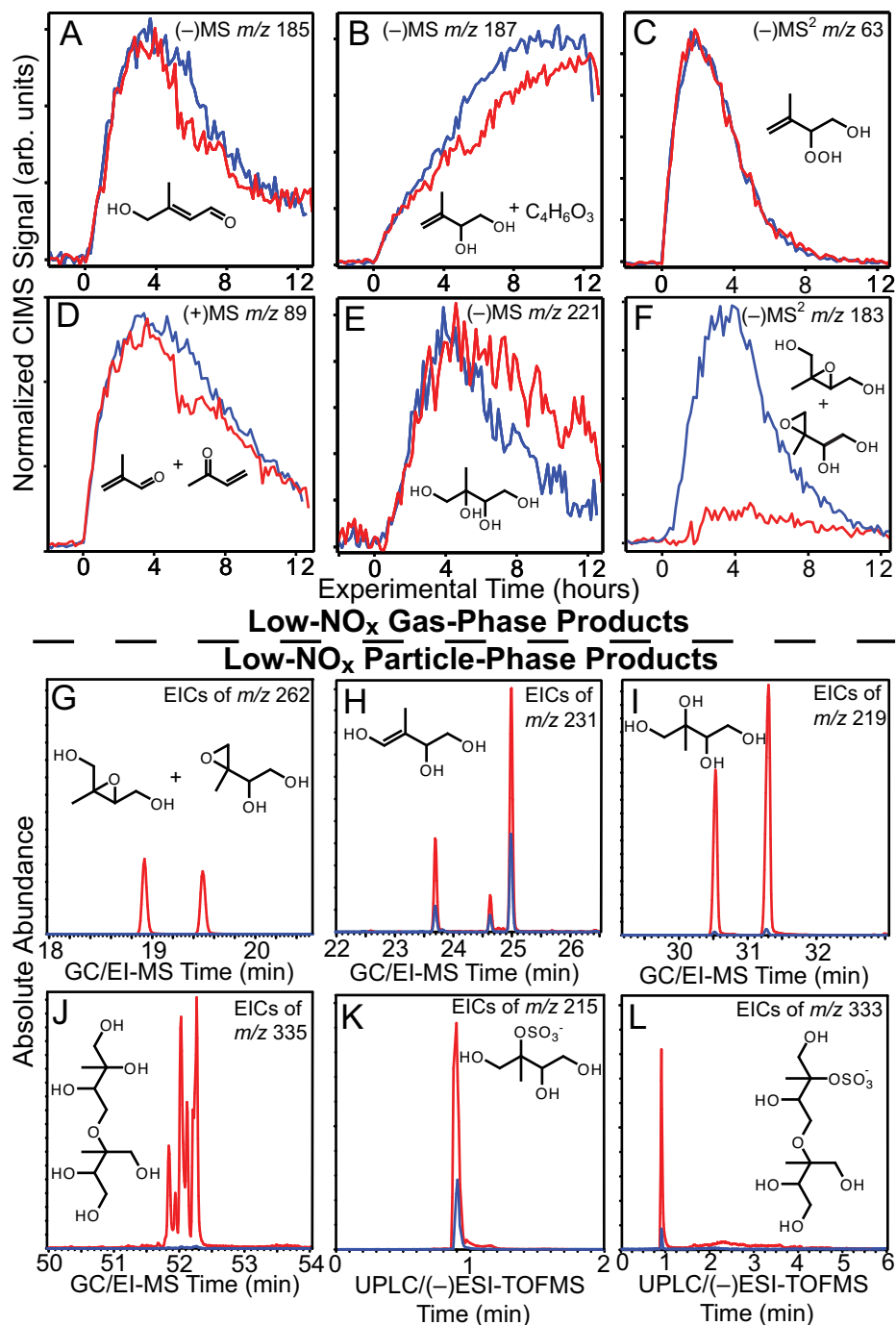


Figure 6.1: Comparison of important gas- and particle-phase products produced from isoprene under low-NO_x conditions in the presence of either neutral (blue lines) or highly acidified (red lines) sulfate seed aerosol. In most cases, only one structural isomer is shown.

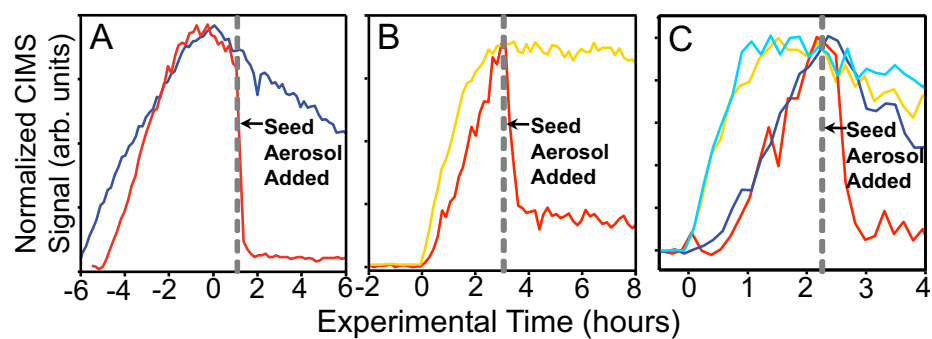


Figure 6.2: (-)CIMS time traces: (A) Reactive uptake of gas-phase BEPOX in the presence of either neutral (blue line) or highly acidified (red line) sulfate seed aerosol under dark conditions. (B) Hydroxy hydroperoxide (orange line) and BEPOX (red line) produced from butadiene under low- NO_x conditions. (C) ISOPOOH (neutral seed = light blue line; highly acidic seed = orange line) and IEPOX (neutral seed = blue line; highly acidic seed = red line) produced from isoprene under low- NO_x conditions. Signals of the IEPOX are normalized to that of the ISOPOOH when lights are turned off.

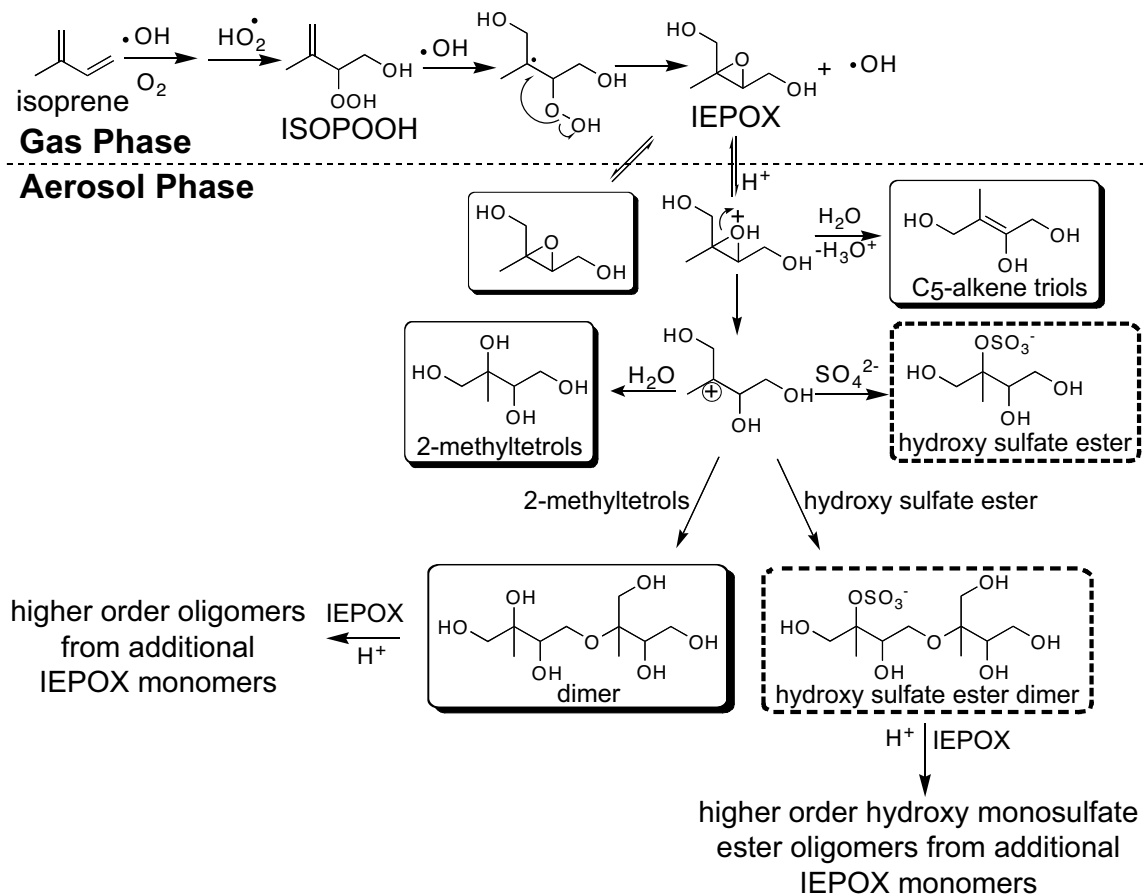


Figure 6.3: Mechanism for the enhancement of SOA formation from isoprene under lower- NO_x conditions due to increased aerosol acidity. SOA constituents in shaded and dashed boxes are observed by GC/MS and UPLC/(-)ESI-TOFMS, respectively. Only the β -IEPOX is considered here, but this also applies to δ -IEPOX.

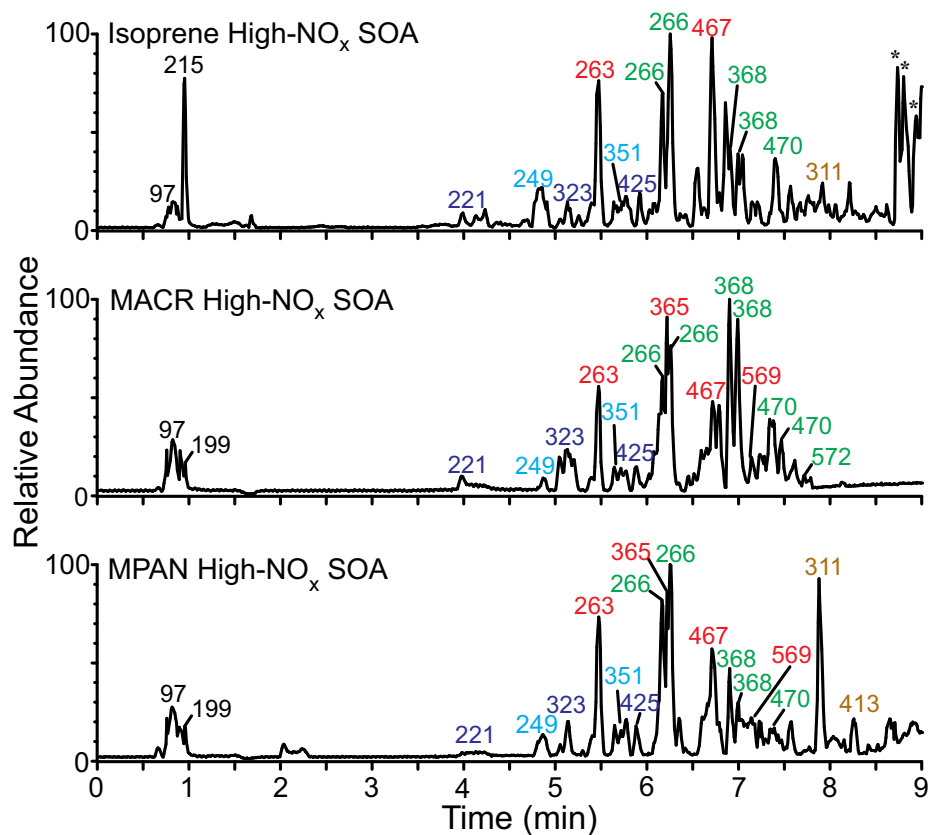


Figure 6.4: UPLC/(-)ESI-TOFMS BPCs. The numbers listed above each peak correspond to the respective $[M-H]^-$ base peak ions. Similar colored $[M-H]^-$ ions are of the same oligoester series (Table 6.1). m/z 97, 199, and 215 correspond to sulfate, an organosulfate of 2-MG (Surratt et al., 2007a), and an organosulfate of 2 methyltetrols (Surratt et al., 2007a,b), respectively.

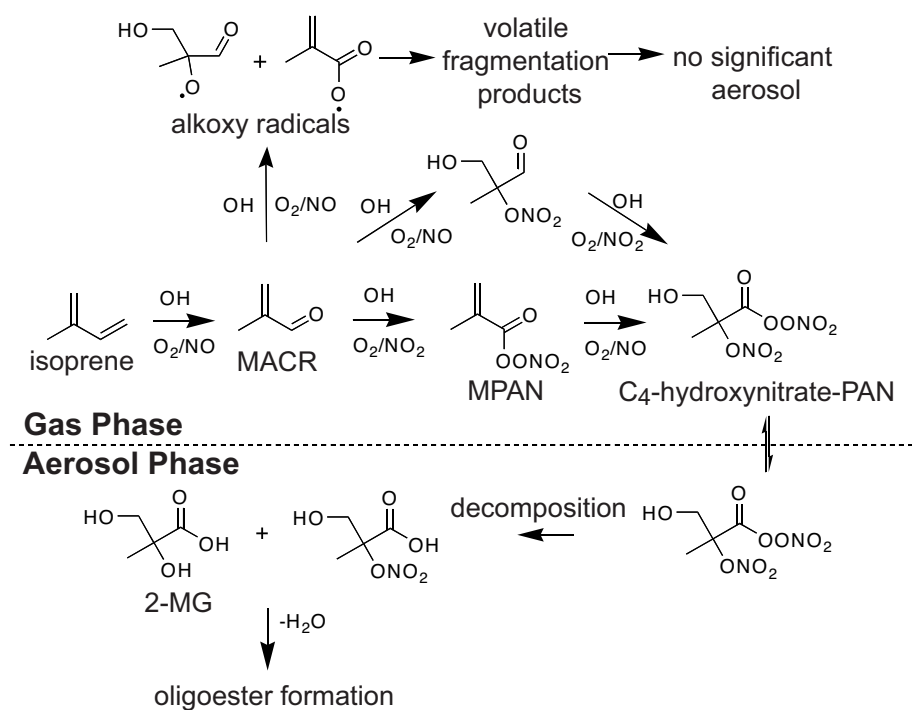


Figure 6.5: Possible chemical mechanism for the formation of isoprene SOA under high- NO_x conditions. Detailed chemical structures of the high- NO_x SOA constituents resulting from the oligoester formation can be found in Table 6.1.

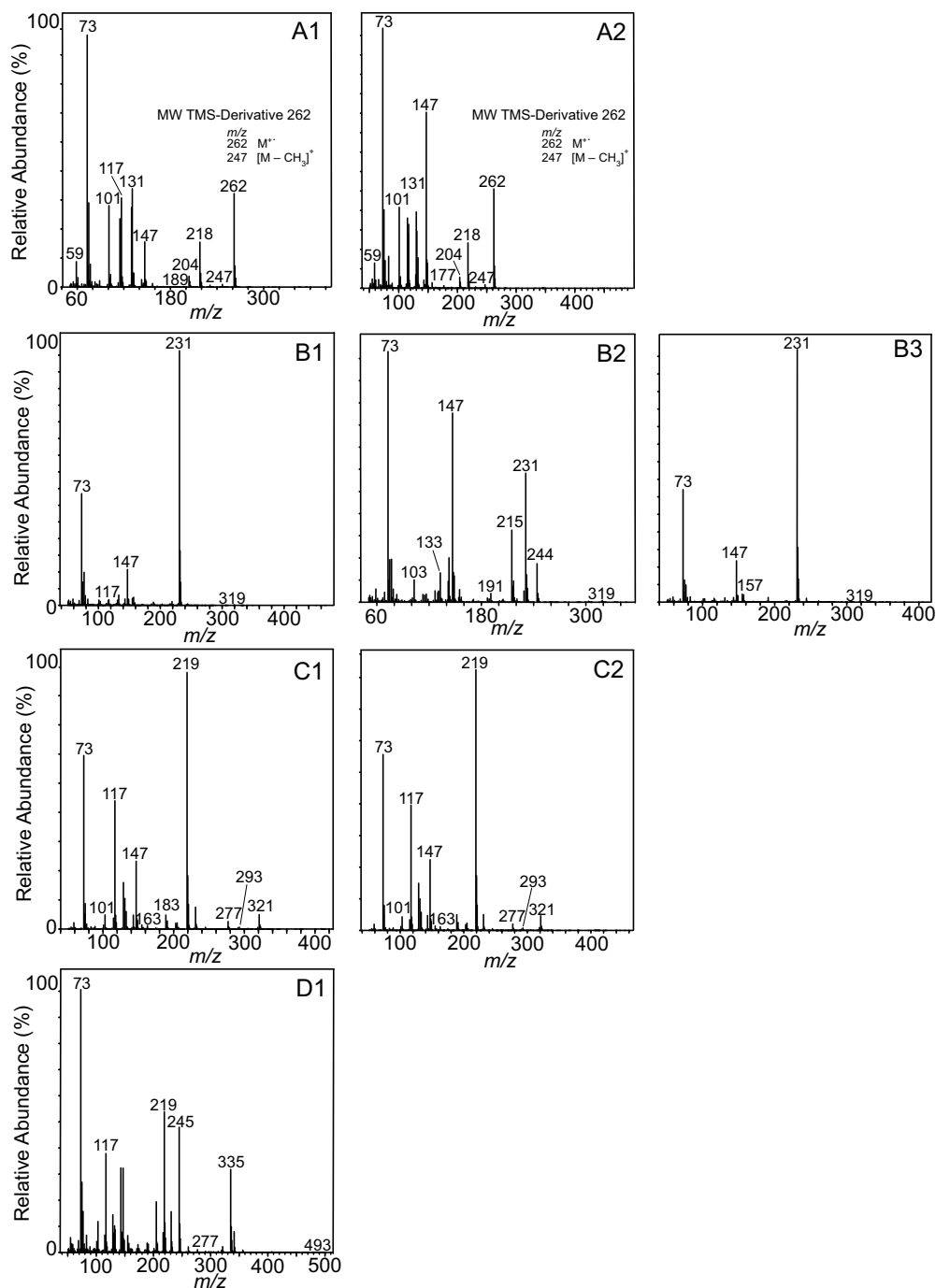


Figure 6.6: GC/EI-MS mass spectra for isoprene low- NO_x SOA constituents formed in the highly acidified sulfate seed aerosol experiment chemically characterized in Fig. 6.6G–J. (A1–A2) Mass spectra corresponding to the IEPOX compounds characterized for the first time in low- NO_x isoprene SOA. (B1–B3) Mass spectra corresponding to the three isomers of the C_5 -alkene triols. (C1–C2) Mass spectra corresponding to the diastereoisomeric 2-methyltetrols. (D1) Averaged mass spectrum corresponding to all 6 major isomers of the previously characterized hemiacetal dimers.

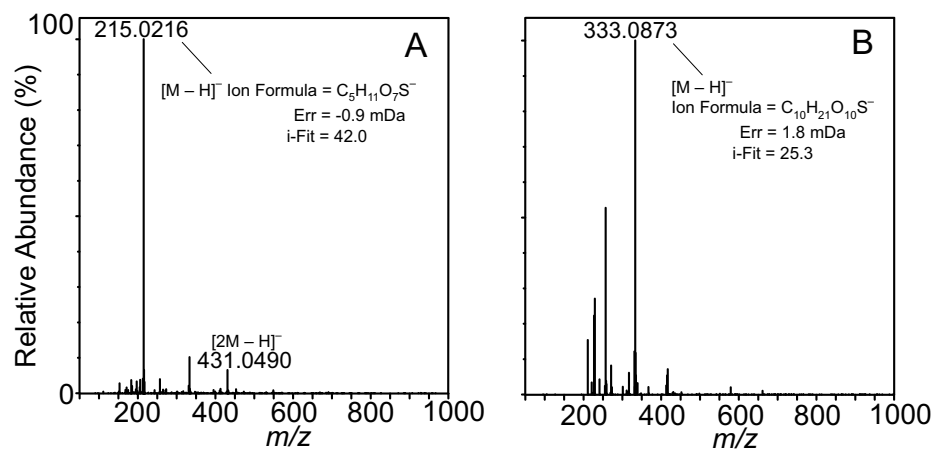


Figure 6.7: UPLC/(-)ESI-TOFMS mass spectra for isoprene low-NO_x SOA constituents formed in the highly acidified sulfate seed aerosol experiment chemically characterized in Fig. 6.6K and Fig. 6.6L, respectively. (A) Mass spectrum corresponding to the organosulfate derivative of the 2-methyltetrols. (B) Mass spectrum corresponding to the organosulfate derivative of the dimer (denoted in prior work as the organosulfate of the hemiacetal dimer). These mass spectra are consistent with prior work (Surratt et al., 2007a; Gómez-González et al., 2008).

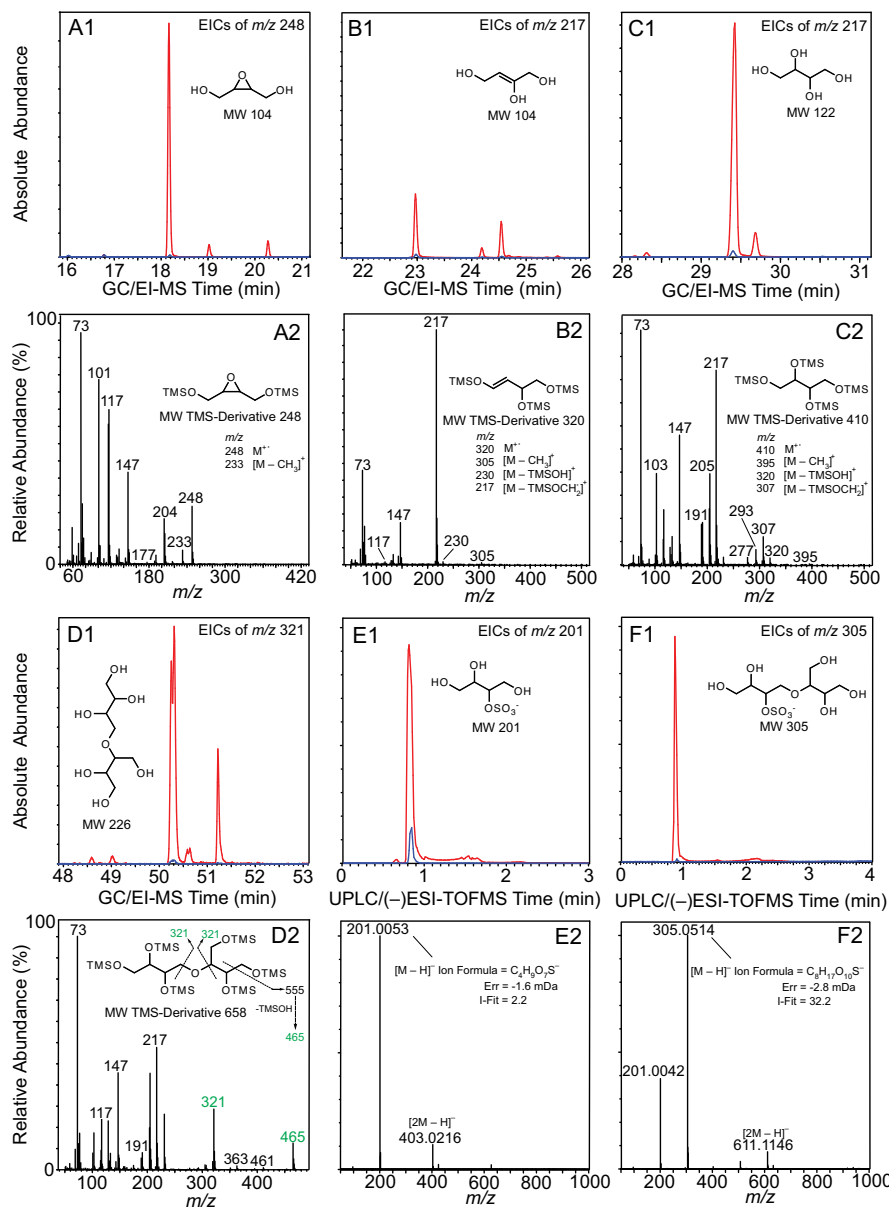


Figure 6.8: (A1–F1) Particle-phase constituents formed from the dark reactive uptake of BEPOX in the presence of either neutral (blue lines) or highly acidic (red lines) sulfate seed aerosol. (A2–F2) Corresponding mass spectra for each chemically characterized particle-phase constituent shown in A1–F1. For simplicity, the mass spectra shown are only those of the most abundant isomers (chromatographic peaks) found in the EICs of A1–F1. All particle-phase constituents shown in A1–F1 are more abundantly formed from the uptake of the BEPOX in the presence of highly acidic sulfate seed aerosol, which is consistent with the low- NO_x isoprene SOA constituents shown in Fig. 6.6. The particle-phase products characterized here were also observed in photooxidation of butadiene under low- NO_x conditions and in the presence of highly acidified sulfate seed aerosol. These data further confirm the role of IEPOX in forming low- NO_x isoprene SOA under acidic conditions.

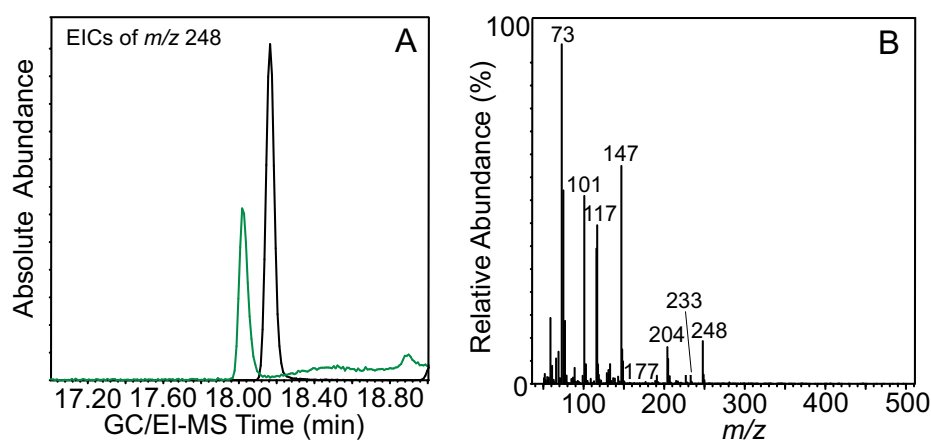


Figure 6.9: (A) GC/MS EICs of m/z 248 from 50 mg of BEPOX dissolved in 0.5 mL of 0.1 M H_2SO_4 in water (green line) and a reactive uptake experiment of BEPOX in the presence of highly acidified sulfate seed aerosol (black line). The two chromatographic peaks differ only slightly in terms of retention time owing to the samples being analyzed by the GC/EI-MS technique on separate days. (B) Corresponding mass spectrum for the chromatographic peak shown in A for the 50 mg BEPOX standard dissolved in 0.5 mL of 0.1 M H_2SO_4 in water (green line). The mass spectrum corresponding to the chromatographic peak shown in A for the reactive uptake experiment of BEPOX in the presence of highly acidified sulfate seed aerosol (black line) is presented in Fig. 6.8A2. This comparison shows that some of the BEPOX remains unreacted in the particle phase and could have resulted there due to semi-volatile partitioning.

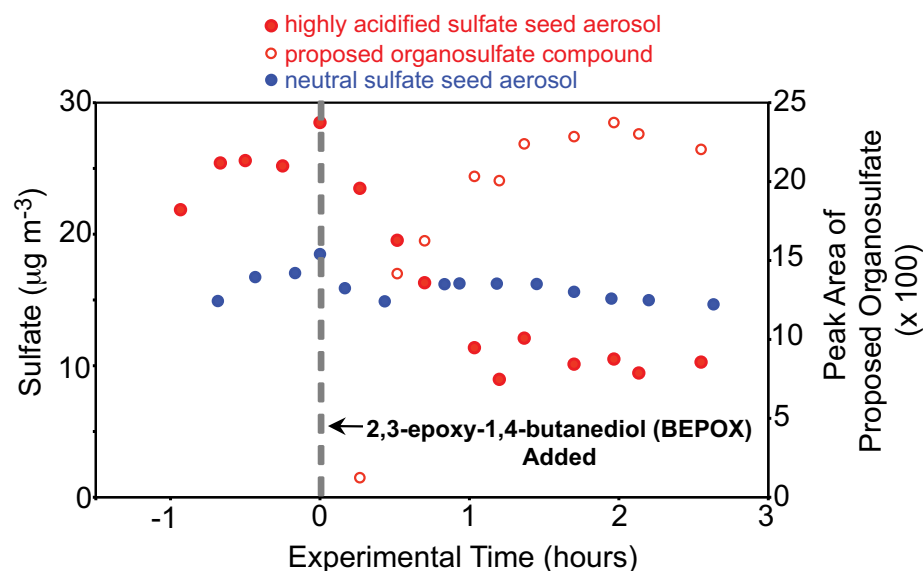


Figure 6.10: PILS/IC time traces of sulfate aerosol mass concentrations observed in experiments examining the reactive uptake of BEPOX in the presence of either neutral or highly acidified sulfate seed aerosol. In addition, a PILS/IC time trace is shown for the peak area of a tentatively assigned organosulfate compound observed only in the SOA formed from the reactive uptake of BEPOX in the presence of highly acidified sulfate seed aerosol. In both the neutral and highly acidified sulfate aerosol experiments, the seed aerosol was injected first and allowed to stabilize. Time zero indicates when the BEPOX was injected. The sulfate aerosol mass concentration decayed by $\sim 58\%$ of its initial loading 1 h after the BEPOX was injected in the presence of highly acidified sulfate seed aerosol. The sulfate aerosol mass concentration remained relatively constant after the injection of BEPOX in the presence of neutral sulfate seed aerosol. The large decay of sulfate mass in the highly acidified sulfate seed aerosol experiment indicates that it is lost due to reaction with BEPOX.

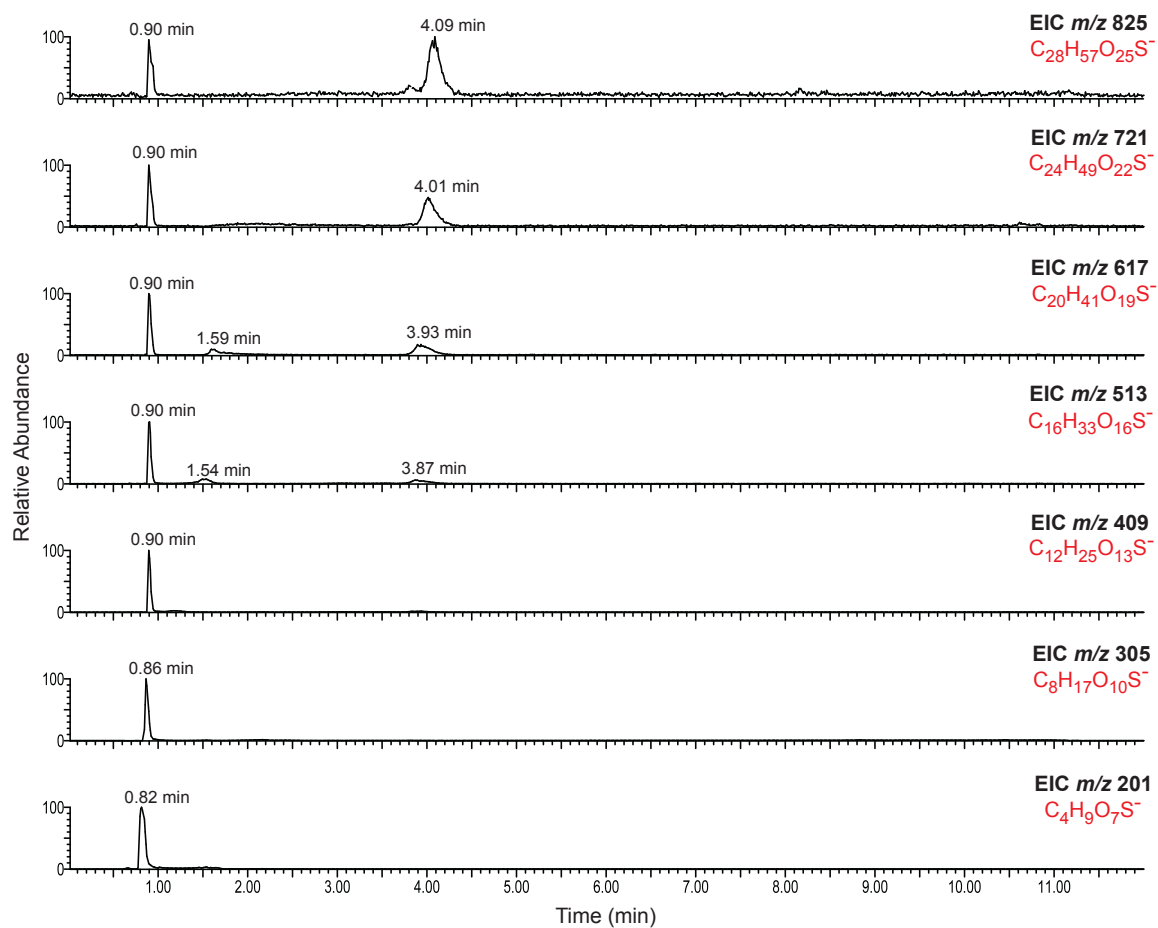


Figure 6.11: UPLC/(-)ESI-TOFMS EICs of organosulfates formed from the reactive uptake of BEPOX in the presence of highly acidified sulfate seed aerosol. EICs of m/z 409 to 825 indicate the formation of high-order (MW) organosulfates. Accurate mass measurements for each observed ion allowed for the determination and verification for the presence of the latter compounds by providing elemental composition (i.e., molecular formula) information. The elemental compositions for each ion are denoted in red. Numbers marked above the chromatographic peaks are the retention times for these compounds.

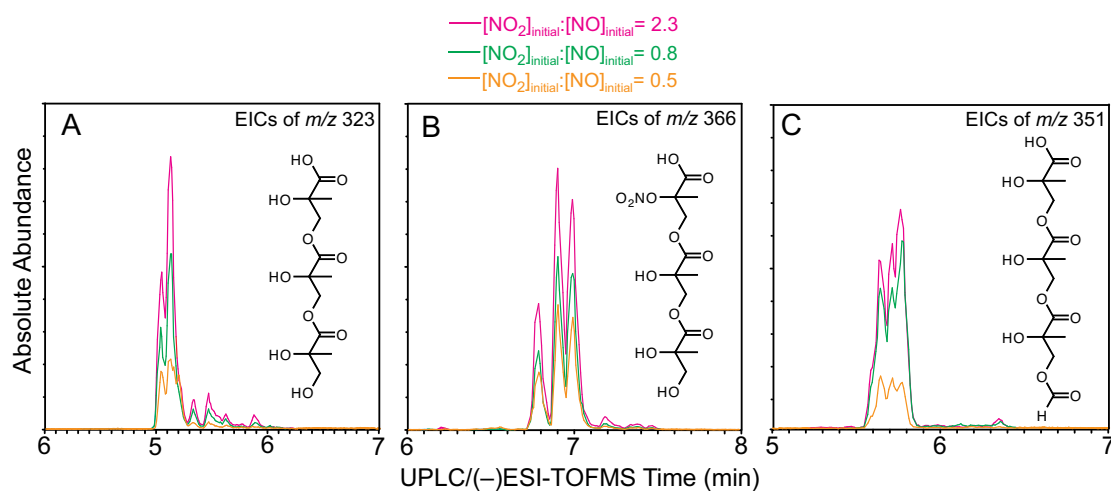


Figure 6.12: UPLC/(-)ESI-TOFMS EICs associated with three major classes of oligoesters previously observed in isoprene high- NO_x SOA (Surratt et al., 2006; Szmigielski et al., 2007). For simplicity, only one structural isomer is shown in each of these EICs. These EICs were obtained from three different experiments in which the photooxidation of the same mixing ratio of MACR was conducted with varying levels of initial $[\text{NO}_2]/[\text{NO}]$ ratio. Increasing the initial $[\text{NO}_2]/[\text{NO}]$ ratio for these high- NO_x MACR experiments shown here results in the enhancement of both the previously characterized high- NO_x SOA constituents and the high- NO_x SOA masses. These enhancements are due to the formation and further reaction of MPAN under high- NO_2 conditions.

Chapter 7

Role of aldehyde chemistry and NO_x concentrations in secondary organic aerosol formation*

*This chapter is prepared for journal submission as "Role of aldehyde chemistry and NO_x concentrations in secondary organic aerosol formation" by A. W. H. Chan, M. N. Chan, J. D. Surratt, P. S. Chhabra, C. L. Loza, J. D. Crounse, L. D. Yee, R. C. Flagan, P. O. Wennberg, J. H. Seinfeld. Copyright 2010 by Authors.

7.1 Abstract

Aldehydes are an important class of products from atmospheric oxidation of hydrocarbons. Isoprene (2-methyl-1,3-butadiene), the most abundantly emitted atmospheric non-methane hydrocarbon, produces a significant amount of secondary organic aerosol (SOA) via methacrolein (a C₄-unsaturated aldehyde) under urban high-NO_x conditions. Previously, we have identified peroxy methacryloyl nitrate (MPAN) as the important intermediate to isoprene and methacrolein SOA in this NO_x regime. Here we show that as a result of this chemistry, NO₂ enhances SOA formation from methacrolein and two other α,β -unsaturated aldehydes, specifically acrolein and crotonaldehyde, a NO_x effect on SOA formation previously unrecognized. Oligoesters of dihydroxycarboxylic acids and hydroxynitrooxycarboxylic acids are observed to increase with increasing NO₂/NO ratio, and previous characterizations are confirmed by both online and offline high-resolution mass spectrometry techniques. Molecular structure also determines the amount of SOA formation, as the SOA mass yields are the highest for aldehydes that are α,β -unsaturated and contain an additional methyl group on the α -carbon. Aerosol formation from 2-methyl-3-buten-2-ol (MBO232) is insignificant, even under high-NO₂ conditions, as PAN (peroxy acyl nitrate, RC(O)OONO₂) formation is structurally unfavorable. At atmospherically relevant NO₂/NO ratios, the SOA yields from isoprene high-NO_x photooxidation are 3 times greater than previously measured at lower NO₂/NO ratios. At sufficiently high NO₂ concentrations, in systems of α,β -unsaturated aldehydes, SOA formation from subsequent oxidation of products from acyl peroxy radicals + NO₂ can exceed that from RO₂ + HO₂ reactions under the same inorganic seed conditions, making RO₂ + NO₂ an important channel for SOA formation.

7.2 Introduction

Organic matter is ubiquitous in atmospheric aerosols and accounts for a major fraction of particulate matter mass (Zhang et al., 2007a). Most particulate organic matter (POM) is secondary in origin, comprising condensable oxidation products of gas-phase volatile organic compounds (VOCs)

(Hallquist et al., 2009). Despite the importance of secondary organic aerosol (SOA), its sources and formation processes are not fully understood. Global modeling studies predict that oxidation of biogenic hydrocarbons dominates the global SOA burden owing to high emissions and efficient SOA production (Chung and Seinfeld, 2002; Kanakidou et al., 2005; Henze and Seinfeld, 2006). This is supported by observations of high levels of modern (hence biogenic) carbon in ambient particulate organic matter, even in urban centers such as Nashville, TN, Tampa, FL, and Atlanta, GA (Lewis et al., 2004; Lewis and Stiles, 2006; Weber et al., 2007). However, field observations have repeatedly shown that SOA formation is highly correlated with anthropogenic tracers, such as CO and acetylene (de Gouw et al., 2005, 2008).

A considerable body of laboratory chamber studies have investigated the dependence of SOA yields (mass of SOA formed per mass of hydrocarbon reacted) on NO_x level, which can vary greatly between urban and remote areas. For photooxidation and ozonolysis of monoterpenes (Hatakeyama et al., 1991; Ng et al., 2007a; Zhang et al., 2007b; Presto et al., 2005), monocyclic (Song et al., 2005; Hurley et al., 2001; Ng et al., 2007b) and polycyclic aromatic compounds (Chan et al., 2009b), SOA yields are larger under low- NO_x conditions; for sesquiterpenes, the reverse is true (Ng et al., 2007a). SOA formation from photooxidation of isoprene exhibits especially complex behavior depending on the NO_x level (Kroll et al., 2006). The effect of NO_x level on SOA formation has generally been attributed to the relative reaction rates of peroxy radicals (RO_2) with NO and HO_2 and the difference in volatilities of the products from the respective pathways (Kroll and Seinfeld, 2008). Under high- NO_x conditions, $\text{RO}_2 + \text{NO}$ dominates and leads to formation of fragmentation products or organic nitrates, which are generally volatile (Presto et al., 2005). On the contrary, the $\text{RO}_2 + \text{HO}_2$ pathway, which is competitive only when $[\text{NO}] \ll 1$ ppb, produces less volatile hydroxyhydroperoxides and peroxy acids, leading to higher SOA yields (Johnson et al., 2005). $\text{RO}_2 + \text{NO}_2$ reactions have not been considered as important for SOA formation due to the short lifetime of peroxy nitrates (< 1 s); the notable exceptions are acyl peroxy nitrates (PANs) and pernitric acid (PNA). As a result, the so-called “high- NO_x ” yields (corresponding to urban NO_x levels) have typically been measured under high-NO conditions. For example, the overall SOA mass yield for isoprene photooxidation

ranges from 1–5% under low-NO_x conditions (Kroll et al., 2006) to 0.2–3% under high-NO_x (high-NO) conditions (Kroll et al., 2005a; Dommen et al., 2006). Owing to the large emissions of isoprene (Guenther et al., 2006), isoprene has been estimated to be the single largest source of SOA globally (Henze and Seinfeld, 2006; Carlton et al., 2009).

In a recent study of the mechanism of SOA formation from isoprene, it was shown that aerosol-phase 2-methylglyceric acid (2-MG) and its oligoesters are produced from methacrolein oxidation through the peroxy methacryloyl nitrate (MPAN) channel, as the SOA from MPAN oxidation is similar in composition to that from high-NO_x oxidation of isoprene and methacrolein (Surratt et al., 2010). Since MPAN is formed from the reversible reaction of methacryloyl peroxy radicals with NO₂, SOA formation can be highly sensitive to the NO₂ concentration, an effect of gas-phase aldehyde chemistry that had previously not been recognized. Given the large emissions and the substantial fraction of isoprene reacting under high-NO_x conditions (a recent modeling study predicts that globally up to two-thirds of isoprene reacts under high-NO_x conditions (Paulot et al., 2009)), it is essential to understand more generally how gas-phase aldehyde chemistry and both NO and NO₂ affect SOA yield and composition. Here we present the results of a systematic study of the effect of NO₂/NO ratio on SOA formation from methacrolein and two other α,β -unsaturated aldehydes, acrolein and crotonaldehyde. In addition, other structurally similar aldehydes and alcohols are studied to provide insight into the reaction mechanism and to establish the role of PAN-type compounds as important SOA intermediates.

7.3 Experimental Section

7.3.1 Experimental protocols

Experiments were carried out in the Caltech dual 28-m³ Teflon chambers. Details of the facilities have been described previously (Cocker et al., 2001; Keywood et al., 2004). Before each experiment, the chambers were flushed with dried purified air for > 24 h (\sim 4–6 air changes), until the particle number concentration < 100 cm⁻³ and the volume concentration < 0.1 μ m³ cm⁻³. In all experiments,

inorganic seed particles were injected by atomization of a 0.015 M aqueous ammonium sulfate solution. The parent hydrocarbon was then introduced into the chamber by injecting a known volume of the liquid hydrocarbon into a glass bulb, and the vapor was carried into the chamber with 5 L min⁻¹ of purified air.

To study the sensitivity of aerosol yields and composition to relative concentrations of NO and NO₂, different OH precursors were used. Use of nitrous acid (HONO) and methyl nitrite (CH₃ONO) as OH precursors allows for SOA yield measurements over a wide range of NO₂/NO ratios. For high NO experiments, OH radicals were generated from photolysis of HONO. HONO was prepared by adding 15 mL of 1 wt% aqueous NaNO₂ dropwise into 30 mL of 10 wt% sulfuric acid in a glass bulb. A stream of dry air was then passed through the bulb, sending HONO into the chamber. During this process, NO and NO₂ formed as side products and were also introduced into the chamber. To achieve high NO₂ concentrations, CH₃ONO was employed as the OH precursor. CH₃ONO was vaporized into an evacuated 500 mL glass bulb and introduced into the chamber with an air stream of 5 L min⁻¹. The mixing ratio of CH₃ONO injected was estimated to be 200–400 ppb, based on the vapor pressure in the glass bulb measured using a capacitance manometer (MKS). In all experiments, varying amounts of NO and NO₂ were also added from gas cylinders (Scott Marrin) both to ensure high-NO_x conditions and to vary the NO₂/NO ratio. For the C₅ unsaturated aldehydes and methylbutenols (MBO), only high NO₂ experiments were conducted. Abbreviations, structures, and OH rate constants (Atkinson and Arey, 2003; Magneron et al., 2002; Tuazon et al., 2005; Fantechi et al., 1998) of the compounds studied are listed in Table 7.1, and initial conditions of the experiments are summarized in Table 7.2.

7.3.2 Materials

The parent hydrocarbons studied and their stated purities are as follows: isoprene (Aldrich, 99%), methacrolein (Aldrich, 95%), acrolein (Fluka, ≥99%), crotonaldehyde (Aldrich, 98%, predominantly *trans*), trans-2-pentenal (Alfa Aesar, 96%), 4-pentenal (Alfa Aesar, 97%), trans-2-methyl-2-butenal (Aldrich, 96+%), 3-methyl-2-butenal (Sigma-Aldrich, 97%), 2-methyl-3-buten-1-ol (Aldrich, 98%),

and 2-methyl-3-buten-2-ol (Aldrich, 98%). CH_3ONO was synthesized following the method described by Taylor et al. (1980). 9 g of NaNO_2 was added to a mixture of 50 mL of methanol and 25 mL of water. 25 mL of 50 wt% sulfuric acid solution was added dropwise into the solution. The CH_3ONO vapor was carried in a small stream of ultra high purity N_2 through a concentrated NaOH solution and an anhydrous CaSO_4 trap to remove any sulfuric acid and water, respectively. The CH_3ONO was then collected in a cold trap immersed in a dry ice/acetone bath (-80°C) and stored under liquid N_2 temperature.

7.3.3 Measurements

Aerosol size distribution, number and volume concentrations were measured with a differential mobility analyzer (DMA, TSI, 3081) coupled with a condensation nuclei counter (TSI, CNC-3760). The volume concentration was corrected for particle wall loss by applying size-dependent first-order loss coefficients, obtained in a separate seed-only experiment, using methods described in Keywood et al. (2004). Aerosol volume concentrations are converted to mass concentrations assuming a density of 1.4 g cm^{-3} (Kroll et al., 2005a). Concentrations of isoprene, methacrolein, methyl vinyl ketone (MVK), acrolein, and crotonaldehyde were monitored using a gas chromatograph with flame ionization detector (GC/FID, Agilent 6890N), equipped with an HP-PLOT Q column ($15 \text{ m} \times 0.53 \text{ mm ID} \times 30 \text{ } \mu\text{m}$ thickness, J&W Scientific). For 2M2B, 3M2B, 2-pentenal, 4-pentenal, MBO231 and MBO232 experiments, the GC/FID was equipped with an HP-5 column ($15 \text{ m} \times 0.53 \text{ mm ID} \times 1.5 \text{ } \mu\text{m}$ thickness, Hewlett Packard). A commercial chemiluminescence NO/NO_x analyzer (Horiba, APNA 360) was used to monitor NO and NO_x . Both HONO and CH_3ONO produce interference on the NO_2 signal from the NO_x monitor. Concentrations of NO and NO_2 are estimated by photochemical modeling (see Appendix). Temperature, RH, and ozone (O_3) were continuously monitored.

A custom-modified Varian 1200 triple-quadrupole chemical ionization mass spectrometer (CIMS) was used to continuously monitor gas-phase species over each experiment. Details of the operation of the CIMS can be found in a number of previous reports (Crounse et al., 2006; Paulot et al.,

2009). The CIMS was operated in negative ion mode, in which CF_3O^- is used as the reagent ion, and in positive ion mode of proton transfer mass spectrometry (PTR-MS). In the negative mode, the reagent ion CF_3O^- clusters with the analyte, R, forming ions at mass-to-charge ratios (m/z) $\text{MW} + 85$ ($\text{R} \cdot \text{CF}_3\text{O}^-$), or, with more acidic species, at m/z $\text{MW} + 19$ ($\text{HF} \cdot \text{R}_{-\text{H}}^-$). In the positive mode, positively charged water clusters, $n(\text{H}_2\text{O})\text{H}^+$, react via proton transfer with the analyte, R, to form the positively charged ion, $\text{R} \cdot n(\text{H}_2\text{O}) \cdot \text{H}^+$. In some cases, tandem mass spectrometry (MS/MS) was used to separate isobaric compounds. In brief, the parent ions selected in the first quadrupole undergo collision-induced dissociation (CID) in the second quadrupole. The parent ions of isobaric compounds can exhibit different CID patterns and yield different daughter ions. Hence, with the third quadrupole acting as a second mass filter for the daughter ions, this allows for separate measurement of these isobaric compounds (see Supplementary Material). The significance of this separation will be discussed in a later section.

Real-time particle mass spectra were collected continuously by an Aerodyne High Resolution Time-of-Flight Aerosol Mass Spectrometer (DeCarlo et al., 2006; Canagaratna et al., 2007), hereby referred to as the AMS. The AMS switched once every minute between the high resolution “W-mode” and the lower resolution, higher sensitivity “V-mode”. The “V-mode” data were analyzed using a fragmentation table to separate sulfate, ammonium, and organic spectra and to time-trace specific mass-to-charge ratios. “W-mode” data were analyzed using a separate high-resolution spectra toolbox known as PIKA to determine the chemical formulas contributing to distinct m/z ratios (DeCarlo et al., 2006).

Aerosol samples were also collected on Teflon filters and analyzed by offline mass spectrometry. Detailed sample collection and extraction protocol are described in Surratt et al. (2008). Filter extraction using 5 mL of high-purity methanol (i.e., LC-MS Chromasolv Grade) was performed by 45 min of sonication. The filter extracts were then analyzed by a Waters ACQUITY ultra performance liquid chromatography (UPLC) system, coupled with a Waters LCT Premier TOF mass spectrometer equipped with an ESI source operated in the negative (–) mode, allowing for accurate mass measurements (i.e., determination of molecular formulas) to be obtained for each

observed ion. Operation conditions and parameters for the UPLC/(-)ESI-TOFMS measurement have been described by Surratt et al. (2008).

7.4 SOA Formation

The importance of isoprene as an SOA source was suggested by identification of 2-methyltetrols and 2-methylglyceric acid (2-MG) in both ambient POM (Claeys et al., 2004; Edney et al., 2005; Ion et al., 2005; Kourtchev et al., 2005) and laboratory aerosol generated from isoprene photooxidation (Edney et al., 2005; Surratt et al., 2006; Szmigielski et al., 2007; Kleindienst et al., 2009). Methacrolein, a first-generation oxidation product of isoprene, has been shown to produce SOA upon further oxidation (Kroll et al., 2006; Surratt et al., 2006) and has been identified as the precursor to aerosol-phase 2-MG and its corresponding oligoester products (Surratt et al., 2006; Szmigielski et al., 2007). A recent study shows aerosol formation from methacrolein oxidation proceeds via subsequent oxidation of MPAN (Surratt et al., 2010). Here we focus our attention on photooxidation of methacrolein under high- NO_x conditions to establish the effect of relative NO and NO_2 concentrations on SOA yields and composition. Acrolein, crotonaldehyde, 2-methyl-2-butenal (2M2B), 3-methyl-2-butenal (3M2B), 2-pentenal, and 4-pentenal differ from methacrolein by one or two methyl groups, and studying their SOA formation provides insight into the mechanism of formation of low-volatility products. Furthermore, aerosol formation from photooxidation of 2-methyl-3-buten-2-ol (MBO232), an atmospherically important unsaturated alcohol (Harley et al., 1998), and structurally similar 2-methyl-3-buten-1-ol (MBO231) is studied to investigate the role of PAN-like compounds in SOA formation.

7.4.1 Methacrolein

Figures 7.1 and 7.2 show typical concentration profiles of various gas-phase species in methacrolein/HONO (high NO) and methacrolein/ CH_3ONO (high NO_2) photooxidation experiments, respectively. In all experiments, NO concentrations remain above 50 ppb during SOA growth, at which conditions $\text{RO}_2 + \text{HO}_2$ or $\text{RO}_2 + \text{RO}_2$ reactions are not competitive with those of RO_2 with NO and NO_2 .

Products of these reactions, such as methacrylic acid and methacrylic peracid, are not observed by CIMS. Instead, hydroxyacetone and methacrolein nitrate, products from $\text{RO}_2 + \text{NO}$ reactions, are observed. During these experiments, RO_2 and HO_2 produced from methacrolein oxidation react with NO to produce NO_2 , which photolyzes to form ozone. As a result, ozone concentrations reach a maximum of up to 126 ppb. Despite relatively high levels of ozone, reaction rates of methacrolein and peroxy methacryloyl nitrate (MPAN) with ozone are still slow compared to those with OH, as efficient photolysis of HONO or CH_3ONO leads to OH concentrations $> 3 \times 10^6 \text{ molec cm}^{-3}$, estimated from the methacrolein decay. For high-NO experiments, the initial decay of methacrolein slows down after 5 h, consistent with the HONO signal (CIMS $(-)$ m/z 66) approaching zero. In these experiments, more than 70% of the initial methacrolein is consumed before SOA growth ceases. In the high- NO_2 experiments, more than 90% of the initial methacrolein is consumed before SOA growth ceases.

Mass concentrations of SOA versus the concentration of methacrolein reacted, so-called “time-dependent growth curves”, are shown in Fig. 7.3. As reported previously, under high-NO conditions (with HONO as the OH precursor), when additional NO is added before irradiation, aerosol formation (mass yield of 1.9 %) from photooxidation of 277 ppb of methacrolein is suppressed (Surratt et al., 2010). In contrast, SOA yields are higher when no additional NO is added (3.0% from 257 ppb methacrolein), and the highest when 350 ppb of additional NO_2 (instead of NO) is injected (5.2% from 285 ppb methacrolein) (Surratt et al., 2010). In all high-NO experiments, the NO_2/NO ratio remains low (< 2), owing to presence of NO impurity in HONO synthesis and production of NO during HONO photolysis. The observed dependence of SOA yields on NO_2/NO ratio is not a result of condensation of nitric acid from $\text{OH} + \text{NO}_2$, as the experiments were conducted under dry ($< 10\% \text{ RH}$) conditions. In confirmation of this conclusion, addition of gas-phase nitric acid in one experiment (09/07/31) did not lead to additional aerosol growth.

In the high- NO_2 experiments, CH_3ONO was used as the OH precursor and lower NO concentrations are expected, owing to relatively pure CH_3ONO synthesis and no net production of NO from CH_3ONO photolysis (see Appendix). Higher SOA yields are observed at higher NO_2/NO ratios; cor-

respondingly, much lower concentrations of methacrolein are required to produce the same amount of SOA (see Fig. 7.3). Also, owing to the high concentrations of CH_3ONO injected, more than 90% of the initial methacrolein is consumed before CH_3ONO is depleted. For example, when 255 ppb of initial methacrolein is oxidized using CH_3ONO as OH precursor (09/09/12), the SOA yields are more than 5 times larger than when a similar amount of methacrolein is reacted using HONO as OH precursor. This rules out a larger extent of reaction as the cause of the high observed SOA yields. HO_2 concentrations quantified from the pernitric acid signal on the CIMS ($(-)$ m/z 98) and modelled NO_2 concentrations do not exceed 60 ppt in all experiments. At organic loadings between 10–20 $\mu\text{g m}^{-3}$, SOA mass yields of methacrolein/high- NO_2 and methacrolein/high-NO photooxidation are roughly 0.19 and 0.03, respectively.

7.4.2 Acrolein and crotonaldehyde

Figures 7.4 and 7.5 show SOA growth curves for acrolein and crotonaldehyde photooxidation, respectively. The SOA yields of these compounds are lower than those of methacrolein, with maximum yields of roughly 0.08 at the highest loadings ($> 100 \mu\text{g m}^{-3}$). These compounds exhibit a similar dependence of SOA growth on NO_2/NO ratio to that of methacrolein: SOA formation is suppressed with addition of NO, and enhanced with addition of NO_2 . SOA yields are highest in the high- NO_2 experiments. Oxidation products analogous to those found in the methacrolein system, such as glycolaldehyde and hydroxynitrates, are observed in the gas phase at similar yields.

7.4.3 Other aldehydes and methylbutenols (MBO)

The growth curves for 2M2B and 3M2B photooxidation are shown in Fig. 7.6. Significant SOA growth is observed for 2M2B (277 ppb) photooxidation under high- NO_2 conditions, with mass yields exceeding 0.35. Similar to methacrolein, 2M2B contains a methyl group in the α -position. Interestingly, photooxidation of 3M2B under similar NO_x conditions and hydrocarbon loadings (207 ppb), produces less SOA (mass yield < 0.01). 3M2B is a structural isomer of 2M2B with the methyl group in the β -position. The trend in SOA yields between 2M2B and 3M2B is consistent with that

observed for methacrolein and crotonaldehyde, their C₄ analogs. The SOA yields from 2-pentenal, a straight-chain α,β -unsaturated aldehyde, are higher than those from 4-pentenal, in which the olefinic bond is not adjacent to the aldehyde group (see Fig. 7.6).

We also carried out MBO232 and MBO231 photooxidation under high-NO₂ conditions. Both MBO's are structurally similar to isoprene and, upon high-NO_x photooxidation, produce an aldehyde (i.e., hydroxy-methylpropanal, HMPR) analogous to methacrolein. Previous results have shown that aerosol formation from MBO232 photooxidation under high-NO conditions is low (Carrasco et al., 2007; Chan et al., 2009a), and here we do not observe SOA growth even at high NO₂/NO ratios. Gas-phase compounds such as glycolaldehyde and HMPR are observed at yields consistent with those published in previous product studies (Carrasco et al., 2007; Chan et al., 2009a). On the other hand, MBO231, a structural isomer with the hydroxyl group in the 1-position, produces a significant amount of SOA (0.8 – 4.2%) upon oxidation under high-NO₂ conditions, comparable to that of isoprene under similar conditions (see Fig. 7.6). Under high-NO conditions, no SOA is formed. To first order, the dependence of SOA yields from MBO231 on NO₂/NO ratio is consistent with that observed in unsaturated aldehydes.

7.5 Chemical Composition of SOA

7.5.1 Offline chemical analysis

In previous work, offline chemical analysis of SOA from photooxidation of isoprene, methacrolein, and MPAN by UPLC/(-)ESI-TOFMS has been presented (Surratt et al., 2010). The same compounds are detected in the methacrolein experiments in this work under both high-NO and high-NO₂ conditions, and are summarized in Table 7.3. Four series of oligoester products from 2-methylglyceric acid (2-MG) and C₄-hydroxynitrooxycarboxylic acid are identified in the SOA. The compounds in the 2-MG oligoester series differ by 102 Da, corresponding to esterification of a 2-MG monomer unit (Surratt et al., 2006). The accurate masses of the identified ions confirm their elemental compositions, and their structures are proposed based on detailed characterization by tandem MS and

GC/MS analyses with prior trimethylsilylation (Szmigielski et al., 2007).

All ions detected by UPLC/(-)ESI-TOFMS in acrolein and crotonaldehyde SOA are listed in the Tables 7.4 and 7.5. It is noteworthy that the identities of detected aerosol-phase products are the same regardless of the OH precursor used. The ions detected in acrolein SOA differ from those found in methacrolein SOA by one methyl group for every monomer unit, and those detected in crotonaldehyde SOA have the same exact mass and elemental composition as those in methacrolein SOA. Detected $[M-H]^-$ ions in SOA from 2M2B and 2-pentenal can also be found in Tables 7.6 and 7.7. No filter sample was collected for 3M2B owing to low aerosol loading. Aerosol-phase products of methacrolein, acrolein, crotonaldehyde, 2M2B, and 2-pentenal are structural analogs of each other, and the structures for the deprotonated ions are proposed based on those characterized previously in isoprene and methacrolein SOA (Surratt et al., 2006; Szmigielski et al., 2007). Interestingly, SOA produced from 4-pentenal is composed of entirely different products, and hence no structures are proposed at this time. The significance of this result will be discussed in a later section.

While the identities of the detected aerosol-phase compounds are independent of the OH precursor, the relative amounts vary greatly and exhibit a strong correlation with NO_2/NO ratio. Figure 7.7 shows the extracted ion signals for the oligoester products detected by UPLC/(-)ESI-TOFMS in the methacrolein high- NO experiments. The amount of identified aerosol-phase components shows the same dependence on NO_2/NO ratio as the total amount of SOA growth. In general, the abundance of each compound decreases when NO is added and increases when NO_2 is added.

7.5.2 Online AMS measurements

AMS V-mode organic spectra of SOA from high- NO_2 photooxidation of isoprene and methacrolein are shown in Fig. 7.8. The mass fragments above m/z 200 likely contain more than 5 carbon atoms, and display a repetitive pattern, indicative of oligomer formation. In addition, 102 Da differences between major peaks were also observed, consistent with previous AMS and LC/MS results (Surratt et al., 2006). Elemental formulas based on accurate mass measurements are determined from high-resolution W-mode data for a number of the major ion peaks observed, as shown in Fig. 7.9. They

correspond to loss of an O^{2-} group from many of the ions detected by UPLC/(-)ESI-TOFMS, confirming their molecular identities (see Table 7.3). The agreement between online and offline high-resolution mass spectrometry confirms that the oligoesters identified are indeed present in the SOA, and that the observations by offline aerosol analysis are not the result of filter sampling artifacts. AMS organic spectra of SOA from oxidation of acrolein and crotonaldehyde show similar features, and accurate mass measurements of a number of the major peaks correspond to the products analogous to the methacrolein system (see Tables 7.4 and 7.5).

7.6 Effect of NO_2/NO Ratios on SOA Yield and Composition

The effect of NO_x concentrations on SOA formation has been the subject of a number of studies (Hatakeyama et al., 1991; Hurley et al., 2001; Presto et al., 2005; Song et al., 2005; Ng et al., 2007a; Zhang et al., 2007b; Ng et al., 2007b; Chan et al., 2009b). For most systems, SOA yields have been shown to be inversely correlated with NO_x concentrations. Under high- NO_x conditions, RO_2 radicals from hydrocarbon oxidation react primarily with NO, resulting in relatively high-volatility organic nitrates and fragmentation products. Vapor pressure calculations show that hydroxyhydroperoxides and carboxylic acids, which dominate the products formed from $\text{RO}_2 + \text{HO}_2$ reactions, have relatively low volatilities (Johnson et al., 2005). As a result, the “ NO_x effect” on SOA formation has been described as a competition of the chemistries for RO_2 between HO_2 (the high-yield pathway) and NO (the low-yield pathway), such that the ratio of HO_2 to NO is critical in determining the branching ratio between these two pathways (Kroll and Seinfeld, 2008; Henze et al., 2008). An exception to this effect is the sesquiterpenes, for which, under high- NO_x conditions, alkoxy radicals preferentially isomerize to form low-volatility multifunctional products (Ng et al., 2007a).

Aerosol yields from isoprene photooxidation are also sensitive to HO_2/NO ratios, with higher yields measured under HO_2 -dominated conditions (using H_2O_2 as OH source) (Kroll et al., 2006) than under NO-dominated conditions (using HONO or NO_x cycling as OH source) (Kroll et al., 2005b; Pandis et al., 1991; Dommen et al., 2006). Addition of NO also suppresses SOA growth in low- NO_x experiments, indicating that the $\text{RO}_2 + \text{NO}$ pathway yields more volatile products, and

hence less SOA (Kroll et al., 2006). However, under the experimental conditions in the present study, $\text{RO}_2 + \text{HO}_2$ reactions are not expected to be significant. Rather, the dependence of SOA yield on the NO_2/NO ratio is consistent with analysis of SOA composition, which is consistent with MPAN, a product of the acyl peroxy radical + NO_2 reaction, being the intermediate in SOA formation.

Based on the proposed mechanism shown in Fig. 7.10, the acyl peroxy radical formed from abstraction of the aldehydic hydrogen atom of an unsaturated aldehyde reacts with either NO or NO_2 . The reversible reaction of RO_2 with NO_2 forms a PAN-type compound (MPAN for methacrolein), which, in the absence of competing reactions, reaches thermal equilibrium. The irreversible reaction of RO_2 with NO leads to fragmentation into CO_2 and a vinyl radical, which subsequently forms volatile gas-phase products, such as formaldehyde and CO (Orlando et al., 1999). At $[\text{OH}] = 2 \times 10^6 \text{ molec cm}^{-3}$, the reaction of MPAN with OH has a rate comparable to that of thermal decomposition (Orlando et al., 2002), and leads to formation of aerosol products. Hence, the SOA formation potential for this system depends critically on the NO_2/NO ratio. High NO_2/NO ratios shift the thermal equilibrium towards the unsaturated PAN, and SOA formation increases as the fraction of PAN reacting with OH radicals increases. At low NO_2/NO ratios, acyl peroxy radicals react predominantly with NO, leading to relatively volatile products.

Previous measurements of isoprene SOA yields under high- NO_x conditions have been carried out using photolysis of HONO (Kroll et al., 2005a) or the recycling of HO_x and NO_x to generate OH (so-called classical photooxidation) (Pandis et al., 1991; Dommen et al., 2006). Low SOA yields were observed as NO concentrations remained high during the experiments. In fact, SOA growth occurred only after NO concentrations decreased to less than 10 ppb (Kroll et al., 2005a; Dommen et al., 2006). It was proposed that after NO has been consumed, aerosol formation commences as the $\text{RO}_2 + \text{HO}_2$ pathway becomes competitive. However, such a mechanism is inconsistent with the major differences in composition observed between high- and low- NO_x SOA products. High- NO_x SOA from isoprene photooxidation is dominated by esterification products of C_4 -carboxylic acids, whereas under low- NO_x conditions, SOA is dominated by peroxides and C_5 -tetrols (Surratt et al., 2006). It is more likely that the decrease in NO concentration (and increase in NO_2 concentration)

leads to a transition from an RO_2+NO dominated regime to an RO_2+NO_2 dominated regime, resulting in significant SOA formation via the MPAN route.

At NO_2/NO ratios (between 3 and 8) higher than in previous studies (and more relevant to urban conditions), SOA yields from isoprene are approximately 3 times larger than previously measured. The yields even exceed those under low- NO_x conditions at the same organic aerosol loadings, as shown in Fig. 7.11. This is, in fact, consistent with observations from Kroll et al. (2006) that at very low NO_x concentrations, addition of NO actually increases SOA yield. It is likely that under very low NO concentrations, the NO_2/NO ratio increases rapidly, as NO is quickly converted to NO_2 . SOA yields are therefore higher than those in the absence of NO, as RO_2 (from methacrolein)+ NO_2 forms SOA more efficiently than RO_2 (from isoprene)+ HO_2 . However, further increasing NO decreases the NO_2/NO ratio. RO_2 (from methacrolein)+NO becomes more dominant, forms volatile products, and leads to a decrease in SOA yield. It must be noted that the effect of RO_2 radical chemistry on SOA formation is complex and can be unique to different systems (Kroll and Seinfeld, 2008). Also, the acidity of the inorganic seed can increase SOA yields significantly: Surratt et al. (2010) shows that SOA yields from isoprene low- NO_x photooxidation can be as high as 0.29. Detailed knowledge of the chemical mechanism is required to predict the effect of NO_x conditions on SOA production.

7.7 Role of PAN in SOA Formation

7.7.1 Unsaturated aldehydes

One can infer from the shapes of the growth curves the relative timescales of the reaction steps of SOA formation. In all high- NO_2 experiments, a greater extent of reaction is achieved than in high-NO experiments, and SOA formation continues after the parent hydrocarbon is completely consumed; this behavior is characterized by a vertical portion (“hook”) at the end of the SOA growth curve. The presence of this vertical portion indicates that SOA formation results from further reaction of first-generation products, which is the rate-limiting step in the mechanism (see Figs. 7.3–7.5). This observation is consistent with our previous results showing that first-generation

products of methacrolein, such as hydroxyacetone and MPAN, are themselves still volatile (Surratt et al., 2010). SOA is instead formed from the further OH reaction of MPAN, which has a comparable rate coefficient to that of methacrolein (Orlando et al., 2002).

Formation of dihydroxycarboxylic acids (e.g., 2-MG), hydroxynitrooxycarboxylic acids, and corresponding oligoesters appears to be important SOA formation pathways for the five α, β -unsaturated aldehydes studied here (methacrolein, acrolein, crotonaldehyde, 2M2B, and 2-pentenal). All of the SOA constituents detected by offline UPLC/(-)ESI-TOFMS in these systems are structural analogs of each other, as confirmed by the online AMS operated in the high-resolution W-mode. Based on similarities in SOA growth trends and composition, we expect that the formation of SOA products proceeds via pathways similar to those elucidated in Surratt et al. (2010) (see Fig. 7.10). Although oxidation of these aldehydes can lead to α -dicarbonyls, such as glyoxal and methylglyoxal, which can undergo reactive uptake under humid conditions (Liggio et al., 2005; Kroll et al., 2005b; Volkamer et al., 2009), these compounds are not expected to contribute significantly to SOA formation under dry conditions. In addition, the AMS spectra for acrolein and crotonaldehyde SOA do not show peaks that are characteristic of glyoxal and its oligomers, as described in Liggio et al. (2005) and Galloway et al. (2009).

While MPAN is clearly the intermediate in SOA formation from methacrolein, the exact mechanism by which MPAN leads to such aerosol-phase products as 2-MG and hydroxynitrooxycarboxylic acids has not been established. From the oligoesters observed in the aerosol phase, it appears that the C_4 backbone of MPAN remains intact. Following OH addition to the double bond, the only known gas-phase pathway that would preserve the carbon backbone is formation of hydroxynitrates. (Fragmentation of the MPAN-alkoxy radical would break up the C_4 backbone and yield smaller products.) The nitrooxy functional groups could then be hydrolyzed to hydroxyl groups (Sato, 2008) to form 2-MG and high-MW oligoesters (Route 3 in Fig. 7.10). However, gas-phase abundances of C_4 - (for methacrolein and crotonaldehyde) or C_5 - (for 2M2B, 3M2B and 2-pentenal) hydroxynitrate-PAN, the supposed SOA intermediate in all these systems, do not correlate with the amount of aerosol formed. Substitution of the α -carbon atom by methyl groups (from crotonaldehyde to methacrolein,

or from 3M2B to 2M2B) leads to an increase in the amount of SOA formed by more than a factor of 4, but no increase in gas-phase signal of the hydroxynitrate-PAN is observed (see Fig. 7.12), implying that it is unlikely the SOA-forming channel.

Another possible mechanism is that after OH addition to the double bond in MPAN, the OH-adduct undergoes intramolecular rearrangement before addition of O₂, leading to formation of 2-MG and oligoesters (Route 1 in Fig. 7.10). Such isomerization can be competitive with O₂ addition, as the O-O bond in the peroxy nitrate moiety is weak. In one experiment (09/12/17), the chambers were flushed with nitrogen to lower the oxygen content to 2%, thereby slowing down addition of O₂ by a factor of 10. Compared to another experiment with 21% O₂ (09/12/16), no increase in aerosol formation is observed, suggesting that SOA formation likely involves O₂ addition to the MPAN-OH adduct, though it is also possible that the intramolecular rearrangement reaction is sufficiently fast that O₂ addition is not competitive at these O₂ levels.

From the trends of SOA formation observed in the unsaturated aldehyde systems, it appears that the chemical environment of the carbon atom adjacent to the aldehyde group plays an important role in determining the extent of SOA formation. Low-volatility oligoesters are formed only when the α - and β -carbon atoms are unsaturated; SOA yields of 4-pentenal, for which the olefinic bond is in the 4-position, are lower than those of 2-pentenal, and the SOA products are not analogous to those found in SOA from α, β -unsaturated aldehydes (see Fig. 7.13). SOA formation is correlated with the fraction of OH addition to the β -carbon atom, which forms a radical at the α site: SOA yields of crotonaldehyde and 2-pentenal (in which OH addition to the β -carbon is favored) exceed those of 3M2B (in which OH addition to the α -carbon is favored), even though 3M2B has an equal or higher molecular weight. This suggests that an interaction responsible for producing low-volatility species occurs between the peroxy nitrate functional group and the α -carbon (likely a radical species) that our experiments are not able to precisely reveal. We hypothesize that the peroxy radical undergoes self cyclization to form a highly reactive dioxketone intermediate, which subsequently reacts with H₂O or HNO₃ heterogeneously to form the low-volatility products observed in the SOA (see Fig. 7.10). This intermediate is likely short-lived, and further work is required to

identify this species and its role in SOA formation.

One possible explanation for the higher SOA yields observed from methacrolein and 2M2B is that for these compounds SOA formation is favored by steric hinderance. With an additional methyl group on the α carbon, steric repulsion causes the methyl group to move away from the neighbouring peroxy nitrate functional group by rotation of the C-C bond. As a result, the intramolecular reaction leading to SOA formation can be enhanced, consistent with the relatively higher SOA yields. For the other α,β -unsaturated aldehydes, this interaction is likely not favored, as the hydrogen atom on the α -carbon is in plane with the peroxy nitrate group in the most stable rotational conformer (see Fig. 7.14). The interaction between the peroxy nitrate group and the added functional group is reduced, corresponding to lower SOA formation. Thermodynamic calculations of the relative stabilities of the conformers are required to confirm this hypothesis.

7.7.2 Methylbutenols (MBO)

MBO232 is a biogenic hydrocarbon potentially important in forest photochemistry (Harley et al., 1998). The SOA yields of MBO232 photooxidation have been shown to be negligible, under both high- and low- NO_x conditions (Carrasco et al., 2007; Chan et al., 2009a). In this study, SOA formation from MBO232 photooxidation is below detection limit, even at high NO_2/NO ratios (which would favor any PAN formation). This is likely linked to the lack of PAN products from MBO232 oxidation. The fate of the alkoxy radical formed from OH-initiated oxidation of MBO232 is shown in Fig. 7.15. Scission of the C-C bond adjacent to the tertiary carbon is favored, leading to high yields of glycolaldehyde ($> 60\%$). Formation of 2-hydroxymethylpropanal (2-HMPR) following scission of the C-C bond adjacent to the primary carbon is not the favored route, and hence the yields of 2-HMPR are relatively low ($< 40\%$). Furthermore, OH oxidation of 2-HMPR proceeds by OH abstraction of the aldehydic hydrogen, but owing to the neighbouring hydroxyl group, decomposition to acetone and CO is favored over addition of O_2 to form an acyl peroxy radical. Carrasco et al. (2006) found no PAN formation from photooxidation of 2-HMPR, despite high NO_2/NO ratios.

MBO231 photooxidation produces, in contrast, substantial amounts of SOA, at mass yields of

0.8 – 4.2%. In MBO231, the hydroxyl group is in the 1-position and is not adjacent to the double bond. Decomposition of the analogous alkoxy radical therefore proceeds by scission of the C-C bond adjacent to the primary carbon, favoring the formation of 1-HMPR; observed HMPR (CIMS $(-)/m/z$ 173) concentrations in MBO231 photooxidation were twice as high as those in MBO232 photooxidation. Also, following abstraction of the aldehydic hydrogen from 1-HMPR, addition of O_2 to form an acyl peroxy radical is favored over decomposition to CO. Under high- NO_2 conditions, the acyl peroxy radical can react with NO_2 to form a C_4 -hydroxy-PAN (see Fig. 7.15). Tandem mass spectrometry was used to distinguish gas-phase C_4 -hydroxy-PAN from the isobaric C_5 dihydroxynitrate, both observed at $(-)/m/z$ 250 (see Supplementary Material for details). The C_5 dihydroxynitrate is a first generation oxidation product of both MBO231 and MBO232 formed from RO_2+NO at 10–15% yields (Chan et al., 2009a). In high- NO photooxidation of MBO231 and high- NO_2 photooxidation of MBO232, no C_4 -hydroxy-PAN was observed in the gas phase, corresponding to negligible aerosol formation. In high- NO_2 photooxidation of MBO231, C_4 -hydroxy-PAN is a major gas-phase product, and SOA formation is significant. The identification of C_4 -hydroxy-PAN is further supported by the ratios of ion signals of m/z 250 to m/z 251, its ^{13}C isotopologue, which indicate that the signal at m/z 250 was dominated by a C_4 compound during MBO231 high- NO_2 photooxidation, and by a C_5 compound during MBO232 photooxidation. Hence, the low SOA yields from MBO232 are due to the lack of PAN formation, illustrating the potentially important role of PAN compounds as SOA intermediates.

7.8 Conclusions

In this work, we systematically investigate the effect of relative NO and NO_2 concentrations on SOA formation from aldehyde photooxidation under high- NO_x conditions. A strong positive correlation of SOA yields with NO_2/NO ratio is observed for methacrolein (a major oxidation product of isoprene responsible for SOA formation) and two related α,β -unsaturated aldehydes, acrolein and crotonaldehyde. Oligoester products from dihydroxycarboxylic acids and hydroxynitrooxycarboxylic acids are also observed to depend on NO_2/NO ratio, confirming that PAN chemistry plays an

important role in formation of these low-volatility products. Offline high-resolution aerosol mass spectrometry reveals that analogous oligoester products are major constituents in SOA formed from all α,β -unsaturated aldehydes studied here. By comparing SOA formation from structurally similar aldehydes, we establish that SOA formation is favored when the α -carbon is substituted by a methyl group and the olefinic bond is in the 2-position, such as in methacrolein and 2M2B. The experimental data suggest that SOA formation proceeds via an intramolecular reaction involving the peroxy nitrate functional group, following the addition of O_2 to the MPAN+OH adduct. No aerosol formation is observed from MBO232, an atmospherically important unsaturated alcohol, even at high NO_2/NO ratios, as PAN formation is structurally unfavorable.

Understanding the overall effect of NO_x on SOA yields is important, as SOA yields can vary greatly depending on NO_x conditions. In most photooxidation systems, addition of OH, followed by O_2 , to an olefinic bond results in formation of a hydroxyperoxy radical. The competition between the RO_2+HO_2 pathway (which forms low-volatility hydroperoxides) and the RO_2+NO pathway (which forms volatile organic nitrates and fragmentation products) determines the SOA yields. In the isoprene-high- NO_x system, owing to the MPAN chemistry, aerosol formation proceeds via OH abstraction of the aldehydic hydrogen from methacrolein. As a result, a competition exists between the reaction of the acyl peroxy radical with NO_2 , leading to the formation of MPAN and SOA, and with NO to form volatile fragmentation products. The present work shows the importance of the RO_2+NO_2 pathway of unsaturated aldehyde photooxidation as a route leading to SOA formation. This could have important implications on SOA formation from other atmospheric compounds, especially those with conjugated double bonds. For example, photooxidation of aromatic compounds (Calvert et al., 2002) can lead to α,β -unsaturated aldehydes, which can form significant amounts of low-volatility products via a PAN intermediate. At atmospherically relevant NO_2/NO ratios, SOA yields from isoprene are 3.1–7.4% at organic aerosol loadings of 3–47 $\mu g\ m^{-3}$; these values are 3 times higher than those previously measured under high-NO conditions. The yields exceed even those measured under low- NO_x conditions. An implication of these results is that atmospheric SOA formation from aldehydes may be significantly underestimated in current models, since an

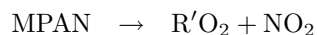
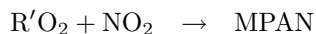
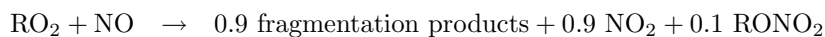
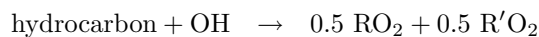
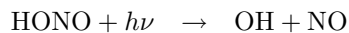
appreciable fraction of SOA is generated in areas where NO_2/NO ratios are high.

Radiocarbon (^{14}C) studies have repeatedly shown that ambient organic aerosol is dominated by biogenic carbon, suggesting that biogenic hydrocarbons are an important source of SOA. However, field measurements have shown that organic aerosol levels tend to be correlated with anthropogenic tracers such as CO and acetylene. From satellite observations one can infer that while the source of carbon in many regions is most likely biogenic, the aerosol formation from biogenic hydrocarbons is significantly enhanced by anthropogenic activities (i.e., NO_x and SO_x emissions (Goldstein et al., 2009)). The present work moves in the direction of reconciling these two seemingly contradictory observations of biogenic carbon versus anthropogenic enhancement. Here we show that the SOA yields from photooxidation of isoprene under atmospherically relevant NO_2/NO ratios are significantly larger than those previously measured under lower NO_2/NO ratios. Moreover, the SOA yields under these conditions are larger than those under low- NO_x conditions, suggesting that SOA formation from isoprene, the most abundantly emitted non-methane biogenic hydrocarbon, can be more efficient in urban high- NO_x plumes than in remote regions.

Appendix: Photochemical modeling to estimate NO and NO_2 concentrations

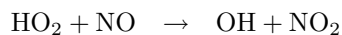
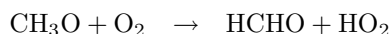
Owing to interference with the NO_2 signal by HONO and CH_3ONO in the chemiluminescence NO_x monitor, we estimate NO and NO_2 concentrations during chamber experiments by photochemical modeling. In experiments in which HONO is the source of OH, the photolysis rate of HONO is estimated from the first-order decay of the m/z 66 signal on the CIMS, which corresponds to the $\text{HF} \cdot \text{ONO}^-$ ion. The initial mixing ratio of HONO was estimated based on the decay of parent hydrocarbon and known rate constants (Atkinson and Arey, 2003; Magneron et al., 2002). Previous comparison to a GC/ NO_2 analyzer allows us to determine the HONO interference on the NO_2 signal, and hence the amount of NO and NO_2 produced during HONO synthesis (Chan et al., 2009b). The initial mixing ratio of NO_2 is therefore the sum of the concentrations of NO_2 impurity from

HONO synthesis (calculated by multiplying the NO₂ signal after HONO injection by a known factor) and additional NO₂ injected (the increase in NO₂ signal from direct injection.) For unsaturated aldehydes, the photochemical model includes the following reactions:



RO₂ denotes the peroxy radical produced by OH addition to the C=C double bond, followed by O₂. R'O₂ denotes the acyl peroxy radical produced by OH abstraction of the aldehydic hydrogen, followed by O₂ addition. These two channels (OH addition and abstraction) have a branching ratio of 1:1 for methacrolein (Tuazon and Atkinson, 1990). Other reactions involving O₃, HO_x, and NO_x are also included in the mechanism. For MBO231 and MBO232, the reactions described in Chan et al. (2009a) are used. The calculated NO₂/NO ratios averaged over the first 200 min of irradiation (the period during which SOA formation occurred) are listed in Table 7.2.

For the high-NO₂ experiments, CH₃ONO was used as the OH precursor:



The photolysis rate of CH₃ONO was estimated by the first-order decay of the CH₃ONO signal on GC/FID. The initial mixing ratio of CH₃ONO was determined from the measured vapor pressure of CH₃ONO in the injection bulb. The modeled decay of the hydrocarbon is consistent with that

observed by GC/FID. FTIR analysis shows no NO or NO₂ impurities are produced during CH₃ONO synthesis ([NO₂] was less than 0.6% of [CH₃ONO]). In the photochemical calculations, the initial NO and NO₂ concentrations are determined from the increase in NO and NO₂ signals from direct injection. The calculated NO₂/NO ratios averaged over the first 100 min of irradiation are listed in Table 7.2.

Acknowledgements

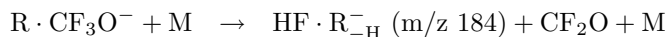
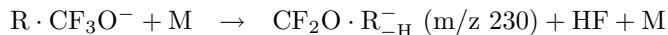
This research was funded by the U.S. Department of Energy Biological and Environmental Research Program DE-FG02-05ER63983, the U.S. Environmental Protection Agency STAR grant RD-83374901, the U.S. National Science Foundation grant ATM-0432377, and the Electric Power Research Institute. This publication has not been formally reviewed by the EPA. The views expressed in this document are solely those of the authors and EPA does not endorse any products mentioned in this publication. The authors would like to thank K. E. Kautzman and A. J. Kwan for experimental assistance, and F. Paulot for helpful discussion.

7.9 Supplementary Material: Negative Chemical Ionization Tandem Mass Spectrometry

Tandem mass spectrometry (MS/MS) in the negative mode of the chemical ionization mass spectrometer has been used in previous studies to separate isobaric compounds (Paulot et al., 2009; Surratt et al., 2010). Details of MS/MS operation are described in Paulot et al. (2009). In brief, the parent ions selected in the first quadrupole enter the second quadrupole, where a small flow of nitrogen is added until the pressure reaches 2.5×10^{-3} hPa. Selected parent ions undergo collision-induced dissociation (CID), and the parent ions of isobaric compounds can exhibit different CID patterns and yield different fragment (daughter) ions. Hence, with the third quadrupole acting as a second mass filter for the daughter ions, this allows for separate measurement of these isobaric compounds. For example, first-generation hydroxy-hydroperoxide and second generation epoxydiol

from isoprene low-NO_x photooxidation both have a molecular weight of 118, and are detected as cluster ions at m/z 203. The hydroxy-hydroperoxide, known as ISOPOOH, has a significant yield of the daughter ion m/z 63, most likely FCO₂⁻, while the epoxydiol, known as IEPOX, is detected at daughter m/z 183, representing a neutral loss of HF from the cluster ion. The individual contribution to the parent ion signal can therefore be separated based on known daughter ions (Paulot et al., 2009).

In the MBO231 and MBO232 experiments, both dihydroxynitrate and hydroxy-PAN are formed during high-NO_x photooxidation. Both compounds have molecular weights of 165, and are detected as the cluster ion at m/z 250. During MBO231 photooxidation, significant daughter ion signals are observed at m/z 's 62, 184, and 230. Both daughter m/z 184 and 230 are formed promptly and the time trends of their signals correlate very well with each other, and likely arise from the same compound. Their signals reach a maximum after 60 minutes of irradiation, and decrease rapidly until the OH precursor is depleted (see Fig. 16 in main text). In all experiments, more OH precursor was injected after 300 minutes of irradiation. Upon further addition of OH precursor, the ion signals at daughter m/z 's 184 and 230 drop by more than 40%. The time trends are consistent with the first-generation C₅-dihydroxynitrate, formed from RO₂ + NO. The CID likely proceeds via the following reactions, resulting in neutral losses of HF and CF₂O to form daughter m/z 's 230 and 184, respectively:



Negative m/z 230 and 184 were also observed in the single MS mode, under both high-NO and high-NO₂ conditions (observed in this work and in Chan et al. (2009a)), suggesting that the fragmentation can also occur without induced collisions in the second quadrupole.

The daughter ion at m/z 62 displayed a distinctly different time trend: the signal increased monotonically until the OH precursor was depleted. In high-NO photooxidation of MBO231, upon

further addition of HONO, the signal of daughter m/z 62 increased slightly. This is characteristic of a second-generation product formed later in the reaction mechanism. In MBO231 photooxidation, the signal of m/z 62 was significantly lower in high-NO experiments than in high-NO₂ experiments, and was insignificant in MBO232 photooxidation. These observations are all consistent with m/z 62 being a characteristic daughter ion for the second-generation C₄-hydroxy-PAN, as formation of PAN is favored by high NO₂/NO ratio. It is likely that the weak PAN functional group fragments to form NO₃⁻ ion (m/z 62), but the fragmentation pathway is currently unclear.

Bibliography

- Atkinson, R. and Arey, J.: Atmospheric degradation of volatile organic compounds, *Chem. Rev.*, 103, 4605–4638, 2003.
- Calvert, J. G., Atkinson, R., Becker, K. H., Kamens, R. M., Seinfeld, J. H., Wallington, T. J., and Yarwood, G.: The mechanisms of atmospheric oxidation of aromatic hydrocarbons, Oxford University Press, 2002.
- Canagaratna, M. R., Jayne, J. T., Jimenez, J. L., Allan, J. D., Alfarra, M. R., Zhang, Q., Onasch, T. B., Drewnick, F., Coe, H., Middlebrook, A., Delia, A., Williams, L. R., Trimborn, A. M., Northway, M. J., DeCarlo, P. F., Kolb, C. E., Davidovits, P., and Worsnop, D. R.: Chemical and microphysical characterization of ambient aerosols with the Aerodyne aerosol mass spectrometer, *Mass. Spec. Rev.*, 26, 185–222, 2007.
- Carlton, A. G., Wiedinmyer, C., and Kroll, J. H.: A review of Secondary Organic Aerosol (SOA) formation from isoprene, *Atmos. Chem. Phys.*, 9, 4987–5005, <http://www.atmos-chem-phys.net/9/4987/2009/>, 2009.
- Carrasco, N., Doussin, J. F., Picquet-Varrault, B., and Carlier, P.: Tropospheric degradation of 2-hydroxy-2-methylpropanal, a photo-oxidation product of 2-methyl-3-buten-2-ol: Kinetic and mechanistic study of its photolysis and its reaction with OH radicals, *Atmos. Environ.*, 40, 2011–2019, 2006.

- Carrasco, N., Doussin, J. F., O'Connor, M., Wenger, J. C., Picquet-Varrault, B., Durand-Jolibois, R., and Carlier, P.: Simulation chamber studies of the atmospheric oxidation of 2-methyl-3-buten-2-ol: Reaction with hydroxyl radicals and ozone under a variety of conditions, *J. Atmos. Chem.*, 56, 33–55, 2007.
- Chan, A. W. H., Galloway, M. M., Kwan, A. J., Chhabra, P. S., Keutsch, F. N., Wennberg, P. O., Flagan, R. C., and Seinfeld, J. H.: Photooxidation of 2-methyl-3-buten-2-ol (MBO) as a potential source of secondary organic aerosol, *Environ. Sci. Technol.*, 43, 4647–4652, 2009a.
- Chan, A. W. H., Kautzman, K. E., Chhabra, P. S., Surratt, J. D., Chan, M. N., Crounse, J. D., Kurten, A., Wennberg, P. O., Flagan, R. C., and Seinfeld, J. H.: Secondary organic aerosol formation from photooxidation of naphthalene and alkylnaphthalenes: implications for oxidation of intermediate volatility organic compounds (IVOCs), *Atmos. Chem. Phys.*, 9, 3049–3060, <http://www.atmos-chem-phys.net/9/4987/2009/>, 2009b.
- Chung, S. H. and Seinfeld, J. H.: Global distribution and climate forcing of carbonaceous aerosols, *J. Geophys. Res.-Atmos.*, 107, doi:10.1029/2001JD001397, 2002.
- Claeys, M., Graham, B., Vas, G., Wang, W., Vermeylen, R., Pashynska, V., Cafmeyer, J., Guyon, P., Andreae, M. O., Artaxo, P., and Maenhaut, W.: Formation of secondary organic aerosols through photooxidation of isoprene, *Science*, 303, 1173–1176, 2004.
- Cocker, D. R., Flagan, R. C., and Seinfeld, J. H.: State-of-the-art chamber facility for studying atmospheric aerosol chemistry, *Environ. Sci. Technol.*, 35, 2594–2601, 2001.
- Crounse, J. D., McKinney, K. A., Kwan, A. J., and Wennberg, P. O.: Measurement of gas-phase hydroperoxides by chemical ionization mass spectrometry, *Anal. Chem.*, 78, 6726–6732, 2006.
- de Gouw, J. A., Middlebrook, A. M., Warneke, C., Goldan, P. D., Kuster, W. C., Roberts, J. M., Fehsenfeld, F. C., Worsnop, D. R., Canagaratna, M. R., Pszenny, A. A. P., Keene, W. C., Marchewka, M., Bertman, S. B., and Bates, T. S.: Budget of organic carbon in a polluted atmo-

- sphere: Results from the New England Air Quality Study in 2002, *J. Geophys. Res.-Atmos.*, 110, D16305, doi:10.1029/2004JD005623, 2005.
- de Gouw, J. A., Brock, C. A., Atlas, E. L., Bates, T. S., Fehsenfeld, F. C., Goldan, P. D., Holloway, J. S., Kuster, W. C., Lerner, B. M., Matthew, B. M., Middlebrook, A. M., Onasch, T. B., Peltier, R. E., Quinn, P. K., Senff, C. J., Stohl, A., Sullivan, A. P., Trainer, M., Warneke, C., Weber, R. J., and Williams, E. J.: Sources of particulate matter in the northeastern United States in summer: 1. Direct emissions and secondary formation of organic matter in urban plumes, *J. Geophys. Res.-Atmos.*, 113, D08301, doi:10.1029/2007JD009243, 2008.
- DeCarlo, P. F., Kimmel, J. R., Trimborn, A., Northway, M. J., Jayne, J. T., Aiken, A. C., Gonin, M., Fuhrer, K., Horvath, T., Docherty, K. S., Worsnop, D. R., and Jimenez, J. L.: Field-deployable, high-resolution, time-of-flight aerosol mass spectrometer, *Anal. Chem.*, 78, 8281–8289, 2006.
- Dommen, J., Metzger, A., Duplissy, J., Kalberer, M., Alfarra, M. R., Gascho, A., Weingartner, E., Prevot, A. S. H., Verheggen, B., and Baltensperger, U.: Laboratory observation of oligomers in the aerosol from isoprene/NO_x photooxidation, *Geophys. Res. Lett.*, 33, L13805, doi:10.1029/2006GL026523, 2006.
- Edney, E. O., Kleindienst, T. E., Jaoui, M., Lewandowski, M., Offenberg, J. H., Wang, W., and Claeys, M.: Formation of 2-methyl tetrols and 2-methylglyceric acid in secondary organic aerosol from laboratory irradiated isoprene/NO_x/SO₂/air mixtures and their detection in ambient PM_{2.5} samples collected in the eastern United States, *Atmos. Environ.*, 39, 5281–5289, 2005.
- Fantechi, G., Jensen, N. R., Hjorth, J., and Peeters, J.: Determination of the rate constants for the gas-phase reactions of methyl butenol with OH radicals, ozone, NO₃ radicals, and Cl atoms, *Int. J. Chem. Kinet.*, 30, 589–594, 1998.
- Galloway, M. M., Chhabra, P. S., Chan, A. W. H., Surratt, J. D., Flagan, R. C., Seinfeld, J. H., and Keutsch, F. N.: Glyoxal uptake on ammonium sulphate seed aerosol: reaction products and reversibility of uptake under dark and irradiated conditions, *Atmos. Chem. Phys.*, 9, 3331–3345, <http://www.atmos-chem-phys.net/9/3331/2009/>, 2009.

- Goldstein, A. H., Koven, C. D., Heald, C. L., and Fung, I. Y.: Biogenic carbon and anthropogenic pollutants combine to form a cooling haze over the southeastern United States, *Proc. Natl. Acad. Sci. USA*, 106, 8835–8840, 2009.
- Guenther, A., Karl, T., Harley, P., Wiedinmyer, C., Palmer, P. I., and Geron, C.: Estimates of global terrestrial isoprene emissions using MEGAN (Model of Emissions of Gases and Aerosols from Nature), *Atmos. Chem. Phys.*, 6, 3181–3210, <http://www.atmos-chem-phys.net/6/3181/2006/>, 2006.
- Hallquist, M., Wenger, J. C., Baltensperger, U., Rudich, Y., Simpson, D., Claeys, M., Dommen, J., Donahue, N. M., George, C., Goldstein, A. H., Hamilton, J. F., Herrmann, H., Hoffmann, T., Iinuma, Y., Jang, M., Jenkin, M. E., Jimenez, J. L., Kiendler-Scharr, A., Maenhaut, W., McFiggans, G., Mentel, T. F., Monod, A., Prevot, A. S. H., Seinfeld, J. H., Surratt, J. D., Szmigielski, R., and Wildt, J.: The formation, properties and impact of secondary organic aerosol: current and emerging issues, *Atmos. Chem. Phys.*, 9, 5155–5236, <http://www.atmos-chem-phys.net/9/5155/2009/>, 2009.
- Harley, P., Fridd-Stroud, V., Greenberg, J., Guenther, A., and Vasconcellos, P.: Emission of 2-methyl-3-buten-2-ol by pines: A potentially large natural source of reactive carbon to the atmosphere, *J. Geophys. Res.-Atmos.*, 103, 25479–25486, 1998.
- Hatakeyama, S., Izumi, K., Fukuyama, T., Akimoto, H., and Washida, N.: Reactions of OH with alpha-pinene and beta-pinene in air – Estimate of global CO production from the atmospheric oxidation of terpenes, *J. Geophys. Res.-Atmos.*, 96, 947–958, 1991.
- Henze, D. K. and Seinfeld, J. H.: Global secondary organic aerosol from isoprene oxidation, *Geophys. Res. Lett.*, 33, L09812, doi:10.1029/2006GL025976, 2006.
- Henze, D. K., Seinfeld, J. H., Ng, N. L., Kroll, J. H., Fu, T. M., Jacob, D. J., and Heald, C. L.: Global modeling of secondary organic aerosol formation from aromatic hydrocarbons: high- vs. low-yield pathways, *Atmos. Chem. Phys.*, 8, 2405–2420, 2008.

- Hurley, M. D., Sokolov, O., Wallington, T. J., Takekawa, H., Karasawa, M., Klotz, B., Barnes, I., and Becker, K. H.: Organic aerosol formation during the atmospheric degradation of toluene, *Environ. Sci. Technol.*, 35, 1358–1366, 2001.
- Ion, A. C., Vermeylen, R., Kourtchev, I., Cafmeyer, J., Chi, X., Gelencser, A., Maenhaut, W., and Claeys, M.: Polar organic compounds in rural PM_{2.5} aerosols from K-puszt, Hungary, during a 2003 summer field campaign: Sources and diel variations, *Atmos. Chem. Phys.*, 5, 1805–1814, <http://www.atmos-chem-phys.net/5/1805/2005/>, 2005.
- Johnson, D., Jenkin, M. E., Wirtz, K., and Martin-Reviejo, M.: Simulating the formation of secondary organic aerosol from the photooxidation of aromatic hydrocarbons, *Environ. Chem.*, 2, 35–48, 2005.
- Kanakidou, M., Seinfeld, J. H., Pandis, S. N., Barnes, I., Dentener, F. J., Facchini, M. C., Van Dingenen, R., Ervens, B., Nenes, A., Nielsen, C. J., Swietlicki, E., Putaud, J. P., Balkanski, Y., Fuzzi, S., Horth, J., Moortgat, G. K., Winterhalter, R., Myhre, C. E. L., Tsigaridis, K., Vignati, E., Stephanou, E. G., and Wilson, J.: Organic aerosol and global climate modelling: a review, *Atmos. Chem. Phys.*, 5, 1053–1123, <http://www.atmos-chem-phys.net/5/1053/2005/>, 2005.
- Keywood, M. D., Varutbangkul, V., Bahreini, R., Flagan, R. C., and Seinfeld, J. H.: Secondary organic aerosol formation from the ozonolysis of cycloalkenes and related compounds, *Environ. Sci. Technol.*, 38, 4157–4164, 2004.
- Kleindienst, T. E., Lewandowski, M., Offenberg, J. H., Jaoui, M., and Edney, E. O.: The formation of secondary organic aerosol from the isoprene + OH reaction in the absence of NO_x, *Atmos. Chem. Phys.*, 9, 6541–6558, <http://www.atmos-chem-phys.net/9/6541/2009/>, 2009.
- Kourtchev, I., Ruuskanen, T., Maenhaut, W., Kulmala, M., and Claeys, M.: Observation of 2-methyltetrols and related photo-oxidation products of isoprene in boreal forest aerosols from Hyytiälä, Finland, *Atmos. Chem. Phys.*, 5, 2761–2770, <http://www.atmos-chem-phys.net/5/2761/2005/>, 2005.

- Kroll, J. H. and Seinfeld, J. H.: Chemistry of secondary organic aerosol: Formation and evolution of low-volatility organics in the atmosphere, *Atmos. Environ.*, 42, 3593–3624, 2008.
- Kroll, J. H., Ng, N. L., Murphy, S. M., Flagan, R. C., and Seinfeld, J. H.: Secondary organic aerosol formation from isoprene photooxidation under high-NO_x conditions, *Geophys. Res. Lett.*, 32, L18808, doi:10.1029/2005GL023637, 2005a.
- Kroll, J. H., Ng, N. L., Murphy, S. M., Varutbangkul, V., Flagan, R. C., and Seinfeld, J. H.: Chamber studies of secondary organic aerosol growth by reactive uptake of simple carbonyl compounds, *J. Geophys. Res.-Atmos.*, 110, D23207, doi:10.1029/2005JD006004, 2005b.
- Kroll, J. H., Ng, N. L., Murphy, S. M., Flagan, R. C., and Seinfeld, J. H.: Secondary organic aerosol formation from isoprene photooxidation, *Environ. Sci. Technol.*, 40, 1869–1877, 2006.
- Lewis, C. W. and Stiles, D. C.: Radiocarbon content of PM_{2.5} ambient aerosol in Tampa, FL, *Aerosol. Sci. Tech.*, 40, 189–196, 2006.
- Lewis, C. W., Klouda, G. A., and Ellenson, W. D.: Radiocarbon measurement of the biogenic contribution to summertime PM-2.5 ambient aerosol in Nashville, TN, *Atmos. Environ.*, 38, 6053–6061, 2004.
- Liggio, J., Li, S. M., and McLaren, R.: Heterogeneous reactions of glyoxal on particulate matter: Identification of acetals and sulfate esters, *Environ. Sci. Technol.*, 39, 1532–1541, 2005.
- Magneron, I., Thevenet, R., Mellouki, A., Le Bras, G., Moortgat, G. K., and Wirtz, K.: A study of the photolysis and OH-initiated oxidation of acrolein and trans-crotonaldehyde, *J. Phys. Chem. A*, 106, 2526–2537, 2002.
- Ng, N. L., Chhabra, P. S., Chan, A. W. H., Surratt, J. D., Kroll, J. H., Kwan, A. J., McCabe, D. C., Wennberg, P. O., Sorooshian, A., Murphy, S. M., Dalleska, N. F., Flagan, R. C., and Seinfeld, J. H.: Effect of NO_x level on secondary organic aerosol (SOA) formation from the photooxidation of terpenes, *Atmos. Chem. Phys.*, 7, 5159–5174, <http://www.atmos-chem-phys.net/7/5159/2007/>, 2007a.

- Ng, N. L., Kroll, J. H., Chan, A. W. H., Chhabra, P. S., Flagan, R. C., and Seinfeld, J. H.: Secondary organic aerosol formation from *m*-xylene, toluene, and benzene, *Atmos. Chem. Phys.*, 7, 3909–3922, <http://www.atmos-chem-phys.net/7/3909/2007/>, 2007b.
- Orlando, J. J., Tyndall, G. S., and Paulson, S. E.: Mechanism of the OH-initiated oxidation of methacrolein, *Geophys. Res. Lett.*, 26, 2191–2194, 1999.
- Orlando, J. J., Tyndall, G. S., Bertman, S. B., Chen, W. C., and Burkholder, J. B.: Rate coefficient for the reaction of OH with $\text{CH}_2=\text{C}(\text{CH}_3)\text{C}(\text{O})\text{OONO}_2$ (MPAN), *Atmos. Environ.*, 36, 1895–1900, 2002.
- Pandis, S. N., Paulson, S. E., Seinfeld, J. H., and Flagan, R. C.: Aerosol formation in the photooxidation of isoprene and beta-pinene, *Atmos. Environ.*, 25, 997–1008, 1991.
- Paulot, F., Crounse, J. D., Kjaergaard, H. G., Kurten, A., St Clair, J. M., Seinfeld, J. H., and Wennberg, P. O.: Unexpected epoxide formation in the gas-phase photooxidation of isoprene, *Science*, 325, 730–733, 2009.
- Presto, A. A., Hartz, K. E. H., and Donahue, N. M.: Secondary organic aerosol production from terpene ozonolysis. 2. Effect of NO_x concentration, *Environ. Sci. Technol.*, 39, 7046–7054, 2005.
- Sato, K.: Detection of nitrooxypolyols in secondary organic aerosol formed from the photooxidation of conjugated dienes under high- NO_x conditions, *Atmos. Environ.*, 42, 6851–6861, 2008.
- Song, C., Na, K. S., and Cocker, D. R.: Impact of the hydrocarbon to NO_x ratio on secondary organic aerosol formation, *Environ. Sci. Technol.*, 39, 3143–3149, 2005.
- Surratt, J. D., Murphy, S. M., Kroll, J. H., Ng, N. L., Hildebrandt, L., Sorooshian, A., Szmigielski, R., Vermeylen, R., Maenhaut, W., Claeys, M., Flagan, R. C., and Seinfeld, J. H.: Chemical composition of secondary organic aerosol formed from the photooxidation of isoprene, *J. Phys. Chem. A*, 110, 9665–9690, 2006.
- Surratt, J. D., Gomez-Gonzalez, Y., Chan, A. W. H., Vermeylen, R., Shahgholi, M., Kleindienst, T. E., Edney, E. O., Offenberg, J. H., Lewandowski, M., Jaoui, M., Maenhaut, W., Claeys, M.,

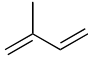
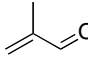
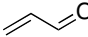
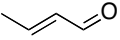
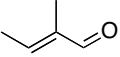
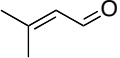
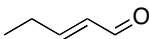
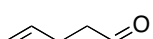
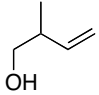
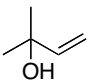
- Flagan, R. C., and Seinfeld, J. H.: Organosulfate formation in biogenic secondary organic aerosol, *J. Phys. Chem. A*, 112, 8345–8378, 2008.
- Surratt, J. D., Chan, A. W. H., Eddingsaas, N. C., Chan, M. N., Loza, C. L., Kwan, A. J., Hersey, S. P., Flagan, R. C., Wennberg, P. O., and Seinfeld, J. H.: Reactive intermediates revealed in secondary organic aerosol formation from isoprene, *Proc. Natl. Acad. Sci. USA*, 107, 6640–6645, 2010.
- Szmigielski, R., Surratt, J. D., Vermeylen, R., Szmigielska, K., Kroll, J. H., Ng, N. L., Murphy, S. M., Sorooshian, A., Seinfeld, J. H., and Claeys, M.: Characterization of 2-methylglyceric acid oligomers in secondary organic aerosol formed from the photooxidation of isoprene using trimethylsilylation and gas chromatography/ion trap mass spectrometry, *J. Mass. Spectrom.*, 42, 101–116, 2007.
- Taylor, W. D., Allston, T. D., Moscato, M. J., Fazekas, G. B., Kozlowski, R., and Takacs, G. A.: Atmospheric photo-dissociation lifetimes for nitromethane, methyl nitrite, and methyl nitrate, *Int. J. Chem. Kinet.*, 12, 231–240, 1980.
- Tuazon, E. C. and Atkinson, R.: A product study of the gas-phase reaction of methacrolein with the OH radical in the presence of NO_x, *Int. J. Chem. Kinet.*, 22, 591–602, 1990.
- Tuazon, E. C., Aschmann, S. M., Nishino, N., Arey, J., and Atkinson, R.: Kinetics and products of the OH radical-initiated reaction of 3-methyl-2-butenal, *Phys. Chem. Chem. Phys.*, 7, 2298–2304, 2005.
- Volkamer, R., Ziemann, P. J., and Molina, M. J.: Secondary organic aerosol formation from acetylene (C₂H₂): seed effect on SOA yields due to organic photochemistry in the aerosol aqueous phase, *Atmos. Chem. Phys.*, 9, 1907–1928, <http://www.atmos-chem-phys.net/9/1907/2009/>, 2009.
- Weber, R. J., Sullivan, A. P., Peltier, R. E., Russell, A., Yan, B., Zheng, M., de Gouw, J., Warneke, C., Brock, C., Holloway, J. S., Atlas, E. L., and Edgerton, E.: A study of secondary organic aerosol

formation in the anthropogenic-influenced southeastern United States, *J. Geophys. Res.-Atmos.*, 112, D13302, doi:10.1029/2007JD008408, 2007.

Zhang, Q., Jimenez, J. L., Canagaratna, M. R., Allan, J. D., Coe, H., Ulbrich, I., Alfarra, M. R., Takami, A., Middlebrook, A. M., Sun, Y. L., Dzepina, K., Dunlea, E., Docherty, K., DeCarlo, P. F., Salcedo, D., Onasch, T., Jayne, J. T., Miyoshi, T., Shimonono, A., Hatakeyama, S., Takegawa, N., Kondo, Y., Schneider, J., Drewnick, F., Borrmann, S., Weimer, S., Demerjian, K., Williams, P., Bower, K., Bahreini, R., Cottrell, L., Griffin, R. J., Rautiainen, J., Sun, J. Y., Zhang, Y. M., and Worsnop, D. R.: Ubiquity and dominance of oxygenated species in organic aerosols in anthropogenically-influenced Northern Hemisphere midlatitudes, *Geophys. Res. Lett.*, 34, L13801, doi:10.1029/2007GL029979, 2007a.

Zhang, Y., Huang, J. P., Henze, D. K., and Seinfeld, J. H.: Role of isoprene in secondary organic aerosol formation on a regional scale, *J. Geophys. Res.-Atmos.*, 112, D20207, doi:10.1029/2007JD008675, 2007b.

Table 7.1: Hydrocarbons studied.

Name	Structure	OH rate constant, $\text{cm}^3 \text{ molec}^{-1} \text{ s}^{-1}$
isoprene		$1 \times 10^{-10} \text{ }^a$
methacrolein		$2.9 \times 10^{-11} \text{ }^a$
acrolein		$2.0 \times 10^{-11} \text{ }^b$
crotonaldehyde (<i>cis</i> and <i>trans</i>)		$3.5 \times 10^{-11} \text{ }^b$
2-methyl-2-butenal (2M2B)		unknown
3-methyl-2-butenal (3M2B)		$6.2 \times 10^{-11} \text{ }^c$
2-pentenal		unknown
4-pentenal		unknown
2-methyl-3-buten-2-ol (MBO232)		unknown
2-methyl-3-buten-1-ol (MBO231)		$3.9 \times 10^{-11} \text{ }^d$

^a Atkinson and Arey (2003)^b Magneron et al. (2002)^c Tuazon et al. (2005)^d Fantechi et al. (1998)

Table 7.2: Experimental conditions and results.

Date ^a (YY/MM/DD)	Compound	[HC] ₀ , ppb	OH precursor	NO _x addition	[NO] ₀ ^b , ppb	[NO ₂] ₀ ^b , ppb	NO ₂ /NO ^c	V ₀ ^d , μm ³ cm ⁻³	ΔM _o ^e , μg m ⁻³	SOA Yield
09/07/14	methacrolein	277	HONO	+NO	725	365	0.5	11.4	10.1	0.019
09/07/16	methacrolein	285	HONO	+NO ₂	296	692	1.7	12.3	24.5	0.052
09/07/19	methacrolein	257	HONO	–	527	407	0.7	12.1	14.4	0.030
09/07/31 ^f	methacrolein	232	HONO	+NO	653	394	0.5	11.7	13.3	0.030
09/09/12	methacrolein	255	CH ₃ ONO	+NO+NO ₂	222	799	10.0	13.9	276.3	0.392
09/09/15	methacrolein	67	CH ₃ ONO	+NO+NO ₂	164	549	5.8	14.8	39.9	0.211
09/09/17	methacrolein	20	CH ₃ ONO	+NO+NO ₂	170	602	3.6	16.0	10.8	0.194
09/09/19	methacrolein	48	CH ₃ ONO	+NO+NO ₂	167	582	4.7	13.2	28.8	0.213
09/09/21	methacrolein	32	CH ₃ ONO	+NO+NO ₂	176	657	4.2	14.4	22.4	0.242
09/12/16	methacrolein	32	CH ₃ ONO	+NO+NO ₂	243	444	2.7	13.9	6.8	0.079
09/12/17 ^g	methacrolein	32	CH ₃ ONO	+NO+NO ₂	233	518	2.7	16.2	6.7	0.075
09/08/08	isoprene	523	HONO	–	312	510	7.7	10.8	65.2	0.044
09/09/23	isoprene	228	CH ₃ ONO	+NO+NO ₂	293	825	8.4	16.0	47.4	0.074
09/09/24	isoprene	94	CH ₃ ONO	+NO+NO ₂	271	735	5.0	14.8	16.0	0.061
09/09/25	isoprene	153	CH ₃ ONO	+NO+NO ₂	316	859	6.1	18.7	27.2	0.064
09/09/27	isoprene	44	CH ₃ ONO	+NO+NO ₂	259	715	4.0	15.8	5.2	0.042
09/09/30	isoprene	33	CH ₃ ONO	+NO+NO ₂	289	768	3.4	18.4	2.9	0.031
09/08/15	acrolein	676	HONO	–	214	389	2.5	13.2	21.3	0.022
09/08/16	acrolein	540	HONO	+NO	550	359	0.8	11.2	4.4	0.006
09/08/17	acrolein	611	HONO	+NO ₂	233	630	2.0	13.2	9.9	0.015
09/09/28	acrolein	220	CH ₃ ONO	+NO+NO ₂	313	830	5.5	19.2	16.6	0.035
09/08/18	crotonaldehyde	293	HONO	–	214	371	2.3	12.1	14.0	0.019
09/08/19	crotonaldehyde	297	HONO	+NO	600	416	1.1	12.3	9.0	0.013
09/08/20	crotonaldehyde	361	HONO	+NO ₂	245	625	2.6	12.2	12.9	0.017
09/09/29	crotonaldehyde	74	CH ₃ ONO	+NO+NO ₂	248	664	3.8	16.4	9.2	0.044
09/12/26	2-pentenal	174	CH ₃ ONO	+NO+NO ₂	230	548	6.7	13.9	18.1	0.03
09/12/27	4-pentenal	191	CH ₃ ONO	+NO+NO ₂	243	488	6.5	15.8	8.2	0.012
09/12/28	2M2B	277	CH ₃ ONO	+NO+NO ₂	240	706	9.3	13.8	376.7	0.391
09/12/29	3M2B	207	CH ₃ ONO	+NO+NO ₂	268	747	8.7	16.1	5.6	0.008
09/12/31	MBO231	589	CH ₃ ONO	+NO+NO ₂	308	493	13.2	16.8	87.6	0.042
10/02/22	MBO231	329	CH ₃ ONO	+NO+NO ₂	351	768	7.8	14.5	21.9	0.019
10/02/24	MBO231	300	HONO	+NO	642	514	1.8	14.2	<2	<0.002
10/02/25	MBO231	378	CH ₃ ONO	+NO+NO ₂	346	793	5.5	17.5	10.7	0.008
10/01/01	MBO232	492	CH ₃ ONO	+NO+NO ₂	251	442	11.4	14.8	<2	<0.002
10/02/23	MBO232	388	CH ₃ ONO	+NO+NO ₂	345	809	8.4	17.1	<2	<0.002

^a All experiments carried out at temperatures of 293–295K and RH of 9–11%^b As measured by chemiluminescence NO_x monitor. Note interference on NO₂ signal from HONO and CH₃ONO^c Estimated by photochemical modeling (see Appendix)^d V₀: volume concentration of ammonium sulfate seed^e ΔM_o: mass concentration of SOA^f Gas-phase nitric acid added during experiment^g Low O₂ experiment

Table 7.3: SOA constituents detected by UPLC/(-)ESI-TOFMS and AMS in methacrolein experiments. All ions were detected in both high-NO and high-NO₂ experiments, unless otherwise noted.

	$[M - H]^-$ ^a	UPLC/ESI-TOFMS Measured Mass	TOFMS Suggested Ion Formula	Error (mDa)	i-Fit	# of 2-MG Monomer Units (n)	Structure	$[M - OH]^+$ ^b	AMS Suggested Ion Formula ^c
Oligoester Series 1		not detected				1		103	C ₄ H ₇ O ₃ ⁺
	221	221.0661	C ₈ H ₁₃ O ₇ ⁻	1.6	0.3	2		205	C ₈ H ₁₃ O ₆ ⁺
	323	323.0979	C ₁₂ H ₁₉ O ₁₀ ⁻	0.1	22.6	3		d	--
	425	425.1290	C ₁₆ H ₂₅ O ₁₃ ⁻	-0.5	48.0	4		d	--
	527 ^e	527.1609	C ₂₀ H ₃₁ O ₁₆ ⁻	-0.3	3.7	5		d	--
Oligoester Series 2	266	266.0507	C ₈ H ₁₂ NO ₉ ⁻	-0.5	32.8	1		d	--
	368	368.0831	C ₁₂ H ₁₈ NO ₁₂ ⁻	0.2	11.4	2		d	--
	470	470.1149	C ₁₆ H ₂₄ NO ₁₅ ⁻	0.3	56.3	3		d	--
	572	572.1510	C ₂₀ H ₃₀ NO ₁₈ ⁻	4.7	1.0	4		d	--
Oligoester Series 3 ^f		not detected				1		131	C ₉ H ₇ O ₄ ⁺ ^g
	249	249.0616	C ₉ H ₁₃ O ₈ ⁻	0.6	2.7	2		233	C ₉ H ₁₃ O ₇ ⁺
	351	351.0912	C ₁₃ H ₁₉ O ₁₁ ⁻	-1.5	46.9	3		d	--
	453	453.1248	C ₁₇ H ₂₅ O ₁₄ ⁻	0.4	63.7	4		d	--
	555 ^e	555.1610	C ₂₁ H ₃₁ O ₁₇ ⁻	4.9	3.0	5		d	--
Oligoester Series 4 ^h		not detected				1		145	C ₈ H ₉ O ₄ ⁺
	263	263.0740	C ₁₀ H ₁₅ O ₈ ⁻	-2.7	4.7	2		247	C ₁₀ H ₁₅ O ₇ ⁺
	365	365.1061	C ₁₄ H ₂₁ O ₁₁ ⁻	-2.3	54.9	3		d	--
	467	467.1434	C ₁₈ H ₂₇ O ₁₄ ⁻	3.3	23.7	4		d	--
	569	569.1711	C ₁₈ H ₂₇ O ₁₄ ⁻	-0.7	20.0	5		d	--
Oligoester Series 5	311	311.0333	C ₈ H ₁₁ N ₂ O ₁₁ ⁻	-3.0	58.9	0		d	--
	413	413.0664	C ₁₂ H ₁₇ N ₂ O ₁₄ ⁻	-1.6	71.9	1		d	--
	515 ^e	515.1039	C ₁₆ H ₂₃ N ₂ O ₁₇ ⁻	4.2	3.6	2		d	--
Other Oligoesters	458 ^e	458.0558	C ₁₂ H ₁₆ N ₃ O ₁₆ ⁻	2.7	3.3	n/a		d	--

^a Observed by UPLC/(-)ESI-TOFMS

^b Observed by AMS V mode

^c Suggested by AMS high-resolution W mode

^d Not observed by AMS, most likely due to fragmentation of nitrate group, or below detection limit

^e Detected in high-NO₂ experiments only

^f This oligoester series involves the esterification with formic acid.

^g C₈H₁₁O₃⁺ also detected

^h This oligoester series involves the esterification with acetic acid.

Table 7.4: SOA constituents detected by UPLC/(-)ESI-TOFMS and AMS in acrolein/high-NO₂ experiments.

	[M - H] ^{-a}	UPLC/ESI-TOFMS Measured Mass	TOFMS Suggested Ion Formula	Error (mDa)	i-Fit	# of Acid Monomer Units (n)	Structure	[M - OH] ^{+b}	AMS Suggested Ion Formula ^c
Oligoester Series 1	105	105.0199	C ₃ H ₅ O ₄ ⁻	1.1	2.1	1		89	C ₃ H ₅ O ₃ ⁺
	193	193.0341	C ₆ H ₉ O ₇ ⁻	-0.7	3.9	2		177	C ₆ H ₉ O ₆ ⁺
	281	281.0493	C ₉ H ₁₃ O ₁₀ ⁻	-1.6	42.9	3		d	--
	369	369.0697	C ₁₂ H ₁₇ O ₁₃ ⁻	2.8	8.5	4		d	--
	457	457.0860	C ₁₅ H ₂₁ O ₁₆ ⁻	3.0	95.9	5		d	--
Oligoester Series 2	238	238.0172	C ₆ H ₈ NO ₉ ⁻	-2.7	8.7	1		d	--
	326	326.0359	C ₉ H ₁₂ NO ₁₂ ⁻	1.6	23.8	2		d	--
	414	414.0539	C ₁₂ H ₁₆ NO ₁₅ ⁻	1.9	51.7	3		d	--
	502	502.0673	C ₁₅ H ₂₀ NO ₁₈ ⁻	-0.7	8.8	4		d	--
	590	590.0826	C ₁₈ H ₂₄ NO ₂₁ ⁻	-1.5	21.4	5		d	--
	678	678.1011	C ₂₁ H ₂₈ NO ₂₄ ⁻	1.0	12.1	6		d	--
	766	766.1182	C ₂₄ H ₃₂ NO ₂₇ ⁻	-3.8	16.7	7		d	--
	854	854.1367	C ₂₇ H ₃₆ NO ₃₀ ⁻	4.5	7.9	8		d	--
Oligoester Series 3^o	133	133.0142	C ₄ H ₅ O ₅ ⁻	0.5	5.4	1		117	C ₄ H ₅ O ₄ ⁺
	221	221.0283	C ₇ H ₉ O ₈ ⁻	-1.4	30.1	2		d	--
	309	309.0453	C ₁₀ H ₁₃ O ₁₁ ⁻	-1.9	0.1	3		d	--
	397	397.0617	C ₁₃ H ₁₇ O ₁₄ ⁻	-0.1	11.4	4		d	--
	485	485.0775	C ₁₆ H ₂₁ O ₁₇ ⁻	-0.4	55.5	5		d	--
Oligoester Series 4^f	147	147.0313	C ₅ H ₇ O ₅ ⁻	-0.9	2.3	1		131	C ₅ H ₇ O ₄ ⁺
	235	235.0457	C ₈ H ₁₁ O ₈ ⁻	-0.7	1.8	2		219	C ₈ H ₁₁ O ₇ ⁺
	323	323.0627	C ₁₁ H ₁₅ O ₁₁ ⁻	1.3	14.4	3		d	--
	411	411.0823	C ₁₄ H ₁₉ O ₁₄ ⁻	4.8	12.6	4		d	--
	499	499.0945	C ₁₇ H ₂₃ O ₁₇ ⁻	1.0	42.9	5		d	--
	587	587.1115	C ₂₀ H ₂₇ O ₂₀ ⁻	1.9	2.1	6		d	--
	675	675.1276	C ₂₃ H ₃₁ O ₂₃ ⁻	2.0	4.0	7		d	--
	763	763.1435	C ₂₆ H ₃₅ O ₂₆ ⁻	1.8	2.3	8		d	--
Oligoester Series 5	851	851.1621	C ₂₉ H ₃₉ O ₂₉ ⁻	4.4	6.4	9		d	--
	283	283.0031	C ₆ H ₇ N ₂ O ₁₁ ⁻	-1.9	12.2	n/a		d	--

^a Observed by UPLC/(-)ESI-TOFMS^b Observed by AMS V mode^c Suggested by AMS high-resolution W mode^d Not observed by AMS, most likely due to fragmentation of nitrate group, or below detection limit^e This oligoester series involves the esterification with formic acid.^f This oligoester series involves the esterification with acetic acid.

Table 7.5: SOA constituents detected by UPLC/(-)ESI-TOFMS and AMS in crotonaldehyde/high-NO₂ experiments.

	$[M - H]^{-a}$	UPLC/ESI-TOFMS Measured Mass	TOFMS Suggested Ion Formula	Error (mDa)	i-Fit	# of Acid Monomer Units (n)	Structure	$[M - OH]^{+b}$	AMS Suggested Ion Formula ^c
Oligoester Series 1	119	119.0342	C ₄ H ₇ O ₄ ⁻	-0.2	1.7	1		103	C ₄ H ₇ O ₃ ⁺
	221	221.0657	C ₈ H ₁₃ O ₇ ⁻	-0.4	18.6	2		205	C ₈ H ₁₃ O ₆ ⁺
Oligoester Series 2	266	266.0484	C ₈ H ₁₂ NO ₉ ⁻	1.3	22.5	1		<i>d</i>	--
	368	368.0819	C ₁₂ H ₁₈ NO ₁₂ ⁻	-1.0	30.3	2		<i>d</i>	--
	470	470.1104	C ₁₆ H ₂₄ NO ₁₅ ⁻	-3.4	34.9	3		<i>d</i>	--
	572	572.1486	C ₂₀ H ₃₀ NO ₁₈ ⁻	2.3	5.1	4		<i>d</i>	--
	674	674.1761	C ₂₄ H ₃₆ NO ₂₁ ⁻	-1.9	10.7	5		<i>d</i>	--
	776	776.2100	C ₂₈ H ₄₂ O ₂₄ ⁻	0.3	10.6	6		<i>d</i>	--
	878	878.2444	C ₃₂ O ₄₈ NO ₂₇ ⁻	3.0	12.1	7		<i>d</i>	--
Oligoester Series 3 ^o	not detected					1		131	C ₅ H ₇ O ₄ ⁺
	249	249.06	C ₉ H ₁₃ O ₈ ⁻	-1.0	1.4	2		233	C ₉ H ₁₃ O ₇ ⁺
	351	351.0937	C ₁₃ H ₁₉ O ₁₁ ⁻	1.3	1.4	3		<i>d</i>	--
	453	453.1255	C ₁₇ H ₂₅ O ₁₄ ⁻	1.1	2.6	4		<i>d</i>	--
	555	555.1592	C ₂₁ H ₃₁ O ₁₇ ⁻	3.1	1.5	5		<i>d</i>	--
	657	657.1909	C ₂₅ H ₃₇ O ₂₀ ⁻	3.1	0.6	6		<i>d</i>	--
Oligoester Series 4 ^f	161	161.0461	C ₆ H ₉ O ₅ ⁻	0.4	2.2	1		145	C ₆ H ₉ O ₄ ⁺
	263	263.0754	C ₁₀ H ₁₅ O ₈ ⁻	-2.1	7.5	2		<i>d</i>	--
	365	365.1087	C ₁₄ H ₂₁ O ₁₁ ⁻	1.5	15	3		<i>d</i>	--
	467	467.1401	C ₁₈ H ₂₇ O ₁₄ ⁻	-4.1	5.7	4		<i>d</i>	--
	569	569.1672	C ₂₂ H ₃₃ O ₁₇ ⁻	-4.6	20.6	5		<i>d</i>	--
	671	671.2040	C ₂₆ H ₃₉ O ₂₀ ⁻	0.5	0.6	6		<i>d</i>	--
Oligoester Series 5	not detected								

^a Observed by UPLC/(-)ESI-TOFMS^b Observed by AMS V mode^c Suggested by AMS high-resolution W mode^d Not observed by AMS, most likely due to fragmentation of nitrate group, or below detection limit^e This oligoester series involves the esterification with formic acid.^f This oligoester series involves the esterification with acetic acid.

Table 7.6: SOA constituents detected by UPLC/(-)ESI-TOFMS in 2M2B/high-NO₂ experiments.

	[M – H] [–]	UPLC/ESI- TOFMS Measured Mass	TOFMS Suggested Ion Formula	Error (mDa)	i-Fit	# of Acid Monomer Units (<i>n</i>)	Structure
Oligoester Series 1	133	133.0509	C ₅ H ₉ O ₄ [–]	0.8	11.5	1	
	249	249.0983	C ₁₀ H ₁₇ O ₇ [–]	0.6	18.0	2	
	365	365.1466	C ₁₅ H ₂₅ O ₁₀ [–]	1.8	16.3	3	
	481	481.1909	C ₂₀ H ₃₃ O ₁₃ [–]	-1.2	64.5	4	
Oligoester Series 2	294	294.0819	C ₁₀ H ₁₆ NO ₉ [–]	-0.6	90.8	1	
	410	410.1299	C ₁₅ H ₂₄ NO ₁₂ [–]	-3.8	12.2	2	
	526	526.1761	C ₂₀ H ₃₂ NO ₁₅ [–]	-1.1	3.2	3	
	641	642.2224	C ₂₅ H ₄₀ NO ₁₈ [–]	-2.1	27.0	4	
Oligoester Series 3^a	not detected					1	
	277	277.0919	C ₁₁ H ₁₇ O ₈ [–]	-0.4	20.5	2	
	393	393.1385	C ₁₆ H ₂₇ O ₁₁ [–]	-1.2	25.8	3	
	509	509.1856	C ₂₁ H ₃₃ O ₁₄ [–]	-1.4	3.1	4	
Oligoester Series 4^b	not detected					1	
	291	291.1083	C ₁₂ H ₁₉ O ₈ [–]	0.3	56.5	2	
	407	407.1536	C ₁₇ H ₂₇ O ₁₁ [–]	-1.7	5.0	3	
	523	523.2034	C ₂₂ H ₃₅ O ₁₄ [–]	0.7	18.1	4	
Oligoester Series 5	not detected						

^a This oligoester series involves the esterification with formic acid.^b This oligoester series involves the esterification with acetic acid.

Table 7.7: SOA constituents detected by UPLC/(-)ESI-TOFMS in 2-pentenal/high-NO₂ experiments.

	[M – H] [–]	UPLC/ESI- TOFMS Measured Mass	TOFMS Suggested Ion Formula	Error (mDa)	i-Fit	# of Acid Monomer Units (<i>n</i>)	Structure
Oligoester Series 1	133	133.0499	C ₅ H ₉ O ₄ [–]	-0.2	1.1	1	
	249	249.0992	C ₁₀ H ₁₇ O ₇ [–]	1.8	12.7	2	
	365	365.1447	C ₁₅ H ₂₅ O ₁₀ [–]	-0.1	9.4	3	
Oligoester Series 2	294	294.0839	C ₁₀ H ₁₆ NO ₉ [–]	1.4	5.2	1	
	410	410.1311	C ₁₅ H ₂₄ NO ₁₂ [–]	1.2	1.9	2	
	526	526.1762	C ₂₀ H ₃₂ NO ₁₅ [–]	-1.0	5.9	3	
	641	642.2251	C ₂₅ H ₄₀ NO ₁₈ [–]	0.6	24.3	4	
Oligoester Series 3^a		not detected				1	
	277	277.0922	C ₁₁ H ₁₇ O ₈ [–]	-0.1	12.5	2	
	393	393.1411	C ₁₆ H ₂₇ O ₁₁ [–]	1.4	14.0	3	
Oligoester Series 4^b		not detected				1	
	291	291.1080	C ₁₂ H ₁₉ O ₈ [–]	0.0	18.5	2	
	407	407.1555	C ₁₇ H ₂₇ O ₁₁ [–]	0.2	10.5	3	
	523	523.2032	C ₂₂ H ₃₅ O ₁₄ [–]	0.5	11.5	4	
Oligoester Series 5		not detected					

^a This oligoester series involves the esterification with formic acid.^b This oligoester series involves the esterification with acetic acid.

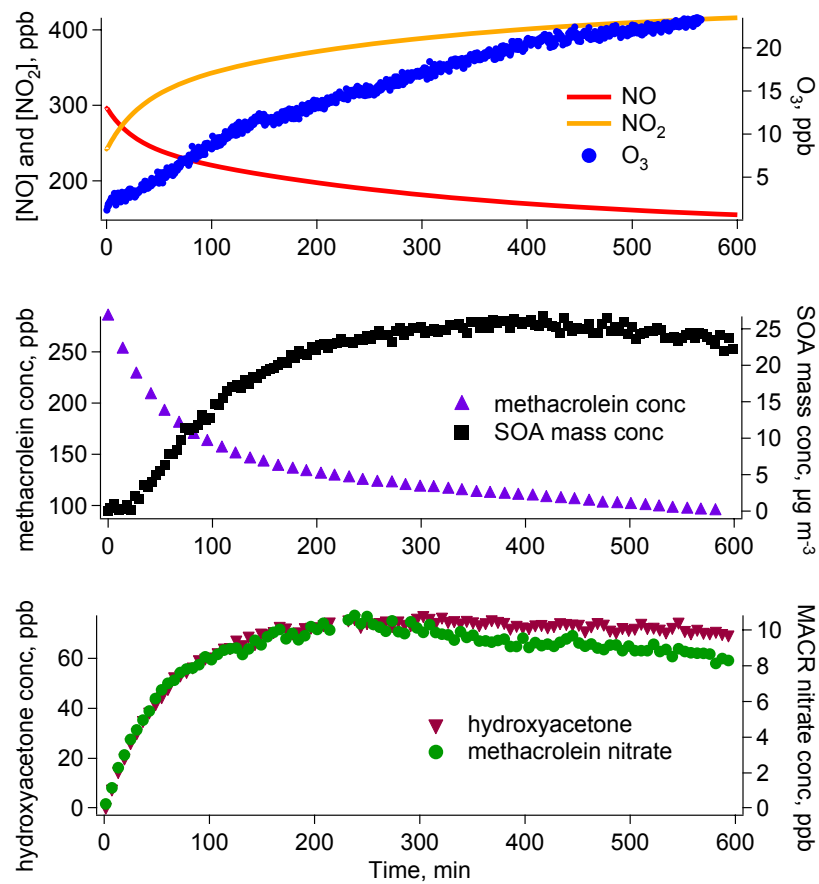


Figure 7.1: Concentration profiles of gas-phase species during a typical methacrolein/high-NO experiment (7/16). In this experiment, additional NO₂ was injected prior to irradiation. Concentrations of NO and NO₂ shown here are calculated from a photochemical model (see Appendix).

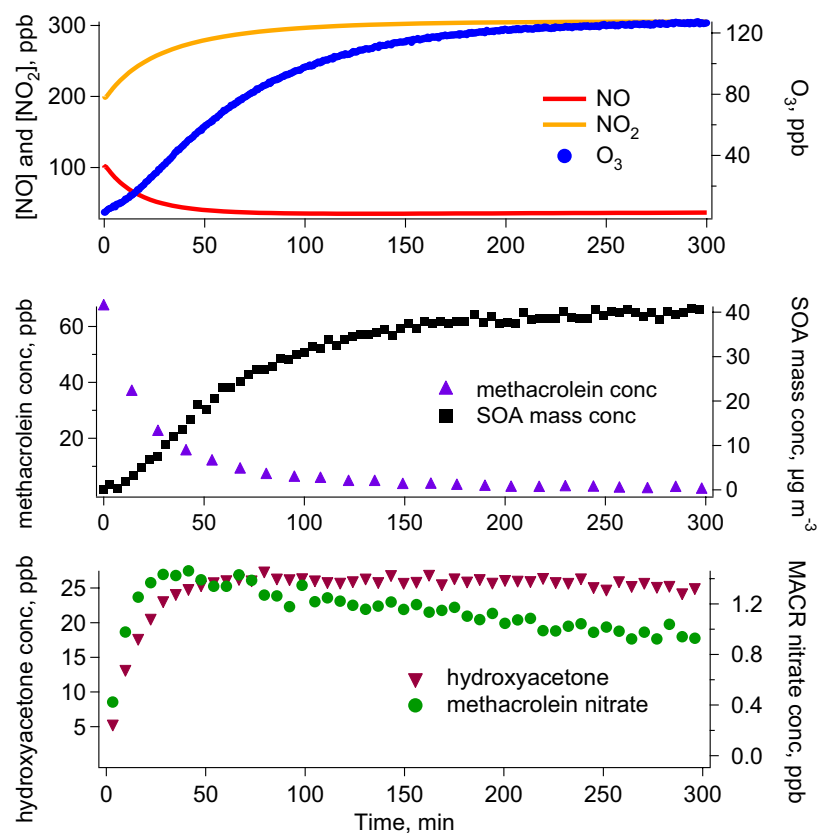


Figure 7.2: Concentration profiles of gas-phase species during a typical methacrolein/high- NO_2 experiment (9/15). Additional NO (100 ppb) and NO_2 (200 ppb) were injected prior to irradiation. Concentrations of NO and NO_2 shown here are calculated from a photochemical model (see Appendix). As a result of the higher OH concentrations from CH_3ONO than from HONO , more methacrolein was reacted and the concentrations of methacrolein nitrate relative to those of hydroxyacetone were lower than those in high- NO experiments, owing to a more rapid consumption by OH .

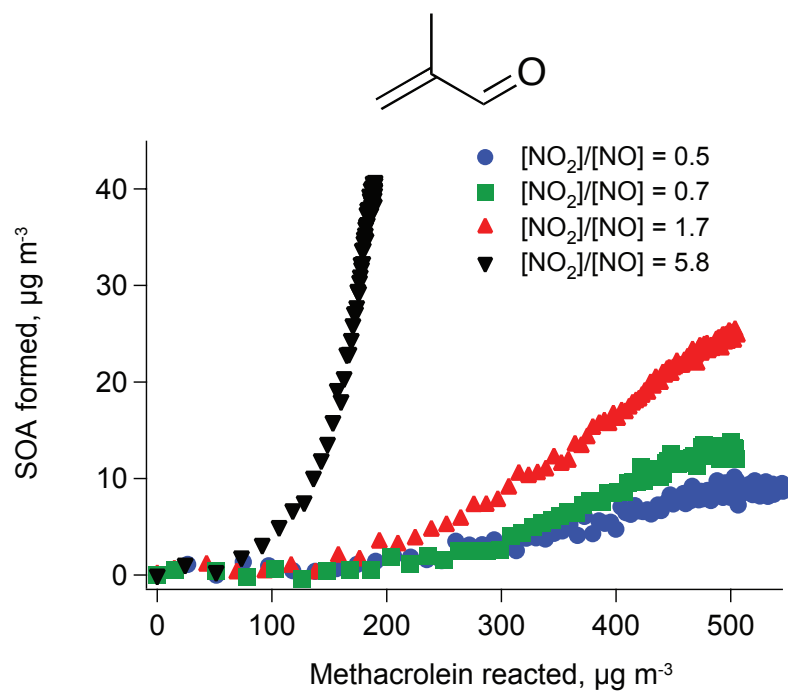


Figure 7.3: Time-dependent SOA growth curves for methacrolein photooxidation. NO_2/NO ratios are computed from photochemical modeling (see Appendix). In the high-NO experiments ($\text{NO}_2/\text{NO} < 2$), HONO was used as the OH precursor, and the NO_2/NO ratio was varied by adding different amounts of NO or NO_2 . In the high- NO_2 experiment, (black triangles), CH_3ONO was used as the OH precursor.

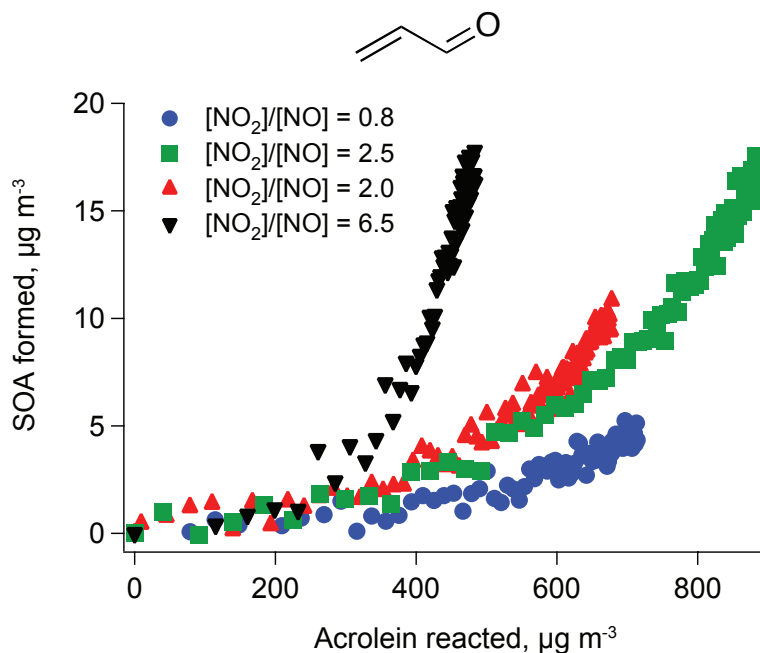


Figure 7.4: Time-dependent SOA growth curves for acrolein photooxidation. Similar to methacrolein photooxidation, NO_2/NO ratios are computed from photochemical modeling (see Appendix). In the high-NO experiments ($\text{NO}_2/\text{NO} < 3$), HONO was used as the OH precursor, and the NO_2/NO ratio was varied by adding different amounts of NO or NO_2 . In the experiment in which NO_2 was added (red triangles), high levels of NO_2 depress OH concentrations, resulting in less acrolein reacted. Concentrations of NO did not drop as rapidly as in other high-NO experiments, leading to a lower NO_2/NO ratio. In the high- NO_2 experiment (black triangles), CH_3ONO was used as the OH precursor.

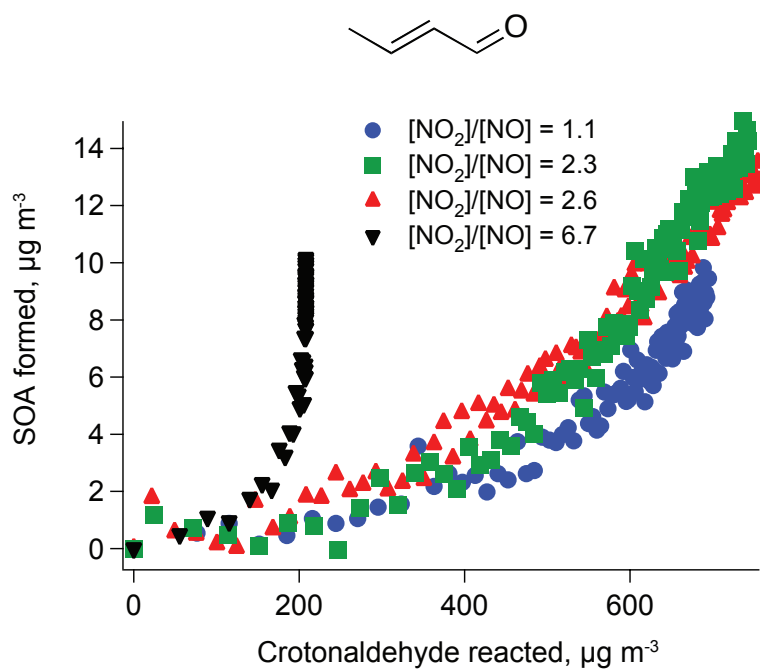


Figure 7.5: Time-dependent SOA growth curves for crotonaldehyde photooxidation. Similar to methacrolein photooxidation, NO_2/NO ratios are computed from photochemical modeling (see Appendix). In the high-NO experiments ($\text{NO}_2/\text{NO} < 3$), HONO was used as the OH precursor, and the NO_2/NO ratio was varied by adding different amounts of NO or NO_2 . In the high- NO_2 experiment (black triangles), CH_3ONO was used as the OH precursor.

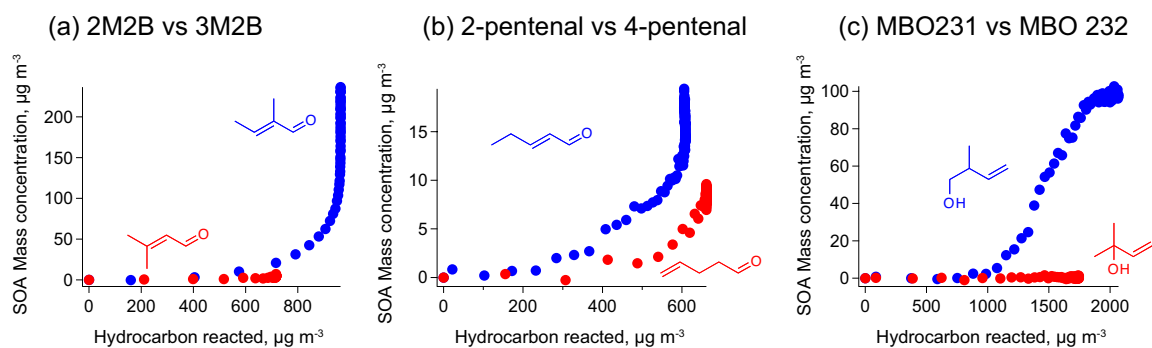


Figure 7.6: Comparisons of time-dependent SOA growth from photooxidation of (a) 2M2B and 3M2B, (b) 2-pentenal and 4-pentenal, and (c) MBO232 and MBO 231 under high- NO_2 conditions. Within each plot, initial concentrations of parent hydrocarbons are comparable (see Table 7.2).

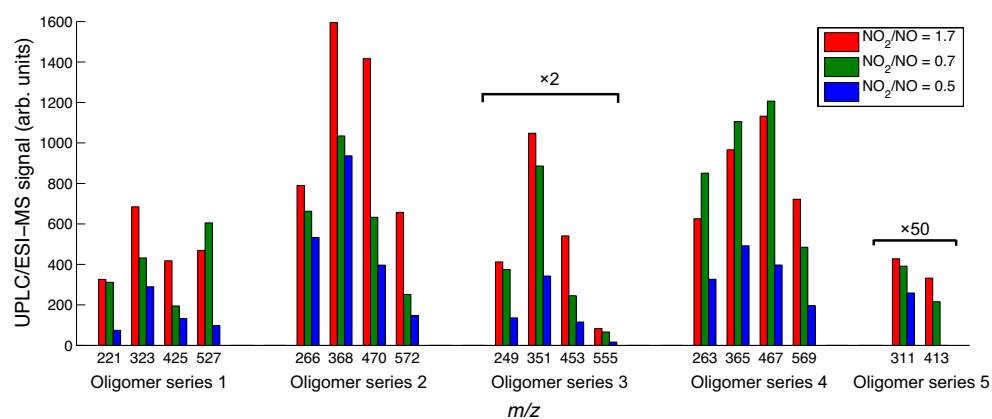


Figure 7.7: Absolute peak areas (normalized by sampling volume) of all deprotonated ions detected by UPLC/(-)ESI-TOFMS in methacrolein/high-NO experiments, listed in Table 7.3. The positive dependence of oligoester abundance on NO_2/NO ratios is consistent with the observed trend in overall SOA growth.

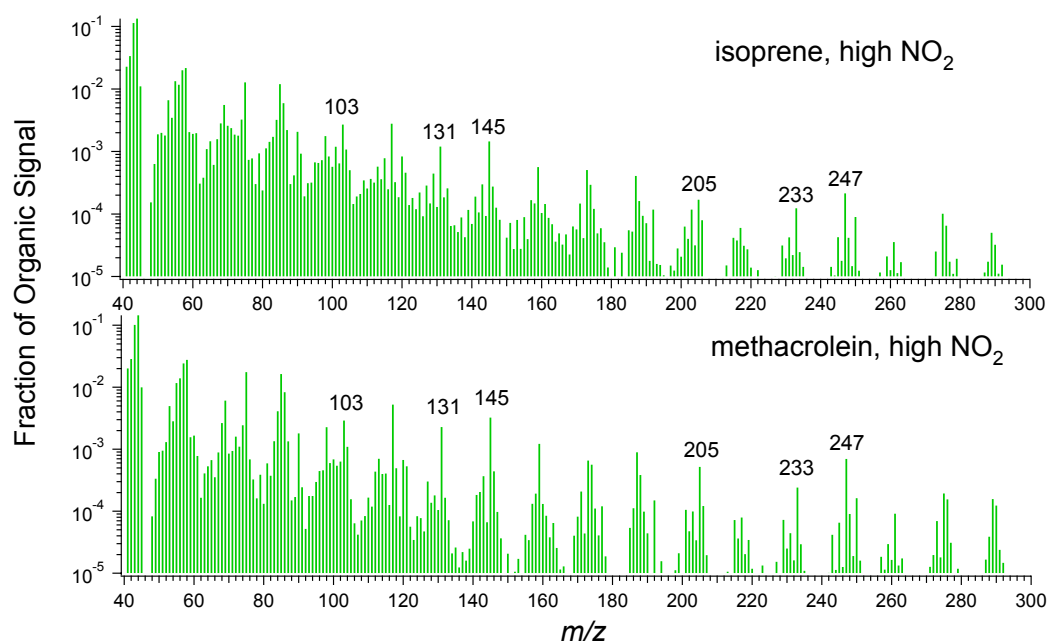


Figure 7.8: AMS V-mode organic spectra of SOA from high- NO_2 photooxidation of isoprene and methacrolein. The labelled ion peaks correspond to the loss of an O^{2-} group from compounds listed in Table 7.3, or the loss of an O^{2-} group and 2-MG monomer units from higher order oligoesters. The accurate masses are confirmed by W-mode high-resolution analysis, as shown in Fig. 7.9. Separation of 102 Da between major peaks is consistent with esterification with a 2-MG monomer.

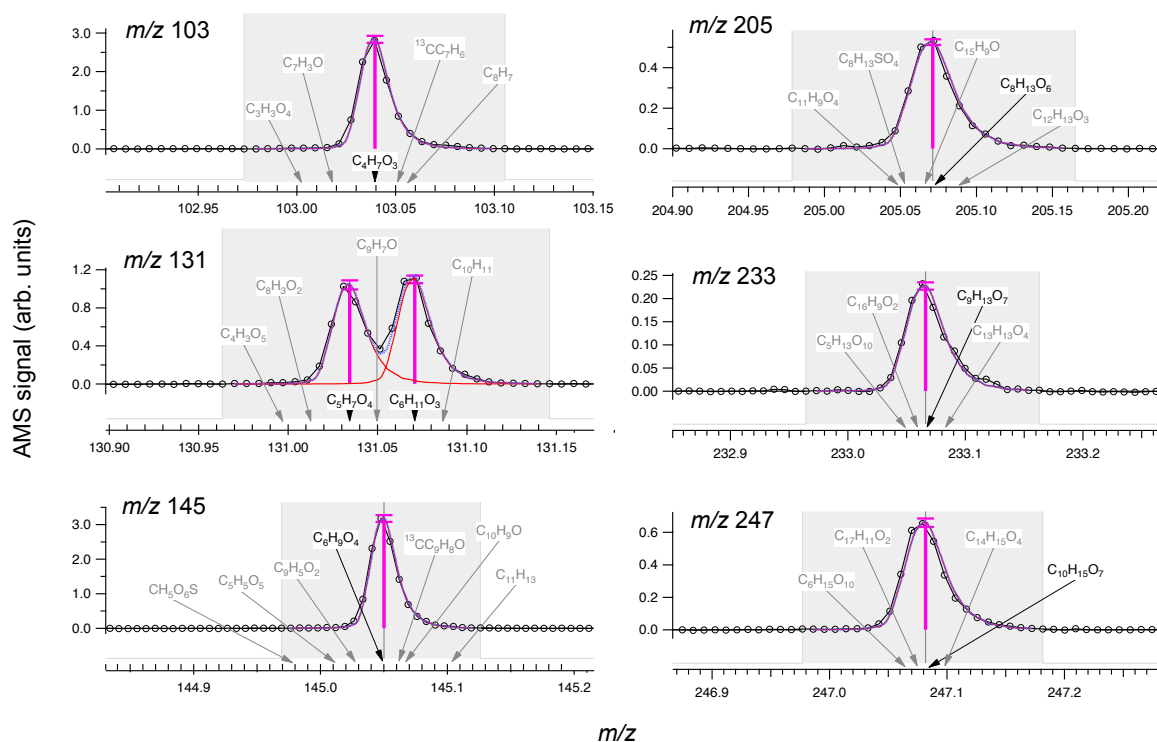


Figure 7.9: High-resolution W-mode AMS peaks of a number of the major fragment ions observed in methacrolein/high- NO_2 experiments. Knowledge of the accurate masses allow assignments of molecular formulas, corresponding to the loss of O^{2-} groups from compounds detected by offline analysis, suggesting that detection of compounds listed in Table 7.3 is not a result of sampling artifacts. m/z 131 contains two different ions, only one of which is consistent with compounds detected by offline UPLC/(–)ESI-TOFMS analysis.

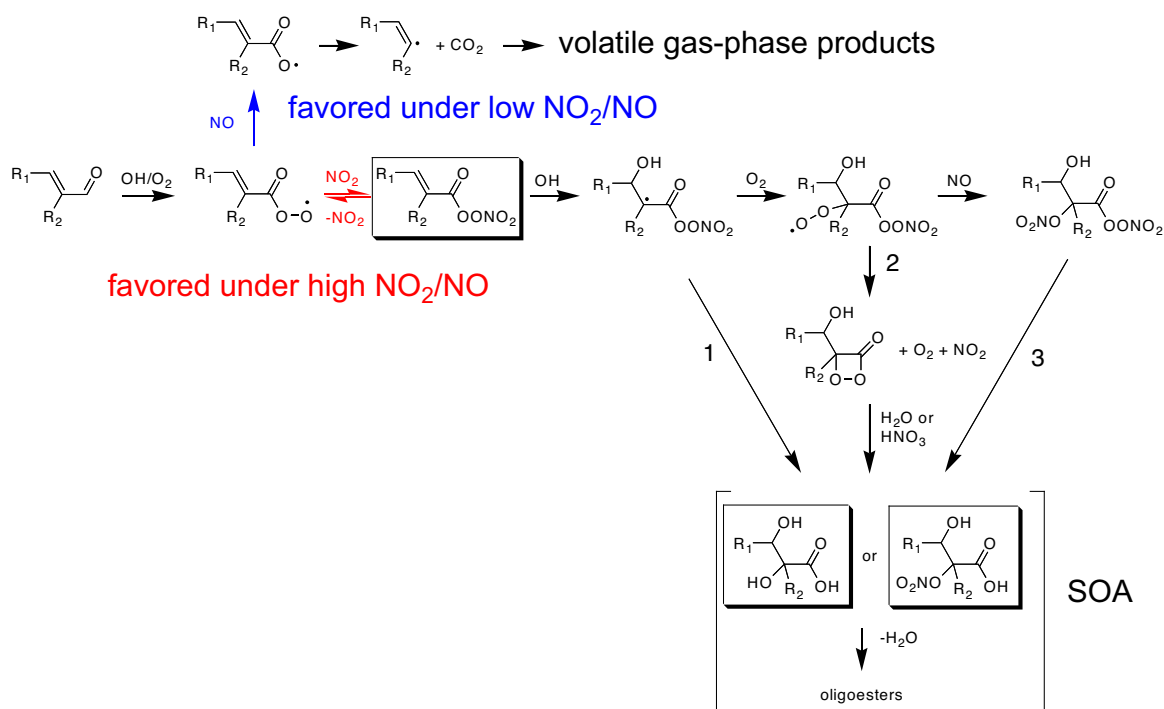


Figure 7.10: Proposed mechanism to form aerosol-phase products from α,β -unsaturated aldehydes. The pathways highlighted in red are favored under high NO_2/NO ratios and lead to aerosol formation. The pathways highlighted in blue are favored under low NO_2/NO ratios and lead to fragmentation into volatile products. Aerosol formation from OH-reaction of unsaturated PANs can proceed via 3 possible routes (routes 1–3), and detailed investigation of each route is discussed in the main text.

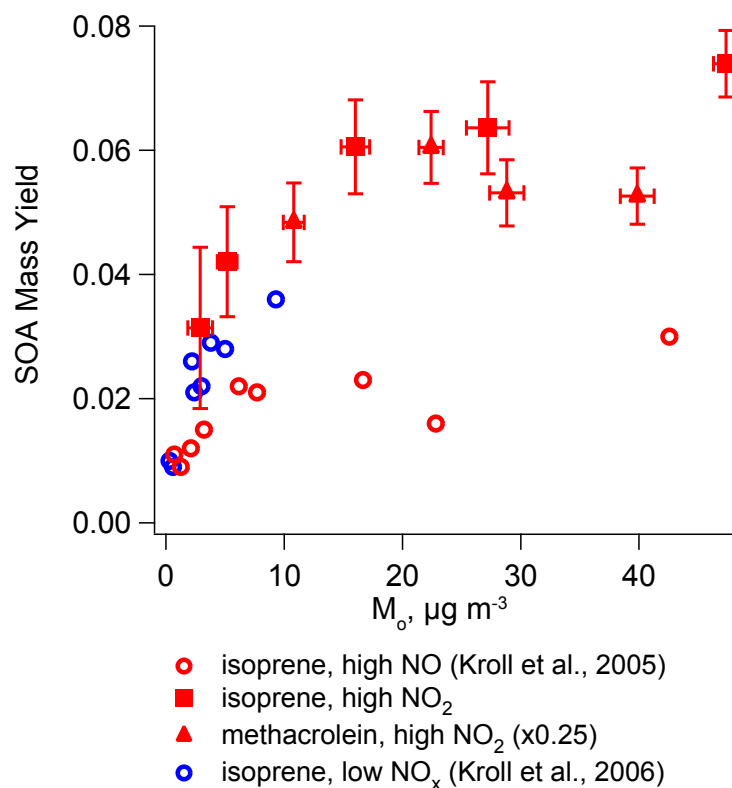


Figure 7.11: SOA mass yields from isoprene photooxidation under neutral seed conditions as a function of organic loading. The solid markers indicate SOA yields measured in this study, using CH_3ONO as the OH precursor under high NO_2/NO ratios (between 3 and 8). The SOA yields for methacrolein (solid red triangles) have been multiplied by 0.25 to account for the gas-phase product yield of methacrolein from isoprene high- NO_x oxidation. The SOA yields measured under high- NO_2/NO conditions are higher than both high-NO (open red circles) and low- NO_x conditions (open blue circles) under neutral seed conditions. With an acidified seed, SOA yields can be as high as 0.29 (Surratt et al., 2010).

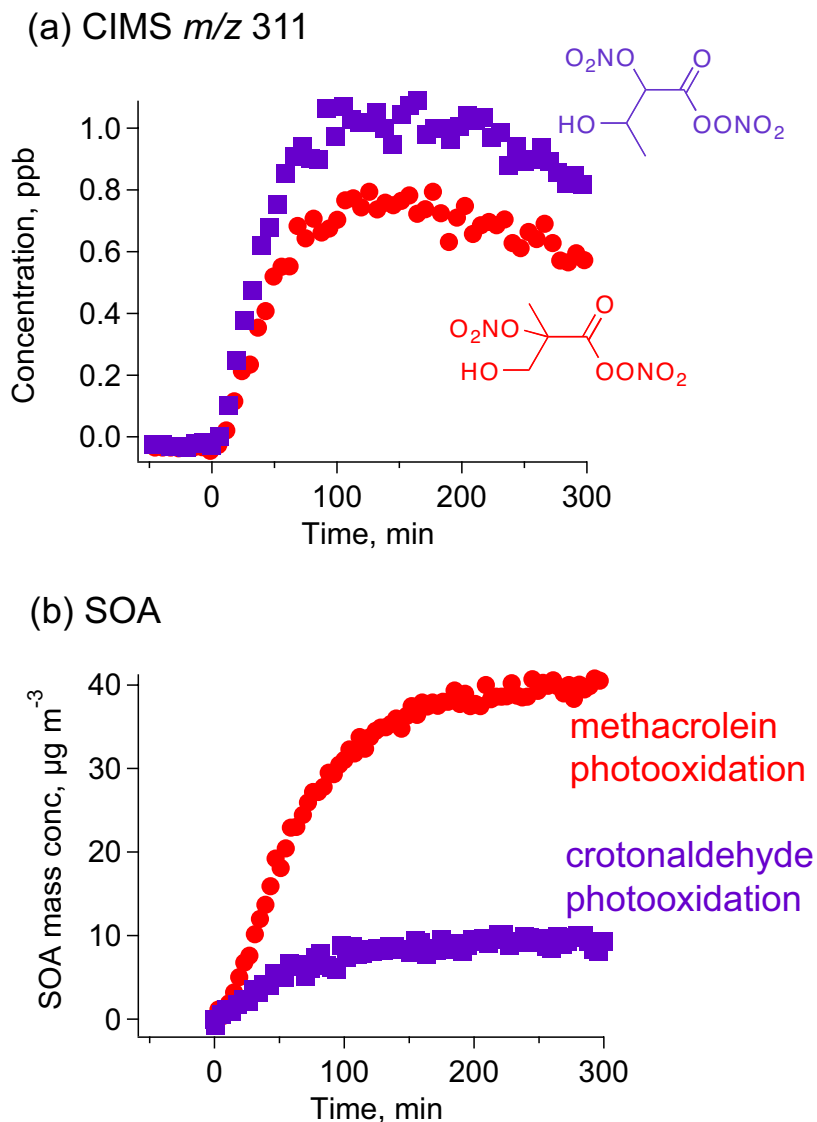


Figure 7.12: Time trends of (a) gas-phase CIMS m/z 311 and (b) SOA growth during high- NO_2 photooxidation of methacrolein (red) and crotonaldehyde (purple). m/z 311 corresponds to the unit mass of CF_3O^- adduct of C₄-hydroxynitrate-PAN. The observed gas-phase signals of C₄-hydroxynitrate-PAN in both experiments are within 20% of each other, but the amount of SOA formed from methacrolein photooxidation is about a factor of 4 higher. A similar difference was observed between 2M2B and 3M2B photooxidation. This suggests that C₄- and C₅-hydroxynitrate-PANs are not precursors to low-volatility aerosol-phase products.

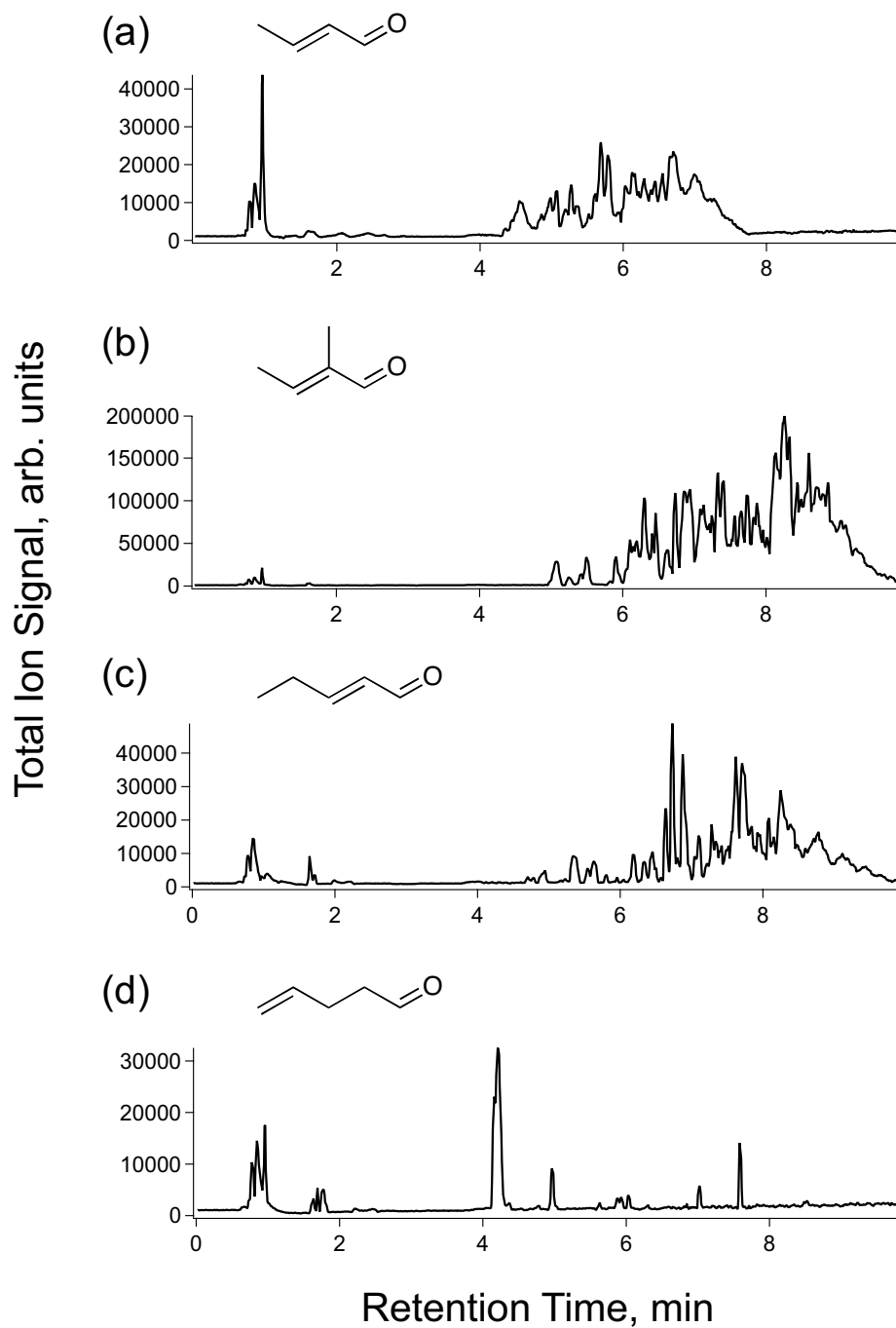
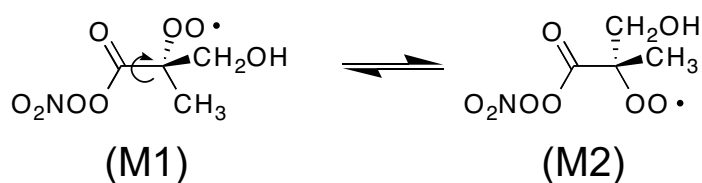


Figure 7.13: UPLC/(-)ESI-TOFMS base peak ion chromatograms (BPCs) for high- NO_2 photooxidation of (a) crotonaldehyde, (b) 2M2B, (c) 2-pentenal, and (d) 4-pentenal. The exact masses and elemental composition of detected $[\text{M}-\text{H}]^-$ ions are listed in Tables 7.5 to 7.7. Compounds detected in crotonaldehyde, 2M2B, and 2-pentenal SOA are likely similar. (SOA products from C_5 2M2B and 2-pentenal are less polar than those from crotonaldehyde, a C_4 compound, and therefore have longer retention times in reverse-phase chromatography.) The chemical composition of 4-pentenal SOA is significantly different from those all 3 other aldehydes, and no oligoester products are detected, suggesting a different SOA formation mechanism.

Methacrolein:



Crotonaldehyde:

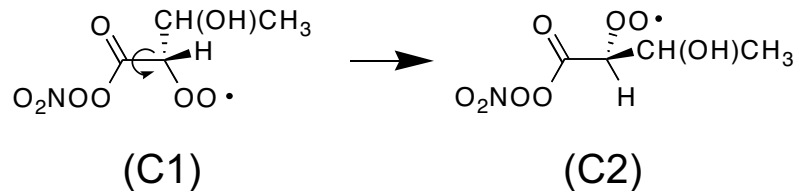
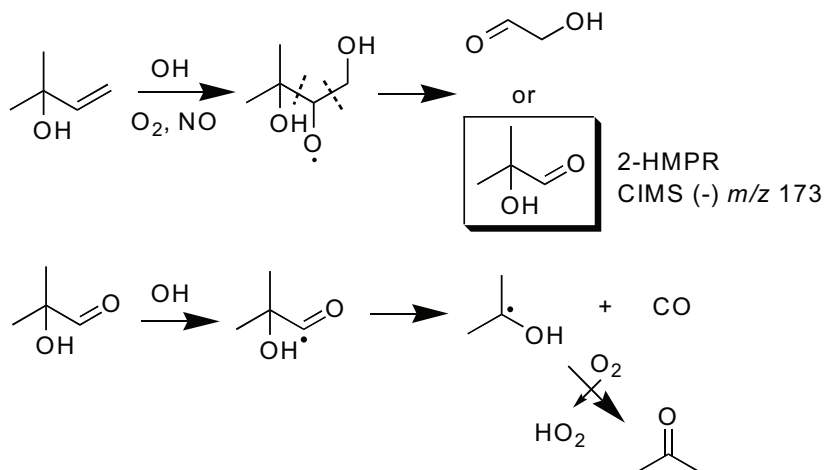


Figure 7.14: Rotational conformers of hypothesized SOA intermediate in methacrolein and crotonaldehyde mechanism. For methacrolein, the methyl group on the α -carbon presents significant steric hinderance, which favors the conformer M2. This increases the interaction between the peroxy radical and the peroxy nitrate group, leading to significant SOA formation. For crotonaldehyde, the hydrogen atom presents much smaller steric hinderance, favoring the conformer C2. As a result, the peroxy radical is out of plane with the PAN group, and the reaction to form SOA can be less favorable.

MBO232:



MBO231:

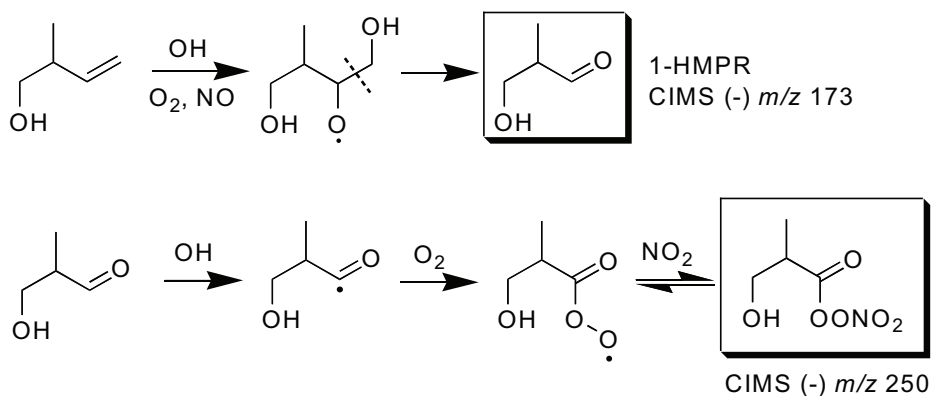


Figure 7.15: Mechanism of MBO231 and MBO232 photooxidation under high- NO_x conditions. The dashed lines indicate possible locations of C-C bond scission under decomposition of alkoxy radicals. For MBO232, 2-HMPR formation is relatively small, as scission of the C-C bond with the 4-carbon is not favored. In addition, the acyl radical from H-abstraction of 2-HMPR rapidly decomposes to CO and acetone. As a result, PAN formation is unlikely. For MBO231, 1-HMPR formation is favored from the decomposition of the alkoxy radical. Furthermore, OH reaction of 1-HMPR leads to an acyl peroxy radical, which reacts with NO_2 to form a C₄-hydroxy-PAN.

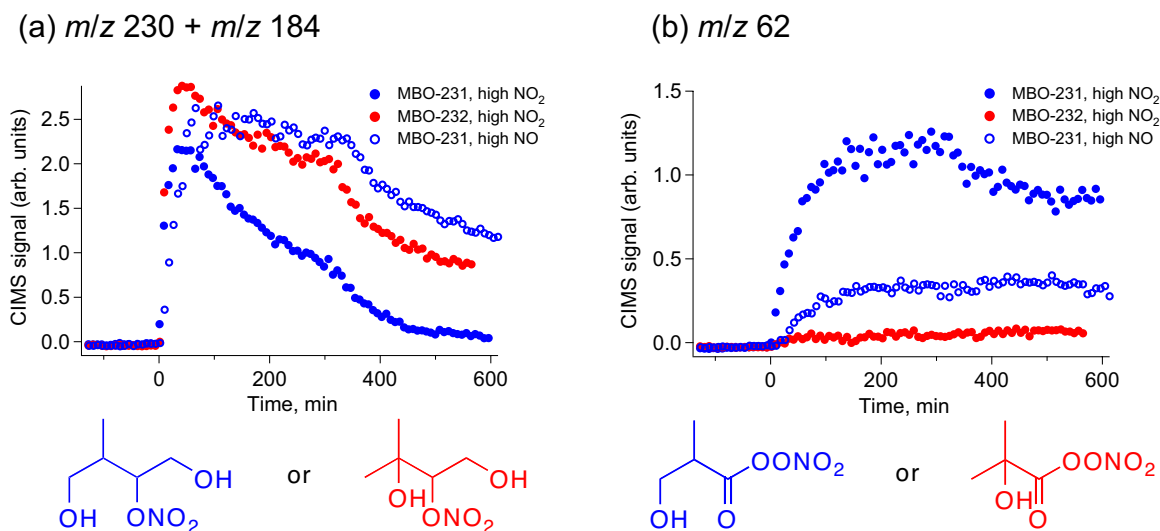


Figure 7.16: Gas-phase ion signals of C_4 -hydroxy-PAN and C_5 -dihydroxynitrate from photooxidation of MBO231 and MBO232, as observed by negative chemical ionization-tandem mass spectrometry of m/z 250. Neutral losses of HF or CF_2O are associated with the C_5 -dihydroxynitrate under CID of the parent ion m/z 250, leading to daughter ions of 230 and 184, respectively. The daughter ion m/z 62, most likely NO_3^- , is associated with the C_4 -hydroxy-PAN. (See Supplementary Material for more details.) After 300 minutes of irradiation, more OH precursor was added to further react oxidation products. PAN formation was observed only from MBO231 oxidation and is positively correlated with NO_2/NO , similar to unsaturated aldehydes.

Chapter 8

Conclusions

SOA formation arising from hydrocarbon oxidation is a complex and dynamic process. In this thesis, a combination of modeling and experimental work is used to study the oxidation reactions of volatile hydrocarbons leading to low-volatility products, as knowledge of these reactions is key to extrapolating experimental findings to understanding ambient aerosol formation.

In Chapters 2 and 3, the current equilibrium partitioning model is extended to include gas- and particle-phase reactions and to establish a kinetic framework for atmospheric SOA models. Using a simplified kinetic model, we illustrate the importance of conducting experiments under relevant kinetic conditions. For example, the induction period associated with subsaturation of semivolatile species can lead to systematic underprediction of SOA yields, as a result of reactive loss in the gas phase. Model predictions are qualitatively consistent with the observed effects of kinetic parameters, such as oxidation rate, preexisting seed particles, and extent of reaction. Distinguishing between reaction mechanisms that lead to similar overall SOA growth behavior requires detailed chemical measurements of gas- and aerosol-phase species, and studies of SOA formation need to be conducted under atmospherically relevant kinetic and equilibrium conditions.

To be able to accurately model ambient SOA formation, the potential sources of SOA also need to be better characterized. While it is shown in Chapter 4 that photooxidation of 2-methyl-3-buten-2-ol (MBO) does not produce significant amounts of aerosol, low-volatility precursors, such as PAHs, can be further oxidized in the gas phase, leading to even more aerosol formation (see Chapter 5). Upon photooxidation, naphthalene and other 2-ring PAHs produce aerosol at substantial mass yields. SOA formation is highly dependent on NO_x conditions, as lower yields and higher volatilities of SOA are observed for high- NO_x photooxidation. This is linked to the ring-opening fragmentation reactions which dominate the fate of peroxy radicals, resulting in greater formation of relatively volatile products as observed by gas-phase mass spectrometry. Together with *n*-alkanes, PAHs are estimated to account for a substantial fraction of SOA formed from oxidation of diesel exhaust and wood burning emissions. To properly account for SOA formation from anthropogenic sources, photooxidation of low-volatility precursors, such as PAH and *n*-alkanes, should therefore be included in atmospheric SOA models, likely increasing the amount of predicted anthropogenic SOA

significantly. Other low-volatility precursors, such as aliphatic aldehydes and large olefins, could also be an important source of SOA, and further study is required to evaluate their potential to form SOA. Better characterization of the emissions of these compounds is also required, as they could potentially contribute a large fraction of SOA.

In this thesis, the processes involved in SOA formation are also studied in detail. In particular, the effect of seed acidity and NO_x can dramatically influence the product distribution observed from hydrocarbon oxidation. In Chapter 6, under low- NO_x conditions, the mechanism by which seed acidity promotes SOA growth is revealed to be acid catalysis of ring-opening reactions of epoxydiols, leading to low-volatility products such as 2-methyltetrols and organosulfates. Under high- NO_x conditions, SOA formation from isoprene proceeds through the MPAN channel. Further oxidation of methacrolein, a first-generation product from isoprene high- NO_x photooxidation, leads to methacryloyl peroxy radicals, which subsequently reacts with NO_2 to form MPAN. Oxidation of MPAN leads to low-volatility acids, nitrates, and oligoesters observed in isoprene high- NO_x SOA.

In Chapter 7, the implications of aldehyde chemistry and the “ NO_x effect” on SOA yields are further explored. It is revealed that the molecular structure of isoprene and methacrolein is conducive to formation of low-volatility products, as the conjugated double bonds and the additional methyl group favor the chemistry to form SOA. In most photooxidation systems, there exists a competition between the $\text{RO}_2 + \text{HO}_2$ pathway (which leads to relatively high SOA yields) and the $\text{RO}_2 + \text{NO}$ pathway (which forms more volatile products) that determines SOA yields. In the isoprene-high- NO_x system, owing to the MPAN chemistry, the present work shows the importance of the $\text{RO}_2 + \text{NO}_2$ pathway of unsaturated aldehyde photooxidation as a route leading to SOA formation. In Chapters 4 and 7, MBO, a C_5 unsaturated alcohol, is found not to be a significant source of SOA, which can be explained by relatively low glyoxal and PAN yields from high- NO_x photooxidation. Under low- NO_x conditions, the low SOA yields from MBO are consistent with the lack of a second double bond to further functionalize the carbon backbone, leading to relatively volatile oxidation products.

The chemistry elucidated in this thesis has important implications on SOA formation from other atmospheric compounds, especially those with conjugated double bonds. For example, photooxi-

dation of aromatic compounds can lead to α,β -unsaturated aldehydes, which can form substantial amounts of low-volatility products via a PAN intermediate. At atmospherically relevant NO_2/NO ratios, SOA yields from isoprene can be up to 3 times higher than those previously measured under high-NO conditions. The yields exceed even those measured under low- NO_x conditions. Atmospheric SOA formation from aldehydes may therefore be significantly underestimated in current models, since an appreciable fraction of SOA is generated in areas where NO_2/NO ratios are high. Further work is required to quantitatively establish the dependence of SOA yields on relative concentrations of NO, NO_2 , and HO_2 such that the effects of oxidation chemistry can be properly represented in atmospheric models.

Appendix A

Secondary organic aerosol formation from *m*-xylene, toluene, and benzene*

*Reproduced with permission from “Secondary organic aerosol formation from *m*-xylene, toluene, and benzene” by N. L. Ng, J. H. Kroll, A. W. H. Chan, P. S. Chhabra, R. C. Flagan, and J. H. Seinfeld, *Atmospheric Chemistry and Physics*, 7 (14), 3909–3922, 2007. Copyright 2007 by Authors. This work is licensed under a Creative Commons License.

Secondary organic aerosol formation from *m*-xylene, toluene, and benzene

N. L. Ng¹, J. H. Kroll^{1,*}, A. W. H. Chan¹, P. S. Chhabra¹, R. C. Flagan¹, and J. H. Seinfeld¹

¹Departments of Chemical Engineering and Environmental Science and Engineering, California Institute of Technology, Pasadena, CA 91125, USA

*now at: Aerodyne Research, Inc. 45 Manning Road, Billerica, MA 01821, USA

Received: 1 March 2007 – Published in Atmos. Chem. Phys. Discuss.: 28 March 2007

Revised: 28 June 2007 – Accepted: 13 July 2007 – Published: 24 July 2007

Abstract. Secondary organic aerosol (SOA) formation from the photooxidation of *m*-xylene, toluene, and benzene is investigated in the Caltech environmental chambers. Experiments are performed under two limiting NO_x conditions; under high-NO_x conditions the peroxy radicals (RO₂) react only with NO, while under low-NO_x conditions they react only with HO₂. For all three aromatics studied (*m*-xylene, toluene, and benzene), the SOA yields (defined as the ratio of the mass of organic aerosol formed to the mass of parent hydrocarbon reacted) under low-NO_x conditions substantially exceed those under high-NO_x conditions, suggesting the importance of peroxy radical chemistry in SOA formation. Under low-NO_x conditions, the SOA yields for *m*-xylene, toluene, and benzene are constant (36%, 30%, and 37%, respectively), indicating that the SOA formed is effectively nonvolatile under the range of $M_o(>10\ \mu\text{g m}^{-3})$ studied. Under high-NO_x conditions, aerosol growth occurs essentially immediately, even when NO concentration is high. The SOA yield curves exhibit behavior similar to that observed by Odum et al. (1996, 1997a, b), although the values are somewhat higher than in the earlier study. The yields measured under high-NO_x conditions are higher than previous measurements, suggesting a “rate effect” in SOA formation, in which SOA yields are higher when the oxidation rate is faster. Experiments carried out in the presence of acidic seed aerosol reveal no change of SOA yields from the aromatics as compared with those using neutral seed aerosol.

aromatic hydrocarbons leads to the production of ozone as well as low-volatility species which then partition into the condensed phase, forming secondary organic aerosol (SOA).

The anthropogenic contribution to global SOA formation is currently estimated to be small, roughly about 10% (Tsigaridis and Kanakidou, 2003). Ambient measurements suggest that SOA formation in the atmosphere is higher than that predicted by current models (Heald et al., 2005, 2006; de Gouw et al., 2005; Volkamer et al., 2006). In addition, it has been suggested that SOA formation from anthropogenic sources is substantially higher than currently thought (de Gouw et al., 2005; Volkamer et al., 2006).

Gas-phase chemistry of aromatic hydrocarbons is dominated by reaction with the OH radical (Calvert et al., 2002). Despite considerable study of the oxidation chemistry of aromatic hydrocarbons, the basic underlying mechanisms of SOA formation and growth from aromatic precursors remain poorly understood. There have been few studies on the molecular composition of SOA from aromatic hydrocarbons (Forstner et al., 1997; Jang and Kamens, 2001; Kleindienst et al., 2004). The carbon balance is poorly constrained; generally, only about 50% of the reacted carbon has been identified as products (Calvert et al., 2002).

SOA formation from individual precursors is typically studied in laboratory chamber experiments. Aerosol yields from the photooxidation of aromatic hydrocarbons have been shown to be highly sensitive to the NO_x level (Hurley et al., 2001; Johnson et al., 2004, 2005; Song et al., 2005); generally, a higher SOA yield is observed under low-NO_x conditions. This general dependence of SOA formation on the NO_x level has been proposed to be the result of differences in concentrations of different oxidants (OH, O₃, and NO₃) (Hurley et al., 2001), or in changes in peroxy radical chemistry (Hatakeyama et al., 1991; Johnson et al., 2004, 2005; Presto et al., 2005; Kroll et al., 2006). In addition, particle-phase reactions have been found to be important processes in SOA formation (Kalberer et al., 2004; Gao et al., 2004a, b;

1 Introduction

Aromatic hydrocarbons contribute an important fraction (~20–30%) of total volatile organic compounds in the urban atmosphere (Calvert et al., 2002). Atmospheric oxidation of

Correspondence to: J. H. Seinfeld
 (seinfeld@caltech.edu)

Tolocka et al., 2004), and the presence of sulfuric acid seed has been shown to lead to increased SOA yields in a number of systems (Jang et al., 2002; Iinuma et al., 2004; Gao et al., 2004a, b; Edney et al., 2005). Odum et al. (1996, 1997a, b) performed an extensive study on aromatic SOA formation. In light of the recent findings on the NO_x dependence and effect of seed aerosol acidity on SOA yields, it is important that SOA formation from aromatics be restudied to establish fully the NO_x dependence and effect of particle acidity on SOA formation.

Most chamber experiments of SOA formation by aromatics involve the irradiation of aromatic/ NO_x mixtures (Izumi and Fukuyama, 1990; Odum et al., 1996, 1997a, b; Hurley et al., 2001; Johnson et al., 2004; Song et al., 2005). In these classical photooxidation experiments, the NO and NO_2 concentrations (hence NO/ NO_2 ratio) constantly change, making it difficult to isolate the effect of NO_x on SOA formation. For example, the decreasing NO concentration over the course of the experiment may lead to a switch from “high- NO_x ” conditions to “low- NO_x ” conditions for the peroxy radical chemistry (Johnson et al., 2004). Another potential complication in interpreting SOA data is that a delay in aerosol formation from the onset of photooxidation has been frequently observed in aromatic systems; in particular, aerosol does not form until the concentration of NO approaches zero. When extrapolating to urban areas where the NO_x level is usually high, this would suggest that aromatics (and other hydrocarbons) do not produce SOA in the atmosphere. The observation that SOA does not form until [NO] approaches zero is not universal, however; in a study of toluene photooxidation by Stroud et al. (2004), aerosol growth is observed even at NO concentrations of 1–3 ppm. Thus the NO_x dependence of SOA yields, which is a crucial parameter for atmospheric modeling, is very poorly understood.

In this work, SOA formation from the photooxidation of *m*-xylene, toluene, and benzene is investigated. A main goal of this study is to establish the NO_x dependence of SOA formation for these aromatic hydrocarbons. In the experiments, SOA formation under two NO_x conditions is studied: (1) high- NO_x experiments in which HONO is used as the OH precursor and the NO_x level at the inception of photooxidation is ~ 1 ppm; and (2) low- NO_x experiments in which H_2O_2 is used as the OH precursor and no NO_x is introduced into the chambers. The background NO_x concentration is < 1 ppb, which is within the uncertainty of the NO_x monitor. By performing experiments at these extreme NO_x limits, the oxidation conditions (initiating oxidant and fate of peroxy radicals) can be maintained relatively constant over the course of the experiment, allowing for the evaluation of the effect of NO_x level on SOA formation. Additionally, the effect of seed aerosol acidity on SOA formation is studied under both high- and low- NO_x conditions. The SOA yield parameters obtained at the two NO_x limits allow one to parameterize the NO_x dependence of SOA formation for use in atmospheric models (Presto et al., 2006).

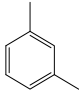
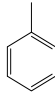
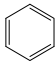
2 Experimental section

Experiments are performed in Caltech’s indoor, dual 28 m^3 Teflon environmental chambers. Details of the facilities have been given elsewhere (Cocker et al., 2001; Keywood et al., 2004). Before each experiment, the chambers are flushed continuously with dry purified air for ~ 24 h. Each chamber has a dedicated Differential Mobility Analyzer (DMA, TSI model 3081) coupled with a condensation nucleus counter (TSI model 3760) for measuring aerosol size distribution, number concentration, and volume concentration. All aerosol growth data are corrected for wall loss, in which size-dependent coefficients determined from inert particle wall loss experiments are applied to the aerosol volume data (Keywood et al., 2004). Generally, the wall loss coefficients range from 10^{-4} to 10^{-2} particles min^{-1} . Temperature, relative humidity (RH), O_3 , NO, and NO_x are continuously monitored. Half of the available black lights are used in the experiments. The initial temperature of the chamber is $\sim 20^\circ\text{C}$. Heating from the lights leads to a temperature increase of approximately 5°C inside the chamber over the course of the experiment. The analytical instruments are located outside the chamber enclosure and are at the temperature of the surrounding room (~ 20 – 22°C). The air may cool slightly as it is sampled from the chamber into the instruments, and the measured aerosol likely corresponds to the gas-particle partitioning at the temperature of the instruments rather than the chamber enclosure. Such small temperature differences are unlikely to affect results significantly.

Seed particles are introduced into the chamber to act as a substrate onto which the gas-phase products may condense. In an earlier work, we have shown that without seed particles, there is an “induction period” in which hydrocarbon is reacted but no aerosol is formed, which has the effect of biasing SOA yield measurements low (Kroll et al., 2007). Therefore, for all experiments in this study seed particles are used to eliminate this effect. Seed particles are generated by atomizing an aqueous solution with a constant-rate atomizer. The nonacid seed consists of $0.015\text{ M } (\text{NH}_4)_2\text{SO}_4$, while the acidic seed contains a mixture of $0.015\text{ M } (\text{NH}_4)_2\text{SO}_4$ and $0.015\text{ M } \text{H}_2\text{SO}_4$. Since all experiments are performed at $\text{RH} \sim 5\%$, which is lower than the crystallization RH (35%) of ammonium sulfate, the nonacid seed is likely a solid (Seinfeld and Pandis, 2006). The initial particle number concentration is about $30\,000\text{ particles cm}^{-3}$, with a geometric mean diameter of about 50 nm . Initial aerosol seed volume is about $15\text{ }\mu\text{m}^3\text{ cm}^{-3}$. After introduction of the seed aerosol, a known volume of the parent hydrocarbon is injected into a glass bulb, and introduced into the chambers by an air stream. The concentration (mixing ratio) of the parent hydrocarbon is monitored with a Hewlett Packard gas chromatograph (model 5890) with flame ionization detection (GC-FID).

In most of the high- NO_x experiments nitrous acid (HONO) serves as the OH precursor. It is introduced into the

Table 1. Aromatic hydrocarbons studied.

Parent Hydrocarbon	Structure	Formula (MW)	k_{OH}^a (cm ³ molec ⁻¹ s ⁻¹)
<i>m</i> -xylene		C ₈ H ₁₀ (106)	2.31 x 10 ⁻¹¹
toluene		C ₇ H ₈ (92)	5.63 x 10 ⁻¹²
benzene		C ₆ H ₆ (78)	1.22 x 10 ⁻¹²

^a: Rate constants were obtained from Calvert et al. (2002).

Table 2. Initial conditions and data for high-NO_x (HONO) experiments.

Expt. No.	Parent Hydrocarbon	T (K)	RH (%)	NO (ppb)	NO ₂ (ppb)	Seed	ΔHC (ppb)	Δ <i>M_o</i> (μg/m ³)	SOA Yield (%) ^a
1	<i>m</i> -xylene	297	5.5	470	473	(NH ₄) ₂ SO ₄	70.9	18.2±1.8	5.9±0.4
2	<i>m</i> -xylene	298	5.7	451	494	(NH ₄) ₂ SO ₄	28.1	4.3±1.2	3.5±0.7
3	<i>m</i> -xylene	298	5.9	432	511	(NH ₄) ₂ SO ₄	132.5	46.4±3.7	8.0±0.3
4	<i>m</i> -xylene	297	5.1	431	514	(NH ₄) ₂ SO ₄	106.1	36.7±2.8	8.0±0.2
5	toluene	298	3.8	421	524	(NH ₄) ₂ SO ₄	30.1	9.1±1.3	8.0±0.7
6	toluene	298	4.3	414	532	(NH ₄) ₂ SO ₄	56.7	23.8±2.2	11.1±0.4
7	toluene	298	4.9	388	559	(NH ₄) ₂ SO ₄	80.2	38.7±3.3	12.8±0.4
8	toluene	298	4.4	373	568	(NH ₄) ₂ SO ₄	50.7	20.9±1.9	10.9±0.5
9	benzene	297	5.2	83	86	(NH ₄) ₂ SO ₄	39.4	35.4±2.7 ^b	28.1±0.9

^a: Stated uncertainties (1σ) are from scatter in particle volume measurements.

^b: Assuming an SOA density of 1.4 g cm⁻³.

chamber after injection of the seed aerosol and parent hydrocarbon. HONO is prepared by dropwise addition of 15 mL of 1% NaNO₂ into 30 mL of 10% H₂SO₄ in a glass bulb. The bulb is then attached to the chamber and a stream of dry air is passed through the bulb into the chamber. NO and NO₂, formed as side products in the preparation of HONO, are also introduced into the chamber, and are measured by a commercial NO_x monitor (Horiba APNA-360, Irvine, CA). Additional NO from a 500 ppm gas cylinder (Scott Marrin, Inc.) is introduced into the chamber after the addition of HONO to achieve a total NO_x level in the chamber of about 1 ppm (upper limit of the NO_x monitor). In some high-NO_x experiments, only NO and NO₂ (from gas cylinders) are added to the chamber. To differentiate these experiments from the high-NO_x experiments in which HONO is used as the OH precursor, we refer to these experiments as classical photooxidation experiments. The majority of the high-NO_x experi-

ments in this study are performed with HONO; only a few classical photooxidation experiments are performed for comparison purposes.

For low-NO_x experiments, H₂O₂ is used as the OH precursor. The background NO_x level in the chamber during the experiment is < 1 ppb. H₂O₂ is introduced into the chamber (prior to introduction of seed particles and parent hydrocarbon) by bubbling air through a 50% H₂O₂ solution for 2.5 h at 5 L/min. The air stream then passes through a particle filter to remove any droplets. The concentration of H₂O₂ in the chamber is not measured; based on the rate of hydrocarbon decay and literature values of σ_{H2O2} and *k*_{OH+H2O2}, we estimate [H₂O₂] to be ~3–5 ppm (Kroll et al., 2006).

Once the seed, parent hydrocarbon, and NO_x concentrations stabilize, reaction is initiated by irradiating the chamber with blacklights. Output from the lights is between 300 and 400 nm, with a maximum at 354 nm. At these wavelengths

Table 3. Initial conditions and data for low-NO_x (H₂O₂) experiments.

Expt. No.	Parent Hydrocarbon	T (K)	RH (%)	Seed	ΔHC (ppb)	ΔM _o (μg/m ³)	SOA Yield (%) ^a
1	<i>m</i> -xylene	298	5.1	(NH ₄) ₂ SO ₄	32.5	53.0±4.2	37.7±0.8
2	<i>m</i> -xylene	298	5.2	(NH ₄) ₂ SO ₄	16.1	24.6±2.2	35.2±1.8
3	<i>m</i> -xylene	298	5.1	(NH ₄) ₂ SO ₄	8.0	12.8±1.7	36.7±2.6
4	<i>m</i> -xylene	297	6.2	(NH ₄) ₂ SO ₄	26.1	40.5±3.4	35.7±1.0
5	toluene	297	6.8	(NH ₄) ₂ SO ₄	32.1	37.4±2.8	30.8±1.7
6	toluene	297	6.2	(NH ₄) ₂ SO ₄	63.9	73.1±5.6	30.2±0.7
7	toluene	298	5.2	(NH ₄) ₂ SO ₄	10.0	11.5±1.6	30.4±4.1
8	toluene	298	5.9	(NH ₄) ₂ SO ₄	23.8	26.7±2.5	29.8±1.6
9	benzene	298	6.6	(NH ₄) ₂ SO ₄	64.7	76.4±5.8 ^b	36.9±0.9

^a: Stated uncertainties (1σ) are from scatter in particle volume measurements.

^b: Assuming an SOA density of 1.4 g cm⁻³.

Table 4. Initial conditions and data for acid/nonacid experiments.

Expt. No.	Parent Hydrocarbon	T (K)	RH (%)	NO _x Condition ^a	Seed	ΔHC (ppb)	ΔM _o (μg/m ³)	SOA Yield (%) ^b
1	<i>m</i> -xylene	297	4.3	Low NO _x	(NH ₄) ₂ SO ₄	60.2	101.3±7.8	38.6±0.5
2	<i>m</i> -xylene	297	4.5	Low NO _x	(NH ₄) ₂ SO ₄ +H ₂ SO ₄	58.8	103.5±8.0	40.4±0.6
3	<i>m</i> -xylene	297	5.0	High NO _x	(NH ₄) ₂ SO ₄	68.9	78.9±5.6 ^c	26.3±0.5
4	<i>m</i> -xylene	298	4.2	High NO _x	(NH ₄) ₂ SO ₄ +H ₂ SO ₄	68.5	78.3±5.4 ^c	26.3±0.4
5	toluene	298	5.9	Low NO _x	(NH ₄) ₂ SO ₄	37.9	41.0±3.0	28.7±0.6
6	toluene	299	4.6	Low NO _x	(NH ₄) ₂ SO ₄ +H ₂ SO ₄	38.9	43.2±3.2	29.5±0.7
7	toluene	296	4.9	High NO _x	(NH ₄) ₂ SO ₄	60.0	43.8±3.6 ^c	19.3±0.4
8	toluene	298	4.9	High NO _x	(NH ₄) ₂ SO ₄ +H ₂ SO ₄	58.2	38.3±3.2 ^c	17.4±0.5

^a: Low NO_x (H₂O₂ only); high NO_x (H₂O₂+about 100 ppb NO added).

^b: Stated uncertainties (1σ) are from scatter in particle volume measurements.

^c: Assuming SOA densities are the same as those determined for HONO experiments (see Table 5).

Table 5. Estimated effective SOA densities.

Parent Hydrocarbon	NO _x Condition	Effective Density (g cm ⁻³) ^a
<i>m</i> -xylene	Low NO _x	1.33±0.10
<i>m</i> -xylene	High NO _x	1.48±0.10
toluene	Low NO _x	1.45±0.10
toluene	High NO _x	1.24±0.10

^a: Stated uncertainties (1σ) are from repeated measurements of ammonium sulfate seed densities.

HONO efficiently photolyzes to OH and NO. By contrast H₂O₂ absorbs only weakly in this wavelength range, requiring the use of ppm concentrations of H₂O₂ to achieve reasonable levels of OH.

The parent aromatics studied (shown in Table 1) and their

stated purities are as follows: *m*-xylene (Aldrich, anhydrous, 99+%), toluene (Aldrich, anhydrous, 99.8%), and benzene (Aldrich, anhydrous, 99.8%). Experimental conditions and results for high-NO_x and low-NO_x experiments are given in Tables 2 and 3, while those for studying the effect of seed acidity on SOA growth are given in Table 4. In calculating SOA yield (defined as the ratio of the mass of organic aerosol formed to the mass of parent hydrocarbon reacted), knowledge of the SOA density is required. By comparing volume distributions from the DMA and mass distributions from an Aerodyne quadrupole Aerosol Mass Spectrometer (AMS), the effective densities for the SOA formed can be estimated (Bahreini et al., 2005). The estimated densities of the SOA formed from different systems are given in Table 5.

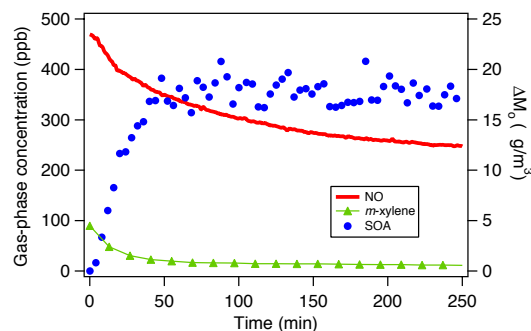


Fig. 1. Typical reaction profile of a high- NO_x experiment in which HONO is used as the OH precursor (initial conditions: 89.3 ppb of *m*-xylene, 470 ppb NO, and 473 ppb NO_2).

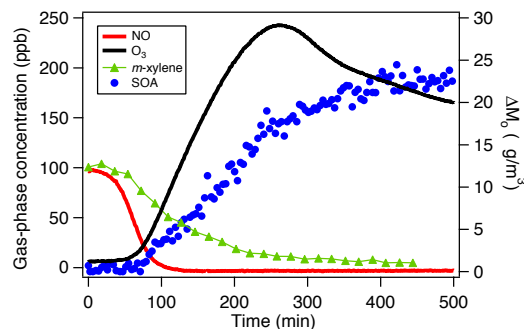


Fig. 2a. Reaction profile of a typical classical photooxidation experiment (initial conditions: 101.6 ppb *m*-xylene, 97 ppb NO, and 26 ppb NO_2).

3 Results

3.1 High- NO_x conditions

Figure 1 shows a typical reaction profile under high- NO_x conditions in which HONO is used as the OH precursor. In this experiment, 89 ppb of *m*-xylene is reacted, and initial NO and NO_2 concentrations are 470 ppb and 473 ppb, respectively. The efficient photolysis of HONO generates high concentrations of OH ($\sim 3 \times 10^7$ molecules cm^{-3} initially), leading to a rapid hydrocarbon decay. This decay slows down after ~ 1 h, suggesting that the HONO is consumed and OH radicals are instead generated through recycling via NO_x/HO_x chemistry. Aerosol growth occurs essentially immediately, even when [NO] is high (100's of ppb). With the high NO concentration, formation of ozone (and hence NO_3 radicals) is suppressed.

Concentration (mixing ratio) profiles from two classical photooxidation experiments with different initial NO_x concentrations are shown in Fig. 2. Figure 2a shows the reaction profile from the photooxidation of 101.6 ppb *m*-xylene, with initial NO and NO_2 concentrations of 97 ppb and 26 ppb, respectively. The hydroxyl radical source in classical photooxidation experiments is likely from the photolysis of HONO, which is formed from the heterogeneous reaction of NO_2 on the chamber wall. The *m*-xylene-OH reaction leads to formation of RO_2 radicals, which react with NO rapidly, converting NO to NO_2 . Ozone is formed from the photolysis of NO_2 , with its concentration increasing rapidly when [NO] falls below ~ 50 ppb. Only when the NO concentration approaches zero does aerosol growth begin, consistent with other classical photooxidation experiments (Izumi and Fukuyama, 1990; Hurley et al., 2001; Johnson et al., 2004; Martin-Reviejo and Wirtz, 2005; Song et al., 2005). The difference between high- NO_x experiments and classical photooxidation experiments will be discussed in Sect. 4.2. Figure 2b shows the reaction profile for the photooxidation of

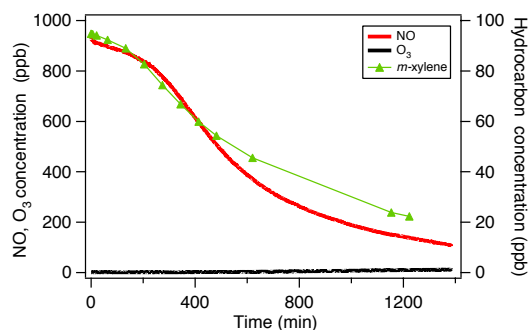


Fig. 2b. Reaction profile of a classical photooxidation experiment in the presence of ~ 1 ppm NO_x (initial conditions: 94.8 ppb *m*-xylene, 878 ppb NO, and 65 ppb NO_2). A negligible amount of ozone is formed during the experiment, and no SOA is formed.

94.8 ppb *m*-xylene, with initial NO and NO_2 concentrations of 878 ppb and 65 ppb, respectively. The NO concentration decreases over the course of the experiment, but does not fall below 100 ppb, even after 20 h. A negligible amount of ozone is formed during the experiment, and no SOA is formed.

For *m*-xylene and toluene, a series of high- NO_x experiments (HONO experiments) with varying initial hydrocarbon concentrations are carried out. The time-dependent “growth curves” (organic aerosol ΔM_0 as a function of hydrocarbon reacted ΔHRC) over the course of the experiment, for four *m*-xylene experiments, with initial hydrocarbon concentrations ranging from 42 to 172 ppb, are shown in Fig. 3. In these experiments, 67–79% of the initial *m*-xylene is consumed. Most of the parent hydrocarbon is consumed in the first hour and the maximum aerosol yield is reached. After that hydrocarbon continues to decay slowly and there is little or no SOA growth, as a result the aerosol yield decreases. Only SOA growth data up to the maximum aerosol yield are shown.

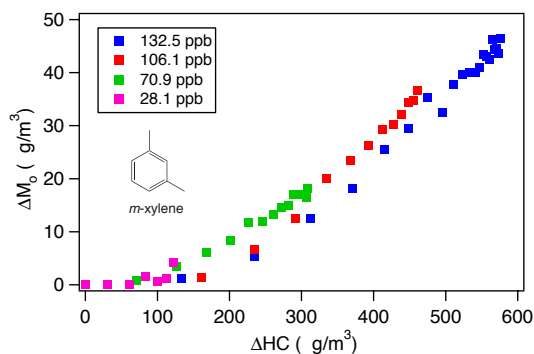


Fig. 3. Time-dependent growth curves for *m*-xylene photooxidation under high- NO_x conditions. The concentrations in the legend refer to the amount of *m*-xylene reacted in each experiment.

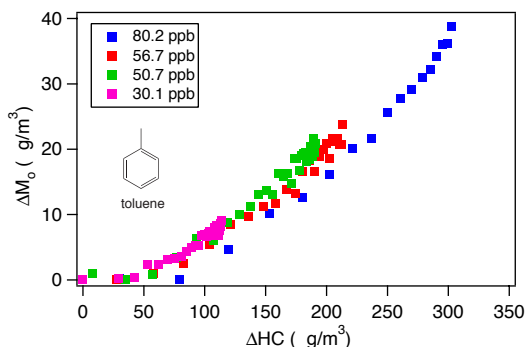


Fig. 4. Time-dependent growth curves for toluene photooxidation under high- NO_x conditions. The concentrations in the legend refer to the amount of toluene reacted in each experiment.

The time-dependent growth curves for four toluene experiments are shown in Fig. 4. The initial toluene concentration ranges from 88 to 270 ppb. Since the toluene-OH reaction rate constant is ~ 4 times lower than that of *m*-xylene-OH, more initial toluene is needed relative to *m*-xylene; only about 30–37% of the initial toluene injected is consumed at the point of maximum aerosol yield. Photooxidation of toluene under high- NO_x conditions results in slightly more SOA growth than for *m*-xylene.

Because benzene reacts slowly with OH radicals ($k = 1.22 \times 10^{-12} \text{ cm}^3 \text{ molecule}^{-1} \text{ s}^{-1}$, Calvert et al., 2002), it is not feasible to carry out photooxidation experiments over a range of initial benzene concentrations unless high levels (ppm) of benzene are used. Thus only a single benzene photooxidation experiment at high NO_x was carried out; at an initial benzene concentration of 337 ppb, only 12% is reacted at the point of maximum aerosol yield. The time-dependent

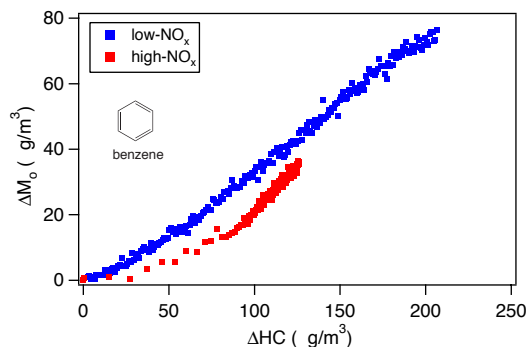


Fig. 5. Time-dependent growth curves for benzene photooxidation under high- and low- NO_x conditions. Under high- NO_x conditions, the initial benzene concentration is 337 ppb (12% reacted). Under low- NO_x conditions, the initial benzene concentration is 395 ppb (16% reacted) and the system has a constant yield of 37%.

growth curve from benzene under high- NO_x conditions (as well as under low- NO_x conditions) is shown in Fig. 5. Hydrocarbon decay slows down at $\Delta\text{HC} \approx 90 \mu\text{g m}^{-3}$, suggesting that HONO is almost completely consumed. After that, OH is generated mainly via NO_x/HO_x chemistry, and hydrocarbon decays at a slower rate resulting in the more closely spaced data points. The slower hydrocarbon oxidation rate after the consumption of HONO may affect the kinetics of SOA growth and contribute to the slight change in the shape of the growth curves.

3.2 Low- NO_x conditions

Under low- NO_x conditions, aerosol growth is observed immediately after initiation of irradiation. The parent hydrocarbon decays at a much slower rate than under high- NO_x conditions, due to the slow production of OH radicals by H_2O_2 photolysis and lack of OH regeneration by NO_x/HO_x cycling. As OH radicals are continually produced, the OH concentration is constant throughout the experiment ($\sim 3 \times 10^6 \text{ molecules cm}^{-3}$). Ozone formation of ~ 10 –15 ppb is observed, possibly owing to residual material released from the chamber walls.

Time-dependent growth curves for four *m*-xylene low- NO_x experiments are shown in Fig. 6, with initial *m*-xylene concentrations ranging from 9 to 37 ppb. About 83–89% of the initial hydrocarbon injected is consumed at the point at which the SOA yield reaches its maximum. From Fig. 6 it is clear that the SOA yield from *m*-xylene photooxidation is constant under low- NO_x conditions, at 36%. Since the *m*-xylene SOA yield is much higher under low- NO_x conditions, a smaller amount of initial parent hydrocarbon is needed to produce the same amount of SOA than under high- NO_x conditions. Comparable time-dependent growth curves for four

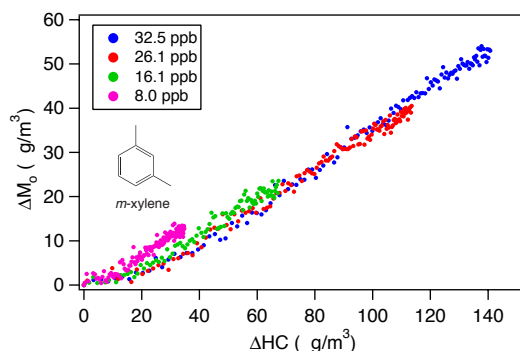


Fig. 6. Time-dependent growth curves for *m*-xylene photooxidation under low- NO_x conditions. The concentrations in the legend refer to the amount of *m*-xylene reacted in each experiment. The system exhibits a constant yield of 36%.

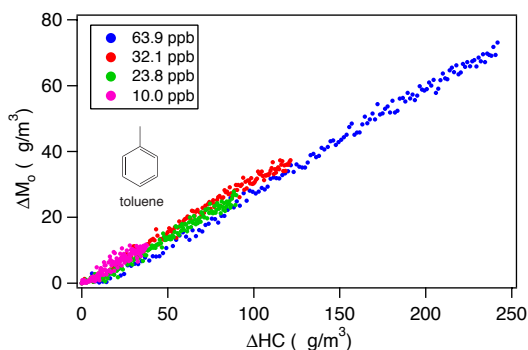


Fig. 7. Time-dependent growth curves for toluene photooxidation under low- NO_x conditions. The concentrations in the legend refer to the amount of toluene reacted in each experiment. The system exhibits a constant yield of 30%.

toluene low- NO_x experiments are shown in Fig. 7. The initial toluene concentration ranges from 21 to 140 ppb. With the slower reactivity of toluene relative to *m*-xylene, only about 45–48% of the initial toluene is consumed. As with *m*-xylene, the aerosol yield (30%) is substantially higher than under high- NO_x conditions.

The time-dependent growth curve for benzene photooxidation is shown in Fig. 5. Similar to *m*-xylene and toluene, benzene photooxidation under low- NO_x conditions results in a constant SOA yield (37%).

3.3 SOA yield parameters

SOA yield has traditionally been described by a semi-empirical model based on absorptive gas-particle partitioning of two semivolatile products (Odum et al., 1996, 1997a, b):

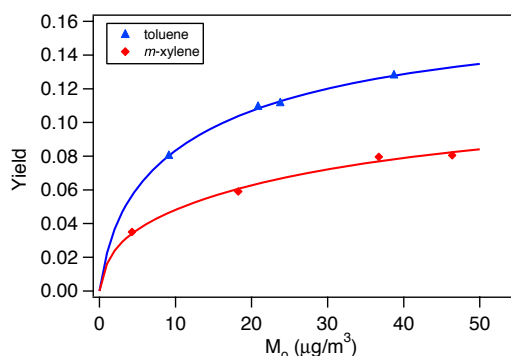


Fig. 8. Yield curves for toluene and *m*-xylene under high- NO_x conditions. The parameters for fitting the yield curves are, toluene: $\alpha_1=0.058$, $K_{om,1}=0.430$, $\alpha_2=0.113$, and $K_{om,2}=0.047$; *m*-xylene: $\alpha_1=0.031$, $K_{om,1}=0.761$, $\alpha_2=0.090$, and $K_{om,2}=0.029$.

$$Y = M_o \left[\frac{\alpha_1 K_{om,1}}{1 + K_{om,1} M_o} + \frac{\alpha_2 K_{om,2}}{1 + K_{om,2} M_o} \right] \quad (1)$$

in which Y is the aerosol yield, M_o is the organic aerosol mass present (equal to ΔM_o in chamber experiments with no absorbing organic mass present initially), α_i is the mass-based gas-phase stoichiometric fraction for semivolatile species i , and $K_{om,i}$ is the gas-particle partitioning coefficient for species i . With this two-product model, Eq. (1) can be fit to experimental yield data to determine values for α_i and $K_{om,i}$, and the resulting plot (Y versus M_o) is generally referred to as a “yield curve”.

For *m*-xylene and toluene, the final SOA yield for each high- NO_x (HONO) experiment is calculated, and the data are fitted to Eq. (1) to obtain the SOA yield parameters. The high- NO_x yield curves for *m*-xylene and toluene are shown in Fig. 8. For all three aromatics (*m*-xylene, toluene, and benzene), the low- NO_x experiments result in a constant aerosol yield (the slope of the “growth curve”), implying the SOA formed can be represented by a single product with very low volatility. Under these conditions the yield curve is simply a horizontal line, and the constant yield corresponds to α_1 in Eq. (1). SOA growth parameters for the three compounds under high- NO_x and low- NO_x conditions are summarized in Table 6.

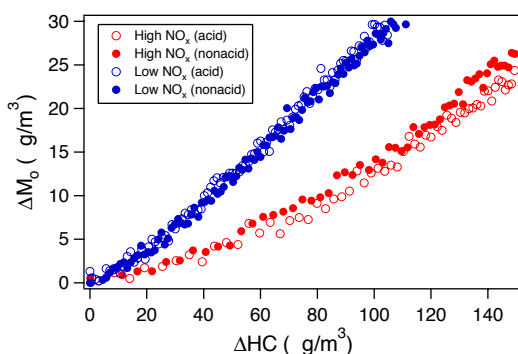
3.4 Acid/nonacid seed experiments

Several *m*-xylene and toluene photooxidation experiments are performed in the presence of acid seed to study the effect of seed acidity on SOA growth. Growth curves for toluene photooxidation under acidic and nonacid conditions are shown in Fig. 9. Regardless of the NO_x level, the time-dependent growth curves from the acid and nonacid experiments are essentially indistinguishable. Therefore, there is

Table 6. Aerosol yield parameters.

Parent Hydrocarbon	NO _x Condition	α_1	$K_{om,1}$ (m ³ μ g ⁻¹)	α_2	$K_{om,2}$ (m ³ μ g ⁻¹)
<i>m</i> -xylene	Low NO _x	0.30	N/A	N/A	N/A
<i>m</i> -xylene	High NO _x	0.031	0.761	0.090	0.029
toluene	Low NO _x	0.36	N/A	N/A	N/A
toluene	High NO _x	0.058	0.430	0.113	0.047
benzene	Low NO _x	0.37	N/A	N/A	N/A
benzene	High NO _x	0.072	3.315	0.888	0.009

N/A: not applicable

**Fig. 9.** Time-dependent growth curves for toluene photooxidation in the presence of neutral seed versus acidic seed.

no evidence that the presence of acidic seed enhances SOA growth in the photooxidation of toluene; similar results are observed for *m*-xylene.

4 Discussion

4.1 Effect of NO_x on SOA yields

Experiments have been performed under two limiting NO_x conditions: (1) high-NO_x experiments in which HONO is used as the OH precursor; and (2) low-NO_x experiments in which H₂O₂ is used as the OH precursor. For all hydrocarbons, considerably more SOA is formed under low-NO_x than high-NO_x conditions (Figs. 3–7). Under high-NO_x conditions, the SOA yields from *m*-xylene and toluene photooxidation are about 10%; they are 36% and 30%, respectively, under low-NO_x conditions. Similar NO_x dependences have been observed in other SOA-forming systems (Hatakeyama et al., 1991; Zhang et al., 1992; Hurley et al., 2001; Johnson et al., 2004; Song et al., 2005; Presto et al., 2005; Kroll et al., 2006). Since O₃ and NO₃ are not formed appreciably under either set of conditions, oxidation is dominated by OH radi-

cals for all experiments, so this NO_x effect cannot be a result of differences in relative oxidant levels (Hurley et al., 2001). Instead the NO_x level likely governs the fate of the organic peroxy radicals formed subsequent to the hydrocarbon-OH reaction, which in turn controls the volatility of molecular products and hence the amount of SOA formed.

Shown in Fig. 10 is the simplified mechanism of the initial steps of toluene-OH reaction, leading to the formation of condensable products. One mechanism by which NO_x levels may affect the products formed in the oxidation of aromatic hydrocarbons is by reaction with the aromatic-OH adduct. The aromatic-OH adduct reacts predominately with O₂ under atmospheric conditions. Under very high levels of NO_x (ppm levels), the adduct+NO can still be neglected (Koch et al., 2006) while the adduct+NO₂ reaction increases in importance, leading to nitrogen-containing ring-retaining products such as nitrobenzene and nitrotoluene (Atkinson et al., 1989; Atkinson and Aschmann, 1994; Koch et al., 2006). The presence of a high concentration of NO_x in the chamber also has an impact on the formation yields of phenol-type compounds, possibly due to the reactions of the aromatic-OH adduct with NO and NO₂. For example, the phenol yield from benzene photooxidation starts to decrease dramatically for [NO₂] > 100 ppb (Volkamer et al., 2002). In the current work, photooxidation of *m*-xylene and toluene is carried out in the presence of ~500 ppb each of NO and NO₂; while for photooxidation of benzene the initial NO₂ concentration is < 100 ppb. At these NO_x levels, the reaction of the aromatic-OH adduct with NO₂ is not expected to be significant (Volkamer et al., 2002; Koch et al., 2006), so such reactions cannot be responsible for the observed effect of NO_x on SOA yield.

Reaction of the aromatic-OH adduct with O₂ results in the formation of peroxy radicals. Theoretical studies have shown that the peroxy radicals preferentially cyclize to form bicyclic radicals, which then react with O₂ to form bicyclic peroxy radicals (Andino et al., 1996; Lay et al., 1996; Suh et al., 2003; Fan et al., 2006), even in the presence of ppm levels of NO (Zhao et al., 2005; Fan et al., 2006). Because of the high energy barrier, the isomerization of bicyclic radicals to form epoxide radicals is unlikely for toluene; only a small of

fraction of epoxy carbonyls are observed in *m*-xylene photooxidation, suggesting that the epoxide radical channel is not important either (Suh et al., 2003; Zhao et al., 2005). As is typical for RO₂ radicals, the fate of the bicyclic peroxy radicals depends mainly on the relative concentrations of NO, HO₂, and RO₂. At the two limiting NO_x conditions of this study, the peroxy radical chemistry is straightforward; under high-NO_x conditions, RO₂ reacts virtually entirely with NO, as NO concentration is high throughout the entire experiment, while under low-NO_x conditions, RO₂ reacts predominantly with HO₂. Based on the Master Chemical Mechanism version 3.1 (MCM v 3.1, <http://www.chem.leeds.ac.uk/Atmospheric/MCM/mcmproj.html>), a simple kinetic simulation shows that under low-NO_x conditions, the RO₂+RO₂ reaction accounts for less than 1% of the RO₂ reacted because of the relative reaction rate constants ($k_{\text{RO}_2+\text{RO}_2}=8.8\times10^{-13}\text{ cm}^3\text{ molecule}^{-1}\text{ s}^{-1}$, $k_{\text{RO}_2+\text{HO}_2}=2.3\times10^{-11}\text{ cm}^3\text{ molecule}^{-1}\text{ s}^{-1}$) as well as the high HO₂ concentration. Thus the larger SOA yields obtained under low-NO_x conditions imply that the products formed via the RO₂+HO₂ partition much more readily into the aerosol phase than those formed via the RO₂+NO reaction. This conclusion is the same as that reached by previous studies (Hatakeyama et al., 1991; Johnson et al., 2004, 2005; Presto et al., 2005; Kroll et al., 2006). That SOA yields are constant under low-NO_x conditions implies that the SOA formed by this channel is effectively nonvolatile under the range of $M_0(>10\text{ }\mu\text{g m}^{-3})$ studied. It is possible that under lower SOA loadings the yields may decrease as some of the products partition back into the gas phase.

In the classical photooxidation experiments carried out in this study and by other researchers (Izumi and Fukuyama, 1990; Hurley et al., 2001; Johnson et al., 2004; Martin-Reviejo and Wirtz, 2005; Song et al., 2005), an “induction period”, a delay between the onset of oxidation and SOA formation, was observed. This too is a likely result of the role of NO_x in peroxy radical chemistry, and hence in product volatility and SOA formation. As illustrated in Fig. 2a, only when [NO] approaches zero does aerosol growth commence. As [NO] approaches zero (from the RO₂+NO and HO₂+NO reactions), the RO₂+HO₂ reaction starts to compete with the RO₂+NO reaction. The fraction of RO₂ which reacts with HO₂, $k_{\text{RO}_2+\text{HO}_2}[\text{HO}_2]/(k_{\text{RO}_2+\text{NO}}[\text{NO}]+k_{\text{RO}_2+\text{HO}_2}[\text{HO}_2])$, can be calculated based on the rate reaction rate constants ($k_{\text{RO}_2+\text{HO}_2}=2.3\times10^{-11}\text{ cm}^3\text{ molecule}^{-1}\text{ s}^{-1}$; $k_{\text{RO}_2+\text{NO}}=8.5\times10^{-12}\text{ cm}^3\text{ molecule}^{-1}\text{ s}^{-1}$) (MCM v 3.1). For instance, at ~ 1 ppb of NO, it only requires 42 ppt of HO₂ for 10% of the RO₂ to react via RO₂+HO₂. Thus it is likely that initial SOA formation results from the RO₂+HO₂ reaction, consistent with the simulations of SOA formation from classical photooxidation experiments of toluene (Johnson et al., 2004). To further study the role of peroxy radical chemistry in the “induction period”, in one of the experiments additional NO was injected after its initial consumption. SOA

growth slows down immediately. This provides strong evidence that the presence of NO suppresses the formation of relatively nonvolatile hydroperoxides (and hence further reactions of hydroperoxides) from the RO₂+HO₂ reaction and results in a lower SOA yield (Johnson et al., 2004, 2005).

The time-dependent growth curves for benzene photooxidation under high- and low-NO_x conditions exhibit the same trend as that of *m*-xylene and toluene, in which more SOA is formed under low-NO_x conditions. Martin-Reviejo and Wirtz (2005) studied the formation of SOA from benzene photooxidation under different NO_x conditions. However, as the NO_x dependence of SOA formation was not systematically studied, it is difficult to draw a definite conclusion on the effect of NO_x on SOA yields from their data. Additionally, the experimental conditions are somewhat different; in particular, the experiments in that study were performed in the absence of seed aerosol while in the current work ammonium sulfate seed aerosol is employed. Kroll et al. (2007) find that SOA yields from the photooxidation of aromatic hydrocarbons are lower when inorganic seed particles are not present initially. The absence of seed particles results in a period in which the hydrocarbon is reacted but no aerosol is formed. The length of the “seed induction period” (and hence the amount of hydrocarbon reacted in this period, $\Delta\text{H/C}$) is likely to be affected by the NO_x levels. Thus the aerosol yields ($\Delta M_0/\Delta\text{H/C}$) obtained by Martin-Reviejo and Wirtz (2005) under different NO_x conditions may be affected by this “seed induction period” and cannot be directly compared.

4.2 Effect of oxidation rate

Under high-NO_x conditions, using HONO as an OH source, we observe SOA formation even when [NO] is several hundreds of ppb (Fig. 1). This is in contrast to results from classical photooxidation experiments, in which essentially no SOA is generated at high NO_x levels, as observed both in the present study (Fig. 2b) and in work by other researchers (Johnson et al., 2004; Song et al., 2005).

The observation of SOA at high NO_x levels suggests that products from the RO₂+NO reactions, such as organic nitrates, are indeed condensable; however they apparently do not partition into the aerosol phase appreciably in the classical photooxidation experiments. A major difference between the HONO experiments (Fig. 1) and classical oxidation experiments (e.g. Fig. 2) is OH level, and hence oxidation rate. HONO photolysis is an efficient source of OH in the wavelength range of our blacklights; thus there is a burst of OH once the lights are turned on, resulting in a rapid rate of *m*-xylene oxidation. In the classical photooxidation experiment, OH is generated mainly from recycling through NO_x and HO_x cycles, and OH concentrations are generally far lower than in the HONO experiments. The large difference in SOA formation in these two cases suggests that SOA yields are

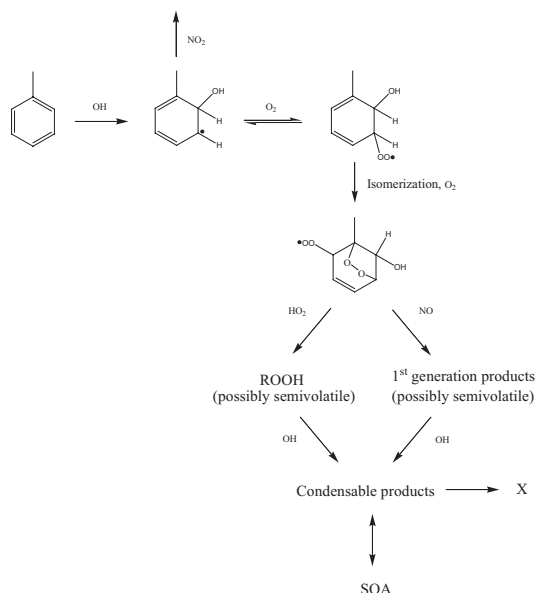


Fig. 10. A simplified SOA formation mechanism for toluene photooxidation. X represents the generic non particle-phase product from all gas-phase loss processes.

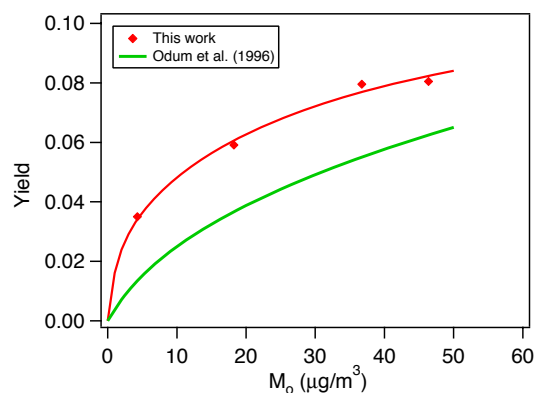


Fig. 11. Comparison of *m*-xylene high- NO_x yield curve obtained in the current work to that from Odum et al. (1996). The yield curve from Odum et al. (1996) has been corrected for the temperature (25°C) of this study and density (1.48 g cm^{-3}) of the SOA.

dependent on the oxidation rate, with faster oxidation rates resulting in higher SOA yields.

This “rate effect” may arise as a result of loss of semivolatiles through processes other than the simple formation and partitioning of semivolatile organics. The loss of semivolatiles has been proposed as one of the mechanisms

for higher SOA yields observed from aromatic photooxidation in the presence of seed aerosols as compared to nucleation experiments (Kroll et al., 2007). In the mechanism shown in Fig. 10, X represents the generic non particle-phase product of all gas-phase loss processes. Possibilities include loss of organic species to the chamber walls, photolysis, and further reactions to form volatile products. With a rapid oxidation rate, the gas-phase concentration of semivolatiles (formed, for example, from the $\text{RO}_2 + \text{NO}$ reaction) increases quickly, and the high concentrations of semivolatiles ensure that aerosol growth ensues even in the presence of semivolatile loss processes (i.e. paths not forming SOA). On the other hand, in classical photooxidation experiments, the slower formation of semivolatiles in the presence of semivolatile sinks will lead to lower SOA growth. If the dominant loss of semivolatiles is deposition to the chamber walls, then conditions in which the effect of wall loss is minimized (i.e. when the reaction is fastest) are expected to be most representative of atmospheric SOA formation. Recently, the effect of particle- and gas-phase reactions of semivolatile products on SOA formation has been examined in a modeling study by Chan et al. (2007), in which the experimental data presented in this work (among other literature data) are fitted to simple kinetic models. Given the importance of the loss of semivolatiles, these loss processes merit further investigation and experimental evidence.

This rate effect also can explain higher SOA yields in the high- NO_x experiments (HONO) compared to the classical photooxidation experiments (Odum et al., 1996), illustrated in Fig. 11. Several classical photooxidation experiments with similar NO_x levels as in Odum et al. (1996) were performed in the present study, with SOA yields comparable to those of Odum et al. (1996). The aerosol yields from Odum et al. (1996) were obtained at a temperature of 35–40°C with an assumed SOA density of 1 g cm^{-3} . In Fig. 11, the yield curve from Odum et al. (1996) has been adjusted based on the temperature (25°C) and SOA density (1.48 g cm^{-3}) obtained in this study. The enthalpy of vaporization employed to convert the SOA yields from the higher temperature in Odum et al. (1996) to the lower temperature in this study is assumed to be 42 kJ mol^{-1} (Chung and Seinfeld, 2002), which is in the range of limited experimental data (Offenberg et al., 2006). The NO_x concentrations (several hundreds of ppb) used by Odum et al. (1996) are lower than those in the current experiments ($\sim 1 \text{ ppm}$). The higher SOA yields obtained here suggest that the enhancement in SOA yield from a faster oxidation rate is greater than the suppression in SOA yield at a higher NO_x concentration.

Significant SOA formation from the rapid oxidation of aromatics under high (ppm) levels of NO_x has also been observed by Stroud et al. (2004), using isopropyl nitrite as an OH source to oxidize toluene. Such results could not be reproduced in the simulations of Johnson et al. (2004), which predicted no SOA formation in the presence of such high NO_x levels, as the $\text{RO}_2 + \text{NO}$ reaction products were found

to be too volatile to partition substantially into the aerosol phase. However, the present work suggests that products of the $\text{RO}_2 + \text{NO}$ reaction are in fact condensable, but contribute to aerosol mass only when oxidation reactions are fast, minimizing the effect of other loss processes. This underscores the need for a better understanding of the behavior of semivolatile organics in the atmosphere, in terms of both physical properties (partitioning coefficients) and chemical reactions (reactive loss processes).

Finally, we note that the pair of high- NO_x experiments (Fig. 1 and Fig. 2b) also provides insight into the extent to which the hydrocarbon/ NO_x (HC/NO_x) ratio characterizes the NO_x level in chamber experiments. Song et al. (2005), for example, report a series of classical photooxidation experiments to study the effect of HC/NO_x ratio on SOA formation from *m*-xylene. It was found that aerosol yields increase with increasing HC/NO_x ratio (i.e. more aerosol growth at lower NO_x levels), which is consistent with the present study. However, the experiments in Fig. 1 and 2b have essentially similar HC/NO_x ratios but exhibit very different SOA growth. Therefore, while the HC/NO_x ratio may be a useful metric for photochemistry for experiments with similar oxidation conditions, it is less useful when comparing systems with very different oxidative conditions, as both oxidation rate and fate of peroxy radicals may differ. Given the importance of the peroxy radical in SOA formation, the NO/HO_2 ratio would be the more appropriate measure of different NO_x levels (Kroll et al., 2006), although continuous measurement of HO_2 is not currently feasible.

4.3 General mechanism of SOA formation

Despite uncertainties in the detailed chemical mechanism of aromatic photooxidation beyond the initial peroxy radical chemistry, we can gain insights into the general SOA formation mechanism and growth kinetics from the shapes of the growth curves under both high- NO_x and low- NO_x conditions (Figs. 3–7). Such curves allow for the identification of the rate-determining steps in SOA formation (Ng et al., 2006). In cases where the initial oxidation step determines the rate of SOA formation (condensable products are first-generation, or are formed extremely rapidly after the initial oxidation), SOA is formed at the same rate of hydrocarbon oxidation, and aerosol growth ceases once the parent hydrocarbon is consumed. In this case, time-dependent growth curves from experiments with different initial hydrocarbon concentrations would overlap, as is the case for α -pinene ozonolysis (Ng et al., 2006). On the other hand, when there are further rate-limiting steps to the formation of condensable products, there is a time lag between hydrocarbon oxidation and SOA formation and the growth curve exhibits a vertical section at the end, as is the case for the ozonolysis and photooxidation of compounds with multiple double bonds (Ng et al., 2006).

Figures 3–7 show the time-dependent growth curves for *m*-xylene, toluene, and benzene photooxidation under high- NO_x and low- NO_x conditions. In all cases, SOA growth is observed immediately after photooxidation commences, resulting in a smooth growth curve from the onset of oxidation. Some hydrocarbon remains unreacted by the end of these experiments. In experiments in which all the hydrocarbon is reacted (not shown), no vertical section in the growth curve is observed, indicating there is no further SOA formation after the complete consumption of the parent hydrocarbon. This indicates that the first oxidation step (oxidation of the parent hydrocarbon) governs the rate of SOA formation.

However, unlike with α -pinene ozonolysis (Ng et al., 2006), the time-dependent growth curves from experiments with different initial aromatic hydrocarbon concentrations do not overlap, and aerosol growth is not the same for a given amount of hydrocarbon reacted (ΔHC). Instead, SOA growth at a given value of ΔHC depends on the initial hydrocarbon concentration (HC_0): experiments with higher HC_0 reach a given ΔHC in a shorter time than those with smaller HC_0 . At smaller HC_0 , during the longer time required to reach the same ΔHC , the first generation products have more time to be oxidized to form condensable products. Therefore, the divergence in growth curves at different initial hydrocarbon concentrations indicates that even though the first step is the rate-limiting in SOA formation, subsequent oxidation steps also occur prior to SOA formation. As discussed in Ng et al. (2006), if subsequent oxidation steps are essentially instantaneous relative to the initial oxidation step, then SOA formation can be treated as a single step and all the growth curves will overlap. In the present study, the growth curves diverge only slightly, indicating that although the second oxidation step is not instantaneous, it is still substantially faster than the initial oxidation step. The formation of SOA by multiple oxidation steps, in which the later steps are substantially faster than the initial oxidation, is consistent with available kinetic data and current understanding of the photooxidation of aromatic hydrocarbons. In general, first-generation products of aromatic photooxidation react about an order of magnitude faster with OH than do their parent hydrocarbons (Calvert et al., 2002). For example, whereas the benzene-OH rate constant is $1.22 \times 10^{-12} \text{ cm}^3 \text{ molecule}^{-1} \text{ s}^{-1}$, the rate constant of the reaction of OH with phenol, a major first-generation reaction product, is $2.7 \times 10^{-11} \text{ cm}^3 \text{ molecule}^{-1} \text{ s}^{-1}$ (Calvert et al., 2002). Our study does not exclude the possibility of formation of SOA from the condensation of first-generation products; however, it suggests that second (or further) generation products contribute significantly to SOA growth.

4.4 Effect of seed acidity

To our knowledge, there are no published data on the effect of seed aerosol acidity on SOA formed from the photooxidation of aromatic VOCs. As shown in Fig. 9, seed particle acidity does not enhance the SOA yield under different NO_x conditions. The composition of the acid and nonacid seed particles, as well as the RH ($\sim 5\%$), are the same as those previously employed in the study of isoprene SOA formation (Surratt et al., 2007); yet, an enhancement in SOA yield is observed for isoprene experiments but not for the aromatics. The chambers are maintained at RH $\sim 5\%$ in this study and so the nonacid seed particles are dry, whereas for acidic seed particles some water might be present. If aerosol water is essential for the acidity effect, its absence might explain the lack of an observed effect in the current study. The dependence of SOA growth on RH is beyond the scope of this work but warrants future investigation.

5 Implication for SOA growth from aromatic hydrocarbons

We report a series of chamber experiments investigating the NO_x dependence and effect of seed aerosol acidity on SOA formation from the photooxidation of aromatic compounds. High- NO_x experiments are performed with HONO as the OH precursor at initial NO_x of ~ 1 ppm. By performing experiments with HONO, SOA is formed under truly high- NO_x conditions, as the NO concentration remains high throughout the entire experiment. In low- NO_x experiments, H_2O_2 is used as the OH precursor and the initial NO_x is < 1 ppb. For each of the aromatic hydrocarbons studied (*m*-xylene, toluene, and benzene), the SOA yields under low- NO_x conditions are significantly larger than those under high- NO_x conditions; this is likely a result of the competition between $\text{RO}_2 + \text{NO}$ and $\text{RO}_2 + \text{HO}_2$ reactions, similar to what has been observed in other studies (Hatakeyama et al., 1991; Johnson et al., 2004, 2005; Presto et al., 2005; Kroll et al., 2006).

In assessing the contribution of aromatic compounds to total ambient SOA, it is important that laboratory conditions are representative of those in the atmosphere. The aromatic SOA yield parameters (α_i and $K_{om,i}$) currently employed in atmospheric models are those obtained by Odum et al. (1996, 1997a, b) almost a decade ago by irradiation of hydrocarbon/ NO_x mixtures. With the profound dependence of NO_x on SOA formation, it is necessary that the effect of NO_x on SOA yields be included in atmospheric models. For instance, compounds like benzene are mainly emitted in source-rich regions; with its slow reactivity, however, benzene can be transported to areas with a lower NO_x level before it reacts substantially, resulting in a higher SOA yield than if it reacted in the immediate vicinity of its sources. By performing experiments at two extreme NO_x conditions, we are able to obtain SOA yield parameters under high- and

low- NO_x conditions, allowing for the parameterization of the NO_x dependence for atmospheric models, based upon the reactivity of organic peroxy radicals. Other than the NO_x effect, the loss of semivolatiles also affects the SOA yields measured. The depletion of semivolatiles by chemical reaction or wall loss may lead to lower SOA formation in the chambers than occurs in the atmosphere. Due to the slower oxidation rate in the classical photooxidation experiments conducted by Odum et al. (1996, 1997a, b), it is likely that their SOA yield parameters underestimate SOA formation from aromatic hydrocarbons in the atmosphere.

Finally, detailed analysis of the chemical composition of aromatic SOA will assist in unraveling the detailed aromatic SOA formation mechanism under both high and low- NO_x conditions. In a forthcoming publication, the chemical composition of aromatic SOA will be explored. Since a wide array of sulfate esters are observed only when acidified inorganic seed aerosols are employed (Surratt et al., 2007), the chemical composition of the SOA formed in nonacid/acid seed experiments may also provide insights into the lack of a seed acidity effect on SOA yields in the present study.

Acknowledgements. This research was funded by the U.S. Environmental Protection Agency Science to Achieve Results (STAR) Program grant number RD-83107501-0, managed by EPA's Office of Research and Development (ORD), National Center for Environmental Research (NCER), and by U.S. Department of Energy Biological and Environmental Research Program DE-FG02-05ER63983.

Edited by: S. Martin

References

- Andino, J. M., Smith, J. N., Flagan, R. C., Goddard III, W. A., and Seinfeld, J. H.: Mechanism of atmospheric photooxidation of aromatics: A theoretical study, *J. Phys. Chem.*, 100, 10967–10980, 1996.
- Atkinson, R., Aschmann, S. M., Arey, J., and Carter, W. P. L.: Formation of ring-retaining products from the OH radical-initiated reactions of benzene and toluene, *Int. J. Chem. Kinet.*, 21, 801–827, 1989.
- Atkinson, R. and Aschmann, S. M.: Products of the gas-phase reactions of aromatic hydrocarbons: effect of NO_2 concentration, *Int. J. Chem. Kinet.*, 26, 929–944, 1994.
- Bahreini, R., Keywood, M. D., Ng, N. L., Varutbangkul, V., Gao, S., Flagan, R. C., and Seinfeld, J. H.: Measurements of secondary organic aerosol (SOA) from oxidation of cycloalkenes, terpenes, and *m*-xylene using an Aerodyne aerosol mass spectrometer, *Environ. Sci. Technol.*, 39, 5674–5688, 2005.
- Calvert, J. G., Atkinson, R., Becker, K. H., Kamens, R. M., Seinfeld, J. H., Wallington, T. J., and Yarwood, G.: *The Mechanisms of Atmospheric Oxidation of Aromatic Hydrocarbons*, Oxford University Press, New York, 556pp., 2002.
- Chan, A. W. H., Kroll, J. H., Ng, N. L., and Seinfeld, J. H.: Kinetic modeling of secondary organic aerosol formation: effects of particle- and gas-phase reactions of semivolatile products, *At-*

- mos. Chem. Phys. Discuss., 7, 7051–7085, 2007, <http://www.atmos-chem-phys-discuss.net/7/7051/2007/>.
- Chung, S. H. and Seinfeld, J. H.: Global distribution and climate forcing of carbonaceous aerosols, *J. Geophys. Res.*, 107, 4407, doi:10.1029/2001JD001397, 2002.
- Cocker III, D. R., Flagan, R. C., and Seinfeld, J. H.: State-of-the-art chamber facility for studying atmospheric aerosol chemistry, *Environ. Sci. Technol.*, 35, 2594–2601, 2001.
- de Gouw, J. A., Middlebrook, A. M., Warneke, C., Goldan, P. D., Kuster, W. C., Roberts, J. M., Fehsenfeld, F. C., Worsnop, D. R., Canagaratna, M. R., Pszenny, A. A. P., Keene, W. C., Marchewka, M., Bertman, S. B., and Bates, T. S.: Budget of organic carbon in a polluted atmosphere: Results from the New England Air Quality Study in 2002, *J. Geophys. Res.*, 110, D16305, doi:10.1029/2004JD005623, 2005.
- Edney, E. O., Kleindienst, T. E., Jaoui, M., Lewandowski, M., Ofenber, J. H., Wang, W., and Claeys, M.: Formation of 2-methyl tetrols and 2-methylglyceric acid in secondary organic aerosol from laboratory irradiated isoprene/NO_x/SO₂/air mixtures and their detection in ambient PM_{2.5} samples collected in the eastern United States, *Atmos. Environ.*, 39, 5281–5289, 2005.
- Fan, J. and Zhang, R.: Atmospheric oxidation mechanism of *p*-xylene: A density function theory study, *J. Phys. Chem. A*, 110, 7728–7737, 2006.
- Forstner, H. J. L., Flagan, R. C., and Seinfeld, J. H.: Secondary organic aerosol from the photooxidation of aromatic hydrocarbons: Molecular composition, *Environ. Sci. Technol.*, 31, 1345–1358, 1997.
- Gao, S., Keywood, M. D., Ng, N. L., Surratt, J. D., Varutbangkul, V., Bahreini, R., Flagan, R. C., and Seinfeld, J. H.: Low-molecule weight and oligomeric components in secondary organic aerosol from the ozonolysis of cycloalkenes and α -pinene, *J. Phys. Chem., A*, 108, 10 147–10 164, 2004a.
- Gao, S., Ng, N. L., Keywood, M. D., Varutbangkul, V., Bahreini, R., Nenes, A., He, J., Yoo, K. Y., Beauchamp, J. L., Hodyss, R. P., Flagan, R. C., and Seinfeld, J. H.: Particle phase acidity and oligomer formation in secondary organic aerosol, *Environ. Sci. Technol.*, 38, 6582–6589, 2004b.
- Hatakeyama, S., Izumi, K., Fukuyama, T., Akimoto, H., Washida, N.: Reactions of OH with α -pinene and β -pinene in air: Estimates of global CO production from the atmospheric oxidation of terpenes, *J. Geophys. Res.*, 96(D1), 947–958, 1991.
- Heald, C. L., Jacob, D. J., Park, R. J., Russell, L. M., Huebert, B. J., Seinfeld, J. H., Liao, H., and Weber, R. J.: A large organic aerosol source in the free troposphere missing from current models, *Geophys. Res. Lett.*, 32, L18809, doi:10.1029/2005GL023831, 2005.
- Heald, C. L., Jacob, D. J., Turquety, S., Hudman, R. C., Weber, R. J., Sullivan, A. P., Peltier, R. E., Atlas, E. L., de Gouw, J. A., Warneke, C., Holloway, J. S., Neuman, J. A., F. Flocke, M., and Seinfeld, J. H.: Concentration and sources of organic carbon aerosols in the free troposphere over North America, *J. Geophys. Res.*, 111(D23), D23S47, doi:10.1029/2006JD007705, 2006.
- Hurley, M. D., Sokolov, O., Wallington, T. J., Takekawa, H., Karsawa, M., Klotz, B., Barnes, I., and Becker, K. H.: Organic aerosol formation during the atmospheric degradation of toluene, *Environ. Sci. Technol.*, 35, 1358–1366, 2001.
- Iinuma, Y., Böge, O., Gnauk, T., and Herrmann, H.: Aerosol-chamber study of the pinene/O₃ reaction: Influence of particle acidity on aerosol yields and products, *Atmos. Environ.*, 38, 761–773, 2004.
- Izumi, K. and Fukuyama, T.: Photochemical aerosol formation from aromatic hydrocarbons in the presence of NO_x, *Atmos. Environ.*, 24A, 1433–1441, 1990.
- Jang, M. and Kamens, R. M.: Characterization of secondary organic aerosol from the photooxidation of toluene in the presence of NO_x and 1-propene, *Environ. Sci. Technol.*, 35, 3626–3639, 2001.
- Jang, M., Czoschke, N. M., Lee, S., and Kamens, R. M.: Heterogeneous atmospheric aerosol production by acid-catalyzed particle-phase reactions, *Science*, 298, 814–817, 2002.
- Johnson, D., Jenkin, M. E., Wirtz, K., and Martín-Reviejo, M.: Simulating the formation of secondary organic aerosol from the photooxidation of toluene, *Environ. Chem.*, 1, 150–165, 2004.
- Johnson, D., Jenkin, M. E., Wirtz, K., and Martín-Reviejo, M.: Simulating the formation of secondary organic aerosol from the photooxidation of aromatic hydrocarbons, *Environ. Chem.*, 2, 35–48, 2005.
- Kalberer, M., Paulsen, S., Sax, M., Steinbacher, M., Dommen, J., Prevot, A. S. H., Fisseha, R., Weingartner, E., Frankevich, V., Zenobi, R., and Baltensperger, U.: Identification of polymers as major components of atmospheric organic aerosols, *Science*, 303, 1659–1662, 2004.
- Keywood, M. D., Varutbangkul, V., Bahreini, R., Flagan, R. C., and Seinfeld, J. H.: Secondary organic aerosol formation from the ozonolysis of cycloalkenes and related compounds, *Environ. Sci. Technol.*, 38, 4157–4164, 2004.
- Kleindienst, T. E., Conner, T. S., McIver, C. D., and Edney, E. O.: Determination of secondary organic aerosol products from the photooxidation of toluene and their implications in ambient PM_{2.5}, *J. Atmos. Chem.*, 47, 79–100, 2004.
- Koch, R., Knispel, R., Elend, M., Siese, M., and Zetzsch, C.: Consecutive reactions of aromatic-OH adducts with NO, NO₂, and O₂: Benzene, toluene, *m*- and *p*-xylene, hexamethylbenzene, phenol, *m*-cresol, and aniline, *Atmos. Chem. Phys. Discuss.*, 6, 7623–7656, 2006, <http://www.atmos-chem-phys-discuss.net/6/7623/2006/>.
- Kroll, J. H., Ng, N. L., Murphy, S. M., Flagan, R. C., and Seinfeld, J. H.: Secondary organic aerosol formation from isoprene photooxidation, *Environ. Sci. Technol.*, 40, 1869–1877, 2006.
- Kroll, J., Chan, A. W. H., Ng, N. L., Flagan, R. C., and Seinfeld, J. H.: Reactions of semivolatile organics and their effects on secondary organic aerosol formation, *Environ. Sci. Technol.*, 41, 3545–3550, 2007.
- Lay, T. H., Bozzelli, J. W., and Seinfeld, J. H.: Atmospheric photochemical oxidation of benzene: Benzene+OH and the benzene-OH adduct, *J. Phys. Chem.*, 100, 6543–6554, 1996.
- Martin-Reviejo, M. and Wirtz, K.: Is benzene a precursor for secondary organic aerosol? *Environ. Sci. Technol.*, 39, 1045–1054, 2005.
- Ng, N. L., Kroll, J. H., Keywood, M. D., Bahreini, R., Varutbangkul, V., Flagan, R. C., Seinfeld, J. H., Lee, A., and Goldstein, A. H.: Contribution of first- versus second-generation products to secondary organic aerosols formed in the oxidation of biogenic hydrocarbons, *Environ. Sci. Technol.*, 40, 2283–2297, 2006.
- Odum, J. R., Hoffmann, T., Bowman, F., Collins, D., Flagan, R. C., and Seinfeld, J. H.: Gas/particle partitioning and secondary

- organic aerosol yields, *Environ. Sci. Technol.*, 30, 2580–2585, 1996.
- Odum, J. R., Jungkamp, T. P. W., Griffin, R. J., Flagan, R. C., and Seinfeld, J. H.: The atmospheric aerosol-forming potential of whole gasoline vapor, *Science*, 276, 96–99, 1997a.
- Odum, J. R., Jungkamp, T. P. W., Griffin, R. J., Forstner, H. J. L., Flagan, R. C., and Seinfeld, J. H.: Aromatics, reformulated gasoline and atmospheric organic aerosol formation, *Environ. Sci. Technol.*, 31, 1890–1897, 1997b.
- Offenberg, J. H., Kleindienst, T. E., Jaoui, M., Lewandowski, M., and Edney, E. O.: Thermal properties of secondary organic aerosols, *Geophys. Res. Lett.*, 33, L03816, doi:10.1029/2005GL024623, 2006.
- Presto, A. A., Huff Hartz, K. E., and Donahue, N. M.: Secondary organic aerosol production from ozonolysis: 2. Effect of NO_x concentration, *Environ. Sci. Technol.*, 39, 7046–7054, 2005.
- Presto, A. A. and Donahue, N. M.: Investigation of α -pinene+ozone secondary organic aerosol formation at low total aerosol mass, *Environ. Sci. Technol.*, 40, 3536–3543, 2006.
- Seinfeld, J. H. and Pandis, S. N.: *Atmospheric Chemistry and Physics: From Air Pollution to Climate Change*, Wiley, New Jersey, 1203pp., 2006.
- Song, C., Na, K., and Cocker III, D. R.: Impact of the hydrocarbon to NO_x ratio on secondary organic aerosol formation, *Environ. Sci. Technol.*, 39, 3143–3149, 2005.
- Stroud, C. A., Makar, P. A., Michelangeli, D. V., Mozurkewich, M., Hastie, D. R., Barbu, A., and Humble, J.: Simulating organic aerosol formation during photooxidation of toluene/NO_x mixtures: Comparing the equilibrium and kinetic assumption, *Environ. Sci. Technol.*, 38, 1471–1479, 2004.
- Suh, I., Zhang, R., Molina, L. T., and Molina, M. J.: Oxidation mechanism of aromatic peroxy and bicyclic radicals from OH-toluene reactions, *J. Am. Chem. Soc.*, 125, 12 655–12 665, 2003.
- Surratt, J. D., Kroll, J. H., Kleindienst, T. E., Edney, E. O., Claeys, M., Sorooshian, A., Ng, N. L., Offenberg, J. H., Lewandowski, M., Jaoui, M., Flagan, R. C., and Seinfeld, J. H.: Evidence for organosulfates in secondary organic aerosol, *Environ. Sci. Technol.*, 41, 517–527, 2007.
- Tolocka, M. P., Jang, M., Ginter, J. M., Cox, F. J., Kamens, R. M., and Johnston M. V.: Formation of oligomers in secondary organic aerosol, *Environ. Sci. Technol.*, 38, 1428–1434, 2004.
- Tsigaridis, K. and Kanakidou, M.: Global modelling of secondary organic aerosols in the troposphere: A sensitivity study, *Atmos. Chem. Phys.*, 3, 1849–1869, 2003, <http://www.atmos-chem-phys.net/3/1849/2003/>.
- Volkamer, R., Klotz, B., Barnes, I., Imamura, T., Wirtz, K., Washida, N., Becker, K. H., and Platt, U.: OH-initiated oxidation of benzene, Part I, phenol formation under atmospheric conditions, *Phys. Chem. Chem. Phys.*, 4, 1589–1610, 2002.
- Volkamer, R., Jimenez, J. L., San Martini, F., Dzepina, K., Zhang, Q., Salcedo, D., Molina, L. T., Worsnop, D. R., Molina, M. J.: Secondary organic aerosol formation from anthropogenic air pollution: Rapid and higher than expected, *Geophys. Res. Lett.*, 33, L17811, doi:10.1029/2006GL026899, 2006.
- Zhang, S., Shaw, M., Seinfeld, J. H., and Flagan, R. C.: Photochemical aerosol formation from α -pinene and β -pinene, *J. Geophys. Res.*, 97, 20 717–20 729, 1992.
- Zhao, J., Zhang, R., Misawa, K., and Shibuya K.: Experimental product study of the OH-initiated oxidation of *m*-xylene, *J. Photochem Photobiol. A*, 199–207, 2005.

Appendix B

Effect of NO_x level on secondary organic aerosol (SOA) formation from the photooxidation of terpenes*

*Reproduced with permission from “Effect of NO_x level on secondary organic aerosol (SOA) formation from the photooxidation of terpenes” by N. L. Ng, P. S. Chhabra, A. W. H. Chan, J. D. Surratt, J. H. Kroll, A. J. Kwan, D. C. McCabe, P. O. Wennberg, A. Sorooshian, S. M. Murphy, N. F. Dalleska, R. C. Flagan, and J. H. Seinfeld, *Atmospheric Chemistry and Physics*, 7 (19), 5159–5174, 2007. Copyright 2007 by Authors. This work is licensed under a Creative Commons License.

Effect of NO_x level on secondary organic aerosol (SOA) formation from the photooxidation of terpenes

N. L. Ng¹, P. S. Chhabra¹, A. W. H. Chan¹, J. D. Surratt², J. H. Kroll³, A. J. Kwan⁴, D. C. McCabe⁴, P. O. Wennberg⁴, A. Sorooshian¹, S. M. Murphy¹, N. F. Dalleska⁴, R. C. Flagan^{1,4}, and J. H. Seinfeld^{1,4}

¹Department of Chemical Engineering, California Institute of Technology, Pasadena, CA 91125, USA

²Department of Chemistry, California Institute of Technology, Pasadena, CA 91125, USA

³Aerodyne Research, Inc., Billerica, MA 01821, USA

⁴Department of Environmental Science and Engineering, California Institute of Technology, Pasadena, CA 91125, USA

Received: 7 June 2007 – Published in Atmos. Chem. Phys. Discuss.: 12 July 2007

Revised: 14 September 2007 – Accepted: 29 September 2007 – Published: 8 October 2007

Abstract. Secondary organic aerosol (SOA) formation from the photooxidation of one monoterpene (α -pinene) and two sesquiterpenes (longifolene and aromadendrene) is investigated in the Caltech environmental chambers. The effect of NO_x on SOA formation for these biogenic hydrocarbons is evaluated by performing photooxidation experiments under varying NO_x conditions. The NO_x dependence of α -pinene SOA formation follows the same trend as that observed previously for a number of SOA precursors, including isoprene, in which SOA yield (defined as the ratio of the mass of organic aerosol formed to the mass of parent hydrocarbon reacted) decreases as NO_x level increases. The NO_x dependence of SOA yield for the sesquiterpenes, longifolene and aromadendrene, however, differs from that determined for isoprene and α -pinene; the aerosol yield under high- NO_x conditions substantially exceeds that under low- NO_x conditions. The reversal of the NO_x dependence of SOA formation for the sesquiterpenes is consistent with formation of relatively low-volatility organic nitrates, and/or the isomerization of large alkoxy radicals leading to less volatile products. Analysis of the aerosol chemical composition for longifolene confirms the presence of organic nitrates under high- NO_x conditions. Consequently the formation of SOA from certain biogenic hydrocarbons such as sesquiterpenes (and possibly large anthropogenic hydrocarbons as well) may be more efficient in polluted air.

1 Introduction

Atmospheric oxidation of certain volatile organic compounds (VOCs) leads to the formation of low volatility species that partition into the condensed phase and form secondary organic aerosol (SOA). Biogenic hydrocarbons, such as isoprene (C_5H_8), monoterpenes ($\text{C}_{10}\text{H}_{16}$), and sesquiterpenes ($\text{C}_{15}\text{H}_{24}$), are important contributors to the total atmospheric burden of SOA owing to their large global emissions and high reactivity with hydroxyl radicals (OH), ozone (O_3), and nitrate radicals (NO_3) (Guenther et al., 1995; Griffin et al., 1999a; Geron et al., 2000; Owen et al., 2001; Atkinson and Arey, 2003; Seinfeld and Pankow, 2003; Kanakidou et al., 2005).

Over the last two decades, numerous laboratory chamber experiments have been conducted to study aerosol formation from biogenic hydrocarbons. Level of odd nitrogen (NO_x) has been found to be highly influential in SOA production for a variety of compounds. Recent studies on isoprene photooxidation, α -pinene ozonolysis, and benzene, toluene, and *m*-xylene photooxidation have demonstrated that aerosol yields are generally highest at low levels of NO_x (Hatakeyama et al., 1991; Kroll et al., 2006; Presto et al., 2005; Song et al., 2005; Ng et al., 2007). These observations are consistent with competitive chemistry of peroxy radicals between NO and HO_2 , with the RO_2+HO_2 reaction producing products of lower volatility than the RO_2+NO reaction (Hatakeyama et al., 1991; Johnson et al., 2004, 2005; Kroll et al., 2005, 2006; Presto et al., 2005; Ng et al., 2007). For example, in α -pinene ozonolysis, Presto et al. (2005) observed relatively volatile organic nitrates under high- NO_x conditions, while less volatile products, such as 10-hydroxypinonic acid, were more abundant under low- NO_x conditions. Although a

Correspondence to: J. H. Seinfeld
(seinfeld@caltech.edu)

decreasing SOA yield with increasing NO_x level has been established for relatively small hydrocarbons (10 carbons or fewer), it is unknown whether larger molecules, such as sesquiterpenes, exhibit a similar NO_x dependence of SOA yield.

In the present study, we focus on two sesquiterpenes, longifolene and aromadendrene, and compare the NO_x-dependence of their SOA formation with that of α -pinene. Longifolene reacts very slowly with ozone (Atkinson and Arey, 2003), making it ideal for the study of OH photooxidation. Moreover, both longifolene and aromadendrene have only one double bond, thus one can infer more easily the general mechanisms of SOA formation than when multiple double bonds are present (Ng et al., 2006). Experiments are conducted under limiting NO_x conditions (high-NO_x conditions in which HONO is used as the OH precursor, and low-NO_x conditions in which H₂O₂ is used as the OH precursor), as well as with intermediate levels of NO_x.

2 Experimental section

Experiments are performed in Caltech's dual 28 m³ Teflon environmental chambers. Details of the facilities are given elsewhere (Cocker et al., 2001; Keywood et al., 2004). Before each experiment, the chambers are flushed continuously with dry purified air for ~24 h. Each chamber has a dedicated Differential Mobility Analyzer (DMA, TSI model 3081) coupled with a condensation nucleus counter (TSI model 3760) for measuring aerosol size distribution, number concentration, and volume concentration. All aerosol growth data are corrected for wall loss, in which size-dependent coefficients determined from inert particle wall loss experiments are applied to the aerosol volume data (Keywood et al., 2004). Temperature, relative humidity (RH), O₃, NO, and NO_x are continuously monitored. The initial temperature of the chamber is ~20°C. Heating from the lights leads to a temperature increase of approximately 5°C inside the chamber over the course of the experiment. The analytical instruments are located outside the chamber enclosure and are at the temperature of the surrounding room (~20–22°C). The air may cool slightly as it is sampled from the chamber into the instruments, and the measured aerosol likely corresponds to the gas-particle partitioning at the temperature of the surrounding room rather than the chamber enclosure. Such small temperature differences are unlikely to affect results significantly.

Seed particles are introduced into the chamber to act as substrates onto which the gas-phase semivolatile products may condense. Seed aerosols are generated from a 0.015 M aqueous ammonium sulfate solution with a constant-rate atomizer, producing initial particle number concentrations of ~25 000 particles cm⁻³, with a geometric mean diameter of ~50 nm, and an initial aerosol seed volume of ~10–15 $\mu\text{m}^3\text{cm}^{-3}$. After introduction of the seed aerosol, a

known volume of the parent hydrocarbon is injected into a glass bulb, and then introduced into the chambers by an air stream. For experiments with α -pinene and longifolene, the concentration (mixing ratio) of the parent hydrocarbon is monitored with a Hewlett Packard gas chromatograph (model 5890) with flame ionization detection (GC-FID). The concentration of longifolene in several experiments is also measured with a Proton Transfer Reaction Mass Spectrometer (PTR-MS), a custom-modified Varian 1200 system (see Appendix A). Owing to the difficulties in measuring aromadendrene with GC-FID, its concentration is measured solely with the PTR-MS. The PTR-MS is calibrated only for aromadendrene.

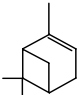
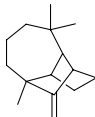
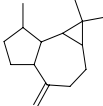
In the high-NO_x experiments nitrous acid (HONO) serves as the OH precursor. HONO is prepared by dropwise addition of 15 mL of 1% NaNO₂ into 30 mL of 10% H₂SO₄ in a glass bulb. After injection of the seed aerosol and parent hydrocarbon, the bulb is then attached to the chamber and a stream of dry air is passed through the bulb, sending HONO into the chamber. NO and NO₂, formed as side products in the preparation of HONO, are also introduced into the chamber, and are measured by a commercial NO_x monitor (Horiba APNA-360, Irvine, CA). Additional NO from a 500 ppm gas cylinder (Scott Marrin, Inc.) is introduced into the chamber after the addition of HONO to achieve a target NO_x level in the chamber of about 1 ppm (upper limit of the NO_x monitor).

For low-NO_x experiments, H₂O₂ serves as the OH precursor. The background NO_x level in the chamber during such experiments is ≤ 2 ppb. H₂O₂ is introduced into the chamber (prior to introduction of seed particles and parent hydrocarbon) by bubbling air through a 50% H₂O₂ solution for 2.5 h at 5 L/min. The concentration of H₂O₂ in the chamber is not measured; based on the rate of hydrocarbon decay and literature values of $\sigma_{\text{H}_2\text{O}_2}$ and $k_{\text{H}_2\text{O}_2}$, we estimate [H₂O₂] to be ~3–5 ppm (Kroll et al., 2006). The air stream then passes through a particle filter to remove any droplets. Variable NO experiments are also carried out, in which a known concentration of NO is introduced into the chamber after the addition of H₂O₂. This allows for the study of SOA formation under intermediate NO_x conditions. It is noted that for these intermediate NO_x experiments, NO goes to zero during the experiment and so there is a switch from high- to low-NO_x conditions over the course of the experiment.

Once the seed, parent hydrocarbon, and NO_x concentrations stabilize, reaction is initiated by irradiating the chamber with blacklights. Output from the lights is between 300 and 400 nm, with a maximum at 354 nm. Half of the available black lights are used in the experiments. At these wavelengths HONO efficiently photolyzes to OH and NO. By contrast, H₂O₂ absorbs only weakly in this wavelength range, requiring the use of ppm mixing ratios of H₂O₂ to achieve target levels of OH.

A comprehensive range of measurements are employed to study the chemical composition of the SOA formed.

Table 1. Parent hydrocarbons used in this study.

Parent Hydrocarbon	Structure	Formula (MW)	k_{OH} (cm ³ molec ⁻¹ s ⁻¹)
α -pinene		C ₁₀ H ₁₆ (136)	5.3×10^{-11} ^a
longifolene		C ₁₅ H ₂₄ (204)	4.8×10^{-11} ^a
aromadendrene		C ₁₅ H ₂₄ (204)	1.5×10^{-10} ^b

^a Rate constants were obtained from Atkinson et al. (2003).

^b Rate constant was estimated from the rate of aromadendrene decay (experiment 1 in Table 4), assuming an OH concentration of 3×10^6 molecule cm⁻³ and that aromadendrene reacts with OH only.

Real-time particle mass spectra are obtained with an Aerodyne quadrupole Aerosol Mass Spectrometer (Q-AMS) (Jayne et al., 2000). A particle-into-liquid sampler (PILS, Brechtel Manufacturing, Inc.) coupled with ion chromatography is employed for quantitative measurements of water-soluble ions in the aerosol phase (Sorooshian et al., 2006). For offline chemical analysis, aerosol samples are collected on Teflon filters (PALL Life Sciences, 47-mm diameter, 1.0- μ m pore size, Teflo membrane) starting at the point when aerosol volume reaches its maximum value. Depending on the total chamber volume concentration of aerosol, the filter sampling time is 2–4 h, which results in ~ 1.5 – 6 m³ of total chamber air sampled. Teflon filter extraction protocols in HPLC-grade methanol have been described previously (Surratt et al., 2006). The resultant filter extracts are then analyzed by high performance liquid chromatography/electrospray ionization-quadrupole mass spectrometry (HPLC/ESI-MS) and electrospray ionization-ion trap mass spectrometry (ESI-ITMS); details of the protocols are described elsewhere (Surratt et al., 2006). Filter extracts are also analyzed by a Waters ACQUITY ultra performance liquid chromatography (UPLC) system, coupled with a Waters LCT Premier time-of-flight (TOF) mass spectrometer (MS) equipped with an electrospray ionization (ESI) source (see Appendix B), allowing for exact mass and tandem MS measurements.

The parent hydrocarbons studied and their stated purities are as follows: α -pinene (Aldrich, 99+%), longifolene (Aldrich, >99%), and aromadendrene (Aldrich, >97%). Ta-

ble 1 lists the structures of the parent hydrocarbons and the rate constants of the compounds for reaction with OH radicals (k_{OH}). Experimental conditions and results for each of the parent hydrocarbons studied are given in Tables 2, 3, and 4. In calculating SOA yield, knowledge of the SOA density is required. By comparing volume distributions from the DMA and mass distributions from the Q-AMS, effective densities for the SOA formed can be estimated (Bahreini et al., 2005; Alfarra et al., 2006). The estimated densities of the SOA formed from different parent hydrocarbons are given in Table 5.

3 Aerosol yields

3.1 α -pinene photooxidation

Under high-NO_x conditions, the efficient photolysis of HONO generates relatively high concentrations of OH ($\sim 2 \times 10^7$ molecules cm⁻³ initially), leading to rapid α -pinene decay. Aerosol growth occurs essentially immediately, even when [NO] is high (100's of ppb). With the high NO concentration throughout the entire experiment, formation of ozone and NO₃ is suppressed.

Under low-NO_x conditions, aerosol growth is also observed immediately after initiation of irradiation. The α -pinene decays at a slower rate than under high-NO_x conditions, owing to the relatively slow production of OH radicals by H₂O₂ photolysis. Ozone formation is observed at an increasing concentration over time (~ 30 ppb at the peak

Table 2. Initial conditions and results for α -pinene experiments.

Expt. No.	NO _x Condition	NO (ppb)	NO ₂ (ppb)	T (K)	RH (%)	Δ HC (ppb) ^a	Δ M ₀ (μ g/m ³) ^b	SOA Yield (%) ^c
1	H ₂ O ₂	0	0	298	5.3	13.8 \pm 0.2	29.3 \pm 2.4	37.9 \pm 3.2
2	H ₂ O ₂	0	1	298	6.2	47.5 \pm 0.8	121.3 \pm 9.4	45.8 \pm 3.6
3	H ₂ O ₂ +NO	198	0	296	6.4	13.1 \pm 0.2	15.6 \pm 1.4	21.2 \pm 2.0
4	HONO	475	463	299	3.3	12.6 \pm 0.2	4.5 \pm 0.9	6.6 \pm 1.4
5	HONO	390	578	298	3.7	46.6 \pm 0.8	40.8 \pm 3.8	15.8 \pm 1.5

^a Stated uncertainties (1 σ) include scatter in GC measurements and GC calibration errors.^b Stated uncertainties (1 σ) are from scatter in particle volume measurements.^c Stated uncertainties are propagated from errors in Δ HC and Δ M₀.**Table 3.** Initial conditions and results for longifolene experiments.

Expt. No.	NO _x Condition	NO (ppb)	NO ₂ (ppb)	T (K)	RH (%)	Δ HC (ppb) ^b	Δ M ₀ (μ g/m ³) ^c	SOA Yield (%) ^d
1	H ₂ O ₂	0	0	298	5.8	4.5 \pm 0.2	28.5 \pm 2.4	75.7 \pm 7.0
2	H ₂ O ₂	0	2	297	6.0	8.4 \pm 0.4	52.5 \pm 4.2	74.4 \pm 6.7
3	H ₂ O ₂	0	2	297	6.3	19.4 \pm 0.8	117.1 \pm 9.3	72.1 \pm 6.5
4	H ₂ O ₂	0	2	299	5.7	24.8 \pm 1.1	148.4 \pm 11.6	71.8 \pm 6.4
5	H ₂ O ₂ +NO	70	31 ^a	297	6.2	3.8 \pm 0.2	35.8 \pm 2.9	111.7 \pm 10.2
6	H ₂ O ₂ +NO	209	26 ^a	297	8.0	4.7 \pm 0.2	43.4 \pm 3.5	110.2 \pm 10.0
7	H ₂ O ₂ +NO	316	0	298	6.4	4.1 \pm 0.2	43.4 \pm 3.5	127.2 \pm 1.5
8	H ₂ O ₂ +NO	394	0	297	6.1	4.8 \pm 0.2	50.0 \pm 4.1	124.9 \pm 11.5
9	H ₂ O ₂ +NO	564	0	297	6.2	3.9 \pm 0.2	51.6 \pm 4.1	157.0 \pm 14.1
10	HONO	428	550	298	3.7	9.7 \pm 0.4	68.3 \pm 5.1	84.0 \pm 7.1
11	HONO	469	502	298	3.7	19.6 \pm 0.9	141.9 \pm 10.3	86.8 \pm 7.3
12	HONO	394	577	299	3.2	26.6 \pm 1.2	213.6 \pm 15.3	96.3 \pm 8.0

^a NO₂ formed due to NO reacting with residual ozone in the chamber.^b Stated uncertainties (1 σ) include scatter in GC measurements and GC calibration errors.^c Stated uncertainties (1 σ) are from scatter in particle volume measurements.^d Stated uncertainties are propagated from errors in Δ HC and Δ M₀.

of aerosol growth), possibly from residual material released from the chamber walls. Based on the reaction rate constants of α -pinene+O₃ ($k_{\text{Ozone}}=8.4\times 10^{-17}$ cm³ molecule⁻¹ s⁻¹, Atkinson et al., 2003) and α -pinene+OH ($k_{\text{OH}}=5.3\times 10^{-11}$ cm³ molecule⁻¹ s⁻¹, Atkinson et al., 2003), and an inferred OH concentration of 3×10^6 molecules cm⁻³ (estimated from longifolene low-NO_x experiments, see Sect. 3.2), it is estimated that an ozone source of ~ 0.1 ppb/min would be required to produce the observed α -pinene decay. It is estimated that only about 35% of the α -pinene reacts by ozonolysis at the point of maximum growth. Therefore, while α -pinene ozonolysis accounts for some of the SOA yield under low-NO_x conditions, it is unlikely that the observed yield differences between high- and low-NO_x conditions (described below) arise solely from the presence of ozone.

Figure 1 shows the time-dependent growth curves (organic aerosol generated, denoted as Δ M₀, as a function of hydrocarbon reacted, Δ HC) for α -pinene under different NO_x conditions. The curves are referred to as “time-dependent growth curves” as each curve represents aerosol growth data for a single experiment over the course of the experiment (Ng et al., 2006). As hydrocarbon measurements are made with a lower frequency than those of particle volume, the α -pinene concentrations shown are obtained by fitting the GC measurements to an exponential decay. In all cases, the initial mixing ratio of α -pinene is about 15 ppb, all of which is consumed by the end of the experiment. It is clear that the aerosol growth under low-NO_x (H₂O₂) conditions substantially exceeds that under high-NO_x (HONO) conditions, while the intermediate NO_x (“H₂O₂+NO”) experiment exhibits an aerosol yield between those of the two extremes. The time-dependent growth curve of the intermediate NO_x

Table 4. Initial conditions and results for aromadendrene experiments.

Expt. No.	NO _x Condition	NO (ppb)	NO ₂ (ppb)	T (K)	RH (%)	ΔHC (ppb) ^a	ΔM ₀ (μg/m ³) ^b	SOA Yield (%)
1	H ₂ O ₂	0	0	299	5.5	5.7±1.2	19.7±2.0	41.7±10
2	H ₂ O ₂ +NO	120	0	298	9.3	5.3±1.2	23.1±2.2	52.0±12.4
3	H ₂ O ₂ +NO	195	0	298	7.7	6.0±1.4	29.3±2.6	58.8±14.4
4	H ₂ O ₂ +NO	517	0	299	7.4	3.2±0.7	22.6±2.2	84.7±20.0

^a Stated uncertainties (1σ) include scatter in PTR-MS measurements and PTR-MS calibration errors.^b Stated uncertainties are derived from scatter in particle volume measurements.**Table 5.** Estimated effective SOA densities.

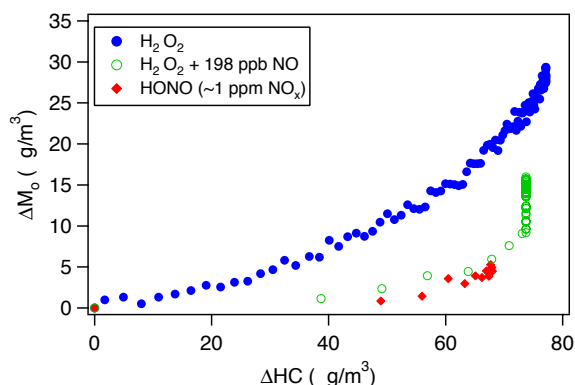
Parent Hydrocarbon	NO _x Condition	Effective Density (g cm ⁻³) ^a
α-pinene	Low-NO _x	1.32±0.10
α-pinene	Intermediate NO _x	1.32±0.10
α-pinene	High-NO _x	1.33±0.10
longifolene	Low-NO _x	1.29±0.10
longifolene	Intermediate NO _x	1.30±0.10
longifolene	High-NO _x	1.40±0.10
aromadendrene	Low-NO _x	1.20±0.10
aromadendrene	Intermediate NO _x	1.35±0.10

^a Stated uncertainties (1σ) are from repeated measurement of ammonium sulfate seed densities.

experiment exhibits a vertical section at the end, indicating that further reactions are contributing to aerosol growth after α-pinene is consumed. We return to this observation in Sect. 5.2.2.

3.2 Longifolene photooxidation

For longifolene, a series of high-NO_x (HONO) experiments and low-NO_x (H₂O₂) experiments with varying initial hydrocarbon concentrations are carried out. The time-dependent growth curves for 3 high-NO_x and 3 low-NO_x experiments, with initial longifolene mixing ratios ranging from ~10 to 30 ppb, are shown in Fig. 2. In contrast to α-pinene photooxidation, longifolene aerosol yields under high-NO_x conditions exceed those under low-NO_x conditions. Under high-NO_x conditions, the maximum SOA yield is about ~100–130% and is reached in ~10 min after initiation of the experiments, with the yield decreasing after that point. It is noted that SOA yield is defined on a mass basis so oxidation (addition of O or N atoms) can lead to yields larger than 100%. Under low-NO_x conditions, SOA yield continues to increase over the course of the experiment, reaching a maximum when all the longifolene is consumed. The final SOA yields of each longifolene low-NO_x experiment lie on a straight line that passes through the origin, indicating that under low-NO_x conditions SOA yield is constant (~75%) under the range of ΔM₀ studied. It is possible that under lower SOA loadings the yields

**Fig. 1.** Time-dependent growth curves for α-pinene photooxidation under different NO_x conditions (Experiments 1, 3 and 4 in Table 2).

may decrease as some of the products partition back into the gas phase. Based on the observed longifolene decay and *k*_{OH} for longifolene, the chamber OH concentration under low-NO_x conditions is estimated to be ~3×10⁶ molecules cm⁻³.

The effect of NO_x on longifolene aerosol formation is further illustrated by the time-dependent growth curves in Fig. 3. In both experiments H₂O₂ is used as the OH precursor and the initial longifolene mixing ratio is 4–5 ppb; in one experiment no extra NO is added, while in the other experiment about 300 ppb of NO is introduced into the chamber after the addition of H₂O₂. Aerosol growth in the presence of ~300 ppb NO is substantially higher. A series of experiments with the same initial longifolene concentration but different initial NO concentrations (~100–600 ppb) are also carried out. Figure 4 shows the final aerosol yield as a function of the initial NO_x concentration. The amount of aerosol formed is highly dependent on the level of NO_x present initially; with ~600 ppb NO, the ultimate aerosol yield is twice that at low-NO_x conditions.

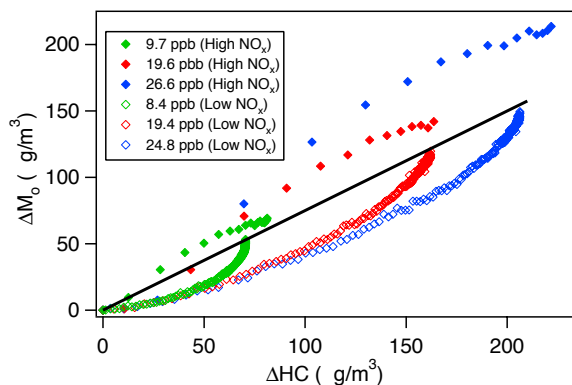


Fig. 2. Time-dependent growth curves for longifolene photooxidation under high- and low- NO_x conditions (Experiments 2, 3, 4, 10, 11, and 12 in Table 3). The mixing ratios in the legend refer to the amount of longifolene reacted in each experiment. The final SOA yields of each low- NO_x experiment lie on a straight line that passes through the origin, indicating that under low- NO_x conditions SOA yield is constant, at $\sim 75\%$.

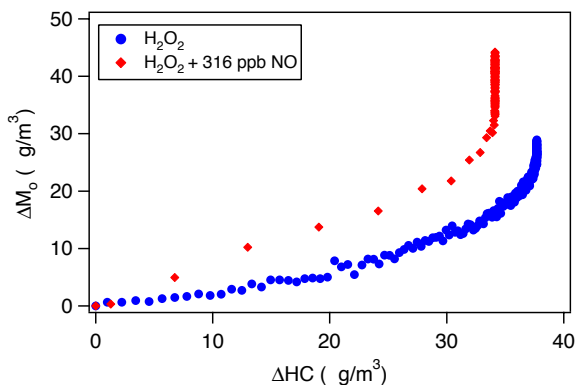


Fig. 3. Time-dependent growth curves for longifolene photooxidation with H_2O_2 as the OH precursor. Aerosol growth in the presence of ~ 300 ppb NO (Experiment 7 in Table 3) significantly exceeds that without NO (Experiment 1 in Table 3).

3.3 Aromadendrene photooxidation

Figure 5 shows the final aerosol yield as a function of initial NO_x concentration for aromadendrene photooxidation. The OH precursor used in these experiments is H_2O_2 and the initial aromadendrene mixing ratio is ~ 5 ppb. It is clear that aromadendrene aerosol yield also increases with NO_x concentration; as with longifolene, with ~ 500 ppb NO , the aerosol yield is approximately double that at low- NO_x conditions.

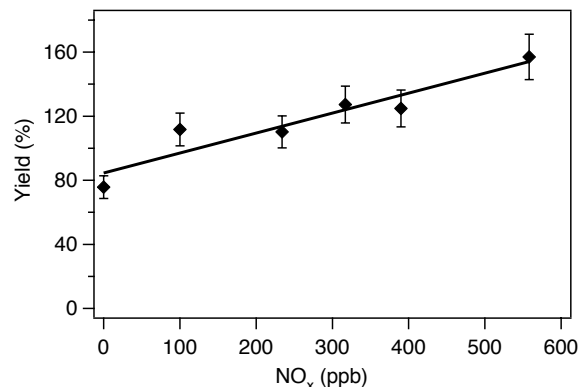


Fig. 4. SOA growth as a function of initial NO_x concentration, for a fixed longifolene concentration (4–5 ppb). Results shown are from Table 3.

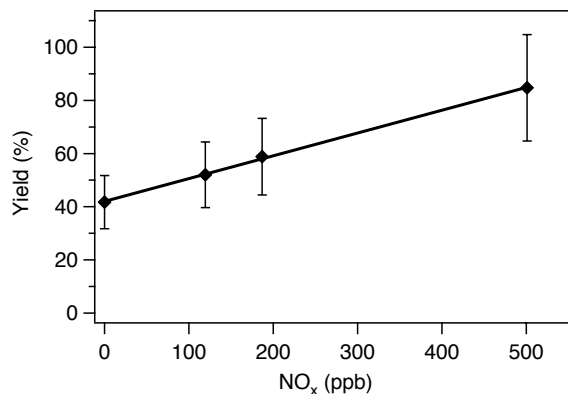


Fig. 5. SOA growth as a function of initial NO_x concentration, at a fixed initial aromadendrene concentration (~ 5 ppb). Results shown are given in Table 4.

4 Chemical composition of SOA

In this section, the measurements of the chemical composition of α -pinene and longifolene SOA are presented. The aromadendrene experiments are performed mainly to verify the observed NO_x dependence for longifolene, in which SOA yield is higher under high- NO_x conditions, and so detailed analysis of the chemical composition of aromadendrene SOA is not pursued.

4.1 Aerosol Mass Spectrometer (Q-AMS) measurements

Figures 6 and 7 show the AMS high- NO_x versus low- NO_x spectrum signal for α -pinene and longifolene photooxidation, respectively. Each mass fragment is normalized by the total signal. For both hydrocarbons, SOA at high NO_x conditions exhibit relatively strong signals at m/z 30 and

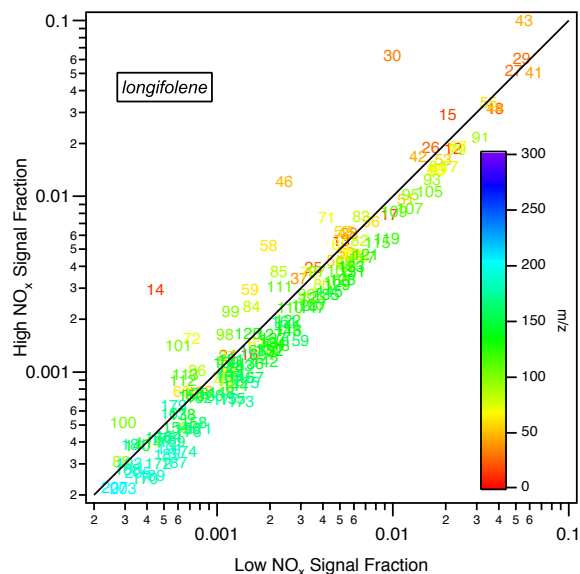


Fig. 7. AMS high-NO_x spectra signal versus low-NO_x spectra signal for longifolene photooxidation. Each mass fragment is normalized by the total signal. The solid black line is the 1:1 line. The spectra are taken when all hydrocarbon has been consumed.

4.2 Offline chemical analysis

All ions detected by the UPLC/ESI-TOFMS instrument from α -pinene and longifolene photooxidation are listed in Tables 6 and 7, respectively. The tables list the exact masses and their likely molecular formulas corresponding to each of the $[M-H]^-$ ions detected (in which M is the molecular weight of the compound). The error between the measured mass and theoretical mass is reported in two different ways, ppm and mDa. For most of the ions observed, the error between the measured and theoretical masses is less than ± 2 mDa and ± 5 ppm, allowing for generally unambiguous identification of molecular formulae. Solvent blanks and control filters are also run on the UPLC/ESI-TOFMS instrument; none of the listed ions is observed in these control samples. The ions listed in Tables 6 and 7 are also detected by HPLC/ESI-MS and ESI-ITMS, confirming that these compounds are not the result of artifact formation in a specific mass spectrometer.

Acidic compounds, such as carboxylic acids and sulfate esters, readily ionize under (–)ESI-MS techniques (Gao et al., 2004; Surratt et al., 2006; Surratt et al., 2007). Hydroxylated compounds, as well as ketones and aldehydes, however, are generally not ionizable unless carboxylic acid and/or sulfate ester moieties are also present within the same molecule. Therefore, it is expected that all ions listed in Tables 6 and 7 are acidic compounds. For the SOA formed in the presence of NO_x (HONO and “H₂O₂+NO” experiments), even-mass

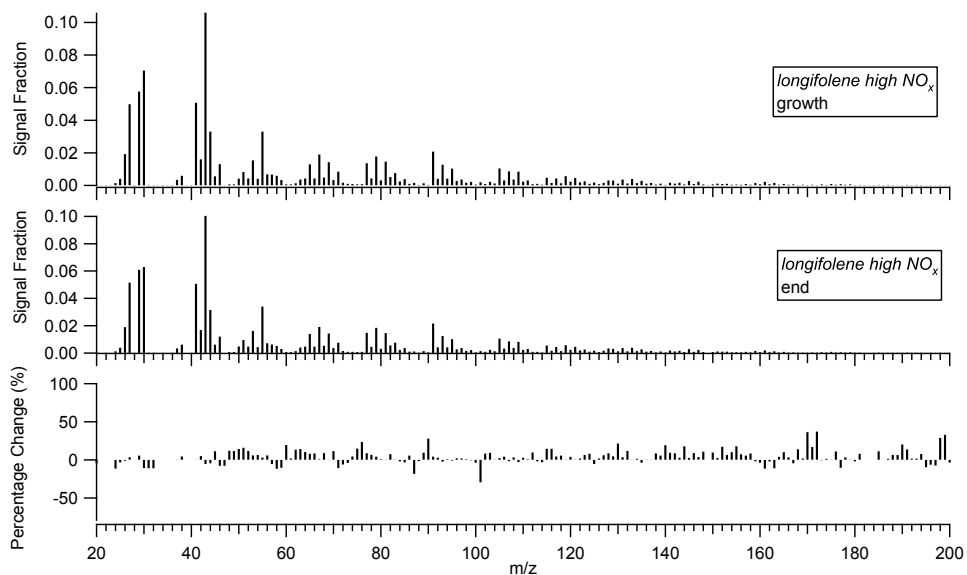


Fig. 8. Change in AMS spectrum over the course of longifolene photooxidation under high- NO_x conditions. Top panel: Fractional contribution of each mass fragment to the total organic and nitrate signal during the growth phase of the experiment. Middle panel: fractional contribution of each mass fragment to the total organic and nitrate signal when all hydrocarbon is consumed. Bottom panel: Percentage change of each mass fragment between the growth phase and the end of the experiment.

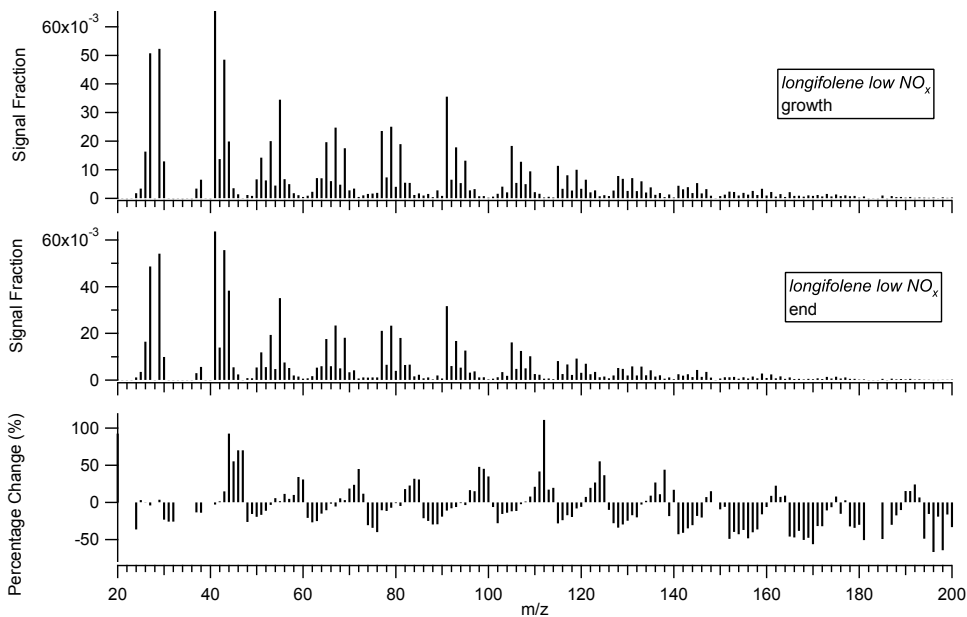


Fig. 9. Change in AMS spectrum over the course of longifolene photooxidation under low- NO_x conditions. Top panel: Fractional contribution of each mass fragment to the total organic and nitrate signal during the growth phase of the experiment. Middle panel: fractional contribution of each mass fragment to the total organic and nitrate signal when all hydrocarbon is consumed. Bottom panel: Percentage change of each mass fragment between the growth phase and the end of the experiment.

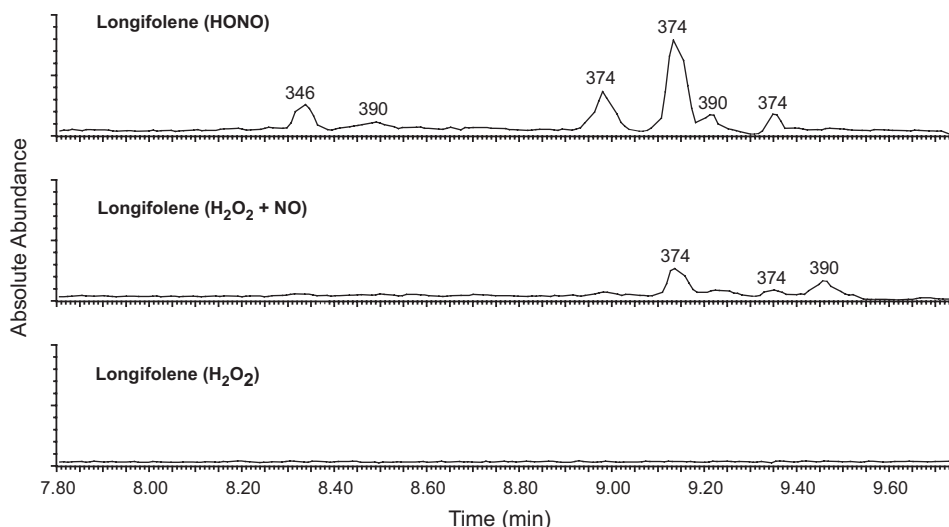


Fig. 10. UPLC/ESI-TOFMS extracted ion chromatograms (EICs) ($=m/z$ 346+374+390) for longifolene photooxidation. The even $[\text{M}-\text{H}]^-$ ions listed above the chromatographic peaks correspond to organic nitrates detected in longifolene SOA. No organic nitrates are detected in the H_2O_2 experiment (low- NO_x condition). The HONO experiment (high- NO_x condition) has the widest array of organic nitrates detected (as shown in Table 7), as well as the largest chromatographic peaks; m/z 372 is the only exception, and is most abundant in the intermediate NO_x experiment. These EICs are directly comparable as the volume of chamber air sampled is approximately the same (2 m^3).

$[\text{M}-\text{H}]^-$ ions are observed in ESI mass spectra, indicating the compound has an odd number of nitrogen atoms, likely within organic nitrate functional groups. Nitrated organics were previously observed in isoprene SOA formed under high- NO_x conditions (both HONO and $\text{H}_2\text{O}_2+\text{NO}$) (Surratt et al., 2006), and are further confirmed by the tandem MS data, which reveals a loss of 63 Da (HNO_3). For α -pinene, only one acidic organic nitrate (m/z 322) is detected in the HONO experiment and none are detected in H_2O_2 and intermediate NO_x experiments. Masses of many ions detected in the α -pinene experiments have been observed in previous laboratory work (Glasius et al., 1999, 2000; Larsen et al., 2001) and field studies (Gao et al., 2006). For longifolene, a much wider array of acidic organic nitrates is detected by the UPLC/ESI-TOFMS instrument in both HONO and intermediate NO_x experiments. For both α -pinene and longifolene, compounds with more carbons than the parent hydrocarbon are observed. Tandem MS data for these C_{12} , C_{16} , and C_{17} acidic organic nitrates reveal a common neutral loss of 60 Da, which possibly corresponds to an acetic acid monomer. Surratt et al. (2006) and Szmigielski et al. (2007) recently showed that particle-phase esterification occurs in isoprene SOA formed under high- NO_x conditions. The observed neutral loss of 60 Da for these acidic organic nitrates suggests that these compounds may be dimers formed by particle-phase esterification.

Figure 10 shows the extracted ion chromatograms (EICs) of m/z 346, 374, and 390 from longifolene oxidation under different NO_x conditions. These m/z values correspond to

acidic organic nitrates, as confirmed by the exact mass data (Table 7) as well as the loss of 63 Da in the tandem MS data. The chromatographic peaks are much larger in the highest NO_x experiment than those in the intermediate NO_x experiment (except m/z 372, not shown); no chromatographic peaks are observed under low- NO_x (H_2O_2) conditions. In addition, for several $[\text{M}-\text{H}]^-$ ions (e.g. m/z 374 and 390) there are several structural isomers present. Additionally, the intensity of non-nitrogen-containing ions (e.g. m/z 223, 239, 253, 255, 267, 269, and 283), are generally larger under low- NO_x conditions.

5 Discussion

5.1 Effect of hydrocarbon size on NO_x dependence

It has been established that NO_x levels exert a major influence on SOA formation (Hatakeyama et al., 1991; Pandis et al., 1991; Zhang et al., 1992, 2006; Hurley et al., 2001; Johnson et al., 2004, 2005; Song et al., 2005; Presto et al., 2005; Kroll et al., 2005, 2006; Ng et al., 2007). For photooxidation of isoprene, SOA yields increase as the NO_x level decreases (Kroll et al., 2006). The proposed mechanism for this observed NO_x dependence is the competitive chemistry of organic peroxy radicals between NO and HO_2 , in which the semivolatile products formed via the RO_2+HO_2 path are less volatile than those formed via the RO_2+NO route (Hatakeyama et al., 1991; Johnson et al., 2004, 2005;

Table 6. α -Pinene acidic SOA components detected by UPLC/ESI-TOFMS.

Experiment	Measured [M - H] ⁻ ion (<i>m/z</i>)	TOFMS suggested molecular formula	Error (mDa)	Error (ppm)	Retention Time (min)
H ₂ O ₂	157.0497	C ₇ H ₉ O ₄ ⁻	-0.4	-2.5	5.09
	169.0873	C ₉ H ₁₃ O ₃ ⁻	0.8	4.7	6.89
	171.0654	C ₈ H ₁₁ O ₄ ⁻	-0.3	-1.8	5.61
	183.1027	C ₁₀ H ₁₅ O ₃ ⁻	0.6	3.3	7.50
	185.0821	C ₉ H ₁₃ O ₄ ⁻	0.7	3.8	6.85
	199.0983	C ₁₀ H ₁₅ O ₄ ⁻	1.3	6.5	6.17
	199.0982	C ₁₀ H ₁₅ O ₄ ⁻	1.2	6.0	6.29
	199.0976	C ₁₀ H ₁₅ O ₄ ⁻	0.6	3.0	6.34
	215.0923	C ₁₀ H ₁₅ O ₅ ⁻	0.4	1.9	5.99
	215.0930	C ₁₀ H ₁₅ O ₅ ⁻	1.1	5.1	7.18
H ₂ O ₂ + NO	231.0885	C ₁₀ H ₁₅ O ₆ ⁻	1.6	6.9	6.80
	157.0499	C ₇ H ₉ O ₄ ⁻	-0.2	-1.3	5.08
	171.0655	C ₈ H ₁₁ O ₄ ⁻	-0.2	-1.2	5.60
	183.1025	C ₁₀ H ₁₅ O ₃ ⁻	0.4	2.2	7.49
	185.0812	C ₉ H ₁₃ O ₄ ⁻	-0.2	-1.1	6.86
	197.0814	C ₁₀ H ₁₃ O ₄ ⁻	0.0	0.0	8.09
	199.0971	C ₁₀ H ₁₅ O ₄ ⁻	0.1	0.5	6.36
	203.0557	C ₈ H ₁₁ O ₆ ⁻	0.1	0.5	5.50
	215.0925	C ₁₀ H ₁₅ O ₅ ⁻	0.6	2.8	6.23
	229.0718	C ₁₀ H ₁₃ O ₆ ⁻	0.6	2.6	6.17
HONO	231.0856	C ₁₀ H ₁₅ O ₆ ⁻	-1.3	-5.6	6.79
	171.0649	C ₈ H ₁₁ O ₄ ⁻	-0.8	-4.7	5.60
	183.1022	C ₁₀ H ₁₅ O ₃ ⁻	0.1	0.5	7.49
	185.0457	C ₈ H ₉ O ₅ ⁻	0.7	3.8	6.63
	187.0606	C ₈ H ₁₁ O ₅ ⁻	0.0	0.0	5.65
	197.0819	C ₁₀ H ₁₃ O ₄ ⁻	0.5	2.5	8.09
	203.0546	C ₈ H ₁₁ O ₆ ⁻	-1.0	-4.9	5.50
	213.0781	C ₁₀ H ₁₃ O ₅ ⁻	1.8	8.4	5.26
	231.0883	C ₁₀ H ₁₅ O ₆ ⁻	1.4	6.1	6.80
	259.1182	C ₁₂ H ₁₉ O ₆ ⁻	0.0	0.0	5.85
	322.1148	C ₁₂ H ₂₀ NO ₉ ⁻	1.0	3.1	7.62

Presto et al., 2005; Kroll et al., 2006; Zhang et al., 2006; Ng et al., 2007). A similar yield dependence on NO_x is observed here for photooxidation of α -pinene (Fig. 1). For an initial α -pinene concentration of ~ 15 ppb, the SOA yield under low-NO_x conditions is about a factor of 3 higher than that under high-NO_x conditions. The observed NO_x dependence is consistent with that of previous studies on α -pinene photooxidation (Hatakeyama et al, 1991) and α -pinene ozonolysis (Presto et al., 2005).

The observed NO_x dependence of SOA yield for the sesquiterpenes, however, is different from that of isoprene and α -pinene (as well as other hydrocarbons with 10 or fewer carbons, such as aromatic species). For longifolene and aromadendrene, aerosol yield increases with increasing NO_x concentration (Figs. 2–5). This reversal of the NO_x dependence of SOA formation could be the result of a number of factors. Figure 11 shows a simplified reaction mechanism involving peroxy radical chemistry. At the two limiting NO_x conditions of this study, the peroxy radical chemistry is relatively well-defined; under high-NO_x conditions, peroxy radicals react virtually entirely with NO, while under low-NO_x conditions, RO₂ reacts predominantly with HO₂. One of the possible explanations for the higher SOA yield under high-NO_x conditions is the formation of large alkoxy radicals that isomerize rather than fragment. Isomerization is plausible if

Table 7. Longifolene acidic SOA components detected by UPLC/ESI-TOFMS.

Experiment	Measured [M - H] ⁻ ion (<i>m/z</i>)	TOFMS suggested molecular formula	Error (mDa)	Error (ppm)	Retention Time (min)
H ₂ O ₂	223.1344	C ₁₃ H ₁₉ O ₃ ⁻	1.0	4.5	8.92
	237.1500	C ₁₄ H ₂₁ O ₃ ⁻	0.9	3.8	9.06
	239.1651	C ₁₄ H ₂₃ O ₃ ⁻	0.4	1.7	10.50
	253.1445	C ₁₄ H ₂₁ O ₄ ⁻	0.5	2.0	9.36
	249.1499	C ₁₅ H ₂₁ O ₄ ⁻	0.8	3.2	9.25
	249.1501	C ₁₅ H ₂₁ O ₄ ⁻	1.0	4.0	10.14
	255.1611	C ₁₄ H ₂₃ O ₄ ⁻	1.5	5.9	9.88
	255.1622	C ₁₄ H ₂₃ O ₄ ⁻	2.6	10.2	8.99
	267.1602	C ₁₅ H ₂₃ O ₄ ⁻	0.6	2.2	8.88
	267.1606	C ₁₅ H ₂₃ O ₄ ⁻	1.0	3.7	9.01
H ₂ O ₂ + NO	267.1611	C ₁₅ H ₂₃ O ₄ ⁻	1.5	5.6	9.28
	267.1601	C ₁₅ H ₂₃ O ₄ ⁻	0.5	1.9	9.70
	269.1392	C ₁₄ H ₂₁ O ₅ ⁻	0.3	1.1	7.71
	283.1561	C ₁₅ H ₂₃ O ₅ ⁻	1.6	5.7	7.35
	313.2018	C ₁₇ H ₂₉ O ₅ ⁻	0.3	1.0	9.20
	223.1337	C ₁₃ H ₁₉ O ₃ ⁻	0.3	1.3	8.92
	239.1649	C ₁₄ H ₂₃ O ₃ ⁻	0.2	0.8	10.49
	265.1442	C ₁₅ H ₂₁ O ₄ ⁻	0.2	0.8	8.93
	269.1401	C ₁₄ H ₂₁ O ₅ ⁻	1.2	4.5	7.72
	316.1396	C ₁₄ H ₂₂ NO ₇ ⁻	0.0	0.0	9.88
HONO	329.1972	C ₁₇ H ₂₉ O ₆ ⁻	0.8	2.4	9.35
	372.1664	C ₁₇ H ₂₆ NO ₈ ⁻	0.6	1.6	10.58
	374.1829	C ₁₇ H ₂₈ NO ₈ ⁻	1.4	3.7	9.14
	374.1829	C ₁₇ H ₂₈ NO ₈ ⁻	1.4	3.7	9.35
	390.1775	C ₁₇ H ₂₈ NO ₉ ⁻	1.1	2.8	9.46
	223.1334	C ₁₃ H ₁₉ O ₃ ⁻	-0.1	-0.4	8.92
	241.1453	C ₁₃ H ₂₁ O ₄ ⁻	1.3	5.4	7.55
	253.1431	C ₁₄ H ₂₁ O ₄ ⁻	-0.9	-3.6	8.02
	269.1394	C ₁₄ H ₂₁ O ₅ ⁻	0.5	1.9	7.18
	269.1408	C ₁₄ H ₂₁ O ₅ ⁻	1.9	7.1	7.71
HONO	342.1930	C ₁₇ H ₂₈ NO ₆ ⁻	1.3	3.8	9.65
	344.1348	C ₁₅ H ₂₂ NO ₈ ⁻	0.3	0.9	8.25
	346.1502	C ₁₅ H ₂₄ NO ₈ ⁻	0.2	0.6	8.34
	360.1674	C ₁₆ H ₂₆ NO ₈ ⁻	1.6	4.4	8.89
	372.1667	C ₁₇ H ₂₆ NO ₈ ⁻	-0.6	-1.6	10.61
	374.1809	C ₁₇ H ₂₈ NO ₈ ⁻	-0.6	-1.6	8.89
	374.1816	C ₁₇ H ₂₈ NO ₈ ⁻	0.1	0.3	9.13
	374.1808	C ₁₇ H ₂₈ NO ₈ ⁻	-0.7	-1.9	9.35
	390.1773	C ₁₇ H ₂₈ NO ₉ ⁻	0.9	2.3	8.49
	390.1778	C ₁₇ H ₂₈ NO ₉ ⁻	1.4	3.6	9.21
	435.1619	C ₁₇ H ₂₇ N ₂ O ₁₁ ⁻	0.4	0.9	9.56

the alkoxy radical has four or more carbon atoms and can form a 6-membered transition state (Baldwin et al., 1977; Carter and Atkinson, 1985). The isomerization pathway leads to the formation of large hydroxycarbonyls, multifunctional products that are likely low in volatility. The relative importance of isomerization increases with the size of alkoxy radicals (Atkinson, 1994, 1997a, b; Atkinson et al., 1995, 1999), and larger compounds could exhibit increasing SOA yields under high-NO_x conditions as a consequence of this mechanism. For example, Lim and Ziemann (2005) measured SOA yields up to $\sim 50\%$ for C₁₅ alkanes in the presence of ppm levels of NO_x. They proposed multiple isomerization steps leading to the formation of multifunctional compounds including nitrooxy, hydroxyl, and carbonyl groups, and it is suggested that the hydroxycarbonyls formed may isomerize to form furan species that can undergo further reactions (Lim and Ziemann, 2005). Gas-phase products that are consistent with the isomerization mechanism have been observed

in α -pinene photooxidation but this pathway does not appear to dominate SOA formation under high- NO_x conditions (Aschmann et al., 1998, 2002), possibly due to the higher volatility of these species.

Higher SOA yields observed under high- NO_x conditions for sesquiterpenes may, secondly, be a result of the formation of relatively nonvolatile organic nitrates, evidence for which appears in both Q-AMS data and filter sample data. In AMS data, m/z 30 (NO^+) and m/z 46 (NO_2^+) signals are commonly associated with nitrate species (organic and inorganic nitrates). For both α -pinene and longifolene, the ratio of the sum of the intensities of ions at m/z 30 and m/z 46 to the total ion intensity is higher under high- NO_x conditions: under low- NO_x conditions, the ratio is very small (2%), under high- NO_x conditions, the ratio is about 15–25%. The ratio of m/z 30 to total mass and the ratio of m/z 46 to total mass show the same trend, indicating m/z 30 and m/z 46 are correlated. It is possible that the signal at m/z 30 could be the result of a non-nitrogen containing organic fragment ion; however, given the observed correlation between m/z 30 and m/z 46 and their small signals under low- NO_x conditions, it appears that there is little interference from organics at these signals. Under high- NO_x conditions, $\sim 10 \mu\text{gm}^{-3}$ of inorganic nitrates, as measured by the PILS/IC, are present in the aerosol. Such nitrates may arise from the partitioning or reactive uptake of gas-phase HNO_3 into the aerosol phase. Assuming no non-nitrate contribution to m/z 30 and m/z 46, the total nitrate content of the SOA is estimated as the sum of the signals at each fragment. It is found that the calculated nitrate content ($\sim 20 \mu\text{gm}^{-3}$) exceeds that measured by PILS/IC, suggesting the presence of organic nitrates.

The filter sample data provide a more direct comparison on the amount of organic nitrates formed in α -pinene and longifolene photooxidation under different NO_x conditions. For both α -pinene and longifolene, no acidic nitrates are observed under low- NO_x conditions, consistent with the lack of NO_x and the prevailing $\text{RO}_2 + \text{HO}_2$ reaction in this case. Organic nitrate yield from the $\text{RO}_2 + \text{NO}$ reaction increases with increasing carbon number (Atkinson et al., 1987; Carter and Atkinson, 1989; O'Brien et al., 1998; Arey et al., 2001; Aschmann et al., 2001; Zhang et al., 2004), and with the larger carbon skeleton the organic nitrates formed will be less volatile, this is consistent with the much wider array and larger quantities of acidic nitrates detected in longifolene photooxidation under high- NO_x conditions compared to the α -pinene experiments. Hence for photooxidation of larger compounds such as sesquiterpenes, the nitrate formation channel may play an important role in SOA formation under high- NO_x conditions. With the formation of large molecular weight compounds with nitrate groups, mass-based SOA yields from longifolene photooxidation under high- NO_x conditions actually exceed 100%.

Lacking appropriate analytical techniques for the detection of non-acidic nitrates, the contribution of these species under high- NO_x conditions cannot be assessed. In α -pinene

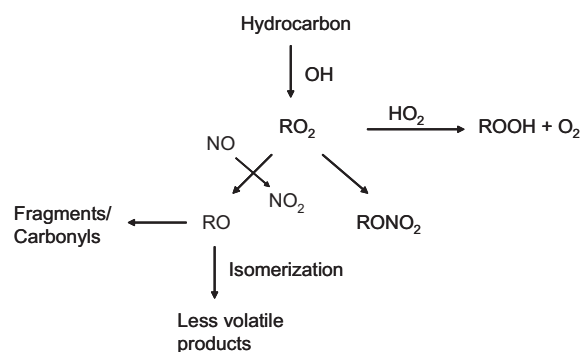


Fig. 11. General schematic of gas-phase peroxy radical chemistry in SOA formation.

photooxidation, hydroxynitrates have been identified in the gas phase using mass spectrometry (Aschmann et al., 1998, 2002). In SOA formation from alkanes under high- NO_x conditions, Lim and Ziemann (2005) found that, while SOA from oxidation of C_{10} alkane contains no δ -hydroxynitrates, nitrates contribute $\sim 40\%$ of the SOA mass for reactions of the C_{15} alkane. It seems likely that higher levels of hydroxynitrates are present in longifolene SOA than in α -pinene SOA.

5.2 General mechanisms of aerosol growth

5.2.1 Loss of semivolatiles

Substantial insight into the general mechanism of SOA formation and growth kinetics can be gained by examining “growth curves”, showing the amount of SOA formed per hydrocarbon reacted (Ng et al., 2006, 2007). Figure 2 shows the time-dependent growth curves from longifolene photooxidation under high- and low- NO_x conditions. The high- NO_x growth curves have a “convex” shape, indicating that aerosol growth slows down as longifolene approaches complete reaction. Similar behavior for longifolene growth was observed previously in our laboratory (Ng et al., 2006); the authors suggested that this atypical growth behavior may have been spurious, as a result of inaccuracies in PTR-MS measurements, owing to interference from product ions, or changes in the aerosol density over the course of the experiment. In this study, in those experiments in which the longifolene concentration is monitored by both GC-FID and PTR-MS, the shape of PTR-MS hydrocarbon decay agrees with that measured by GC-FID. The density of the aerosol is estimated during oxidation by comparing Q-AMS and DMA data. It is found that the SOA density decreases slightly ($< 5\%$) over the course of the experiment, however, such a small decrease in density is within experimental uncertainty and cannot account for the observed atypical growth behavior.

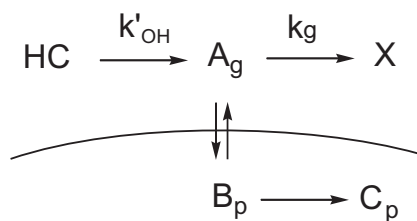


Fig. 12. A kinetic scheme depicting the competition between gas-particle partitioning and irreversible loss of the gas-phase semivolatiles. X represents the product of generic loss of semivolatile species A_g by chemical reaction, and/or loss to chamber walls. k'_{OH} is the pseudo-first-order rate constant ($k'_{OH}=k_{OH}[OH]$) for photooxidation of the parent hydrocarbon; k_g is the first-order rate constant of loss of semivolatiles.

Deceleration in SOA growth can arise from the loss of semivolatiles by photolysis, further reaction with OH to form volatile products, or irreversible loss to chamber walls. Such processes reduce the amount of gas-phase semivolatiles that partition into the aerosol phase. The effect on SOA growth of gas-phase reaction forming more volatile species has been examined in a recent modeling study (Chan et al., 2007). Figure 12 shows a kinetic scheme depicting the competition between gas-particle partitioning and irreversible loss of the gas-phase semivolatiles. X represents the product of generic loss of semivolatile species A_g ; k'_{OH} is the pseudo-first-order rate constant ($k'_{OH}=k_{OH}[OH]$) for reaction of the parent hydrocarbon; and k_g is the first-order rate constant of loss of semivolatiles. When fitting the observed aerosol growth with this simple kinetic model, it is estimated that k_g is about 5 times larger than k'_{OH} . At the estimated OH concentration of $\sim 2 \times 10^7$ molecules cm^{-3} under high-NO_x conditions, k'_{OH} for longifolene is $\sim 9.6 \times 10^{-4} \text{ s}^{-1}$. A major difference in SOA composition under high- and low-NO_x conditions is the presence of organic nitrates under high-NO_x conditions. Thus the loss of organic nitrates (among other gas-phase species) may play a role in the observed deceleration in aerosol growth. The reaction rate constants of small alkyl nitrates with OH are generally of the order of $10^{-13} \text{ cm}^3 \text{ molecule}^{-1} \text{ s}^{-1}$ (hence pseudo-first-order reaction rate of $\sim 10^{-6} \text{ s}^{-1}$) and their photolysis rates have been measured to be $\sim 1 \times 10^{-6} \text{ s}^{-1}$ (Talukdar et al., 1997; Finlayson-Pitts and Pitts, 2000). Although the OH reaction rate and photolysis rate of organic nitrates are much slower than the oxidation rate of longifolene, both rates are expected to increase with carbon number (Talukdar et al., 1997; Finlayson-Pitts and Pitts, 2000; Treves and Rudich, 2003). Hence, it is possible that gas-phase reaction of C₁₅ organic nitrates may be occurring at an appreciable rate. Further study on the OH reaction rate constant and photolysis rate of larger nitrates would be useful in evaluating the importance of gas-phase nitrate chemistry in aerosol formation.

Such a deceleration in SOA growth is not observed in longifolene low-NO_x experiments. This is in contrast to the rapid decrease in aerosol volume observed in isoprene photooxidation under low-NO_x conditions, in which photolysis and/or further reactions of organic hydroperoxides may be occurring (Kroll et al., 2006). There is evidence for further reactions with longifolene low-NO_x SOA as well: the AMS m/z 44 (CO_2^+) mass fraction increases over the course of the experiment (Fig. 9), indicating the SOA is being further oxidized. Unlike with isoprene photooxidation, however, the compounds formed from the further oxidation of longifolene products are likely sufficiently nonvolatile to remain in the particle phase. The photochemistry of larger and more complex hydroperoxides merits further investigation.

5.2.2 SOA formation from higher generation products

In Figs. 1 and 3, the growth curves of α -pinene and longifolene photooxidation exhibit a “hook” at the end of the intermediate NO_x experiments, indicating that aerosol growth continues after the complete consumption of the parent hydrocarbon. Organic mass measured by the Q-AMS increases even after all the hydrocarbon is consumed, indicating that this additional aerosol growth is not a result of condensation of inorganic nitrate. Continued aerosol growth can arise from further gas-phase reactions of reactive oxidation products, such as aldehydes and furans, etc., or from further particle-phase reactions. In the intermediate NO_x experiments, the NO concentration goes to zero within 20 min after the commencement of photooxidation, owing to the rapid reaction of NO and peroxy radicals (HO_2 and other peroxy radicals). As a result, a transition from high-NO_x to low-NO_x conditions occurs over the course of the experiment, and the final aerosol formed is potentially a mixture of the products formed under both conditions. It is possible that particle-phase reactions, such as the formation of peroxyhemiacetals from hydroperoxides and aldehyde species, may be contributing to the further aerosol growth observed in the intermediate NO_x experiments (Johnson et al., 2004, 2005).

6 Implications

A series of chamber experiments investigating the NO_x dependence of SOA formation from the photooxidation of one monoterpene and two sesquiterpenes is reported here. SOA formation from monoterpenes such as α -pinene is found to have a similar NO_x dependence as isoprene (as well as other hydrocarbons with 10 or fewer carbons, such as aromatic species), in which the aerosol yields are substantially higher under low-NO_x conditions. The NO_x dependence of SOA formation from the two sesquiterpenes is, however, markedly different; for longifolene and aromadendrene, aerosol yields are at their maximum under high-NO_x conditions. The reason for this reversal of the NO_x dependence, while not

unequivocally established here, may be the result of production of highly nonvolatile organic nitrates, the existence of which is suggested by both Q-AMS and filter sample data, and/or isomerization of alkoxy radicals to form low-volatility multifunctional organics.

The increase in SOA yield from photooxidation of the larger biogenic hydrocarbons under high-NO_x conditions could have implications in terms of the effect of anthropogenically influenced air masses on biogenic SOA formation. In the recent study of de Gouw et al. (2005), it is suggested that over the western Atlantic the majority of the measured organic aerosol is from secondary anthropogenic sources, a conclusion that is somewhat at odds with the radiocarbon measurements that indicate high fractions of “modern” (presumably biogenic) carbon (e.g. Klinedinst and Currie, 1999; Weber et al., 2007). If the production of SOA from biogenic hydrocarbons is enhanced in the presence of NO_x, observations of enhanced SOA correlated with anthropogenic sources can occur, even for organic carbon of biogenic origin. Large anthropogenic hydrocarbons may exhibit a similar NO_x behavior as that of the sesquiterpenes studied, as suggested by the substantial SOA yields from the OH-initiated reaction of large alkanes in the presence of ppm levels of NO_x (Lim and Ziemann, 2005). If the NO_x behavior observed for longifolene and aromadendrene extends to other sesquiterpenes as well as larger alkanes, the contribution to the total SOA from these compounds in polluted air may actually be higher than previously estimated (Griffin et al., 1999a, b; Carreras-Sospedra et al., 2005; de Gouw et al., 2005).

In this study, we have investigated the NO_x dependence of SOA formation from photooxidation of only the monoterpene α -pinene and two sesquiterpenes, each containing one double bond. SOA formation from compounds with two or more double bonds can exhibit characteristics that suggest significant contributions from multiple generation products (Ng et al., 2006) and this may have impacts on the NO_x dependence. It is clear that the effect of NO_x on SOA yields from the complete suite of atmospherically relevant aerosol-forming hydrocarbons should be evaluated thoroughly.

Appendix A

Description of PTR-MS technique

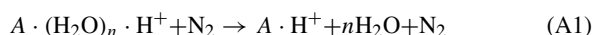
For PTR-MS sampling, a constant flow of ~ 2.5 standard liters per minute (slm) is drawn from the chamber through PFA tubing. The residence time in the inlet tubing is roughly 1 s. A small portion of the flow, 93 standard cubic centimeters per minute (sccm), is pulled through a glass critical orifice into a 2.54-cm diameter glass flow tube, in which this sample flow is diluted with dry N₂ (1.6 slm) to maintain the flow tube pressure at 35 mbar. This dilution minimizes confounding effects owing to large concentrations of hydrogen

peroxide and other compounds typically used or produced in chamber experiments.

In the flow tube, analyte ionization occurs in a manner similar to that described by Crounse et al. (2006) for negative ionization. N₂ (400 sccm) flows through an ion source cup composed of a cylindrical silver foil lined with ²¹⁰Po and sealed with gold. α bombardment from the ²¹⁰Po, coupled with trace water present in the N₂, leads to the formation of positively charged clusters, e.g. (H₂O)_{*n*}H⁺. The electric potentials of the ion source components are set such that these positively charged clusters then pass through a 6.35 mm aperture into the 35 mbar flow tube, flowing perpendicular to the sample flow. The clusters then react via proton transfer with the analyte (e.g. aromadendrene) in the sample flow to form aromadendrene-H⁺ and higher order water clusters.

Across the flow tube from the ion source, a pinhole aperture (diameter 0.34 mm) allows a portion of the ions and neutral gas (~ 30 sccm) to flow into the mass spectrometer, a Varian 1200 tandem mass spectrometer. The spectrometer was modified by removing the electron impact source and extending the hexapole ion guide that leads to the quadrupole mass analyzer to the pinhole aperture. For these measurements, the mass spectrometer was operated exclusively in one-dimensional mass spectrometry mode.

In order to simplify the mass spectra, a DC potential of -10 V (relative to the pinhole aperture) is applied to the hexapole. This offset pulls ions into the hexapole, where the pressure is relatively high owing to the neutral gas flow (chiefly N₂) through the pinhole. The ions therefore undergo high energy collisions with the neutral gas molecules which dissociate water clusters of analyte A:



Thus, species are predominantly observed at $m/z = M+1$, where *M* is the molecular mass of the species. Hydrates, A·(H₂O)_{*m*}·H⁺, particularly *m*=1, are also observed for some species, though not for aromadendrene or longifolene.

Each day, the PTR-MS sensitivity towards aromadendrene was determined by sampling standard mixtures of aromadendrene in teflon bags filled with 50 L zero air. The sensitivity was determined to be linear from 0 ppb to at least 5 ppb. Also, because of the large amounts of H₂O₂ utilized in the experiments, the sensitivity as a function of H₂O₂ was determined, with [H₂O₂] measured by operating the Varian 1200 in negative ionization mode, exploiting the reaction of CF₃O[−] with H₂O₂ (Crounse et al., 2006). Thus, the sensitivity determined from H₂O₂-free standards was corrected for sampling from the chamber when H₂O₂ was present.

The uncertainty of aromadendrene measurements using PTR-MS is estimated to be $\sim \pm 22\%$, based on the scatter of replicate data and background measurements and uncertainties in the H₂O₂ correction.

Appendix B

Description of UPLC/ESI-TOFMS technique

Filter extracts (in 1:1 (v/v) solvent mixture of methanol and 0.1% aqueous acetic acid solution) are analyzed by a Waters ACQUITY ultra performance liquid chromatography (UPLC) system, coupled with a Waters LCT Premier time-of-flight (TOF) mass spectrometer (MS) equipped with an electrospray ionization (ESI) source. The ESI source on this instrument contains two individual sprays; one spray is for the eluent and the other is for the lock-mass correction. Optimum ESI conditions are found using a 2.5 kV capillary voltage, 40 V sample cone voltage, 350°C desolvation temperature, 130°C source temperature, 20 L h⁻¹ cone gas flow rate, and a 650 L h⁻¹ desolvation gas flow rate. Data are collected from *m/z* 50–1000 in the negative (–) ionization mode using the TOFMS operated in the W geometry reflectron mode. The W reflectron mode offers the highest mass resolution, which is approximately 12 000, and allows for exact mass measurements to be conducted on detected SOA components. The chromatographic separations are carried out on a Waters ACQUITY HPLC HSS (high strength silica) column (2.1 × 100 mm, 1.8 μm particle size) at 45°C using a gradient elution scheme. The eluent composition is (A) 0.1% acetic acid in water and (B) 0.1% acetic acid in methanol; both eluents are high purity solvents (LC-MS ChromaSolv Grade, Sigma-Aldrich). In the 12-min gradient elution program used, the concentration of eluent B is 0% for the first 2 min, increased to 90% from 2 to 10 min, held at 90% from 10 to 10.2 min; and then decreased back to 0% from 10.2 to 12 min. The flow rate of the eluent is 0.3 mL min⁻¹ and the sample injection volume is 2 μL. At the beginning of each analysis period, the TOFMS is calibrated using a 1:1 (v/v) solvent mixture of acetonitrile and 0.1% phosphoric acid aqueous solution. During each chromatographic run, 2 ng/μL of leucine enkephalin (MW=555) is used for the lock-mass spray for lock-mass correction to obtain accurate masses for each SOA component eluting from the column. The lock-mass syringe pump is operated at 20 μL min⁻¹. In addition to the lock-mass spray, the dynamic range enhancement feature of this mass spectrometer is applied to prevent dead time, which affects mass accuracy, from occurring. As confirmation of the UPLC/ESI-TOFMS technique, a standard sample containing known isoprene and α-pinene sulfate esters previously characterized by Surratt et al. (2007) are analyzed. The known elemental compositions (i.e. molecular formulas) of the previously characterized sulfate esters (Surratt et al., 2007) are in excellent agreement with their measured exact masses (i.e. within ±2 mDa or ±2 ppm). In addition to exact mass measurements, further insights into the structures of the SOA components are obtained by generating tandem MS data, which are generated by increasing the first aperture voltage on the TOFMS from 10 V to 25 V.

Acknowledgements. This research was funded by U.S. Department of Energy Biological and Environmental Research Program grant DE-FG02-05ER63983. This material is based in part on work supported by the National Science Foundation (NSF) under grant ATM-0432377. The Waters LCT Premier XT time-of-flight mass spectrometer interfaced to a Waters UPLC system was purchased in 2006 with a grant from the National Science Foundation, Chemistry Research Instrumentation and Facilities Program (CHE-0541745). The LCQ Ion Trap mass spectrometer was purchased in 1997 with funds from the National Science Foundation through the CRIF program (CHE-9709233). J. D. Surratt is supported in part by the U.S. EPA under the STAR Graduate Fellowship Program. A. J. Kwan acknowledges the support of a NSF graduate research fellowship. The authors would like to thank M. Shahgohli of the Chemistry Department at Caltech for her useful communications regarding high-resolution mass spectrometry.

Edited by: A. Nenes

References

- Alfarra, M. R., Paulsen, D., Gysel, M., Garforth, A. A., Dommen, J., Prevot, A. S. H., Worsnop, D. R., Baltensperger, U., and Coe, H.: A mass spectrometric study of secondary organic aerosols formed from the photooxidation of anthropogenic and biogenic precursors in a reaction chamber, *Atmos. Chem. Phys.*, 6, 5279–5293, 2006, <http://www.atmos-chem-phys.net/6/5279/2006/>.
- Arey, J., Aschmann, S. M., Kwok, E. S. C., and Atkinson, R.: Alkyl nitrates, hydroxyalkyl nitrates and hydroxycarbonyl formation from the NO_x – air photooxidation of C₅–C₈ n-alkanes, *J. Phys. Chem. A*, 105, 1020–1027, 2001.
- Aschmann, S. M., Arey, J., and Atkinson, R.: Atmospheric chemistry of three C₁₀ alkanes, *J. Phys. Chem. A*, 105, 7598–7606, 2001.
- Aschmann, S. M., Atkinson, R., and Arey, J.: Products of reaction of OH radicals with α-pinene, *J. Geophys. Res.*, 107(D14), 4191, doi:10.1029/2001JD001098, 2002.
- Aschmann, S. M., Reissell, A., Atkinson, R., and Arey, J.: Products of the gas phase reactions of the OH radical with α- and β-pinene in the presence of NO, *J. Geophys. Res.*, 103(D19), 4191, 25 553–25 561, 1998.
- Aschmann, S. M., Reissell, A., Atkinson, R., and Arey, J.: Products of the gas phase reactions of the OH radical with a- and b-pinene in the presence of NO, *J. Geophys. Res.*, 103(D19), 25 553–25 561, 1998.
- Atkinson, R., Kwok, E. S. C., Arey, J., and Aschmann, S. M.: Reactions of alkoxy radicals in the atmosphere, *Faraday Discuss.*, 100, 23–37, 1995.
- Atkinson, R. and Arey, J.: Gas-phase tropospheric chemistry of biogenic volatile organic compounds: a review, *Atmos. Environ.*, 37, S197–S219, 2003.
- Atkinson, R., Aschmann, S. M., and Winer, A. M.: Alkyl nitrate formation from the reaction of a series of branched RO₂ radicals with NO as a function of temperature and pressure, *J. Phys. Chem.*, 5, 91–102, 1987.
- Atkinson, R., Baulch, D. L., Cox, R. A., Hampson, R. F., Kerr, J. A., Rossi, M. J., and Troe, J.: Evaluated kinetic and photochemical

- data for atmospheric chemistry, organic species, supplement VII, *J. Phys. Chem. Ref. Data.*, 28, 2, 1999.
- Atkinson, R.: Atmospheric reactions of alkoxy and β -hydroxyalkoxy radicals, *Int. J. Chem. Kinet.*, 29, 99–111, 1997a.
- Atkinson, R.: Gas phase tropospheric chemistry of organic compounds, *J. Phys. Chem. Ref. Data, Monogr.*, 2, 11–216, 1994.
- Atkinson, R.: Gas phase tropospheric chemistry of volatile organic compounds: 1. Alkanes and Alkenes, *J. Phys. Chem. Ref. Data.*, 215–290, 1997b.
- Baldwin, A. C., Barker, J. R., Golden, D. M., and Hendry, D. G.: Photochemical smog – rate parameter estimates and computer simulations, *J. Phys. Chem.*, 81, 2483–2492, 1977.
- Bahreini, R., Keywood, M. D., Ng, N. L., Varutbangkul, V., Gao, S., Flagan, R. C., and Seinfeld, J. H.: Measurements of secondary organic aerosol (SOA) from oxidation of cycloalkenes, terpenes, and m-xylene using an Aerodyne aerosol mass spectrometer, *Environ. Sci. Technol.*, 39, 5674–5688, 2005.
- Carreras-Sospedra, M., Griffin, R. J., and Dabdub, D.: Calculations of incremental secondary organic aerosol reactivity, *Environ. Sci. Technol.*, 39, 1724–1730, 2005.
- Carter, W. P. L. and Atkinson, R.: Alkyl nitrate formation from the atmospheric photooxidation of alkanes; a revised estimation, *J. Phys. Chem.*, 8, 165–173, 1989.
- Carter, W. P. L. and Atkinson, R.: Atmospheric chemistry of alkanes, *J. Atmos. Chem.*, 3, 377–405, 1985.
- Chan, A. W. H., Kroll, J. H., Ng, N. L., and Seinfeld, J. H.: Kinetic modeling of secondary organic aerosol formation: effect of particle- and gas-phase reactions of semivolatile products, *Atmos. Chem. Phys. Discuss.*, 7, 7051–7085, 2007, <http://www.atmos-chem-phys-discuss.net/7/7051/2007/>.
- Cocker III, D. R., Flagan, R. C., and Seinfeld, J. H.: State-of-the-art chamber facility for studying atmospheric aerosol chemistry, *Environ. Sci. Technol.*, 35, 2594–2601, 2001.
- Crounse, J. D., McKinney, K. A., Kwan, A. J., and Wennberg, P. O.: Measurements of gas-phase hydroperoxides by chemical ionization mass spectrometry, *Anal. Chem.*, 78, 6726–6732, 2006.
- de Gouw, J. A., Middlebrook, A. M., Warneke, C., Goldan, P. D., Kuster, W. C., Roberts, J. M., Fehsenfeld, F. C., Worsnop, D. R., Canagaratna, M. R., Pszenny, A. A. P., Keene, W. C., Marchewka, M., Bertman, S. B., and Bates, T. S.: Budget of organic carbon in a polluted atmosphere: Results from the New England Air Quality Study in 2002, *J. Geophys. Res.*, 110, D16305, doi:10.1029/2004JD005623, 2005.
- Finlayson-Pitts, B. J. and Pitts, J. N.: Chemistry of the upper and lower atmosphere: theory, experiments and applications, Academic Press, San Diego, 220–221, 2000.
- Gao, S., Keywood, M. D., Ng, N. L., Surratt, J. D., Varutbangkul, V., Bahreini, R., Flagan, R. C., and Seinfeld, J. H.: Low-molecular weight and oligomeric components in secondary organic aerosol from the ozonolysis of cycloalkenes and α -pinene, *J. Phys. Chem. A*, 108, 10 147–10 164, 2004.
- Gao, S., Surratt, J. D., Knipping, E. M., Edgerton, E. S., Shahgholi, M., and Seinfeld, J. H.: Characterization of polar organic components in fine aerosols in the southeastern United States: Identity, origin, and evolution, *J. Geophys. Res.*, 111, D14314, doi:10.1029/2005JD006601, 2006.
- Geron, C., Rasmussen, R., Arnts, R. R., and Guenther, A.: A review and synthesis of monoterpene speciation from forests in the United States, *Atmos. Environ.*, 34, 1761–1781, 2000.
- Glasius, M., Duane, M., and Larsen, B. R.: Determination of polar terpene oxidation products in aerosols by liquid chromatography-ion trap mass spectrometry, *J. Chrom. A.*, 833, 121–135, 1999.
- Glasius, M., Lahaniati, M., Calogirou, A., Di Bella, D., Jensen, N. R., Hjorth, J., Kotzias, D., and Larsen, B. R.: Carboxylic acids in secondary aerosols from oxidation of cyclic monoterpenes by ozone, *Environ. Sci. Technol.*, 34, 1001–1010, 2000.
- Griffin, R. J., Cocker, D. R., Flagan, R. C., Seinfeld, J. H., and Dabdub, D.: Estimate of global atmospheric organic aerosol formation from the oxidation of biogenic hydrocarbons, *Geophys. Res. Lett.*, 26, 17, 2721–2724, 1999a.
- Griffin, R. J., Cocker, D. R., Flagan, R. C., and Seinfeld, J. H.: Organic aerosol formation from the oxidation of biogenic hydrocarbons, *J. Geophys. Res.*, 104(D3), 3555–3567, 1999b.
- Guenther, A., Hewitt, C. N., Erickson, D., Fall, R., Geron, C., Graedel, T., Harley, P., Klinger, L., Lerdau, M., McKay, W. A., Pierce, T., Scholes, B., Steinbrecher, R., Tallamraju, R., Taylor, T., and Zimmerman, P.: A global model of natural volatile organic compound emission, *J. Geophys. Res.*, 100(D5), 8873–8892, 1995.
- Hatakeyama, S., Izumi, K., Fukuyama, T., Akimoto, H., and Washida, N.: Reactions of OH with α -pinene and β -pinene in air: Estimates of global CO production from the atmospheric oxidation of terpenes, *J. Geophys. Res.*, 96(D1), 947–958, 1991.
- Hurley, M. D., Sokolov, O., Wallington, T. J., Takekawa, H., Karasawa, M., Klotz, B., Barnes, I., and Becker, K. H.: Organic aerosol formation during the atmospheric degradation of toluene, *Environ. Sci. Technol.*, 35, 1358–1366, 2001.
- Jayne, J. T., Leard, D. C., Zhang, X., Davidovits, P., Smith, K. A., Kolb, C. E., and Worsnop, D. W.: Development of an Aerosol Mass Spectrometer for size and composition analysis of submicron particles, *Aerosol Sci. Tech.*, 33, 49–70, 2000.
- Johnson, D., Jenkin, M. E., Wirtz, K., and Martín-Reviejo, M.: Simulating the formation of secondary organic aerosol from the photooxidation of aromatic hydrocarbons, *Environ. Chem.*, 2, 35–48, 2005.
- Johnson, D., Jenkin, M. E., Wirtz, K., and Martín-Reviejo, M.: Simulating the formation of secondary organic aerosol from the photooxidation of toluene, *Environ. Chem.*, 1, 150–165, 2004.
- Kanakidou, M., Seinfeld, J. H., Pandis, S. N., Barnes, I., Dentener, F. J., Facchini, M. C., Van Dingenen, R., Evers, B., Nenes, A., Swietlicki, E., Pautaud, J. P., Balkanski, Y., Fuzzi, S., Horth, J., Moortgat, G. K., Winterhalter, R., Myhre, C. E. L., Tsigaridis, K., Vignati, E., Stephanou, E. G., and Wilson, J.: Organic aerosol and global climate modeling: a review, *Atmos. Chem. Phys.*, 5, 1053–1123, 2005, <http://www.atmos-chem-phys.net/5/1053/2005/>.
- Keywood, M. D., Varutbangkul, V., Bahreini, R., Flagan, R. C., and Seinfeld, J. H.: Secondary organic aerosol formation from the ozonolysis of cycloalkenes and related compounds, *Environ. Sci. Technol.*, 38, 4157–4164, 2004.
- Klinedinst, D. B. and Currie, L. A.: Direct quantification of PM_{2.5} fossil and biomass carbon within the northern front range air quality study's domain, *Environ. Sci. Technol.*, 33, 4146–4154, 1999.
- Kroll, J. H., Ng, N. L., Murphy, S. M., Flagan, R. C., and Seinfeld, J. H.: Secondary organic aerosol formation from isoprene photooxidation under high-NO_x conditions, *J. Geophys. Res.*, 32,

- L18808, doi:10.1029/2005GL023637, 2005.
- Kroll, J. H., Ng, N. L., Murphy, S. M., Flagan, R. C., and Seinfeld, J. H.: Secondary organic aerosol formation from isoprene photooxidation, *Environ. Sci. Technol.*, 40, 1869–1877, 2006.
- Larsen, B. R., Di Bella, D., Glasius, M., Winterhalter, R., Jensen, N. R., and Hjorth, J.: Gas-phase OH oxidation of monoterpenes: Gaseous and particulate products, *J. Atmos. Chem.*, 38, 231–276, 2001.
- Lim, Y. B. and Ziemann, P. J.: Products and mechanism of secondary organic aerosol formation from reactions of *n*-alkanes with OH radicals in the presence of NO_x, *Environ. Sci. Technol.*, 39, 9229–9236, 2005.
- Ng, N. L., Kroll, J. H., Keywood, M. D., Bahreini, R., Varutbangkul, V., Flagan, R. C., Seinfeld, J. H., Lee, A., and Goldstein, A. H.: Contribution of first- versus second-generation products to secondary organic aerosols formed in the oxidation of biogenic hydrocarbons, *Environ. Sci. Technol.*, 40, 2283–2297, 2006.
- Ng, N. L., Kroll, J. H., Chan, A. W. H., Chhabra, P. S., Flagan, R. C., and Seinfeld, J. H.: Secondary organic aerosol formation from *m*-xylene, toluene, and benzene, *Atmos. Chem. Phys. Discuss.*, 7, 4085–4126, 2007, <http://www.atmos-chem-phys-discuss.net/7/4085/2007/>.
- O'Brien, J. M., Czuba, E., Hastie, D. R., Francisco, J. S., and Shepson, P. B.: Determination of the hydroxy nitrate yields from the reaction of C₂–C₆ alkenes with OH in the presence of NO, *J. Phys. Chem.*, 102, 8903–8908, 1998.
- Odum, J. R., Hoffmann, T., Bowman, F., Collins, D., Flagan, R. C., and Seinfeld, J. H.: Gas/particle partitioning and secondary organic aerosol yields, *Environ. Sci. Technol.*, 30, 2580–2585, 1996.
- Odum, J. R., Jungkamp, T. P. W., Griffin, R. J., Forstner, H. J. L., Flagan, R. C., and Seinfeld, J. H.: Aromatics, reformulated gasoline and atmospheric organic aerosol formation, *Environ. Sci. Technol.*, 31, 1890–1897, 1997.
- Owen, S. M., Boissard, C., and Hewitt, C. N.: Volatile organic compounds (VOCs) emitted from 40 Mediterranean plant species: VOC speciation and extrapolation to habitat scale, *Atmos. Environ.*, 35, 5393–5409, 2001.
- Pandis, S. N., Paulson, S. E., Seinfeld, J. H., and Flagan, R. C.: Aerosol formation in the photooxidation of isoprene and β -pinene, *Atmos. Environ.*, 25A, 997–1008, 1991.
- Presto, A. A., Huff Hartz, K. E., and Donahue, N. M.: Secondary organic aerosol production from ozonolysis: 2. Effect of NO_x concentration, *Environ. Sci. Technol.*, 39, 7046–7054, 2005.
- Seinfeld, J. and Pankow, J. F.: Organic atmospheric particulate material, *Annu. Rev. Phys. Chem.*, 54, 121–140, 2003.
- Song, C., Na, K., and Cocker III, D. R.: Impact of the hydrocarbon to NO_x ratio on secondary organic aerosol formation, *Environ. Sci. Technol.*, 39, 3143–3149, 2005.
- Sorooshian, A., Brechtel F. J., Ma, Y. L., Weber R. J., Corless, A., Flagan, R. C., and Seinfeld, J. H.: Modeling and characterization of a particle-into-liquid sampler (PILS), *Aerosol Sci. Tech.*, 40, 396–409, 2006.
- Surratt, J. D., Kroll, J. H., Kleindienst, T. E., Edney, E. O., Claeys, M., Sorooshian, A., Ng, N. L., Offenberg, J. H., Lewandowski, M., Jaoui, M., Flagan, R. C., and Seinfeld, J. H.: Evidence for organosulfates in secondary organic aerosol, *Environ. Sci. Technol.*, 41, 517–527, 2007.
- Surratt, J. D., Murphy, S. M., Kroll, J. H., Ng, N. L., Hildebrandt, L., Sorooshian, A., Szmigielski, R., Vermeylen, R., Maenhaut, W., Claeys, M., Flagan, R. C., and Seinfeld, J. H.: Chemical composition of secondary organic aerosol formed from the photooxidation of isoprene, *J. Atmos. Chem.*, 31, 9665–9690, 2006.
- Szmigielski, R., Surratt, J. D., Vermeylen, R., Szmigielska, K., Kroll, J. H., Ng, N. L., Murphy, S. M., Sorooshian, A., Seinfeld, J. H., and Claeys, M.: Characterization of 2-methylglyceric acid oligomers in secondary organic aerosol formed from the photooxidation of isoprene using trimethylsilylation and gas chromatography/ion trap mass spectrometry, *J. Mass Spectrom.*, 42, 101–116, 2007.
- Talukdar, R. K., Herndon, S. C., Burkholder, J. B., Roberts, J. M., and Ravishankara, A. R.: Atmospheric fate of several alkyl nitrates, *J. Chem. Soc., Faraday Trans.*, 93, 2787–2796, 1997.
- Treves, K. and Rudich, Y.: The atmospheric fate of C₃–C₆ hydroxyalkyl nitrates, *J. Phys. Chem. A*, 107, 7809–7817, 2003.
- Weber, R. J., Sullivan, A., Peltier, R. E., Russell, A., Yan, B., Zheng, M., de Gouw, J., Warneke, C., Brock, C., Holloway, J. S., Atlas, E. L., and Edgerton, E.: A study of secondary organic aerosol formation in the anthropogenic-influenced southeastern USA, *J. Geophys. Res.*, 112, D13302, doi:10.1029/2007JD008408, 2007.
- Zhang, J., Dransfield, T., and Donahue, N. M.: On the mechanism for nitrate formation via the peroxy radical + NO reaction, *J. Phys. Chem. A*, 108, 9082–9095, 2004.
- Zhang, J., Hartz, K. E. H., Pandis, S. N., and Donahue, N. M.: Secondary organic aerosol formation from limonene ozonolysis: Homogeneous and heterogeneous influences as a function of NO_x, *J. Phys. Chem. A*, 110, 11 053–11 063, 2006.
- Zhang, S. H., Shaw, M., Seinfeld, J. H., and Flagan, R. C.: Photochemical aerosol formation from α -pinene and β -pinene, *J. Geophys. Res.*, 97(D18), 20 717–20 729, 1992.

Appendix C

Organosulfate formation in biogenic secondary organic aerosol*

*Reproduced with permission from “Organosulfate Formation in Biogenic Secondary Organic Aerosol by Jason D. Surratt, Yadian Gómez-González, Arthur W. H. Chan, Reinhilde Vermeylen, Mona Shahgholi, Tadeusz E. Kleindienst, Edward O. Edney, John H. Offenberg, Michael Lewandowski, Mohammed Jaoui, Willy Maenhaut, Magda Claeys, Richard C. Flagan, and John H. Seinfeld, *Journal of Physical Chemistry A*, 112 (36), 8345–8378, 2008. Copyright 2008 by the American Chemical Society.

Organosulfate Formation in Biogenic Secondary Organic Aerosol

Jason D. Surratt,[†] Yadian Gómez-González,[‡] Arthur W. H. Chan,[§] Reinhilde Vermeylen,[‡] Mona Shahgholi,[†] Tadeusz E. Kleindienst,[‡] Edward O. Edney,[‡] John H. Offenberg,[‡] Michael Lewandowski,[‡] Mohammed Jaoui,[#] Willy Maenhaut,[¶] Magda Claeys,[‡] Richard C. Flagan,^{§,+} and John H. Seinfeld^{*,§,+}

Department of Chemistry, California Institute of Technology, Pasadena, California 91125, Department of Pharmaceutical Sciences, University of Antwerp (Campus Drie Eiken), Universiteitsplein 1, BE-2610 Antwerp, Belgium, Department of Chemical Engineering, California Institute of Technology, Pasadena, California 91125, National Exposure Laboratory, Office of Research and Development, Environmental Protection Agency, Research Triangle Park, North Carolina 27711, Alion Science and Technology, P.O. Box 1231, Research Triangle Park, North Carolina 27709, Department of Analytical Chemistry, Institute for Nuclear Sciences, Ghent University, Proeftuinstraat 86, BE-9000 Gent, Belgium, and Department of Environmental Science and Engineering, California Institute of Technology, Pasadena, California 91125

Received: March 17, 2008; Revised Manuscript Received: May 16, 2008

Organosulfates of isoprene, α -pinene, and β -pinene have recently been identified in both laboratory-generated and ambient secondary organic aerosol (SOA). In this study, the mechanism and ubiquity of organosulfate formation in biogenic SOA is investigated by a comprehensive series of laboratory photooxidation (i.e., OH-initiated oxidation) and nighttime oxidation (i.e., NO₃-initiated oxidation under dark conditions) experiments using nine monoterpenes (α -pinene, β -pinene, *d*-limonene, *l*-limonene, α -terpinene, γ -terpinene, terpinolene, Δ^3 -carene, and β -phellandrene) and three monoterpenes (α -pinene, *d*-limonene, and *l*-limonene), respectively. Organosulfates were characterized using liquid chromatographic techniques coupled to electrospray ionization combined with both linear ion trap and high-resolution time-of-flight mass spectrometry. Organosulfates are formed only when monoterpenes are oxidized in the presence of acidified sulfate seed aerosol, a result consistent with prior work. Archived laboratory-generated isoprene SOA and ambient filter samples collected from the southeastern U.S. were reexamined for organosulfates. By comparing the tandem mass spectrometric and accurate mass measurements collected for both the laboratory-generated and ambient aerosol, previously uncharacterized ambient organic aerosol components are found to be organosulfates of isoprene, α -pinene, β -pinene, and limonene-like monoterpenes (e.g., myrcene), demonstrating the ubiquity of organosulfate formation in ambient SOA. Several of the organosulfates of isoprene and of the monoterpenes characterized in this study are ambient tracer compounds for the occurrence of biogenic SOA formation under acidic conditions. Furthermore, the nighttime oxidation experiments conducted under highly acidic conditions reveal a viable mechanism for the formation of previously identified nitrooxy organosulfates found in ambient nighttime aerosol samples. We estimate that the organosulfate contribution to the total organic mass fraction of ambient aerosol collected from K-puszt, Hungary, a field site with a similar organosulfate composition as that found in the present study for the southeastern U.S., can be as high as 30%.

1. Introduction

The atmospheric oxidation of volatile organic compounds (VOCs) leads to secondary organic aerosol (SOA) formation through low-volatility products that partition into the aerosol phase. SOA can contribute a significant fraction to the organic mass found in tropospheric fine particulate matter (PM_{2.5}, with aerodynamic diameter < 2.5 μ m);¹ high concentrations of PM_{2.5} are known to have adverse health effects² and play a role in global climate change.³ Of the known SOA precursor classes of VOCs, biogenic volatile organic compounds (BVOCs), which

include isoprene (2-methyl-1,3-butadiene, C₅H₈) and monoterpenes (C₁₀H₁₆), contribute significantly to the global SOA budget^{1,4,5} owing to their high reactivities with atmospheric oxidants, such as hydroxyl radicals (OH), ozone (O₃), and nitrate radicals (NO₃), and their large global emission rates.⁶

Laboratory work has shown that several factors need to be considered in order to understand and predict SOA formation mechanisms from BVOCs; these include the NO_x level,^{4,7–15} acidity of inorganic seed aerosol,^{16–26} relative humidity (RH),^{27–29} and temperature.^{30–32} Enhancements in laboratory-generated SOA from isoprene and α -pinene have recently been observed at increased acidity of preexisting sulfate seed aerosol.^{17–24,33} Acid-catalyzed particle-phase reactions,^{16–20} some of which lead to the formation of high molecular weight (MW) species through oligomerization, have been proposed to explain these observed enhancements. Detailed chemical analysis of laboratory-generated aerosol has revealed several types of particle-phase reactions contributing to SOA formation, including peroxy-hemiacetal formation,^{34,35} acetal/hemiacetal formation,^{16,36} hy-

* To whom correspondence should be addressed. Phone: (626) 395-4635. Fax: (626) 796-2591. E-mail: seinfeld@caltech.edu.

[†] Department of Chemistry, California Institute of Technology, Pasadena.

[‡] University of Antwerp.

[§] Department of Chemical Engineering, California Institute of Technology.

[‡] Environmental Protection Agency.

[#] Alion Science and Technology.

[¶] Ghent University.

⁺ Department of Environmental Science and Engineering, California Institute of Technology.

dration followed by polymerization,¹⁶ aldol condensation,^{16,36} and organic esterification.^{33,37–40} Many of these reactions have been observed when particle-phase acidity is derived from sulfuric acid; however, recent work has shown that photochemically generated organic acids are a sufficient source of acidity, especially under dry conditions.^{28,33,37,41} The importance of particle-phase reactions to ambient SOA formation remains uncertain as currently there is no chemical evidence for their respective products, and with the exception of organic esterification, many of these reactions are not thermodynamically favorable under ambient conditions.^{42–44} Additionally, some of these reactions may not be kinetically favorable in the atmosphere, as recently shown by Casale et al.⁴⁵ for aldol condensation reactions of aliphatic aldehydes.

Organosulfate formation (i.e., sulfate esters and/or sulfate derivatives) has recently been shown to occur in laboratory-generated SOA produced from the oxidation of several BVOCs, including isoprene,^{23,24,46} α -pinene,^{23,26,46,47} limonene,²⁵ and β -pinene,²⁶ and by the reactive uptake of known volatile aldehydes, such as glyoxal⁴⁸ and pinonaldehyde,^{49,50} in the presence of acidified sulfate seed aerosol. In addition, mass spectrometric evidence exists for organosulfates and nitrooxy organosulfates in ambient aerosol; however, direct evidence as to the sources and mechanism of formation for these compounds is lacking.^{47,51,52} Recent work from the Caltech laboratory, as well as the U.S. Environmental Protection Agency (EPA) and University of Antwerp laboratories, has shown that organosulfate formation occurs from isoprene and α -pinene in both laboratory-generated SOA and ambient aerosol collected from the southeastern U.S.²³ and K-puszta, Hungary.⁴⁶ This work has identified ambient tracer compounds for the occurrence of biogenic SOA formation under acidic conditions as well as a relevant particle-phase reaction. Additionally, Iinuma et al.²⁶ have reported organosulfate formation from β -pinene in ambient aerosol and identified new organosulfates of monoterpenes likely containing two double bonds (e.g., limonene); however, laboratory experiments that confirm the initially proposed structures for the latter compounds were lacking. Interestingly, Iinuma et al.²⁶ showed that previously identified monoterpene nitrooxy organosulfates were detected only in nighttime samples, suggesting the importance of nighttime chemistry (i.e., NO₃ radical oxidation chemistry) to SOA formation. Despite these recent advances in identifying organosulfate formation in SOA, the ubiquity and abundance of organosulfates in ambient aerosol remain unclear. In addition, formation mechanisms and sources of several previously detected organosulfates in ambient aerosol are unknown.

In the present work, we investigate in detail the mechanism of organosulfate formation in biogenic SOA on the basis of a series of laboratory oxidation experiments under varying particle-phase acidities and oxidative conditions. Laboratory photooxidation (i.e., OH-initiated oxidation) experiments were conducted using nine monoterpenes: α -pinene, β -pinene, *d*-limonene, *l*-limonene, α -terpinene, γ -terpinene, β -phellandrene, Δ^3 -carene, and terpinolene. In addition, laboratory nighttime oxidation (i.e., NO₃-initiated oxidation) experiments were conducted using three monoterpenes (α -pinene, *d*-limonene, and *l*-limonene). Filters were collected from all of the laboratory experiments for off-line chemical composition analysis. Furthermore, archived isoprene SOA and ambient filter samples collected from prior studies^{33,47} were reexamined for organosulfates using highly sensitive and advanced mass spectrometric techniques. Both high-performance liquid chromatography (HPLC) combined with electrospray ionization (ESI)-linear ion

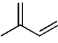
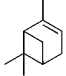
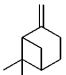
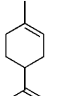
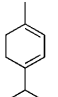
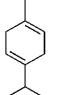
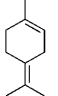
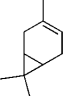
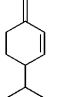
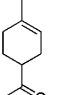
trap mass spectrometry (LITMS) and ultra performance liquid chromatography (UPLC) combined with ESI high-resolution time-of-flight mass spectrometry (TOFMS), which provide tandem MS (i.e., structural elucidation) and accurate mass measurements (i.e., elemental composition/molecular formulas), respectively, were employed to characterize the detailed chemical structures of the organosulfates; particular attention was focused on those compounds detected in both laboratory-generated SOA and ambient aerosol collected from the Southeastern Aerosol Research and Characterization (SEARCH) network in the southeastern U.S. during the June 2004 campaign. In a previous study from our laboratories, many of the chemical structures of the compounds detected during the June 2004 campaign remained uncharacterized because of the use of less-advanced mass spectrometric techniques as compared to those in the current study; it was found that many of these compounds were likely secondary in nature and resulted from terpene oxidation.⁴⁷ As will be presented, many of these previously uncharacterized products, as well as newly identified compounds, are found to be organosulfates of isoprene and of prevalent monoterpenes, including α -pinene, β -pinene, and limonene-like monoterpenes (i.e., monoterpenes, such as myrcene and ocimene, containing at least two or more double bonds, with the requirement of one of these double bonds being in a terminal position).

2. Experimental Section

2.1. Chamber Experiments. Organosulfate formation was studied in SOA generated from the following nine monoterpenes: α -pinene (98+%, Sigma–Aldrich), β -pinene (98%, Lancaster), *d*-limonene (puriss. p.a. terpene standard for GC, $\geq 99\%$, Fluka), *l*-limonene (puriss. p.a. terpene standard for GC, $\geq 99\%$, Fluka), α -terpinene (purum $\geq 95\%$, Fluka), γ -terpinene (puriss. p.a. terpene standard for GC, $\geq 98.5\%$, Fluka), terpinolene (purum $\geq 97\%$, Fluka), Δ^3 -carene (puriss. p.a. terpene standard for GC, $\geq 98.5\%$, Fluka), and β -phellandrene/*d*-limonene standard mixture (40:60 v/v, generously provided by Professor Roger Atkinson of the University of California, Riverside).⁵³ To establish better understanding of organosulfate formation in limonene SOA, the further oxidation of limonaketone (4-acetyl-1-methylcyclohexene, C₉H₁₄O, Sigma–Aldrich, library of rare chemicals), which is a known first-generation gas-phase product from limonene,⁵⁴ was conducted in a single photooxidation experiment. In addition to these monoterpenes, organosulfate formation was reexamined in isoprene SOA; archived isoprene SOA samples were available from both the Caltech and EPA chamber experiments and were used for the high-resolution MS analysis to confirm previous identifications. Details of the experimental conditions employed for the generation of isoprene SOA can be found elsewhere;^{4,13,23,33} it should be noted that the EPA isoprene SOA came from the EPA-199 stage 2 photooxidation experiment, in which experimental conditions (i.e., 1598 ppb of initial isoprene, 475 ppb of initial NO_x, and 200 ppb of SO₂) were previously outlined in Surratt et al.²³ and were used solely for the tandem MS analysis of organosulfates of isoprene. Table 1 lists the chemical structures of isoprene and of the monoterpenes studied, as well as the rate constants of these VOCs for reaction with OH, O₃, and NO₃.⁵⁵ Table 2 summarizes the experimental conditions and results for the suite of monoterpene oxidation experiments conducted.

All monoterpene experiments were performed in the Caltech dual 28 m³ Teflon environmental chambers. Details of the facilities have been described elsewhere.^{56,57} Before each

TABLE 1: Biogenic Volatile Organic Compounds Studied

compound	structure	formula (MW)	k_{OH}^a $\text{cm}^3 \text{molec}^{-1} \text{s}^{-1}$	$k_{\text{O}_3}^{a,b,c}$ $\text{cm}^3 \text{molec}^{-1} \text{s}^{-1}$	$k_{\text{NO}_3}^{a,d}$ $\text{cm}^3 \text{molec}^{-1} \text{s}^{-1}$
isoprene		C_5H_8 (68)	9.9×10^{-11}	1.3×10^{-17}	7.0×10^{-13}
α -pinene		$\text{C}_{10}\text{H}_{16}$ (136)	5.3×10^{-11}	8.4×10^{-17}	6.2×10^{-12}
β -pinene		$\text{C}_{10}\text{H}_{16}$ (136)	7.4×10^{-11}	1.5×10^{-17}	2.5×10^{-12}
limonene		$\text{C}_{10}\text{H}_{16}$ (136)	1.7×10^{-10}	2.1×10^{-16}	1.2×10^{-11}
α -terpinene		$\text{C}_{10}\text{H}_{16}$ (136)	3.6×10^{-10}	2.1×10^{-14}	1.4×10^{-10}
γ -terpinene		$\text{C}_{10}\text{H}_{16}$ (136)	1.8×10^{-10}	1.4×10^{-16}	2.9×10^{-11}
terpinolene		$\text{C}_{10}\text{H}_{16}$ (136)	2.3×10^{-10}	1.9×10^{-15}	9.7×10^{-11}
Δ^3 -carene		$\text{C}_{10}\text{H}_{16}$ (136)	8.8×10^{-11}	3.7×10^{-17}	9.1×10^{-12}
β -phellandrene		$\text{C}_{10}\text{H}_{16}$ (136)	1.7×10^{-10}	4.7×10^{-17}	8.0×10^{-12}
limonaketone		$\text{C}_9\text{H}_{14}\text{O}$ (138)	-	2.7×10^{-16}	-

^a Rate constants were obtained from Atkinson and Arey⁵⁵ (and references therein). ^b No ozonolysis experiments were conducted; however, rates are reported here to show that under the conditions of the chamber experiments, OH and NO₃ radicals dominate the initial oxidation of the BVOCs during photooxidation and nighttime oxidation experiments, respectively. ^c The rate constant for limonaketone was measured by Donahue et al.⁵⁴ ^d α -Pinene and *d*-*l*-limonene were the only three BVOCs for which reactions with NO₃ radicals were studied.

experiment, the chambers were flushed continuously for at least 24 h. The aerosol number concentration, size distribution, and volume concentration were measured by a differential mobility analyzer (DMA, TSI model 3081) coupled with a condensation nucleus counter (TSI model 3760). All aerosol growth data were corrected for wall loss, in which size-dependent particle loss coefficients were determined from inert particle loss experiments.⁵⁷ The temperature, relative humidity, and concentrations of O₃, NO, and NO_x were continuously monitored.

Seed particles were generated by atomizing an aqueous solution with a constant-rate atomizer. The neutral seed consisted of 15 mM (NH₄)₂SO₄, while the acidic seed contained a mixture

of 15 mM (NH₄)₂SO₄ and 15 mM H₂SO₄, and the highly acidic seed contained a mixture of 30 mM MgSO₄ and 50 mM H₂SO₄. The initial particle number concentration was about 20 000 particles cm⁻³, with a geometric mean diameter of ~55 (for the neutral and acid seed) or ~70 nm (for the highly acidic seed). The initial seed volume was ~15 $\mu\text{m}^3 \text{cm}^{-3}$. After introduction of the seed aerosol, a known volume of the parent hydrocarbon was injected into a glass bulb and introduced into the chambers by an air stream. The mixing ratio of the hydrocarbon was monitored with a gas chromatograph (Agilent model 6890N) coupled with a flame ionization detector (GC-FID).

TABLE 2: Summary of Experimental Conditions and Organosulfate Formation from Monoterpene Oxidation Chamber Experiments

hydrocarbon	initial [HC] (ppb)	oxidant precursor ^d	seed type ^b	initial [NO] (ppb)	initial [NO ₂] (ppb)	initial [O ₃] (ppb)	T ^c (°C)	RH ^c (%)	total SOA volume ^c (μm ³ cm ⁻³)	[M - H] ⁻ detected organosulfate ions (m/z)
α-pinene	41	H ₂ O ₂	neutral	<2	<2	2	31.2	3.8	82	none detected
α-pinene	46	H ₂ O ₂	highly acidic	<2	<2	2	26.4	5.5	145	237, 279 ^d , 281, 297
α-pinene	47	H ₂ O ₂ /NO	neutral	303	4	3	25.6	7.2	104	none detected
α-pinene	61	H ₂ O ₂ /NO	acidic	488	12	3	27.1	4.3	151	279 ^d , 342
α-pinene	53	H ₂ O ₂ /NO	highly acidic	507	5	3	25.7	5.7	189	223, 227 ^d , 237, 249 ^d , 265, 279 ^d , 294 ^d , 310 ^d , 342
α-pinene	81	HONO	neutral	463	447	2	23.8	<4.5	78	none detected
α-pinene	78	HONO	acidic	509	468	2	29.1	3.4	62	265, 279 ^d , 310 ^d , 342
α-pinene	104	HONO	highly acidic	522	429	<2	25.2	4.5	96	247, 249 ^d , 265, 279 ^d , 294 ^d , 310 ^d , 342
α-pinene	~100	NO ₂ + O ₃ /dark	neutral	<2	170	45	20.3	6.3	52	none detected
α-pinene	~100	NO ₂ + O ₃ /dark	highly acidic	<2	212	47	21.0	5.8	107	247, 249 ^d , 279 ^d , 294 ^d , 310 ^d , 339, 355
d-limonene	93	HONO	acidic	499	479	3	27.1	4.0	92	251, 281, 312, 330, 389
d-limonene	91	H ₂ O ₂ /NO	highly acidic	504	<2	2	27.2	5.0	340	312, 328
d-limonene	~100	NO ₂ + O ₃ /dark	highly acidic	<2	140	54	19.0	5.8	525	239 ^d , 249, 251, 267, 279, 296 ^d , 312, 326, 328, 373 ^d
l-limonene	86	H ₂ O ₂ /NO	highly acidic	508	12	2	27.8	4.4	186	239 ^d , 249, 251, 267, 279, 281, 296 ^d , 312, 326, 330, 373
l-limonene	~50	NO ₂ + O ₃ /dark	highly acidic	<2	186	38	21.4	5.4	373	239 ^d , 279, 312, 328, 389
β-phellandrene	~100 (total)	H ₂ O ₂ /NO	highly acidic	428	<2	<2	26.9	3.7	169	239 ^d , 251, 267, 296 ^d , 326, 238, 373
l-d-limonene mixture										
limonaketone	~150	H ₂ O ₂ /NO	highly acidic	<2	494	<2	26.8	5.9	384	249, 251, 267, 296 ^d , 312
α-terpinene	141	HONO	acidic	489	479	4	26.6	3.8	57	265, 281, 283, 297, 373
α-terpinene	123	H ₂ O ₂ /NO	highly acidic	505	10	<2	26.5	4.9	153	253, 265, 279, 281, 283, 294, 297, 310, 342, 373
γ-terpinene	85	H ₂ O ₂ /NO	highly acidic	497	8	3	26.4	8.3	142	279, 310, 373
terpinolene	34	H ₂ O ₂ /NO	highly acidic	483	17	<2	25.5	8.6	101	249, 265, 281, 283, 294, 297, 326, 373
β-pinene	62	H ₂ O ₂ /NO	highly acidic	469	<2	3	26.2	5.9	232	249 ^d , 263, 279 ^d , 281, 283, 294 ^d , 310 ^d , 326, 342
Δ ³ -carene	~100	H ₂ O ₂ /NO	highly acidic	496	<2	<2	26.6	3.7	123	342 ^e

^a H₂O₂ and HONO serve as OH radical sources in photooxidation experiments. The NO₂ + O₃ reaction serves as the NO₃ radical source in dark experiments. ^b Atomizing solution compositions: neutral = 15 mM (NH₄)₂SO₄; acidic = 15 mM (NH₄)₂SO₄ + 15 mM H₂SO₄; highly acidic = 30 mM MgSO₄ + 50 mM H₂SO₄. ^c Averaged over the course of filter sampling. ^d At least one of the isomers has the same RT and exact mass as compared to those of the corresponding ion detected in the field samples collected from the southeastern U.S. (see Table 8S, Supporting Information). ^e Unlike Tables 1S–6S (Supporting Information), no separate table for this monoterpene is provided, owing to the fact that there was only one organosulfate isomer observed. RT = 6.59 min; measured mass = 342.0329; mDa error = 3.3 mDa; ppm error = 9.6 ppm; elemental composition = C₁₀H₁₆NO₁₀S⁻.

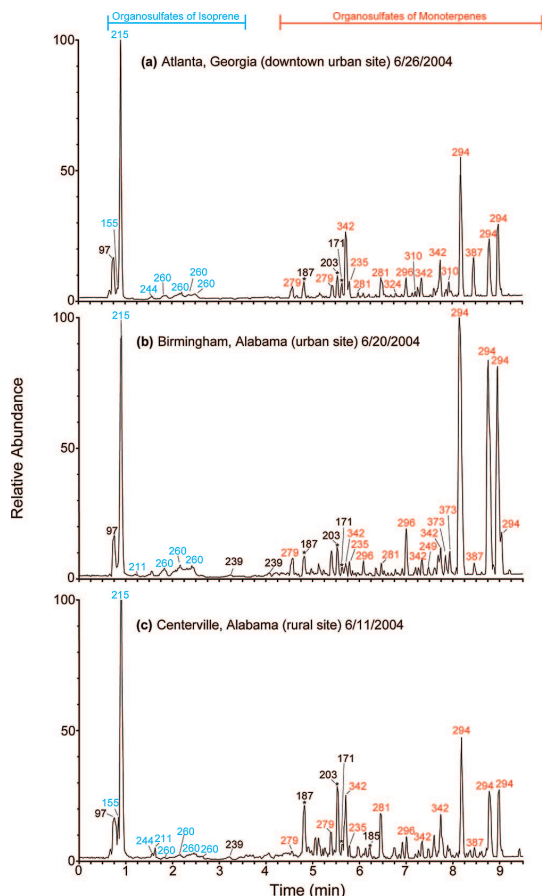


Figure 1. UPLC/(-)ESI-TOFMS base peak chromatograms (BPCs) for filter extracts of $\text{PM}_{2.5}$ aerosol collected from the SEARCH network during the June 2004 campaign. Chromatographic peaks are marked with corresponding $[M - H]^-$ ion. Besides the m/z 97 (i.e., inorganic sulfate) peak and peaks marked with an asterisk, which correspond to known SOA acidic products (i.e., m/z 187, azelaic acid; m/z 203, 3-methyl-1,2,3-butanetricarboxylic acid; m/z 171, norpinic acid; m/z 185, pinic acid), all other peaks correspond to organosulfates or nitroxy organosulfates formed from the oxidation of isoprene and/or monoterpenes. The source of the m/z 239 organosulfates remains unknown. Although most of the chromatographic peaks correspond to organosulfates, this does not mean that all of the organic mass on the filters is from these compounds. Due to the use of methanol as the extraction solvent, the type of chromatographic column, and the mobile phase system employed, some of the organic mass on the filter will not be extracted and/or observed by the UPLC/(-)ESI-TOFMS technique due to some of the organic mass not being eluted from the column or not being detected in the negative ion mode.

In the monoterpene photooxidation experiments, aerosol was generated under either high-, intermediate-, or low- NO_x conditions. Of the monoterpenes investigated, α -pinene was the only compound studied over all NO_x conditions, thus providing a model system for organosulfate formation from monoterpenes. The experimental protocols are similar to those in previous NO_x -dependence studies.^{14,15} In the high- NO_x experiments, nitrous acid (HONO) was used as the source of oxidant (OH). HONO was prepared by dropwise addition of 15 mL of 1 wt% NaNO_2 into 30 mL of 10 wt% H_2SO_4 in a glass bulb and introduced into the chambers with an air stream. Additional NO from a

500 ppm gas cylinder (Scott Marrin, Inc.) was added until the total concentration of NO_x was ~ 1 ppm (upper limit of NO_x monitor). This relatively high concentration was used in the high- NO_x experiments to prevent a switch in NO_x regimes (i.e., high- to low- NO_x conditions) during the course of oxidation. In the low- NO_x experiments, hydrogen peroxide (H_2O_2) served as the OH precursor. Prior to the introduction of seed particles and the parent hydrocarbon, about 3–5 ppm of H_2O_2 was introduced into the chambers by bubbling a 50% aqueous H_2O_2 solution for 2.5 h at 5 L min^{-1} . In most experiments, 300–500 ppb of NO was introduced into the chamber after addition of H_2O_2 . In these experiments, the concentration of NO drops to zero rapidly during the experiment, resulting in a switch from high- to low- NO_x conditions. These latter experiments are designated as intermediate- NO_x experiments (denoted as $\text{H}_2\text{O}_2/\text{NO}$ in the text). In all of the photooxidation experiments, the reaction was initiated by irradiating the chamber with black-lights, after the concentrations of the seed, parent hydrocarbon, and NO_x stabilized.

To study the nighttime chemistry of selected monoterpenes (i.e., α -pinene, *d*-limonene, and *l*-limonene), oxidation by nitrate radicals (NO_3) was performed in the dark. O_3 at a level of 200 ppb, generated with a UV lamp ozone generator (EnMet Corporation, MI), was injected into the chambers at 5 L min^{-1} after introduction of the seed particles. Approximately 600 ppb of NO_2 was then added. When the O_3 concentration dropped to ~ 45 ppb, the parent hydrocarbon was introduced into the chambers, marking the beginning of the experiment. On the basis of the concentrations of NO_2 and O_3 employed, it is estimated that about 500 ppt of NO_3 radical was initially present; on the basis of the applicable rate constants, NO_3 initially dominates the oxidation of the monoterpenes rather than O_3 . The initial concentration of the hydrocarbon was estimated from the volume of hydrocarbon injected.

2.2. Chamber Filter Sample Collection and Extraction Protocols. Duplicate Teflon filters (PALL Life Sciences, 47 mm diameter, $1.0 \mu\text{m}$ pore size, teflo membrane) were collected from each of the monoterpene chamber experiments for off-line chemical analysis. The flow rate for filter collection was ~ 17 and 23 L min^{-1} for the first and second filter samplers, respectively. The difference between flow rates for the two filter samplers was found not to affect the chemical characterization results as the total mass sampled on the duplicate filters was approximately the same for each experiment. Filter sampling was initiated when the aerosol volume reached its maximum (constant) value, as determined by the DMA. Depending on the total volume concentration of aerosol in the chamber, the duration of filter sampling was 2–3.5 h, which resulted in ~ 1.6 – 4.6 m^3 of total chamber air sampled.

Teflon filters used for the high-resolution mass spectrometry (MS) analysis were extracted in 5 mL of high-purity methanol (LC-MS CHROMASOLV-grade, Sigma–Aldrich) by 45 min of sonication. Methanol extracts were blown dry under a gentle N_2 stream at ambient temperature. Dried residues were then reconstituted with $500 \mu\text{L}$ of a 1:1 (v/v) solvent mixture of 0.1% acetic acid in water (LC-MSCHROMASOLV-grade, Sigma–Aldrich) and 0.1% acetic acid in methanol (LC-MS CHROMASOLV-grade, Sigma–Aldrich). Blank Teflon filters were extracted and treated in the same manner as the samples; none of the organosulfates detected in the filter samples collected from the chamber experiments were observed in these blanks, indicating that organosulfates were not introduced during sample storage and/or preparation. Furthermore, to ensure that organosulfate formation was not an artifact simply formed from the collection

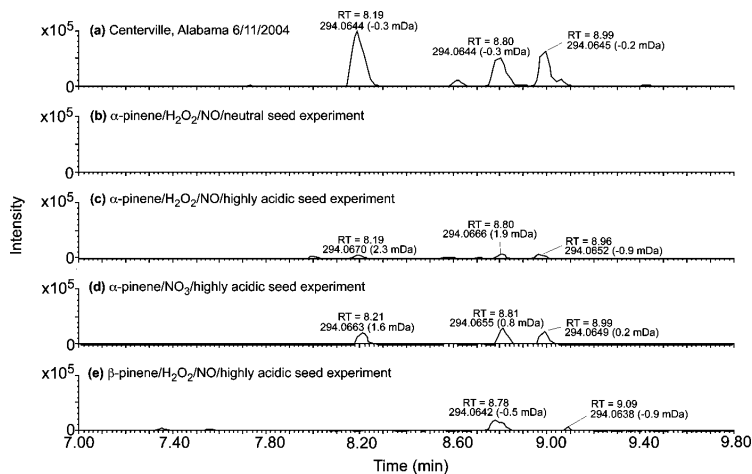


Figure 2. UPLC/(−)ESI-TOFMS extracted ion chromatograms (EICs) of m/z 294. The RTs, accurate masses, and mDa errors between the theoretical masses of the TOFMS suggested molecular formulas, and the accurate masses of the detected m/z 294 ions are listed above each chromatographic peak. All of the chromatographic peaks highlighted in the figure share the same elemental composition of $C_{10}H_{16}NO_5S^-$. In order to form the m/z 294 nitrooxy organosulfates in the monoterpene photooxidation experiments, the presence of both NO_x (i.e., intermediate- NO_x or high- NO_x levels) and highly acidified sulfate seed aerosol is required (Table 2). Additionally, the m/z 294 nitrooxy organosulfates can form from the nighttime (NO_3 -initiated) oxidation of α -pinene; however, the presence of highly acidified sulfate seed aerosol is also required (Table 2). Although the β -pinene experiment produced one of the m/z 294 isomers observed in the ambient aerosol, in subsequent figures, the tandem MS data reveal that α -pinene is the only monoterpene examined in this study that appears to be the sole source of these compounds in ambient aerosol collected from the southeastern U.S. Besides the suite of monoterpenes examined in this study, other known highly emitted monoterpenes (e.g., myrcene and ocimene)^{79,80} in the southeastern U.S. should be examined in future experiments to determine their potential for forming the m/z 294 nitrooxy organosulfates in organic aerosol.

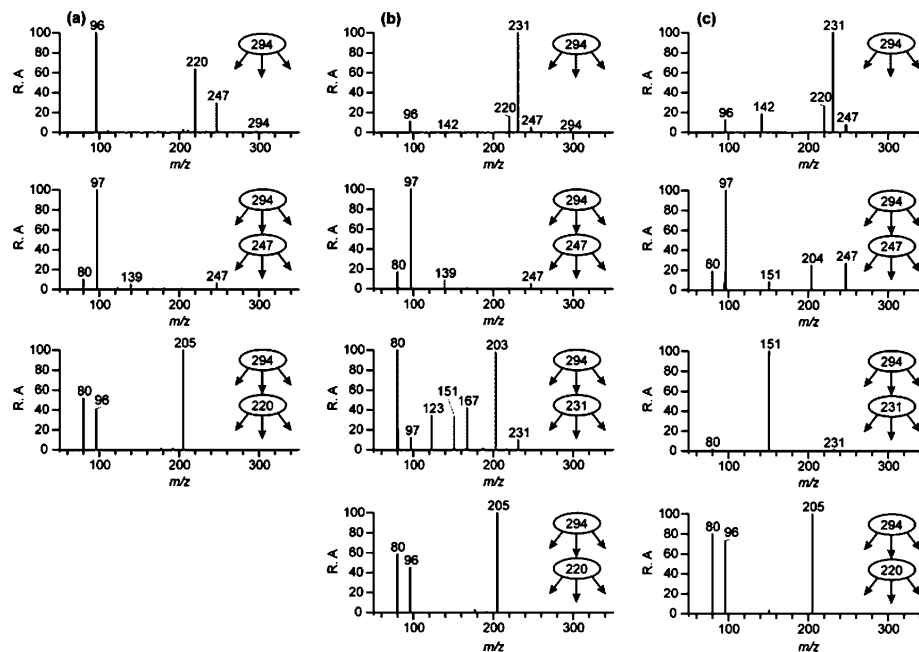


Figure 3. MS²/MS³ data obtained for *m/z* 294 compounds from an α -pinene/NO₃/highly acidic seed experiment with RTs of (a) 37.6, (b) 43.6, and (c) 45.3 min. These compounds are denoted in the text and Scheme 1 by 1(295), 2(295), and 3(295), respectively.

of seed aerosol onto filter media, blank filters were collected under dark conditions from the Caltech chamber containing typical experimental well-mixed concentrations of the VOC (i.e., individual runs of isoprene and α -pinene), seed aerosol, and the OH precursor (i.e., H_2O_2 or HONO) and were extracted and

analyzed by our high-resolution MS technique. The chamber air mixture was sampled on these blanks for the same duration as a sample filter. Besides the observation of inorganic sulfate, no organosulfates characterized in the present study or significant contaminants were observed by the high-resolution MS technique.

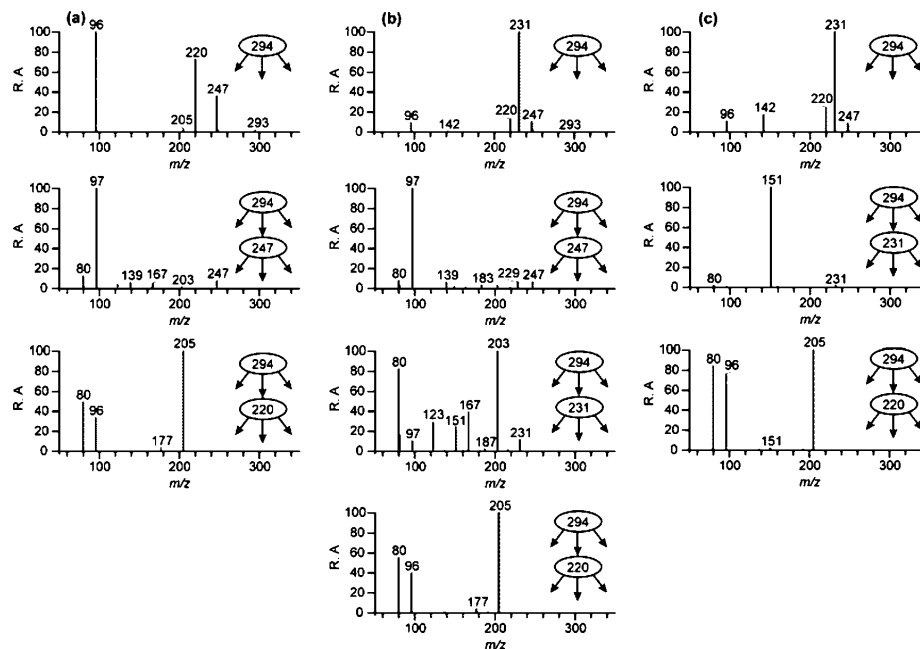


Figure 4. MS²/MS³ data obtained for *m/z* 294 compounds from a SEARCH sample (BHM 6/20/04) with RTs of (a) 37.4, (b) 43.4, and (c) 45.1 min. These compounds are denoted in the text and Scheme 1 by **1**(295), **2**(295), and **3**(295), respectively.

nique from these blank filters, consistent with the lack of observed aerosol growth under dark conditions. Additionally, it is worth mentioning that our initial study on organosulfate formation also included several quality control tests to ensure that organosulfate formation occurred only during SOA formation.²³ All Teflon filters used for high-resolution MS analysis were examined within 1–2 days of the filter extraction/sample preparation. Following their initial analysis, sample extract solutions were stored at -20°C . Several samples were reanalyzed a month after their initial extraction and showed no signs of degradation due to hydrolysis, a result consistent with previous work.²⁶ Additionally, it should be noted that a prior systematic study has shown that extractions of aliphatic sulfate esters and sulfonic acids in deionized water do not release any detectable inorganic sulfate by ion chromatography.⁵⁸

Teflon filters used for linear ion trap mass spectrometry analysis were extracted two times for 30 min in an ultrasonic bath with 20 mL of methanol. The extracts were combined and concentrated in a rotary evaporator at 35 °C to approximately 1 mL, filtered through a Teflon filter (0.45 μm), evaporated to dryness under a N₂ stream at ambient temperature, and reconstituted in 300 μL of a solvent mixture of methanol/water (2:1; v/v). Quality control tests were made to ensure that the filtration step did not introduce artifacts or interferences.

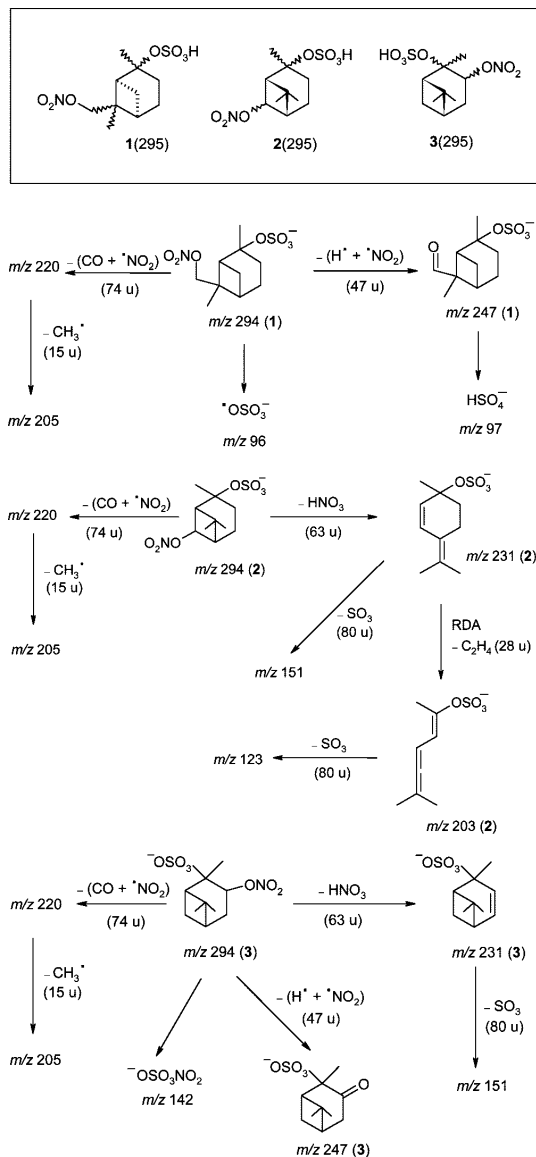
2.3. Ambient Aerosol Sample Collection and Extraction

Protocols. Details of the SEARCH network, which includes descriptions of each site, sample collection protocols, and gas- and particle-phase measurements conducted, can be found elsewhere.^{59,60} In the present study, archived quartz fiber filters collected from the June 2004 campaign⁴⁷ were analyzed and were collected from the following three sites: Birmingham, Alabama (BHM, urban site), Centerville, Alabama (CTR, rural site), and Atlanta, Georgia (JST, Jefferson Street, downtown urban site). Quartz fiber filter extraction and sample preparation procedures have been described elsewhere;⁴⁷ however, it should

be noted that solid-phase extraction (SPE) was not employed in the current study to desalt the ambient filter samples before MS analysis. This was not done because of the risk of removing early eluting organosulfates of isoprene in C₁₈ reversed phase LC, therefore preventing their detection by MS.

2.4. Ultra Performance Liquid Chromatography/Electrospray Ionization Time-of-Flight High-Resolution Mass Spectrometry (UPLC/ESI-TOFMS). Both chamber and field sample extracts were analyzed by a Waters ACQUITY ultra performance liquid chromatography (UPLC) system, coupled to a Waters LCT Premier XT time-of-flight mass spectrometer (TOFMS) equipped with an electrospray ionization (ESI) source. The ESI source on this instrument contains two individual orthogonal sprays; one spray is for the column eluent, and the other is for lock-mass correction. Optimum ESI conditions were found using a 2.5 kV capillary voltage, 40 V sample cone voltage, 350 °C desolvation temperature, 130 °C source temperature, 20 L h⁻¹ cone gas flow rate, and 650 L h⁻¹ desolvation gas flow rate. Data were collected from *m/z* 50 to 1000 in the negative (−) ionization mode with the TOFMS instrument operated in the W geometry reflection mode. The W reflectron mode offers the highest mass resolution, which is approximately 12 000, and allows for accurate mass measurements to be conducted on detected organosulfates, resulting in the determination of elemental compositions for these compounds. All organosulfates were detected as their deprotonated molecules ([M − H][−]). The chromatographic separations were carried out using a Waters ACQUITY UPLC HSS (high-strength silica) column (2.1 × 100 mm, 1.8 μm particle size) at 45 °C. The mobile phases consisted of (A) 0.1% acetic acid in water (LC-MS CHROMASOLV-grade, Sigma–Aldrich) and (B) 0.1% acetic acid in methanol (LC-MS CHROMASOLV-grade, Sigma–Aldrich). The applied 12 min gradient elution program was as follows: The concentration of eluent B was 0% for the first 2 min, increased to 90% from 2 to 10 min, held at 90%

SCHEME 1



from 10 to 10.2 min, and then decreased back to 0% from 10.2 to 12 min. The flow rate and sample injection volume were 0.3 mL min⁻¹ and 2 μ L, respectively.

The Waters ACQUITY UPLC HSS column was selected to separate organosulfates in this study because of its increased retention of water-soluble polar organosulfates as compared to the Waters ACQUITY BEH C₁₈ column. The latter column is essentially analogous to that of the C₁₈ HPLC column previously employed by Surratt et al.^{23,24} Both C₁₈ columns failed to separate inorganic sulfate from many of the organosulfates of isoprene previously identified in these studies. On the Waters ACQUITY UPLC HSS column, a separation was achieved between inorganic sulfate (detected as m/z 97 and its adduct m/z 195), which elutes first from the column (Figure 1, RT 0.79 min), and the organosulfates of the 2-methyltetrols previously

identified by Surratt et al.^{23,24} (Figure 1, RT 0.91 min). Separation was achieved as a result of trifunctionally bonded (T3) C₁₈ alkyl residues on this column, which prevent stationary phase collapse when a 100% aqueous mobile phase is used, thus resulting in better retention of water-soluble polar organic compounds. The newly acquired separation between inorganic sulfate and organosulfates of isoprene further confirms that these latter compounds are not artifacts formed in the electrospray ionization source during MS analysis due to coelution.

At the beginning of each analysis period, the TOFMS instrument was calibrated using a 1:1 (v/v) solvent mixture of acetonitrile and 0.1% phosphoric acid aqueous solution. During each chromatographic run, 2 ng μ L⁻¹ leucine enkephalin (MW = 555) was used for the lock-mass spray for lock-mass correction to obtain accurate masses for each SOA component eluting from the column. The lock-mass syringe pump was operated at 20 μ L min⁻¹. In addition to using the lock-mass spray, the dynamic range enhancement feature of this mass spectrometer was applied to prevent dead time, which decreases mass accuracy, from occurring. Data were acquired and processed using the MassLynx version 4.1 software. As a confirmation that the accurate mass measurement was reliable from the UPLC/(-)ESI-TOFMS technique, a standard sample containing known isoprene and α -pinene organosulfates previously characterized by Surratt et al.²³ was analyzed. The known elemental compositions (i.e., molecular formulas) of the previously characterized organosulfates²³ were in excellent agreement with their measured exact masses (i.e., within ± 2 mDa or ± 2 ppm, which is excellent for small molecules). In addition to accurate mass measurements, further insights into the structures of the organosulfates were obtained by generating tandem MS data, which was done by increasing the first aperture voltage on the TOFMS instrument from 10 to 25 V; however, it should be noted that the tandem MS data generated from the linear ion trap instrument, as will be described in the next section, was the preferred method for this type of analysis. The tandem MS analysis conducted on the UPLC/ESI-TOFMS instrument served only as a further confirmation of the presence of a sulfate or nitrooxy group.

2.5. High-Performance Liquid Chromatography/Electrospray Ionization Linear Ion Trap Mass Spectrometry (HPLC/ESI-LITMS). Selected chamber and field sample extracts were also analyzed by a Thermo Fisher Surveyor plus HPLC system (pump and autosampler) coupled to a Thermo Fisher LXQ linear ion trap analyzer equipped with an electrospray ionization source. Data were acquired and processed using Xcalibur version 2.0 software. A Waters Atlantis dC18 column (3 μ m; 2.1 \times 150 mm; 3 μ m particle size) was employed, which is similar to the Waters ACQUITY UPLC HSS column used for UPLC/ESI-TOFMS analysis, except that the stationary phase contained difunctionally instead of trifunctionally bonded C₁₈ alkyl chains. The mobile phases consisted of acetic acid 0.1% (v/v) (A) and methanol (B). The applied 45 min gradient elution program was as follows: The concentration of eluent B was kept at 3% for 2 min, then increased to 90% in 18 min, kept at 90% for 10 min, then decreased to 3% in 5 min, and kept at 3% for 10 min. The injection volume and flow rate were 5 μ L and 0.2 mL min⁻¹, respectively.

The linear ion trap was operated under the following conditions: sheath gas flow (nitrogen), 50 arbitrary units; auxiliary gas flow (nitrogen), 5 arbitrary units; source voltage, -4.5 kV; capillary temperature, 350 $^\circ$ C; and maximum ion injection time, 200 ms. For MS² and MS³ experiments, an isolation width of 2 m/z units and a normalized collision energy

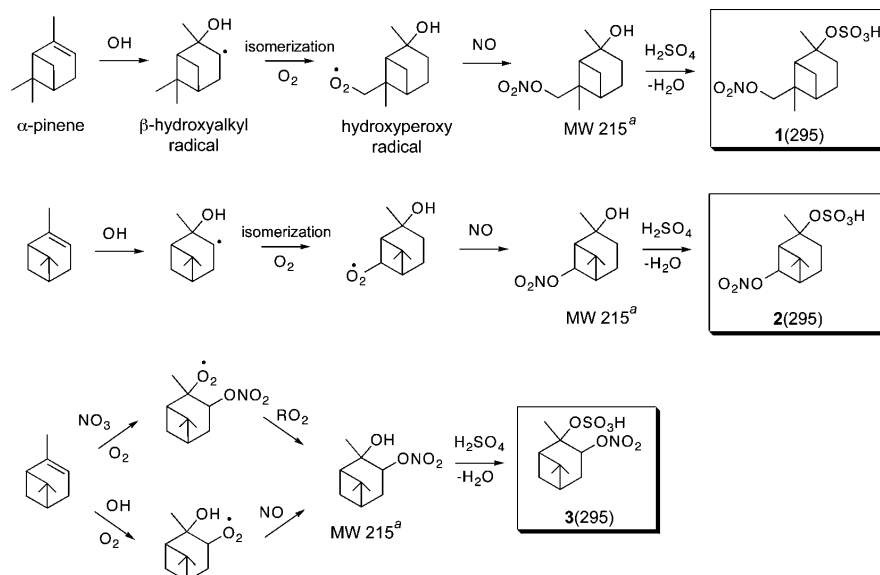


Figure 5. Proposed formation mechanism for the three major isomers of the m/z 294 nitrooxy organosulfates observed in ambient aerosol from the oxidation of α -pinene. Numerals 1–3(295) correspond to the isomeric structural assignments based upon the explanations shown in Scheme 1 for the observed product ions formed in the tandem MS experiments. For isomers 1 and 2(295), it remains unclear how the NO_3 -initiated oxidation produces these compounds in the presence of highly acidified sulfate seed aerosol. Footnote *a*: Aschmann et al.^{74,75} observed a hydroxynitrate of this MW in the gas phase from the OH-initiated oxidation of α -pinene in the presence of NO.

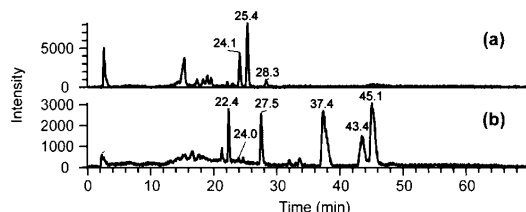


Figure 6. MS^2 (m/z 296) TICs obtained from (a) a d -limonene/ H_2O_2 /NO/highly acidic seed experiment and (b) a SEARCH sample (BHM 6/20/04).

level of 35% were applied. The $[\text{M} - \text{H}]^-$ signal optimization was done by introducing a $50 \mu\text{g mL}^{-1}$ malic acid standard solution.

3. Atmospheric Significance of Organosulfates

In the subsequent sections, the detailed chemical characterization of several high-mass organosulfates detected in ambient fine aerosol collected from the southeastern U.S. will be presented; however, before presenting our detailed chemical characterization results, we estimate the total contribution of organosulfates to aerosol collected during summertime conditions from an independent European field site to demonstrate the potential significance of these compounds to ambient organic aerosol formation. Although authentic and/or suitable surrogate standards are not currently available to quantify the characterized organosulfates by the UPLC/(–)ESI-TOFMS and HPLC/(–)ESI-LITMS techniques employed in the present study, an upper-limit estimate of the contribution from organosulfates to the particulate organic matter (OM) can be derived from the analysis of aerosol samples for total sulfur and water-soluble sulfate. Water-soluble sulfate is commonly measured by ion chromatography (IC), and organosulfates do not appear in this type of

measurement, consistent with previous work.²³ Total sulfur can be measured by X-ray emission techniques, such as X-ray fluorescence (XRF) or particle-induced X-ray emission spectrometry (PIXE), and this measurement will include the sulfur from water-soluble sulfate and other inorganic sulfur species (e.g., sulfite), the insoluble sulfur that may be associated with primary biogenic particles,⁶¹ and also the sulfur of the organosulfates. Subtracting the IC sulfate sulfur from the XRF or PIXE sulfur can thus provide an upper limit for the sulfur that is associated with organosulfates. XRF, PIXE, and IC analyses have an associated uncertainty on the order of 5% or more; therefore, the uncertainty that is associated with the difference can be substantial. Even though such data sets were not available for the SEARCH samples analyzed in the present study, one can estimate the maximum amount of sulfur associated with organosulfates for PM_{10} samples that were collected during a 2003 summer field campaign at the forested site of K-pusztá in Hungary,^{62,63} where organosulfates found in the K-pusztá aerosol are generally the same as those characterized in the present study and are likely present in substantial concentrations.⁴⁶ The difference between the PIXE sulfur data and the IC sulfate sulfur data for the 63 PM_{10} samples ranged from 32 to 850 ng m^{-3} and was, on average, 330 ng m^{-3} , which represents 20% of the average PIXE total PM_{10} sulfur concentration (Maenhaut, unpublished results). The average concentration of particulate organic carbon (OC) in the PM_{10} samples of the campaign was $5.8 \mu\text{g m}^{-3}$, which, using an OC-to-OM conversion factor of 1.8 that was adopted for the site,⁶³ corresponds to $10.4 \mu\text{g m}^{-3}$ of OM. The mass percentages of sulfur in some common BSOA organosulfates, that is, those of the characterized 2-methyltetrols and the nitrooxy organosulfates from α -pinene SOA with a MW of 295, are 14.8 and 10.8%, respectively. Using the latter percentage, the 330 ng m^{-3} of nonsulfate sulfur mentioned above would correspond to $3.1 \mu\text{g m}^{-3}$ of OM for the 2003 summer campaign at K-pusztá and thus represents about 30% of the total

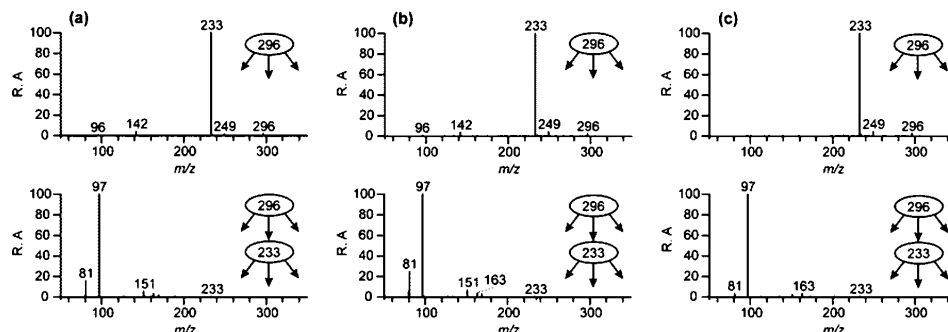
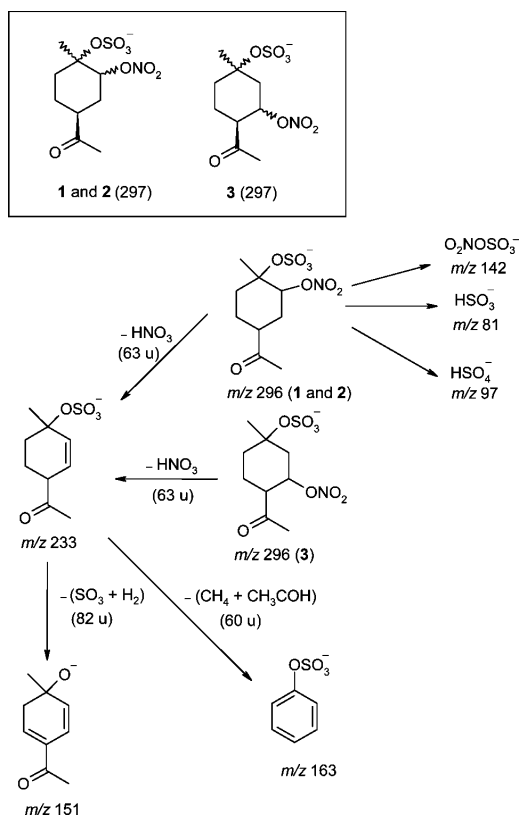


Figure 7. MS²/MS³ data obtained for the three *m/z* 296 compounds from a *d*-limonene/ H_2O_2 /NO/highly acidic seed experiment with RTs of 24.1, 25.4, and 28.3 min. The compounds are denoted by **1–3**(297) in the text and Scheme 2.

SCHEME 2



PM₁₀ OM. Despite the uncertainties associated with this estimate, it is clear that organosulfates may be responsible for a sizable fraction of ambient OM. In addition to our estimates, Lukács et al.⁶⁴ recently showed that organosulfates in water-soluble fine aerosol, also collected from the K-pusztá field site during the 2006 summer campaign, contribute 6–12% to the total sulfur concentration. Due to the likely importance of these estimates, it is essential that the detailed chemical characterization of organosulfates be conducted as this will lead to improved understanding of their formation pathways in ambient organic aerosol. In the following sections, we first present the results of our laboratory chamber experiments in order to reveal conditions under which organosulfate formation is favorable.

Even though our chamber experiments employ higher VOC mixing ratios, higher levels of seed aerosol acidity, and drier conditions than typically observed in the atmosphere, it will be shown that many of the laboratory-generated organosulfates are also detected in the ambient aerosol collected from the southeastern U.S. Those organosulfates detected in both laboratory-generated and ambient organic aerosol will then be the focus of our detailed chemical characterization efforts. Since most of these compounds are characterized for the first time, a substantial amount of analytical detail is provided.

4. Laboratory-Generated Organosulfates

4.1. Monoterpene Oxidation Experiments. Experimental conditions and results of the monoterpene oxidation experiments are summarized in Table 2. As in recent work,^{23,46} only two types of organosulfates are considered in the present study (i) sulfate esters formed from the particle-phase esterification of a semivolatile product containing one or more hydroxyl groups by sulfuric acid and (ii) sulfate derivatives formed from a semivolatile product containing an aldehyde or a keto group and sulfuric acid. The latter organosulfates require gem-diol formation followed by esterification with sulfuric acid.

As stated previously, organosulfates were identified by using both UPLC/(–)ESI-TOFMS and HPLC/(–)ESI-LITMS techniques. Accurate mass measurements for all of the organosulfate ions listed in Table 2 are provided in Tables 1S–6S (Supporting Information); however, as noted in Table 2, no separate table for accurate mass measurements is provided for the Δ³-carene experiment owing to the fact that only one organosulfate isomer was identified at *m/z* 342 using the UPLC/(–)ESI-TOFMS technique. The differences between the theoretical masses of the TOFMS suggested molecular formulas and the measured masses found in Tables 1S–6S (Supporting Information) are minimal and are generally well within acceptable errors (i.e., approximately ±1–2 mDa and/or ±5 ppm error). The accurate mass data shown in these tables indicate that these ions have molecular formulas containing at least one sulfur atom and, on the basis of the degree of oxidation indicated by their respective molecular formulas, suggest the presence of a sulfate group. Additionally, some of these ions were also found to contain at least one nitrogen atom, thus being identified as nitroxy organosulfates. In addition to the accurate mass data, MS² spectra for all of the organosulfate ions listed in Table 2 showed prominent *m/z* 97 (HSO_4^-) product ions, as well as *m/z* 80 (SO_3^-) product ions in some cases, both of which have been previously shown to serve as indicator ions for the presence of a sulfate group.^{23–26,51,65,66} MS² product ion spectra for all nitroxy organosulfates yield a neutral loss of 63 u (HNO_3 ; nitric

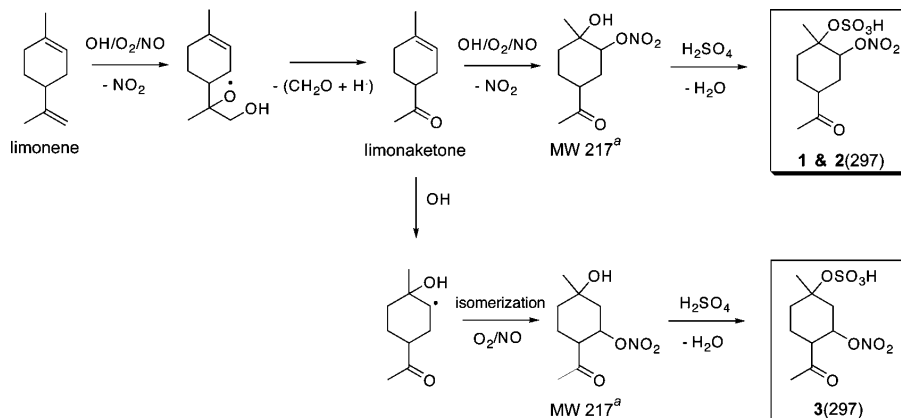


Figure 8. Proposed formation mechanism for the three major m/z 296 nitrooxy organosulfates observed from the photooxidation of limonene/limonaketone in the presence of NO_x and highly acidified sulfate seed aerosol. Numerals 1–3(297) correspond to the isomeric structural assignments based upon the explanations shown in Scheme 2 for the observed product ions formed in the tandem MS experiments. Footnote a: Lee et al.⁸² observed an organic nitrate species of this MW in the gas phase from the photooxidation of limonene in the presence of NO_x as the $[\text{M} + \text{H}]^+$ ion using PTR-MS.

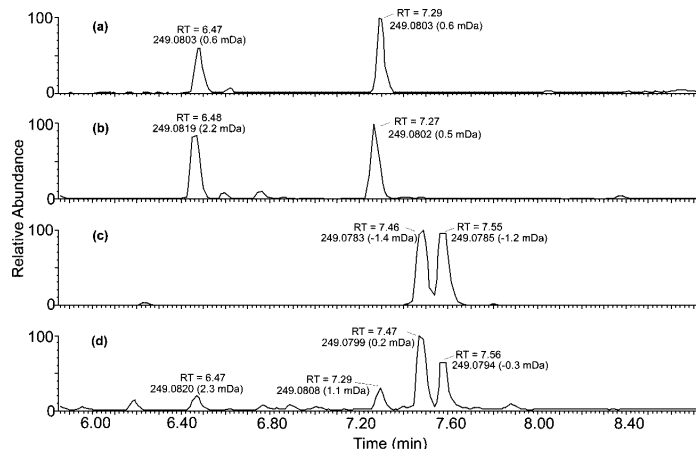


Figure 9. UPLC/(-)ESI-TOFMS extracted ion chromatograms (EICs) of m/z 249 for the following: (a) α -pinene/ NO_3 /highly acidic seed experiment; (b) α -pinene/ $\text{H}_2\text{O}_2/\text{NO}$ /highly acidic seed experiment; (c) β -pinene/ $\text{H}_2\text{O}_2/\text{NO}$ /highly acidic seed experiment; (d) SEARCH sample collected from the CTR field site on 6/11/2004. The RTs, accurate masses, and mDa errors between the theoretical masses of the TOFMS suggested molecular formulas, and the accurate masses of the detected m/z 249 ions are listed above each chromatographic peak. All of the chromatographic peaks highlighted in the figure share the same elemental composition of $\text{C}_{10}\text{H}_{17}\text{O}_5\text{S}^-$. α -/ β -Pinene were the only monoterpenes found in this study to produce the m/z 249 organosulfates with the same RTs, accurate masses, and elemental compositions as those observed in the SEARCH field samples.

acid), further confirming the presence of a nitrooxy group. On the basis of these accurate mass and tandem MS results, all of the $[\text{M} - \text{H}]^-$ ions listed in Table 2 were classified only as organosulfates and/or nitrooxy organosulfates.

Detailed study of organosulfate formation in laboratory-generated SOA produced from the photooxidation (i.e., OH-initiated oxidation) and/or nighttime oxidation (i.e., NO_3 -initiated oxidation) of monoterpenes has been limited. Previous work, in collaboration with the EPA laboratory, observed organosulfates, as well as nitrooxy organosulfates, from the photooxidation of α -pinene in the presence of NO_x and SO_2 .²³ Limited experiments were conducted in this prior study; specifically, a series of experiments in which mixtures of hydrocarbons (toluene, isoprene) containing α -pinene were irradiated in the presence of NO_x and, for selected experiments, in the presence of SO_2 . Organosulfates of α -pinene were observed in this prior

study only when both α -pinene and SO_2 were present; particle-phase acidity was generated from the photochemical conversion of SO_2 to condensable H_2SO_4 . Owing to the complexity of this previous study (i.e., the use of hydrocarbon mixtures to investigate organosulfate formation from α -pinene), organosulfate formation in α -pinene SOA was investigated in much greater detail in the present work.

A number of α -pinene experiments were conducted, in which both the acidity of the sulfate seed aerosol and the oxidation conditions employed were varied (Table 2). Organosulfates were formed only when α -pinene was oxidized (under light or dark conditions) in the presence of acidic and/or highly acidic sulfate seed aerosol; higher acidity led to a wider array of organosulfate products detected, consistent with prior work.^{23–26} In the photooxidation experiments, organosulfate formation occurred at all NO_x levels examined, a result previously observed in

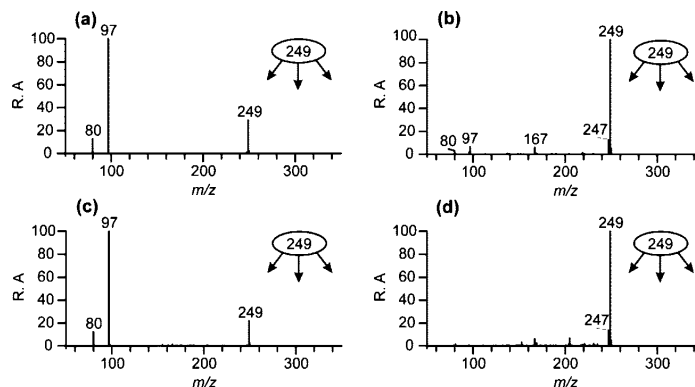


Figure 10. MS² spectra obtained for the two m/z 249 compounds with RTs of 31.2 and 32.2 min from (a, b) a β -pinene/H₂O₂/NO/highly acidic seed experiment and (c, d) a SEARCH sample (BHM 6/20/04). The compounds are denoted by 1(250) and 2(250) in the text, Figure 12, and Scheme 3.

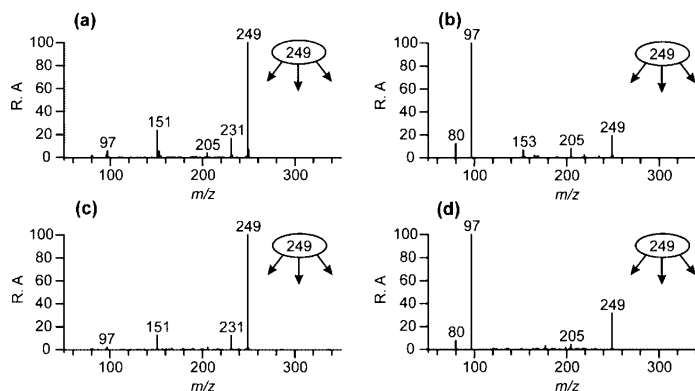


Figure 11. MS² spectra obtained for the two m/z 249 compounds with RTs of 24.4 and 29.3 min from (a, b) a α -pinene/H₂O₂/NO/highly acidic seed experiment and (c, d) a SEARCH sample (CTR 6/11/04). The compounds are denoted by 3(250) and 4(250) in the text, Figure 12, and Scheme 3. The ion at m/z 205 is due to an interference.

isoprene SOA.²³ Additionally, nitrooxy organosulfates were observed only under either intermediate- or high-NO_x conditions (denoted as H₂O₂/NO and HONO, respectively). This thorough investigation of organosulfate formation from α -pinene served as a model system for the experimental design of other monoterpenes examined in this study. In particular, since no organosulfate formation from α -pinene was observed under neutral sulfate seed aerosol conditions, which is consistent with previous work,^{25,26} all other monoterpene experiments were conducted only under acidic and/or highly acidic conditions. For the remaining monoterpene experiments, intermediate-NO_x conditions were employed (in most cases) to favor the formation of both organosulfates and nitrooxy organosulfates, as previously observed in isoprene SOA.²³ As shown in Tables 1S–6S (Supporting Information), organosulfates and nitrooxy organosulfates of all monoterpenes studied under these conditions were detected. Tentative structures and likely precursor oxidation products for many of these organosulfates are given in these tables; however, in subsequent sections, detailed chemical characterization will focus only on those ions detected in both laboratory-generated and ambient aerosol.

4.2. Isoprene Oxidation Experiments. Recent work from our laboratories has examined the detailed chemical composition of isoprene SOA formed under differing combinations of NO_x levels and sulfate seed aerosol acidities.^{23,24,33,37} In these previous

studies, organosulfates of isoprene were observed at all NO_x levels and in the presence of sulfate seed aerosol. Interestingly, organosulfates of isoprene were observed in the presence of neutral sulfate seed aerosol,²³ differing from the behavior of the monoterpenes examined in the present study; however, isoprene produced a wider array of organosulfates with enhanced acidity of the sulfate seed aerosol. Chemical characterization of these products was conducted using less-advanced mass spectrometric approaches as compared to the present study. No high-resolution (–)ESI-MS data were obtained in the initial study by Surratt et al.²³ As a further confirmation of the initial identifications made in the latter study, Table 7S (Supporting Information) shows the accurate mass measurements obtained in the present study for previously observed organosulfates of isoprene formed in the Caltech isoprene chamber experiments. With the exception of the nitrooxy organosulfates of isoprene detected at m/z 244, in conjunction with recent detailed tandem MS analysis,^{23,46} the $[M - H]^-$ ion formulas, as determined from the accurate mass data, correspond exactly to the deprotonated forms of the previously proposed isoprene organosulfate structures, hence now providing a more complete characterization of these chamber-generated SOA products. As for the monoterpene organosulfates, only those organosulfates of isoprene detected in both laboratory-generated and ambient aerosol will be further discussed and thoroughly characterized in

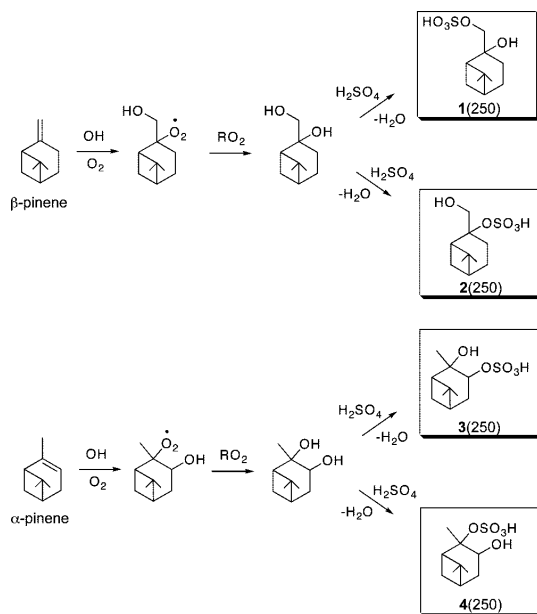


Figure 12. Proposed formation mechanism for the four m/z 249 organosulfates observed in ambient aerosol from the OH-initiated oxidation of β -pinene and α -pinene. Numerals 1–2(250) correspond to the isomeric structural assignments for the m/z 249 β -pinene organosulfates, which are based upon the explanations for the observed product ions formed in the tandem MS experiments (Figure 10). Iinuma et al.²⁶ also observed the formation of isomer 1(250) from a β -pinene ozonolysis acid seed experiment and detected this same isomer in a Norway-spruce-dominated forest in Bavaria, Germany. Numerals 3–4(250) correspond to the isomeric structural assignments for the m/z 249 α -pinene organosulfates, which are based upon the explanations for the observed product ions formed in the tandem MS experiments (Figure 11).

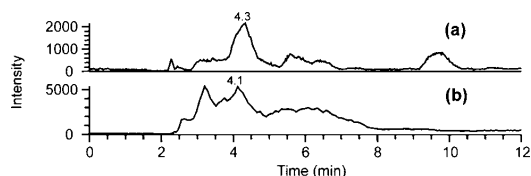


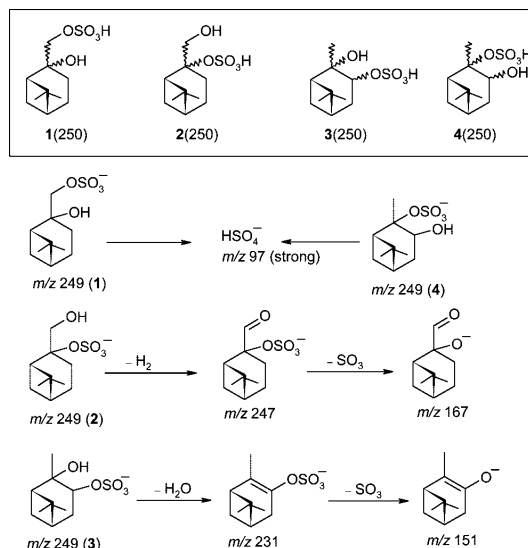
Figure 13. MS^2 (m/z 227) TICs obtained from (a) an α -pinene/ H_2O_2 /NO/highly acidic seed experiment and (b) a SEARCH sample (BHM 6/20/04).

subsequent sections; particular attention is focused on those ions detected for the first time in ambient aerosol.

5. Organosulfates in Ambient Aerosol

Figure 1 shows the UPLC/(–)ESI-TOFMS base peak ion chromatograms (BPCs) for 24 h integrated ambient aerosol samples collected from three different sites, and on three different days, across the southeastern U.S. during the summer of 2004. Several of the chromatographic peaks in these BPCs are labeled with their respective $[M - H]^-$ ion. Comparison of these BPCs demonstrates that the chemical composition of $PM_{2.5}$ in this region is rather constant during summertime polluted conditions, consistent with our initial investigation of this region.⁴⁷ It should be noted that not all organosulfates detected are labeled in this figure; Table 8S (Supporting Information)

SCHEME 3



shows the accurate mass data for all organosulfates detected in each analyzed field sample.

In our previous study, the chemical composition of aerosol collected from this region was investigated; however, very few organic components identified in Figure 1 (and Table 8S, Supporting Information) were fully characterized, and in some cases, they were not even detected, owing to the use of less-sensitive mass spectrometric approaches.⁴⁷ Besides the identification of known terpenic acids (denoted with an asterisk in Figure 1), such as norpinic (MW 172), pinic (MW 186), and pinonic (MW 184) acids, as well as the commonly observed MW 204 compound found in ambient aerosol,^{47,67–70} which was recently characterized as 3-methyl-1,2,3-butanetricarboxylic acid,⁷¹ only one organosulfate (i.e., m/z 294) was identified in this previous study.⁴⁷ In addition to characterizing m/z 294 as a nitrooxy organosulfate of α -pinene,²³ recent work has reported that ions at m/z 215 and 260 shown in Figure 1 (as well as m/z 199, not shown) are organosulfates of isoprene;^{23,46} specifically, it was found that m/z 215, 260, and 199 corresponded to organosulfates of the 2-methyltetrols, nitrooxy organosulfates of the 2-methyltetrol mononitrates, and organosulfates of 2-methylglyceric acid, respectively. It should be noted that both the 2-methyltetrols and 2-methylglyceric acid have been previously identified as tracer compounds for the occurrence of SOA formation in ambient aerosol from isoprene photooxidation.^{21,72} In the following sections, detailed mass spectrometric evidence is presented, characterizing most of the previously uncharacterized and partially characterized organic components observed in the field samples (Figure 1) as organosulfates of monoterpenes and isoprene. Except for the organosulfates of glyoxal (i.e., m/z 155) and methylglyoxal (i.e., m/z 169), which could form from the oxidation of both anthropogenic and biogenic VOCs in the presence of acidified sulfate seed aerosol, all other organosulfates characterized in this study appear to be unique tracer compounds for the occurrence of biogenic SOA formation under acidic conditions.

5.1. Organosulfates of Monoterpenes in Ambient Aerosol.

5.1.1. m/z 294. $[M - H]^-$ ions at m/z 294 have been observed using (–)ESI-MS techniques in ambient $PM_{2.5}$ collected from several regions of the U.S.^{23,47} as well as Europe^{26,46,51,73} and

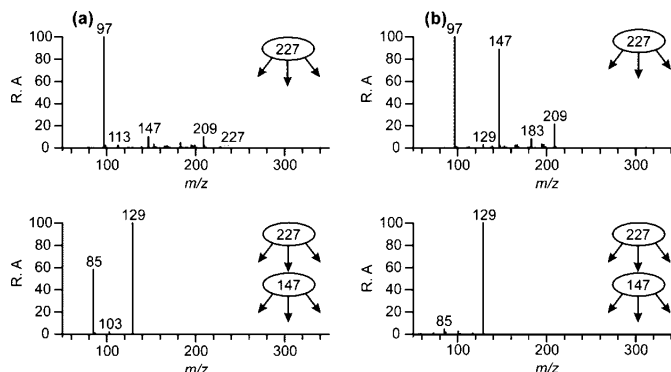
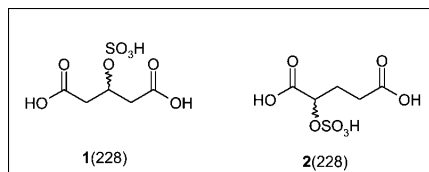


Figure 14. MS²/MS³ data for the *m/z* 227 compounds from (a) an α -pinene/H₂O₂/NO/highly acidic seed experiment with a RT of 4.3 min and (b) a SEARCH sample (BHM 6/20/04) with a RT of 4.1 min.

SCHEME 4



have been only partially characterized as nitrooxy organosulfates using high-resolution and tandem MS. It should be noted that it is critical that the latter MS techniques be used in combination when establishing the chemical identity of an unknown compound measured by (−)ESI-MS as many isobaric compounds (i.e., compounds of the same molecular mass but of different elemental composition) exist in ambient organic aerosol, and as a result, low-resolution MS instruments (e.g., quadrupole and ion trap mass analyzers) will not allow the determination of the mass difference between isobaric compounds.

By using a surrogate standard, the total *m/z* 294 nitrooxy organosulfate aerosol mass concentration (i.e., sum of three major isomers observed) was previously estimated to range from 27 to 140 ng m^{−3} for all days and field sites analyzed from the southeastern U.S.,⁴⁷ resulting in this ion being the most abundant organic species detected by (−)ESI-MS for this region. However, it is noted that the latter is only true when the filters are extracted in methanol. There may be other more-abundant organic components in ambient aerosol collected from this region not extractable by methanol, as well as not observed in the (−)ESI-MS analysis due to not being eluted from the chromatographic column previously employed or not being detected in the negative ion mode.

(−)ESI-TOFMS accurate mass data for the *m/z* 294 ions indicated that the [M − H][−] ion formula is C₁₀H₁₆NO₇S[−],^{26,47} consistent with the accurate mass data shown in Table 8S (Supporting Information). On the basis of these ion formulas, it was suggested that monoterpenes (C₁₀H₁₆) serve as a likely source for these ambient nitrooxy organosulfates.^{26,47} Surratt et al.²³ recently reported that the *m/z* 294 nitrooxy organosulfates detected in southeastern U.S. aerosol could arise from the photooxidation of α -pinene in the presence of NO_x and SO₂ (i.e., acidified sulfate seed aerosol); however, it was noted in this prior study, as well as in that of Iinuma et al.,²⁶ that other monoterpenes might also contribute to the formation of these compounds. Interestingly, previous studies have found that these compounds were more abundant in nighttime samples collected

from Europe, indicating that an additional formation mechanism is possible (i.e., NO₃-initiated oxidation).^{26,46} No such distinction between daytime and nighttime chemistry could be made in previous studies from the SEARCH campaign,^{23,47} nor in the present study, owing to the fact that the samples were collected over a 24 h integrated period.

Figure 2 compares the UPLC/(−)ESI-TOFMS extracted ion chromatograms (EICs) of *m/z* 294 obtained from one representative SEARCH field sample (CTR 6/11/04) and four selected monoterpene oxidation experiments, including α -pinene/H₂O₂/NO/neutral seed, α -pinene/H₂O₂/NO/highly acidic seed, α -pinene/NO₃/highly acidic seed, and β -pinene/H₂O₂/NO/highly acidic seed experiments, respectively. It is noted that the *m/z* 294 compounds were detected for all days in which samples were collected from each SEARCH field site (Table 8S, Supporting Information), consistent with our previous field study.⁴⁷ Although isomeric *m/z* 294 nitrooxy organosulfates were also formed in the α -terpinene and terpinolene photooxidation experiments conducted under highly acidic conditions (Tables 3S and 5S, Supporting Information), these two monoterpenes are not considered as possible sources for these nitrooxy organosulfates found in the SEARCH samples since the retention times (RTs) of their single isomers do not correspond to those of the ambient samples. The photooxidation and nighttime oxidation of α -pinene in the presence of highly acidic seed aerosol is shown in Figure 2 to produce three *m/z* 294 nitrooxy organosulfates with the same RTs and accurate masses as those observed in the SEARCH samples (RTs of 8.19, 8.80, and 8.99 min; Figure 2a). As shown in Figure 2b, the photooxidation of α -pinene in the presence of neutral sulfate seed aerosol does not produce *m/z* 294 compounds, which was also the result for the α -pinene/NO₃/neutral seed experiment (Table 2). Additionally, Figure 2c shows that the β -pinene/H₂O₂/NO/highly acidic seed experiment produced one *m/z* 294 nitrooxy organosulfate isomer with the same RT and accurate mass found in the field samples; however, tandem MS data will be discussed subsequently in order to confirm whether α -pinene, as well as β -pinene, are, in fact, the monoterpene precursors required for the formation of these compounds in ambient aerosol.

Figures 3 and 4 show MS²/MS³ data obtained with the HPLC/(−)ESI-LITMS technique for the three *m/z* 294 compounds formed in the α -pinene/NO₃/highly acidic seed experiment and MS²/MS³ data for the three *m/z* 294 compounds present from a selected SEARCH sample (CTR 6/20/04), respectively. MS² data similar to those for the α -pinene/NO₃/highly acidic seed

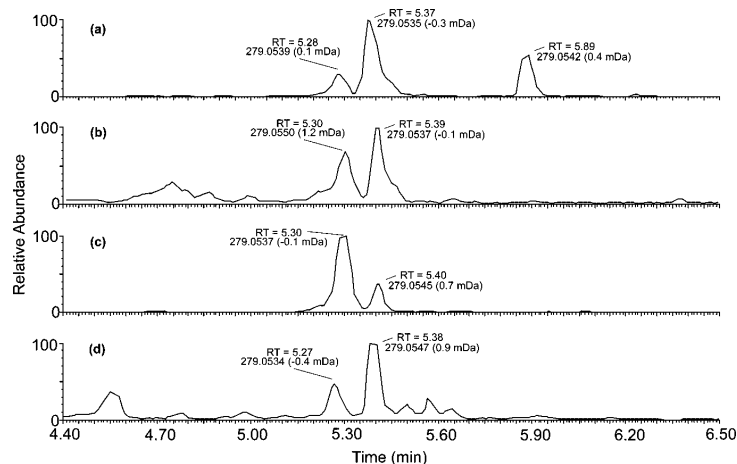


Figure 15. UPLC/ESI-TOFMS extracted ion chromatograms (EICs) of m/z 279 for the following: (a) α -pinene/ H_2O_2 /NO/highly acidic seed experiment; (b) α -pinene/NO/highly acidic seed experiment; (c) β -pinene/ H_2O_2 /NO/highly acidic seed experiment; and (d) a SEARCH sample collected from the CTR field site on 6/11/2004. The RTs, accurate masses, and mDa errors between the theoretical masses of the TOFMS suggested molecular formulas, and the accurate masses of the detected m/z 279 ions are listed above each chromatographic peak. All of the chromatographic peaks highlighted in the figure share the same elemental composition of $\text{C}_{10}\text{H}_{15}\text{O}_7\text{S}^-$.

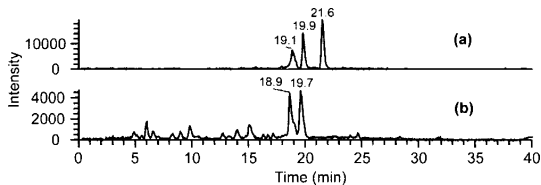


Figure 16. MS^2 (m/z 279) TICs obtained from (a) an α -pinene/ H_2O_2 /NO/highly acidic seed experiment and (b) a SEARCH sample (CTR 6/11/04). The compounds with RTs of 19.1 (or 18.9) and 19.9 min are denoted by **1**(280) and **2**(280) in the text and Scheme 5.

experiment were also obtained in the case of the α -pinene/ H_2O_2 /NO/highly acidic seed experiment (see Figure 1S, Supporting Information); in addition, similar MS^2 data were also recorded for two other field samples (JST 6/26/04 and BHM 6/20/04; data not shown). Comparison of these data establishes that the NO_3 and H_2O_2 /NO highly acidic sulfate seed experiments yield the same m/z 294 nitrooxy organosulfates as those present in the field samples and originate from either the nighttime oxidation or photooxidation of α -pinene, with the latter in the presence of NO_x .

Isomeric structural assignments, taking into account that these compounds originate from the oxidation of α -pinene, and explanations for the formation of product ions produced in the tandem MS data supporting these structural assignments are outlined in Scheme 1 [where numerals **1**–**3**(295) indicate the protonated compounds proposed]; however, in the absence of reference compounds, these attributions should be regarded as tentative. The m/z 294 MS^2 product spectra of compounds **2** and **3**(295) are very similar, suggesting positional isomers with sulfate and nitrate groups at different positions. The m/z 294 MS^2 spectra for compounds **2** and **3**(295) contain an abundant m/z 231 ion due to the loss of 63 u (HNO_3), which shows a different fragmentation behavior for the two compounds; in the case of compound **2**(295), multiple product ions are formed upon MS^3 of the m/z 231 ion, while in the case of compound **3**(295), m/z 151 is the only product ion. The abundant m/z 203 ion in the m/z 294 \rightarrow m/z 231 MS^3 spectrum of compound **2**(295) corresponds to the loss of 28 u ($\text{CH}_2=\text{CH}_2$). This can be

explained by a retro-Diels–Alder (RDA) fragmentation and points to a nitrooxy group at the secondary carbon position of the 2,2-dimethylcyclobutane ring. On the other hand, the m/z 142 ion in the m/z 294 MS^2 spectrum of compound **3**(295) points to neighboring OSO_3^- and ONO_2 groups and thus supports the proposed structure shown in Scheme 1. In regards to compound **1**(295), it is noted that the m/z 294 MS^2 spectrum is remarkably similar to those shown in Figure 2S (Supporting Information) for β -pinene SOA; however, the product ions at m/z 247, 220, and 96 exhibit different relative abundances, consistent with isomeric differences, and indicate that β -pinene is not responsible for the formation of these nitrooxy organosulfates in ambient aerosol. This conclusion is further supported by the MS^3 data, which reveal more distinct differences between compound **1**(295) and the two m/z 294 compounds present in β -pinene SOA. The m/z 247 ion (loss of HNO_2) in the m/z 294 MS^2 spectrum of compound **1**(295) is consistent with a primary nitrooxy group, while the base peak at m/z 96 (SO_4^{2-}) points to a sulfate group at a tertiary position. The absence of a m/z 151 ion suggests that a hydrogen required for loss of HNO_3 is not available at a neighboring position within compound **1**(295). The abundant m/z 220 ion can be explained by the combined loss of CO and a NO_2^+ radical (74 u); however, a simple mechanism for this fragmentation could not be formulated.

On the basis of the interpretation of both the accurate mass and tandem MS data, Figure 5 shows the proposed formation mechanism for the three major isomers of the m/z 294 nitrooxy organosulfates observed in ambient aerosol. As previously shown for pinonaldehyde,^{49,50} a known first-generation gas-phase product from α -pinene oxidation, it is proposed that isomeric hydroxynitrate gas-phase products of MW 215 from α -pinene reactively uptake onto acidified sulfate seed aerosol through esterification of the hydroxyl group with sulfuric acid, yielding the characterized nitrooxy organosulfates shown in Scheme 1. Prior work done by Aschmann et al.^{74,75} has detected a hydroxynitrate species of MW 215 in the gas phase produced from an α -pinene photooxidation experiment conducted in the presence of NO when using an atmospheric pressure ionization tandem mass spectrometer and, as a result, supporting the

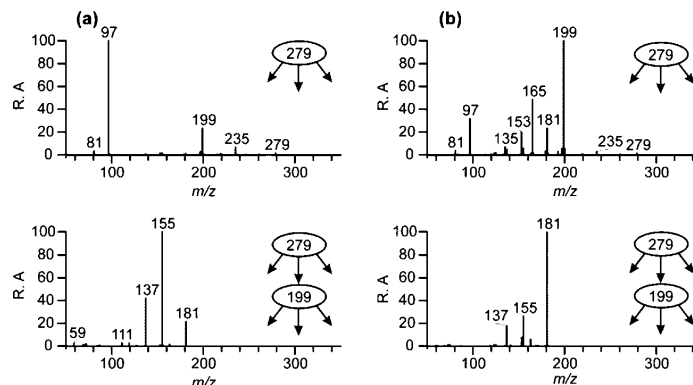


Figure 17. MS²/MS³ data for (a) the first- (19.1 min) and (b) second-eluting (19.9 min) *m/z* 279 compounds from the α -pinene/H₂O₂/NO/highly acidic seed experiment.

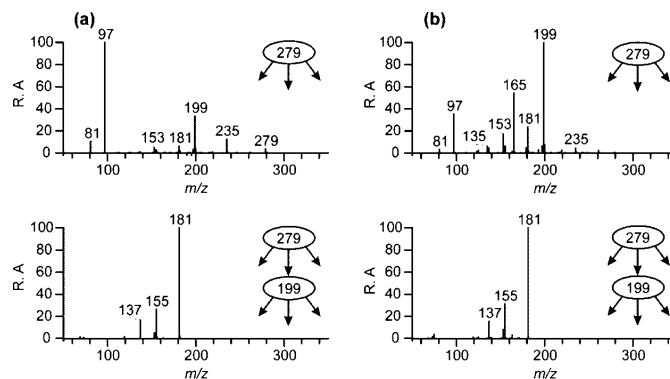


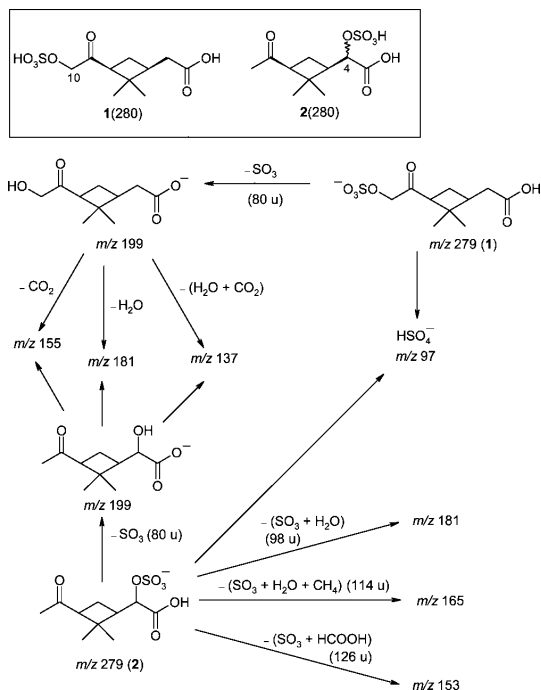
Figure 18. MS²/MS³ data for (a) the first- (19.1 min) and (b) second-eluting (19.9 min) *m/z* 279 compounds from the β -pinene/H₂O₂/NO/highly acidic seed experiment.

feasibility of our proposed reaction mechanism; in addition, Jay and Stieglitz⁷⁶ also observed hydroxynitrates from the NO₃-initiated oxidation of α -pinene using gas chromatography(GC)/mass spectrometry(MS) and FTIR analysis. Despite the structure for the hydroxynitrate gas-phase precursor of compound **3**(295) being the only isomer conforming to known RO₂ chemistry, other structural isomers of the hydroxynitrate likely correspond to the detailed chemical structures shown in Scheme 1. In order to form compounds **1** and **2**(295) from the photooxidation of α -pinene in the presence of NO_x, we propose that the β -hydroxyalkyl radical that forms after the initial OH radical addition to the double bond isomerizes the radical by H-abstraction to another carbon within the α -pinene skeleton (or undergoes a hydrogen rearrangement), followed by the immediate reaction with O₂ to form the respective hydroxyperoxy radicals shown in Figure 5. Similar isomerization behavior has been proposed by Jay and Stieglitz⁷⁶ for β -nitrooxyalkyl radicals formed from the NO₃-initiated oxidation of α -pinene; however, it remains unclear at this time how such an isomerization would yield the hydroxynitrates needed to produce compounds **1** and **2**(295) under nighttime oxidation conditions, even though the MS data clearly show that both nighttime and daytime chemistry of α -pinene produce the same three isomers of the *m/z* 294 nitrooxy organosulfates. Conversely, we only discuss and propose the formation of compounds **1** and **2**(295) from the photooxidation pathway in Figure 5. Upon the formation of the hydroxyperoxy radicals from the isomerization of the initial β -hydroxyalkyl radical and subsequent addition of O₂, under intermediate- and/

or high-NO_x conditions, the former radicals react with NO to yield the hydroxynitrate precursors shown for compounds **1** and **2**(295). Alternatively, previous work has shown that large hydroxyalkoxy (RO) radicals, produced from the reaction of the RO₂ radical with NO, readily isomerize rather than fragment,^{12,74,75} especially if the RO radical has at least four or more carbons and can form a six-membered transition state.^{77,78} The isomerization of the RO radical was not considered in the present study, owing to the fact that if the initial RO radical of α -pinene isomerizes, as previously observed by Aschmann et al.,^{74,75} this results in the formation of a dihydroxyalkyl radical. The latter radical immediately reacts with O₂ to form a dihydroxyperoxy radical, and in the presence of NO, it forms a dihydroxynitrate gas-phase product of MW 231, thus failing to explain the formation of compounds **1** and **2**(295) from the photooxidation of α -pinene.

Recent emission data show that α -pinene is the most abundant monoterpene emitted from loblolly pine (*Pinus taeda* L.), which is one of the most predominant timber species found in southeastern U.S. forests, followed by β -pinene, myrcene, *d*-limonene, and β -phellandrene.^{79,80} Considering our chemical characterization results and the known emission rates from loblolly pine, it appears that the *m/z* 294 nitrooxy organosulfates that we observe in the SEARCH field samples arise solely from either the photooxidation of α -pinene in the presence of NO_x or the nighttime oxidation of α -pinene, both of which require the presence of acidified sulfate seed aerosol. It should be noted that future laboratory chamber experiments of myrcene and

SCHEME 5



ocimene are needed in order to determine their potential contribution to the m/z 294 nitrooxy organosulfates found in ambient aerosol, especially considering that new emission data for the U.S. indicate that these two monoterpenes are emitted abundantly from deciduous (broadleaf) and coniferous (needle) trees.⁸¹ Additionally, it would be worthwhile to analyze nighttime-segregated filter samples collected from the SEARCH network to evaluate the importance of nighttime chemistry to the formation of the m/z 294 nitrooxy organosulfates.

5.1.2. m/z 296. Previous field studies have reported $[M - H]^-$ ions at m/z 296 when using $(-)$ ESI-MS techniques to characterize organic aerosol collected from both the southeastern and southwestern U.S.^{47,52} Despite the recent identification of a m/z 296 compound as a nitrooxy organosulfate in southwestern U.S. aerosol,⁵² the source and formation mechanism of this compound remained unclear in both regions previously studied. Figure 3S (Supporting Information) compares the UPLC/ $(-)$ ESI-TOFMS EICs of m/z 296 obtained from three selected monoterpene oxidation experiments, which includes the *d*-limonene/ H_2O_2 /NO/highly acidic seed, β -phellandrene + *d*-limonene mixture/ H_2O_2 /NO/highly acidic seed, and limonaketone/ H_2O_2 /NO/highly acidic seed experiments, to that of one representative SEARCH field sample (JST 6/26/04). Although not shown, it should be noted that the *l*-limonene/ H_2O_2 /NO/highly acidic seed experiment also produced three m/z 296 compounds with the same RTs and accurate masses as those highlighted in Figure 3S (Supporting Information) for the *d*-limonene experiments. From all of the monoterpene oxidation experiments conducted, *d*-*l*-limonene and β -phellandrene, as well as limonaketone ($C_9H_{14}O$), which is a known first-generation oxidation product of limonene,^{54,82} were the only precursors in this study to produce m/z 296 compounds; specifically, the photooxidation of these BVOC precursors in the presence of NO_x and highly acidified sulfate seed aerosol

produced these compounds. Interestingly, no m/z 296 compounds formed in the NO_3 /highly acidic seed experiments of *d*- and *l*-limonene, which is likely attributable to the large nucleation events observed at the start of these experiments; specifically, the NO_3 -initiated oxidation of these monoterpenes led to a large number of particles being formed by nucleation and, as a result, likely prevented the formation of the m/z 296 compounds by not allowing for the reactive uptake of the gas-phase semivolatile products onto the acidified sulfate seed aerosol. Accurate mass data for all chromatographic peaks highlighted in Figure 3S (Supporting Information) indicate that the $[M - H]^-$ ion formulas for both the laboratory-generated (Figure 3Sa–c, Supporting Information) and ambient m/z 296 compounds (Figure 3Sd, Supporting Information) are $C_9H_{14}NO_8S^-$.

Figure 6 shows the m/z 296 MS^2 TICs obtained using the HPLC/ $(-)$ ESI-TOFMS technique for the *d*-limonene/ H_2O_2 /NO/highly acidic seed experiment and a SEARCH sample (BHM 6/20/04). As observed in the UPLC/ $(-)$ ESI-TOFMS EICs of m/z 296 (Figure 3S, Supporting Information), the RTs for the three m/z 296 compounds in *d*-limonene SOA were slightly shifted to longer times when compared to that for the ambient m/z 296 compounds. It is noted that the signals observed between 36 and 48 min in Figure 6b are due to $^{34}S/^{18}O$ isotopic contributions of m/z 294 α -pinene SOA nitrooxy organosulfates that are very abundant in the ambient sample. The MS^2/MS^3 data for the three m/z 296 compounds from *d*-limonene SOA (Figure 6a) eluting at 24.1, 25.4, and 28.3 min are given in Figure 7a–c, respectively. It can be seen that the m/z 296 MS^2 and m/z 296 \rightarrow m/z 233 MS^3 spectra are remarkably similar for the three compounds in *d*-limonene SOA. Tentative structures based on the interpretation of both the MS^2/MS^3 (Figure 7) and accurate mass data for the three m/z 296 compounds observed in *d*-limonene SOA and explanations for the observed product ions supporting these structural assignments are given in Scheme 2 [where numerals 1–3(297) indicate the protonated compounds proposed]. The m/z 233 ion is explained by the loss of HNO_3 (63 u), indicating that a hydrogen is available for HNO_3 loss in the three compounds. The two first-eluting compounds [1 and 2(297)] also reveal a weak m/z 142 ion, indicating that the sulfate and nitrooxy groups are spatially close. Furthermore, in addition to m/z 97 [HSO_4^-], it can be seen that the m/z 296 \rightarrow m/z 233 MS^3 spectra show a m/z 81 ion corresponding to HSO_3^- . It is worth noting that this ion is not formed from the corresponding m/z 294 α -pinene derivatives, where instead m/z 80 [SO_3^{--}] is generated upon fragmentation of m/z 231.

In order to further support the proposed structures shown in Scheme 2 and gain insight into the formation mechanism of these compounds in *d*-limonene SOA, a limonaketone/ H_2O_2 /NO/highly acidic seed experiment was conducted. As shown in Figure 3S (Supporting Information), this experiment (Figure 3Sc, Supporting Information) produced three m/z 296 compounds with the same RTs and accurate masses as those observed in the *d*-limonene and β -phellandrene + *d*-limonene experiments (Figures 3Sa and 3Sb, respectively, Supporting Information). Additionally, comparison of the MS^2/MS^3 data collected for the three m/z 296 compounds observed in both the *d*-limonene (Figure 7) and limonaketone (Figure 4S, Supporting Information) H_2O_2 /NO/highly acidic seed experiments show comparable mass spectral properties and, as a result, conclusively indicate that the further oxidation of limonaketone in the presence of NO_x and highly acidified sulfate seed aerosol produces these m/z 296 nitrooxy organosulfates in *d*-limonene SOA. On the basis of the interpretation of both the accurate

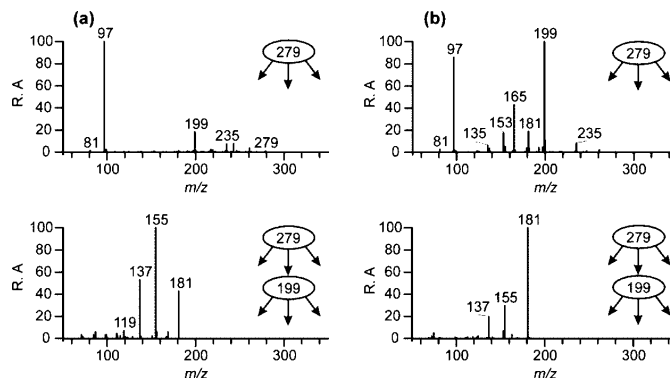


Figure 19. MS²/MS³ data for the first- (18.9 min) and second-eluting (19.7 min) m/z 279 compounds from the SEARCH sample (CTR 6/11/04).

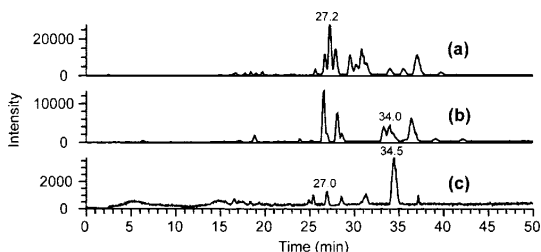


Figure 20. MS² (m/z 310) TICs obtained from (a) an α -pinene/ H_2O_2 /NO/highly acidic seed experiment, (b) a β -pinene/ H_2O_2 /NO/highly acidic seed experiment, and (c) a SEARCH sample (BHM 6/20/04). The compounds with RTs of 27.0 and 34.5 min from the ambient sample are denoted by 1 and 2(311) in the text and Scheme 6.

mass and tandem MS data, Figure 8 shows the proposed formation mechanism for the three major m/z 296 nitrooxy organosulfates observed in the laboratory-generated *d*-limonene SOA. As proposed for the m/z 294 α -pinene derivatives, the m/z 296 compounds are formed from the reactive uptake of isomeric hydroxynitrate gas-phase products by esterification of the hydroxyl groups with sulfuric acid. Notably, previous gas-phase measurements using proton-transfer reaction (PTR)-MS for *d*-limonene/ NO_x photooxidation experiments observed an organic nitrate species of MW 217 in the gas phase,⁸² thus further supporting the proposed reaction mechanism. Compounds 1 and 2(297) are likely stereoisomers (i.e., enantiomers) formed directly from the reactive uptake of the hydroxynitrate that results from the reaction of the RO_2 radical of limonaketone with NO; however, analogous to the proposed formation mechanism of compounds 1 and 2(295) in α -pinene SOA, compound 3(297) likely forms from the hydroxynitrate that results from isomerization (i.e., hydrogen rearrangement) of the β -hydroxyalkyl radical of limonaketone.

The three m/z 296 compounds observed in the ambient sample (Figure 3Sd, Supporting Information, and Figure 6b) were initially considered as *d*-limonene SOA products since their elemental compositions (i.e., $C_9H_{14}NO_8S^-$) were exactly the same as those observed in the limonene SOA experiments (Figure 3Sa–c, Supporting Information). Despite some differences in the RTs, careful inspection of the MS²/MS³ data shown in Figure 5S (Supporting Information) revealed notable differences in the mass spectral properties of the ambient m/z 296 compounds as compared to those in the *d*-limonene SOA experiments (Figure 7). The trace m/z 296 compound eluting

at 24.0 min in Figure 6b corresponds with the second-eluting m/z 296 compound from *d*-limonene SOA [2(297)]. Comparison of their respective MS²/MS³ spectra (Figure 7b and Figure 5Sb, Supporting Information) supports this conclusion; the MS² spectrum obtained for the trace m/z 296 compound in the ambient sample reveals some additional interfering ions (i.e., at m/z 237, 179, and 137) compared to that of *d*-limonene SOA, but the m/z 296 \rightarrow m/z 233 MS³ spectra compare reasonably well, suggesting that the precursor of this compound is likely *d*-limonene. However, the two other major m/z 296 compounds from the ambient sample have RTs at 22.4 and 27.5 min that are different from those of the *d*-limonene SOA compounds. The third-eluting compounds from both samples have slightly different RTs (difference of only 0.8 min), but their MS²/MS³ data are virtually similar, suggesting a very close structural relationship. These results allowed us to conclude that the m/z 296 compounds observed in the ambient samples could originate from limonene-like monoterpene precursors; specifically, these precursors require the presence of two or more double bonds, with at least one of these double bonds located at a terminal position, whereupon oxidation of this bond type under intermediate-/high- NO_x conditions, allows for the formation of a C_9 ketone/aldehyde precursor. Importantly, it should be noted that the other monoterpenes with two double bonds (i.e., α - γ -terpinene and terpinolene), neither of which are at a terminal position, which were examined in the present study (Table 2), did not produce m/z 296 compounds.

As previously noted, emissions of myrcene have been measured to be substantial during summertime conditions from loblolly pine (*Pinus taeda* L.).^{79,80} Even though α - and β -pinene are the most abundant monoterpenes emitted from this prevalent timber species found in the southeastern U.S., prior studies have shown that myrcene is emitted more abundantly than limonene,^{79,80} making myrcene a likely candidate for the source of the major m/z 296 compounds found in ambient aerosol collected from this region. It would be worthwhile to evaluate whether myrcene, as well as ocimene (a known isomer of myrcene that is abundantly emitted from broadleaf trees),⁸¹ serves as the precursor for the m/z 296 compounds observed in ambient aerosol by conducting further laboratory investigations. In addition, it should be kept in mind that there are still unknown terpene-like compounds in the atmosphere that show substantial OH reactivity and remain to be identified.⁸³

5.1.3. m/z 249. Figure 9 compares the UPLC/(–)ESI-TOFMS EICs of m/z 249 obtained from three selected monoterpene oxidation experiments, which include α -pinene/ NO_3 /highly

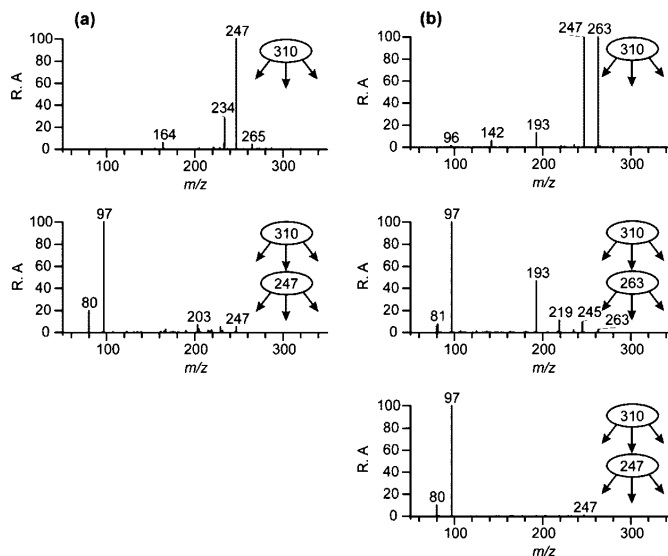
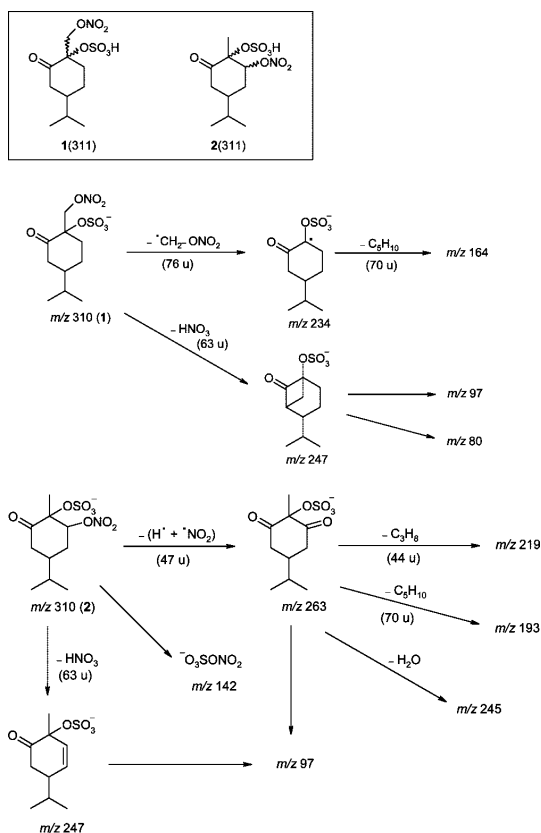


Figure 21. MS²/MS³ data for the *m/z* 310 compounds with RTs of (a) 27.0 min and (b) 34.5 min from the SEARCH sample (BHM 6/20/04).

SCHEME 6



acidic seed, α -pinene/H₂O₂/NO/highly acidic seed, and β -pinene/H₂O₂/NO/highly acidic seed experiments, to that of one representative SEARCH field sample (CTR 6/11/04). Accurate mass data for all chromatographic peaks highlighted in this

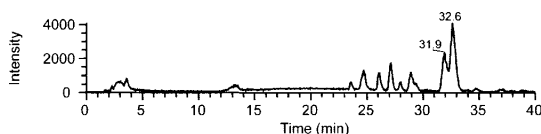


Figure 22. MS² (*m/z* 373) TIC obtained from a SEARCH sample (BHM 6/20/04). The compounds with RTs of 31.9 and 32.6 min are denoted by **1**(374) and **2**(374) in the text and Scheme 7.

figure indicate that the $[M - H]^-$ ion formula for both the laboratory-generated (Figure 9a–c) and ambient *m/z* 249 compounds (Figure 13d) is C₁₀H₁₇O₅S[−]. Even though other monoterpenes shown in Tables 1S–6S (Supporting Information) also produced *m/z* 249 compounds (i.e., *d*-*l*-limonene and terpinolene), α - and β -pinene were the only monoterpenes in this study to produce these compounds with the same RTs as those detected in filter samples collected from the SEARCH network (Table 8S, Supporting Information), and as a result, detailed tandem MS experiments were conducted in order to confirm that α -pinene and/or β -pinene were the source of these compounds in ambient aerosol collected from the southeastern U.S.

Figure 10 shows the MS² spectra for the two *m/z* 249 compounds from the β -pinene/H₂O₂/NO/highly acidic seed experiment and a SEARCH sample (BHM 6/20/04), which have exactly the same RTs (i.e., 24.4 and 29.3 min using the HPLC/ESI-LITMS technique). In addition, Figure 11 shows the MS² spectra for the two *m/z* 249 compounds from the α -pinene/H₂O₂/NO/highly acidic seed experiment and a SEARCH sample (CTR 6/11/04), which also have exactly the same RTs (i.e., 31.2 and 32.2 min using the HPLC/ESI-LITMS technique). It should be noted that the two ambient *m/z* 249 compounds with the same RTs as those found in the α -pinene SOA were not detected in every field sample using the UPLC/(−)ESI-TOFMS technique (Table 8S, Supporting Information); in fact, only trace amounts were observed for those samples containing these compounds, differing from the relatively large signals observed for the β -pinene *m/z* 249 organosulfates in ambient aerosol. It can be seen that the *m/z* 249 MS² spectra of the compounds from both the β -pinene and ambient samples with the same RTs perfectly

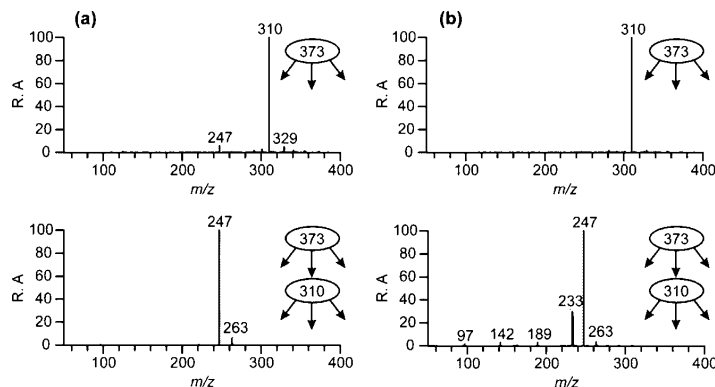
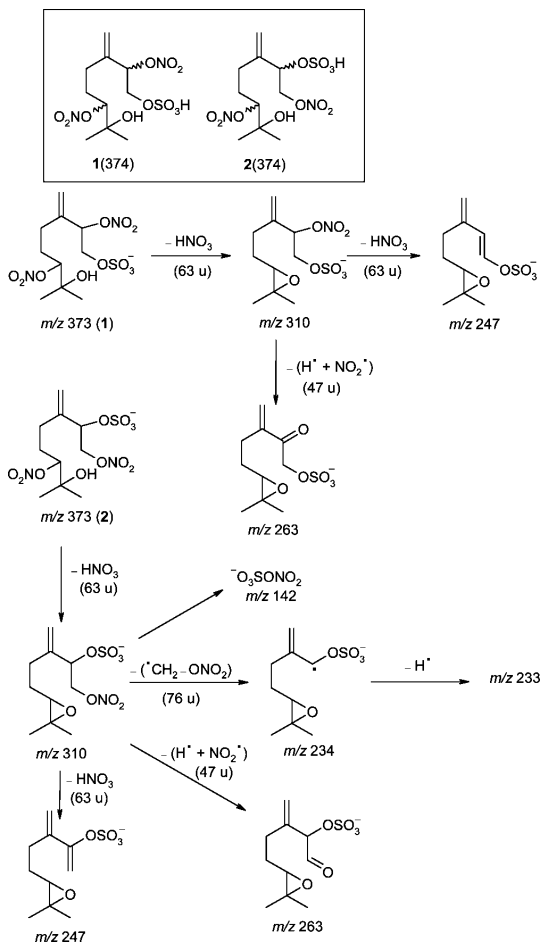


Figure 23. MS²/MS³ data for the *m/z* 373 compounds with RTs of (a) 31.9 min and (b) 32.6 min from a SEARCH sample (BHM 6/20/04).

SCHEME 7



agree. Plausible isomeric structures are given in Figure 12 and Scheme 3 [where numerals 1–4(250) indicate the protonated compounds proposed]; the second-eluting β -pinene compound 2(250) is assigned to the isomer with a terminal hydroxyl group based on the loss of a hydrogen molecule giving rise to *m/z* 247 and subsequent loss of SO₃ (80 u) yielding *m/z* 167 in its

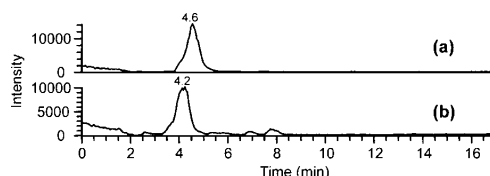


Figure 24. MS² (*m/z* 244) TICs obtained from (a) an isoprene/NO₃/SO₂ EPA photooxidation experiment and (b) a SEARCH sample (CTR 6/11/04).

m/z 249 MS² spectrum. The fragmentation behavior of both β -pinene isomers [i.e., compounds 1 and 2(250)] is distinctly different with regard to the formation of *m/z* 97 [HSO₄[−]]; while *m/z* 97 is virtually absent from the *m/z* 249 MS² spectrum of the second-eluting isomer 2(250), the formation of *m/z* 97 is favored in the first-eluting isomer 1(250), resulting in the base peak. The α -pinene isomers [i.e., compounds 3 and 4(250)] also reveal a quite different fragmentation behavior. The *m/z* 249 MS² spectrum of the first-eluting α -pinene isomer shows *m/z* 249 as base peak and product ions at *m/z* 231 and 151 due to the loss of water and the combined loss of water and SO₃, respectively. As in the case of the β -pinene isomers, notable abundance differences are observed for *m/z* 97 [HSO₄[−]]; while *m/z* 97 is virtually absent from the *m/z* 249 MS² spectrum of the first-eluting isomer 3(250), the formation of *m/z* 97 is favored in the second-eluting isomer 4(250).

In addition to the tentatively proposed structures, Figure 12 shows the proposed reaction scheme for the formation of the *m/z* 249 organosulfates observed in ambient aerosol collected from the southeastern U.S. The oxidation of α - and β -pinene is expected to occur primarily through reaction with OH radicals, owing to the fact that H₂O₂ was employed as the OH radical source in both photooxidation experiments; however, as shown in Figure 9a, α -pinene + NO₃ cannot be ruled as a source for compounds 3 and 4(250) until nighttime-segregated samples from the southeastern U.S. are analyzed. On the basis of the latter result, β -pinene + NO₃ may also contribute to the formation of compounds 1 and 2(250); thus, this route cannot be excluded as a possible source at this time. Even though negligible amounts of O₃ were initially present at the start of each experiment, O₃ formation occurs during the course of the experiments, resulting from the photochemical conversion of NO to NO₂. In the case of β -pinene, even at ~500 ppb of O₃, which is the maximum mixing ratio of O₃ when β -pinene is still present, the reaction rate of β -pinene + OH is still nine times that of β -pinene + O₃. As previously observed in isoprene

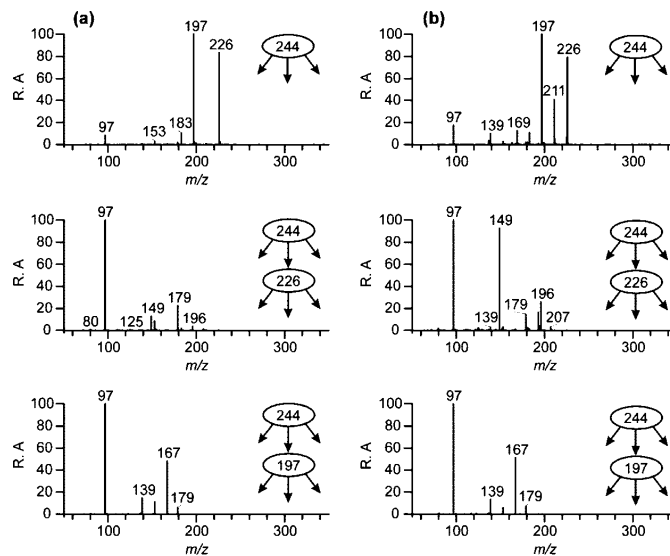


Figure 25. MS²/MS³ data for the *m/z* 244 compounds from (a) an isoprene/NO₃/SO₂ EPA photooxidation experiment and (b) a SEARCH sample (CTR 6/11/04).

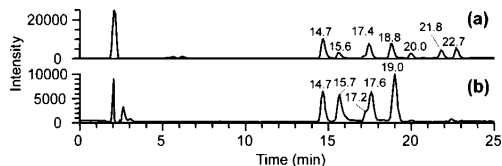


Figure 26. MS² (*m/z* 305) TICs obtained from (a) from an isoprene/NO₃/SO₂ EPA photooxidation experiment and (b) a SEARCH sample (CTR 6/11/04). The compounds with RTs of 15.7 and 19.0 min in the ambient sample are denoted by **2**(306) and **4**(306) in the text and Scheme 9.

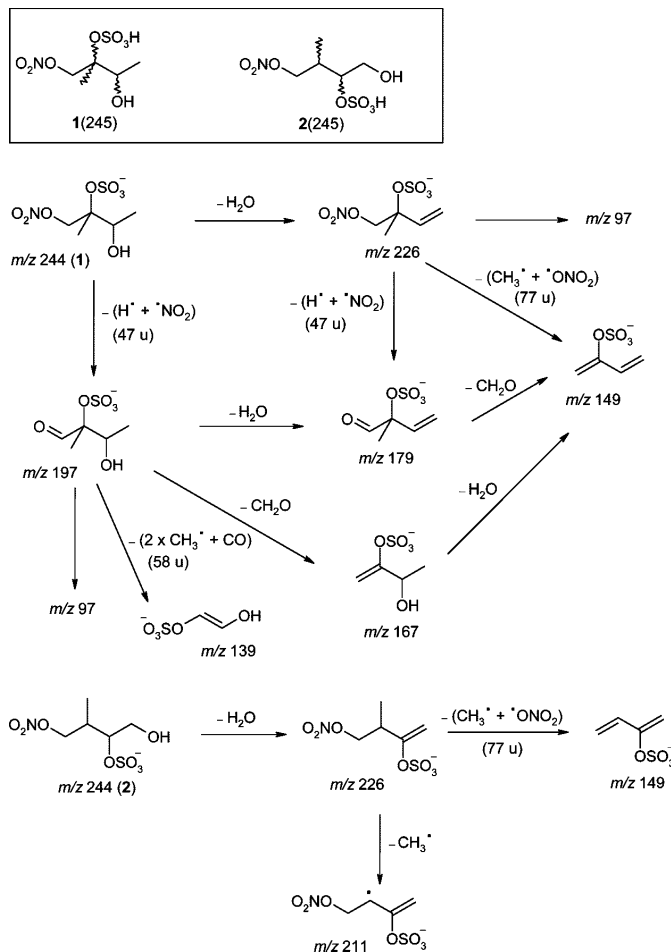
photooxidation experiments,^{4,13,33} the NO mixing ratio needs to approach zero before significant levels of O₃ form; however, by this time, most of the hydrocarbon is typically reacted away by OH radicals.

Although we propose that the OH radical oxidation is primarily responsible for the formation of the *m/z* 249 organosulfates in southeastern U.S. aerosol, Iinuma et al.²⁶ have shown that β -pinene ozonolysis in the presence of acidified sulfate seed aerosol can also produce compound **1**(250) in PM_{2.5} aerosol from a German Norway-spruce-dominated forest; specifically, similar tandem MS and accurate mass data were obtained for compound **1**(250) of this study, suggesting that O₃ may play a role in forming these compounds under polluted conditions. Instead of forming the *m/z* 249 organosulfates by reactive uptake of pinanediol gas-phase intermediates, as shown in Figure 12, Iinuma et al.²⁶ have proposed that these compounds also form by the reactive uptake of β -pinene oxide when the oxidation of β -pinene is initiated by O₃. Interestingly, this prior study found that α -pinene ozonolysis in the presence of acidic seed particles exhibited a distinctly different behavior; specifically, this experiment did not produce a corresponding organosulfate at *m/z* 249, which was attributed to α -pinene + O₃ likely following a ring-opening primary ozonide pathway rather than a ring-retaining oxirane pathway (like that for β -pinene) owing to the fact that the α -pinene primary ozonide structure is relatively strained.

Similar to previous work done with glyoxal and pinonaldehyde,^{48–50} it would be worthwhile to perform reactive uptake experiments using the pinanediol and epoxide intermediates only in the presence of acidified sulfate seed aerosol, as this could help establish the reaction mechanism responsible for the formation of these organosulfates in ambient aerosol. Considering that the α -pinene/NO₃/highly acidic seed experiment (Figure 9a) also produced the *m/z* 249 α -pinene organosulfates detected in ambient aerosol (Figure 9d), as well as α -pinene oxide being detected in the gas phase at measurable yields under nighttime oxidation conditions,^{84–86} it will be crucial to analyze nighttime-segregated filter samples collected from the SEARCH network in order to evaluate the importance of this reaction pathway to the formation of these compounds in ambient aerosol. Additionally, β -pinene/NO₃/highly acidic seed experiments should be conducted in the future, owing to the fact that measurable quantities of β -pinene oxide have also been observed in the gas phase from β -pinene + NO₃ reactions.⁸⁷ Further work should also investigate the source for the differences in the relative abundances of the *m/z* 249 α - and β -pinene organosulfates.

5.1.4. *m/z* 227. Figures 13 and 14 show *m/z* 227 MS² TICs obtained from the α -pinene/H₂O₂/NO/highly acidic seed experiment and a SEARCH sample (BHM 6/20/04) and MS²/MS³ data for the *m/z* 227 compounds from the α -pinene SOA sample and *m/z* 227 compounds eluting at the same RT from the ambient sample, respectively. In a prior study by Gómez-González et al.,⁴⁶ polar early-eluting *m/z* 227 compounds from K-pusztas aerosol with comparable RTs as those found in the present study were identified as sulfate esters of 2- and 3-hydroxyglutaric acid, as shown in Scheme 4 [where numerals **1** and **2**(228) indicate the protonated forms of 3- and 2-hydroxyglutaric acids, respectively], of which 3-hydroxyglutaric acid was attributed to an α -pinene SOA product⁸⁸ and 2-hydroxyglutaric acid was proposed to be an oxidation product of unsaturated fatty acids. It can be seen in the *m/z* 227 \rightarrow *m/z* 147 MS³ spectrum of the α -pinene SOA product (Figure 14a) that both *m/z* 129 and *m/z* 85 are produced, which are characteristic product ions of deprotonated 2- and 3-hydroxy-

SCHEME 8



glutaric acid,⁴⁶ respectively; these data indicate that the *m/z* 227 α-pinene SOA product is a mixture of sulfated 2- and 3-hydroxyglutaric acids. Furthermore, the UPLC/(−)ESI-TOFMS accurate mass data indicated that the elemental composition of both the laboratory-generated and ambient *m/z* 227 compounds is C₅H₇O₈S[−], confirming that these compounds are likely formed from either 2- or 3-hydroxyglutaric acids in ambient aerosol.

The *m/z* 227 MS²/MS³ data obtained from the SEARCH sample (BHM 6/20/04) are comparable with those reported from K-pusztai aerosol.⁴⁶ It is noted that *m/z* 129 dominates the *m/z* 227 → *m/z* 147 MS³ spectrum (Figure 14b), indicating that sulfated 2-hydroxyglutaric acid is the prevalent isomer in the SEARCH sample. This suggests that 2-hydroxyglutaric acid has precursors other than α-pinene, possibly unsaturated fatty acids as proposed in our prior study.⁴⁶ Besides the α-pinene/H₂O₂/NO/highly acidic seed experiment, none of the other monoterpenes studied in the present work produced laboratory-generated *m/z* 227 organosulfates (see Tables 2 and Tables 1S–6S, Supporting Information); however, owing to substantial emission rates of myrcene and ocimene in the southeastern U.S. during summertime conditions,^{79–81} future laboratory experiments are needed to determine their potential for the formation of *m/z* 227 organosulfates found in ambient aerosol. Additionally, from our

experimental work, it appears that the formation of the *m/z* 227 α-pinene organosulfates in ambient aerosol requires the presence of NO_x, consistent with recent work showing that the 3-hydroxyglutaric acid precursors, and likely 2-hydroxyglutaric acid, form from the further oxidation of *cis*-pinonic acid by OH radicals in the presence of NO.^{88,89}

5.1.5. *m/z* 279. Even though recent work identified a *m/z* 279 compound as an organosulfate in southwestern U.S. aerosol,⁵² the source and formation mechanism of this compound remained unclear. Our initial characterization of organic aerosol collected from the SEARCH network did not observe an ion at *m/z* 279, likely owing to the lower sensitivity of the (−)ESI-MS techniques employed.⁴⁷ Figure 15 compares the UPLC/(−)ESI-TOFMS EICs of *m/z* 279 obtained from three selected monoterpene oxidation experiments, which include α-pinene/H₂O₂/NO/highly acidic seed, α-pinene/NO₃/highly acidic seed, and β-pinene/H₂O₂/NO/highly acidic seed experiments, to that of one representative SEARCH field sample (CTR 6/11/04). Accurate mass data for all chromatographic peaks highlighted in this figure indicate that the [M − H][−] ion formula for both the laboratory-generated (Figure 15a–c) and ambient *m/z* 279 compounds (Figure 15d) is C₁₀H₁₅O₇S[−]. Although other monoterpene oxidation experiments (i.e., *d*-*l*-limonene and α-*l*-

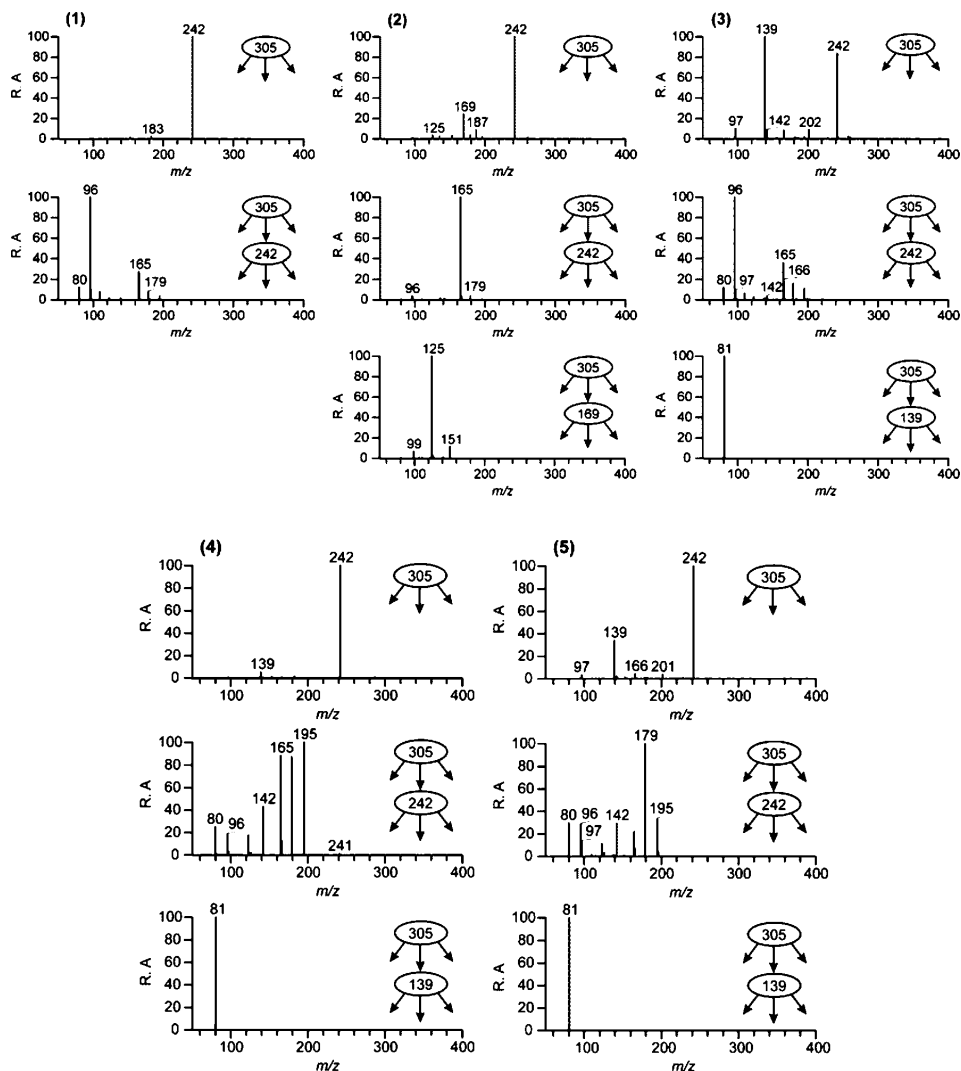


Figure 27. MS²/MS³ data obtained for the five first-eluting *m/z* 305 compounds from an isoprene/NO_x/SO₂ EPA photooxidation experiment. It is noted that MS²/MS³ data obtained for the three last-eluting *m/z* 305 compounds from the same isoprene experiment (Figure 26a) are shown in Figure 8S (Supporting Information).

terpinene) produced *m/z* 279 SOA compounds with the same elemental compositions as those observed in ambient aerosol, α - and β -pinene were the only monoterpenes in this study to produce these compounds with the same RTs as those detected in all SEARCH filter samples (Table 8S, Supporting Information), and as a result, detailed tandem MS experiments were conducted in order to confirm that α - and β -pinene were the source of these compounds.

Figures 16–19 show *m/z* 279 MS² TICs from an α -pinene/H₂O₂/NO/highly acidic seed experiment and a SEARCH sample (CTR 6/11/04) and MS²/MS³ data for the two first-eluting *m/z* 279 compounds from the α -pinene and β -pinene SOA samples and the two *m/z* 279 compounds eluting at the same RTs in the ambient sample, respectively. It can be seen that the *m/z* 279 MS² spectra are distinctly different for the two first-eluting α -pinene SOA products (Figure 17); *m/z* 97 [HSO₄⁻] is the base peak in the case of the first-eluting compound 1(280), while

m/z 199 due to loss of SO₃ dominates the *m/z* 279 MS² spectrum of the second-eluting isomer 2(280). Different possible isomeric structures corresponding to sulfated hydroxypinonic acids can be suggested for the *m/z* 279 compounds. In this respect, it is worth mentioning that 10-hydroxypinonic acid (MW 200) has been reported by Larsen et al.⁹⁰ as a photooxidation product formed through reaction of the OH radical of both α - and β -pinene but that multiple isomers of MW 200 were observed in each case. In addition, three isomeric hydroxypinonic acids with hydroxyl groups at the 1-, 4-, and 10-positions have been considered as α -pinene SOA products formed under photooxidation and ozonolysis conditions by Winterhalter et al.⁹¹ It can be seen that the MS²/MS³ data of the α -pinene SOA compounds (Figure 17) and those eluting at the same RTs of the ambient sample (Figure 19) are fairly similar. However, comparison of the MS²/MS³ data of the α -pinene SOA compounds (Figure 17) with those of the β -pinene SOA compounds with exactly

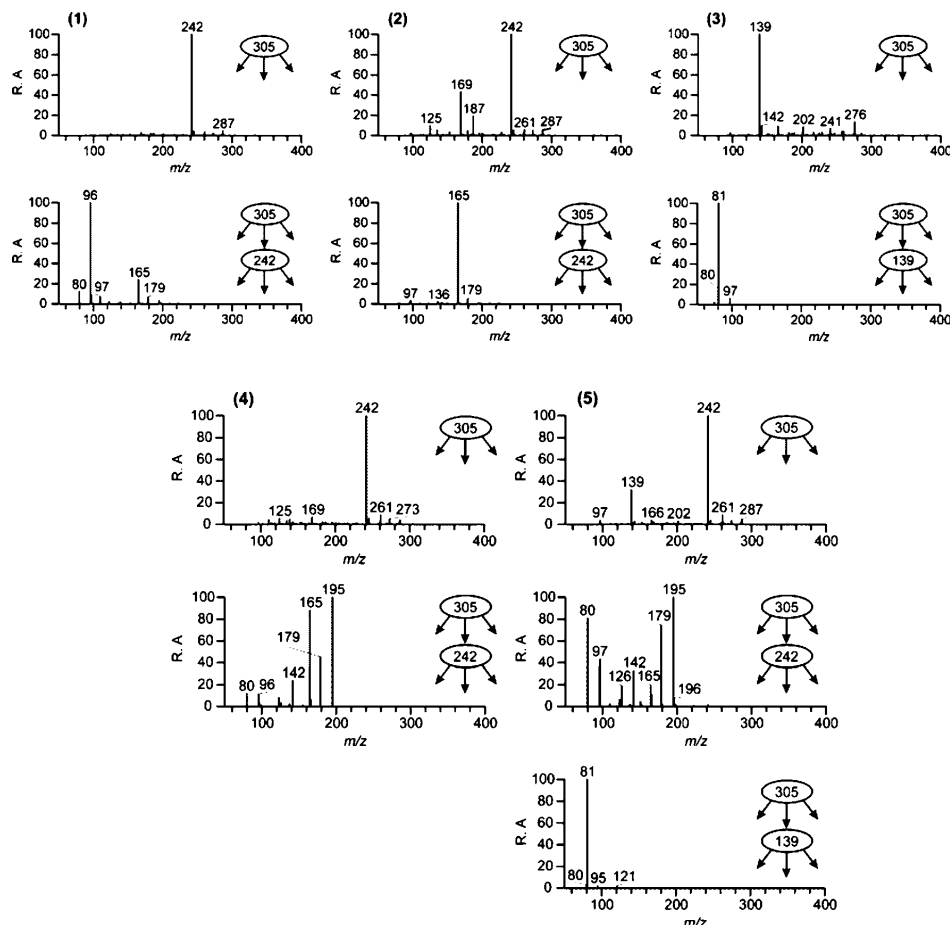


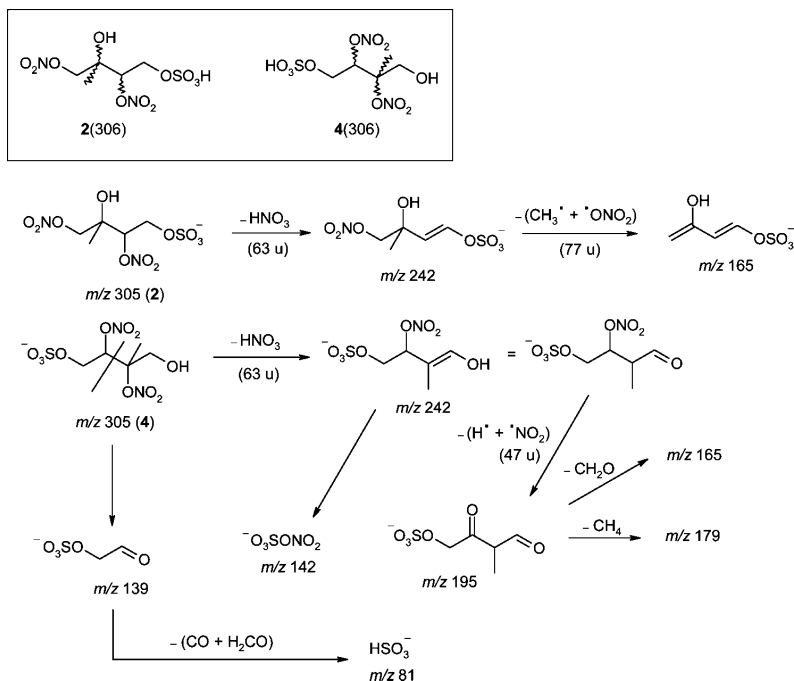
Figure 28. MS²/MS³ data obtained for the five m/z 305 compounds from a SEARCH sample (CTR 6/11/04).

the same RTs reveals some differences which are, at present, not understood; more specifically, the m/z 279 \rightarrow m/z 199 MS³ spectra are similar in the case of the β -pinene compounds, in contrast to those obtained for the α -pinene compounds. On the basis of the interpretation of the MS²/MS³ data and the known elemental composition of the m/z 279 ions determined from the accurate mass measurements, tentative structures and explanations for the observed product ions are proposed in Scheme 5 [where numerals 1 and 2(280) indicate the protonated compounds proposed] for the two m/z 279 organosulfates found in southeastern U.S. organic aerosol. Additional research is required to confirm the chemical structures of the m/z 279 compounds and understand the MS behaviors of these compounds.

5.1.6. m/z 310. Figures 20 and 21 show m/z 310 MS² TICs obtained from the α - and β -pinene/H₂O₂/NO/highly acidic seed experiments and a representative SEARCH sample (BHM 6/20/04) and MS²/MS³ data for the two major m/z 310 compounds from the ambient sample, respectively. MS²/MS³ data for the m/z 310 compounds eluting at similar RTs from the α - and β -pinene SOA samples are given in Figure 6S (Supporting Information). Interestingly, in addition to α - and β -pinene, the α - and γ -terpinene/H₂O₂/NO/highly acidic seed experiments also produced m/z 310 compounds (Tables 3S and 4S, Supporting Information); however, their RTs did not correspond to any of

the ambient m/z 310 compounds and, as a result, were not considered as possible sources for these compounds. It is worth noting that the MS²/MS³ data for the selected compounds from the α - and β -pinene SOA, as well as those from the ambient sample, are strikingly different. On the basis of these data, it may be concluded that the m/z 310 compounds from the ambient sample originate from BVOC precursors other than α - and β -pinene, even though both the laboratory and ambient m/z 310 compounds share a common elemental composition of C₁₀H₁₆NO₈S⁻ (Tables 1S, 6S, and 8S, Supporting Information). In the following discussion, we will consider only the two m/z 310 compounds from the ambient sample. The m/z 310 MS² spectrum of the first-eluting compound 1(311) contains m/z 247 due to loss of HNO₃, consistent with the presence of a nitrooxy group, while the m/z 310 \rightarrow m/z 247 MS³ spectrum reveals m/z 97 [HSO₄⁻] and m/z 80 [SO₃⁻], characteristic features of a sulfate group. Another characteristic fragmentation is the loss of 76 u (m/z 234), corresponding to a CH₂-ONO₂ radical and pointing to a terminal CH₂-ONO₂ group. The m/z 310 MS² spectrum of the second-eluting major compound 2(311) shows m/z 142, indicating that the sulfate and nitrooxy groups in the molecule are proximate. Other diagnostic ions include m/z 263 due the combined loss of H and NO₂ radicals, and m/z 245, 219, and 193 due to a subsequent loss of H₂O, C₃H₈, and C₅H₁₀,

SCHEME 9



respectively. Taking into account the fragmentation behaviors and the elemental compositions, tentative structures are proposed for the m/z 310 compounds from the ambient sample in Scheme 6 [where numerals 1 and 2(311) indicate the protonated compounds proposed]. The major nitrooxy organosulfate compound 2(311) can be related to p -menth-6-en-2-one, a known constituent of the essential oil of many plants, e.g., *Eucalyptus* species.⁹² Additionally, as suggested for the m/z 294, 296, and 279 organosulfates, photooxidation experiments of myrcene and ocimene in the presence of NO_x and acidified sulfate seed aerosol may provide additional insights into the sources of the m/z 310 compounds, especially owing to their high emission strengths from coniferous and deciduous trees during summertime conditions in the U.S.^{79–81}

5.1.7. *m/z* 373. Iinuma et al.²⁶ previously determined that the elemental composition of $[M - H]^-$ ions at *m/z* 373 detected in ambient aerosol collected from a forested site in Europe by (-)ESI-MS techniques is $C_{10}H_{17}N_2O_{11}S^-$. This prior study observed these compounds only in nighttime samples. On the basis of the mass spectral behaviors of these previously detected compounds, tentative structures were proposed containing two nitrooxy groups, and monoterpenes containing two double bonds (e.g., limonene) were suggested as the BVOC precursors; however, no laboratory experiments were conducted to confirm these structures.

Figure 7S (Supporting Information) compares the UPLC/(-)ESI-TOFMS EICs of m/z 373 obtained from two monoterpene experiments conducted in the present study, which include the *d*-limonene/H₂O₂/NO/highly acidic seed and β -phellandrene + *d*-limonene/H₂O₂/highly acidic seed experiments, to that of one representative SEARCH field sample (BHM 6/20/04). Accurate mass data for all chromatographic peaks highlighted in this figure indicates that the $[M - H]^-$ ion formula for both the laboratory-generated (Figure 7Sa-b, Supporting Information)

and ambient m/z 373 compounds (Figure 7Sc, Supporting Information) is $C_{10}H_{17}N_2O_{11}S^-$. In addition to *d*-limonene and β -phellandrene, the photooxidation of all other monoterpenes containing two double bonds, which included α -terpinene, γ -terpinene, and terpinolene (Tables 3S–5S, respectively, Supporting Information), also produced m/z 373 compounds with the same elemental compositions as those observed in the ambient samples (Table 8S, Supporting Information); however, none of these compounds have the same RTs as those found in the ambient samples, indicating that some other monoterpene not examined in the present study is likely the source. Unlike the photooxidation experiments, it is worth noting that the *d*-limonene/ NO_3 /highly acidic experiment did not produce m/z 373 compounds, likely resulting from the large nucleation event observed at the start of the experiment and, as a result, preventing the reactive uptake of gas-phase precursors. From our set of laboratory data (Tables 2 and 1S–6S, Supporting Information), it now appears that monoterpenes with one double bond do not contribute to the formation of these compounds in ambient aerosol.

To gain insight into the source of the compounds, Figures 22 and 23 show m/z 373 MS² TICs obtained from a representative SEARCH sample (BHM 6/20/04) and the MS²/MS³ data for the two major compounds **1** and **2**(373) found in the ambient aerosol, respectively; it should be noted that both the HPLC/(−)ESI-LITMS and UPLC/(−)ESI-TOFMS techniques observed these two major late-eluting m/z 373 compounds (Figures 22 and 7Sc, Supporting Information). In agreement with the findings of Iinuma et al.,²⁶ the m/z 373 MS² spectra are very similar for the two compounds, revealing m/z 310 (loss of HNO₃) as the base peak. Subsequent fragmentation of m/z 310 proceeds through a second loss of HNO₃, affording m/z 247. In the case of compound **2**(373), the m/z 373 → m/z 310 MS³ spectrum also shows an ion at m/z 234 due to the loss of a

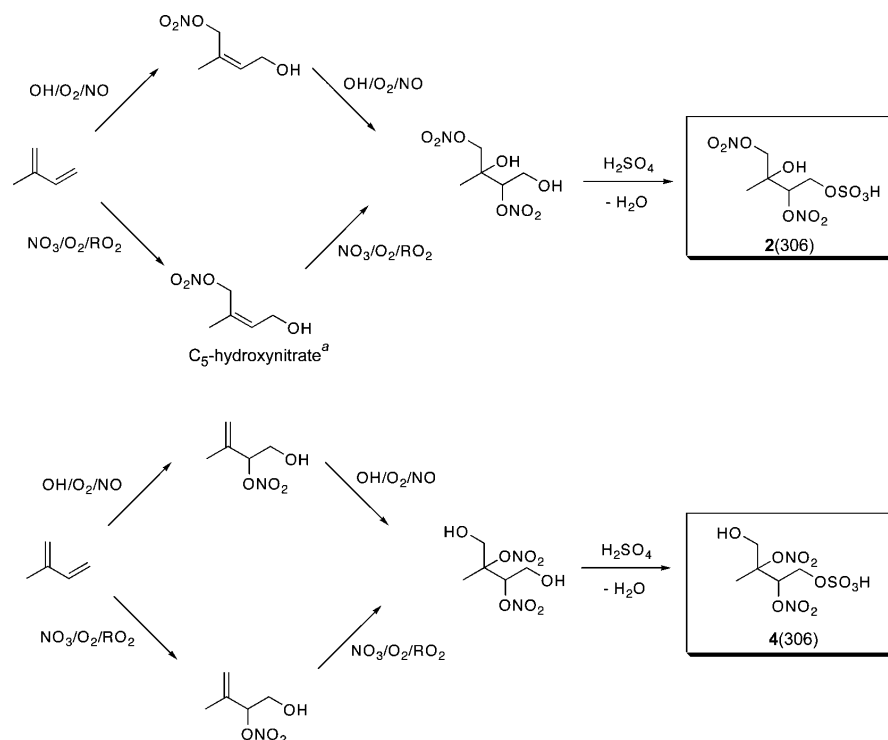


Figure 29. Proposed formation mechanism for the two major m/z 305 nitrooxy organosulfate isomers observed in ambient aerosol (Figure 26b) from either the photooxidation of isoprene in the presence of NO_3 or the NO_3 -initiated oxidation of isoprene under dark conditions, with both in the presence of acidified sulfate seed aerosol. Numerals 2 and 4(306) correspond to the isomeric structural assignments based upon the explanations shown in Scheme 9 for the observed product ions formed in the tandem MS experiments. Footnote *a*: Ng et al.⁹³ observed a hydroxynitrate species of this MW in the gas phase from the NO_3 -initiated oxidation of isoprene under dark conditions as the $[\text{M} + \text{CF}_3\text{O}^-]$ ion using chemical ionization MS.

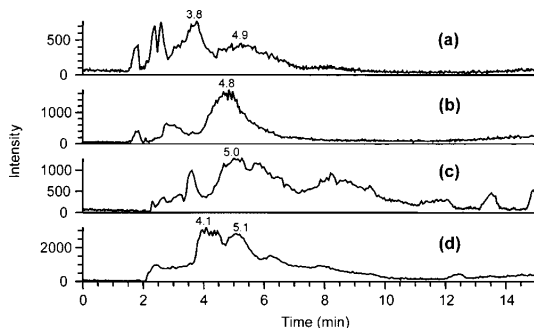


Figure 30. MS² (m/z 334 and 332) TICs obtained from (a, c) an isoprene/ NO_3/SO_2 EPA photooxidation experiment and (b, d) a SEARCH sample (CTR 6/11/04), respectively.

$\text{CH}_2\text{-ONO}_2$ radical (76 u) and m/z 233 due to subsequent loss of a hydrogen radical. Furthermore, the weak m/z 142 ion suggests that the sulfate and nitrooxy groups in the m/z 310 precursor ion are spatially close. Taking into account this fragmentation behavior and the elemental compositions determined from the accurate mass measurements (Table 8S, Supporting Information), a tentative structure with a myrcene skeleton is proposed in Scheme 7 [where numerals 1 and 2(374) indicate the protonated compounds proposed] for the m/z 373 compounds from the ambient sample. Since myrcene is one of the five major monoterpenes that are emitted from the loblolly

pine (*Pinus taeda* L.),^{79,80} a species native to the southeastern U.S., it would be worthwhile to evaluate whether myrcene serves as a precursor for the m/z 373 compounds. Additionally, other monoterpenes with multiple double bonds, such as ocimene, should also be evaluated in future laboratory experiments.

5.1.8. Uncharacterized Organosulfates Detected at m/z 239, 281, 283, 324, 326, 342, and 387 in SEARCH Samples Likely Attributable to Monoterpenes. In addition to the ions already characterized in this study, close examination of Table 8S (Supporting Information) reveals that many other $[\text{M} - \text{H}]^-$ ions detected in the field samples by the UPLC/(-)ESI-TOFMS technique have elemental compositions containing 9 or 10 carbon atoms, which indicate monoterpenes as a potential source. The $[\text{M} - \text{H}]^-$ ion formulas determined from the UPLC/(-)ESI-TOFMS accurate mass data were $\text{C}_{10}\text{H}_{17}\text{O}_7\text{S}^-$, $\text{C}_9\text{H}_{15}\text{O}_8\text{S}^-$, $\text{C}_{10}\text{H}_{14}\text{NO}_9\text{S}^-$, $\text{C}_{10}\text{H}_{16}\text{NO}_9\text{S}^-$, $\text{C}_{10}\text{H}_{16}\text{NO}_{10}\text{S}^-$, and $\text{C}_{10}\text{H}_{15}\text{N}_2\text{O}_{12}\text{S}^-$ for m/z 281, 283, 324, 326, 342, and 387, respectively. Although both m/z 239 isomers observed in the SEARCH samples have an elemental composition of $\text{C}_7\text{H}_{11}\text{O}_7\text{S}^-$, which does not clearly support a monoterpene source, the early eluting isomer has the same RT and elemental composition as that of the *d*-limonene SOA m/z 239 compound; however, additional research and characterization is needed in order to confirm *d*-limonene as the source of this early eluting compound. Notably, Lee et al.⁸² observed a gas-phase product of MW 142 from the photooxidation of *d*-limonene in the presence of NO_x and suggested that this product corresponds

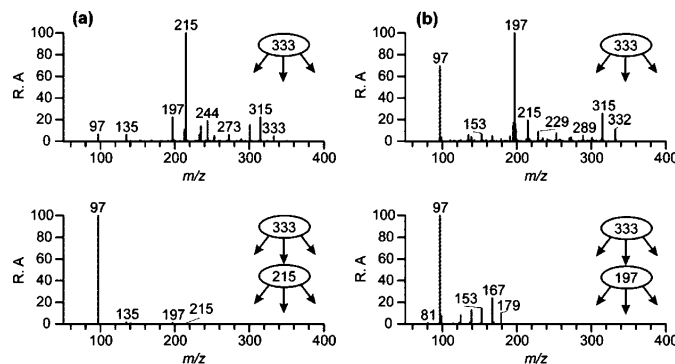


Figure 31. MS²/MS³ data obtained for the m/z 333 compounds from an isoprene/NO₂/SO₂ EPA photooxidation experiment eluting at (a) 3.8 and (b) 4.2 min.

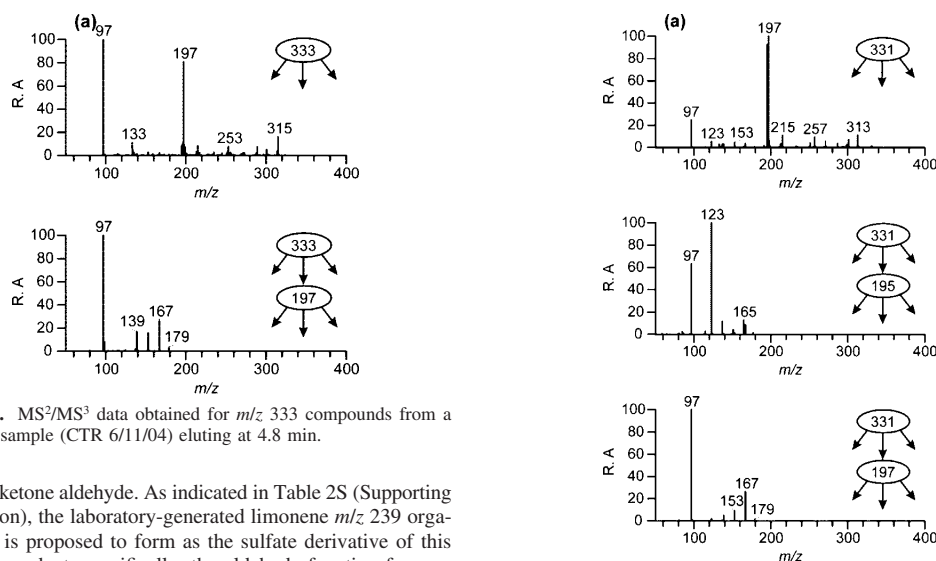


Figure 32. MS²/MS³ data obtained for m/z 333 compounds from a SEARCH sample (CTR 6/11/04) eluting at 4.8 min.

to a C₇-diketone aldehyde. As indicated in Table 2S (Supporting Information), the laboratory-generated limonene m/z 239 organosulfate is proposed to form as the sulfate derivative of this MW 142 product; specifically, the aldehyde function forms a gem-diol followed by esterification with sulfuric acid.

The m/z 281 compounds observed in the SEARCH samples have the same elemental composition of the single isomer previously observed in SOA produced from the ozonolysis of *d*-limonene in the presence of acidic seed aerosol;²⁵ however, it was found in the present study that the m/z 281 compounds produced in the *d*-limonene SOA (Table 2S, Supporting Information) do not have the same RTs as those in the ambient samples (Table 8S, Supporting Information). Further work is needed to confirm whether limonene or a limonene-like precursor is the source of these compounds. Although other monoterpenes, including α -pinene (i.e., only the H₂O₂/highly acidic seed experiment), *l*-limonene, α -terpinene, terpinolene, and β -pinene, examined in this study produced m/z 281 compounds with the same elemental compositions as those observed in the ambient aerosol, these monoterpenes are not considered as the source of these compounds owing to the differences in the RTs.

The m/z 283 organosulfate was detected only on one day (6/17/04) from the BHM SEARCH site (Table 8S, Supporting Information). Although the α -terpinene/H₂O₂/NO/highly acidic seed experiment produced one m/z 283 compound with the same elemental composition (i.e., C₉H₁₅O₈S⁻) as the compound observed in the ambient sample, this monoterpene was not considered as a source for this compound owing to the

Figure 33. MS²/MS³ data obtained for m/z 331 compounds from an isoprene/NO₂/SO₂ EPA photooxidation experiment eluting at 5.0 min.

differences in the RTs. Additionally, the β -pinene and terpinolene experiments produced m/z 283 compounds; however, these monoterpenes were also ruled out as potential sources for this compound in the ambient aerosol due to the differences in the elemental compositions. On the basis of the current laboratory findings (Tables 1S–6S, Supporting Information), monoterpenes with more than one double bond, such as myrcene and ocimene, are candidate precursors of this compound.

Despite the absence of m/z 324 nitrooxy organosulfates in the current set of monoterpene experiments (Table 2), several of the monoterpenes, including *d*-limonene, *l*-limonene, terpinolene, and β -pinene, were found to produce m/z 326 nitrooxy organosulfates. The accurate mass data for all of these laboratory-generated m/z 326 compounds indicate that these ions have an elemental composition of C₁₀H₁₆NO₉S⁻, consistent with the ambient compounds (Table 8S, Supporting Information); however, the oxidation of these monoterpenes did not produce these compounds with the same RTs and corresponding tandem MS data. As for the m/z 283 compound, our laboratory data suggest that an unidentified monoterpene is the likely source for the m/z 326 nitrooxy organosulfates.

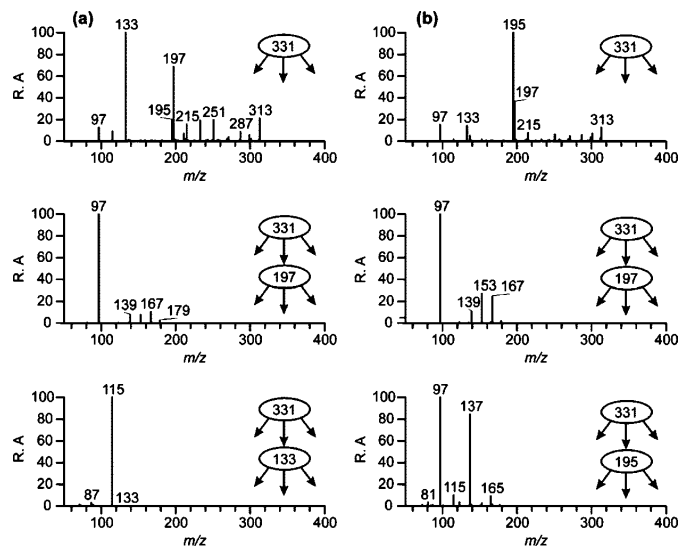
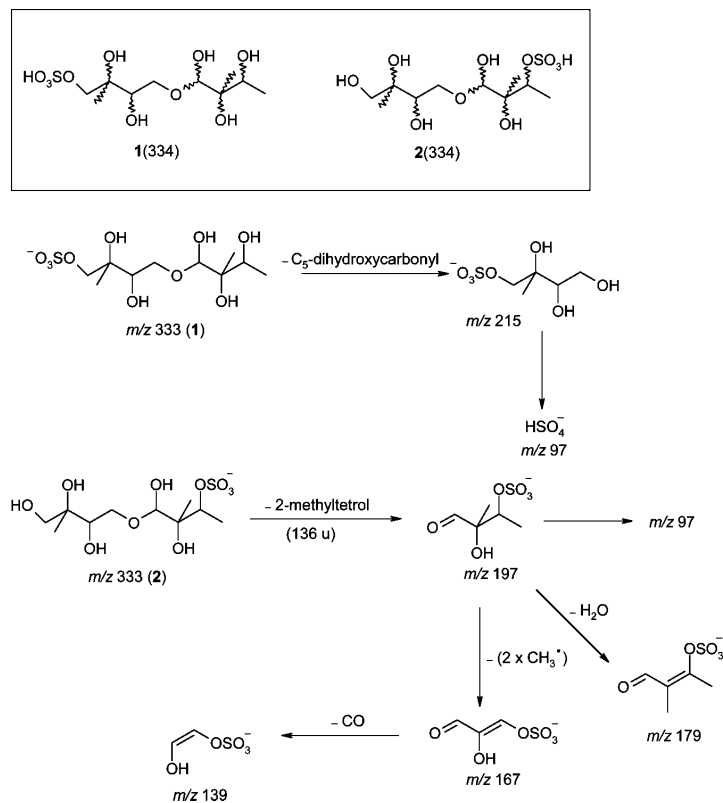


Figure 34. MS²/MS³ data obtained for m/z 331 compounds from a SEARCH sample (CTR 6/11/04) eluting at (a) 4.1 and (b) 5.1 min.

SCHEME 10



Iinuma et al.²⁶ previously detected m/z 342 compounds in aerosol collected from a forested site in Germany with the same elemental compositions (i.e., $C_{10}H_{16}NO_{10}S^-$) as those observed in the SEARCH field samples. Interestingly, this prior study observed the m/z 342 nitrooxy organosulfates only in nighttime

samples. None of the monoterpene (i.e., α -pinene, d -limonene, and l -limonene) nighttime oxidation experiments in the present study produced m/z 342 compounds; however, the photooxidation of α -pinene, β -pinene, and α -terpinene in the presence of NO_x and highly acidic seed aerosol did produce m/z 342

compounds with the same elemental compositions as those observed in the ambient samples. Although the latter experiments produced m/z 342 compounds, the monoterpenes examined in the present study are not considered as sources for these compounds in ambient aerosol owing to the differences in the RTs and in the tandem MS data. Further experimental work is needed in order to confirm and identify the source of the m/z 342 nitrooxy organosulfates, especially since these compounds have relatively large signals and many isomeric forms in the ambient aerosol.

Similar to the m/z 342 compounds, the m/z 387 compound was previously observed using (–)ESI-MS techniques in our initial characterization of ambient PM_{2.5} collected from the southeastern U.S.; however, the formation mechanism and structure of this compound were also not determined. As shown in Figure 1, the m/z 387 compound was abundantly detected on some days in the ambient aerosol. Although none of the monoterpene oxidation experiments formed a m/z 387 nitrooxy organosulfate, it is likely that this compound is formed from a monoterpene (e.g., myrcene) not examined in the current study since its elemental composition (i.e., C₁₀H₁₅N₂O₁₂S[–]) determined from the accurate mass measurements (Table 8S, Supporting Information) suggests a monoterpene part.

5.2. Organosulfates of Isoprene in Ambient Aerosol.

5.2.1. m/z 244. Figures 24 and 25 show m/z 244 MS² TICs obtained from an isoprene/NO_x/SO₂ EPA photooxidation experiment and a SEARCH sample (CTR 6/11/04) and MS²/MS³ data for the m/z 244 compounds from both samples, respectively. As shown in Tables 7S and 8S (Supporting Information), both the Caltech isoprene/H₂O₂/NO/acidic seed and isoprene/HONO/neutral seed experiments also produced m/z 244 compounds with the same RTs and elemental compositions (i.e., C₅H₁₀NO₈S[–]) as those observed in the SEARCH samples. Even though not previously detected in ambient aerosol, Surratt et al.²³ previously proposed that these laboratory-generated compounds formed from the esterification of a hydroxyl group contained within a 2-methylglyceric acid nitrate with sulfuric acid. This previous proposal now appears incorrect owing to the elemental compositions determined from the accurate mass data collected in the present study (Tables 7S and 8S, Supporting Information) as well as the MS²/MS³ data not supporting such a structure.

It can be seen that the m/z 244 MS² spectra shown in Figure 25 reveal some differences; the spectrum obtained for the ambient sample is more complex, however. In both cases, m/z 226 and 197, due to the loss of water and the combined loss of hydrogen and NO₂ radicals, respectively, are the most abundant product ions. Furthermore, it can be noted that the m/z 244 → m/z 197 MS³ spectra are similar and, moreover, show the same product ions as the m/z 260 → m/z 197 MS³ spectra obtained for nitrooxy organosulfates of 2-methyltetrols in the prior study by Gómez-González et al.⁴⁶ This leads us to propose nitrooxy organosulfate structures of C₅-alkane triols for the m/z 244 compounds. On the basis of the interpretation of the MS²/MS³ data and the known elemental composition of the m/z 244 ions determined from the accurate mass measurements, tentative structures and explanations for the observed product ions are proposed in Scheme 8 [where numerals **1** and **2**(245) indicate the protonated compounds proposed]. In the case of the isoprene SOA sample, the mass spectral behavior of the m/z 244 compound can be addressed with a structure of a nitrooxy organosulfate of 2-methyl-1,2,3-butanetriol **1**(245). In regards to the m/z 244 MS² spectrum of the ambient sample, it can be noted that an ion at m/z 211 is present, corresponding to the combined loss of water and a methyl radical. This suggests that

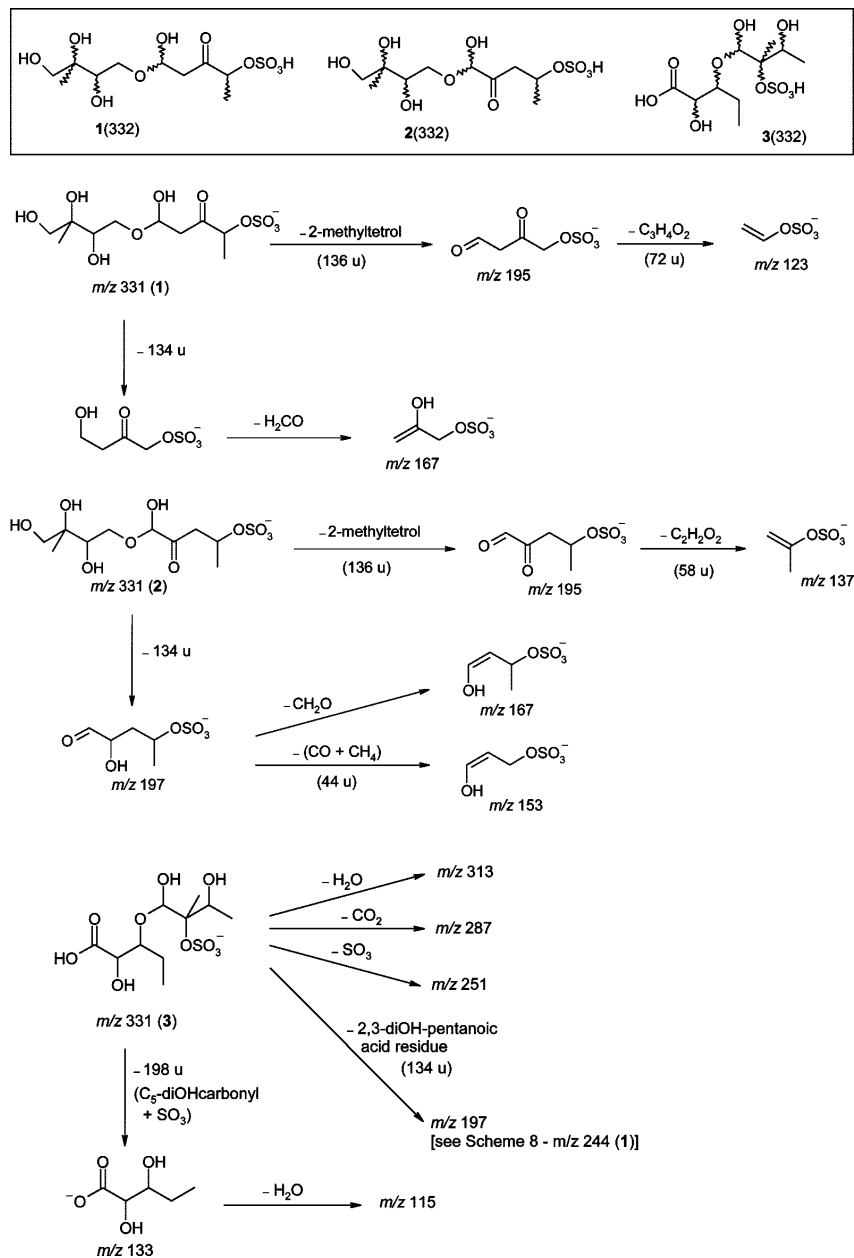
the ambient sample contains one or more additional m/z 244 isomeric compounds; the structure of a nitrooxy organosulfate of 3-methyl-1,2,4-butanetriol **2**(245) allows us to explain quite readily m/z 211 in the m/z 244 MS² spectrum, as well as the abundant m/z 149 ion in the m/z 244 → m/z 226 MS³ spectrum. The formation of C₅-alkane triols through photooxidation of isoprene has, to our knowledge, not yet been documented in the literature.

5.2.2. m/z 305. Figures 26–28 show m/z 305 MS² TICs obtained from an isoprene/NO_x/SO₂ EPA photooxidation experiment and a SEARCH sample (CTR 6/11/04) and MS²/MS³ data for the m/z 305 compounds from both samples, respectively. The m/z 305 compounds correspond to 2-methyltetrols containing one sulfate and two nitrooxy groups; hence, many stereo- and positional isomers are possible, as shown by the number of chromatographic peaks in Figure 26. Recent work of the Caltech laboratory has shown that the NO₃-initiated oxidation of isoprene under dark conditions, in the presence of either nonacidified or highly acidified sulfate seed aerosol, also produces m/z 305 compounds.⁹³ The further oxidation of a C₅-hydroxynitrate, a known first-generation gas-phase product, by NO₃ was shown to yield a dihydroxydinitrate that subsequently reacts in the particle phase by esterification with sulfuric acid. Interestingly, UPLC/(–)ESI-TOFMS accurate mass measurements made in this prior study indicated that the elemental composition of these ions is C₅H₉N₂O₁₁S[–],⁹³ consistent with the accurate mass measurements made for the m/z 305 compounds found in both the SEARCH (Table 8S, Supporting Information) and Caltech isoprene SOA samples (Table 7S, Supporting Information), and, as a result, shows that either the photooxidation (in the presence of NO_x) or nighttime oxidation of isoprene in the presence of sulfate seed aerosol leads to the formation of these compounds.

While eight isomeric m/z 305 compounds are detected in the laboratory SOA sample (Figure 26a), only the five first-eluting isomers are seen in the ambient samples. In the following discussion, we will address only the structures of two of the five major m/z 305 isomers from the ambient sample, namely, those with RTs of 15.7 min [**2**(306)] and 19.0 min [**4**(306)]. Possible structures for these compounds are proposed and supported in Scheme 9 [where numerals **2** and **4**(306) indicate the protonated compounds proposed]; insufficient MS structural information was available in the case of the three other isomers. Four of the major m/z 305 compounds from the ambient sample have m/z 242 as the base peak in their respective MS² spectra (Figure 28), corresponding to the loss of HNO₃ (63 u). In regards to compound **2**(306), the ion at m/z 165 due to the combined loss of CH₃ and ONO₂ radicals (77 u) in the m/z 305 → m/z 242 MS³ spectrum is consistent with a nitrooxy group and a methyl substituent at neighboring positions. The ion at m/z 139 in the m/z 305 MS² spectrum of compound **4**(306) points to a sulfated nitrooxy diol part and a terminal sulfate group. Furthermore, the m/z 305 → m/z 242 MS³ spectrum reveals ions at m/z 142, indicating that the sulfate and nitrooxy group in the m/z 242 precursor ion are proximate, at m/z 195, due to the combined loss of a hydrogen and a NO₂ radical (47 u), and, at m/z 179 and 165, which can be attributed to further loss of CH₄ and CH₂O, respectively, from m/z 195.

On the basis of the interpretation of both the accurate mass and tandem MS data, Figure 29 shows the proposed formation mechanism for the two characterized m/z 305 nitrooxy organosulfates [i.e., compounds **2** and **4**(306)] observed in the ambient aerosol. In conjunction with our previous analysis of SOA produced from the NO₃-initiated oxidation of isoprene

SCHEME 11



under dark conditions in the presence of sulfate seed aerosol,⁹³ it now appears that both the photooxidation (in the presence of NO_x) and the nighttime oxidation of isoprene could yield these products in ambient aerosol; however, nighttime-segregated samples need to be analyzed from the SEARCH network in order to determine which pathway is more important for ambient aerosol. As for many of the ions already discussed, these nitrooxy organosulfates should form from the particle-phase esterification of one of the hydroxyl groups contained within a dihydroxy dinitrate with sulfuric acid.

5.2.3. *m/z* 333 and 331. Figures 30–34 show *m/z* 333 and 331 MS² TICs obtained from an isoprene/NO_x/SO₂ EPA photooxidation experiment and a SEARCH sample (CTR 6/11/04) and MS²/MS³ data for *m/z* 333 and 331 compounds from both samples. Surratt et al.²³ tentatively identified the *m/z* 333 compounds as the sulfated form of hemiacetals formed between 2-methyltetrols and a C₅-dihydroxycarbonyl, that is, 1,2-dihydroxy-3-methylbutane-4-one. It can be seen that the *m/z* 333 compounds elute as broad peaks in both samples, which is as expected since many stereo- and positional isomers are

possible. In this respect, it is worth mentioning that six partly resolved hemiacetal dimers could be observed by GC/MS with prior trimethylsilylation for SOA from an isoprene photooxidation experiment at low- NO_x .³³ Again, as in the case of the m/z 244 and 305 compounds discussed above, isomeric differences can be noted between the m/z 333 compounds from isoprene SOA and the ambient sample. The m/z 333 MS^2 spectra for the middle sections of the peaks with RTs of 3.8 and 4.9 min from isoprene SOA reveal clear differences for the relative abundances of the product ions at m/z 215 and 197, indicating that the sulfate group is primarily located in the 2-methyltetrol and C_5 -dihydroxycarbonyl part for the isomeric mixtures with RTs of 3.8 and 4.9 min, respectively. Possible structures for m/z 333 compounds are given and supported in Scheme 10 [where numerals 1 and 2(334) indicate the protonated compounds proposed]; accurate mass measurements of both the Caltech laboratory-generated and SEARCH m/z 333 compounds indicates that these ions share the same elemental composition of $\text{C}_{10}\text{H}_{20}\text{O}_{10}\text{S}^-$ and, as a result, further confirm the proposed structures. The m/z 333 $\rightarrow m/z$ 215 MS^3 spectrum obtained for the m/z 333 isomeric mixture eluting at 3.8 min is exactly the same as the m/z 215 MS^2 spectrum reported in the prior study by Gómez-González et al.⁴⁶ for sulfated 2-methyltetrol isomers, demonstrating that the sulfate group in the m/z 333 compounds is located in the 2-methyltetrol part. It is noted that the m/z 333 $\rightarrow m/z$ 197 MS^3 spectrum of the m/z 333 compounds eluting at 4.9 min is strikingly similar to the m/z 244 $\rightarrow m/z$ 197 MS^3 spectrum of the m/z 244 compounds. This led us to revise the structure of the C_5 -dihydroxycarbonyl part as 2,3-dihydroxy-2-methylbutane-1-one. It is worth mentioning that the C_5 -dihydroxycarbonyl part, tentatively attributed to 1,2-dihydroxy-3-methylbutane-4-one in the prior study by Surratt et al.,³³ was based on MS data of trimethylsilyl derivatives obtained in a preceding study for the corresponding nonsulfated products with MW 254. It was verified here that the latter MS data are also consistent with the new revised C_5 -dihydroxycarbonyl structure. The m/z 333 $\rightarrow m/z$ 197 MS^3 spectrum reveals m/z 97 [HSO_4^-] as base peak and product ions at m/z 179, 167, 153, and 139, which are all readily explained with the revised sulfated C_5 -dihydroxycarbonyl structure.

In regards to the m/z 331 compounds, it can be seen that the m/z 331 MS^2 spectra (Figures 33 and 34) show features that are similar to those of the m/z 333 compounds, that is, the presence of m/z 215 and 197, of which the latter ion shows exactly the same fragmentation behavior as that for the m/z 333 compounds. In addition, a product ion at m/z 195 can be observed in the m/z 331 MS^2 spectra; however, the fate of this ion is not the same for isoprene SOA and the ambient sample. While m/z 331 fragments to m/z 123 in isoprene SOA (Figure 33), fragmentation to m/z 137 occurs for the ambient sample (Figure 34b). Possible structures for the m/z 331 compounds from isoprene SOA (RT of 5 min) [1(332)] and the ambient sample (RT of 5.1 min) [2(332)], taking into account their fragmentation behaviors, are given in Scheme 11 [where numerals 1–3(332) indicate the protonated compounds proposed]. The proposed C_5 -hydroxydicarbonyl part in the m/z 331 compound from the ambient sample likely has a precursor that is different from isoprene. The m/z 331 compound with a RT of 4.1 min [3(332)] from the ambient sample shows m/z 133 as a base peak in its MS^2 spectrum, an ion that was elucidated in the prior study by Gómez-González et al.⁴⁶ and attributed to a sulfate derivative of 4,5-dihydroxypentanoic acid, which is believed to originate from the photooxidation of 4-pentenal, which in turn may result from the oxidative decay of unsaturated

fatty acids. The m/z 331 $\rightarrow m/z$ 133 MS^3 spectrum perfectly agrees with the m/z 133 MS^2 spectrum reported for sulfated 4,5-dihydroxypentanoic acid in the cited study. A possible structure for the first-eluting m/z 331 compound [3(332)] in the ambient sample is presented in Scheme 11.

5.2.4. Other Organosulfates of Isoprene Detected at m/z 155, 169, 211, 213, and 260. Similar to previously characterized organic aerosol collected from K-puszt, Hungary, and an isoprene/ NO_x / SO_2 EPA photooxidation experiment,⁴⁶ the $[\text{M} - \text{H}]^-$ ions at m/z 155 and 169 detected in the SEARCH (Table 8S, Supporting Information) and the Caltech laboratory-generated isoprene SOA samples (Table 7S, Supporting Information) are attributed to organosulfates (i.e., sulfate derivatives) of glyoxal and methylglyoxal, respectively. The accurate mass measurements obtained for the m/z 155 and 169 compounds in the latter two samples indicate that the elemental compositions of these ions are $\text{C}_2\text{H}_3\text{O}_6\text{S}^-$ and $\text{C}_3\text{H}_5\text{O}_6\text{S}^-$, respectively. MS^2 product ion spectra (not shown) for both of these organosulfates show a major product ion at m/z 97 [HSO_4^-], consistent with prior work⁴⁶ and the neutral nature of the nonsulfated part of these compounds, as well as further confirming our characterization. It is worth mentioning that Gómez-González et al.⁴⁶ observed two chromatographic peaks for m/z 155 glyoxal organosulfates; the first-eluting compound coeluted with inorganic sulfate and was explained by reaction of glyoxal and inorganic sulfate in the electrospray ionization source, while the second-eluting compound was attributed to the α -hydroxysulfate ester of glyoxal present in the sample. In addition, this prior study also considered the noncovalent adduct formed between glyoxal and sulfuric acid; theoretical calculations indicate that the organosulfate of glyoxal exists in the α -hydroxysulfate ester (i.e., sulfate derivative) form rather than the noncovalent adduct form. As shown in Figure 1, chromatographic separation was achieved between inorganic sulfate and the organosulfate of glyoxal in the present study, providing further confirmation that the organosulfate of glyoxal is not an artifact or noncovalent adduct formed in the electrospray ionization source. Our previous characterization of organic aerosol collected from the June 2004 SEARCH campaign failed to detect the organosulfates of glyoxal and methylglyoxal, owing to the solid-phase extraction (SPE) technique employed to desalt the filter samples before MS analysis.⁴⁷ Interestingly, from our detailed investigation of organosulfate formation in both isoprene and monoterpene SOA (Tables 2 and Tables 1S–7S, Supporting Information), it appears that isoprene is the only BVOC in this study to yield organosulfates of glyoxal and methylglyoxal; this is an important finding, owing to the fact that recent global estimates indicate that isoprene oxidation is the most important precursor for both dicarbonyls (i.e., contributing 47% of glyoxal and 79% of methylglyoxal globally).⁹⁴ As shown in Table 7S (Supporting Information), only the photooxidation of isoprene under intermediate ($\text{H}_2\text{O}_2/\text{NO}$)- and/or high (HONO)-NO_x conditions in the presence of sulfate seed aerosol produces the organosulfates of glyoxal and methylglyoxal, suggesting that this pathway is responsible for a large fraction of these compounds found in ambient aerosol. Oxidation of anthropogenic VOCs, such as aromatic compounds and acetylene, are also known to be a significant source of glyoxal and methylglyoxal⁹⁴ and, as a result, may potentially contribute to the organosulfate formation of both of these compounds. Laboratory chamber experiments are needed in order to establish whether organosulfates of glyoxal and methylglyoxal form from the oxidation of aromatics in the presence of acidified sulfate seed aerosol.

Organosulfates at m/z 211 and 213 have previously been observed in ambient aerosol collected from K-puszt, Hungary; however, chemical structures were elucidated only for the m/z 213 organosulfates, resulting in the source of the m/z 211 remaining unknown.⁴⁶ In this prior study, the m/z 213 compounds were attributed to isomeric organosulfates of 4,5-dihydroxypentanoic and 2,3-dihydroxypentanoic acids, and it was suggested that 4-pentenal, a likely gas-phase product from the oxidative decay of unsaturated fatty acids, and 2-pentenal, a photolysis product of the plant leaf volatile Z-3-hexenal, were the VOC precursors for these organosulfates. Notably, we find that both the Caltech isoprene/ H_2O_2 /acidic seed photooxidation experiment and the SEARCH samples contain m/z 213 organosulfates (Tables 7S and 8S, respectively, Supporting Information) with the same elemental composition (i.e., $C_5H_9O_7S^-$) as those previously observed by Gómez-González et al.⁴⁶ for K-puszt aerosol. In addition to sharing the same elemental composition, the m/z 213 organosulfates detected in both the Caltech isoprene/ H_2O_2 /acidic seed experiment and the SEARCH samples were found to have the same RTs, suggesting that isoprene is a likely source for these compounds. It should be noted that the m/z 213 compounds were not detected by Gómez-González et al.⁴⁶ in the aerosol collected from an isoprene/ NO_x /SO₂ EPA photooxidation experiment. It appears that the photooxidation of isoprene under low- NO_x (or NO_x -free) conditions in the presence of acidified sulfate seed aerosol produces m/z 213 organosulfates in ambient aerosol; however, work is needed in order to further characterize these products as well as identify their detailed formation mechanism. Although the source for the m/z 211 compounds remained unknown in K-puszt aerosol analyzed by Gómez-González et al.,⁴⁶ the Caltech isoprene/ H_2O_2 /acidic seed experiment (Table 7S, Supporting Information) produced a m/z 211 organosulfate with the same elemental composition (i.e., $C_5H_7O_7S^-$) and RT as that of one of the isomeric m/z 211 compounds detected in the SEARCH samples (Table 8S, Supporting Information). Interestingly, the three remaining, later-eluting isomeric m/z 211 organosulfates observed in the SEARCH samples were not detected in the Caltech isoprene photooxidation experiments, suggesting that some other VOC precursor, such as unsaturated fatty acids, are responsible for the formation of these compounds. It is noted that isoprene was the only BVOC in this study to produce the m/z 211 and 213 organosulfates in the laboratory-generated BSOA.

Although m/z 260 compounds have been previously detected and thoroughly characterized as isomeric organosulfates of the 2-methyltetrol mononitrates in K-puszt aerosol⁴⁶ and in isoprene SOA,^{23,46} these compounds were not previously detected in the initial analysis of aerosol collected from the SEARCH network,⁴⁷ owing to the use of less-advanced mass spectrometric techniques. As shown in Tables 7S and 8S (Supporting Information), the accurate mass measurements indicate that these compounds have an elemental composition of $C_5H_{10}NO_9S^-$, confirming the initial characterization of these compounds in SOA as well as identifying isoprene as the VOC precursor.

6. Conclusions

The presence of organosulfates and nitrooxy organosulfates of both monoterpenes and isoprene in ambient samples is confirmed. With the exception of the organosulfates of glyoxal and methylglyoxal, our results indicate that all of the organosulfates characterized in this study should be considered as unique tracers for the occurrence of biogenic SOA formation under acidic conditions. Owing to the fact that glyoxal and

methylglyoxal are also oxidation products from anthropogenic VOCs (such as aromatics, e.g., toluene), oxidation experiments of these VOCs under acidic conditions are needed in order to confirm whether they serve as additional sources of organosulfates of glyoxal and methylglyoxal in ambient fine aerosol.

Laboratory studies of isoprene and monoterpene oxidation have tended to employ levels of seed aerosol acidity that exceed those expected in ambient aerosol. These studies have established seed aerosol acidity either by adding sulfuric acid to ammonium sulfate solutions or by oxidizing gas-phase SO₂, resulting in sulfate aerosol mass. These approaches leave it unclear as to whether organosulfate formation is dependent upon either the sulfate aerosol mass concentration or acidity. In this regard, Surratt et al.²³ found that organosulfates and nitrooxy organosulfates of isoprene form in the presence of nonacidified sulfate seed aerosol; however, it was found that as the sulfuric acid concentration increased in the atomization solution, so did the number of organosulfate and nitrooxy organosulfate products. Further work is required to elucidate the extent to which the sulfate aerosol mass concentration, level of acidity, and ionic strength affect the organosulfate formation potential from isoprene and monoterpenes in ambient aerosol. Furthermore, it has been suggested that organosulfate formation occurs on the acidic surface (and not in the bulk) of a fine ambient aerosol particle as a result of condensation of semivolatile organic vapors and subsequent reaction with sulfuric acid and gives rise to a refractory organic film.^{64,95} It would be worthwhile to confirm in further studies with suitable analytical techniques (e.g., transmission electron microscopy) the occurrence of organosulfates on the surface of ambient fine aerosols.

Acknowledgment. Research at Caltech was funded by the U.S. Department of Energy Biological and Environmental Research Program (Grant DE-FG02-05ER63983) and U.S. Environmental Protection Agency Science to Achieve Results (STAR) Grant RD-83374901. Research at the University of Antwerp and Ghent University was supported by the Belgian Federal Science Policy Office (Contract SD/AT/02A), the Research Foundation—Flanders (FWO), and the Special Research Funds of both universities. The Waters UPLC-LCT Premier XT time-of-flight mass spectrometer was purchased in 2006 with a grant from the National Science Foundation, Chemistry Research Instrumentation and Facilities Program (CHE-0541745). The Electric Power Research Institute provided support for the SEARCH network field samples. This article has been jointly developed and published by the EPA and the California Institute of Technology. It was produced under Cooperative Agreement CR-83194001 and is subject to 40 CFR 30.36. The article has been reviewed by EPA personnel under EPA scientific and technical peer review procedures and approved for joint publication based on its scientific merit, technical accuracy, or contribution to advancing public understanding of environmental protection. However, the Agency's decision to publish the article jointly with Caltech is intended to further the public purpose supported by Cooperative Agreement No. CR-83194001 and not to establish an official EPA rule, regulation, guidance, or policy through the publication of this article. The U.S. Environmental Protection Agency through its Office of Research and Development also funded research described here under Contract EP-D-05-065 to Alion Science and Technology. Jason D. Surratt was supported, in part, by the U.S. Environmental Protection Agency (EPA) under the STAR Graduate Fellowship Program. We would like to thank Professor Roger Atkinson of the University of California,

Riverside for providing the standard needed for the β -phellandrene/*d*-limonene photooxidation experiment.

Supporting Information Available: Tables containing the detailed accurate mass measurements for all experiments conducted in Table 2, MS² data for the three *m/z* 294 nitrooxy organosulfates formed in the α -pinene/H₂O₂/NO/highly acidic seed experiment, MS²/MS³ data for the *m/z* 294 nitrooxy organosulfates formed in the β -pinene/H₂O₂/NO/highly acidic seed experiment, UPLC/(−)ESI-TOFMS EICs of *m/z* 296 for three selected limonene experiments and one SEARCH field site, MS²/MS³ data for the three *m/z* 296 nitrooxy organosulfates formed in the limonaketone/H₂O₂/NO/highly acidic seed experiment, MS²/MS³ data for the three *m/z* 296 nitrooxy organosulfates found in the BHM field site, MS²/MS³ data for the *m/z* 310 nitrooxy organosulfates from an α -pinene/H₂O₂/NO/highly acidic seed experiment and a β -pinene/H₂O₂/NO/highly acidic seed experiment, UPLC/(−)ESI-TOFMS EICs of *m/z* 373 for two selected limonene experiments and one SEARCH field site, and MS²/MS³ data for the three last-eluting *m/z* 305 compounds from an isoprene/NO₂/SO₂ EPA photooxidation experiment. This material is available free of charge via the Internet at <http://pubs.acs.org>.

References and Notes

- (1) Kanakidou, M.; Seinfeld, J. H.; Pandis, S. N.; Barnes, I.; Dentener, F. J.; Facchini, M. C.; Van Dingenen, R.; Ervens, B.; Nenes, A.; Nielsen, C. J.; Swietlicki, E.; Putaud, J. P.; Balkanski, Y.; Fuzzi, S.; Horth, J.; Moortgat, G. K.; Winterhalter, R.; Myhre, C. E. L.; Tsigaridis, K.; Vignati, E.; Stephanou, E. G.; Wilson, J. *Atmos. Chem. Phys.* **2005**, *5*, 1053.
- (2) Pope, C. A., III; Burnett, R. T.; Thun, M. J.; Calle, E. E.; Krewski, D.; Ito, K.; Thurston, G. D. *J. Am. Med. Assoc.* **2002**, *287*, 1132.
- (3) Intergovernmental Panel on Climate Change (IPCC). *Climate Change: The Scientific Basis*; Cambridge University Press: Cambridge, U.K., 2001.
- (4) Kroll, J. H.; Ng, N. L.; Murphy, S. M.; Flagan, R. C.; Seinfeld, J. H. *Environ. Sci. Technol.* **2006**, *40*, 1869.
- (5) Henze, D. K.; Seinfeld, J. H. *Geophys. Res. Lett.* **2006**, *33*, L09812.
- (6) Guenther, A.; Hewitt, C. N.; Erickson, D.; Fall, R.; Geron, C.; Graedel, T.; Harley, P.; Klinger, L.; Lerdau, M.; McKay, W. A.; Pierce, T.; Scholes, B.; Steinbrecher, R.; Tallamraju, R.; Taylor, T.; Zimmerman, P. J. *Geophys. Res.* **1995**, *100*, 8873.
- (7) Hatakeyama, S.; Izumi, K.; Fukuyama, T.; Akimoto, H.; Washida, N. *J. Geophys. Res.* **1991**, *96*, 947.
- (8) Johnson, D.; Jenkin, M. E.; Wirtz, K.; Martín-Reviejo, M. *Environ. Chem.* **2004**, *1*, 150.
- (9) Johnson, D.; Jenkin, M. E.; Wirtz, K.; Martín-Reviejo, M. *Environ. Chem.* **2005**, *2*, 35.
- (10) Song, C.; Na, K.; Cocker, D. R., III. *Environ. Sci. Technol.* **2005**, *39*, 3143.
- (11) Presto, A. A.; Huff Hartz, K. E.; Donahue, N. M. *Environ. Sci. Technol.* **2005**, *39*, 7046.
- (12) Lim, Y. B.; Ziemann, P. J. *Environ. Sci. Technol.* **2005**, *39*, 9229.
- (13) Kroll, J. H.; Ng, N. L.; Murphy, S. M.; Flagan, R. C.; Seinfeld, J. H. *Geophys. Res. Lett.* **2005**, *32*, L18808.
- (14) Ng, N. L.; Kroll, J. H.; Chan, A. W. H.; Chhabra, P. S.; Flagan, R. C.; Seinfeld, J. H. *Atmos. Chem. Phys.* **2007**, *7*, 3909.
- (15) Ng, N. L.; Chhabra, P. S.; Chan, A. W. H.; Surratt, J. D.; Kroll, J. H.; Kwan, A. J.; McCabe, D. C.; Wennberg, P. O.; Sorooshian, A.; Murphy, S. M.; Dalleska, N. F.; Flagan, R. C.; Seinfeld, J. H. *Atmos. Chem. Phys.* **2007**, *7*, 5159.
- (16) Jang, M.; Czoschke, N. M.; Lee, S.; Kamens, R. M. *Science* **2002**, *298*, 814.
- (17) Iinuma, Y.; Böge, O.; Gnauk, T.; Herrmann, H. *Atmos. Environ.* **2004**, *38*, 761.
- (18) Gao, S.; Ng, N. L.; Keywood, M.; Varutbangkul, V.; Bahreini, R.; Nenes, A.; He, J.; Yoo, K. Y.; Beauchamp, J. L.; Hodyss, R. P.; Flagan, R. C.; Seinfeld, J. H. *Environ. Sci. Technol.* **2004**, *38*, 6582.
- (19) Gao, S.; Keywood, M.; Ng, N. L.; Surratt, J. D.; Varutbangkul, V.; Bahreini, R.; Flagan, R. C.; Seinfeld, J. H. *J. Phys. Chem. A* **2004**, *108*, 10147.
- (20) Tolocka, M. P.; Jang, M.; Ginter, J. M.; Cox, F. J.; Kamens, R. M.; Johnston, M. V. *Environ. Sci. Technol.* **2004**, *38*, 1428.
- (21) Edney, E. O.; Kleindienst, T. E.; Jaoui, M.; Lewandowski, M.; Offenberg, J. H.; Wang, W.; Claeys, M. *Atmos. Environ.* **2005**, *39*, 5281.
- (22) Kleindienst, T. E.; Edney, E. O.; Lewandowski, M.; Offenberg, J. H.; Jaoui, M. *Environ. Sci. Technol.* **2006**, *40*, 3807.
- (23) Surratt, J. D.; Kroll, J. H.; Kleindienst, T. E.; Edney, E. O.; Claeys, M.; Sorooshian, A.; Ng, N. L.; Offenberg, J. H.; Lewandowski, M.; Jaoui, M.; Flagan, R. C.; Seinfeld, J. H. *Environ. Sci. Technol.* **2007**, *41*, 517.
- (24) Surratt, J. D.; Lewandowski, M.; Offenberg, J. H.; Jaoui, M.; Kleindienst, T. E.; Edney, E. O.; Seinfeld, J. H. *Environ. Sci. Technol.* **2007**, *41*, 5363.
- (25) Iinuma, Y.; Müller, C.; Böge, O.; Gnauk, T.; Herrmann, H. *Atmos. Environ.* **2007**, *41*, 5571.
- (26) Iinuma, Y.; Müller, C.; Berndt, T.; Böge, O.; Claeys, M.; Herrmann, H. *Environ. Sci. Technol.* **2007**, *41*, 6678.
- (27) Seinfeld, J. H.; Erdakos, G. B.; Asher, W. E.; Pankow, J. F. *Environ. Sci. Technol.* **2001**, *35*, 1806.
- (28) Dommen, J.; Metzger, A.; Duplissy, J.; Kalberer, M.; Alfara, M. R.; Gascho, A.; Weingartner, E.; Prevot, A. S. H.; Verheggen, B.; Baltensperger, U. *Geophys. Res. Lett.* **2006**, *33*, L13805.
- (29) Jonsson, Å. M.; Hallquist, M.; Ljunström, E. *Environ. Sci. Technol.* **2006**, *40*, 188.
- (30) Takekawa, H.; Minoura, H.; Yamazaki, S. *Atmos. Environ.* **2003**, *37*, 3413.
- (31) Stanier, C. O.; Pathak, R. K.; Pandis, S. N. *Environ. Sci. Technol.* **2007**, *41*, 2756.
- (32) Pathak, R. K.; Stanier, C. O.; Donahue, N. M.; Pandis, S. N. *J. Geophys. Res.* **2007**, *112*, D03201.
- (33) Surratt, J. D.; Murphy, S. M.; Kroll, J. H.; Ng, N. L.; Hildebrandt, L.; Sorooshian, A.; Szmigielski, R.; Vermeylen, R.; Maenhaut, W.; Claeys, M.; Flagan, R. C.; Seinfeld, J. H. *J. Phys. Chem. A* **2006**, *110*, 9665.
- (34) Tobias, H. J.; Ziemann, P. J. *Environ. Sci. Technol.* **2000**, *34*, 2105.
- (35) Docherty, K. S.; Wu, W.; Lim, Y. B.; Ziemann, P. J. *Environ. Sci. Technol.* **2005**, *39*, 4049.
- (36) Garland, R. M.; Elrod, M. J.; Kincaid, K.; Beaver, M. R.; Jimenez, J. L.; Tolbert, M. A. *Atmos. Environ.* **2006**, *40*, 6863.
- (37) Szmigielski, R.; Surratt, J. D.; Vermeylen, R.; Szmigielska, K.; Kroll, J. H.; Ng, N. L.; Murphy, S. M.; Sorooshian, A.; Seinfeld, J. H.; Claeys, M. *J. Mass Spectrom.* **2007**, *42*, 101.
- (38) Hamilton, J. F.; Lewis, A. C.; Reynolds, J. C.; Carpenter, L. J.; Lubben, A. *Atmos. Chem. Phys.* **2006**, *6*, 4973.
- (39) Müller, L.; Reinig, M.-C.; Warnke, J.; Hoffmann, T. *Atmos. Chem. Phys.* **2008**, *8*, 1423.
- (40) Altieri, K. E.; Seitzinger, S. P.; Carlton, A. G.; Turpin, B. J.; Klein, G. C.; Marshall, A. G. *Atmos. Environ.* **2008**, *42*, 1476.
- (41) Kalberer, M.; Paulsen, D.; Sax, M.; Steinbacher, M.; Dommen, J.; Prevot, A. S. H.; Fisseha, R.; Weingartner, E.; Frankevich, V.; Zenobi, R.; Baltensperger, U. *Science* **2004**, *303*, 1659.
- (42) Barsanti, K. C.; Pankow, J. F. *Atmos. Environ.* **2004**, *38*, 4371.
- (43) Barsanti, K. C.; Pankow, J. F. *Atmos. Environ.* **2005**, *39*, 6597.
- (44) Barsanti, K. C.; Pankow, J. F. *Atmos. Environ.* **2006**, *40*, 6676.
- (45) Casale, M. T.; Richman, A. R.; Elrod, M. J.; Garland, R. M.; Beaver, M. R.; Tolbert, M. A. *Atmos. Environ.* **2007**, *41*, 6212.
- (46) Gómez-González, Y.; Surratt, J. D.; Cuyckens, F.; Szmigielski, R.; Vermeylen, R.; Jaoui, M.; Lewandowski, M.; Offenberg, J. H.; Kleindienst, T. E.; Edney, E. O.; Blockhuys, F.; Van Alsenoy, C.; Maenhaut, W.; Claeys, M. *J. Mass Spectrom.* **2008**, *43*, 371.
- (47) Gao, S.; Surratt, J. D.; Knipping, E. M.; Edgerton, E. S.; Shahgholi, M.; Seinfeld, J. H. *J. Geophys. Res.* **2006**, *111*, D14314.
- (48) Liggio, J.; Li, S.-M.; McLaren, R. *Environ. Sci. Technol.* **2005**, *39*, 1532.
- (49) Liggio, J.; Li, S.-M. *Geophys. Res. Lett.* **2006**, *33*, L13808.
- (50) Liggio, J.; Li, S.-M. *J. Geophys. Res.* **2006**, *111*, D24303.
- (51) Romero, F.; Oehme, M. *J. Atmos. Chem.* **2005**, *52*, 283.
- (52) Reemtsma, T.; These, A.; Venkatachari, P.; Xia, X.; Hopke, P. K.; Springer, A.; Linscheid, M. *Anal. Chem.* **2006**, *78*, 8299.
- (53) Hakola, H.; Shorees, B.; Arey, J.; Atkinson, R. *Environ. Sci. Technol.* **1993**, *27*, 278.
- (54) Donahue, N. M.; Tischuk, J. E.; Marquis, B. J.; Huff Hartz, K. E. *Phys. Chem. Chem. Phys.* **2007**, *9*, 2991.
- (55) Atkinson, R.; Arey, J. *Chem. Rev.* **2003**, *103*, 14605.
- (56) Cocker, D. R., III; Flagan, R. C.; Seinfeld, J. H. *Environ. Sci. Technol.* **2001**, *35*, 2594.
- (57) Keywood, M. D.; Varutbangkul, V.; Bahreini, R.; Flagan, R. C.; Seinfeld, J. H. *Environ. Sci. Technol.* **2004**, *38*, 4157.
- (58) Alewell, C. *Plant Soil* **1993**, *149*, 141.
- (59) Hansen, D. A.; Edgerton, E. S.; Hartsell, B. E.; Jansen, J. J.; Kandasamy, N.; Hidy, G. M.; Blanchard, C. L. *J. Air Waste Manage. Assoc.* **2003**, *53*, 1460.
- (60) Edgerton, E. S.; Hartsell, B. E.; Saylor, R. D.; Jansen, J. J.; Hansen, D. A.; Hidy, G. M. *J. Air Waste Manage. Assoc.* **2005**, *55*, 1527.
- (61) Graham, B.; Guyon, P.; Maenhaut, W.; Taylor, P. E.; Ebert, M.; Matthias-Maser, S.; Mayol-Bracero, O. L.; Godoi, R. H. M.; Artaxo, P.; Meixner, F. X.; Lima Moura, M. A.; Ega D'Almeida Rocha, C. H.; Van Grieken, R.; Glovsky, M. M.; Flagan, R. C.; Andreae, M. O. *J. Geophys. Res.* **2003**, *108*, 4765.

- (62) Ocskay, R.; Salma, I.; Wang, W.; Maenhaut, W. *J. Environ. Monit.* **2006**, 8, 300.
- (63) Maenhaut, W.; Raes, N.; Chi, X.; Cafmeyer, J.; Wang, W. *X-Ray Spectrom.* **2008**, 37, 193.
- (64) Lukács, H.; Gelencsér, A.; Hoffer, A.; Kiss, G.; Horváth, K.; Hartyáni, Z. *Atmos. Chem. Phys. Discuss.* **2008**, 8, 6825.
- (65) Boss, B.; Richling, E.; Herderich, R.; Schreier, P. *Phytochemistry* **1999**, 50, 219.
- (66) Metzger, K.; Rehberger, P. A.; Erben, G.; Lehmann, W. D. *Anal. Chem.* **1995**, 67, 4178.
- (67) Kubátová, A.; Vermeylen, R.; Claeys, M.; Cafmeyer, J.; Maenhaut, W.; Roberts, G.; Artaxo, P. *Atmos. Environ.* **2000**, 34, 5037.
- (68) Warnke, J.; Bandur, R.; Hoffmann, T. *J. Aerosol Sci.*, Supplement, Abstracts of EAC; **2004**, S21.
- (69) Kourtchev, I.; Ruuskanen, T.; Maenhaut, W.; Kulmala, M.; Claeys, M. *Atmos. Chem. Phys.* **2005**, 5, 2761.
- (70) Edney, E. O.; Kleindienst, T. E.; Conner, T. S.; McIver, C. D.; Corse, E. W.; Weathers, W. S. *Atmos. Environ.* **2003**, 37, 3947.
- (71) Szmigielski, R.; Surratt, J. D.; Gómez-González, Y.; Van der Veken, P.; Kourtchev, I.; Vermeylen, R.; Blockhuys, F.; Jaoui, M.; Kleindienst, T. E.; Lewandowski, M.; Offenberg, J. H.; Edney, E. O.; Seinfeld, J. H.; Maenhaut, W.; Claeys, M. *Geophys. Res. Lett.* **2007**, 34, L24811. doi: 10.1029/2007GL031338.
- (72) Claeys, M.; Graham, B.; Vas, G.; Wang, W.; Vermeylen, R.; Pashynska, V.; Cafmeyer, J.; Guyon, P.; Andreae, M. O.; Artaxo, P.; Maenhaut, W. *Science* **2004**, 303, 1173.
- (73) Kiss, G.; Tombácz, E.; Varga, B.; Alsberg, T.; Persson, L. *Atmos. Environ.* **2003**, 37, 3783.
- (74) Aschmann, S. M.; Reissell, A.; Atkinson, R.; Arey, J. *J. Geophys. Res.* **1998**, 103, 22553.
- (75) Aschmann, S. M.; Atkinson, R.; Arey, J. *J. Geophys. Res.* **2002**, 107, 4191.
- (76) Jay, K.; Stieglitz, L. *Chemosphere* **1989**, 19, 1939.
- (77) Baldwin, A. C.; Barker, J. R.; Golden, D. M.; Hendry, D. G. *J. Phys. Chem.* **1977**, 81, 2483.
- (78) Cartier, W. P. L.; Atkinson, R. *J. Atmos. Chem.* **1985**, 3, 377.
- (79) Kim, J.-C. *Atmos. Environ.* **2001**, 35, 3279.
- (80) Helmig, D.; Ortega, J.; Guenther, A.; Herrick, J. D.; Geron, C. *Atmos. Environ.* **2006**, 40, 4150.
- (81) Sakulyanontvittaya, T.; Duhl, T.; Wiedinmyer, C.; Helmig, D.; Matsunaga, S.; Potosnak, M.; Milford, J.; Guenther, A. *Environ. Sci. Technol.* **2008**, 42, 1623.
- (82) Lee, A.; Goldstein, A. H.; Kroll, J. H.; Ng, N. L.; Varutbangkul, V.; Flagan, R. C.; Seinfeld, J. H. *J. Geophys. Res.* **2006**, 111, D17305.
- (83) Di Carlo, P.; Brune, W. H.; Martinez, M.; Harder, H.; Leshner, R.; Ren, X.; Thornberry, T.; Carroll, M. A.; Young, V.; Shepson, P. B.; Riemer, D.; Apel, E.; Campbell, C. *Science* **2004**, 304, 722.
- (84) Alvarado, A.; Tuazon, E. C.; Aschmann, S. M.; Atkinson, R.; Arey, J. *J. Geophys. Res.* **1998**, 103, 25541.
- (85) Berndt, T.; Böge, O.; Stratmann, F. *Atmos. Environ.* **2003**, 37, 3933.
- (86) Berndt, T.; Böge, O. *J. Chem. Soc., Faraday Trans.* **1997**, 93, 3021.
- (87) Berndt, T.; Böge, O.; Hermann, M. *Proceedings of EUROTRAC Symposium 98*; Borrell, P. M., Borrell, P. M. Eds.; WIT Press: Southampton, U.K., 1999; Vol. 1, pp 79–83.
- (88) Claeys, M.; Szmigielski, R.; Kourtchev, I.; Van der Veken, P.; Vermeylen, R.; Maenhaut, W.; Jaoui, M.; Kleindienst, T. E.; Lewandowski, M.; Offenberg, J. H.; Edney, E. O. *Environ. Sci. Technol.* **2007**, 41, 1628.
- (89) Hallquist, M.; Wenger, J.; Baltensperger, U.; Rudich, Y.; Simpson, D.; Claeys, M.; Dommen, J.; Donahue, N. M.; George, C.; Goldstein, A. H.; Hamilton, J. F.; Herrmann, H.; Hoffmann, T.; Iinuma, Y.; Jang, M.; Jenkin, M. E.; Jimenez, J.-L.; Kiendler-Scharr, A.; Maenhaut, W.; McFiggans, G.; Mentel, T.; Monod, A.; Prévôt, A. S. H.; Seinfeld, J. H.; Surratt, J. D.; Szmigielski, R.; Wildt, J. *Atmos. Chem. Phys. Discuss.* **2008**, to be submitted.
- (90) Larsen, B. R.; Di Bella, D.; Glasius, M.; Winterhalter, R.; Jensen, N. R.; Hjorth, J. *J. Atmos. Chem.* **2001**, 38, 231.
- (91) Winterhalter, R.; Van Dingenen, R.; Larsen, B. R.; Jensen, N. R.; Hjorth, J. *Atmos. Chem. Phys. Discuss.* **2003**, 3, 1.
- (92) Sutherland, M. D.; Webb, L. J.; Wells, J. W. *Aust. J. Chem.* **1960**, 13, 357.
- (93) Ng, N. L.; Kwan, A. J.; Surratt, J. D.; Chan, A. W. H.; Chhabra, P. S.; Sorooshian, A.; Pye, H. O. T.; Crounse, J. D.; Wennberg, P. O.; Flagan, R. C.; Seinfeld, J. H. *Atmos. Chem. Phys.* **2008**, 8, 4117.
- (94) Fu, T.-M.; Jacob, D. J.; Wittrock, F.; Burrows, J. P.; Vrekoussis, M.; Henze, D. K. *J. Geophys. Res.* **2008**, in press.
- (95) Pósfai, M.; Molnár, A. *EMU Notes in Mineralogy* **2000**, 2, 197.

Appendix D

Secondary organic aerosol (SOA) formation from reaction of isoprene with nitrate radicals (NO_3)*

*Reproduced with permission from “Secondary Organic Aerosol (SOA) formation from reaction of isoprene with nitrate radicals (NO_3)” by N. L. Ng, A. J. Kwan, J. D. Surratt, A. W. H. Chan, P. S. Chhabra, A. Sorooshian, H. O. T. Pye, J. D. Crounse, P. O. Wennberg, R. C. Flagan, and J. H. Seinfeld, *Atmospheric Chemistry and Physics*, 8 (14), 4117–4140, 2008. Copyright 2008 by Authors. This work is licensed under a Creative Commons License.

Secondary organic aerosol (SOA) formation from reaction of isoprene with nitrate radicals (NO₃)

N. L. Ng¹, A. J. Kwan², J. D. Surratt¹, A. W. H. Chan¹, P. S. Chhabra¹, A. Sorooshian¹, H. O. T. Pye¹, J. D. Crounse¹, P. O. Wennberg^{2,3}, R. C. Flagan^{1,2}, and J. H. Seinfeld^{1,2}

¹Division of Chemistry and Chemical Engineering, California Institute of Technology, Pasadena, CA 91125, USA

²Division of Engineering and Applied Science, California Institute of Technology, Pasadena, CA 91125, USA

³Division of Geological and Planetary Sciences, California Institute of Technology, Pasadena, CA 91125, USA

Received: 3 January 2008 – Published in Atmos. Chem. Phys. Discuss.: 15 February 2008

Revised: 3 July 2008 – Accepted: 3 July 2008 – Published: 1 August 2008

Abstract. Secondary organic aerosol (SOA) formation from the reaction of isoprene with nitrate radicals (NO₃) is investigated in the Caltech indoor chambers. Experiments are performed in the dark and under dry conditions (RH<10%) using N₂O₅ as a source of NO₃ radicals. For an initial isoprene concentration of 18.4 to 101.6 ppb, the SOA yield (defined as the ratio of the mass of organic aerosol formed to the mass of parent hydrocarbon reacted) ranges from 4.3% to 23.8%. By examining the time evolutions of gas-phase intermediate products and aerosol volume in real time, we are able to constrain the chemistry that leads to the formation of low-volatility products. Although the formation of ROOR from the reaction of two peroxy radicals (RO₂) has generally been considered as a minor channel, based on the gas-phase and aerosol-phase data it appears that RO₂+RO₂ reaction (self reaction or cross-reaction) in the gas phase yielding ROOR products is a dominant SOA formation pathway. A wide array of organic nitrates and peroxides are identified in the aerosol formed and mechanisms for SOA formation are proposed. Using a uniform SOA yield of 10% (corresponding to M_o≅10 μg m⁻³), it is estimated that ~2 to 3 Tg yr⁻¹ of SOA results from isoprene+NO₃. The extent to which the results from this study can be applied to conditions in the atmosphere depends on the fate of peroxy radicals in the nighttime troposphere.

1 Introduction

Isoprene is the most abundant non-methane hydrocarbon emitted into the atmosphere with a global emission of ~500 Tg yr⁻¹ (Guenther et al., 1995; Guenther et al., 2006). In the troposphere, isoprene reacts with hydroxyl radicals (OH), ozone (O₃), and nitrate radicals (NO₃). Owing to its high concentration and reactivity with OH radicals, isoprene plays an important role in the photochemistry occurring within the atmospheric boundary layer. Recently, it has been shown that the photooxidation of isoprene leads to the formation of low volatility species that condense to form SOA (Claeys et al., 2004; Edney et al., 2005; Kroll et al., 2005; Dommen et al., 2006; Kroll et al., 2006; Surratt et al., 2006); SOA yields as high as ~3% have been observed (Kroll et al., 2005; Kroll et al., 2006). Global SOA production from isoprene photooxidation has been estimated to be about 13 Tg yr⁻¹ (Henze et al., 2007).

Although emission of isoprene from vegetation is triggered by sunlight and increases with light intensity and temperature (e.g. Sharkey et al., 1996), the isoprene mixing ratio has been observed to peak in early evening in several field studies, with a measured mixing ratio up to a few ppb (Curren et al., 1998; Starn et al., 1998; Stroud et al., 2002; Steinbacher et al., 2005). After sunset, the isoprene mixing ratio drops rapidly, and it has been suggested that the reaction with nitrate radicals, NO₃, is a major contributor to isoprene decay at night (Curren et al., 1998; Starn et al., 1998; Stroud et al., 2002; Steinbacher et al., 2005). Typical NO₃ radical mixing ratios in boundary layer continental air masses range between ~10 to ~100 ppt (Platt and Janssen, 1995; Smith et al., 1995; Heintz et al., 1996; Carslaw et al., 1997). However, concentrations as high as



Correspondence to: J. H. Seinfeld
 (seinfeld@caltech.edu)

several hundred ppt have been observed over northeastern USA and Europe (Platt et al., 1981; von Friedeburg et al., 2002; Brown et al., 2006; Penkett et al., 2007). Given the rapid reaction rate between isoprene and NO₃ radicals ($k_{\text{NO}_3} = 7 \times 10^{-13} \text{ cm}^3 \text{ molecule}^{-1} \text{ s}^{-1}$ at $T = 298 \text{ K}$, IUPAC), it is likely that NO₃ radicals play a major role in the nighttime chemistry of isoprene.

The kinetics and gas-phase products of the isoprene-NO₃ reaction have been the subject of several laboratory and theoretical studies (Jay and Stieglitz, 1989; Barnes et al., 1990; Skov et al., 1992; Kwok et al., 1996; Berndt and Böge, 1997; Suh et al., 2001; Zhang et al., 2002; Fan et al., 2004). In many studies, C₅-nitrooxycarbonyl is identified as the major first-generation gas-phase reaction product (Jay and Stieglitz, 1989; Skov et al., 1992; Kwok et al., 1996; Berndt and Böge, 1997). Other compounds such as C₅-hydroxynitrate, C₅-nitrooxyhydroperoxide, and C₅-hydroxycarbonyl have also been identified (Kwok et al., 1996); C₅-hydroxynitrate has also been measured in ambient air with concentrations in the lower ppt range at a few ng m⁻³ (Werner et al., 1999). According to the experimental study by Barnes et al. (1990), the yield for nitrate-containing compounds from the reaction of isoprene and NO₃ radicals can be as high as 80%. A recent modeling study in conjunction with observations from the ICARTT field campaign suggests that ~50% of the total isoprene nitrates production occurs via reaction of isoprene and NO₃ radicals (Horowitz et al., 2007).

Little is known beyond the formation of the first-generation products of the reaction of NO₃ with isoprene. The isoprene nitrates and other first-generation products still contain a double bond, and it is likely that the further oxidation of these species will lead to low volatility products that can contribute to SOA formation at nighttime.

In this work, SOA formation from the reaction of isoprene with NO₃ radicals is investigated. Laboratory chamber experiments are performed in the dark using N₂O₅ as a source of NO₃ radicals. Aerosol yields are obtained over a range of initial isoprene concentrations (mixing ratios). By examining the time evolutions of aerosol volume and different intermediate gas-phase products, we are able to constrain the chemistry that leads to the formation of low-volatility products. Mechanisms for SOA formation are proposed and chemical composition data of the SOA formed are also presented.

2 Experimental section

Experiments are carried out in the Caltech dual 28 m³ Teflon chambers. A detailed description of the facility is provided elsewhere (Cocker et al., 2001; Keywood et al., 2004). Before each experiment, the chambers are flushed continuously for over 24 h. Aerosol number concentration, size distribution, and volume concentration are measured by a Differential Mobility Analyzer (DMA, TSI model 3081) coupled with a condensation nucleus counter (TSI model 3760).

All aerosol growth data are corrected for wall loss, in which size-dependent particle loss coefficients are determined from inert particle wall loss experiments (Keywood et al., 2004). Temperature, relative humidity (RH), O₃, NO, and NO_x are continuously monitored. Experiments are performed in the dark at room temperature (20–21°C) and under dry conditions (RH < 10%).

In most experiments, seed aerosols are introduced into the chamber to act as a substrate onto which the gas-phase products may condense. Seed aerosols are generated by atomizing an aqueous solution with a constant-rate atomizer. The seed solution consists of 0.015 M (NH₄)₂SO₄. In a few experiments, acidic seed is used, consisting of 0.03 M MgSO₄ and 0.05 M H₂SO₄. The initial particle number concentration is ~20 000 particles cm⁻³, with a geometric mean diameter of ~50 nm. The initial seed volume is 10–12 μm³ cm⁻³. In some experiments, no seed particles are added and aerosols are formed via nucleation. After introduction of the seed aerosols (in seeded experiments), a known volume of isoprene (Aldrich, 99%) is injected into a glass bulb and introduced into the chamber by an air stream. The mixing ratio of isoprene is monitored with a gas chromatograph equipped with a flame ionization detector (GC-FID, Agilent model 6890N). The column used is a bonded polystyrene-divinylbenzene based column (HP-PLLOT Q, 15 m × 0.53 mm, 40 μm thickness, J&W Scientific). The oven temperature is held at 60°C for 0.5 min, ramped at 35°C min⁻¹ to 200°C, and held constant for 3.5 min.

The thermal decomposition of N₂O₅ serves as a source of NO₃ radicals in these experiments. N₂O₅ is prepared and collected offline by mixing a stream of nitric oxide (≥ 99.5%, Matheson Tri Gas) with a stream of ozone in a glass bulb (Davidson et al., 1978):



Ozone is generated by flowing oxygen through an ozonizer (OREC model V10-0, Phoenix, AZ) at ~1 L min⁻¹. The mixing ratio of ozone is measured by a UV/VIS spectrometer (Hewlett Packard model 8453) to be ~2%. The flow rate of nitric oxide into the glass bulb is adjusted until the brown color in the bulb disappears. The N₂O₅ is trapped for 2 h in an acetone-dry ice bath (approximately at -80°C; cold enough to trap N₂O₅ but not O₃, as condensed O₃ can explode upon warming and is extremely dangerous) as a white solid, and stored between experiments under liquid nitrogen temperature. Once the seed and isoprene concentrations in the chamber stabilize, reaction is initiated by vaporizing N₂O₅ into an evacuated 500 mL glass bulb and introduced into the chamber with an air stream of 5 L min⁻¹.

The amount of N₂O₅ injected is estimated based on the vapor pressure in the glass bulb, which is measured using a capacitance manometer (MKS); this amount corresponds to an initial mixing ratio of ~1 ppm in the chamber. The thermal decomposition of N₂O₅ forms NO₂ and NO₃ radicals. Impurities in the N₂O₅ starting material are quantified by FTIR spectroscopy (Nicolet model Magna 550). N₂O₅ is vaporized into an evacuated pyrex cell (18 cm in length and 300 cm³) with CaF₂ windows. Spectra are collected immediately upon addition over the 1000 cm⁻¹ to 4000 cm⁻¹ window allowing for quantification of NO₂ (1616 cm⁻¹ band) and HNO₃ (3550 cm⁻¹ band) impurities.

A custom-modified Varian 1200 Chemical Ionization Mass Spectrometer (CIMS) is used to continuously monitor the concentrations of various gas-phase intermediates and products over the course of the experiments. The CIMS instrument is operated mainly in negative mode using CF₃O⁻ as a reagent ion, which selectively clusters with compounds having high fluorine affinity (e.g., acidic compounds and many hydroxy- and nitrooxy- carbonyls), forming ions at *m/z* MW+85. In some experiments, the CIMS instrument is also operated in the positive mode using H₂O as a reagent ion forming ions at *m/z* MW+1. The ionization schemes are as follows:

Negative chemical ionization: CF₃O⁻ + HB → CF₃O⁻ · HB

Positive chemical ionization: H₃O⁺ + D → D · H⁺ + H₂O
(where D has a proton affinity > H₂O)

The term “product ion” is used throughout this manuscript to describe the ionized products formed through the above chemical reaction schemes. Typically, we scan from *m/z* 50 to 400. More details about the CIMS technique are given in Crounse et al. (2006) and Ng et al. (2007a). Because authentic standards are not available for the major products, sensitivities are not experimentally determined. We estimate the collision rate of CF₃O⁻ with these products (which determines the sensitivity) with the empirical method of Su and Chesnavich (1982), which bases its predictions on an analyte's dipole moment and polarizability. Dipole moments and polarizabilities are calculated with the Spartan06 quantum package, and are based on molecular structures optimized with the B3LYP/6-31G(d) method. Further details on estimating CIMS sensitivities based on quantum calculations are described in Paulot et al. (2008). As isomers would have different polarities and hence different sensitivities, in estimating the concentrations it is assumed that the NO₃ attack at C₁-position to C₄-position is 5.5:1 (See Sect. 4.1).

Aerosol physical and chemical properties are monitored by many instruments. Real-time particle mass spectra are obtained with an Aerodyne quadrupole Aerosol Mass Spectrometer (Q-AMS) (Jayne et al., 2000). A Particle-Into-Liquid Sampler (PILS, Brechtel Manufacturing, Inc.) coupled with ion chromatography (IC) is employed for quantitative measurements of water-soluble ions in the aerosol phase

(Sorooshian et al., 2006). Duplicate Teflon filters (PALL Life Sciences, 47-mm diameter, 1.0-μm pore size, teflo membrane) are collected from a selected number of experiments for offline chemical analysis. Filter sampling is initiated when the aerosol volume reaches its maximum value. Depending on the total volume concentration of aerosol in the chamber, the filter sampling time is 2–4 h, which results in ~2–5 m³ of total chamber air sampled. Teflon filters used for high-resolution electrospray ionization-time-of-flight mass spectrometry (ESI-TOFMS) analysis are extracted in 5 mL of high-purity methanol (LC-MS CHROMASOLV-Grade, Sigma-Aldrich) by 45 min of sonication. Methanol sample extracts are then blown dry under a gentle N₂ stream (without added heat) once the filters are removed and archived at -20°C. Dried residues are then reconstituted with 500 mL of a 1:1 (v/v) solvent mixture of 0.1% acetic acid in water (LC-MS CHROMASOLV-Grade, Sigma-Aldrich) and 0.1% acetic acid in methanol (LC-MS CHROMASOLV-Grade, Sigma Aldrich). All resultant filter extracts are analyzed by a Waters ACQUITY ultra performance liquid chromatography (UPLC) system, coupled to a Waters LCT Premier XT time-of-flight mass spectrometer (TOFMS) equipped with an ESI source that is operated in the negative (-) ionization mode. Detailed operating conditions for the UPLC/(-)ESI-TOFMS instrument have been described previously (Ng et al., 2007a). A Waters ACQUITY UPLC HSS column is selected to separate the SOA components because of its increased retention of water-soluble polar organics; separation is achieved as a result of trifunctionally-bonded (T3) C₁₈ alkyl residues on this column, which prevent stationary phase collapse when a 100% aqueous mobile phase is used and result in better retention of water-soluble polar organic compounds. In addition to the UPLC/(-)ESI-TOFMS analysis, all remaining Teflon filters are extracted and analyzed for total peroxide content (sum of ROOR and ROOH) by using an iodometric-spectroscopic method (Docherty et al., 2005; Surratt et al., 2006).

To study the mechanism of SOA formation, in several experiments the experimental protocols are slightly modified: (1) An excess amount of isoprene (relative to N₂O₅ concentration) is injected into the chamber to prevent the further reaction of first-generation gas-phase products, allowing these products to be detected more readily; (2) After the addition of isoprene, pulses of N₂O₅ are introduced into the chamber to study the evolution of different intermediate gas-phase products; (3) With isoprene well mixed in the chamber, N₂O₅ is introduced slowly to maximize the self-reaction of peroxy radicals (see Sect. 4.2). This is achieved by first injecting N₂O₅ into a 65 L Teflon bag; then an air stream of 1 L min⁻¹ is passed through the Teflon bag to introduce N₂O₅ into the chamber over a 7 h period. We refer to this as the “slow N₂O₅ injection experiment”; and (4) With N₂O₅ well mixed in the chamber, isoprene is introduced slowly to maximize the reaction between peroxy radicals and nitrate radicals (see Sect. 4.2). This is achieved by first injecting isoprene into a

4120

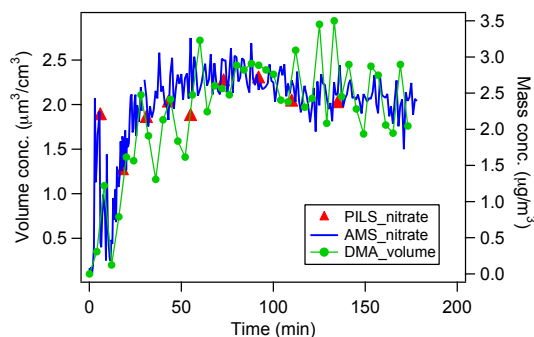


Fig. 1. Time profiles of aerosol volume, inorganic nitrate measured by PILS/IC, and nitrate signals from Q-AMS in a blank experiment (~ 1 ppm N₂O₅, ammonium sulfate seed, no isoprene).

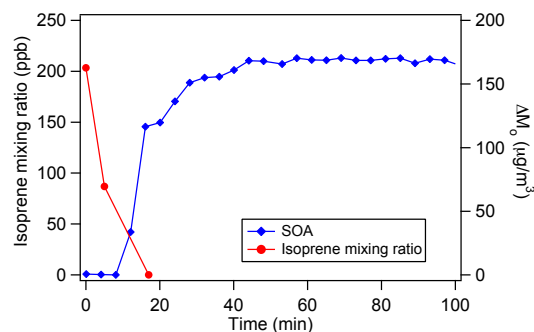


Fig. 2. Reaction profile of the oxidation of an initial mixture containing 203.4 ppb isoprene ($573 \mu\text{g}/\text{m}^3$).

65 L Teflon bag, and then introduced into the chamber with an air stream of 1 L min^{-1} for 7 h. We refer to this as the “slow isoprene injection experiment”.

Experimental conditions and results are given in Table 1. In calculating SOA yield (defined as the ratio of the organic aerosol mass formed to the mass of parent hydrocarbon reacted), knowledge of the SOA density is required. By comparing volume distributions from the DMA and mass distributions from the Q-AMS, the effective density for the SOA formed can be estimated (Bahreini et al., 2005; Alfara et al., 2006).

3 Results

3.1 Blank experiments

Blank experiments are performed to ensure that the aerosol growth observed is from the reaction of isoprene with NO₃ radicals. In these experiments, ~ 1 ppm N₂O₅ is introduced

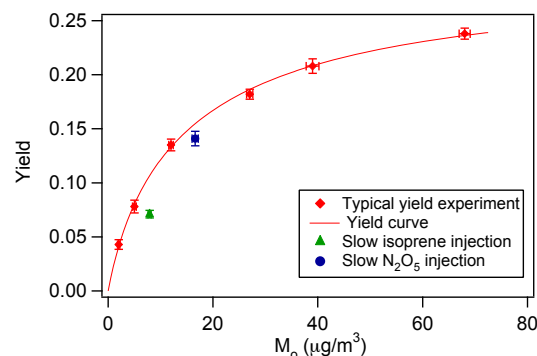


Fig. 3. SOA yield data and yield curve for isoprene-NO₃ reaction. Also shown are SOA yields from the slow N₂O₅ injection experiment and slow isoprene injection experiment.

into chamber after the addition of ammonium sulfate seed aerosol (with no isoprene present). As shown in Fig. 1, aerosol volume increases by $\sim 2 \mu\text{m}^3 \text{ cm}^{-3}$ within an hour after the introduction of N₂O₅. About $2.5 \mu\text{g m}^{-3}$ of inorganic nitrate is measured by PILS/IC, which agrees well with the amount of nitrates detected by Q-AMS. FTIR analysis indicates the presence of $\sim 10\%$ HNO₃ and 4% NO₂ impurity in the N₂O₅ prepared, thus the nitrates measured by PILS/IC and Q-AMS likely arise from the partitioning or reactive uptake of gas-phase HNO₃ into the aerosol phase, or HNO₃ produced from heterogeneous hydrolysis of N₂O₅. As in the Q-AMS analysis, no organic species are detected in the filter samples collected from these blank experiments.

3.2 Aerosol yields

A series of experiments with different initial isoprene concentrations are carried out (these are referred to as “typical yield experiments” hereafter). The initial isoprene concentration ranged from 18.4 to 203.4 ppb. Figure 2 shows the reaction profile of the oxidation of an initial mixture containing 203.4 ppb isoprene. Since the chamber is NO_x-free at the beginning of the experiment, once N₂O₅ is introduced into the chamber the equilibrium in Reaction (3) favors the formation of NO₃. This generates a relatively high concentration of NO₃ radicals and results in rapid isoprene decay. Aerosol growth is observed and aerosol volume continues to increase even after all the isoprene is consumed. Owing to the rapid isoprene decay and the relatively long time between each GC measurement (12 min), the isoprene decay over time is captured only in experiments in which the initial isoprene concentration is > 100 ppb. Based on the observed isoprene decay in these experiments and the isoprene-NO₃ rate constant k_{NO_3} , the average NO₃ concentration in the chamber is estimated to be ~ 140 ppt.

Table 1. Initial conditions and results for yield experiments.

Date	T (K)	RH (%)	ΔHC (ppb) ^a	ΔM_o ($\mu\text{g}/\text{m}^3$) ^b	SOA Yield (%)
8/9/07	294	5.1	101.6 \pm 0.6	68.1 \pm 1.1	23.8 \pm 0.5
8/10/07	293	4.7	30.2 \pm 0.1	11.5 \pm 0.4	13.5 \pm 0.5
8/11/07	294	5.4	67.1 \pm 0.1	39.3 \pm 1.2	20.8 \pm 0.7
8/12/07	293	6.0	51.7 \pm 0.2	26.7 \pm 0.6	18.2 \pm 0.5
8/13/07	294	5.7	18.4 \pm 0.1	2.2 \pm 0.2	4.3 \pm 0.5
8/14/07	294	5.5	21.8 \pm 0.1	4.8 \pm 0.4	7.8 \pm 0.6
10/4/2007 ^c	293	5.5	39.5 \pm 0.1 ^d	7.9 \pm 0.3	7.1 \pm 0.6
10/25/2007 ^e	294	6.4	42.0 \pm 0.1	16.6 \pm 0.6	14.1 \pm 0.7

^a Stated uncertainties (1σ) are from scatter in isoprene measurements.

^b Stated uncertainties (1σ) are from scatter in particle volume measurements.

^c Slow isoprene injection experiment.

^d Concentration estimated based on a separate calibration experiment (see Sect. 3.2); the uncertainty in the measured isoprene concentration is assumed to be the same as in the slow N₂O₅ injection experiment.

^e Slow N₂O₅ injection experiment.

The SOA yield of each experiment (Table 1) is shown in Fig. 3. The density of the SOA is determined to be 1.42 g cm⁻³. The amount of inorganic nitrate detected by PILS/IC in each experiment ranges from 1.6 to 2.6 $\mu\text{g m}^{-3}$, which is approximately equal to that measured in the blank experiments. In calculating SOA yield, the organic aerosol mass is corrected for the amount of inorganic nitrate measured in each experiment. For convenience, SOA yields can be parameterized by a semi-empirical model based on absorptive gas-particle partitioning of two semivolatile products (Odum et al., 1996, 1997a,b):

$$Y = \Delta M_o \left[\frac{\alpha_1 K_{om,1}}{1 + K_{om,1} M_o} + \frac{\alpha_2 K_{om,2}}{1 + K_{om,2} M_o} \right] \quad (4)$$

in which Y is the aerosol yield, ΔM_o is the organic aerosol mass produced, M_o is the organic aerosol mass present (equal to ΔM_o in chamber experiments with no absorbing organic mass present initially), α_i is the mass-based gas-phase stoichiometric fraction for semivolatile species i , and $K_{om,i}$ is the gas-particle partitioning coefficient for species i . With this two-product model, Eq. (4) is fit to the experimental yield data (data with $\Delta M_o < 100 \mu\text{g m}^{-3}$) and the yield parameters obtained are: $\alpha_1 = 0.089$, $\alpha_2 = 0.203$, $K_{om,1} = 0.182 \text{ m}^3 \mu\text{g}^{-1}$, and $K_{om,2} = 0.046 \text{ m}^3 \mu\text{g}^{-1}$. For an organic aerosol mass of $\sim 10 \mu\text{g m}^{-3}$, the aerosol yield is $\sim 10\%$.

Also shown in Fig. 3 are aerosol yields from the slow isoprene/N₂O₅ injection experiments. Since the PILS/IC is not employed in these experiments, in calculating SOA yields it is assumed that the amount of inorganic nitrate formed in these slow injection experiments is roughly the same as that in other experiments. For the slow isoprene injection experiment, no isoprene is observed by GC-FID, indicating that once the isoprene enters the chamber, it is quickly consumed by reaction with NO₃. The time profile of isoprene

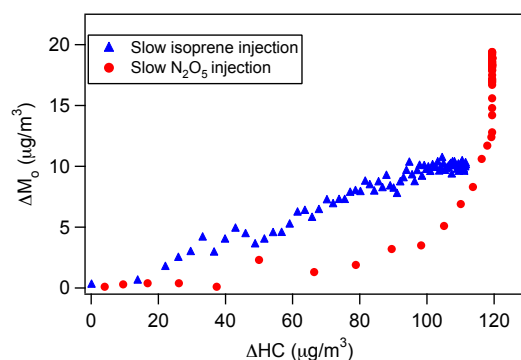


Fig. 4. Time-dependent growth curves for the slow N₂O₅ injection experiment and slow isoprene injection experiment (last two experiments in Table 1).

injection is obtained in a separate experiment, in which the same amount of isoprene is added into the chamber without N₂O₅ present. Assuming the amount of isoprene injected into the chamber is the same as the isoprene reacted, the amount of isoprene reacted over the course of the slow isoprene experiment can be deduced. As seen in Fig. 3, the SOA yield from the slow N₂O₅ injection experiment is roughly the same as those in the other yield experiments; the yield from the slow isoprene injection experiment, however, is lower.

The time-dependent “growth curves” (organic aerosol, ΔM_o , as a function of hydrocarbon reacted, ΔHC) over the course of the slow N₂O₅ injection experiment and the slow isoprene injection experiment are shown in Fig. 4. As hydrocarbon measurements are made with a lower frequency than particle volume, the isoprene concentrations shown are obtained by interpolating GC-FID measurements. In both

4122

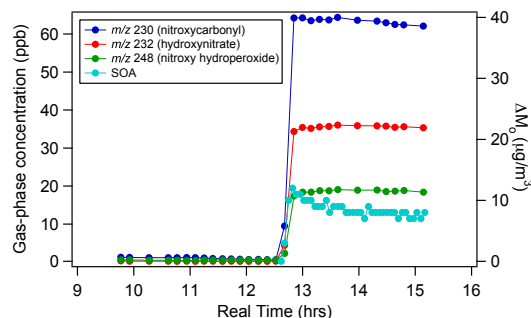


Fig. 5. Time profiles of the major gas-phase products (m/z 230, 232, and 248) and the corresponding aerosol growth from the excess isoprene experiment.

experiments about 40 ppb of isoprene is consumed, the only difference being the order of isoprene/ N_2O_5 injection. From Fig. 4 it is clear that as the reaction proceeds, more aerosol is formed in the slow isoprene injection experiment for the same amount of isoprene reacted. However, the final SOA yield under the slow N_2O_5 injection conditions is higher due to continued aerosol formation even after the complete consumption of isoprene. The presence of a “hook” at the end of the growth curve for the slow N_2O_5 injection experiment indicates that further reactions are contributing to aerosol growth after isoprene is consumed (Ng et al., 2006). Higher generation products also contribute to the aerosols formed in the slow isoprene injection experiment; however, their contributions are not readily observed in the growth curve owing to the way the experiment is conducted. This is further discussed in Sect. 4.3.

3.3 Gas-phase measurements

The CIMS technique measures the concentrations of different gas-phase products over the course of the experiments. A series of experiments is carried out to study the mechanisms of SOA formation by varying the relative amount of isoprene and N_2O_5 injected and monitoring the time evolution of the intermediate products. Shown in Fig. 5 are the time profiles of three major gas-phase products and the corresponding aerosol growth from the excess isoprene experiment. In this experiment, ~ 120 ppb of N_2O_5 is first injected into the chamber, followed by the introduction of ~ 800 ppb isoprene. The initial concentration of isoprene is estimated based on the volume of the isoprene injected and the chamber volume. Once isoprene is injected, a number of product ions are formed immediately, with m/z 230, 232, and 248 being the most dominant ones. Several minor product ions at m/z 185, 377, and 393 are also observed (not shown). With the presence of excess isoprene, it is expected that the three major products detected are first-generation products.

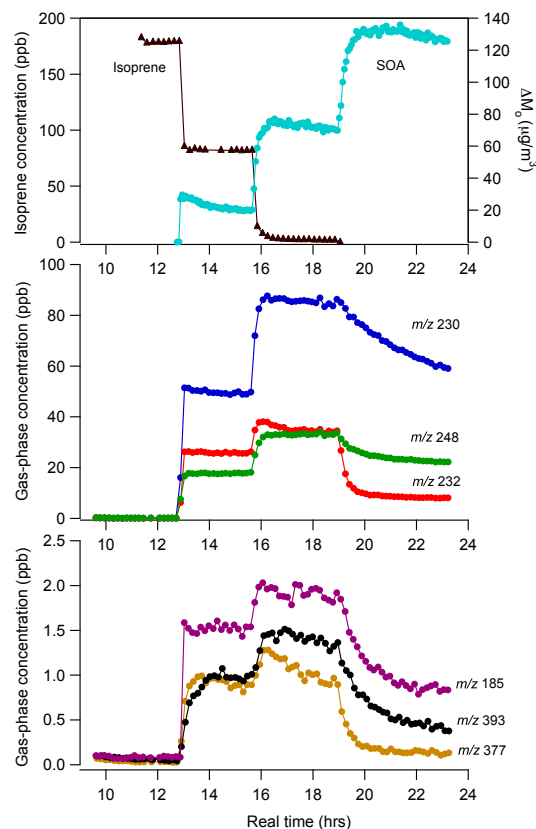


Fig. 6. Time evolution of various gas-phase products in the staggered N_2O_5 injection experiment (Isoprene is first injected into the chamber, followed by the addition of 3 pulses of N_2O_5 : ~ 120 , 50, and 210 ppb). The top panel shows the isoprene decay and aerosol formation; the middle panel shows the time profiles of the three major first-generation products (m/z 230, 232, and 248); the bottom panel shows the time profiles of three minor products (m/z 185, 377, and 393). (The likely identities for these products are shown in Fig. 11).

Their further reaction is suppressed, as indicated by the relatively constant concentrations of the product ions once they are formed. At the end of the experiment, 725 ppb of isoprene is measured by GC-FID. A small amount of aerosol is formed instantaneously, likely from the condensation of relatively nonvolatile first-generation products, or from further generation products that are formed at a relatively rapid rate.

To study further the evolution of the gas-phase products, an experiment is performed in which pulses of N_2O_5 are introduced into the chamber (with isoprene present) (Fig. 6). The top panel shows the isoprene decay and aerosol formation; the middle panel shows the time profiles of the three major first-generation products (m/z 230, 232, and 248); the

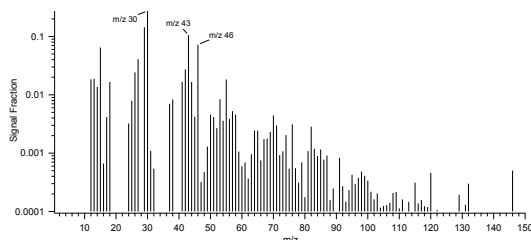


Fig. 7. A typical AMS spectrum for SOA formed in typical yield experiments.

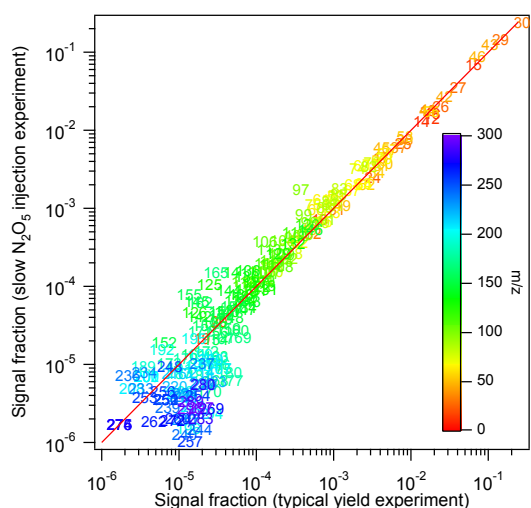


Fig. 8. AMS spectra signal from the slow N₂O₅ injection experiment versus a typical yield experiment. Each mass fragment is normalized by the total signal. The solid red line is the 1:1 line. Note that the higher masses ($m/z > 165$) are dominated by noise.

bottom panel shows the time profiles of three minor products (m/z 185, 377, and 393). In this experiment, 179 ppb of isoprene is first injected into the chamber, followed by the addition of 3 pulses of N₂O₅ (~120, 50, 210 ppb). The observations after the addition of the first pulse of N₂O₅ are similar to the excess isoprene experiment described above. With the addition of ~120 ppb N₂O₅, 97 ppb of isoprene is reacted away, m/z 230, 232, and 248 are formed with concentrations of 49.8 ppb, 26.1 ppb, and 17.3 ppb, respectively. Because of the lack of authentic standards, the concentrations are uncertain. Similar to the data in Fig. 5, the concentrations of these product ions stay relatively constant owing to the presence of excess isoprene. The minor products at m/z 185, 377, and 393, are formed with the concentrations 1.4 ppb, 0.9 ppb, and 0.9 ppb, respectively. Because the sum of the ion concentra-

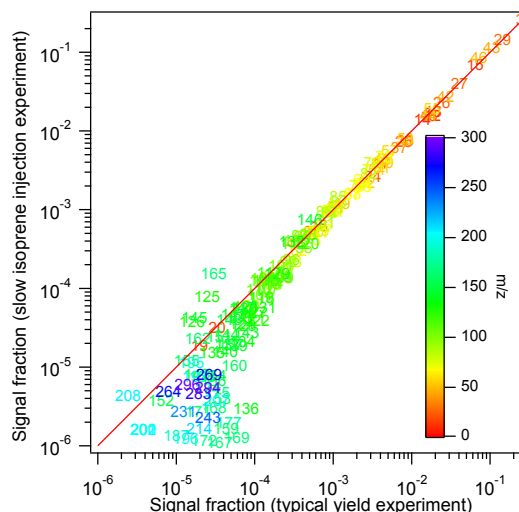


Fig. 9. AMS spectra signal from the slow isoprene injection experiment versus a typical yield experiment. Each mass fragment is normalized by the total signal. The solid red line is the 1:1 line. Note that the higher masses ($m/z > 165$) are dominated by noise.

tions derived from our estimated sensitivities is equal to the reacted isoprene, our estimated sensitivity must represent a lower limit for the actual sensitivity of the CIMS technique to these compounds. It is noted that the m/z 393 ion is formed with a relatively slower rate than all other product ions. A small amount of aerosol is observed. At $t=15:40$, a second pulse of N₂O₅ (~50 ppb) is introduced into the chamber and the remaining 82 ppb isoprene is completely consumed. As seen from Fig. 6, the concentrations of all intermediate products increase accordingly and more aerosol is produced. The last pulse of N₂O₅ (~210 ppb) is added at $t=19:00$. Since all isoprene has been consumed, the additional NO₃ radicals react mainly with the first-generation products, as indicated by the decay of m/z 230, 232, and 248, 185, 377, and 393 ions. Of all of the observed products, it appears that m/z 232 and 377 ions are the most reactive with NO₃ radicals, and their decays in excess NO₃ are strongly correlated with aerosol growth. The rest of the product ions display relatively slower decay kinetics. The decay of the major product ion at m/z 230 does not appear to correlate with aerosol growth, as the concentration of the m/z 230 ion continues to decrease throughout the experiment but there is no further aerosol growth. Since the CIMS instrument has only 0.5 AMU resolution and it cannot distinguish products of similar or identical molecular weight, it is likely that many of observed ions comprise isomers formed from the NO₃ attack at different positions. The fact that many of the observed product ions show two distinct decay time scales indicates that these isomers have substantially different reactivity towards NO₃ radicals.

3.4 Chemical composition of SOA

3.4.1 Aerosol Mass Spectrometer (Q-AMS) measurements

Figure 7 shows the AMS spectrum of SOA formed in the typical yield experiments. Each mass fragment is normalized by the total signal. The SOA exhibits relatively high signals at m/z 30, 43, and 46. The signals at m/z 30 and 46 likely correspond to NO⁺(30) and NO₂⁺(46) fragments from the nitrates in the aerosol. The spectrum shown in Fig. 7 is obtained when aerosol volume reaches its maximum value; the spectrum obtained several hours after aerosol volume peaks shows minimal changes in the mass fractions of different fragments, indicating that the aerosol composition is not changing significantly over time.

Figure 8 shows the mass spectrum of the slow N₂O₅ injection experiment versus a typical yield experiment; Fig. 9 shows the mass spectrum of the slow isoprene injection experiment versus a typical yield experiment. As shown in both figures, the mass fragments fall on the 1:1 line, suggesting a similar SOA composition under the three different experimental conditions. At higher mass to charge ratios the plots drift below the one-to-one line and it appears that the typical experiments have stronger signals at higher m/z 's. However, the signals at these masses (>165) are strongly dominated by noise and cannot be interpreted as differences between the spectra.

3.4.2 Offline chemical analysis

Figure 10 shows the representative UPLC/(–)ESI-TOFMS base peak ion chromatograms (BPCs) for different types of experiments conducted. The numbers denoted above the selected chromatographic peaks correspond to the most abundant negative ions observed in their respective mass spectra. Comparison of the BPCs shown in Fig. 10 indicates that the compositions of the SOA are quite similar for the typical yield experiment, slow isoprene injection experiment, and the acid seed experiment, suggesting a common SOA formation pathway. The SOA composition from the excess isoprene experiment, however, is different from these experiments. This will be discussed further in Sect. 4.4.

Accurate mass measurements for all ions observed by the UPLC/(–)ESI-TOFMS technique for a typical yield experiment are listed in Table 2. The error between the measured mass and theoretical mass is reported in two different ways, ppm and mDa. Overall, the error between the measured and theoretical masses is found to be less than ±2 mDa and ±5 ppm, allowing for generally unambiguous identification of molecular formulae. None of the listed ions is observed in solvent blanks and control filters. By combining the elemental SOA composition (i.e. TOFMS suggested ion formula) data and the gas-phase data from CIMS, structures for each of the SOA components are also proposed. As shown in Table 2, the types of compounds formed included

nitrooxy-organic acids, hydroxynitrates, nitrooxy-organic peroxides (e.g. nitrooxy-hydroxyperoxides), and nitrooxy-organosulfates. It should be noted that the data presented in Table 2 are also applicable to all other types of experiments conducted in this study; however, none of the organosulfates are observed in the nucleation experiments, consistent with previous work (Liggio et al., 2005; Liggio et al., 2006; Surratt et al., 2007a,b; Iinuma et al., 2007a,b). Surprisingly, previously characterized organosulfates of the 2-methyltetrols and the 2-methyltetrol mono-nitrates detected at m/z 215 and m/z 260 (not listed in Table 2), respectively, which are produced from the photooxidation of isoprene in the presence of acidified sulfate seed aerosol (Surratt et al., 2007a,b; Gómez-González et al., 2007), are also observed in the acid seed experiment shown in Fig. 10, suggesting that nighttime oxidation of isoprene in the presence of acidic seed may also be a viable pathway for these known ambient tracer compounds.

Owing to the implementation of reverse-phase chromatography, the SOA components that are more hydrophilic elute from the column the earliest, while the more hydrophobic components elute the latest. It is clear from Table 2 that compounds with the same carbon number and general functionality (i.e. carboxylic acid, alcohol, or organosulfate), but differing number of nitrooxy groups, exhibit distinctly different chromatographic behaviors. The presence of more nitrooxy groups appears to increase the retention time of the SOA compound. For example, it is found that m/z 194 organic acid compound (C₅H₈NO₇[–]) containing one nitrooxy group elutes earlier than that of the m/z 239 organic acid compounds (C₅H₇N₂O₉[–]) containing two nitrooxy groups. Similarly, the m/z 305 organosulfate (C₅H₉N₂O₁₁S[–]) elutes earlier than that of the m/z 349 organosulfate (C₅H₈N₃O₁₃S[–]).

SOA components that are either nitrooxy-organic acids or nitrooxy-organosulfates are detected strongly as the [M–H][–] ion, consistent with previous work (Surratt et al., 2006; Surratt et al., 2007a,b; Gao et al., 2004a,b; Gao et al., 2006), whereas the hydroxynitrates and nitrooxy-hydroxyperoxides are detected as both the [M–H][–] and [M–H + C₂H₄O₂][–] ions, with the latter acetic acid adduct ion, in most cases, being the base peak ion (i.e. dominant ion). The acetic acid adduct ions for the hydroxynitrates and the nitrooxy-hydroxyperoxides are formed owing to the presence of acetic acid in the UPLC mobile phase. Previous studies have shown that non-acidic hydroxylated species (such as the 2-methyltetrols) and organic peroxides formed from the photooxidation of isoprene (Claeys et al., 2004; Edney et al., 2005; Surratt et al., 2006) are either undetectable or yield weak negative ions when using (–)ESI-MS techniques. However, it appears that the co-presence of nitrooxy groups in the hydroxylated SOA components allow for these compounds to become acidic enough to be detected by the UPLC/(–)ESI-TOFMS technique, or allow for adduction with acetic acid. Further confirmation for the presence of organic peroxides in the isoprene SOA produced from NO₃ oxidation is provided by the iodometric-spectroscopic measurements shown

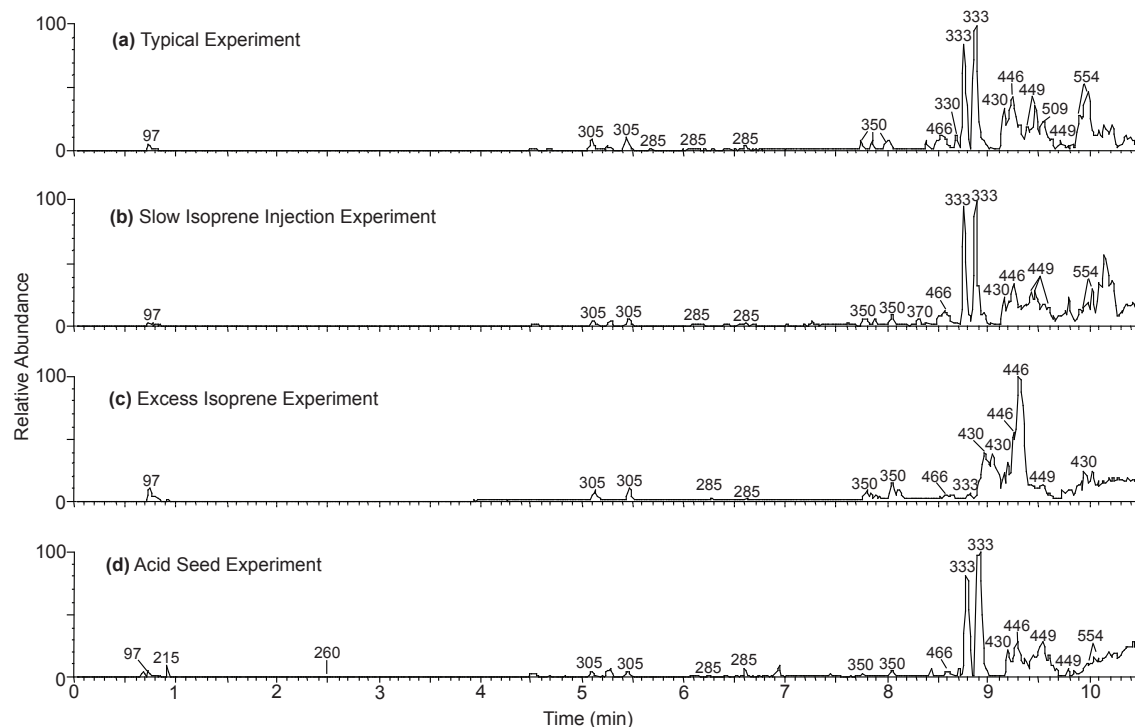


Fig. 10. UPLC/(-)ESI-TOFMS base peak ion chromatograms (BPCs) for the following isoprene-NO₃ oxidation experiments: **(a)** 200 ppb isoprene+1 ppm N₂O₅+seed aerosol generated from 15 mM (NH₄)₂SO₄ atomizing solution; **(b)** 300 ppb isoprene+1 ppm N₂O₅+seed aerosol generated from 15 mM (NH₄)₂SO₄ atomizing solution; **(c)** 1.2 ppm isoprene+700 ppb N₂O₅+seed aerosol generated from 15 mM (NH₄)₂SO₄ atomizing solution; **(d)** 200 ppb isoprene+1 ppm N₂O₅+seed aerosol generated from 30 mM MgSO₄+50 mM H₂SO₄ atomizing solution. The numbers indicated above the selected chromatographic peaks correspond to the most abundant negative ion, which is either the [M-H]⁻ or [M-H+C₂H₄O₂]⁻ ion.

in Table 3. Based upon the UPLC/(-)ESI-TOFMS measurements shown in Table 2, an average molecular weight of 433 for the organic peroxides is assumed for the calculations shown in Table 3. The contribution of organic peroxides to the SOA mass concentration is found to be fairly reproducible for duplicate typical experiments (i.e., 8/22/07 and 10/24/07). The amount of organic peroxides in the excess isoprene experiment is below detection limits. Owing to the lack of authentic standards, there are large uncertainties associated with the quantification of these products in the aerosol phase. This is further discussed in Sect. 4.4.

4 Gas-phase chemistry and SOA formation

4.1 Formation of various gas-phase products

As seen from Figs. 5 and 6, the three major first-generation products formed from isoprene-NO₃ reaction are the *m/z* 230, 232, and 248 ions. Since the CIMS technique uses

CF₃O⁻ (anionic mass 85 Da) as the reagent ion, compounds are detected at a *m/z* value of their molecular weight (MW) plus 85. The product ions at *m/z* 230, 232, and 248 likely correspond to C₅-nitrooxycarbonyl (MW 145), C₅-hydroxynitrate (MW 147), and C₅-nitrooxyhydroperoxide (MW 163). These products have been observed in previous studies (Jay and Stieglitz, 1989; Skov et al., 1992; Kwok et al., 1996; Berndt and Böge, 1997) and their formation from the isoprene-NO₃ reaction is relatively straightforward (Fig. 11). The reaction proceeds by NO₃ addition to the C=C double bond, forming four possible nitrooxyalkyl radicals depending on the position of the NO₃ attack. Previous studies suggest that NO₃ radicals predominantly attack isoprene in the 1-position, with a branching ratio (C₁-position/C₄-position) varying between 3.5 and 7.4 (Skov et al., 1992; Berndt and Böge, 1997; Suh et al., 2001). As mentioned before, the average branching ratio (5.5:1) is used in estimating the sensitivities of the compounds measured by CIMS. In Fig. 11, only the nitrooxyalkyl radical formed from the C1

Table 2. SOA products identified using UPLC/(–)ESI-TOFMS.

Retention Time (min)	Measured [M–H] [–] Ion (<i>m/z</i>)	TOFMS Suggested [M–H] [–] Ion Formula	Error (mDa, ppm)	Measured [M–H+C ₂ H ₄ O ₂] [–] Ion (<i>m/z</i>)	TOFMS Suggested [M–H+C ₂ H ₄ O ₂] [–] Ion Formula	Error (mDa, ppm)	Proposed Structure ^a
3.68 ^b	194.0310	C ₅ H ₈ NO ₇ [–]	0.9, 4.6	^c			
4.52 ^b	239.0137	C ₅ H ₇ N ₂ O ₉ [–]	–1.5, –6.3				
5.09 ^d	304.9946	C ₅ H ₉ N ₂ O ₁₁ S [–]	1.9, 6.2				
5.24 ^b	239.0152	C ₅ H ₇ N ₂ O ₉ [–]	0.0, 0.0				
5.43 ^d	304.9944	C ₅ H ₉ N ₂ O ₁₁ S [–]	1.7, 5.6				
6.07	225.0350	C ₅ H ₉ N ₂ O ₈ [–]	–0.9, –4.0				
6.12	225.0342	C ₅ H ₉ N ₂ O ₈ [–]	–1.7, –7.6				
6.60	225.0375	C ₅ H ₉ N ₂ O ₈ [–]	1.6, 7.1		285.0676	C ₇ H ₁₃ N ₂ O ₁₀ [–]	0.6, 2.1
7.75 ^d	349.9775	C ₅ H ₈ N ₃ O ₁₃ S [–]	–0.3, –0.9				
7.85 ^d	349.9764	C ₅ H ₈ N ₃ O ₁₃ S [–]	0.2, 0.6				
8.00 ^d	349.9784	C ₅ H ₈ N ₃ O ₁₃ S [–]	–0.4, –1.1				
8.48 ^d	466.0268	C ₁₀ H ₁₆ N ₃ O ₁₆ S [–]	1.7, 3.6				
8.54 ^d	466.0264	C ₁₀ H ₁₆ N ₃ O ₁₆ S [–]	1.3, 2.8				
8.72 ^d	466.0237	C ₁₀ H ₁₆ N ₃ O ₁₆ S [–]	–1.4, –3.0				
8.76 ^e	270.0199	C ₅ H ₈ N ₃ O ₁₀ [–]	–1.1, –4.1	330.0393	C ₇ H ₁₂ N ₃ O ₁₂ [–]	–2.8, –8.5	
8.81 ^d	466.0237	C ₁₀ H ₁₆ N ₃ O ₁₆ S [–]	–1.4, –3.0				
8.85 ^e	270.0204	C ₅ H ₈ N ₃ O ₁₀ [–]	–0.6, –2.2	330.0379	C ₇ H ₁₂ N ₃ O ₁₂ [–]	–4.2, –12.7	
9.15	370.0734	C ₁₀ H ₁₆ N ₃ O ₁₂ [–]	0.9, 2.4	430.0940	C ₁₂ H ₂₀ N ₃ O ₁₄ [–]	–0.5, –1.2	
9.19	386.0678	C ₁₀ H ₁₆ N ₃ O ₁₃ [–]	–0.5, –1.3	446.0888	C ₁₂ H ₂₀ N ₃ O ₁₅ [–]	–0.6, –1.3	
9.24	370.0732	C ₁₀ H ₁₆ N ₃ O ₁₂ [–]	–0.2, –0.5	430.0937	C ₁₂ H ₂₀ N ₃ O ₁₄ [–]	–0.8, –1.9	
9.25	386.0683	C ₁₀ H ₁₆ N ₃ O ₁₃ [–]	–0.2, –0.5	446.0893	C ₁₂ H ₂₀ N ₃ O ₁₅ [–]	–0.1, –0.2	
9.37	449.0637	C ₁₀ H ₁₇ N ₄ O ₁₆ [–]	–0.3, –0.7	509.0854	C ₁₂ H ₂₁ N ₄ O ₁₈ [–]	0.3, 0.6	
9.41	386.0684	C ₁₀ H ₁₆ N ₃ O ₁₃ [–]	0.1, 0.3	446.0903	C ₁₂ H ₂₀ N ₃ O ₁₅ [–]	0.9, 2.0	
9.45	449.0653	C ₁₀ H ₁₇ N ₄ O ₁₆ [–]	1.3, 2.9	509.0853	C ₁₂ H ₂₁ N ₄ O ₁₈ [–]	0.2, 0.4	
9.90 ^f	494.0537	C ₁₀ H ₁₆ N ₅ O ₁₈ [–]	4.7, 9.5	554.0669	C ₁₂ H ₂₀ N ₅ O ₂₀ [–]	–3.3, –6.0	
9.98 ^f	494.0518	C ₁₀ H ₁₆ N ₅ O ₁₈ [–]	2.8, 5.7	554.0676	C ₁₂ H ₂₀ N ₅ O ₂₀ [–]	–2.6, –4.7	

^a Structural isomers containing nitrate, sulfate, or hydroxyl groups at other positions are likely; for simplicity, only one isomer is shown.

^b These compounds appear to be very minor SOA products due to very small chromatographic peak areas, confirming that the further oxidation of the nitrooxycarbonyl and hydroxycarbonyl first-generation gas-phase products do not yield significant quantities of SOA.

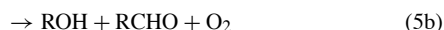
^c A blank cell indicates that the detected SOA product had no observable acetic acid adduct ion (i.e. [M–H+C₂H₄O₂][–]).

^d These organosulfate SOA products were observed only in experiments employing either (NH₄)₂SO₄ (i.e. neutral) or MgSO₄ + H₂SO₄ (i.e. acidic) seed aerosol. These organosulfate SOA products were also observed in the excess isoprene experiments.

^e In addition to the acetic acid adduct ion, these compounds also had a significant adduct ion at [M–H+HNO₃][–] (*m/z* 333), indicating that these compounds are likely not very stable due to the fragmentation of one of the NO₃ groups during the MS analysis.

^f These compounds were only weakly detected in the excess isoprene experiments.

attack is shown. The nitrooxyalkyl radicals then react with O₂ to form RO₂ radicals, which react further with HO₂, RO₂, or NO₃ radicals under the experimental conditions in this study. The reaction of RO₂ radicals and HO₂ radicals leads to the formation of C₅-nitrooxyhydroperoxide (*m/z* 248). The reaction of two RO₂ radicals (self reaction or cross reaction) has three different possible channels:



The second channel results in the formation of C₅-nitrooxycarbonyl (*m/z* 230) and C₅-hydroxynitrate (*m/z* 232). According to channel (5b), these two products should be formed with a 1:1 ratio; however, C₅-nitrooxycarbonyl can also be formed from alkoxy radicals (alkoxy radicals formed through RO₂+RO₂ reaction or RO₂+NO₃ reaction). In Fig. 6, 49.8 ppb of C₅-nitrooxycarbonyl and 26.1 ppb of C₅-hydroxynitrate are formed after the addition of the first pulse of N₂O₅, indicating ~24 ppb of C₅-nitrooxycarbonyl is formed from the reaction of alkoxy radicals. The branching ratios for the reaction of small peroxy radicals have been investigated in previous studies. It is found that the branching ratio for channel (5a) for methylperoxy and ethylperoxy radicals is ~0.3–0.4 and ~0.6, respectively (Lightfoot et al., 1992; Wallington et al., 1992; Tyndall et al., 1998). It is

Experiment Date	Seeded ^a / Nucleation	[Isoprene] (ppb)	[N ₂ O ₅] (ppm)	SOA Volume Growth Observed ^b ($\mu\text{m}^3/\text{cm}^3$)	Total SOA Mass Concentration ^c ($\mu\text{g}/\text{m}^3$)	Peroxide Aerosol Mass Concentration ($\mu\text{g}/\text{m}^3$)	Contribution of Peroxides to the SOA Mass Concentration Observed (%)
8/22/07	AS	200	1	102	145	46	32
8/30/07	AMS	200	1	123	174	40	23
10/22/07 ^d	AS	1200	0.7	70	100	b.d.l. ^e	f
10/23/07	nucleation	200	1	125	177	31	17
10/24/07	AS	200	1	111	158	47	30
10/27/07 ^g	AS	300	1	110	156	47	30

^b Averaged over the course of filter sampling.

^c Assuming a SOA density of 1.42 g/cm³. This was based on DMA and Q-AMS measurements.

^d Excess isoprene experiment.^e Below detection limits.

^f No observable contribution of organic peroxides to the SOA mass concentration.

^g Slow injection of isoprene in this experiment to enhance the $\text{RO}_2 + \text{NO}_3$ reaction pathway.

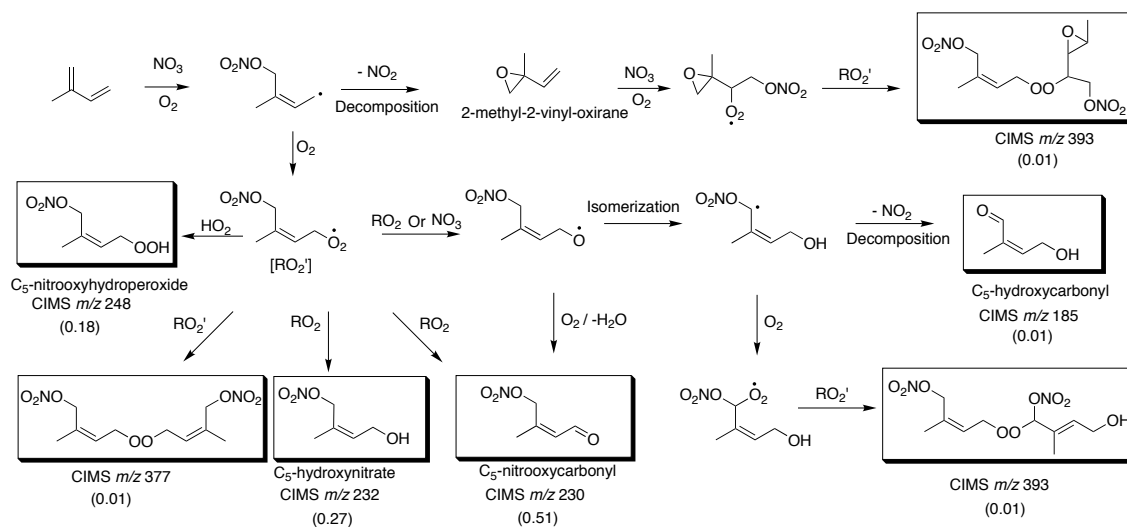


Fig. 11. Proposed mechanisms for the formation of various gas-phase intermediate product ions observed by CIMS. Multiple structural isomers are possible. In this figure, RO₂' refers to the isoprene peroxy radical (nitrooxyperoxy radical), RO₂ refer to a generic peroxy radical. The numbers in the parentheses refer to the molar yields of the products. It is noted that the sensitivity for *m/z* 393 is not calculated; instead, it is assumed that the sensitivity (and hence the sum of the molar yields of the two isomers shown, since *m/z* 377 and *m/z* 393 are formed with the same concentration) to be the same as that for *m/z* 377.

likely that the isoprene peroxy radicals react via this pathway to form alkoxy radicals and contribute to the “extra” 24 ppb of C₅-nitrooxycarbonyl. This observation is indicative that most RO₂ radicals react with other RO₂ radicals instead with NO₃ or HO₂ radicals.

Other than C₅-nitrooxycarbonyl, C₅-hydroxynitrate, and C₅-nitrooxyhydroperoxide, three other minor products (*m/z* 185, 377 and 393 ions) are also observed as intermediate products. The proposed mechanisms for the formation of

these gas-phase products are also shown in Fig. 11. Although channel (5c) in the RO₂+RO₂ reaction is found to be minor for small peroxy radicals such as methylperoxy and ethylperoxy radicals (Kan et al., 1980; Niki et al., 1981, 1982; Wallington et al., 1989; Tyndall et al., 1998; Tyndall et al., 2001), the product ion at m/z 377 could be the corresponding ROOR product formed from the self reaction of isoprene peroxy radicals. The product ion at m/z 185 likely corresponds to the C₅-hydroxycarbonyl. It has been observed

4128

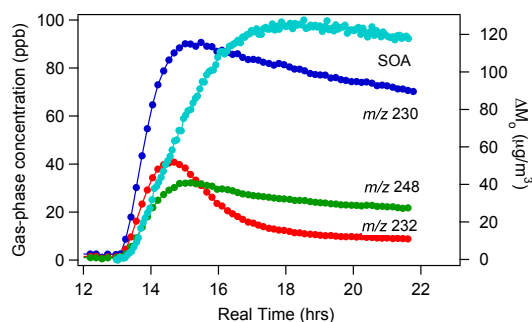


Fig. 12. Time profiles of the major gas-phase products (m/z 230, 232, and 248) and the corresponding aerosol growth from the slow N_2O_5 injection experiment. Note that this experiment has a higher initial isoprene concentration (~ 200 ppb) compared to the one shown in Fig. 4.

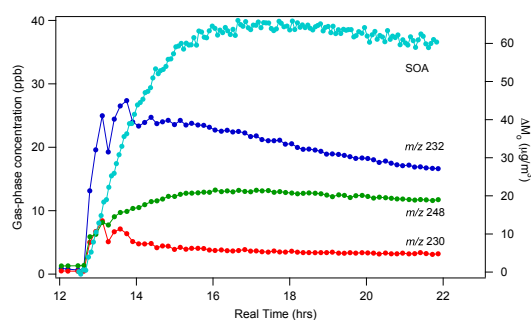


Fig. 13. Time profiles of the major gas-phase products (m/z 230, 232, and 248) and the corresponding aerosol growth from the slow isoprene injection experiment. Note that this experiment has a higher initial isoprene concentration (~ 200 ppb) compared to the one shown in Fig. 4.

in previous studies and it likely arises from the isomerization of nitrooxyalkoxy radicals through a 6-member transition state to form a hydroxynitrooxy alkyl radical, which then decomposes to form NO_2 and C₅-hydroxycarbonyl (Kwok et al., 1996). Such isomerization has also been proposed to occur in the photooxidation of isoprene (Paulson and Seinfeld, 1992; Carter and Atkinson, 1996; Dibble, 2002). It is possible that the hydroxynitrooxy alkyl radical formed proceeds to react with O_2 to form a peroxy radical, which then reacts with the isoprene peroxy radical to form the product ion at m/z 393. The product ion at m/z 393 shows a slower rate of formation (Fig. 6) compared to other product ions suggesting that it might also be formed from the further oxidation of a first-generation product. 2-methyl-2-vinyl-oxirane has been observed from isoprene- NO_3 reaction in previous studies at 20 mbar in helium (Berndt and Böge, 1997) and 20 Torr in argon (Skov et al., 1994), respectively. When operated in positive mode with H_3O^+ as the reagent ion (products are observed at $m/z = MW + 1$), CIMS shows a protonated molecule at m/z 85. Although the epoxide yield is found to be $< 1\%$ of the total reacted isoprene at atmospheric pressure (Skov et al., 1994), the signal at m/z 85 can arise in part from the epoxide. The further oxidation of the epoxide results in the formation of an epoxide peroxy radical, which can react with the isoprene peroxy radical to form the peroxide at m/z 393. It is noted that a product ion at m/z 246 is detected in CIMS, which could arise from the corresponding carbonyl product formed from the reactions of two epoxide peroxy radicals, or from the fragmentation of the epoxide alkoxy radicals. Unlike m/z 393, which decays after the addition of the last pulse of N_2O_5 , m/z 246 stays relatively constant suggesting that it is not being further oxidized by NO_3 radicals. To examine further the possibility of peroxide formation (m/z 377 and 393) in the gas phase, an experiment is conducted using 1,3-butadiene as the parent hydrocarbon. The analogous

product ions for the 1,3-butadiene system, i.e. m/z 349 and 365, are observed in CIMS, providing further indication that the formation of ROOR products from two RO_2 radicals is occurring in the gas phase. Further details of the gas-phase chemistry of isoprene and 1,3-butadiene will be forthcoming in a future manuscript.

4.2 Effect of peroxy radical chemistry on SOA yield

The SOA yield ranges from 4.3% to 23.8% for an initial isoprene concentration of 18.4 to 101.6 ppb in the typical yield experiments. While the SOA yield from the slow N_2O_5 injection experiment is roughly the same as that in the typical yield experiments, the SOA yield from the slow isoprene injection experiment is lower (Fig. 3). In both cases, ~ 40 ppb of isoprene is consumed, the main difference being the relative importance of $RO_2 + RO_2$ reaction versus $RO_2 + NO_3$ reaction in each system. In the slow N_2O_5 injection experiment, a relatively small amount of NO_3 is available in the chamber. Once RO_2 radicals are formed, it is expected that they would react primarily with other RO_2 radicals instead of NO_3 radicals owing to the presence of a relatively higher isoprene concentration in the chamber. On the other hand, the slow isoprene injection experiment favors $RO_2 + NO_3$ reaction owing to the presence of excess N_2O_5 in the chamber. Thus the higher SOA yield observed in the slow N_2O_5 injection experiment suggests the products formed via $RO_2 + RO_2$ reaction partition more readily into the aerosol phase, or the $RO_2 + RO_2$ reaction forms products that further react and contribute significantly to aerosol growth. The fact that the SOA yield from the slow N_2O_5 injection experiment is roughly the same as in the typical yield experiments implies that $RO_2 + RO_2$ reaction dominates in typical yield experiments.

The time profile for the three major first-generation gas phase products and SOA growth from the slow N_2O_5 injection experiment and slow isoprene injection experiment are

shown in Figs. 12 and 13, respectively. It is noted that this pair of experiments has a higher initial isoprene concentration (~200 ppb) compared to the pair of experiments shown in Fig. 4. In both cases, once the first-generation products are formed they can react further with NO₃ radicals, making it difficult to estimate the formation yields of these products based on the measured concentrations. The extent to which these products react further is expected to be higher in the slow isoprene injection experiment owing to the presence of excess NO₃ in chamber; this is consistent with the relatively lower concentrations of first-generation products observed. As mentioned before, it is possible that the CIMS signal at the observed m/z comprises isomers formed from the NO₃ attack at positions other than the C1 carbon. Such isomers have slightly different structures but they could exhibit a very different reaction rate towards NO₃ radicals. For instance, studies have shown that the reaction rates of NO₃ radicals with unsaturated alcohols and unsaturated carbonyl compounds can vary by several orders of magnitude depending on the position of the substituted methyl group (Noda et al., 2002; Canosa-Mas et al., 2005). It is possible that the minor products formed from NO₃ attack at other positions react much slower with NO₃ radicals, hence the concentrations of the observed product ions do not decay to zero towards the end of the experiment. At the end of the experiment, about 8 ppb and 3 ppb of C₅-hydroxynitrate is left in the slow N₂O₅ injection experiment and slow isoprene injection experiment, respectively. Assuming the amount of reactive isomers and unreactive (or relatively slow reacting) isomers are formed in the same ratio in the slow N₂O₅ injection experiment and the slow isoprene injection experiment, we can deduce that a relatively higher concentration of reactive C₅-hydroxynitrate (as well as the two other first-generation products) is formed in the slow N₂O₅ injection experiment. This is consistent with the larger extent of RO₂+RO₂ reaction (which forms C₅-hydroxynitrate) and the higher SOA yield observed in the slow N₂O₅ injection experiment, as it appears that C₅-hydroxynitrate is an effective SOA precursor (Fig. 6).

4.3 Growth curves: multiple steps in SOA formation

By examining the time-dependent growth curves (organic aerosol, ΔM_o , as a function of hydrocarbon reacted, ΔH_C) we can gain insights into the general mechanisms of SOA formation (Ng et al., 2006, 2007a,b). Figure 4 shows the time-dependent growth curves for the slow N₂O₅ injection experiment and the slow isoprene injection experiment, respectively. For the slow N₂O₅ injection experiment, the initial aerosol growth likely arises from the condensation of first-generation products as the presence of excess isoprene in the chamber suppresses their further oxidation. If higher generation products do contribute to SOA formation, they would have to be formed at relatively fast rates. After isoprene is consumed, aerosol mass continue to increase and results in a “hook” in the growth curve. This indicates that

secondary products (or higher generation products) also contribute significantly to SOA formation. The same observation can be made if we examine the reaction profile of a typical yield experiment (Fig. 2): there is further SOA growth after all isoprene is reacted away, indicating that the further oxidation of first generation products are contributing to SOA formed. These observations are consistent with the fact that the decay of first-generation products observed in CIMS (especially the m/z 232 and m/z 377 ions) is strongly anticorrelated with further SOA growth (Fig. 6). On the other hand, the slow isoprene injection experiment does not allow us to differentiate the contribution of first- and second-generation products to SOA formation. With the presence of excess NO₃ radicals in the chamber, the first-generation products formed in the slow isoprene injection experiment would be further oxidized once they are formed. The SOA growth observed throughout this experiment is from the partitioning of these highly oxidized and nonvolatile products. Hence, at the beginning of the experiment, for the same amount of ΔH_C , the amount of SOA formed in this experiment is higher than that in the slow N₂O₅ injection experiment, in which the aerosol growth is probably from the condensation of relatively more volatile first-generation products. Both the AMS data and filter sample data (Figs. 8, 9, and 10) show a very similar composition for the final SOA formed in slow N₂O₅ injection experiment and the slow isoprene injection experiment, suggesting a common SOA forming channel. Based on the previous discussion on the effect of peroxy radical chemistry on SOA yields, it is likely that the RO₂+RO₂ reaction is the SOA-forming channel in both cases; such a reaction occurs to a large extent in the slow N₂O₅ injection experiments and results in the formation of more SOA.

4.4 Proposed mechanisms of SOA formation

The combination of CIMS gas-phase data and elemental SOA composition data provides substantial insights into the mechanisms of SOA formation. Shown in Figs. 14–17 are the proposed SOA formation mechanisms from the further oxidation of the various gas-phase products measured by CIMS. The compounds in the boxes are the SOA products detected by UPLC/(–)ESI-TOFMS. Owing to multiple chromatographic peaks observed in the UPLC/(–)ESI-TOFMS extracted ion chromatograms (EICs) for the negative ions of the proposed SOA products, structural isomers are likely; however, for simplicity we show only one possible isomer for each product formed from a particular reaction pathway. Many of the SOA products detected are formed from the further oxidation of first- or higher-generation products, which is consistent with the observation of continual SOA growth after the complete consumption of isoprene (hence a “hook” in the growth curve). With the large number of nitrate-substituted compounds detected by UPLC/(–)ESI-TOFMS technique, it is also not surprising that AMS shows strong signals at m/z 30 (NO⁺) and m/z 46 (NO₂⁺).

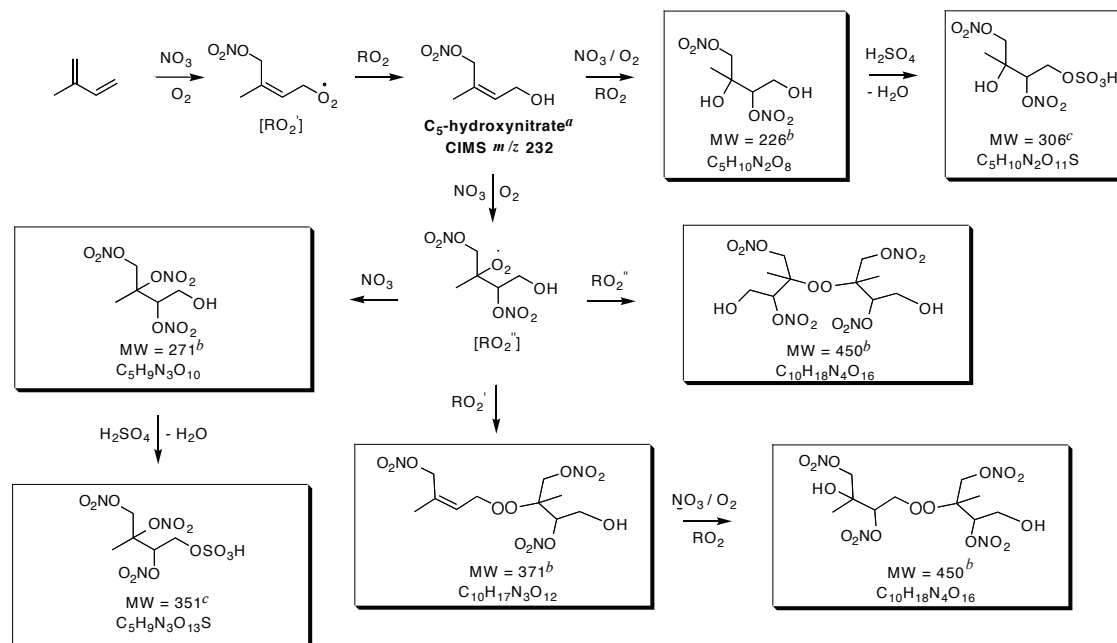


Fig. 14. Proposed mechanism for SOA formation from the formation and decay of the C₅-hydroxynitrate gas-phase product formed from the isoprene + NO₃ reaction. Boxes indicate UPLC/(–)ESI-TOFMS detected SOA products; molecular formulas were confirmed by the accurate mass data provided by the UPLC/(–)ESI-TOFMS. Multiple structural isomers are possible, consistent with the multiple chromatographic peaks observed in the extracted ion chromatograms; however, only one structural isomer is shown for simplicity. ^a This first-generation gas-phase product was previously observed by Jay and Stieglitz (1989), Skov et al. (1992), Kwok et al. (1996), and Berndt and Böge (1997); this gas-phase product was detected as the [M+CF₃O][–] ion by the CIMS instrument. ^b These particle-phase compounds were detected as both their [M–H][–] and [M–H+C₂H₄O₂][–] ions; the acetic acid adduct ([M–H+C₂H₄O₂][–]) ion was, in most cases, the molecular ion (i.e. dominant ion). ^c These organosulfate compounds were detected as their [M–H][–] ions and were observed only in ammonium sulfate and acidified magnesium sulfate seeded experiments.

Shown in Figs. 14 and 15 are the proposed SOA formation pathways from the further oxidation of the *m/z* 232 (i.e. C₅-hydroxynitrate) and 377 gas-phase product ions (as detected by CIMS). The decay of these two products has been found to be strongly correlated with aerosol growth (Fig. 6), which is consistent with the large number of SOA products formed from their further oxidation. The further oxidation of these two gas-phase products also yields SOA compounds of the same molecular weight (compounds of MW 371 and 450). Although *m/z* 393 is a minor gas-phase product, the further oxidation of this compound leads to formation of several SOA products (Fig. 16). As mentioned before, there are two possible formation routes for *m/z* 393, and the further oxidation of both products is shown in Fig. 16. The further oxidation of the *m/z* 393 ion appears to yield SOA products that are specific only to this gas-phase product: these include the SOA products of MW 387 and 467.

Figure 17 shows the proposed SOA formation mechanisms from three other gas-phase products (*m/z* 185, *m/z* 230, and *m/z* 277); the further oxidation of these product ions leads to relatively minor SOA products. Although C₅-nitrooxycarbonyl (*m/z* 230) is the most abundant gas-phase product detected by CIMS, its further oxidation is not well correlated with aerosol growth (Fig. 6). The further oxidation of *m/z* 230 yields an SOA product at MW 240. This organic acid product is found to be quite minor when examining the peak area in its corresponding extracted ion chromatogram (EIC). It is noted that no SOA products are detected from the further oxidation of the C₅-nitrooxyhydroperoxide (*m/z* 248) (also a major gas-phase product); it is possible that these hydroperoxide products are not acidic enough to be detected by the UPLC/(–)ESI-TOFMS technique, or degrade during sample workup and/or analysis procedures. It has been shown that hydroxycarbonyl

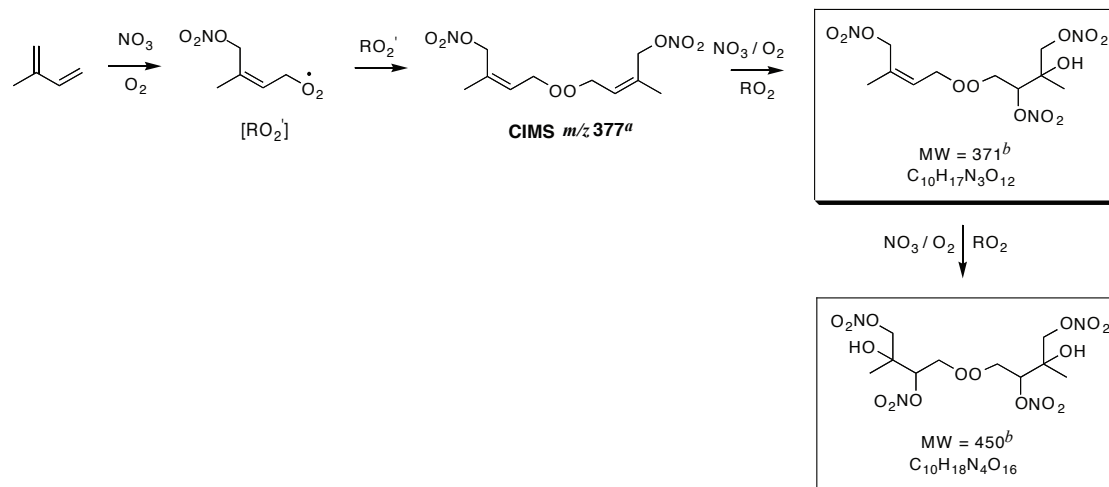


Fig. 15. Proposed mechanism for SOA formation from the formation and decay of the CIMS *m/z* 377 gas-phase product formed from the isoprene+NO₃ reaction. Boxes indicate UPLC/(–)ESI-TOFMS detected SOA products; molecular formulas were confirmed by the accurate mass data provided by the UPLC/(–)ESI-TOFMS. Multiple structural isomers are possible, consistent with the multiple chromatographic peaks observed in the extracted ion chromatograms; however, only one structural isomer is shown for simplicity. ^a This first-generation gas-phase product was detected as the [M + CF₃O][–] ion by the CIMS instrument. ^b These particle-phase compounds were detected as both their [M–H][–] and [M–H+C₂H₄O₂][–] ions; the acetic acid adduct ([M–H+C₂H₄O₂][–]) ion was, in most cases, the molecular ion (i.e. dominant ion).

plays a key role in SOA formation from the reaction of linear alkenes with NO₃ radicals (Gong et al., 2005), however, in the isoprene-NO₃ system, the further oxidation of the minor gas-phase product C₅-hydroxycarbonyl (*m/z* 185) leads to the formation of only one minor aerosol product at MW 195. Some evidence for the formation of a C₅-dinitrate first-generation gas-phase product is indicated from the CIMS and UPLC/(–)ESI-TOFMS data. This first-generation gas-phase product has been observed previously by Werner et al. (1997). The CIMS shows a weak signal at *m/z* 277, which could be associated to the dinitrate product; we do not know, however, whether the negative ion efficiently clusters with such compounds. Further evidence for the dinitrate gas-phase product is provided by the UPLC/(–)ESI-TOFMS detection of an SOA product at MW 495, which could result from the further oxidation of a C₅-dinitrate precursor. The precursor compound before the last oxidation step shown in this mechanism in Fig. 17 may exist in the particle phase; however, this compound is not likely to be detected by the UPLC/(–)ESI-TOFMS technique owing to the lack of acidic hydrogens from neighboring hydroxyl and/or carboxyl groups.

The SOA products highlighted in Figs. 14–17 are observed in all major experiments conducted; however, not all of these products are strongly detected in the excess isoprene experiment (Fig. 10c). With the presence of excess isoprene, further oxidations of first-generation products should be minimal and no significant SOA formation is expected. The reaction rate of isoprene and NO₃ radicals is $k_{\text{NO}_3} = 7 \times 10^{-13} \text{ cm}^3 \text{ molecule}^{-1} \text{ s}^{-1}$. To our knowledge, the reaction rate of the first-generation products and NO₃ radicals has not been studied. The structure of *m/z* 232 (C₅-hydroxynitrate) is similar to 3-methyl-2-buten-1-ol (MBO321), except that the γ -carbon has one nitro group and one methyl group substitution instead of two methyl group substitutions. The reaction rate coefficient of MBO321 and NO₃ radicals is $k_{\text{NO}_3} = 1 \times 10^{-12} \text{ cm}^3 \text{ molecule}^{-1} \text{ s}^{-1}$. It is found that the reaction rate with NO₃ radicals increases with increasing number of methyl groups at the γ -carbon (Noda et al., 2002), which is in accordance with the stabilization theory for leaving groups discussed in Atkinson (1997) and Noda et al. (2000). With reference to this, we would expect the reaction rate of C₅-hydroxynitrate and NO₃ radicals to be slower than that of MBO321 due to the presence of the electron withdrawing nitro group. Hence, it is likely that the reaction rate of isoprene and NO₃ radicals and C₅-hydroxynitrate and NO₃ radicals are roughly in the same range. The relative production rate of first- and second-generation products will then be the ratio of the

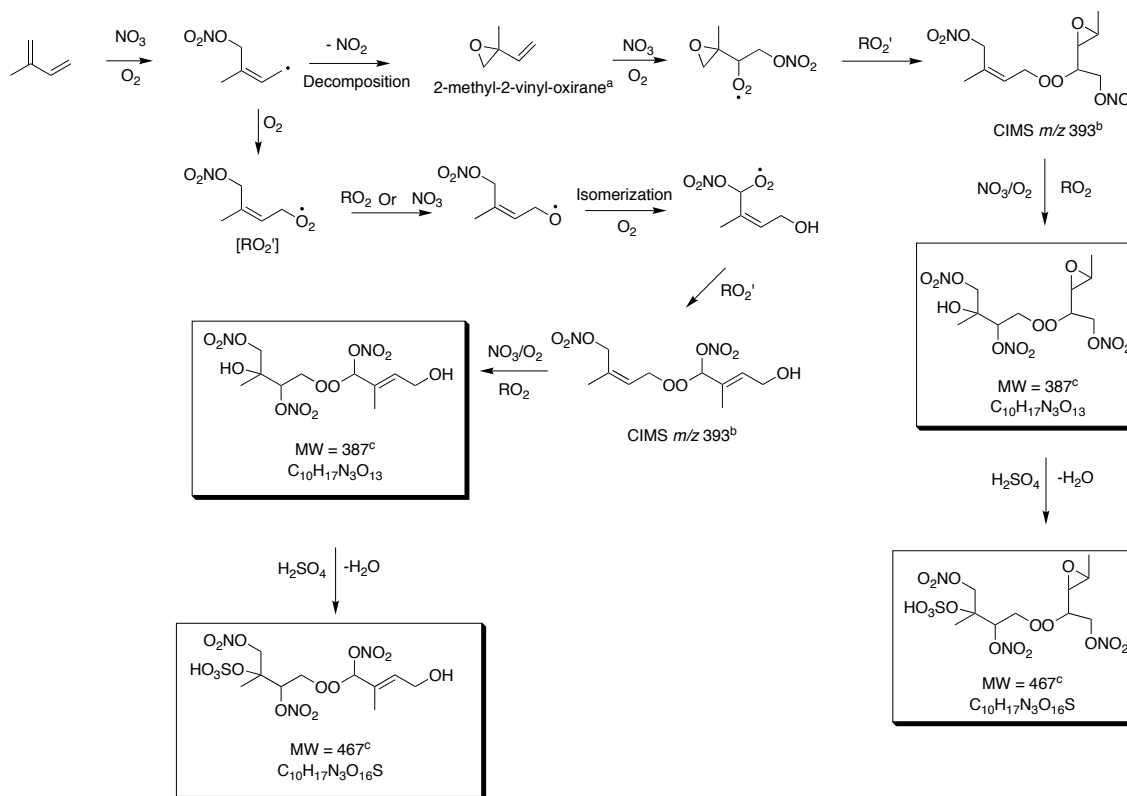
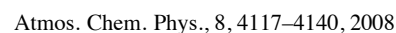


Fig. 16. Proposed mechanism for SOA formation from the formation and decay of the CIMS *m/z* 393 gas-phase product formed from the isoprene+NO₃ reaction. Boxes indicate UPLC/(–)ESI-TOFMS detected SOA products; molecular formulas were confirmed by the accurate mass data provided by the UPLC/(–)ESI-TOFMS. Multiple structural isomers are possible, consistent with the multiple chromatographic peaks observed in the extracted ion chromatograms; however, only one structural isomer is shown for simplicity. ^a This first-generation gas-phase product was detected as the [M+H]⁺ ion by the CIMS instrument; this gas-phase product was previously observed by Berndt and Böge (1997) and could also be 2-(1-methyl-vinyl)oxirane. ^b This gas-phase product was detected as the [M+CF₃O][–] ion. ^c These particle-phase compounds were detected as both their [M–H][–] and [M–H+C₂H₄O₂][–] ions; the acetic acid adduct ([M–H+C₂H₄O₂][–]) ion was, in most cases, the molecular ion (i.e. dominant ion). ^d This organosulfate compound was detected as its [M–H][–] ion and was observed only in the ammonium sulfate and acidified magnesium sulfate seeded experiments.

concentrations of isoprene and first-generation products, and aerosol can be formed either from the condensation of relatively non-volatile first-generation products (e.g. *m/z* 393) or higher generation products that are formed relatively fast in the gas-phase. It appears from the UPLC/(–)ESI-TOFMS data that enough RO₂+RO₂ chemistry is occurring to yield many of the products shown in Figs. 14–17. When comparing the UPLC/(–)ESI-TOFMS BPCs (Fig. 10) of all experiments, it is clear that the *m/z* 430 and *m/z* 446 are the dominant ions in the excess isoprene experiment, while *m/z* 333 is the dominant chromatographic peak in other experiments. The chromatographic peak at *m/z* 430 corresponds to the acetic acid cluster ion for the compound at MW 371, which can be formed from the further oxidation of CIMS *m/z* 232

and 377 ions (Figs. 14 and 15). The chromatographic peak at *m/z* 446 corresponds to the acetic acid cluster ion for the compound at MW 387, which is formed from the further oxidation of CIMS *m/z* 393 (Fig. 16). The detection of these two SOA products (MW 371 and MW 387) suggests that further oxidation of *m/z* 232, 377, and 393 is occurring in the excess isoprene experiment and contributing to SOA growth. Studies have shown that NO₃ uptake on organic surfaces (even to saturated organic surfaces) be quite rapid (Moise et al., 2002; Knopf et al., 2006; Rudich et al., 2007). Hence, it is also possible that CIMS *m/z* 393 (a first-generation product according to one of the formation routes) is nonvolatile enough that it partitions into the aerosol phase and its further oxidation proceeds heterogeneously. Chromatographic peaks



17), possibly owing to the lack of nitrooxy groups which seem to induce acidity and/or increase the adductive abilities of organic peroxides with acetic acid during the ESI-MS analysis. Overall, it appears that the isoprene-NO₃ SOA is much more similar to the previously studied low-NO_x isoprene SOA. More specifically, it appears that both contain a large amount of organic peroxides, organosulfates (if conducted in the presence of sulfate seed aerosol), and neutral hydroxylated compounds, such as the hydroxynitrates observed in Fig. 14 (e.g. MW 226 and 271 products).

As discussed earlier, the formation yields of ROOR from the reaction of two peroxy radicals is very low for small peroxy radicals (Kan et al., 1980; Niki et al., 1981, 1982; Wallington et al., 1989; Tyndall et al., 1998, 2001). However, according to both gas-phase and aerosol-phase data in this study, it appears that the RO₂+RO₂ reaction (self reaction or cross-reaction) in the gas phase yielding ROOR products is an important SOA formation pathway. Such reaction has been proposed to form low-volatility diacyl peroxides in the SOA formed from cyclohexene ozonolysis (Ziemann, 2002). In the case of self-reaction of peroxy radicals, the molecular weight of the product is essentially doubled, providing an efficient way to form products of low volatility. Based on the iodimetric spectroscopic method the contributions of peroxides (ROOH+ROOR) to the total SOA formed is 17–32% (Table 3). We can estimate the mass yield of peroxides based on their percentage contribution to total SOA and the SOA yield for each of the experiments in Table 3. It is found that the mass yield of peroxides range from ~6–10%. For the two experiments (i.e., 8/22/07 and 10/24/07) that are carried out under similar conditions as those in the yield experiments, the mass yield of peroxide is 8%.

Based on the shape of the Odum yield curve (Fig. 3), it is expected that the products are semivolatile. Hence, the relatively large contribution of nonvolatile peroxides in the aerosol phase appears to be inconsistent with the observed yield curve behavior. It is evident from the UPLC/(–)ESI-TOFMS data that there exists a wide array of peroxides in the aerosol composition, however, we need to caution that there are large uncertainties associated with the quantification of peroxides owing to the lack of authentic standards. Based on the standard deviations of the measurements, the uncertainty is at least 10%, yet if we take into account the following factors it is expected that the true uncertainty would be larger. In estimating the percentage contribution of peroxides, an average molecular weight of 433 for peroxides is used. The peroxides formed would largely depend on the branching ratio of various reactions and this number may not reflect the molecular weights of the wide array of peroxides formed. Also, the iodimetric spectroscopic method does not allow the distinction between ROOH and ROOR products. Hence, the contribution of the low volatility ROOR products may not be as high as estimated. ROOH standards were run in the ESI-TOFMS to examine the possibility of ROOH further reacting in the mass spectrometer to form ROOR and no ROOR

products were detected. As mentioned before, it appears that the presence of nitrooxy groups in ROOR products aids their detection in the MS. Since the ROOH standards used do not have a nitrooxy group, unfortunately we cannot rule out the possibility that ROOR products are formed but just not being detected. Finally, it is worth noting that the initial isoprene concentrations in the yield experiments are much lower than those experiments in which SOA composition is measured. In performing the yield experiments, the initial isoprene concentrations are kept relatively low so as to be closer to atmospheric levels. Because of the lower initial isoprene concentration (hence lower aerosol loading), the partitioning of various products would be different and it is likely that level of peroxides would be lower in the yield experiments. Nevertheless, the higher concentration experiments are necessary to produce enough aerosols for filter analysis and to map out the complete spectrum of oxidation products.

To fully elucidate the relationship between the actual products identified and those inferred from fitting the yield data would require a modeling study that is beyond the scope of this work. However, we emphasize that there are large uncertainties associated with the quantification of peroxides and it is likely that their contributions to total SOA can be overestimated. Indeed, if the mass yield for these nonvolatile peroxides were lower (for instance, ~2%), this would agree well with the observed yield curve behavior. The measurement of peroxides certainly warrants further study. This work serves as a good example in showing that caution must be taken when interpreting experiments with low aerosol yields, especially when a relatively minor pathway may be responsible for forming the aerosols.

5 Approximate estimate of global production of SOA from isoprene+NO₃

The global chemical transport model GEOS-Chem (v. 7-04-11) (<http://www-as.harvard.edu/chemistry/trop/geos/>) is used to estimate, roughly, global SOA formation from the isoprene+NO₃ reaction. The current version of GEOS-Chem treats mechanistically SOA formation from isoprene+OH, monoterpenes and sesquiterpenes, and aromatics; here we will estimate SOA formation from isoprene+NO₃ by using an approximate, uniform SOA yield of 10% (corresponding to $M_o \approx 10 \mu\text{g m}^{-3}$ in Fig. 3). It is noted that this yield is quite uncertain and the importance of peroxy radical self reactions in this study suggest that the SOA yield in the atmosphere will be highly sensitive to the nature of the nighttime peroxy radical chemistry. Here, we seek to obtain only a “back-of-the-envelope” estimate.

Two global isoprene emissions are available in GEOS-Chem: GEIA (Global Emission Inventory Activity) (Guenther et al., 1995) and MEGAN (Model of Emissions and Gases from Nature) (Guenther et al., 2006). Both models require, as input, meteorological data such as temperature

to calculate the amount isoprene emitted. For the present estimate, the meteorological fields employed by Wu et al. (2007), generated by the Goddard Institute for Space Studies (GISS) General Circulation Model III, are used. Meteorological conditions correspond approximately to those of year 2000.

Table 4 presents the annual emissions of isoprene as predicted by each of the emission models, together with the amount of isoprene predicted to react via OH, O₃, and NO₃, the global burden, and lifetime. We note that there is a significant difference between the annual isoprene emissions predicted by the earlier and newer emission models. Isoprene+OH accounts for 300 to 400 Tg yr⁻¹ of isoprene consumption. Henze et al. (2007) predict that annual SOA production from isoprene+OH is about 13 Tg yr⁻¹ (based on the MEGAN inventory and GEOS-4 meteorological fields, which are assimilated fields from actual year 2004). Note that SOA production from isoprene+OH, or any other pathway for that matter, is sensitive to the production of SOA from other hydrocarbon precursors since gas-aerosol partitioning depends on the total organic aerosol mass.

If we take as a rough estimate a 10% SOA yield from the isoprene+NO₃ pathway from the results in Table 4, 2 to 3 Tg yr⁻¹ of SOA results from isoprene+NO₃. This rate of production would make SOA from isoprene+NO₃ as significant as that from sesquiterpenes, biogenic alcohols, and aromatics, each of which is estimated to produce about 2 to 4 Tg yr⁻¹ of SOA based on yields measured in chamber studies (Henze et al., 2007). As a reference, the global SOA production is estimated to be 10–70 Tg yr⁻¹ (Kanakidou et al., 2005). Recently, Goldstein et al. (2007) provided several alternative approaches to estimate global SOA production: 510–910 Tg C yr⁻¹ based on the global mass balance of VOC removal, 225–575 Tg C yr⁻¹ based on SOA deposition plus oxidation, 140–540 Tg C yr⁻¹ based on comparison with the sulfate budget, and 223–615 Tg C yr⁻¹ required to maintain the assumed global mean vertical SOA distribution. If we assume mass carbon/mass organics=0.5, the lower limit for SOA production from these estimates would be 280 Tg yr⁻¹, which is much larger than that estimated from chamber SOA yields. Still, the 3 Tg yr⁻¹ of SOA estimated for the isoprene + NO₃ system is worth noticing. Owing to efficient photodissociation, NO₃ achieves its highest concentrations at night. By contrast, isoprene emissions are assumed to be zero at night in both emission models. Consequently, the isoprene+NO₃ reaction occurs only at night, involving isoprene that remains unreacted after each daytime period.

We caution that the estimates above are obtained at the crudest level of approximation, in which a globally uniform SOA yield of 10% from isoprene+NO₃ is applied. As we note from Table 4, there is also a substantial difference between predictions of the two available isoprene emission models; the more recent MEGAN model represents an improved level of understanding over the earlier GEIA model. Predictions of SOA formation from the isoprene+NO₃ path-

Table 4. Global estimation of isoprene using GEOS-Chem.

	Emission Model	
	GEIA ^a	MEGAN ^b
Isoprene emission (Tg/y)	507	389
Global isoprene burden (Tg)	1.7	1.7
Isoprene lifetime (days)	1.2	1.6
Isoprene reacted (Tg/y) by		
Isoprene+OH	407	304
Isoprene+O ₃	69	62
Isoprene+NO ₃	29	21

^a Modification of GEIA for GEOS-Chem are described at Bey et al. (2001c). Original GEIA reference is Guenther et al. (1995).

^b Guenther et al. (2006).

way are, of course, highly dependent on ambient NO₃ radical concentrations. Nitrate radical concentrations predicted in the current simulations vary from about 0.1 ppt in remote regions of South America to 20 ppt or more in the southeastern USA (in August). Future work will address the simulation of SOA formation from isoprene+NO₃ following the microphysical treatment in GEOS-Chem.

6 Implications

We report a series of chamber experiments investigating the formation of secondary organic aerosols from the reaction of isoprene with nitrate radicals. For an initial isoprene concentration of 18.4 to 101.6 ppb, the SOA yield ranges from 4.3% to 23.8% (typical yield experiments). The SOA yield from the slow N₂O₅ injection experiment (RO₂+RO₂ reaction dominates) is much higher than that from the slow isoprene injection experiment (RO₂+NO₃ dominates), implying that RO₂+RO₂ is a more effective channel of forming SOA. The SOA yield from the slow N₂O₅ experiment is roughly the same as that in the typical yield experiments, suggesting that SOA yields obtained in this study likely represent conditions in which peroxy-peroxy radical reactions are favored. Using a uniform SOA yield of 10% (corresponding to $M_o \cong 10 \mu\text{g m}^{-3}$), ~2 to 3 Tg yr⁻¹ of SOA results from isoprene+NO₃, which is about 1/4 of the amount of SOA estimated to be formed from isoprene+OH (~13 Tg yr⁻¹) (Henze et al., 2007).

The extent to which the results from this study can be applied to conditions in the atmosphere depends on the relative importance of the various reaction pathways of peroxy radicals in the nighttime atmosphere: RO₂+RO₂, RO₂+NO₃, RO₂+NO, and RO₂+HO₂. However, the fate of peroxy radicals in the atmosphere is uncertain owing to the large uncertainties in the reaction rate constants and ambient concentrations of the radicals (Skov et al., 1992; Kirchner and Stockwell, 1996; Bey et al., 2001a, b; Vaughan et al., 2006). For

instance, a modeling study by Kirchner and Stockwell (1996) suggests that the RO₂+NO₃ reaction is the dominant pathway at night; 77% and 90% of the total RO₂ at night is predicted to react with NO₃ in polluted atmosphere and rural air (mixed with aged air), respectively. The other pathways are not as important; while RO₂+RO₂ can account for about 8–23% of the total RO₂ reaction, RO₂+HO₂ only accounts for 6–10%, and RO₂+NO is minimal (0–1%) (Kirchner and Stockwell, 1996). These results are at odds with the study by Bey et al. (2001a,b), which suggests that NO₃ radicals are not involved significantly in the propagation of RO₂ radicals (<5%). Instead, RO₂+NO (77%) and RO₂+RO₂ (40%) are dominant in the mixed layer in the urban and rural areas, respectively. Although there is no definite conclusion as to which reaction pathway dominates in the nighttime atmosphere, both studies seem to suggest that RO₂+HO₂ is relatively not as important. In this work, we investigated situations in which either RO₂+RO₂ or RO₂+NO₃ dominates. In both cases the RO₂+HO₂ reaction is expected to be a minor channel and thus this is in line with the modeling studies. Although RO₂+NO is not considered in this study, this reaction produces the same alkoxy radical as in the RO₂+NO₃ reaction. It is likely that it would result in similar products as those in the case where the RO₂+NO₃ reaction dominates. Currently, only the reaction rate constants for small, relatively simple RO₂ radicals with NO₃ radicals have been reported (e.g. Biggs et al., 1994; Daele et al., 1995; Canosa-Mas et al., 1996; Vaughan et al., 2006) and they are roughly in the range of $(1-3) \times 10^{-12} \text{ cm}^3 \text{ molecule}^{-1} \text{ s}^{-1}$. With the oxidation of various volatile organic compounds by O₃ and NO₃ under nighttime conditions, it is expected that multifunctional peroxy radicals would be prevalent; the reaction rates of these complex peroxy radicals warrant future study. Furthermore, more field measurements on the concentrations of various radicals would also help to constrain the relative importance of the different reaction pathways.

In this study, we have shown that the formation of ROOR from the reaction of two peroxy radicals is an effective SOA-forming channel based on gas-phase data and elemental SOA composition data. If the results from this study can be applied to other systems (i.e., the reaction of NO₃ radicals with other volatile organic compounds), the organic peroxides could possibly be formed in all systems; they may not have been identified previously owing to the lack of suitable analytical techniques such as accurate mass measurements from high resolution MS. Since the formation of ROOR from two peroxy radicals has always been considered as a minor channel, the reaction has not been widely studied. Ghigo et al. (2003) ruled out the direct formation of products (RO, ROH, RCHO) from the tetroxide intermediate ROOOOR. Instead, they proposed that the tetroxide breaks up into a weakly bound complex of two RO radicals and O₂, which then fall apart or undergoes intersystem crossing to form the corresponding alcohol and carbonyl products. The formation of ROOR was not discussed in Ghigo et al. (2003)

owing to little experimental evidence for the production of ROOR. However, the observation of ROOR formation in this study suggests that this reaction does occur and is potentially important for aerosol formation. As pointed out by Dibble (2008), the mechanism proposed by Ghigo (2003) would seem to allow for easy production of ROOR from the RO-RO-O₂ complex. Therefore, it appears that there are at least two possible pathways for ROOR formation: it can either be formed through the RO-RO-O₂ complex as suggested by Dibble (2008), or there may exist a direct pathway for ROOR formation from ROO+ROO. Certainly more work is needed regarding the formation, detection, and quantification of ROOR products.

It is also worth noting that while most NO₃ chemistry occurs at night, it can also be important during the day at specific locations. Recently, a study by Fuentes et al. (2007) suggested substantial formation of NO₃ radicals can take place in forested environments with moderate to high levels of BVOC production, resulting in a significant oxidation of isoprene and terpenes by NO₃ radicals. For instance, approximately 60% of the terpenes react with NO₃ radicals within the canopy. Clearly, more study is needed to evaluate the importance of NO₃ chemistry of biogenic hydrocarbons under different environments and time of the day.

Acknowledgements. This research was funded by US Department of Energy Biological and Environmental Research Program DE-FG02-05ER63983. This material is based in part on work supported by the National Science Foundation (NSF) under grant ATM-0432377. The Waters LCT Premier XT time-of-flight mass spectrometer interfaced to a Waters UPLC system was purchased in 2006 with a grant from the National Science Foundation, Chemistry Research Instrumentation and Facilities Program (CHE-0541745). The LCQ Ion Trap mass spectrometer was purchased in 1997 with funds from the National Science Foundation through the CRIF program (CHE-9709233). J. D. Surratt is supported in part by the US EPA under the STAR Graduate Fellowship Program. A. J. Kwan and H. O. T. Pye acknowledge the support of NSF graduate research fellowships. The authors would like to thank C. D. Vecitis, J. Cheng, and M. R. Hoffmann for use of and aid with their ozonizer and UV-VIS spectrometer; to K. Takematsu and M. Okumura for helpful advice on preparing N₂O₅; to J. H. Kroll and M. Claeys for helpful discussions and suggestions; to M. N. Chan for assistance with filter sample collection; to H. G. Kjaergaard and F. Paulot for performing the quantum calculations and estimating the sensitivities of CIMS to various gas-phase products; and to Y. Yu and the reviewers for helpful comments on the manuscript.

Edited by: S. Martin

References

- Alfarra, M. R., Paulsen, D., Gysel, M., Garforth, A. A., Dommen, J., Prevot, A. S. H., Worsnop, D. R., Baltensperger, U., and Coe, H.: A mass spectrometric study of secondary organic aerosols formed from the photooxidation of anthropogenic and biogenic precursors in a reaction chamber, *Atmos. Chem. Phys.*, 6, 5279–5293, 2006, <http://www.atmos-chem-phys.net/6/5279/2006/>.
- Bahreini, R., Keywood, M. D., Ng, N. L., Varutbangkul, V., Gao, S., Flagan, R. C., and Seinfeld, J. H.: Measurements of secondary organic aerosol (SOA) from oxidation of cycloalkenes, terpenes, and m-xylene using an Aerodyne aerosol mass spectrometer. *Environ. Sci. Technol.*, 39, 5674–5688, 2005.
- Barnes, I., Bastian, V., Becker, K. H., and Tong, Z.: Kinetics and products of the reactions of NO₃ with monoalkenes, dialkenes, and monoterpenes, *J. Phys. Chem.*, 94, 2413–2419, 1990.
- Berndt, T. and Böge, O.: Gas-Phase reaction of NO₃ radicals with isoprene: A kinetic and mechanistic study, *Inter. J. Chem. Kinet.*, 29, 755–765, 1997.
- Bey, I., Aumont, B., and Toupance, G.: A modeling study of the nighttime radical chemistry in the lower continental troposphere. 1. Development of a detailed chemical mechanism including nighttime chemistry, *J. Geophys. Res.*, 106(D9), 9959–9990, 2001a.
- Bey, I., Aumont, B., and Toupance, G.: A modeling study of the nighttime radical chemistry in the lower continental troposphere. 2. Origin and evolution of HO_x, *J. Geophys. Res.*, 106(D9), 9991–10001, 2001b.
- Bey, I., Jacob, D. J., Yantosca, R. M., Logan, J. A., Field, B. D., Fiore, A. M., Li, Q. B., Liu, H. G. Y., Mickley, L. J., and Schultz, M. G.: Global modeling of tropospheric chemistry with assimilated meteorology: Model description and evaluation, *J. Geophys. Res.*, 106(D19), 23 073–23 095, 2001c.
- Biggs, P., Canosa-Mas, C. E., Fracheboud, J. M., Shallcross, D. E., and Wayne, R. P.: Investigation into the kinetics and mechanisms of the reaction of NO₃ with CH₃ and CH₃O at 298K between 0.6 Torr and 8.5 Torr – is there a chain decomposition mechanism in operation, *J. Chem. Soc., Faraday Trans.*, 90, 1197–1204, 1994.
- Brown, S. S., Ryerson, T. B., Wollny, A. G., Brock, C. A., Peltier, R., Sullivan, A. P., Weber, R. J., Dube, W. P., Trainer, M., Meagher, J. F., Fehsenfeld, F. C., and Ravishankara, A. R.: Variability in nocturnal nitrogen oxide processing and its role in regional air quality, *Science*, 311, 5757, 67–70, 2006.
- Canosa-Mas, C. E., Flugge, M. L., King, M. D., and Wayne, R. P.: An experimental study of the gas-phase reaction of the NO₃ radical with $\alpha\beta$ unsaturated carbonyl compounds, *Phys. Chem. Chem. Phys.*, 7, 643–650, 2005.
- Canosa-Mas, C. E., King, M. D., Lopez, R., Percival, C. J., Wayne, R. P., Shallcross, D. E., Pyle, J. A., and Daele, V.: Is the reaction CH₃C(O)O₂ and NO₃ important in the night-time troposphere? *J. Chem. Soc., Faraday Trans.*, 92, 2211–2222, 1996.
- Carslaw, N., Carpenter, L. J., Plane, J. M. C., Allan, B. J., Burgess, R. A., Clemitshaw, K. C., Coe, H., and Penkett, S. A.: Simultaneous measurements of nitrate and peroxy radicals in the marine boundary layer, *J. Geophys. Res.*, 102, 18 917–18 933, 1997.
- Carter, W. P. L. and Atkinson, R.: Development and evaluation of a detailed mechanism for the atmospheric reactions of isoprene and NO_x, *Int. J. Chem. Kinet.*, 28, 497–530, 1996.
- Claeys, M., Graham, B., Vas, G., Wang, W., Vermeylen, R., Pashynska, V., Cafmeyer, J., Guyon, P., Andreae, M. O., Artaxo, P., and Maenhaut, W.: Formation of secondary organic aerosols through photooxidation of isoprene, *Science*, 303, 1173–1176, 2004.
- Cocker III, D. R., Flagan, R. C., and Seinfeld, J. H.: State-of-the-art chamber facility for studying atmospheric aerosol chemistry, *Environ. Sci. Technol.*, 35, 2594–2601, 2001.
- Crounse, J. D., McKinney, K. A., Kwan, A. J., and Wennberg, P. O.: Measurements of gas-phase hydroperoxides by chemical ionization mass spectrometry, *Anal. Chem.*, 78, 6726–6732, 2006.
- Curren, K., Gillespie, T., Steyn, D., Dann, T., and Wang, D.: Biogenic isoprene in the Lower Fraser Valley, British Columbia, *J. Geophys. Res.*, 103, D19, 25467–25477, 1998.
- Daele, V., Laverdet, G., Lebras, G., and Poulet, G.: Kinetics of the reactions of CH₃O+NO, CH₃O+NO₃, and CH₃O₂+NO₃, *J. Phys. Chem.*, 99, 1470–1477, 1995.
- Davidson, J. A., Viggiano, A. A., Howard, C. J., Fehsenfeld, F. C., Albritton, D. L., and Ferguson, E. E.: Rate constants for the reaction of O₃⁺, NO₂⁺, NO⁺, H₃O⁺, CO₃⁺, NO₂⁺, and halide ions with N₂O₅ at 300 K, *J. Chem. Phys.*, 68, 2085–2087, 1978.
- Dibble, T. S.: Isomerization of OH-isoprene adducts and hydroxylalkoxy isoprene radicals, *J. Phys. Chem.*, 106(28), 6643–6650, 2002.
- Dibbe T. S.: Failures and limitations of quantum chemistry for two key problems in the atmospheric chemistry of peroxy radicals, *Atmos. Environ.*, in press, 2008.
- Docherty, K., Wu, W., Lim, Y., and Ziemann, P.: Contributions of Organic Peroxides to Secondary Aerosol Formed from Reactions of Monoterpenes with O₃, *Environ. Sci. Technol.*, 39, 4049–4059, 2005.
- Dommen, J., Metzger, A., Duplissy, J., Kalberer, M., Alfarra, M. R., Gascho, A., Weingartner, E., Prevot, A. S. H., Verheggen, B., and Baltensperger, U.: Laboratory observation of oligomers in the aerosol from isoprene/NO_x photooxidation, *Geophys. Res. Lett.*, 33, L13805, doi:10.1029/2006GL026523, 2006.
- Edney, E. O., Kleindienst, T. E., Jaoui, M., Lewandowski, M., Offenberg, J. H., Wang, W., and Claeys, M.: Formation of 2-methyl tetrols and 2-methylglyceric acid in secondary organic aerosol from laboratory irradiated isoprene/NO_x/SO₂/air mixtures and their detection in ambient PM_{2.5} samples collected in the eastern United States, *Atmos. Environ.*, 39, 5281–5289, 2005.
- Fan, J. and Zhang, R.: Atmospheric oxidation mechanism of isoprene, *Environ. Chem.*, 1, 140–149, doi:10.1071/EN04045, 2004.
- Fuentes, J. D., Wang, D., Rowling, D. R., Potosnak, M., Monson, R. K., Goliff, W. S., and Stockwell, W. R.: Biogenic hydrocarbon chemistry within and above a mixed deciduous forest, *J. Atmos. Chem.*, 56, 165–185, 2007.
- Gao, S., Keywood, M. D., Ng, N. L., Surratt, J. D., Varutbangkul, V., Bahreini, R., Flagan, R. C., and Seinfeld, J. H.: Low molecular weight and oligomeric components in secondary organic aerosol from the ozonolysis of cycloalkenes and α -pinene, *J. Phys. Chem. A*, 108, 10 147–10 164, 2004a.
- Gao, S., Ng, N. L., Keywood, M. D., Varutbangkul, V., Bahreini, R., Nenes, A., He, J., Yoo, K. Y., Beauchamp, J. L., Hodyss, R. P., Flagan, R. C., and Seinfeld, J. H.: Particle phase acidity and oligomer formation in secondary organic aerosol, *Environ. Sci. Technol.*, 38, 6582–6589, 2004b.
- Gao, S., Surratt, J. D., Knipping, E. M., Edgerton, E. S., Shahgholi, M., and Seinfeld, J. H.: Characterization of polar organic com-

- ponents in fine aerosols in the southeastern United States: Identity, origin, and evolution, *J. Geophys. Res.*, 111, D14314, doi:10.1029/2005JD006601, 2006.
- Ghigo, G., Maranzana, A., and Tonachini, G.: Combustion and atmospheric oxidation of hydrocarbons: Theoretical study of the methyl peroxy self-reaction, *J. Chem. Phys.*, 118, 23, 2003.
- Goldstein, A. H. and Galbally, I. E.: Known and unexplored organic constituents in the earth's atmosphere, *Environ. Sci. Technol.*, 41, 1514–1521, 2007.
- Gong, H., Matsunaga, A., and Ziemann, P.: Products and mechanism of secondary organic aerosol formation from reactions of linear alkenes with NO₃ radicals, *J. Phys. Chem.*, 109, 4312–4324, 2005.
- Gómez-González, Y., Surratt, J. D., Cuyckens, F., Szmigielski, R., Vermeylen, R., Jaoui, M., Lewandowski, M., Offenberg, J. H., Kleindienst, T. E., Edney, E. O., Blockhuys, F., Van Alsenoy, C., Maenhaut, W. and Claeys, M.: Characterization of organosulfates from the photooxidation of isoprene and unsaturated fatty acids in ambient aerosol using liquid chromatography/(–) electrospray ionization mass spectrometry, *J. Mass Spectrom.*, 43(3), 371–382, doi:10.1002/jms.1329, 2007.
- Guenther, A., Hewitt, C. N., Erickson, D., Fall, R., Geron, C., Graedel, T., Harley, P., Klinger, L., Lerdau, M., McKay, W. A., Pierce, T., Scholes, B., Steinbrecher, R., Tallamraju, R., Taylor, J., and Zimmerman, P.: A global-model of natural volatile organic compound emissions, *J. Geophys. Res.*, 100(D5), 8873–8892, 1995.
- Guenther, A., Karl, T., Harley, P., Wiedinmyer, C., Palmer, P. I., and Geron, C.: Estimates of global terrestrial isoprene emissions using MEGAN (Model of Emissions of Gases and Aerosols from Nature), *Atmos. Chem. Phys.*, 6, 3181–3210, 2006, <http://www.atmos-chem-phys.net/6/3181/2006/>.
- Heintz, F., Platt, U., Flentje, H., and Dubois, R.: Long-term observation of nitrate radicals at the tor station, Kap Arkona (Rügen), *J. Geophys. Res.*, 101(D17), 22 891–22 910, 1996.
- Henze, D. K., Seinfeld, J. H., Ng, N. L., Kroll, J. H., Fu, T.-M., Jacob, D. J., and Heald, C. L.: Global modeling of secondary organic aerosol formation from aromatic hydrocarbons: high- vs. low-yield pathways, *Atmos. Chem. Phys.*, 8, 2405–2420, 2008, <http://www.atmos-chem-phys.net/8/2405/2008/>.
- Horowitz, L. W., Fiore, A. M., Milly, G. P., Cohen, R. C., Perring, A., Wooldridge, P. J., Hess, P. G., Emmons, L. K., and Lamarque, J.: Observational constraints on the chemistry of isoprene nitrates over the eastern United States, *J. Geophys. Res.*, 112, D12S08, doi:10.1029/2006JD007747, 2007.
- Iinuma, Y., Müller, C., Berndt, T., Böge, O., Claeys, M., and Herrmann, H.: Evidence for the existence of organosulfates from β -pinene ozonolysis in ambient secondary organic aerosol, *Environ. Sci. Technol.*, 41, 6678–6683, 2007b.
- Iinuma, Y., Müller, C., Böge, O., Gnauk, T., and Herrmann, H.: The formation of organic sulfate esters in the limonene ozonolysis secondary organic aerosol (SOA) under acidic conditions, *Atmos. Environ.*, 41, 5571–5583, 2007a.
- Jay, K. and Stieglitz, L.: The gas phase addition of NO_x to olefins, *Chemosphere*, 19, 1939–1950, 1989.
- Jayne, J. T., Leard, D. C., Zhang, X., Davidovits, P., Smith, K. A., Kolb, C. E., and Worsnop, D. W.: Development of an Aerosol Mass Spectrometer for size and composition analysis of submicron particles, *Aerosol Sci. Technol.*, 33, 49–70, 2000.
- Kan, C. S., Calvert, J. G., and Shaw, J. H.: Reactive channels of the CH₃O₂–CH₃O₂ reaction, *J. Phys. Chem.*, 84, 3411–3417, 1980.
- Kanakidou, M., Seinfeld, J. H., Pandis, S. N., Barnes, I., Dentener, F. J., Facchini, M. C., Van Dingenen, R., Ervens, B., Nenes, A., Nielsen, C. J., Swietlicki, E., Putaud, J. P., Balkanski, Y., Fuzzi, S., Horth, J., Moortgat, G. K., Winterhalter, R., Myhre, C. E. L., Tsigaridis, K., Vignati, E., Stephanou, E. G., and Wilson, J.: Organic aerosol and global climate modelling: a review, *Atmos. Chem. Phys.*, 5, 1053–1123, 2005, <http://www.atmos-chem-phys.net/5/1053/2005/>.
- Keywood, M. D., Varutbangkul, V., Bahreini, R., Flagan, R. C., and Seinfeld, J. H.: Secondary organic aerosol formation from the ozonolysis of cycloalkenes and related compounds, *Environ. Sci. Technol.*, 38, 4157–4164, 2004.
- Kirchner, F. and Stockwell, W. R.: Effect of peroxy radical reactions on the predicted concentrations of ozone, nitrogenous compounds, and radicals, *J. Geophys. Res.*, 101(D15), 21 007–21 022, 1996.
- Knopf, D. A., Mak, J., Gross, S., and Bertram, A. K.: Does atmospheric processing of saturated hydrocarbon surfaces by NO₃ lead to volatilization?, *Geophys. Res. Lett.*, 33, L17816, doi:10.1029/2006GL026884, 2006.
- Kroll, J. H., Ng, N. L., Murphy, S. M., Flagan, R. C., and Seinfeld, J. H.: Secondary organic aerosol formation from isoprene photooxidation under high-NO_x conditions, *J. Geophys. Res.*, 32, L18808, doi:10.1029/2005GL023637, 2005.
- Kroll, J. H., Ng, N. L., Murphy, S. M., Flagan, R. C., and Seinfeld, J. H.: Secondary organic aerosol formation from isoprene photooxidation, *Environ. Sci. Technol.*, 40, 1869–1877, 2006.
- Kwok, E. S. C., Aschmann, S. M., Arey, J., and Atkinson, R.: Product formation from the reaction of the NO₃ radical with isoprene and rate constants for the reactions of methacrolein and methyl vinyl ketone with the NO₃ radical, *Inter. J. Chem. Kinet.* 28, 925–934, 1996.
- Liggio, J. and Li, S. M.: Organosulfate formation during the uptake of pinonaldehyde on acidic sulfate aerosols, *Geophys. Res. Lett.*, 33, L13808, doi:10.1029/2006GL026079, 2006.
- Liggio, J., Li, S. M., and McLaren, R.: Heterogeneous reactions of glyoxal on particulate matter: Identification of acetals and sulfate esters, *Environ. Sci. Technol.*, 39, 1532–1541, 2005.
- Lightfoot, P. D., Cox, R. A., Crowley, J. N., Destriau, M., Hayman, G. D., Jenkin, M. E., Moortgat G. K., and Zabel, F.: Organic peroxy radicals – kinetics, spectroscopy and tropospheric chemistry, *Atmos. Environ.*, 26, 1805–1961, 1992.
- Moise, T., Talukdar, R. K., Frost, G. J., Fox, R. W., and Rudich, Y.: Reactive uptake of NO₃ by liquid and frozen organics, *J. Geophys. Res.*, 107(D2), 4014, doi:10.1029/2001JD000334, 2002.
- Ng, N. L., Chhabra, P. S., Chan, A. W. H., Surratt, J. D., Kroll, J. H., Kwan, A. J., McCabe, D. C., Wennberg, P. O., Sorooshian, A., Murphy, S. M., Dalleska, N. F., Flagan, R. C., and Seinfeld, J. H.: Effect of NO_x level on secondary organic aerosol (SOA) formation from the photooxidation of terpenes, *Atmos. Chem. Phys.*, 7, 5159–5174, 2007a, <http://www.atmos-chem-phys.net/7/5159/2007/>.
- Ng, N. L., Kroll, J. H., Chan, A. W. H., Chhabra, P. S., Flagan, R. C., and Seinfeld, J. H.: Secondary organic aerosol formation from *m*-xylene, toluene, and benzene, *Atmos. Chem. Phys.*, 7, 3909–3922, 2007b, <http://www.atmos-chem-phys.net/7/3909/2007/>.

- Ng, N. L., Kroll, J. H., Keywood, M. D., Bahreini, R., Varutbangkul, V., Flagan, R. C., Seinfeld, J. H., Lee, A., and Goldstein, A. H.: Contribution of first- versus second-generation products to secondary organic aerosols formed in the oxidation of biogenic hydrocarbons, *Environ. Sci. Technol.*, 40, 2283–2297, 2006.
- Niki, H., Maker, P. D., Savage, C. M., and Breitenbach L.P.: Fourier Transform Infrared studies of the self-reaction of CH₃O₂ radicals, *J. Phys. Chem.*, 85, 877–881, 1981.
- Niki, H., Maker, P. D., Savage, C. M., and Breitenbach L.P.: Fourier Transform Infrared studies of the self-reaction of C₂H₅O₂ radicals, *J. Phys. Chem.*, 86, 3825–3829, 1982.
- Noda, J., Nyman, G., and Langer S.: Kinetics of the gas-phase reaction of some unsaturated alcohols with the nitrate radical, *J. Phys. Chem.*, 106, 945–951, 2002.
- Odum, J. R., Hoffmann, T., Bowman, F., Collins, D., R. C. Flagan, R. C., and Seinfeld, J. H.: Gas/particle partitioning and secondary organic aerosol yields, *Environ. Sci. Technol.*, 30, 2580–2585, 1996.
- Odum, J. R., Jungkamp, T. P. W., Griffin, R. J., Flagan, R. C., and Seinfeld, J. H.: The atmospheric aerosol-forming potential of whole gasoline vapor, *Science*, 276, 96–99, 1997a.
- Odum, J. R., Jungkamp, T. P. W., Griffin, R. J., Forstner, H. J. L., Flagan, R. C., and Seinfeld, J. H.: Aromatics, reformulated gasoline and atmospheric organic aerosol formation, *Environ. Sci. Technol.*, 31, 1890–1897, 1997b.
- Paulot, F., Crounse, J. D., Kjaergaard, H. G., Kroll, J. H., Seinfeld, J. H., and Wennberg, P. O.: Isoprene photooxidation mechanism: resonance channels and implications for the production of nitrates and acids, accepted, *Atmos. Chem. Phys. Discuss.*, 2008.
- Paulson, S. E. and Seinfeld, J. H.: Development and evaluation of a photooxidation mechanism for isoprene, *J. Geophys. Res.*, 97(D18), 20 703–20 715, 1992.
- Penkett, S. A., Burgess, R. A., Coe, H., Coll, I., Hov, Ø., Lindskog, A., Schmidbauer, N., Solberg, S., Roemer, M., Thijssse, T., Beck, J., and Reeves C. E.: Evidence for large average concentrations of the nitrate radical (NO₃) in Western Europe from the HANSA hydrocarbon database, *Atmos. Environ.*, 41, 3465–3478, 2007.
- Platt, U. and Janssen, C.: Observation and role of the free radicals NO₃, ClO, BrO and IO in the troposphere, *Faraday Discuss.*, 100, 175–198, 1995.
- Platt, U., Perner, D., Schroder, J., Kessler, C., and Toennissen, A.: The diurnal variation of NO₃, *J. Geophys. Res.*, 86, 11 965–11 970, 1981.
- Rudich, Y., Donahue, N. M., and Mentel, T. F.: Aging of organic aerosol: Bridging the gap between laboratory and field studies, *Annu. Rev. Phys. Chem.*, 58, 321–352, 2007.
- Sharkey, T. D., Singsaas, E. L., Vanderveer, P. J., and Geron, C.: Field measurements of isoprene emission from trees in response to temperature and light, *Tree Physiol.*, 16, 649–654, 1996.
- Skov, H., Benter, Th., Schindler, R. N., Hjorth, J., and Restelli, G.: Epoxide formation in the reactions of the nitrate radical with 2,3-dimethyl-2-butene, cis- and trans-2-butene and isoprene, *Atmos. Environ.*, 28, 1583–1592, 1994.
- Skov, H., Hjorth, J., Lohse, C., Jensen, N. R. and Restelli, G.: Products and mechanisms of the reactions of the nitrate radical (NO₃) with isoprene, 1,3-butadiene and 2,3-dimethyl-1,3-butadiene in air, *Atmos. Environ.*, 26A(15), 2771–2783, 1992.
- Smith, N., Plane, J. M. C., Nien, C. F., and Solomon, P. A.: Night-time radical chemistry in the San-Joaquin Valley, *Atmos. Environ.*, 29, 2887–2897, 1995.
- Sorooshian, A., Brechtel F. J., Ma, Y. L., Weber R. J., Corless, A., Flagan, R. C., and Seinfeld, J. H.: Modeling and characterization of a particle-into-liquid sampler (PILS), *Aerosol Sci. Technol.*, 40, 396–409, 2006.
- Starn, T. K., Shepson, P. B., Bertman, S. B., Riemer, D. D., Zika, R. G. and Olszyna, K.: Nighttime isoprene chemistry at an urban-impacted forest site, *J. Geophys. Res.*, 103(D17), 22 437–22 447, 1998.
- Steinbacher, M., Dommen, J., Ordóñez, C., Reimann, S., Gruebler, F. C., Staehelin, J., Andreani-Aksoyoglu, S., and Prevot, A. S. H.: Volatile organic compounds in the Po Basin. Part B: Biogenic VOCs, *J. Atmos. Chem.*, 51, 293–315, 2005.
- Stroud, C. A., Roberts, J. M., Williams E. J., Hereid, D., Angevine, W. M., Fehsenfeld, F. C., Wisthaler, A., Hansel, A., Martinez-Harder, M., Harder, H., Brune, W. H., Hoenninger, G., Stutz, J., and White, A. B.: Nighttime isoprene trends at an urban forested site during the 1999 Southern Oxidant Study, *J. Geophys. Res.*, 107(D16), 4291, doi:10.1029/2001JD000959, 2002.
- Su, T. and Chesnavich, W. J.: Parametrization of the ion–polar molecule collision rate constant by trajectory calculations, *The Journal of Chemical Physics*, 76, 5183, 1982.
- Suh, I., Lei, W., and Zhang, R.: Experimental and theoretical studies of isoprene reaction with NO₃, *J. Phys. Chem.*, 105, 6471–6478, 2001.
- Surratt, J. D., Kroll, J. H., Kleindienst, T. E., Edney, E. O., Claeys, M., Sorooshian, A., Ng, N. L., Offenberg, J. H., Lewandowski, M., Jaoui, M., Flagan, R. C., and Seinfeld, J. H.: Evidence for organosulfates in secondary organic aerosol, *Environ. Sci. Technol.*, 41, 517–527, 2007a.
- Surratt, J. D., Lewandowski, M., Offenberg, J. H., Jaoui, M., Kleindienst, T. E., Edney, E. O., and Seinfeld, J. H.: Effect of acidity on secondary organic aerosol formation from isoprene, *Environ. Sci. Technol.*, 41, 5363–5369, 2007b.
- Surratt, J. D., Murphy, S. M., Kroll, J. H., Ng, N. L., Hildebrandt, L., Sorooshian, A., Szmigielski, R., Vermeylen, R., Maenhaut, W., Claeys, M., Flagan, R. C., and Seinfeld, J. H.: Chemical composition of secondary organic aerosol formed from the photooxidation of isoprene, *J. Phys. Chem. A*, 110, 9665–9690, 2006.
- Szmigielski, R., Surratt, J. D., Vermeylen, R., Szmigielska, K., Kroll, J. H., Ng, N. L., Murphy, S. M., Sorooshian, A., Seinfeld, J. H., and Claeys, M.: Characterization of 2-methylglyceric acid oligomers in secondary organic aerosol formed from the photooxidation of isoprene using trimethylsilylation and gas chromatography/ion trap mass spectrometry, *J. Mass Spectrom.*, 42, 101–116, 2007.
- Tyndall, G. S., Cox, R. A., Granier, C., Lesclaux, R., Moortgat, G. K., Pilling, M. J., Ravishankara, A. R., and Wallington, T. J.: Atmospheric chemistry of small peroxy radicals, *J. Geophys. Res.*, 106(D11), 12 157–12 182, 2001.
- Tyndall, G. S., Wallington, T. J., and Ball, J. C.: FTIR product study of the reactions of CH₃O₂+CH₃O₂ and CH₃O₂+O₃, *J. Phys. Chem.*, 102, 2547–2554, 1998.
- Vaughan, S., Canosa-Mas, C. E., Pfrang, C., Shallcross, D. E., Watson, L., and Wayne, R. P.: Kinetic studies of reactions of the nitrate radical (NO₃) with peroxy radicals (RO₂): an indirect

4140

- source of OH at night? *Phys. Chem. Chem. Phys.*, 8, 3749–3760, 2006.
- von Friedeburg, C., Wagner, T., Geyer, A., Kaiser, N., Platt, U., Vogel, B. and Vogel, H.: Derivation of tropospheric NO₃ profiles using off-axis differential optical absorption spectroscopy measurements during sunrise and comparison with simulations, *J. Geophys. Res.*, 107(D13), 4168, doi:10.1029/2001JD000481, 2002.
- Wallington, T. J., Dagaut, P., and Kurylo, M. J.: Ultraviolet absorption cross-sections and reaction kinetics and mechanisms for peroxy radicals in the gas phase, *Chem. Rev.*, 92, 667–710, 1992.
- Wallington, T. J., Gierczak, C. A., Ball, J. C., and Japar, S. M.: Fourier Transform Infrared studies of the self-reaction of C₂H₅O₂ radicals in air at 295 K, *Int. J. Chem. Kinet.*, 21, 1077–1089, 1989.
- N. L. Ng et al.: SOA formation from isoprene-NO₃ reaction
- Werner, G., Kastler, J., Looser, R., and Ballschmiter, K.: Organic nitrates of isoprene as atmospheric trace compounds, *Angew. Chem. Int. Ed.*, 38(11), 1634–1637, 1999.
- Wu, S. L., Mickley, L. J., Jacob, D. J., Logan, J. A., Yantosca, R. M., and Rind, D.: Why are there large differences between models in global budgets of tropospheric ozone? *J. Geophys. Res.*, 112(D5), D05302, doi:10.1029/2006JD007801, 2007.
- Zhang, D. and Zhang, R.: Unimolecular decomposition of nitrooxyalkyl radicals from NO₃-isoprene reaction, *J. Chem. Phys.*, 116(22), 9721–9728, 2002.
- Ziemann, P.: Evidence for low-volatility diacyl peroxides as a nucleating agent and major component of aerosol formed from reactions of O₃ with cyclohexene and homologous compounds, *J. Phys. Chem.*, 106, 4390–4402, 2002.

Appendix E

Glyoxal uptake on ammonium sulphate seed aerosol: reaction products and reversibility of uptake under dark and irradiated conditions*

*Reproduced with permission from “Glyoxal uptake on ammonium sulphate seed aerosol: reaction products and reversibility of uptake under dark and irradiated conditions” by M. M. Galloway, P. S. Chhabra, A. W. H. Chan, J. D. Surratt, R. C. Flagan, J. H. Seinfeld, and F. N. Keutsch, *Atmospheric Chemistry and Physics*, 9 (10), 3331–3345, 2009. Copyright 2009 by Authors. This work is licensed under a Creative Commons License.

Glyoxal uptake on ammonium sulphate seed aerosol: reaction products and reversibility of uptake under dark and irradiated conditions

M. M. Galloway¹, P. S. Chhabra², A. W. H. Chan², J. D. Surratt³, R. C. Flagan^{2,4}, J. H. Seinfeld^{2,4}, and F. N. Keutsch¹

¹Dept. of Chemistry, University of Wisconsin-Madison, Madison, WI, USA

²Dept. of Chemical Engineering, California Institute of Technology, Pasadena, CA, USA

³Dept. of Chemistry, California Institute of Technology, Pasadena, CA, USA

⁴Dept. of Environmental Science and Engineering, California Institute of Technology, Pasadena, CA, USA

Received: 7 October 2008 – Published in Atmos. Chem. Phys. Discuss.: 12 December 2008

Revised: 14 May 2009 – Accepted: 19 May 2009 – Published: 25 May 2009

Abstract. Chamber studies of glyoxal uptake onto ammonium sulphate aerosol were performed under dark and irradiated conditions to gain further insight into processes controlling glyoxal uptake onto ambient aerosol. Organic fragments from glyoxal dimers and trimers were observed within the aerosol under dark and irradiated conditions. Glyoxal monomers and oligomers were the dominant organic compounds formed under the conditions of this study; glyoxal oligomer formation and overall organic growth were found to be reversible under dark conditions. Analysis of high-resolution time-of-flight aerosol mass spectra provides evidence for irreversible formation of carbon-nitrogen (C-N) compounds in the aerosol. We have identified 1H-imidazole-2-carboxaldehyde as one C-N product. To the authors' knowledge, this is the first time C-N compounds resulting from condensed phase reactions with ammonium sulphate seed have been detected in aerosol. Organosulphates were not detected under dark conditions. However, active photochemistry was found to occur within aerosol during irradiated experiments. Carboxylic acids and organic esters were identified within the aerosol. An organosulphate, which had been previously assigned as glyoxal sulphate in ambient samples and chamber studies of isoprene oxidation, was observed only in the irradiated experiments. Comparison with a laboratory synthesized standard and chemical considerations strongly suggest that this organosulphate is glycolic acid sulphate, an isomer of the previously proposed glyoxal sulphate.

Our study shows that reversibility of glyoxal uptake should be taken into account in SOA models and also demonstrates the need for further investigation of C-N compound formation and photochemical processes, in particular organosulphate formation.

1 Introduction

Organic aerosol has been detected in substantial concentrations in urban and rural atmospheres (Zhang et al., 2007). Secondary organic aerosol (SOA) contributes significantly to particulate matter, though current models considerably underestimate SOA formation (de Gouw et al., 2005; Heald et al., 2005; Volkamer et al., 2006). In order to understand the possible health and climate effects of particulate matter, it is critical that the physical and chemical models of SOA formation be improved. Glyoxal (GL) is produced by a wide variety of biogenic and anthropogenic volatile organic compounds (VOCs), many of which are SOA precursors, and is considered a tracer for SOA formation. One current model estimates global GL production of 45 Tg/yr, with roughly half due to isoprene photooxidation (Fu et al., 2008), and another estimates 56 Tg/yr of global GL production with 70% being produced from biogenic hydrocarbon oxidation (Myriokefalitakis et al., 2008). In addition to acting as a tracer for SOA formation, GL has been suggested as a direct contributor to SOA (Sorooshian et al., 2006; Volkamer et al., 2007, 2009; Carlton et al., 2007; Ervens et al., 2008; Fu et al., 2008). A study comparing observed and modelled GL has suggested that GL could contribute at least 15% of the SOA



Correspondence to: F. N. Keutsch
 (keutsch@wisc.edu)

in Mexico City (Volkamer et al., 2007), while a study using the GEOS-Chem model found the modelled GL contribution to SOA to be 2.6 Tg C/year out of a total of 29 Tg C/year (Fu et al., 2008).

Despite existing research aimed at elucidating SOA formation by GL, further quantification of SOA yields as a function of conditions such as relative humidity, irradiation, gas-phase GL mixing ratio, and seed aerosol composition and pH are required in order to allow for the application of laboratory findings to ambient conditions. On a more fundamental level, it is desirable to achieve a detailed understanding of the processes contributing to SOA formation from GL as a function of the above conditions. GL is also promising as an interesting model system for compounds that can yield SOA via purely physical absorption processes and via complex condensed phase processes, such as oligomerization, organosulphate formation, condensation, and photochemical reactions.

The standard models that have been employed to explain organic gas-particle partitioning have generally assumed physical absorption processes (Pankow, 1994a,b; Odum et al., 1996). On this basis, GL, the smallest dicarbonyl, should have virtually no SOA yield because of its high vapour pressure (220 Torr at 20°C, Kielhorn et al., 2004). However, GL partitions strongly to aqueous condensed-phase systems, which is reflected in a surprisingly high effective Henry's law constant, $K_{\text{H,aq}}^* = 3.6 \times 10^5 \text{ M/atm}$ for seawater (Zhou and Mopper, 1990) and $4.19 \times 10^5 \text{ M/atm}$ in water (Ip et al., 2009). The effective Henry's law constant of GL is higher than that of atmospherically relevant monocarboxylic acids including glyoxylic acid, $K_{\text{H,aq}}^* = 1 \times 10^4 \text{ M/atm}$ (Ip et al., 2009), the acid that results from oxidation of one of the aldehyde groups in GL. Glycolic acid, an isomer of glyoxal monohydrate, also has a lower effective Henry's law constant of $2.83 \times 10^4 \text{ M/atm}$ (Ip et al., 2009). The high effective Henry's law constant of GL has been explained by the hydration of the aldehyde groups, producing an effectively lower vapour pressure species in aqueous solution. In addition to the physical absorption processes, particle-phase chemical reactions have been identified as a possible driving force for uptake. Carbonyl containing species are known to participate in aldol, acetal, and esterification reactions, which form low volatility compounds that add to SOA mass. Field and laboratory studies have also yielded evidence for the formation of high molecular weight products within SOA (Gross et al., 2006; Reinhardt et al., 2007; Denkenberger et al., 2007) and it is well known that GL will polymerize in the presence of water (Whipple, 1970; Loeffler et al., 2006).

These properties of GL, together with its production via oxidation of many VOCs, have inspired chamber investigations into GL partitioning onto a variety of seed particles (Jang et al., 2002; Liggio et al., 2005a,b; Kroll et al., 2005; Corrigan et al., 2008; Volkamer et al., 2009). Liggio et al. (2005b) have demonstrated reactive uptake of GL onto several different types of seed aerosol using an Aero-

dyne aerosol mass spectrometer (AMS). This study suggested that GL uptake onto ammonium sulphate (AS) aerosol is irreversible and enhanced with acidified seed. However, Kroll et al. (2005) observed negligible acid effect and reversible GL uptake onto AS seed aerosol that is possibly controlled by ionic strength. The authors concluded that GL uptake obeys a modified effective Henry's Law at equilibrium ($K_{\text{H,AS}}^* = 2.6 \times 10^7 \text{ M/atm}$; using a density of 1 g/cm^3 to convert volume growth to organic mass and normalizing by the seed volume). Both Liggio et al. (2005b) and Kroll et al. (2005) observed hydration and oligomerization of GL within aerosol and, in addition, Liggio et al. (2005b) proposed irreversible formation of the organosulphate of GL (GL sulphate) to explain certain peaks in the AMS mass spectra. Volkamer et al. (2009) demonstrated that acetylene is an SOA precursor and estimated that almost all particle phase organic growth was due to its oxidation product, GL. SOA yields were shown to correlate with the liquid water content (LWC) of the AS seed. Therefore, the authors introduced a modified definition of molarity, calculating GL concentrations with respect to LWC fraction of the seed volume, which gave $K_{\text{H,AS}}^{**} = 1.65 \times 10^8 \text{ M/atm}$. Evaluating the data from Kroll et al. (2005) in this manner gives $K_{\text{H,AS}}^{**} = 1.07 \times 10^8 \text{ M/atm}$. However, in addition to the larger effective Henry's law constant in the study of Volkamer et al. (2009), this uptake in the presence of OH radicals and UV light was achieved in 90 s compared to many hours under dark conditions in the work by Kroll et al. (2005).

The difference between the Henry's law constant of water and AS aerosol is substantial and the reasons for this are not well understood. Recently, Ip et al. (2009) found that the effective Henry's Law increases with increasing sulphate concentration. At a sodium sulphate ionic strength of 0.03 mol/L (M) , $K_{\text{H}}^* = 2.40 \times 10^7 \text{ M/atm}$. This is 50 times higher than $K_{\text{H,aq}}^*$ and 12 times higher than with a sodium chloride ionic strength of 0.05 M . Ip et al. (2009) concluded that the presence of sulphate has a greater effect on the effective Henry's Law than ionic strength alone. Increasing the ionic strength of sulphate to 0.225 M increases the K_{H}^* to the point that it could not be measured, a value suggested to be $\geq 10^9 \text{ M/atm}$. This sulphate concentration is still substantially lower than that in the AS aerosol studies, but the suggested effective Henry's law constant is substantially larger than for the AS aerosol. It is possible that with increasing sulphate concentration and thus decreasing LWC, K_{H}^* of GL first increases up to a maximum and then decreases again. A similar effect was found by Ip et al. (2009) for sodium chloride solutions. This indicates that the amount of GL partitioning to the condensed phase is dependent on more than just the LWC over the entire range of sulphate concentrations. The mechanism that is at work is still unknown, and the importance of this observation over the more limited sulphate concentration range of ambient aerosol is unclear.

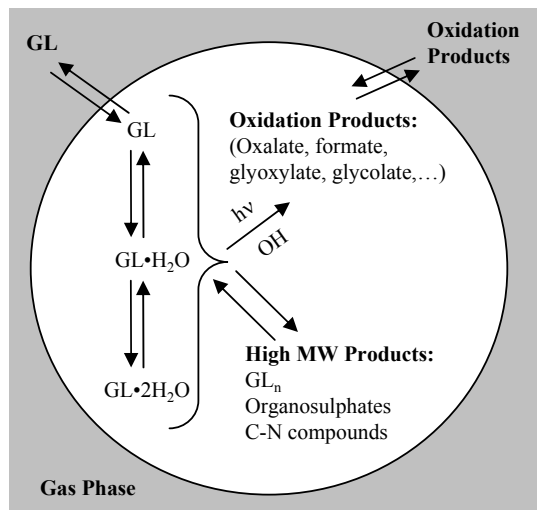


Fig. 1. Processes contributing to GL uptake on AS seed aerosol. GL=GL monomer; GL·H₂O=monohydrate; GL·2H₂O=dihydrate; high molecular weight (MW) products include GL_n, organosulphates, and carbon-nitrogen containing compounds; oxidation products include oxalate, formate, glyoxylate, and glycolate and their oxidation products.

Bulk studies have also provided valuable insight into the aqueous GL system. Carlton et al. (2007) performed photochemical reactions of GL and hydrogen peroxide and demonstrated that SOA yield from GL depends on photochemical processing. Recent work by Nozière et al. (2009) showed that GL reacts to form high molecular weight compounds and postulated that the ammonium ion is a catalyst for condensed phase GL reactions such as oligomerization. In a different study, Shapiro et al. (2009) showed that light absorbing complexes were observed in solutions containing AS and GL but not in sodium sulphate or sodium chloride solutions, indicating that nitrogen is central to the formation of light absorbing complexes.

In light of these investigations, it is clear that particle-phase chemistry plays a crucial role in the gas/particle partitioning of GL, though the processes controlling uptake are still not clear. In this study, we examine the uptake processes onto wet AS seed aerosol using a variety of instrumentation in dark conditions and in the presence of light. Figure 1 shows the major processes that could be contributing to GL uptake. The processes that have been identified by previous studies are:

1. GL-hydrate formation is fast and reversible (Schweitzer et al., 1998). Hydration equilibria up to GL·2H₂O, the dominant form of GL in dilute aqueous solutions, are included in $K_{H,aq}^*$ (Zhou and Mopper, 1990). Some

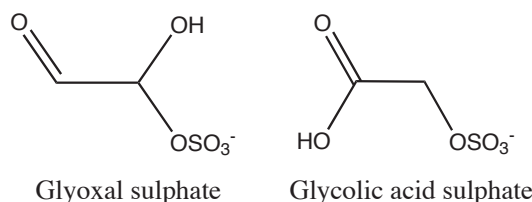


Fig. 2. Proposed structures for *m/z* 155; glyoxal sulphate and glycolic acid sulphate.

studies have demonstrated correlation of organic growth with water content of aerosol (Volkamer et al., 2009), whereas others have shown growth at extremely low water content and noted that GL·*n*H₂O concentrations appear to be independent of gas-phase GL concentrations (Corrigan et al., 2008).

2. Glyoxal oligomers (GL_n) have been detected by time-of-flight and quadrupole AMS studies of aerosol growth from GL uptake in chamber experiments (Kroll et al., 2005; Liggio et al., 2005b); no definitive evidence for GL_n in field samples has been found, likely due to analytical challenges. GL_n formation is reversible and slow (many minutes to hour timescales) in aqueous GL/H₂O solutions (Whipple, 1970; Fratzke and Reilly, 1986), and there are indications from a previous study that it is reversible in AS aerosol (Kroll et al., 2005).
3. The proposed GL sulphate (C₂H₃SO₆⁻, Fig. 2) is of much interest as it has been detected via filter sampling methods in field samples (Surratt et al., 2007, 2008; Gómez-González et al., 2008) and in chamber studies of isoprene oxidation under intermediate- to high-NO_x conditions (Surratt et al., 2008). The formation conditions for C₂H₃SO₆⁻ as well as its contribution to $K_{H,AS}^*$ are unclear. Irreversible formation of C₂H₃SO₆⁻ would not contribute to $K_{H,AS}^*$, however, reversible formation would have an effect on $K_{H,AS}^*$.

In this study we aim to investigate the processes contributing to overall GL uptake as well as which of these processes are effectively reversible, meaning reversible over aerosol lifetimes. These questions are important for evaluating applicability of laboratory studies to ambient conditions and net SOA yields from GL. If most GL uptake is effectively reversible, the organic aerosol will revolatilize at lower GL gas-phase concentrations upon transport away from GL sources or at night. Net SOA yields from a specific process will be higher if that process is irreversible.

Table 1. Experimental conditions of dark experiments.

	Seed ^a	[GL] ^b ppb _v	RH	Temp K	LWC ^c	Seed volume ^d , <i>V</i> μm ³ /cm ³	Δ <i>V</i> μm ³ /cm ³	<i>M</i> _{GL} ^e μg/cm ³
1	AS	131	65%	294	43%	84.0	18.8	31.8
2	AS	67	56%	293	37%	67.0	10.7	18.1
3	AS	182	56%	293	37%	87.0	40.4	68.3
4	AS	400 ^f	70%	293	47%	146.0	35.0	59.2
5	AS/SA	400 ^f	70%	293	49%	94.0	104.0	176
6	MgSO ₄ /SA	400 ^f	70%	293	67%	149.0	114.0	193
7	AS	none	70%	294	47%	77.0 ^g	--	--

^a AS=ammonium sulphate, SA=sulphuric acid^b 20% uncertainty on gas phase glyoxal values^c Calculated using ISORROPIA (Nenes et al., 1998)^d As measured by the DMA and corrected for wall loss^e Calculated assuming $\rho=1.69$ g/cm³^f Estimated^g Not wall loss corrected**Table 2.** Experimental conditions of irradiated experiments.

	Seed ^a	[GL] ^b ppb _v	RH Initial	RH Final	Temp Initial, K	Temp Final, K	LWC ^c Initial	LWC ^c Final	Seed volume ^d , <i>V</i> μm ³ /cm ³	Δ <i>V</i> μm ³ /cm ³
8	AS	86.2	66.0%	42.6%	293.0	299.4	43.7%	28.4%	81.0	-14.0
9	AS/Fe	128	64.6%	42.5%	292.8	299.3	43.0%	28.4%	78.9	-13.5
10	AS	127	55.7%	37.9%	292.8	299.4	36.7%	25.2%	87.0	-12.0
11	AS	none	59.6%	54.7%	293.1	294.4	39.4%	36.0%	62.3 ^e	--

^a AS=ammonium sulphate, Fe=Fe₂(SO₄)₃^b 20% uncertainty on gas phase glyoxal values^c Calculated using ISORROPIA (Nenes et al., 1998)^d As measured by the DMA and corrected for wall loss^e Not wall loss corrected

2 Experimental procedures

Experiments were performed in Caltech's indoor, dual 28 m³ Teflon environmental chambers (Cocker et al., 2001; Keywood et al., 2004). The experimental conditions are summarized in Tables 1 and 2. Each chamber has a dedicated Differential Mobility Analyzer (DMA, TSI model 3081) coupled with a condensation nucleus counter (TSI model 3760) for measuring aerosol size distribution, and number and volume concentration. Temperature, relative humidity (RH), O₃, NO, and NO_x were continuously monitored. AS seed particles were generated by atomization of a 0.015 M aqueous AS solution using a constant rate atomizer. Acidic seed particles were generated by atomization of a 0.015 M aqueous AS solution containing 0.015 M sulphuric acid. GL was prepared by heating a mixture of solid GL trimer dihydrate (Sigma, minimum 97%) and phosphorus pentoxide (P₂O₅)

to ~160°C under vacuum. The monomer was collected in an LN₂ trap as a yellow solid and stored overnight at -20°C. Before each experiment, the frozen monomer was allowed to vaporize into a 500 mL glass bulb and introduced into the chamber using a gentle air stream. The chamber was kept at ~60% RH. The concentration of an inert tracer, cyclohexane, was monitored using a gas-chromatograph with flame ionization detector (GC-FID, Agilent 6890N).

Dark experiments typically began by introducing gas-phase GL into a dark chamber and allowing the concentration to equilibrate over ~10 h. Approximately 160 ppb_v (part-per-billion by volume) of cyclohexane was also added as a tracer for dilution. Once the gas-phase GL concentration reached a steady state, AS seed was introduced and the resulting organic growth was monitored by both the DMA and a high resolution time-of-flight AMS (HR-ToF-AMS, hereby referred to as AMS). After organic growth levelled off, the

chamber air mass was diluted with clean hydrocarbon-free air to investigate the reversibility of uptake. The amount of dilution was calculated by monitoring the cyclohexane concentration with the GC-FID. In some experiments, AS seed was added first and then GL, though the results are the same.

Experiments with irradiation began similarly to dark experiments but when the addition of GL or AS seed was complete, the chamber lights were turned on. No external OH or NO_x source was added, and no dilution was performed in irradiated experiments.

Two blank experiments (Exp. 7 and 11) were conducted in which wet AS seed was atomized into a humid chamber without GL present. A negligible organic signal was measured in the absence of radiation, most likely due to background organics from the chamber walls. Under irradiation, miniscule organic growth was observed.

2.1 Teflon filter collection and offline chemical analysis

Teflon filters (PALL Life Sciences, 47 mm diameter, 1.0 μm pore size, teflo membrane) were collected from each experiment for offline chemical analysis. Filter sampling was initiated when the aerosol volume reached its maximum (constant) value, as determined by the DMA. Depending on the total volume concentration of aerosol in the chamber, the duration of filter sampling was 3.6–4.1 h, which resulted in ~5.1–5.8 m³ of total chamber air sampled. Collected filters were extracted in high-purity methanol, dried, and then reconstituted with 250 μL of a 1:1 (v/v) solvent mixture of 0.1% acetic acid in water and 0.1% acetic acid in methanol (Surratt et al., 2008). All filter extracts were analyzed by a Waters ACQUITY ultra performance liquid chromatography (UPLC) system, coupled to a Waters LCT Premier XT time-of-flight mass spectrometer (TOFMS) equipped with an electrospray ionization (ESI) source. The ESI source was operated in both negative (–) and positive (+) ion mode; acidic GL SOA components were detected in the negative ion mode, whereas C–N compounds (e.g. imidazoles) were detected in the positive ion mode. All other operating conditions for this technique have been fully described elsewhere (Surratt et al., 2008).

Blank Teflon filters were extracted and treated in the same manner as the samples; none of the SOA products detected on the filter samples collected from the GL chamber experiments were observed in these blanks, indicating that these SOA components were not introduced during sample storage and/or preparation. Furthermore, to ensure that the SOA components observed were not an artefact formed from the collection of gaseous GL onto filter media, a blank filter was collected under dark conditions from the chamber containing a well mixed concentration of GL (~2 ppm_v) and analyzed with UPLC/ESI-HR-TOFMS. This blank was sampled for the same duration as a sample filter. No SOA components characterized in the present study or significant contaminants were observed, consistent with the lack of observed aerosol

growth in the absence of light and AS seed aerosol. All filters used for UPLC/ESI-HR-TOFMS analysis were examined within 1–2 days of the filter extraction/sample preparation. Following their initial analysis, sample extract solutions were stored at –20°C. Selected samples were reanalyzed a month after initial extraction and showed no signs of degradation.

2.2 Aerodyne aerosol mass spectrometer

Real-time particle mass spectra were collected continuously by the AMS, which is described in detail elsewhere (DeCarlo, 2006; Canagaratna et al., 2007, and references therein). The AMS switched once every minute between a high resolution “W-mode” and a lower resolution, higher sensitivity “V-mode”. The “V-mode” data were analyzed using a fragmentation table to separate out sulphate, ammonium, and organic spectra and to time-trace specific mass-to-charge ratios. “W-mode” data were analyzed using a separate high-resolution spectra toolbox known as PIKA to determine the chemical formulas contributing to distinct mass-to-charge ratios (DeCarlo, 2006). Since GL easily fragments to produce CH₂O⁺, the fragmentation table was corrected so that the organic signal at *m/z* 30 was equal to its total signal minus the contribution from air. The nitrate contribution was changed to approximately 1.3 times the nitrate signal at *m/z* 46 as this was the 30/46 ratio during ammonium nitrate calibrations.

To determine elemental ratios, the computational toolbox known as Analytical Procedure for Elemental Separation (APES) was used. This toolbox applies the analysis procedure described in Aiken et al. (2007) to the high-resolution “W-mode data”. The particle-phase signal of CO⁺ and the organic contribution to H_xO⁺ ions were estimated as described in Aiken et al. (2008).

2.3 Madison laser-induced phosphorescence instrument

Gas-phase GL was detected with high specificity via Laser-Induced Phosphorescence (LIP) using the Madison LIP Instrument described in Huisman et al. (2008). This instrument utilizes a White-type multipass cell in a 2-pass configuration with gated photon counting and is highly sensitive, permitting specific, direct, in situ measurement of GL with a one-minute limit of detection (3σ) of 6 ppt_v (part-per-trillion by volume) per minute in a 32-pass configuration.

3 Results

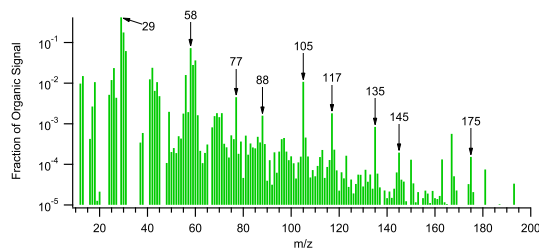
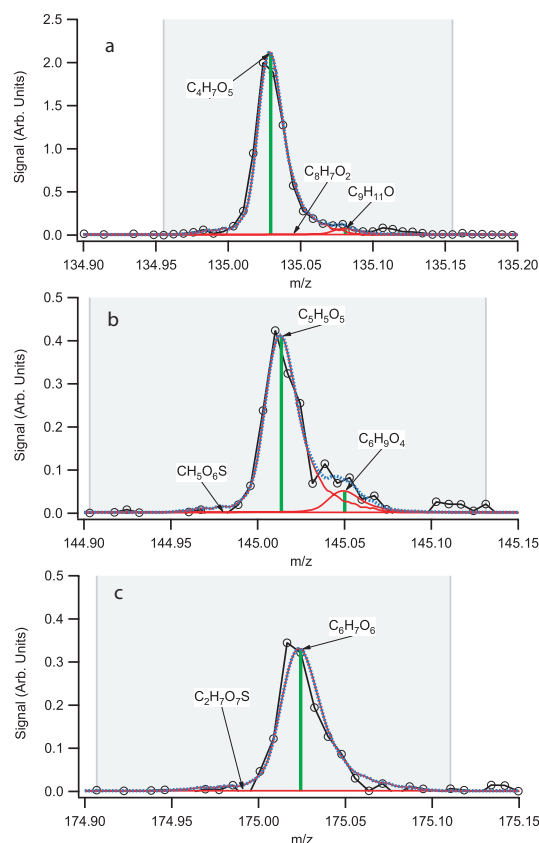
3.1 Glyoxal uptake in the absence of light

For a typical experiment, gas-phase GL was present in the chamber and equilibrated with the chamber walls prior to the

Table 3. GL fragments observed via AMS and suggested structures from which the fragments are formed.

m/z	Fragment Formula	Suggested Structure
29	CHO^+	
58	$\text{C}_2\text{H}_2\text{O}_2^+$	
77	$\text{C}_2\text{H}_5\text{O}_3^+$	
88	$\text{C}_3\text{H}_4\text{O}_3^+$	
105	$\text{C}_3\text{H}_5\text{O}_4^+$	
117	$\text{C}_4\text{H}_5\text{O}_4^+$	
135	$\text{C}_4\text{H}_7\text{O}_5^+$	
145	$\text{C}_5\text{H}_5\text{O}_5^+$	
175	$\text{C}_6\text{H}_7\text{O}_6^+$	

introduction of AS seed particles. Organic growth began immediately upon particle addition, and reached a maximum after approximately 10 h; over this time period, sulphate and ammonium decreased due to particle wall losses. A representative unit-mass AMS spectrum is shown in Fig. 3. The fragments of interest to this study are summarized in Tables 3 and 4. The most significant fragments are m/z 44, 58, 68, 135, 145, and 175. The observed fragments are in general accord with those observed by Liggio et al. (2005a), though certain masses such as m/z 192 and 193 have lower signals in this study. Proposed precursor structures for the fragment masses marked in Fig. 3 are listed in Table 3. The fragment chemical formulae are unequivocally confirmed by the high-resolution spectra obtained in “W-mode”, verifying many of the assignments made by Liggio et al. (2005a). Masses listed in Table 3 which are larger than or equal to m/z 77 represent ion fragments of oligomers; as an example, the high-resolution peak for m/z 135 is shown in Fig. 4a. In the high resolution spectra, the only fragment ion found to contain both sulphur and carbon is m/z 79 (CH_3SO_2^+); however, the signal intensity is similar to that in the blank experiment (Exp. 7). Filter sample analysis did not detect any organosulphates under dark conditions in neutral (Exp. 4) or acidic seed (Fig. 5c, Exp. 5 and 6), as can be seen in the comparison between experiments carried out under irradiated conditions (Fig. 5a, Exp. 10) and experiments performed in the dark (Fig. 5b, Exp. 3).

**Fig. 3.** Representative unit-mass AMS spectrum. Distinct GL and GL oligomer marker peaks are shown. The compound from which each fragment was formed is listed in Table 3.**Fig. 4.** High-resolution (“W-mode”) AMS peaks allow unequivocal assignment of a $\text{C}_4\text{H}_7\text{O}_5^+$ formula to the m/z 135, $\text{C}_5\text{H}_5\text{O}_5^+$ formula to the m/z 145, and $\text{C}_6\text{H}_7\text{O}_6^+$ formula to the m/z 175 fragment ions.

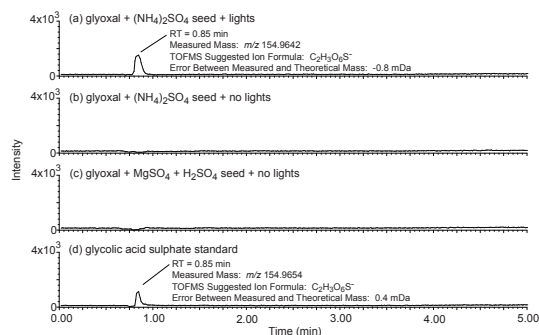


Fig. 5. UPLC/ESI-TOFMS extracted ion chromatograms (EICs) of m/z 155 for selected GL experiments. The comparison of these EICs reveals that glycolic acid sulphate only forms under irradiated conditions when using AS seed aerosol. Comparison of the retention time (RT) and mass (m/z) of the compound detected in panel (a) and the glycolic acid sulphate standard, (d), unequivocally shows that glycolic acid sulphate is being formed in the presence of light, but not in neutral, (b), or acidic, (c), dark experiments.

After particle growth has stopped, the chamber was diluted with clean air (Exp. 1 and 3) to investigate the reversibility of GL uptake. Upon dilution, the concentrations of tracer, gas-phase GL, and particle-phase organic, sulphate, and ammonium decreased. To remove the effect of the decrease in overall particle volume due to wall loss and to dilution, the organic and several marker signals are normalized to sulphate. This normalized signal is proportional to the condensed phase concentration of each species. The normalized organic signal and GL markers at m/z 58 and m/z 105 decrease after dilution by 15–25% and 18–30%, respectively. The gas-phase GL concentration decreased by 25–40% of the initial concentration and the overall organic signal decreased relative to the tracer signal. Figure 6 shows this for a typical dilution experiment (Exp. 3).

Several fragments were observed by the AMS to have different temporal characteristics (and thus uptake kinetics) than the total organic or GL_n signal. Relatively strong signals occurred at m/z 41, 68, 69, and 70. Weaker signals, approximately 5–10 times lower in magnitude, were also detected at other masses, the largest fragment occurring at m/z 96. The signal at m/z 68 increased immediately upon seed injection and grew steadily, even after no further change in total organic growth was observable within the uncertainty of that measurement. Furthermore, during dilution, the signal continued to increase when normalized to the sulphate signal. These compounds contribute only $\sim 0.5\%$ of total organic mass measured by the AMS, but the sensitivity for these compounds or the GL_n has not been calibrated, and it is unlikely such a calibration can be achieved for the oligomers. Dilution has very little effect on the relative growth of m/z 68, implying that the reactions are irreversible with respect to the

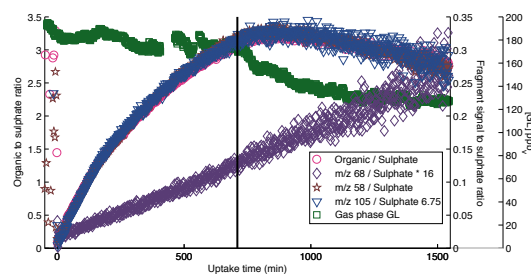


Fig. 6. The time traces of total organic, m/z 58, 105, and 68 fragment ions normalized by the sulphate ion signal along with gas phase GL concentrations for a dilution experiment (Exp. 3). Dilution begins at the black vertical line. Upon dilution, the normalized organic and GL (m/z 58 and 105) marker signals decrease by 30%, and 17%, respectively, which is less than the 25% reduction in gas-phase GL concentrations. However, the system has clearly not equilibrated and thus further loss of particle-phase GL is expected. In contrast to the reversible behaviour of total organic and GL and GL oligomer growth, the growth of the m/z 68 (imidazole) marker has markedly different characteristics, indicating irreversible uptake.

lifetime of chamber aerosol. The high-resolution spectra obtained with the AMS in “W-mode” show unequivocally that these fragments originate from compounds containing carbon and nitrogen, as discussed below. Filter sample analysis also showed the presence of several nitrogen containing species in positive mode, including a species with m/z 97.

3.2 Glyoxal uptake in the presence of light

The AMS spectra in irradiated experiments initially resembled those of dark uptake experiments, with many of the same marker fragments prominent, but then changed quickly. As under non-irradiated conditions, gaseous GL partitioned immediately to the AS seed under UV light. The organic signal increased quickly upon addition of AS aerosol, but began to decrease soon after irradiation began. Upon reaching a maximum, the GL marker signal decayed faster than wall loss and the maximum is reached earlier than in the experiments under dark conditions. No dilution was performed in the irradiated experiments. The fractional contribution of m/z 44 and m/z 68 increased upon irradiation (Fig. 7). The irradiation resulted in a temperature increase of $\sim 5^\circ\text{C}$ and a drop in relative humidity (see Table 2). As a result, the liquid water content (LWC) was lowered and the total aerosol volume decreased, which made it impossible to determine the mass of GL taken up into the aerosol from the DMA data. The fragment with m/z 44 can be confidently assigned as CO_2^+ , and in AMS spectra is considered an indicator of the oxidation state of organic aerosol. Its increase in irradiated experiments points to the fact that the amount of oxidized organic species is increasing in these experiments.

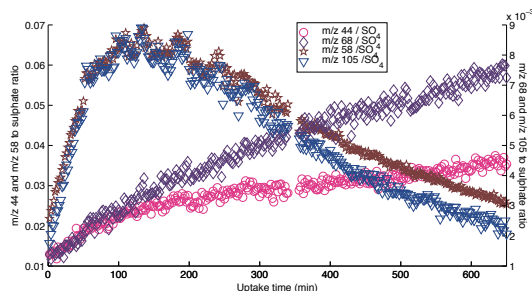


Fig. 7. The sulphate normalized GL and GL oligomer marker signals m/z 58 and 105 increase rapidly on introduction of seed aerosol under irradiated conditions, but decrease rapidly without any dilution taking place, which is in marked difference to the dark experiments. The m/z 44, and in particular, 68 marker signals increase steadily during these experiments, indicating oxidation of the organic fraction of the aerosol and continued imidazole formation.

In agreement with this, numerous highly oxidized organic species were detected via the UPLC/ESI-HR-TOFMS analysis, including glyoxylic, glycolic, and formic acids. Filter sample analysis also showed the presence of a sulphur containing compound with m/z 155. No OH source was added in these experiments but a small amount of OH is potentially being produced via photolysis of GL, resulting in formation of the carboxylic acids. In one experiment, Fe was added to the seed (Exp. 9). The results closely resembled those of the other irradiated experiments (Exp. 8 and 10). Although carboxylic acids are formed, the O:C ratio of the organic fraction of the aerosol is not increasing but rather decreasing. In contrast the H:C and N:C ratios both increase in these experiments. The ammonium fraction of the aerosol is excluded in the calculation of N:C ratio.

4 Discussion

4.1 Organosulphate formation

The fragment ions m/z 145 and 175, which were previously assigned the formulas $\text{CH}_5\text{O}_6\text{S}^+$ and $\text{C}_2\text{H}_7\text{O}_7\text{S}^+$, respectively by Liggio et al. (2005a), were unequivocally determined to be $\text{C}_5\text{H}_5\text{O}_5\text{S}^+$ and $\text{C}_6\text{H}_7\text{O}_6\text{S}^+$, respectively (Fig. 4a and b) with the AMS in “W-mode”. The detection of these fragments demonstrates the existence of trimers or larger GL_n in the aerosol. Liggio et al. (2005a) suggested that these fragments correspond to fragmentation products of GL sulphates formed from a proposed aqueous reaction of sulphate or bisulphate with GL. If this proposed mechanism were correct, it would be the only evidence prior to the work presented here for the formation of GL sulphates in chamber aerosol resulting from GL uptake. The current study is in the unique position to unambiguously determine the chemi-

cal formulas of both fragment ions due to the employment of the high-resolution “W-mode”, which is not possible with a quadrupole AMS. No sulphate esters were detected by the UPLC/ESI-HR-TOFMS analysis of filter samples in non-irradiated conditions with neutral or acidic seed (Fig. 5b and 5c). This evidence suggests that GL sulphate does not form in dark GL uptake experiments with AS seed.

Our results do not rule out that sulphates were formed in the study by Liggio et al. (2005b), and our irradiated experiments clearly demonstrate that organosulphates can form. Figure 5a shows that m/z 155, which corresponds to glycolic acid sulphate ($\text{C}_2\text{H}_3\text{SO}_6^-$, see below), is measured in filter samples obtained during irradiated experiments (Exp. 8 and 10). The AMS did not detect this sulphate, most likely due to a high degree of fragmentation. The same organosulphate (as judged by elution time and formula) $\text{C}_2\text{H}_3\text{SO}_6^-$ has previously been detected in filter samples from isoprene photooxidation experiments conducted in the Caltech chamber (Surratt et al., 2008) under intermediate- and high- NO_x conditions, which favour GL production, but only with acidic seed. Ambient organic aerosol collected from K-puszt, Hungary (Gómez-González et al., 2008) and from the southeastern US (Surratt et al., 2008) has also been found to contain this $\text{C}_2\text{H}_3\text{SO}_6^-$ organosulphate. In the previous work this sulphate was proposed to be GL sulphate. In all of these studies the filter extraction was performed in methanol. As sulphate is a better leaving group than methoxy, it appeared likely that the initially proposed GL sulphate would not be observed with the methanol extraction method, as it should dissociate. Thus, isomers of $\text{C}_2\text{H}_3\text{SO}_6^-$ were investigated and glycolic acid sulphate was chosen as a likely candidate since this sulphate should be more stable in methanol and as a different glycolic acid ester was proposed as one of the products of the light induced experiments in the work presented here, which suggests that a pathway for glycolic acid production exists. We subsequently synthesized the glycolic acid sulphate and verified that the mass and elution time of the standard and the $\text{C}_2\text{H}_3\text{SO}_6^-$ sulphate observed in this and previous studies were identical using UPLC/ESI-HR-TOFMS (Fig. 5d). This analysis shows that previous assignments of glyoxal sulphate that were obtained via filter extraction involving methanol or related solvents, such as in the chamber and ambient aerosol studies mentioned above, should be revisited as carbonyl sulphates are not stable under these conditions. However, this does not rule out the existence of carbonyl sulphates under the conditions present in aerosol.

This is the first report of glycolic acid sulphate measured in chamber filter samples of GL uptake, and one of the few organosulphates to be positively identified in ambient aerosol. Acid catalysis has been traditionally been implicated in the formation of organosulphates. However, this study shows no sulphate formation under acidic conditions in the absence of light (Exp. 5 and 6) and recent studies have questioned this pathway for lower tropospheric conditions and instead proposed an epoxide pathway (Minerath et al., 2008;

Table 4. Fragments containing both carbon and nitrogen observed and suggested chemical formulas. The masses detected by UPLC/(+)ESI-TOFMS were detected in the protonated form.

	<i>m/z</i>	Fragment formula
Strong ions	41	C ₂ H ₃ N ⁺
	68	C ₃ H ₄ N ₂ ⁺
	69	C ₃ H ₃ NO ⁺
	70	C ₃ H ₄ NO ⁺
Weak ions	46	CH ₄ NO ⁺
	52	C ₃ H ₂ N ⁺
	53	C ₃ H ₃ N ⁺
	57	C ₂ H ₃ NO ⁺
	68	C ₃ H ₂ NO ⁺
	96	C ₄ H ₄ N ₂ O ⁺
ESI	97	C ₄ H ₅ N ₂ O ⁺
	115	C ₄ H ₇ N ₂ O ₂ ⁺
	129	C ₅ H ₉ N ₂ O ₂ ⁺
	159	C ₆ H ₁₁ N ₂ O ₃ ⁺
	173	C ₇ H ₁₃ N ₂ O ₃ ⁺
	184	C ₇ H ₁₀ N ₃ O ₃ ⁺

Minerath and Elrod, 2009). In contrast, the glycolic acid sulphate formation observed in this work requires a light induced pathway as it is only observed in the presence of light (Exp. 8 and 10), even in neutral seed aerosol. Although the identification of C₂H₃SO₆[−] as glycolic acid sulphate reconciles the expected chemical stability to methanol extraction, it is unclear how glycolic acid or its sulphate are formed, although the increasing *m/z* 44 marker shows that there is active oxidative chemistry occurring in the presence of UV light. However, glycolic acid is not an oxidation product of GL but rather a disproportionation product. We are currently investigating the pathway for glycolic acid sulphate formation, which is unlikely to involve an epoxide.

4.2 Carbon-nitrogen containing compound formation

Although no significant AMS fragments containing both sulphur and carbon are found, several fragments in the high-resolution spectra are found to contain nitrogen together with carbon, hydrogen and occasionally oxygen (Table 4). In addition, filter samples analyzed with UPLC/ESI-HR-TOFMS in positive mode showed compounds containing carbon and nitrogen (C-N compounds), listed in Table 4. The identification of the species corresponding to the chemical formulae listed in Table 4 is ongoing but we have achieved a positive identification of three masses in the AMS spectra; the strong signals at *m/z* 41 (C₂H₃N) and 68 (C₃H₄N₂, Fig. 8a), and a weaker signal at *m/z* 96 (C₄H₄N₂O, Fig. 8b). The carrier of *m/z* 97 from the filter samples also had the formula C₄H₄N₂O (after the subtraction of a proton) in high-resolution positive

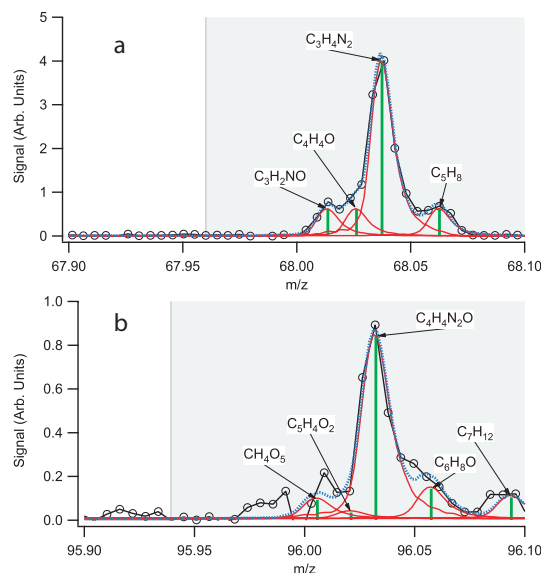


Fig. 8. High-resolution (W-mode) AMS peaks allow unequivocal assignment of a C₃H₄N₂⁺ formula to the *m/z* 68, C₄H₄N₂O⁺ formula to the *m/z* 96 fragment ions.

mode ESI and had the same elution time as a standard of 1H-imidazole-2-carboxaldehyde (Sigma-Aldrich). The AMS fragments are also consistent with 1H-imidazole-2-carboxaldehyde. The high-resolution masses observed with UPLC/ESI-HR-TOFMS and the AMS, the AMS fragmentation pattern and the observed elution time provide strong support for the assignment of the carrier of this signal to 1H-imidazole-2-carboxaldehyde. In further support of this finding, the general Debus mechanism for imidazole formation (see following paragraph) predicts the formation of 1H-imidazole-2-carboxaldehyde as shown in Fig. 9. Other C-N containing products were observed, but have not been positively identified. The production of a very stable aromatic compound such as an imidazole may be the thermodynamic driving force behind this reaction and explains why carbon-nitrogen containing fragments are observed in the AMS. This is in contrast to the case of organic nitrates, which fragment easily via loss of the nitrogen moiety.

Since no NO_x was present or added to the chamber before GL addition, the only source of labile nitrogen is ammonium from AS. Therefore, the C-N ions likely arise from fragmentation of products of a reaction between GL and ammonium. Although the ammonium ion is not a nucleophile and is not expected to react with GL, there will be a non-negligible concentration of ammonia in equilibrium with ammonium at the pH found in AS aerosol. The reaction of GL and ammonia is an established organic reaction for synthesis of imidazole and was described in 1858 (Debus, 1858). In view of recent

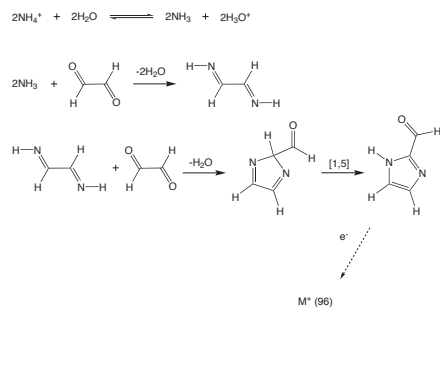


Fig. 9. Proposed formation mechanism of 1H-imidazole-2-carboxaldehyde and observed m/z 68 and 96 fragment ion.

literature describing the observation of light absorbing complexes and higher molecular weight compounds from reaction of bulk solutions containing AS and GL (Nozière et al., 2009; Shapiro et al., 2009), it is interesting to note the observations by Debus (1858). Debus (1858) describes formation of a brown solution as well as two colourless products; imidazole ($\text{C}_3\text{H}_4\text{N}_2$) and $\text{C}_6\text{H}_6\text{N}_4$, most likely 2,2'-bi-1H-imidazole, which is available commercially as a coloured compound. Thus the reaction of GL with ammonia has a long history. In addition to reaction with ammonia, the reaction of GL with AS in bulk solution is well established. In fact, a method for reaction of GL with formaldehyde and AS in bulk aqueous solution with 69% yield has been published and patented (Schulze, 1973). The author states the yield of imidazole is surprisingly high, which could be a result of catalytic activity by ammonium (proposed recently by Nozière et al., 2009) in addition to being a reactant, although this is complicated by the pronounced effect of anions on GL (Ip et al., 2009). A similar method for the production of 2,2'-bi-1H-imidazole in bulk aqueous solution via reaction of GL in AS with 43–54% yield has also been published and patented (Cho et al., 2003). Thus, reaction of GL with AS in bulk solutions to form coloured compounds has a well established history. Other studies have addressed the effect of added gas-phase ammonia (Na et al., 2006, 2007), organic amines (Angelino et al., 2001; Murphy et al., 2007; Silva et al., 2008), and amino acids (De Haan et al., 2009) on SOA formation as well as bulk phase reactions between AS and GL (Nozière et al., 2009; Shapiro et al., 2009) and amino acids and GL (De Haan et al., 2009), but to the authors' knowledge, imidazole compounds have not been previously detected in AS seed aerosol chamber studies. The mass spectrum published by Liggio et al. (2005a) does not show a peak at m/z 68. However, subsequent to the initial publication of our work, De Haan et al. (2009) identified substituted imidazole compounds formed from the reaction of GL and amino acids in both the bulk phase and in solid

phase aerosols. We report the first observation of the formation of C-N containing compounds from reaction of a carbonyl in AS seed aerosol, but this finding is not surprising given the recent findings by De Haan et al. (2009) and the well established chemistry reported for bulk solutions.

Little experimental data are available on the physical properties of 1H-imidazole-2-carboxaldehyde, though it is predicted to have a vapour pressure of 1.43×10^{-3} Torr (SciFinder Scholar, 2008). Under mildly acidic conditions, this molecule would be protonated, lowering the vapour pressure and making it a viable candidate for an SOA constituent. The pK_B of imidazole is 7, so 50% will be protonated in neutral solutions. Thus at the pH of AS (~ 5) most of the imidazole will be protonated and the low volatility is evidenced by the fact that the carrier of the m/z 68 signal does not repartition to the gas phase in the dilution or irradiated experiments. The imidazole and other C-N compounds only contribute a small amount to the total organic mass. It is possible that reaction of other α -dicarbonyls and aldehydes could increase this contribution. However, as mentioned above, some of the reaction products of GL and AS are strongly light absorbing (Shapiro et al., 2009) and even amounts that do not add significantly to SOA mass could affect aerosol optical properties. As the imidazole is formed irreversibly, it could be used as a tracer for atmospheric carbonyl-nitrogen reactivity with implications for changing aerosol optical properties.

4.3 Overall organic growth and glyoxal oligomer formation

Analysis of the AMS spectra collected indicates strong evidence for GL_n within the aerosol (see Fig. 3). It is important to note that fragments with one or two carbons do not necessarily arise only from GL monomers in the particle phase. They can also be fragmentation products of larger oligomers; thus C1 and C2 fragments are a result of fragmentation of at least a monomer, C3 and C4 fragments are the result of fragmentation from at least a dimer, and so on. The GL and GL_n mass fragments stop growing in parallel with overall organic growth and show analogous behaviour to total organic growth upon dilution. Organic growth in our study reached a plateau, providing evidence for a steady-state point, which could either be due to a depletion of a reactant in an intrinsically irreversible process or because equilibrium, with a corresponding modified effective Henry's law constant, is achieved. The dilution experiments, in which the chamber air mass was diluted with GL-free air, provide key evidence that this plateau is not caused by the depletion of a reactant. The dilution process itself reduces the gas-phase GL concentration and aerosol number density and thus total aerosol volume but does not change the composition of the aerosol phase. However, if the aerosol-phase composition was achieved via equilibrium with the gas-phase GL, reduction of the gas-phase GL concentration via dilution disturbs this equilibrium. As a result the aerosol-phase organic

content immediately after dilution is higher than the equilibrium value for the reduced gas phase concentration would predict. The system will respond by re-partitioning GL to the gas-phase. In our dilution experiments, which reduce the gas-phase GL concentration by 25–40% (Fig. 6), the organic:sulphate ratio decreases by 15–25%, which shows that organic aerosol content decreases relative to sulphate, implying a loss of GL from the aerosol phase. This shows that GL uptake onto AS aerosol is reversible; GL will partition from the aerosol to gas phase in the event of lowered gas phase concentrations in the case of reversible uptake. The fact that the aerosol phase organic content decreased a little less than the gas-phase GL concentration is expected from the (slow) kinetics.

For the dark GL uptake experiments, only C-N compounds, GL and GL_n were identified, while no organosulphate was found. C-N compounds are clearly formed irreversibly since no loss from the aerosol was seen upon dilution. The fact that they only contribute a small part of the organic AMS signal and that overall organic growth as well as GL and GL_n growth are reversible, suggests strongly that overall growth is dominated by GL and GL_n. The studies by Liggio et al. (2005a,b) were conducted on timescales (~4 h) in which equilibrium was not yet achieved in our studies. We have therefore compared our organic growth during the first 4 h with that of Liggio et al. (2005a,b) for experiments at similar relative humidities of 49% (Liggio et al., 2005a,b) and 55% (this study) and gas-phase GL concentrations of 5.1 ppb_v (Liggio et al., 2005a,b) and ~70 ppb_v (this study). The organic/sulphate ratio after 4 h in the work by Liggio et al. (2005a) is ~16, which is more than an order of magnitude larger than in this study (~0.35), and we expect that the difference would have been even larger if we had employed the lower GL mixing ratios of the work by Liggio et al. (2005a,b). Although the first two hours of our data can be interpreted with a linear slope the curvature of 2–4 hrs in the study presented here shows a decreasing uptake rate in agreement with the fact that equilibrium is achieved after about 10 h. It is hard to interpret a clear curvature in the work by Liggio et al. (2005a). The average aerodynamic diameter of the seed aerosol in the study by Liggio et al. (2005a) is initially smaller and thus the uptake rate per volume of seed aerosol is expected to be faster than in this study, but it is unlikely that this alone can explain the discrepancy. In a more recent study, Volkamer et al. (2009) showed that photochemical uptake was higher within 90 s than over several hours in our study and the study of Kroll et al. (2005). The presence of OH in the study by Volkamer et al. (2009) represents a significant difference, which could explain the large difference in uptake rate. However, we also currently cannot determine a particular reason why the non-irradiated studies potentially show two different types of uptake (irreversible and reversible) at different rates, information that is critical if understanding of these processes is to be applied to ambient studies.

Although the primary focus of this work are the condensed phase reactions of GL and the reversibility of uptake onto AS aerosol, effective Henry's Law values for GL were also calculated. Kroll et al. (2005) assumed a unit density of 1 g/cm³ and used the seed volume to calculate aerosol GL concentrations. In this manner the authors obtained a value of $K_{H,mod}^* = 2.6 \times 10^7$ M/atm. However, the densities of GL trimer dihydrate (in our lab) and GL aerosol derived from drying aerosolized 40% w/w GL solutions (D. De Haan, personal communication, 2009) have since been measured. These densities were determined to be 1.67 g/cm³ and 1.71 g/cm³, respectively. Therefore, the density of GL used in this work is $\rho = 1.69$ g/cm³, which is likely a lower limit due to partial molar volume effects in solution. Using this density, we calculate an effective Henry's Law value of 3.4×10^7 M/atm for the data from Kroll et al. (2005) and a value between 4.2×10^7 M/atm and 7.0×10^7 M/atm from this study. The study by Volkamer et al. (2009) used a density of $\rho = 2$ g/cm³ and used the fraction of seed volume corresponding to LWC to calculate a modified GL concentration. In this manner they obtained a value of $K_{H,mod}^{**} = 1.65 \times 10^8$ M/atm. Using this method and density, we calculate a value between 1.51×10^8 M/atm and 2.52×10^8 M/atm for our study, reflecting the experimental uncertainty. However, it should be noted that the two studies were conducted under different conditions, as the study Volkamer et al. (2009) had an OH source present, and thus the corresponding Henry's Law constants cannot be directly compared. More work is needed to determine the effect of GL concentration, AS and LWC on the effective Henry's Law constant of GL.

4.4 Glyoxal uptake under irradiated conditions

We present the first analysis of organic reaction products formed during irradiated GL uptake with AS seed aerosol. Within the framework of Fig. 1, the light induced reactions that are occurring should add additional product channels in the condensed phase, so a higher uptake would be expected under irradiated conditions. No OH source was added in our study and thus conditions are not identical to those employed by Volkamer et al. (2009). However, there is a marked difference in the fate of GL in the particle phase for the irradiated conditions compared to dark conditions in our study, even without an added OH source: an organosulphate and organic acids are formed. As discussed earlier, the organosulphate formation is a result of a light induced mechanism, as can be seen in the lack of organosulphate formed even in highly acidic aerosol under non-irradiated conditions.

The relative signal strength of m/z 44, an indicator of oxidized organic aerosol in the AMS spectra, shows that a substantial amount of oxidized organics are formed over the duration of the irradiated experiments. This is supported by the organic acids found in filter sample analysis: formic, glyoxylic and glycolic acids, the latter a disproportionation

product of GL, all of which have smaller Henry's law constants than GL. The formic acid and glycolic acid are observed as an ester, a higher molecular weight condensation product. Although no OH source was added, the observation of glyoxal oxidation products strongly indicates that the irradiation resulted in radical chemistry. Whether this chemistry occurred via OH or some other radical mechanism cannot be ascertained. If oxidation to more volatile products, such as glyoxylic acid, is not significantly faster than condensation (e.g. the formic-glycolic acid ester, or oxidation to oxalic acid, which can form SOA), the net SOA yield under irradiated conditions should be higher than under dark conditions as additional product channels are available. These additional product channels also make Henry's law analysis of uptake inapplicable. In contrast to the study of Volkamer et al. (2009), which generally found increased uptake and uptake rate but had an OH source, overall organic growth was reduced under irradiated conditions in this study as compared to dark conditions. Enhanced loss of particle-phase GL in the presence of light was observed, but while it is possible that rapid oxidation to higher volatility compounds, such as formic and glyoxylic acid, and subsequent partitioning of these to the gas phase is competing with the formation of GL_n and reaction of the oxidation products to higher molecular weight compounds, it is also possible that increasing temperature upon irradiation causes significant amounts of GL to repartition to the gas phase. This is supported by the fact that the O:C ratio started to decrease once the chambers were irradiated. As the chambers heated, GL (O:C=1:1, H:C=1:1) and possibly high volatility glyoxal oxidation products are revolatilized to the gas phase, leaving behind irreversibly formed compounds such as imidazoles (O:C=1:4, N:C=1:2 and H:C=1:1) and low volatility carboxylic acids. This loss of GL, together with the lack of loss of imidazole, explains the increase in the N:C ratio and an increase in the H:C ratio, both of which are seen in these experiments. It is important to note that heating the chambers does not result in efflorescence of the aerosol, as this would trap the GL within the aerosol and increase oligomer formation (Loeffler et al., 2006), which is not observed. GL photolysis in the gas phase is also possible; however, since the walls act as a substantial reservoir of GL that is at steady state with the gas phase, this is less likely. In fact, during the irradiated GL uptake experiment shown in Fig. 7, the gas-phase GL concentrations remained constant at ~150 ppb_v throughout the experiment. A quantitative comparison of SOA yields between dark and irradiated conditions is not possible for this work due to the different experimental conditions.

4.5 Implications to ambient aerosol

GL and other α -dicarbonyls, such as methylglyoxal, are common oxidation products of both biogenic and anthropogenic VOCs. The concentration of these α -dicarbonyls is

typically highest during the day and thus SOA formation under irradiated conditions should be more important than under dark conditions. However, for a detailed understanding of the processes depicted in Fig. 1 and their contribution to SOA formation under ambient conditions, it is desirable to address these processes separately, therefore an analysis of GL uptake under both dark and irradiated conditions is helpful. While uptake and aerosol phase chemistry of GL and other α -dicarbonyls may differ, understanding GL is instructive as a model for understanding the chemistry involved in other systems for model and experimental studies. Our study shows that GL uptake involves both reversible processes, such as growth via GL monomer and oligomers, and irreversible processes, such as C-N compound formation and oxidation reactions under irradiated conditions. The reversible processes are likely less relevant to ambient SOA formation as they will repartition GL to the gas phase upon decreasing GL gas-phase concentrations, such as night time or transport away from GL sources. However, they provide a pathway for uptake of GL into the particle phase, allowing the irreversible processes to proceed. The majority of organic growth in the chamber studies under dark conditions occurs via GL uptake with subsequent oligomer formation, but ambient GL concentrations are substantially lower (2–3 orders of magnitude), so it is less likely the organic character of the aerosol will involve multiple GL molecules such as oligomers and 1H-imidazole-2-carboxaldehyde. However, it is likely that reactions with other aldehydes will occur. Aldehydes and α -dicarbonyls are ubiquitous, and the discovery of this new C-N reaction pathway allows for the potential production of many different imidazole compounds. While methylglyoxal is the most abundant α -dicarbonyl, GL is likely the most important α -dicarbonyl for formation of imidazoles due to the fact that the Henry's law constant for GL is larger than that for methylglyoxal ($K_{H, \text{aq}, \text{MGL}}^* = 3.2 \times 10^4 \text{ M/atm}$), and thus it partitions more strongly to aqueous aerosol. However, Matsunaga et al. (2004) detected higher levels of methylglyoxal than GL in ambient particulate matter, indicating that the high gas phase mixing ratios of methylglyoxal may make it an important contributor to SOA formation. As the underlying reasons for the large difference between $K_{H, \text{aq}}^*$ and $K_{H, \text{mod}}^*$ are not known, it is difficult to estimate the Henry's law constant for methylglyoxal for AS seed aerosol. Kroll et al. (2005) did not observe any organic growth for methylglyoxal, but the growth from imidazoles, which proceeds via an α -dicarbonyl monomer, might have been below the detection threshold. Even small amounts of the newly discovered light absorbing compounds, in particular C-N compounds, in aerosol can influence the optical properties of the aerosol due to their strong absorptive properties (Shapiro et al., 2009). In this context it is interesting to note that Barnard et al. (2008) found enhanced absorption of "brown carbon" aerosol in Mexico City that added about 40% absorption to that of black carbon. Imidazoles are an ideal tracer for these C-N

compounds, due to the ubiquitous nature of their precursors, as described above. This study suggests that methods should be developed to allow analysis of field aerosol samples with respect to this class of compound, and potentially also for compounds derived from methylglyoxal, which is typically present in higher concentrations in areas in which biogenic VOC chemistry dominates (Spaulding et al., 2003). This study also shows that irradiated conditions produce oxidation products of GL even in the absence of an added OH source. However, the monomers found in this study, such as formic acid, glycolic acid and glyoxylic acids, have lower Henry's law constants than GL and thus will not necessarily increase SOA yields. An exception would be the production of oxalic acid and higher molecular weight compounds, such as organosulphates, which would increase SOA yields.

5 Conclusions

This study provides new insights into processes that can contribute to SOA formation from GL and the degree of reversibility of these processes. Reversibility is judged with respect to the experimental timescales, which were as long as 26 h after initiation of organic growth. We demonstrate that:

1. GL does not form a sulphate (i.e. organosulphate of GL) that can be detected using methods based on filter extraction. It is likely that carbonyl sulphates are in general not stable enough to be identified with filter extraction methods. Previous assignments of such compounds should be revisited,
2. $\text{C}_2\text{H}_3\text{SO}_6^-$, which has been found in ambient samples, corresponds to glycolic acid sulphate. It is not formed under dark conditions with neutral or acidic AS seed aerosol and was only observed in irradiated experiments. The glycolic acid sulphate was identified by comparison with a laboratory synthesized standard,
3. carbon-nitrogen containing compounds form irreversibly with AS seed aerosol,
4. overall GL uptake and GL oligomer formation in the particle phase are reversible for neutral AS seed aerosol in the dark for the experimental conditions of this study,
5. there is clear evidence for active photochemistry for GL uptake under irradiated conditions, including formation of glyoxylic acid, glycolic acid, formic acid, and glycolic acid sulphate.

Further studies are required to evaluate imidazoles as tracers of carbonyl-ammonium chemistry that produces strongly light absorbing aerosol products. Studies are ongoing to elucidate the formation of condensed-phase oxidation products and, in particular, glycolic acid sulphate and the contribution of these compounds to SOA.

Acknowledgements. The authors are grateful to Tehshik Yoon for his helpful discussions about organic synthesis. This work was supported by the Camille and Henry Dreyfus Foundation, the NDSEG-ARO, the US Department of Energy grant DE-FG02-05ER63 983 and US Environmental Protection Agency STAR grant RD-83 374 901. It has not been formally reviewed by EPA. The views expressed in this document are solely those of the authors and the EPA does not endorse any products in this publication. Development of the Madison-LIP instrument was supported by the National Science Foundation, Division of Atmospheric Sciences, Atmospheric Chemistry Program (grant 0724 912), and the NDSEG-ARO. The Waters UPLC-LCT Premier XT time-of-flight mass spectrometer was purchased in 2006 with a grant from the National Science Foundation, Chemistry Research Instrumentation and Facilities Program (CHE-0 541 745).

Edited by: V. F. McNeill

References

- Aiken, A. C., DeCarlo, P. F., and Jimenez, J. L.: Elemental analysis of organic species with Electron Ionization High-Resolution Mass Spectrometry, *Anal. Chem.*, 79, 8350–8358, doi:10.1021/ac071150w, 2007.
- Aiken, A. C., DeCarlo, P. F., Kroll, J. H., Worsnop, D. R., Huffman, J. A., Docherty, K., Ulbrich, I. M., Mohr, C., Kimmel, J. R., Sueper, D., Zhang, Q., Sun, Y., Trimborn, A., Northway, M., Ziemann, P. J., Canagaratna, M. R., Onasch, T. B., Alfarra, R., Prevot, A. S. H., Dommen, J., Duplissy, J., Metzger, A., Baltensperger, U., and Jimenez, J. L.: O/C and OM/OC ratios of primary, secondary, and ambient organic aerosols with High Resolution Time-of-Flight Aerosol Mass Spectrometry, *Environ. Sci. Technol.*, 42, 4478–4485, doi:10.1021/es703009q, 2008.
- Angelino, S., Suess, D. T., and Prather, K. A.: Formation of aerosol particles from reactions of secondary and tertiary alkylamines: Characterization by aerosol time-of-flight mass spectrometry, *Environ. Sci. Technol.*, 35, 3130–3138, doi:10.1021/es0015444, 2001.
- Barnard, J. C., Volkamer, R., and Kassianov, E. I.: Estimation of the mass absorption cross section of the organic carbon component of aerosols in the Mexico City Metropolitan Area, *Atmos. Chem. Phys.*, 8, 6665–6679, 2008, <http://www.atmos-chem-phys.net/8/6665/2008/>.
- Canagaratna, M. R., Jayne, J. T., Jimenez, J. L., Allan, J. D., Alfarra, M. R., Zhang, Q., Onasch, T. B., Drewnick, F., Coe, H., Middlebrook, A., Delia, A., Williams, L. R., Trimborn, A. M., Northway, M. J., DeCarlo, P. F., Kolb, C. E., Davidovits, P., and Worsnop, D. R.: Chemical and microphysical characterization of ambient aerosols with the Aerodyne Aerosol Mass Spectrometer, *Mass. Spectrom. Rev.*, 26, 185–222, doi:10.1002/mas.20115, 2007.
- Carlton, A. G., Turpin, B. J., Altieri, K. E., Seitzinger, S., Reff, A., Lim, H. J., and Ervens, B.: Atmospheric oxalic acid and SOA production from glyoxal: Results of aqueous photooxidation experiments, *Atmos. Environ.*, 41, 7588–7602, doi:10.1016/j.atmosenv.2007.05.035, 2007.
- Cho, J. R., Cho, S. G., Goh, E. M., and Kim, J. K.: Procédé de préparation du 2,2'-bi-1H-imidazole à partir du glyoxal et d'un sel d'ammonium, 0304378, 2003.

- Cocker, D. R., Flagan, R. C., and Seinfeld, J. H.: State-of-the-art chamber facility for studying atmospheric aerosol chemistry, *Environ. Sci. Technol.*, 35, 2594–2601, doi:10.1021/es0019169, 2001.
- Corrigan, A. L., Hanley, S. W., and De Haan, D. O.: Uptake of glyoxal by organic and inorganic aerosol, *Environ. Sci. Technol.*, 42, 4428–4433, doi:10.1021/es7032394, 2008.
- de Gouw, J. A., Middlebrook, A. M., Warneke, C., Goldan, P. D., Kuster, W. C., Roberts, J. M., Fehsenfeld, F. C., Worsnop, D. R., Canagaratna, M. R., Pszenny, A. A. P., Keene, W. C., Marchewka, M., Bertman, S. B., and Bates, T. S.: Budget of organic carbon in a polluted atmosphere: Results from the New England air quality study in 2002, *J. Geophys. Res.-Atmos.*, 110, D16305, doi:10.1029/2004JD005623, 2005.
- De Haan, D. O., Corrigan, A. L., Smith, K. W., Stroik, D. R., Turley, J. J., Lee, F. E., Tolbert, M. A., Jimenez, J. L., Cordova, K. E. and Ferrell, G. R.: Secondary organic aerosol-forming reactions of glyoxal with amino acids, *Environ. Sci. Technol.*, 43, 2818–2824, doi:10.1021/es803534f, 2009.
- Debus, H.: Ueber die einwirkung des ammoniaks auf glyoxal, *Annalen der Chemie und Pharmacie*, 107, 199–208, doi:10.1002/jlac.18581070209, 1858.
- DeCarlo, P. F., Kimmel, J. R., Trimborn, A., Northway, M. J., Jayne, J. T., Aiken, A. C., Gonin, M., Furber, K., Horvath, T., Docherty, K. S., Worsnop, D. R., and Jimenez, J. L.: Field-deployable, high-resolution, time-of-flight aerosol mass spectrometer, *Anal. Chem.*, 78, 8281–8289, doi:10.1021/ac061249n, 2006.
- Denkenberger, K. A., Moffet, R. C., Holecek, J. C., Rebotier, T. P., and Prather, K. A.: Real-time, single-particle measurements of oligomers in aged ambient aerosol particles, *Environ. Sci. Technol.*, 41, 5439–5446, doi:10.1021/es0703291, 2007.
- Ervens, B., Carlton, A. G., Turpin, B. J., Altieri, K. E., Kreidenweis, S. M., and Feingold, G.: Secondary organic aerosol yields from cloud-processing of isoprene oxidation products, *Geophys. Res. Lett.*, 35, L02816, doi:10.1029/2007GL031828, 2008.
- Fratzke, A. R. and Reilly, P. J.: Thermodynamic and kinetic analysis of the dimerization of aqueous glyoxal, *Int. J. Chem. Kinet.*, 18, 775–789, 1986.
- Fu, T. M., Jacob, D. J., Wittrock, F., Burrows, J. P., Vrekousis, M., and Henze, D. K.: Global budgets of atmospheric glyoxal and methylglyoxal, and implications for formation of secondary organic aerosols, *J. Geophys. Res.-Atmos.*, 113, D15303, doi:10.1029/2007JD009505, 2008.
- Gómez-González, Y., Surratt, J. D., Cuyckens, F., Szmigielski, R., Vermeylen, R., Jaoui, M., Lewandowski, M., Offenberg, J. H., Kleindienst, T. E., Edney, E. O., Blockhuys, F., Van Alsenoy, C., Maenhaut, W., and Claeys, M.: Characterization of organosulfates from the photooxidation of isoprene and unsaturated fatty acids in ambient aerosol using liquid chromatography/(-) electrospray ionization mass spectrometry, *J. Mass. Spectrom.*, 43, 371–382, doi:10.1002/jms.1329, 2008.
- Gross, D. S., Galli, M. E., Kalberer, M., Prevot, A. S. H., Dommen, J., Alfarra, M. R., Duplissy, J., Gaeggeler, K., Gascho, A., Metzger, A., and Baltensperger, U.: Real-time measurement of oligomeric species in secondary organic aerosol with the aerosol time-of-flight mass spectrometer, *Anal. Chem.*, 78, 2130–2137, doi:10.1021/ac0601381, 2006.
- Hastings, W. P., Koehler, C. A., Bailey, E. L., and DeHaan, D. O.: Secondary organic aerosol formation by glyoxal hydration and oligomer formation: humidity effects and equilibrium shifts during analysis, *Environ. Sci. Technol.*, 39, 8728–8735, doi:10.1021/es0504461, 2005.
- Herald, C. L., Jacob, D. J., Park, R. J., Russell, L. M., Huebert, B. J., Seinfeld, J. H., Liao, H., and Weber, R. J.: A large organic aerosol source in the free troposphere missing from current models, *Geophys. Res. Lett.*, 32, L18809, doi:10.1029/2005GL023831, 2005.
- Huisman, A. J., Hottel, J. R., Coens, K. L., DiGangi, J. P., Galloway, M. M., Kammrath, A., and Keutsch, F. N.: Laser-induced phosphorescence for the in situ detection of glyoxal at part per trillion mixing ratios, *Anal. Chem.*, 80, 5884–5891, doi:10.1021/ac800407b, 2008.
- Ip, H. S. S., Huang, X. H. H., and Yu, J. Z.: Effective Henry's law constants of glyoxal, glyoxylic acid, and glycolic acid, *Geophys. Res. Lett.*, 36, L01802, doi:10.1029/2008GL036212, 2009.
- Jang, M. S., Czoschke, N. M., Lee, S., and Kamens, R. M.: Heterogeneous atmospheric aerosol production by acid-catalyzed particle-phase reactions, *Science*, 298, 814–817, doi:10.1126/science.1075798, 2002.
- Keywood, M. D., Varutbangkul, V., Bahreini, R., Flagan, R. C., and Seinfeld, J. H.: Secondary organic aerosol formation from the ozonolysis of cycloalkenes and related compounds, *Environ. Sci. Technol.*, 38, 4157–4164, doi:10.1021/es035363o, 2004.
- Kielhorn, J., Pohlentz-Michel, C., Schmidt, S., and Mangelsdorf, I.: Concise International Chemical Assessment Document 57: Glyoxal, 57, 2004.
- Kroll, J. H., Ng, N. L., Murphy, S. M., Varutbangkul, V., Flagan, R. C., and Seinfeld, J. H.: Chamber studies of secondary organic aerosol growth by reactive uptake of simple carbonyl compounds, *J. Geophys. Res.*, 110, D23207, doi:10.1029/2005JD006004, 2005.
- Liggio, J., Li, S., and McLaren, R.: Heterogeneous reactions of glyoxal on particulate matter: Identification of acetals and sulphate esters, *Environ. Sci. Technol.*, 39, 1532–1541, doi:10.1021/es048375y, 2005a.
- Liggio, J., Li, S., and McLaren, R.: Reactive uptake of glyoxal by particulate matter, *J. Geophys. Res.*, 110, D10304, doi:10.1029/2004JD005113, 2005b.
- Loeffler, K. W., Koehler, C. A., Paul, N. M., and De Haan, D. O.: Oligomer formation in evaporating aqueous glyoxal and methyl glyoxal solutions, *Environ. Sci. Technol.*, 40, 6318–6323, doi:10.1021/es060810w, 2006.
- Matsunaga, S., Mochida, M., and Kawamura, K.: Variation on the atmospheric concentrations of biogenic carbonyl compounds and their removal processes in the Northern Forest at Moshiri, Hokkaido Island in Japan, *J. Geophys. Res.*, 109, D04302, doi:10.1029/2003JD004100, 2004.
- Minerath, E. C. and Elrod, M. J.: Assessing the potential for diol and hydroxy sulfate ester formation from the reaction of epoxides in tropospheric aerosols, *Environ. Sci. Technol.*, 43, 1386–1392, doi:10.1021/es8029076, 2009.
- Minerath, E. C., Casale, M. T., and Elrod, M. J.: Kinetics feasibility study of alcohol sulfate esterification reactions in tropospheric aerosols, *Environ. Sci. Technol.*, 42, 4410–4415, 2008.
- Murphy, S. M., Sorooshian, A., Kroll, J. H., Ng, N. L., Chhabra, P., Tong, C., Surratt, J. D., Knipping, E., Flagan, R. C., and Seinfeld, J. H.: Secondary aerosol formation from atmospheric reactions of aliphatic amines, *Atmos. Chem. Phys.*, 7, 2313–2337, 2007.

- <http://www.atmos-chem-phys.net/7/2313/2007/>.
- Myriokefalitakis, S., Vrekoussis, M., Tsigaridis, K., Wittrock, F., Richter, A., Brühl, C., Volkamer, R., Burrows, J. P., and Kanakidou, M.: The influence of natural and anthropogenic secondary sources on the glyoxal global distribution, *Atmos. Chem. Phys.*, 8, 4965–4981, 2008, <http://www.atmos-chem-phys.net/8/4965/2008/>.
- Na, K., Song, C., Switzer, C., and Cocker, D. R.: Effect of ammonia on secondary organic aerosol formation from alpha-pinene ozonolysis in dry and humid conditions, *Environ. Sci. Technol.*, 41, 6096–6102, doi:10.1021/es061956y, 2007.
- Na, K., Song, C., and Cocker, D. R.: Formation of secondary organic aerosol from the reaction of styrene with ozone in the presence and absence of ammonia and water, *Atmos. Environ.*, 40, 1889–1900, doi:10.1016/j.atmosenv.2005.10.063, 2006.
- Nenes, A., Pandis, S. N., and Pilinis, C.: ISORROPIA: A new thermodynamic equilibrium model for multiphase multi-component inorganic aerosols, *Aquat. Geochem.*, 4, 123–152, doi:10.1023/A:1009604003981, 1998.
- Nozière, B., Dziedzic, P., and Córdoba, A.: Products and kinetics of the liquid-phase reaction of glyoxal catalyzed by ammonium ions (NH_4^+), *J. Phys. Chem. A*, 113, 231–237, 2009.
- Odum, J. R., Hoffmann, T., Bowman, F., Collins, D., Flagan, R. C., and Seinfeld, J. H.: Gas/particle partitioning and secondary organic aerosol yields, *Environ. Sci. Technol.*, 30, 2580–2585, doi:10.1021/es950943+, 1996.
- Pankow, J. F.: An absorption-model of gas-particle partitioning of organic-compounds in the atmosphere, *Atmos. Environ.*, 28, 185–188, 1994a.
- Pankow, J. F.: An absorption-model of the gas aerosol partitioning involved in the formation of secondary organic aerosol, *Atmos. Environ.*, 28, 189–193, 1994b.
- Reinhardt, A., Emmenegger, C., Gerrits, B., Panse, C., Dommen, J., Baltensperger, U., Zenobi, R., and Kalberer, M.: Ultrahigh mass resolution and accurate mass measurements as a tool to characterize oligomers in secondary organic aerosols, *Anal. Chem.*, 79, 4074–4082, doi:10.1021/ac062425v, 2007.
- Schweitzer, F., Magi, L., Mirabel, P., and George, C.: Uptake rate measurements of methanesulfonic acid and glyoxal by aqueous droplets, *J. Phys. Chem. A*, 102, 593–600, doi:10.1021/jp972451k, 1998.
- SciFinder Scholar: Calculated using Advanced Chemistry Development (ACD/Labs) Software V8.14 for Solaris (1994–2008 ACD/Labs), last access: 26 September 2008.
- Silva, P. J., Erupe, M. E., Price, D., Elias, J., Malloy, Q. G. J., Li, Q., Warren, B., and Cocker, D. R.: Trimethylamine as precursor to secondary organic aerosol formation via nitrate radical reaction in the atmosphere, *Environ. Sci. Technol.*, 42, 4689–4696, doi:10.1021/es703016v, 2008.
- Shapiro, E. L., Szprengiel, J., Sareen, N., Jen, C. N., Giordano, M. R., and McNeill, V. F.: Light-absorbing secondary organic material formed by glyoxal in aqueous aerosol mimics, *Atmos. Chem. Phys.*, 9, 2289–2300, 2009, <http://www.atmos-chem-phys.net/9/2289/2009/>.
- Schulze, H.: Imidazole Synthesis, 113684, 1973.
- Sorooshian, A., Varutbangkul, V., Brechtel, F. J., Ervens, B., Feingold, G., Bahreini, R., Murphy, S. M., Holloway, J. S., Atlas, E. L., Buzorius, G., Jonsson, H., Flagan, R. C., and Seinfeld, J. H.: Oxalic acid in clear and cloudy atmospheres: Analysis of data from International Consortium for Atmospheric Research on Transport and Transformation 2004, *J. Geophys. Res.-Atmos.*, 111, D23S45, doi:10.1029/2005JD006880, 2006.
- Spaulding, R. S., Schade, G. W., Goldstein, A. H., and Charles, M. J.: Characterization of secondary atmospheric photooxidation products: Evidence for biogenic and anthropogenic sources, *J. Geophys. Res.*, 108, 4247, doi:10.1029/2002JD002478, 2003.
- Surratt, J. D., Gómez-González, Y., Chan, A. W. H., Vermeylen, R., Shahgholi, M., Kleindienst, T. E., Edney, E. O., Offenberg, J. H., Lewandowski, M., Jaoui, M., Maenhaut, W., Claeys, M., Flagan, R. C., and Seinfeld, J. H.: Organosulfate formation in biogenic secondary organic aerosol, *J. Phys. Chem. A*, 112, 8345–8378, doi:10.1021/jp802310p, 2008.
- Surratt, J. D., Kroll, J. H., Kleindienst, T. E., Edney, E. O., Claeys, M., Sorooshian, A., Offenberg, J. H., Lewandowski, M., Jaoui, M., Flagan, R. C., and Seinfeld, J. H.: Evidence for organosulfates in secondary organic aerosol, *Environ. Sci. Technol.*, 41, 517–527, doi:10.1021/es062081q, 2007.
- Volkamer, R., Jimenez, J. L., San Martini, F., Dzepina, K., Zhang, Q., Salcedo, D., Molina, L. T., Worsnop, D. R., and Molina, M. J.: Secondary organic aerosol formation from anthropogenic air pollution: Rapid and higher than expected, *Geophys. Res. Lett.*, 33, L17811, doi:10.1029/2006GL026899, 2006.
- Volkamer, R., San Martini, F., Molina, L. T., Salcedo, D., Jimenez, J. L., and Molina, M. J.: A missing sink for gas-phase glyoxal in Mexico City: Formation of secondary organic aerosol, *Geophys. Res. Lett.*, 34, L19807, doi:10.1029/2007GL030752, 2007.
- Volkamer, R., Ziemann, P. J., and Molina, M. J.: Secondary Organic Aerosol Formation from Acetylene (C_2H_2): seed effect on SOA yields due to organic photochemistry in the aerosol aqueous phase, *Atmos. Chem. Phys.*, 9, 1907–1928, 2009, <http://www.atmos-chem-phys.net/9/1907/2009/>.
- Whipple, E. B.: The structure of glyoxal in water, *J. Am. Chem. Soc.*, 92, 7183–7186, doi:10.1021/ja00727a027, 1970.
- Zhang, Q., Jimenez, J. L., Canagaratna, M. R., Allan, J. D., Coe, H., Ulbrich, I., Alfarra, M. R., Takami, A., Middlebrook, A. M., Sun, Y. L., Dzepina, K., Dunlea, E., Docherty, K. S., DeCarlo, P. F., Salcedo, D., Onasch, T., Jayne, J. T., Miyoshi, T., Shimojo, A., Hatakeyama, S., Takegawa, N., Kondo, Y., Schneider, J., Drewnick, F., Borrmann, S., Weimer, S., Demerjian, K., Williams, P., Bower, K., Bahreini, R., Cottrell, L., Griffin, R. J., Rautiainen, J., Sun, J. Y., Zhang, Y. M., and Worsnop, D. R.: Ubiquity and dominance of oxygenated species in organic aerosols in anthropogenically-influenced Northern Hemisphere midlatitudes, *Geophys. Res. Lett.*, 34, L13801, doi:10.1029/2007GL029979, 2007.
- Zhou, X. and Mopper, K.: Apparent partition coefficients of 15 carbonyl compounds between air and seawater and between air and freshwater, implications for air-sea exchange, *Environ. Sci. Technol.*, 24, 1864–1869, doi:10.1021/es00082a013, 1990.

Appendix F

Modeling of secondary organic aerosol yields from laboratory chamber data*

*Reproduced with permission from “Modeling of secondary organic aerosol yields from laboratory chamber data” by M. N. Chan, A. W. H. Chan, P. S. Chhabra, J. D. Surratt, and J. H. Seinfeld, *Atmospheric Chemistry and Physics*, 9 (15), 5669–5680, 2009. Copyright 2009 by Authors. This work is licensed under a Creative Commons License.

Modeling of secondary organic aerosol yields from laboratory chamber data

M. N. Chan¹, A. W. H. Chan², P. S. Chhabra², J. D. Surratt², and J. H. Seinfeld^{1,2}

¹Division of Engineering and Applied Science, California Institute of Technology, Pasadena, CA, USA

²Division of Chemistry and Chemical Engineering, California Institute of Technology, Pasadena, CA, USA

Abstract. Laboratory chamber data serve as the basis for constraining models of secondary organic aerosol (SOA) formation. Current models fall into three categories: empirical two-product (Odum), product-specific, and volatility basis set. The product-specific and volatility basis set models are applied here to represent laboratory data on the ozonolysis of α -pinene under dry, dark, and low-NO_x conditions in the presence of ammonium sulfate seed aerosol. Using five major identified products, the model is fit to the chamber data. From the optimal fitting, SOA oxygen-to-carbon (O/C) and hydrogen-to-carbon (H/C) ratios are modeled. The discrepancy between measured H/C ratios and those based on the oxidation products used in the model fitting suggests the potential importance of particle-phase reactions. Data fitting is also carried out using the volatility basis set, wherein oxidation products are parsed into volatility bins. The product-specific model is most likely hindered by lack of explicit inclusion of particle-phase accretion compounds. While prospects for identification of the majority of SOA products for major volatile organic compounds (VOCs) classes remain promising, for the near future empirical product or volatility basis set models remain the approaches of choice.

tween the gas and particle phases (Pankow, 1994a,b; Odum et al., 1996; Hallquist et al., 2009). Gas-particle partitioning of each compound is described by an equilibrium partitioning coefficient, K_p ,

$$K_p = \frac{P}{GM} \sim \frac{1}{c^*} \quad (1)$$

where G is the mass concentration per unit volume of air ($\mu\text{g m}^{-3}$) of the semivolatile species in the gas phase, P is the mass concentration per unit volume of air ($\mu\text{g m}^{-3}$) of the semivolatile species in the particle phase, and M is the mass concentration per unit volume of air ($\mu\text{g m}^{-3}$) of the total absorbing particle phase. The equilibrium partitioning coefficient, K_p ($\text{m}^3 \mu\text{g}^{-1}$), is inversely proportional to the saturation vapor concentration, c^* ($\mu\text{g m}^{-3}$), of the pure semivolatile compound (see Appendix A). M refers only to the portion of the particulate matter participating in absorptive partitioning (organic aerosol into which semivolatile organics can partition and the aqueous portion of the particles in the case of water-soluble organics). Note that as long as some absorbing mass is present, some fraction of a given semivolatile compound partitions into the particle phase, even if its gas-phase concentration is below its saturation vapor concentration, c^* .

Oxidation of a parent VOC leads to a variety of semivolatile products, each with its own saturation vapor concentration. Moreover, the semivolatile oxidation products may be formed from first- or higher generation gas-phase reactions, and the products themselves may react further in the gas phase to yield compounds of either lower (in the case of addition of more functional groups) or greater (in the case in which the carbon backbone of the molecule is cleaved) volatility.

1 Introduction

Laboratory chamber data are needed to determine secondary organic aerosol (SOA) yields from volatile organic compounds (VOCs). The fundamental concept on which all descriptions of SOA formation lies is that SOA comprises a mixture of semivolatile organic compounds that partition be-



Correspondence to: J. H. Seinfeld
 (seinfeld@caltech.edu)

The fraction F of a semivolatile compound in the particle phase can be expressed in terms of K_p or c^* as

$$F = \frac{P}{G + P} = \frac{MK_p}{1 + MK_p} = \frac{1}{1 + c^*/M} \quad (2)$$

As the amount of absorbing material (M) increases, compounds of greater volatility (larger c^* , smaller K_p) will partition increasingly into the particle phase. When $c^*=M$, half of the semivolatile mass resides in the particle phase. If $M \gg c^*$, essentially all of the semivolatile species is in the particle phase.

In the first basic model of SOA formation, Odum et al. (1996) represented the process of SOA formation by n semivolatile products and showed that the SOA yield Y , defined as the mass of aerosol formed per mass of hydrocarbon reacted, can be expressed as

$$Y = M \sum_i \frac{\alpha_i K_{p,i}}{1 + MK_{p,i}} \quad (3)$$

where α_i is the mass-based stoichiometric coefficient for product i (mass of i produced per mass of parent VOC reacted). Note that Y can exceed 1.0 as a result of the increase of molecular mass of oxidation products (the designation "aerosol mass fraction" is also used for Y). Equation (3) is an equilibrium model in that it relates the amount of each product formed to the amount of VOC reacted regardless of number of chemical steps involved. While, in principle, n can be as large as desired, in the application of the Odum model usually $n=2$. The two products are not necessarily associated with actual compounds, and the 4 parameters, α_1 , α_2 , $K_{p,1}$, and $K_{p,2}$, are estimated by optimal fitting of Eq. (3) to the data.

SOA forms when gas-phase oxidation products of a hydrocarbon precursor partition between the gas and particle phases. Products with lower vapor pressures partition preferentially to the particle phase; compounds that are more highly functionalized tend to have lower vapor pressures. The degree of partitioning to the particle phase depends also on the quantity of absorbing organic material in that phase into which the compounds can condense; as the mass of absorbing material increases, compounds of higher vapor pressure that tend not to partition to the particle phase under low mass loadings do so at the higher mass loadings. The result is that SOA at low mass loading tends to be enriched in the least volatile (and most oxygenated) products (Bahreini et al., 2005; Shilling et al., 2008). In typical chamber experiments, a range of initial hydrocarbon precursor concentrations is employed in order to determine SOA yields as a function of the mass concentration of organic particles generated. When chamber experiments are conducted over a range of initial VOC concentrations, such experiments afford a view of the full spectrum of oxidation products, thereby facilitating the formulation of chemical mechanisms.

Laboratory chamber studies are limited in duration to about 12 h or so, as constrained by particle deposition on the

chamber walls, whereas the typical atmospheric lifetime of a particle is considerably longer. Chamber studies capture the initial multi-hour VOC oxidation but not that which takes place on a multi-day time scale. The sequence of reactions and associated SOA formation that occur over the duration of a chamber experiment can be termed as the *chamber phase*. (Stanier et al. (2008) have referred to this as the "prompt" phase.) The chamber or prompt phase chemistry begins with oxidant (OH, O₃, NO₃) attack on the VOC, initiating a series of reactions, which can depend critically on NO_x level, leading to semivolatile products. Experimentally-derived SOA yields reflect the extent of SOA formation over the chamber phase. Reactions that occur on a time scale longer than a chamber experiment can be termed the *aging phase*, during which the following processes may occur: (1) particle-phase accretion reactions that convert semivolatile condensed products to essentially non-volatile compounds; (2) gas-phase oxidation reactions of chamber phase semivolatile products that are too slow to be important during the chamber phase but are capable of producing compounds of even lower volatility over the aging phase; and (3) gas-particle reactions that convert some particulate material to volatile products. Over the typical time scale and spatial grid scale of atmospheric models, SOA formation occurring on the chamber phase time scale can be considered as taking place essentially instantaneously, suggesting that an equilibrium partitioning model for this phase is appropriate. Over the longer aging time scale, the equilibrium partitioning can be considered to be slowly perturbed as chemical aging takes place.

2 Form of SOA model

If a number of products accounting for a significant fraction of the total mass of SOA have been identified, these major products can serve as SOA surrogates in a product-specific model (Pankow et al., 2001; Seinfeld et al., 2001). Upon estimating the vapor pressures, the values of K_p of the major products can be determined. For the product-specific model, major identified particle-phase products are chosen as SOA surrogates to represent other chemically similar compounds, and to give a reasonable approximation of gas/particle partitioning of all other products (Pankow et al., 2001). The simulated SOA composition may allow a first approximation of the properties of SOA (e.g., water uptake and cloud condensation nuclei activity). The SOA composition changes with organic mass loading, and the amount of hydrocarbon precursors reacted can be tracked. Using the simulated SOA composition, one can also calculate the aerosol oxygen-to-carbon (O/C) and hydrogen-to-carbon (H/C) ratios at different loadings. Simulated ratios for O/C and H/C can be compared with those measured.

An alternative approach is the *volatility basis set*, in which the range of products is specified in terms of volatility bins (Donahue et al., 2006; Stanier et al., 2008). The product

volatilities can be segmented into order-of-magnitude volatility bins (expressed as values of c^*). Since SOA products are grouped into volatility bins, specific information about the chemical composition of SOA is not required. For the volatility basis set, Stanier et al. (2008) present a methodology for selecting the maximum and minimum values of c^* , and logarithmic spacing between c^* values then determines the number of volatility bins.

Either treatment has the potential to reproduce the measured concentrations of major reaction products (both gas-phase and particle-phase), even in the absence of details of major particle-phase reactions. On the other hand, if an equilibrium state is not attained during the chamber phase, the kinetics of gas-phase and particle-phase reactions determine the SOA composition. In such cases, development of kinetic models in which reaction products undergo reactions in both gas-phase and particle-phase is needed to describe the SOA formation (Chan et al., 2007).

The goal of this work is to evaluate the product-specific approach to SOA modeling, using a system that has been relatively well characterized in the laboratory: ozonolysis of α -pinene. Because of a general lack of complete product identification for any SOA system, as well as uncertainty about the properties of the products, in practical terms, parameters in the model need to be determined by optimal fitting of the model to chamber data.

3 Ozonolysis of α -pinene

3.1 Product-specific model

Ozonolysis of α -pinene is, in many respects, an excellent test case for an SOA model. A number of experimental studies exist in the literature, and relatively complete product identification has been carried out. Oxocarboxylic acids, hydroxy oxocarboxylic acids, dicarboxylic acids, oxoaldehydes, and organic peroxides are the major classes of SOA products identified (Yu et al., 1999; Docherty et al., 2005). For the purposes of evaluating the product-specific model it is assumed that there are five major products: pinonic acid, pinic acid, pinonaldehyde, a hydroperoxide, and terpenylic acid (Table 1). These compounds are chosen to reflect the current understanding of the gas-phase products formed in the ozonolysis of α -pinene.

The vapor pressure of a product i is estimated by using a group contribution method developed by Pankow and Asher (2008). At a given temperature, the $K_{p,i}$ of the product i is determined by assuming that its activity coefficient, γ_i , is unity, and the molecular weight of product i is taken as the mean molecular weight of the surrogate mixture, \overline{MW} , as a first approximation. These assumptions may be reasonable as the range of molecular weights of products is small (168–200 g mol⁻¹, see Table 1) and the amount of water present in the particle phase is not significant under dry conditions

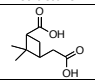
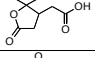
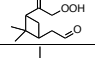
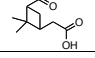
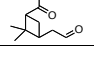
(<5%–40% RH). Bilde and Pandis (2001) measured the vapor pressure of semivolatile products formed from oxidation of biogenic monoterpenes using a laminar flow reactor with uncertainty of $\pm 50\%$. They reported a vapor pressure of 1.989×10^{-10} atm for pinic acid at 293 K, which is comparable to the estimated value (4.605×10^{-10} atm) using the Pankow and Asher (2008) model. At a given temperature, the estimated vapor pressures of the major products using the Pankow and Asher (2008) model are lower than that estimated by Jenkin (2004). Hence, the present estimated K_p values of major products are larger than those reported by Jenkin (2004). For example, Jenkin (2004) estimated a higher vapor pressure of pinic acid of 4.7×10^{-4} torr (or 6.18×10^{-7} atm) at 298 K compared to that reported by Bilde and Pandis (2001) (4.213×10^{-10} atm).

When the vapor pressure estimation is carried out for the α -pinene/ozone system, two sets of two products each are estimated to have very similar K_p values. For example, at 293 K, the estimated value of K_p of hydroxy pinonic acid ($K_p=0.2802$) is very close to that of pinic acid ($K_p=0.2822$), and the estimated K_p of pinonic acid ($K_p=0.0018$) is close to that of hydroxy pinonaldehyde ($K_p=0.0017$). In such a case, two products of essentially identical vapor pressures cannot be distinguished, and a single product is chosen to represent the two products. Pinonic acid is chosen to represent the pinonic acid, norpinonic acid, hydroxy pinonaldehyde, and isomers. Pinic acid is chosen to represent pinic acid, norpinic acid, hydroxy pinonic acid, and isomers.

The basic chamber data are considered to be in the form of particle mass concentration as a function of VOC reacted. The actual chamber data are in the form of aerosol volume concentration. Aerosol density needed to convert volume to mass concentration is estimated by comparing the aerosol number distribution measured by a differential mobility analyzer with that obtained from the Aerodyne Aerosol Mass Spectrometer (AMS), through the theoretical relationship between mobility diameter and vacuum aerodynamic diameter. Ng et al. (2006) have shown that for the oxidation of a number of hydrocarbons with a single double bond, the growth curve for one experiment over the course of the experiment (“time-dependent growth curve”) follows that of final SOA growth over different experiments. This suggests that in this case the time-dependent SOA growth data can also be used for model data fitting.

Data from ozonolysis of α -pinene are obtained from experiments conducted under dry, dark, and low-NO_x conditions in the presence of dry (NH₄)₂SO₄ particles (Ng et al., 2006; Pathak et al., 2007; Shilling et al., 2008). The SOA yield data cover a range of organic mass loading (0.5–411 $\mu\text{g m}^{-3}$) and are used for the parameterization to model the SOA yield relevant to atmospheric conditions (Presto and Donahue, 2006). An effective SOA density of 1.25 g cm⁻³ is applied for conversion of volume to mass concentration in determination of SOA yield. It is noted that Shilling

Table 1. Major products chosen to represent the ozonolysis of α -pinene under dry, dark, and low- NO_x conditions in the presence of dry ammonium sulfate particles. ^a Vapor pressure is determined at 293 K using a model developed by Pankow and Asher (2008). K_p is determined at 293 K with the assumption of activity coefficient of the products equal to one and the molecular weight of product i is used as mean molecular weight in organic absorbing phase, as a first approximation. ^b (Claeys et al., 2009) ^c The enthalpy of vaporization, ΔH_v (kJ mol^{-1}) of the product is estimated by plotting the estimated vapor pressure of the product against temperature. The ΔH_v of the product can be estimated from the slope of the line following the Clausius-Clapeyron equation.

Product	Chemical structure	O/C	H/C	ΔH_v^c	Product-Specific Model				Volatility Basis Set		
					$(K_p \times 1 \text{ case})$		$(K_p \times 100 \text{ case})$		$K_p (c^*)$	α	α from Product-Specific Model ($K_p \times 100 \text{ case}$)
Pinic acid $\text{C}_{10}\text{H}_{18}\text{O}_4$ (MW: 186)		0.444	1.556	99.89	0.2822 (3.544)	0.2308	28.22 (0.0354)	0.0563	100 (0.01)	0.0707	0.0563 (Pinic acid: $c^* = 0.0354$)
Terpenylic acid ^b $\text{C}_{10}\text{H}_{18}\text{O}_4$ (MW: 172)		0.5	1.5	76.73	0.0332 (30.12)	0.0172	3.32 (0.3012)	0.0132	10 (0.1)	0.0110	0.0131 (Terpenylic acid: $c^* = 0.3012$)
Hydroperoxide $\text{C}_{10}\text{H}_{18}\text{O}_4$ (MW: 200)		0.4	1.6	83.99	0.0029 (344.8)	0.0181	0.29 (3.448)	0.0173	1 (1)	0.0120	0.0172 (Hydroperoxide: $c^* = 3.448$)
Pinonic acid $\text{C}_{10}\text{H}_{18}\text{O}_3$ (MW: 184)		0.3	1.6	81.72	0.0018 (555.6)	0.6883	0.18 (5.556)	0.1573	0.1 (10)	0.1603	0.1573 (Pinonic acid: $c^* = 5.556$)
									0.01 (100)	0.0210	-
Pinonaldehyde $\text{C}_{10}\text{H}_{18}\text{O}_2$ (MW: 168)		0.2	1.6	69.53	1.145×10^{-5} (87334)	1	1.145×10^{-3} (873.34)	0.9380	0.001 (1000)	0.9554	0.9380 (Pinonaldehyde: $c^* = 873.34$)

et al. (2009) reported a higher effective SOA density ($1.73\text{--}1.4\text{ g cm}^{-3}$) at low organic mass loading ($0.5\text{--}7\text{ }\mu\text{g m}^{-3}$). The SOA yield data from Shilling et al. (2008) are adjusted to 293 K, using a temperature correction factor suggested by Pathak et al. (2007). Generally, the time-dependent SOA yield data reported by Ng et al. (2006) are in good agreement with the final SOA yield data reported by Pathak et al. (2007) and Shilling et al. (2008) but are lower than those reported by Shilling et al. (2008) for organic mass loadings less than $2\text{ }\mu\text{g m}^{-3}$. Measurement uncertainties may explain part of the variability in SOA yield data reported by Ng et al. (2006) at low organic mass loading.

Data, plotted as SOA yield, Y , versus organic mass loading, M , are shown in Fig. 1. The SOA yield increases rapidly at low organic mass loading and more slowly at high organic mass loading. Shown in Fig. 1 are the optimal fits to the product-specific and volatility basis set models. In order to evaluate the effect of uncertainty in K_p values, results are shown for the estimated values of K_p (termed $K_p \times 1$ case) and the estimated values of K_p increased by a factor of 100 (termed $K_p \times 100$ case). Previous modeling studies on this system have also shown that an overall increase of K_p of all products of a factor on the order of 10^2 is needed to explain the partitioning (Jenkin, 2004; Chen and Griffin, 2005). In each case, the α_i values are determined by optimal fitting to the data. Different sets of α_i values produce essentially the same goodness of fit to the overall mass yield. The sets can be discriminated according to how well they fit the SOA composition as compared to that measured. The α_i values are chosen to give the best fit to experimental SOA yields

and SOA composition. As shown in Fig. 1, the predicted SOA yields agree well with the experimental SOA yield data in both $K_p \times 1$ and $K_p \times 100$ cases. The $K_p \times 100$ case gives a better estimation of SOA yields at low organic mass loading than the $K_p \times 1$ case. However, the optimized curves underpredict the SOA yield data reported by Shilling et al. (2008) when the organic mass loading is less than $\sim 2\text{ }\mu\text{g m}^{-3}$.

For the $K_p \times 1$ case, the predicted SOA yields are lower than the measured ones at low organic mass loading. The data fitting produces the unrealistic result that the mass yield of the pinonaldehyde is unity. The sum of fitted molar yields exceeds 1. One likely explanation is the uncertainty in the estimation of the K_p of major products (vapor pressure and activity coefficient). The estimated vapor pressure of the products using the group contribution method is too high, and the products are estimated to be too volatile. In order to match experimental SOA yields, large mass yields of the products are predicted so that a significant amount of the products is partitioned into the particle phase. This results in unrealistically high mass yields of the products. Another likely explanation is that other products (gas-phase and/or particle-phase) of higher K_p (and lower volatilities) are present. Particle-phase reaction products (e.g., oligomers and esters), which are likely present, tend to have higher molecular weights and lower volatilities (Gao et al., 2004; Iinuma et al., 2004; Müller et al., 2008), effectively enhancing the K_p values (Kroll and Seinfeld, 2005). For example, an ester, which is formed between pinic acid and hydroxy pinonic acid, has been detected (Müller et al., 2008). At 293 K, the estimated K_p of the ester is 4.96×10^5 , which is

much larger than that of hydroxy pinonic acid ($K_p=0.2802$) and of pinic acid ($K_p=0.2822$).

3.2 Volatility basis set model

The volatility basis set model is also applied to fit the experimental SOA yields. The estimated volatility (or c^*) of products spans from 0.035 to $873 \mu\text{g m}^{-3}$. A volatility basis set of six volatility bins is chosen and the volatility bins are separated by an order-of-magnitude (c^* : 0.01, 0.1, 1, 10, 100, and $1000 \mu\text{g m}^{-3}$). The mass of aerosol in bin i is obtained by optimal fitting to the experimental SOA yield data. Figure 1 shows that for the volatility basis set, the predicted SOA yields agree well with the experimental SOA yield data, even at low organic mass loading ($<0.5 \mu\text{g m}^{-3}$). This suggests that products with volatility as low as $c^*=0.01 \mu\text{g m}^{-3}$ (or $K_p=100 \mu\text{g}^{-1} \text{m}^3$) are present. The quantity of aerosol in the volatility bin i is in good agreement with that of the product i with similar K_p or c^* (Table 1) in the $K_p \times 100$ case. Overall, the volatility basis set produces the smallest fitting error of SOA yield prediction over the whole range of organic mass loading (mean absolute fractional error, $\text{err}=0.1572$) compared to the $K_p \times 1$ case ($\text{err}=0.1688$) and the $K_p \times 100$ case ($\text{err}=0.1598$).

3.3 Temperature dependence of SOA yield

We also investigate temperature dependence of SOA yield using the product-specific model (only the $K_p \times 100$ case which gives a better description of SOA yields is shown). The temperature-dependent vapor pressure of the products can be estimated using the group contribution method developed by Pankow and Asher (2008). The temperature dependence of the structural groups ($b(T)$) are assumed to follow $b(T)=B_1/T+B_2+B_3T+B_4 \ln T$. The B coefficients are obtained by optimal fitting to a number of compounds. In the calculation of the K_p , it is assumed that the activity coefficient is unity and the molecular weight of the product is taken as the mean molecular weight of the surrogate mixture. The α values determined at 293 K are assumed to be constant over the temperature range studied (273–313 K). The enthalpy of vaporization, ΔH_v of the products can also be estimated by the group contribution method. By plotting the estimated vapor pressure of the product against the temperature, the ΔH_v of the product can be estimated from the slope of the line following the Clausius-Clapeyron equation (see Appendix A). Estimated values of ΔH_v of major products are listed in Table 1.

As shown in Fig. 2, the predicted SOA yield increases as the temperature decreases, as lower temperature favors the partitioning of gas-phase reaction products into the particle phase. The model predicts a stronger temperature dependence of SOA yield than that observed by Pathak et al. (2007). The predicted SOA yields agree well with those measured at 293 and 303 K. The mean absolute fractional

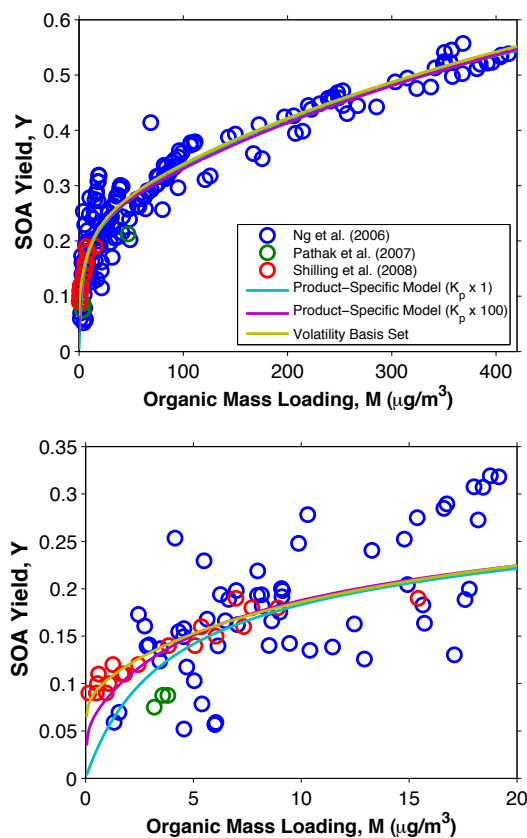


Fig. 1. SOA yield from ozonolysis of α -pinene at different organic mass loading, M . Data represent experiments conducted under dry, dark, and low- NO_x conditions in the presence of dry ammonium sulfate particles (Ng et al., 2006; Pathak et al., 2007; Shilling et al., 2008). Top panel: organic mass loading: $0\text{--}411 \mu\text{g m}^{-3}$; bottom panel: organic mass loading: $0\text{--}20 \mu\text{g m}^{-3}$. SOA yield data are adjusted to 293 K, using a temperature correction factor. Lines show the model fit with the parameters given in Table 1.

error between the measured and predicted SOA yields, err , is 0.1666 and 0.0895 at 293 and 303 K, respectively. On the other hand, the predicted SOA yields are higher than those measured at 288 K ($\text{err}=0.6728$) and 273 K ($\text{err}=0.6266$) but slightly lower than those measured at 313 K ($\text{err}=0.1968$).

In the product-specific model, the temperature dependence of the vapor pressure of major products is estimated directly using the group contribution method (Pankow and Asher, 2008). In this approach, uncertainties in the vapor pressure estimation method will lead to uncertainties in data fitting. Uncertainty in the vapor pressure estimation using the group contribution method is likely one factor contributing to a relatively large deviation between measured and predicted values at lower temperatures in the present study.

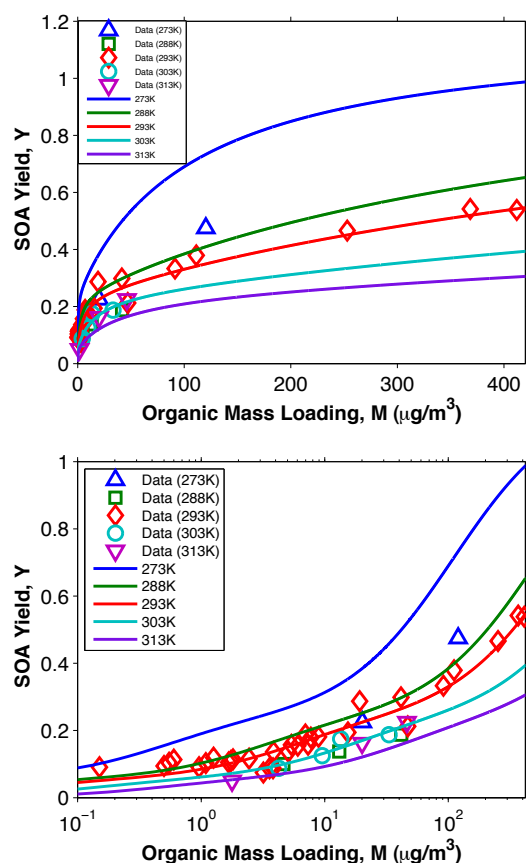


Fig. 2. Temperature dependence of SOA yield of ozonolysis of α -pinene obtained from experiments conducted under dry, dark, and low- NO_x conditions in the presence of dry ammonium sulfate particles. Data (293 K) are the final SOA yields from Ng et al. (2006), Pathak et al. (2007) and Shilling et al. (2008). Data from Shilling et al. (2008) have been adjusted to 293 K. Data at other temperatures are obtained from Pathak et al. (2007). The lines show the model fit at different temperatures for the $K_p \times 100$ case.

4 SOA composition

At a given temperature and organic mass loading, M , the mass yield of the product i , Y_i can be determined as:

$$Y_i = \frac{M_i}{\Delta H C} = \frac{M K_{p,i}}{1 + M K_{p,i}} \alpha_i \quad (4)$$

where the mass-based stoichiometric coefficient of the product i , α_i , is obtained from the parameterization of SOA yield data using the product-specific model (Table 1). M_i is the concentration of product i in the particle phase ($\mu\text{g m}^{-3}$). The SOA yield, Y , is the sum of the mass yields of all prod-

ucts (SOA yield, $Y = \sum_i Y_i$, at a given organic mass loading. The ratio of mass yield of product i to total yield (Y_i/Y) is the relative contribution of the product i to the total SOA yield (or total SOA mass).

Figure 3 shows the predicted relative contributions of the products to the SOA yield at different organic mass loading for the $K_p \times 100$ case. The predicted SOA composition is compared to the measured concentration of the corresponding classes of compounds in chamber experiments. Yu et al. (1999) reported the product distribution of ozonolysis of α -pinene at 306 K and organic mass loading of $38.8 \mu\text{g m}^{-3}$: hydroxy pinonic acid (17.7%), pinic acid and norpinic acid (22.5%), pinonic acid and norpinonic acid, and isomers (36.5%), hydroxy pinonaldehyde (15.9%), and pinonaldehyde and norpinonaldehyde (7.4%). It is noted that organic peroxides, particle-phase reaction products (e.g., oligomers and esters), and terpenylic acid were not reported in Yu et al. (1999). Docherty et al. (2005) estimated that organic peroxides contribute $\sim 47\%$ of the SOA mass at high organic mass loading. The concentration of terpenylic acid in chamber SOA has not been reported previously (Claeys et al., 2009). A smaller effective density of 1 g cm^{-3} was used to calculate the SOA mass in Yu et al. (1999). This change in density will increase the reported percentage of products. In addition, the relative abundance of products reported by Yu et al. (1999) may be overestimated if the organic peroxides, terpenylic acid, or other unidentified products contribute significantly to the SOA mass at the given organic mass loading.

As shown in the bottom panel of Fig. 3, for the $K_p \times 100$ case, the predicted percentage of pinonic acid is about 51%, which is close to the sum of the percentages of pinonic acid and norpinonic acid and isomers and hydroxy pinonaldehyde (52.4%). The predicted percentage of pinonaldehyde is also close to that of pinonaldehyde and norpinonaldehyde (7.4%). On the other hand, the predicted percentage of pinic acid is about 28%, which is smaller than the sum of the percentages of pinic acid and norpinic acid and hydroxy pinonic acid (40.2%). For organic peroxides, using a hydroperoxide as surrogate gives $\sim 7\%$ of SOA yield, which is lower than that reported by Docherty et al. (2005) at high organic mass loading. The percentage of terpenylic acid contributes about 5% of the SOA yield. Overall, the $K_p \times 100$ case may give a good first estimation of the gas/particle partitioning and composition of the SOA products at the given organic mass loading and temperature.

5 O/C and H/C ratios

The chemical composition of SOA formed from ozonolysis of α -pinene has been recently characterized by an Aerodyne high-resolution time-of-flight aerosol mass spectrometer (HR-ToF-AMS) at 298 K (Shilling et al., 2009). This characterization provides measurement of the O/C and H/C ratios at different organic mass loadings; these data provide

additional information about the SOA composition and impose important constraints on the SOA parameterization. As shown in Figs. 4 and 5, the data show that the O/C ratio decreases as the organic mass loading increases, while the H/C ratio increases (Shilling et al., 2009). This observation indicates, as expected, that the SOA is more oxygenated at low organic mass loading than at high organic mass loading.

O/C and H/C ratios of the SOA can also be determined from the predicted SOA composition. At a given organic mass loading, the number of moles of product i , m_i can be calculated from its particle-phase mass concentration and molecular weight. The number of carbon atoms, $n_{C,i}$, (O/C) $_i$ and (H/C) $_i$ ratios of the product i are known (Table 1). The O/C and H/C ratios of the SOA can be determined as follows:

$$\text{O/C} = \frac{\sum_i m_i \cdot n_{C,i} \cdot (\text{O/C})_i}{\sum_i m_i \cdot n_{C,i}} \quad (5)$$

$$\text{H/C} = \frac{\sum_i m_i \cdot n_{C,i} \cdot (\text{H/C})_i}{\sum_i m_i \cdot n_{C,i}} \quad (6)$$

At 298 K, for the $K_p \times 1$ case (Fig. 4, upper panel), the modeled O/C ratios decrease from ~ 0.44 to ~ 0.36 as the organic mass loading increases from $0.5 \mu\text{g m}^{-3}$ to $150 \mu\text{g m}^{-3}$. The predicted O/C ratios are higher than those in Shilling et al. (2009), except at low organic mass loading ($< 1 \mu\text{g m}^{-3}$). The predicted ratios decrease less rapidly as the organic mass loading increases. For the $K_p \times 100$ case (Fig. 4, lower panel), the predicted O/C ratios agree quite well with those measured; predicted O/C ratios decrease from 0.43 to 0.30 as the organic mass loading increases. On the other hand, in both $K_p \times 1$ and $K_p \times 100$ cases, the predicted H/C ratios exceed those measured at these loadings (Fig. 5).

The O/C ratios of selected major products range from 0.2 to 0.5, which cover the range of the experimental O/C ratios. On the other hand, the H/C ratios of the selected major products range from 1.5 to 1.6, which exceed the reported H/C ratios (1.38–1.51). Using the experimentally identified gas-phase reaction products, the predicted H/C ratios do not match those reported at low organic mass loading. Notably, the H/C ratios of the major SOA products identified in the literature range from 1.5 to 1.6. In addition to uncertainties in determination of the O/C and H/C ratios, the formation of oligomers or organic peroxides will shift the H/C ratio without greatly affecting the O/C ratio (Shilling et al., 2009). Formation of esters can alter the H/C and O/C ratios (Müller et al., 2008). The discrepancy in the H/C ratios based on known gas-phase products and those measured stresses the potential importance of particle-phase reactions on the determination of SOA yield and composition in the ozonolysis of α -pinene under dry, dark, and low- NO_x conditions.

Figures 4 and 5 also show the temperature dependence of the O/C and H/C ratios in the temperature range (273–313 K). For the both $K_p \times 1$ and $K_p \times 100$ cases (Fig. 4),

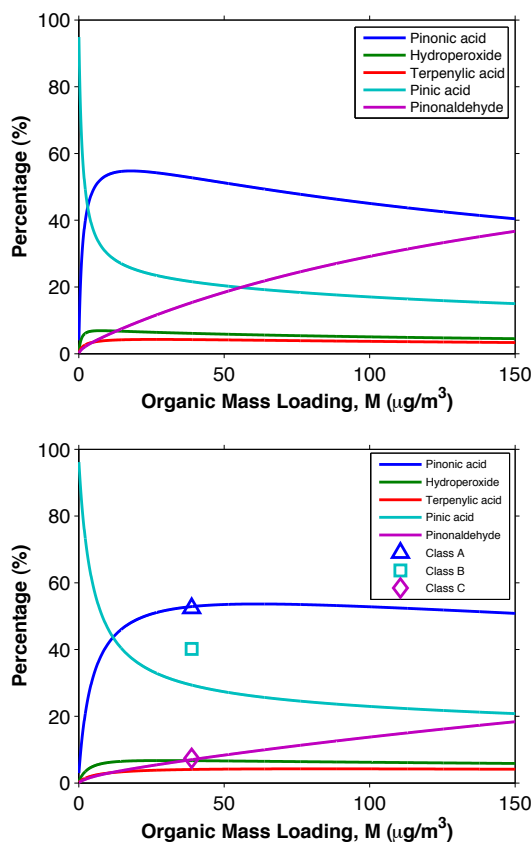


Fig. 3. Relative contributions of the modeled products to the SOA yield at different organic mass loadings for $K_p \times 100$ case at different temperatures (solid lines). Top panel: 293 K; bottom panel: 306 K; Class A data point refers to the sum of the percentages of pinonic acid, norpinonic acid and isomers, and hydroxy pinonaldehyde (Yu et al., 1999); Class B data point refers to the sum of the percentages of pinic acid, norpinic acid, and hydroxy pinonic acid (Yu et al., 1999); Class C data point refers to the sum of the percentages of pinonaldehyde and norpinonaldehyde (Yu et al., 1999).

the modeled O/C ratio increases when the temperature increases. On the other hand, the modeled H/C ratio decreases when the temperature increases (Fig. 5). At a higher temperature, the less volatile gas-phase products which are usually more oxygenated (i.e., usually a higher O/C ratio and a lower H/C ratio) partition preferentially into the particle phase. As shown in Fig. 3 ($K_p \times 100$ case), the contribution of pinic acid, which is the least volatile product and is more oxygenated, increases when the temperature increases from 293 to 306 K. On the other hand, the relative abundance of pinonaldehyde, which is the most volatile product and is the least oxygenated, decreases with increasing temperature.

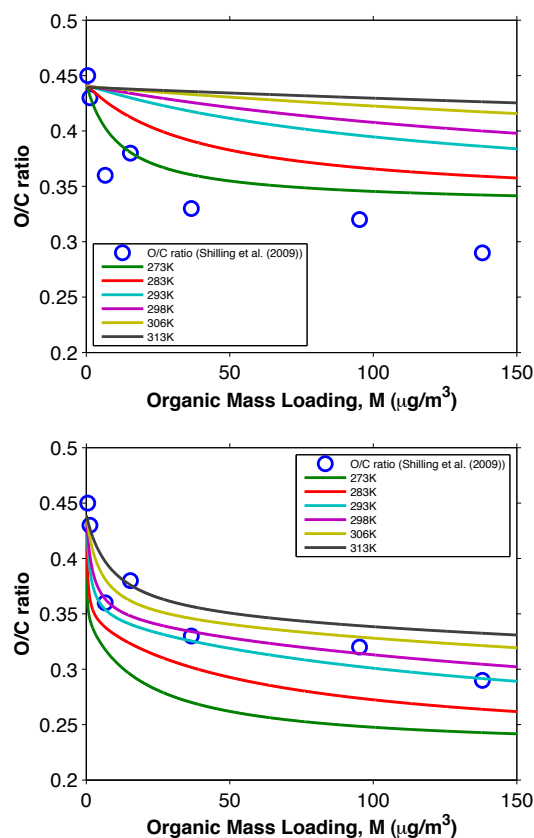


Fig. 4. O/C ratio of SOA formed from the ozonolysis of α -pinene under dry, dark, and low- NO_x conditions in the presence of dry ammonium sulfate particles as a function of organic mass loading, M , at different temperatures. Top panel: $K_p \times 1$ case; bottom panel: $K_p \times 100$ case; Blue open circles represent measured O/C ratios reported by Shilling et al. (2009) at 298 K.

The effect of particle-phase reactions on O/C and H/C ratios at different temperatures is not considered.

We also report here on an α -pinene ozonolysis experiment conducted in the Caltech laboratory chamber under dry, dark, and low- NO_x conditions in the presence of dry $(\text{NH}_4)_2\text{SO}_4$ particles to generate a data set comparable to that of Shilling et al. (2008, 2009). The chemical composition of the SOA was continuously monitored using an Aerodyne HR-ToF-AMS. Details of the experiment are given in Appendix B. Figure 6 shows the time evolution of α -pinene concentration, organic mass loading, and aerosol O/C and H/C ratios. Once the ozone is injected, α -pinene oxidation commences, and the organic mass loading increases almost immediately. When α -pinene is completely reacted, organic aerosol mass loading remains unchanged. These observations are consistent with those reported by Ng et al. (2006).

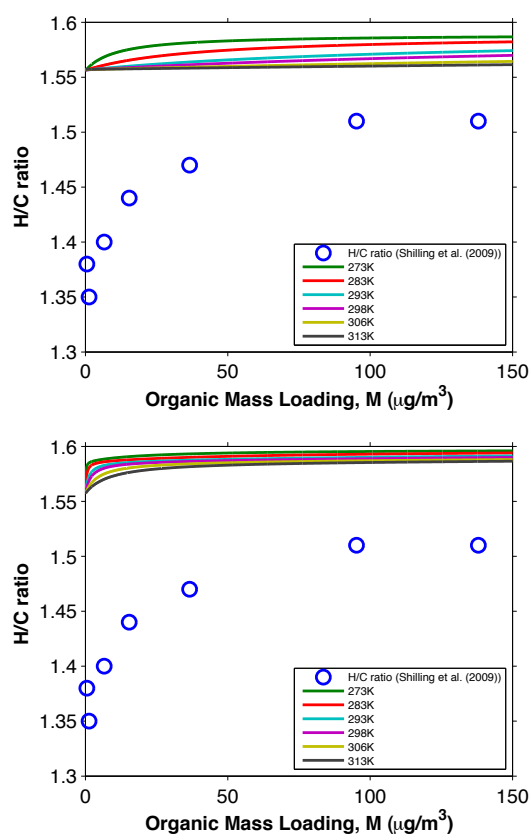


Fig. 5. H/C ratio of SOA formed from the ozonolysis of α -pinene under dry, dark, and low- NO_x conditions in the presence of dry ammonium sulfate particles as a function of organic mass loading, M , at different temperatures. Top panel: $K_p \times 1$ case; bottom panel: $K_p \times 100$ case; Blue open circles represent measured H/C ratios reported by Shilling et al. (2009) at 298 K.

Measured O/C and H/C ratios as a function of organic mass loading are shown in Fig. 7. The data scatter reflects the inherent uncertainty in measurement of O/C and H/C ratios at low organic mass loading. Generally, the H/C ratio increases as time increases, while the O/C ratio decreases. The trends in O/C and H/C ratios are in good agreement with those reported by Shilling et al. (2009). The absolute values of the O/C ratios are slightly lower than those reported by Shilling et al. (2009), but well within the experimental uncertainty. When all α -pinene is consumed and the SOA growth has leveled out ($\sim 58 \mu\text{g m}^{-3}$), O/C and H/C ratios and fragment mass spectrum (not shown here) remain unchanged. As discussed by Ng et al. (2006), the first oxidation step in the ozonolysis of α -pinene (a hydrocarbon with a single double bond) is most likely the rate-determining step in SOA formation. Either the condensable products are the initial reaction

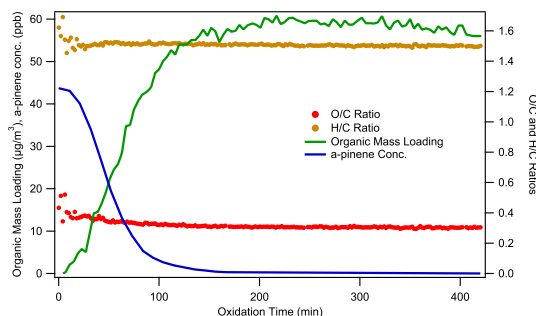


Fig. 6. Time evolution of α -pinene concentration, organic mass loading, and O/C and H/C ratios during ozonolysis of α -pinene under dry, dark, and low- NO_x conditions in the presence of dry ammonium sulfate particles. Experiment conducted in the Caltech laboratory chamber. Conditions given in Appendix B.

products of the parent hydrocarbon oxidation (first- or higher generation products), or subsequent reactions (in either the gas or particle phase) proceed at relatively fast rates. Thus, the instantaneous product spectrum can be considered as that at equilibrium during the chamber phase.

To determine the extent to which an equilibrium state is achieved, the chemical composition of SOA can be measured by the Aerodyne HR-ToF-AMS over the course of the chamber experiments. The change in element-to-carbon ratios (e.g., O/C, H/C ratios) can provide insight about the change in SOA composition. If the ratios or the mass spectra do not vary with time, this may suggest that an equilibrium state is achieved within the timescale of the chamber experiment. In that case, major experimentally identified products (both particle-phase and gas-phase reaction products) can be chosen as SOA surrogates in the product-specific model. In addition, the O/C, H/C, N/C, or S/C ratios can be calculated from the detailed gas-chemistry model coupled with gas/particle partitioning theory.

Recently, Dzepina et al. (2009) suggest that the O/C ratio and volatility can be used to compare modeled and measured SOA. The authors calculate O/C ratios using various models and compare these to the measured O/C ratios of ambient Mexico City aerosol. They find that O/C ratios predicted by different models do not agree and are generally lower than the measured ratios.

In the present study, we show that although good agreement in O/C ratio between observations and predictions can exist, a discrepancy in H/C ratio is not removed by data fitting. Hence, in addition to the O/C ratio, other element-to-carbon ratios such as H/C are important for modeling fitting and comparison. S/C and N/C ratios could be used once accurate determinations can be made using the AMS. These element-to-carbon ratios can also be calculated using detailed gas-chemistry models coupled with gas/particle par-

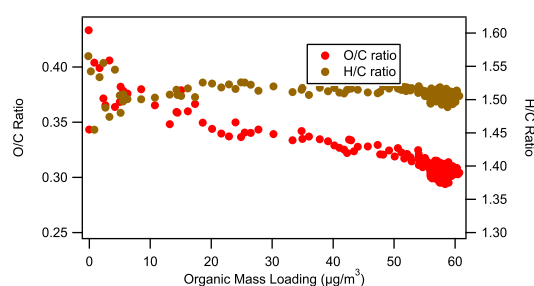


Fig. 7. O/C and H/C ratios of SOA formed from the ozonolysis of α -pinene under dry, dark, and low- NO_x conditions in the presence of dry ammonium sulfate particles as function of organic mass loading, M . Experiment conducted in the Caltech laboratory chamber. Conditions given in Appendix B.

tituting theory and can be used as additional constraints on the SOA parameterization in chamber experiments and modeling studies.

6 Discussion

SOA yields from volatile organic compounds are determined from laboratory chamber data. Gas-particle partitioning of semivolatile oxidation products forms the basis of all current models of SOA formation. As identification of aerosol-phase products has become feasible using advanced mass spectrometric techniques, we investigate the extent to which a product-specific model, certain parameters of which are determined from chamber data, can be used to represent SOA formation. In the present work we address this question using data on SOA formation in the α -pinene/ozone system. While the product specific model can be fitted to available chamber data, fitting of the product-specific model required increasing estimated equilibrium partitioning coefficients by two orders of magnitude, and the predicted fractional contributions of the selected products to SOA are unreasonable in several respects and no better than a fitting of the data to a volatility basis set representation.

The performance of the product-specific model is most likely hindered by lack of explicit inclusion of particle-phase accretion compounds that are almost certainly present but have yet to be identified in this system. Prospects for identification of the majority of SOA products for major VOC classes remain promising. However, for the near future, empirical product Odum-type or volatility basis set models remain the approaches of choice.

Appendix A

The gas-particle partitioning coefficient

The gas-particle partitioning coefficient for compound i to a condensed phase of i only is given by (Pankow, 1994a,b)

$$K_{p,i} = \frac{RT}{10^6 MW_i p_{L,i}^o} \quad (\text{A1})$$

where $R=8.2 \times 10^{-5} \text{ m}^3 \text{ atm mol}^{-1} \text{ K}^{-1}$, MW_i =molecular weight of i (g mol^{-1}) and $p_{L,i}^o$ is the vapor pressure of pure i as a liquid (atm). When multiple condensed-phase compounds exist

$$K_{p,i} = \frac{RTf}{10^6 \overline{MW} \zeta_i p_{L,i}^o} \quad (\text{A2})$$

where f =weight fraction of the total particulate matter that is the absorbing phase, \overline{MW} is the mean molecular weight of the absorbing organic phase (g mol^{-1}), and ζ_i =mole-fraction based activity coefficient. $K_{p,i}$ varies as a function of T , through both its explicit dependence on T as well as the strong dependence of $p_{L,i}^o$ on T . The value of $K_{p,i}$ is also influenced by ζ_i and \overline{MW} owing to the types and amounts of condensed-phase compounds.

The vapor pressure of each component obeys the Clausius-Clapeyron equation,

$$p_{L,i}^o(T) = p_{L,i}^o(T_o) \exp \left[-\frac{\Delta H_{v,i}}{R} \left(\frac{1}{T} - \frac{1}{T_o} \right) \right] \quad (\text{A3})$$

For a set of compounds at a given T , $p_{L,i}^o$ tends to decrease with increasing $\Delta H_{v,i}$.

The variation of gas-partitioning coefficient with temperature results from variation of $p_{L,i}^o$ as well as the explicit dependence on T ,

$$\begin{aligned} \frac{K_{p,i}(T)}{K_{p,i}(T_o)} &= \left(\frac{T}{T_o} \right) \frac{p_{L,i}^o(T_o)}{p_{L,i}^o(T)} \\ &= \left(\frac{T}{T_o} \right) \exp \left[-\frac{\Delta H_{v,i}}{R} \left(\frac{1}{T} - \frac{1}{T_o} \right) \right] \end{aligned} \quad (\text{A4})$$

Following Pankow and Chang (2008), one may choose $\Delta H_v=100 \text{ kJ mol}^{-1}$ as a “reference” $\Delta H_{v,i}$ value, so that any $\Delta H_{v,i}$ can be written as a multiple of the reference value, $\Delta H_{v,i}=a_i \times 100 \text{ kJ mol}^{-1}$. For $T_o=293 \text{ K}$, for $a=1$, a 10 K decrease in T leads to

$$\begin{aligned} \frac{K_{p,i}(283)}{K_{p,i}(293)} &= \left(\frac{283}{293} \right) \exp \left[-\frac{100}{R} \left(\frac{1}{283} - \frac{1}{293} \right) \right] \\ &= 4.1 \end{aligned} \quad (\text{A5})$$

Thus, for a compound with $\Delta H_v=100 \text{ kJ mol}^{-1}$, a 10 K decrease in temperature leads to a factor of 4 increase in $K_{p,i}$. For a compound with $a_i=0.5$, the increase of $K_{p,i}$ for a 10 K decrease in T is \sim a factor of 2. Note that the factor (T/T_o) exerts only a minor effect compared to that from the temperature dependence of $p_{L,i}^o$.

Appendix B

Measurement of O/C and H/C ratios of SOA from α -pinene ozonolysis

To provide an additional set of data on the O/C ratio of SOA generated from α -pinene ozonolysis, an experiment was performed in one of the dual Caltech 28-m³ Teflon chambers. Details of the facility have been described elsewhere (Cocker et al., 2001; Keywood et al., 2004). Before the experiment, the chamber was flushed continuously with dry, purified air for at least 24 h. Aerosol number concentration, size distribution, and volume concentrations were measured by a differential mobility analyzer (DMA, TSI model 3081) coupled with a condensation nucleus counter (TSI model 3760). Ammonium sulfate seed particles were generated by atomizing an aqueous solution of 0.015 M $(\text{NH}_4)_2\text{SO}_4$ with a constant-rate atomizer. The volume concentration of the seed particles was $12 \mu\text{m}^3 \text{ cm}^{-3}$.

The parent hydrocarbon, α -pinene, and an OH scavenger, cyclohexane, were then introduced separately by injecting known volumes of the liquid hydrocarbon into a glass bulb, subsequently carried into the chamber by an air stream at 5 L min^{-1} . The mixing ratio of α -pinene was monitored with a gas chromatograph coupled with a flame ionization detector (GC-FID, Agilent model 6890N). The initial mixing ratio of α -pinene was 44 ppb. The estimated mixing ratio of cyclohexane was 37 ppm, which corresponds to a rate of cyclohexane + OH 100 times faster than that of α -pinene + OH.

Ozone was generated with a UV lamp ozone generator (EnMet Corporation, MI), and monitored with a commercial ozone analyzer (Horiba Instruments, CA). Ozone injection was stopped after the ozone concentration reached 180 ppb. The aerosol growth data were corrected for wall deposition of particles. First-order size dependent wall loss coefficients were determined from a separate seed-only experiment. The final SOA volume was $46 \mu\text{m}^3 \text{ cm}^{-3}$, as measured by the DMA.

Real-time particle mass spectra were collected continuously by an Aerodyne High Resolution Time-of-Flight Aerosol Mass Spectrometer (HR-ToF-AMS). The HR-ToF-AMS is described in detail elsewhere (Canagaratna et al., 2007) and references therein). The HR-ToF-AMS switched once every minute between the high resolution “W-mode” and the lower resolution, higher sensitivity “V-mode”. The “V-mode” data were analyzed using a fragmentation table to separate sulfate, ammonium, and organic spectra and to time-trace specific mass-to-charge ratios. “W-mode” data were analyzed using a separate high-resolution spectra toolbox known as PIKA to determine the chemical formulas contributing to distinct mass-to-charge ratios (DeCarlo et al., 2006).

To determine elemental ratios, the computational toolbox Analytical Procedure for Elemental Separation (APES) was used. This toolbox applies the analysis procedure described

in Aiken et al. (2007) to the high-resolution “W-mode” data. The particle-phase signal of CO^+ and the organic contribution to H_xO^+ ions were estimated as described in Aiken et al. (2008). It is noted that chamber air is cleaned through a series of chemical denuders and filters. Fourier transform infrared spectroscopy measurements show that the concentrations of CO_2 in the chamber air is nominally the same as that in the atmosphere. Due to the relatively large SOA loadings generated in this study, the sensitivity of the O/C calculation to the CO_2 concentration input is relatively small.

Acknowledgements. This work was supported by the Office of Science (BER), U.S. Department of Energy, Grant No. DE-FG02-05ER63983 and the U.S. Environmental Protection Agency under STAR Agreement RD-833749. It has not been formally reviewed by the EPA. The views expressed in this document are solely those of the authors and the EPA does not endorse any products or commercial services mentioned in this publication.

Edited by: A. Nenes

References

- Aiken, A. C., DeCarlo, P. F., and Jimenez, J. L.: Elemental analysis of organic species with electron ionization high-resolution mass spectrometry, *Anal. Chem.*, 79, 8350–8358, 2007.
- Aiken, A. C., DeCarlo, P. F., Kroll, J. H., Worsnop, D. R., Huffman, J. A., Docherty, K. S., Ulbrich, I. M., Mohr, C., Kimmel, J. R., Sueper, D., Sun, Y., Zhang, Q., Trimborn, A., Northway, M., Ziemann, P. J., Canagaratna, M. R., Onasch, T. B., Alfarra, M. R., Prevot, A. S. H., Dommen, J., Duplissy, J., Metzger, A., Baltensperger, U., and Jimenez, J. L.: O/C and OM/OC ratios of primary, secondary, and ambient organic aerosols with high-resolution time-of-flight aerosol mass spectrometry, *Environ. Sci. Technol.*, 42, 4478–4485, 2008.
- Bahreini, R., Keywood, M. D., Ng, N. L., Varutbangkul, V., Gao, S., Flagan, R. C., Seinfeld, J. H., Worsnop, D. R., and Jimenez, J. L.: Measurements of secondary organic aerosol from oxidation of cycloalkenes, terpenes, and m-xylene using an Aerodyne aerosol mass spectrometer, *Environ. Sci. Technol.*, 39, 5674–5688, 2005.
- Bilde, M. and Pandis, S. N.: Evaporation rates and vapor pressures of individual aerosol species formed in the atmospheric oxidation of alpha- and beta-pinene, *Environ. Sci. Technol.*, 35, 3344–3349, 2001.
- Canagaratna, M. R., Jayne, J. T., Jimenez, J. L., Allan, J. D., Alfarra, M. R., Zhang, Q., Onasch, T. B., Drewnick, F., Coe, H., Middlebrook, A., Delia, A., Williams, L. R., Trimborn, A. M., Northway, M. J., DeCarlo, P. F., Kolb, C. E., Davidovits, P., and Worsnop, D. R.: Chemical and microphysical characterization of ambient aerosols with the aerodyne aerosol mass spectrometer, *Mass. Spectrom. Rev.*, 26, 185–222, 2007.
- Chan, A. W. H., Kroll, J. H., Ng, N. L., and Seinfeld, J. H.: Kinetic modeling of secondary organic aerosol formation: effects of particle- and gas-phase reactions of semivolatile products, *Atmos. Chem. Phys.*, 7, 4135–4147, 2007, <http://www.atmos-chem-phys.net/7/4135/2007/>.
- Chen, J. J. and Griffin, R. J.: Modeling secondary organic aerosol formation from oxidation of alpha-pinene, beta-pinene, and d-limonene, *Atmos. Environ.*, 39, 7731–7744, 2005.
- Claeys, M., Iinuma, Y., Szmigielski, R., Surratt, J. D., Blockhuys, F., Van Alsenoy, C., Böge, O., Sierau, B., Gómez-González, Y., Vermeylen, R., Van der Veken, P., Shahgholi, M., Chan, A. W. H., Herrmann, H., Seinfeld, J. H., and Maenhaut, W.: Terpenylic acid and related compounds from the oxidation of α -pinene: Implications for new particle formation and growth above forests, *Environ. Sci. Technol.*, in press, 2009.
- Cocker, D. R., Flagan, R. C., and Seinfeld, J. H.: State-of-the-art chamber facility for studying atmospheric aerosol chemistry, *Environ. Sci. Technol.*, 35, 2594–2601, 2001.
- DeCarlo, P. F., Kimmel, J. R., Trimborn, A., Northway, M. J., Jayne, J. T., Aiken, A. C., Gonin, M., Fuhrer, K., Horvath, T., Docherty, K. S., Worsnop, D. R., and Jimenez, J. L.: Field-deployable, high-resolution, time-of-flight aerosol mass spectrometer, *Anal. Chem.*, 78, 8281–8289, 2006.
- Docherty, K. S., Wu, W., Lim, Y. B., and Ziemann, P. J.: Contributions of organic peroxides to secondary aerosol formed from reactions of monoterpenes with O₃, *Environ. Sci. Technol.*, 39, 4049–4059, 2005.
- Donahue, N. M., Robinson, A. L., Stanier, C. O., and Pandis, S. N.: Coupled partitioning, dilution, and chemical aging of semivolatile organics, *Environ. Sci. Technol.*, 40, 2635–2643, 2006.
- Dzepina, K., Volkamer, R. M., Madronich, S., Tulett, P., Ulbrich, I. M., Zhang, Q., Cappa, C. D., Ziemann, P. J., and Jimenez, J. L.: Evaluation of new secondary organic aerosol models for a case study in Mexico City, *Atmos. Chem. Phys. Discuss.*, 9, 4417–4488, 2009, <http://www.atmos-chem-phys-discuss.net/9/4417/2009/>.
- Gao, S., Keywood, M., Ng, N. L., Surratt, J., Varutbangkul, V., Bahreini, R., Flagan, R. C., and Seinfeld, J. H.: Low-molecular-weight and oligomeric components in secondary organic aerosol from the ozonolysis of cycloalkenes and alpha-pinene, *J. Phys. Chem. A*, 108, 10147–10164, 2004.
- Hallquist, M., Wenger, J. C., Baltensperger, U., Rudich, Y., Simpson, D., Claeys, M., Dommen, J., Donahue, N. M., George, C., Goldstein, A. H., Hamilton, J. F., Herrmann, H., Hoffmann, T., Iinuma, Y., Jang, M., Jenkin, M. E., Jimenez, J. L., Kiendler-Scharr, A., Maenhaut, W., McFiggans, G., Mentel, Th. F., Monod, A., Prévôt, A. S. H., Seinfeld, J. H., Surratt, J. D., Szmigielski, R., and Wildt, J.: The formation, properties and impact of secondary organic aerosol: current and emerging issues, *Atmos. Chem. Phys.*, 9, 5155–5235, 2009, <http://www.atmos-chem-phys.net/9/5155/2009/>.
- Iinuma, Y., Böge, O., Gnauk, T., and Herrmann, H.: Aerosol-chamber study of the alpha-pinene/O₃ reaction: influence of particle acidity on aerosol yields and products, *Atmos. Environ.*, 38, 761–773, 2004.
- Jenkin, M. E.: Modelling the formation and composition of secondary organic aerosol from α - and β -pinene ozonolysis using MCM v3, *Atmos. Chem. Phys.*, 4, 1741–1757, 2004, <http://www.atmos-chem-phys.net/4/1741/2004/>.
- Keywood, M. D., Varutbangkul, V., Bahreini, R., Flagan, R. C., and Seinfeld, J. H.: Secondary organic aerosol formation from the ozonolysis of cycloalkenes and related compounds, *Environ. Sci. Technol.*, 38, 4157–4164, 2004.

- Kroll, J. H. and Seinfeld, J. H.: Representation of secondary organic aerosol laboratory chamber data for the interpretation of mechanisms of particle growth, *Environ. Sci. Technol.*, 39, 4159–4165, 2005.
- Müller, L., Reinnig, M.-C., Warnke, J., and Hoffmann, Th.: Unambiguous identification of esters as oligomers in secondary organic aerosol formed from cyclohexene and cyclohexene/alpha-pinene ozonolysis, *Atmos. Chem. Phys.*, 8, 1423–1433, 2008, <http://www.atmos-chem-phys.net/8/1423/2008/>.
- Ng, N. L., Kroll, J. H., Keywood, M. D., Bahreini, R., Varutbangkul, V., Flagan, R. C., Seinfeld, J. H., Lee, A., and Goldstein, A. H.: Contribution of first- versus second-generation products to secondary organic aerosols formed in the oxidation of biogenic hydrocarbons, *Environ. Sci. Technol.*, 40, 2283–2297, 2006.
- Odum, J. R., Hoffmann, T., Bowman, F., Collins, D., Flagan, R. C., and Seinfeld, J. H.: Gas/particle partitioning and secondary organic aerosol yields, *Environ. Sci. Technol.*, 30, 2580–2585, 1996.
- Pankow, J. F.: An absorption-model of gas-particle partitioning of organic-compounds in the atmosphere, *Atmos. Environ.*, 28, 185–188, 1994a.
- Pankow, J. F.: An absorption-model of the gas aerosol partitioning involved in the formation of secondary organic aerosol, *Atmos. Environ.*, 28, 189–193, 1994b.
- Pankow, J. F. and Asher, W. E.: SIMPOL.1: a simple group contribution method for predicting vapor pressures and enthalpies of vaporization of multifunctional organic compounds, *Atmos. Chem. Phys.*, 8, 2773–2796, 2008, <http://www.atmos-chem-phys.net/8/2773/2008/>.
- Pankow, J. F. and Chang, E. I.: Variation in the sensitivity of predicted levels of atmospheric organic particulate matter (OPM), *Environ. Sci. Technol.*, 42, 7321–7329, 2008.
- Pankow, J. F., Seinfeld, J. H., Asher, W. E., and Erdakos, G. B.: Modeling the formation of secondary organic aerosol. 1. Application of theoretical principles to measurements obtained in the alpha-pinene/, beta-pinene/, sabinene/, Delta(3)-carene/, and cyclohexene/ozone systems, *Environ. Sci. Technol.*, 35, 1164–1172, 2001.
- Pathak, R. K., Stanier, C. O., Donahue, N. M., and Pandis, S. N.: Ozonolysis of alpha-pinene at atmospherically relevant concentrations: Temperature dependence of aerosol mass fractions (yields), *J. Geophys. Res.-Atmos.*, 112, D03201, doi:10.1029/2006JD007436, 2007.
- Presto, A. A. and Donahue, N. M.: Investigation of alpha-pinene plus ozone secondary organic aerosol formation at low total aerosol mass, *Environ. Sci. Technol.*, 40, 3536–3543, 2006.
- Seinfeld, J. H., Erdakos, G. B., Asher, W. E., and Pankow, J. F.: Modeling the formation of secondary organic aerosol (SOA). 2. The predicted effects of relative humidity on aerosol formation in the alpha-pinene-, beta-pinene-, sabinene-, Delta(3)-Carene-, and cyclohexene-ozone systems, *Environ. Sci. Technol.*, 35, 1806–1817, 2001.
- Shilling, J. E., Chen, Q., King, S. M., Rosenoern, T., Kroll, J. H., Worsnop, D. R., McKinney, K. A., and Martin, S. T.: Particle mass yield in secondary organic aerosol formed by the dark ozonolysis of alpha-pinene, *Atmos. Chem. Phys.*, 8, 2073–2088, 2008, <http://www.atmos-chem-phys.net/8/2073/2008/>.
- Shilling, J. E., Chen, Q., King, S. M., Rosenoern, T., Kroll, J. H., Worsnop, D. R., DeCarlo, P. F., Aiken, A. C., Sueper, D., Jimenez, J. L., and Martin, S. T.: Loading-dependent elemental composition of alpha-pinene SOA particles, *Atmos. Chem. Phys.*, 9, 771–782, 2009, <http://www.atmos-chem-phys.net/9/771/2009/>.
- Stanier, C. O., Donahue, N., and Pandis, S. N.: Parameterization of secondary organic aerosol mass fractions from smog chamber data, *Atmos. Environ.*, 42, 2276–2299, 2008.
- Yu, J. Z., Cocker, D. R., Griffin, R. J., Flagan, R. C., and Seinfeld, J. H.: Gas-phase ozone oxidation of monoterpenes: Gaseous and particulate products, *J. Atmos. Chem.*, 34, 207–258, 1999.

Appendix G

Chemical composition of gas- and aerosol-phase products from the photooxidation of naphthalene*

*Reproduced with permission from “Chemical composition of gas- and aerosol-phase products from the photooxidation of naphthalene” by K. E. Kautzman, J. D. Surratt, M. N. Chan, A. W. H. Chan, S. P. Hersey, P. S. Chhabra, N. F. Dalleska, P. O. Wennberg, R. C. Flagan, and R. H. Seinfeld, *Journal of Physical Chemistry A*, 114 (2), 913–934, 2010. Copyright 2010 by the American Chemical Society.

Chemical Composition of Gas- and Aerosol-Phase Products from the Photooxidation of Naphthalene

K. E. Kautzman,[†] J. D. Surratt,[†] M. N. Chan,[‡] A. W. H. Chan,[†] S. P. Hersey,[‡] P. S. Chhabra,[†] N. F. Dalleska,[‡] P. O. Wennberg,^{‡,§} R. C. Flagan,^{†,§} and J. H. Seinfeld^{*,†,§}

Division of Chemistry and Chemical Engineering, Division of Engineering and Applied Science, and Division of Geological and Planetary Sciences, California Institute of Technology, Pasadena, CA

Received: September 3, 2009; Revised Manuscript Received: October 15, 2009

The current work focuses on the detailed evolution of the chemical composition of both the gas- and aerosol-phase constituents produced from the OH-initiated photooxidation of naphthalene under low- and high-NO_x conditions. Under high-NO_x conditions ring-opening products are the primary gas-phase products, suggesting that the mechanism involves dissociation of alkoxy radicals (RO) formed through an RO₂ + NO pathway, or a bicyclic peroxy mechanism. In contrast to the high-NO_x chemistry, ring-retaining compounds appear to dominate the low-NO_x gas-phase products owing to the RO₂ + HO₂ pathway. We are able to chemically characterize 53–68% of the secondary organic aerosol (SOA) mass. Atomic oxygen-to-carbon (O/C), hydrogen-to-carbon (H/C), and nitrogen-to-carbon (N/C) ratios measured in bulk samples by high-resolution electrospray ionization time-of-flight mass spectrometry (HR-ESI-TOFMS) are the same as the ratios observed with online high-resolution time-of-flight aerosol mass spectrometry (HR-ToF-AMS), suggesting that the chemical compositions and oxidation levels found in the chemically-characterized fraction of the particle phase are representative of the bulk aerosol. Oligomers, organosulfates (R-OSO₃), and other high-molecular-weight (MW) products are not observed in either the low- or high-NO_x SOA; however, in the presence of neutral ammonium sulfate seed aerosol, an organic sulfonic acid (R-SO₃), characterized as hydroxybenzene sulfonic acid, is observed in naphthalene SOA produced under both high- and low-NO_x conditions. Acidic compounds and organic peroxides are found to account for a large fraction of the chemically characterized high- and low-NO_x SOA. We propose that the major gas- and aerosol-phase products observed are generated through the formation and further reaction of 2-formylcinnamaldehyde or a bicyclic peroxy intermediate. The chemical similarity between the laboratory SOA and ambient aerosol collected from Birmingham, Alabama (AL) and Pasadena, California (CA) confirm the importance of PAH oxidation in the formation of aerosol within the urban atmosphere.

1. Introduction

A large fraction (80–90% in some locations) of atmospheric organic aerosol is secondary in origin.¹ The formation of secondary organic aerosol (SOA) results from the formation of low-vapor-pressure products in the oxidation of volatile organic compounds (VOCs), where the resultant low-vapor-pressure oxidation products partition between the gas and aerosol phases. Many VOCs, such as monoterpenes (e.g., α -pinene) and single-ringed aromatic hydrocarbons (e.g., toluene), are known to produce SOA. However, the mass of SOA observed in many locations cannot be accounted for by known precursor VOC, suggesting that many sources of SOA are not yet identified or well characterized.^{2–4} Recent identification of isoprene oxidation as a significant source of SOA,^{5–12} the role of NO_x in forming SOA from the oxidation of aromatics^{13–15} and other hydrocarbons,^{16–18} the effects of aerosol acidity and heterogeneous chemistry (e.g., oligomer^{19–27} and organosulfate formation^{24,28–32}), and the contribution of glyoxal to SOA formation^{24,33–35} have provided significant insights into potential missing and poorly characterized sources of SOA. Additionally, Robinson et al.³⁶

have shown that primary organic aerosol (POA), previously considered as nonvolatile, contains gas-phase components of intermediate volatility that themselves are sources of SOA.

Although it is traditionally assumed that small volatile aromatic organic compounds, such as toluene and benzene, are the primary precursors for anthropogenic SOA, it has recently been shown that substantial contributions to SOA formation may also come from compounds of lower volatility,³⁶ such as polycyclic aromatic hydrocarbons (PAHs). PAHs account for a significant portion of the semivolatile gas-phase emissions from diesel fuels,³⁷ with substantial emissions also being produced from gasoline engines,³⁸ wood burning,^{39,40} and cooking sources.^{41,42} Photooxidation of PAHs has been shown to produce high-MW, low-vapor-pressure, oxygenated compounds.^{40,43–47} The nitro PAHs, specifically nitronaphthalenes, have been observed in ambient particulate matter⁴⁸ and are of particular importance due to their expected role as carcinogens.^{49–52}

We have previously reported SOA yields, defined as the ratio of mass of SOA formed, ΔM_o , to the mass of hydrocarbon reacted, ΔHC , from the photooxidation of naphthalene, 1-methylnaphthalene (1-MN), 2-methylnaphthalene (2-MN), and 1,2-dimethylnaphthalene (1,2-DMN) as a function of organic mass loading under both high- and low-NO_x conditions.¹⁵ Yields for high-NO_x conditions were observed between 0.19 and 0.30 for

* Author to whom correspondence should be addressed. Phone: (626) 395-4635, Fax: (626) 796-2591, E-mail: seinfeld@caltech.edu.

[†] Division of Chemistry and Chemical Engineering.

[‡] Division of Engineering and Applied Science.

[§] Division of Geological and Planetary Sciences.

TABLE 1: Instruments Employed in Chamber Experiments^a

instrumentation	measurement	time resolution	detection limit/range
hygrometer (capacitance probe)	temperature	online	10–50 °C
Vaisala HMP233	humidity	online	5–95%
chemiluminescent NO _x analyzer	NO, NO ₂ concentrations	online	2 ppb
luminol NO _x analyzer	concentration of NO ₂ separated from PAN by GC	online	5 ppb
O ₃ analyzer	ozone concentration	online	2 ppb
differential mobility analyzer (DMA)	aerosol number concentration, size distribution, and volume concentration	4 min	0.2 μm ³ cm ⁻³ , 15–780 nm
gas chromatography/flame ionization detector (GC/FID)	parent hydrocarbon concentration	12 min	~1 ppb ^b
chemical ionization mass spectrometry (CIMS)	gas-phase oxidation products	~9 min	~0.1 ppb ^b , unit mass resolution
gas chromatography/electron ionization-time-of-flight mass spectrometry (GC/EL-TOFMS)	gas-phase oxidation products, structural identification	semionline, off-line	0.5 ppb ^b , resolution ~7000
ultra performance liquid chromatography/electrospray ionization-time-of-flight mass spectrometry (UPLC/ESI-TOFMS)	particle-phase products, structural identification	off-line	1 ng m ⁻³ ^b , resolution ~12 000
high performance liquid chromatography/electrospray ionization-ion trap mass spectrometry (HPLC/ESI-ITMS)	particle-phase products, structural identification	off-line	1 ng m ⁻³ ^b , unit mass resolution
high-resolution time-of-flight aerosol mass spectrometry (HR-ToF-AMS)	particle-phase composition	online	0.03 μg m ⁻³ , 50–600 nm
particle into liquid sampler-ion chromatography (PILS-IC)	water-soluble aerosol composition	online	~0.1 μg m ⁻³ ^b

^a Instruments employed at the Caltech dual chamber environmental facility. ^b Detection limits dependent on identity of target species.

naphthalene, 0.19 and 0.39 for 1-MN, 0.26 and 0.45 for 2-MN, and constant at 0.31 for 1, 2-DMN, at aerosol mass loadings between 10 and 40 μg m⁻³. Under low-NO_x conditions, yields were found to be 0.73, 0.68, and 0.58, for naphthalene, 1-MN, and 2-MN, respectively. Gas-phase products were tentatively identified, and trends involving ring-opening versus ring-retaining oxidation mechanisms were established. Calculations of SOA formation from these PAHs demonstrated that these precursors may contribute significantly to the amount of urban SOA. The suite of instruments associated with the Caltech dual indoor environmental chamber facility (Table 1), by which the data to be presented were obtained, permits a thorough analysis of the generation of SOA commencing with the oxidation of the gas-phase hydrocarbon to the formation of SOA. Here we describe the detailed evaluation of the chemical composition of both the gas- and aerosol-phase constituents produced from the photooxidation of naphthalene, the most abundant PAH in the urban atmosphere.⁴⁸

2. Experimental Section

2.1. Chamber Experiments. All experiments were carried out in the Caltech dual 28 m³ Teflon chambers. Details of the facilities have been described previously.^{53,54} Before each experiment, the chambers were flushed with dried purified air for >24 h, until the particle number concentration was <100 cm⁻³ and the volume concentration was <0.1 μm³ cm⁻³. In most experiments, ammonium sulfate seed aerosol was used to promote condensation of low volatility oxidation products. The seed aerosol was generated by atomization of a 0.06 M aqueous ammonium sulfate solution. The hydrocarbon was introduced into the chamber by flowing purified air through an FEP tube packed with solid naphthalene at 1 L min⁻¹.

For high-NO_x experiments (NO > 350 ppb initially) nitrous acid (HONO) was used as the OH precursor. HONO was prepared by adding 10 mL of 1 wt % aqueous NaNO₂ dropwise into 20 mL of 10 wt % sulfuric acid in a glass bulb. A stream

of dry air was then passed through the bulb, sending HONO into the chamber. During this process, NO and NO₂ formed as side products and were also introduced into the chamber. NO/NO_x was measured with a commercial chemiluminescence NO_x monitor (Horiba, APNA-360). In some experiments, NO₂ was monitored by a gas chromatograph with luminol detector (University of California, Riverside, CA) in which NO₂ and peroxyacetyl nitrate (PAN) were separated by gas chromatography and detected by chemiluminescence of reaction with luminol.⁵⁵ Reaction of HONO with luminol is unlikely, and thus no interference with the NO₂ signal is expected. The NO₂ measurement from the NO_x monitor is higher due to interferences from HONO. The injection of HONO was stopped when the mixing ratio of NO₂ reached about 80 ppb in the chamber as measured by the Riverside NO₂ monitor. Additional NO was added until total NO was about 400 ppb. For all experiments, the concentrations of NO and NO₂ remained approximately constant over the course of photooxidation, and ozone (O₃) concentrations remained insignificant. For low-NO_x experiments, hydrogen peroxide (H₂O₂) was used as the OH precursor. Prior to atomization of the ammonium sulfate seed, H₂O₂ was introduced by bubbling purified air through a 50% aqueous H₂O₂ solution for 2.5 h at 5 L min⁻¹ resulting in a mixing ratio of 2–8 ppm of H₂O₂.

The aerosol number concentrations, size distributions, and volume concentrations were measured by a differential mobility analyzer (DMA, TSI model 3081) coupled with a condensation nuclei counter (TSI, CNC-3760). After allowing for all concentrations to stabilize, irradiation was initiated. The temperature (*T*), relative humidity (RH), and concentrations of O₃, NO, and NO_x were continuously monitored. Table 2 summarizes the experimental conditions for the series of naphthalene oxidation experiments conducted.

2.2. Gas-Phase Measurements.

2.2.1. Gas Chromatography/Flame-Ionization Detection (GC/FID). The concentration of naphthalene was continuously monitored by GC/FID. Chamber air was sampled into a 10 mL

TABLE 2: Experimental Conditions from Chamber Experiments

	initial naphthalene (ppb)	oxidant precursor ^a	initial NO ₂ (ppb)	initial NO (ppb)	initial O ₃ (ppb)	T (°C) ^b	RH (%) ^b	initial seed volume (μm ³ /cm ³)	end volume (μm ³ /cm ³)
1	60	H ₂ O ₂	0	0	6	26	6	14	143
2	25	H ₂ O ₂	0	3	4	26	19	26	50
3	20	H ₂ O ₂	0	2	2	24	10	11	38
4	20	H ₂ O ₂	0	1	1	24	13	11	40
5	48	HONO	166	401	3	28	5	16	65
6	30	HONO	245	455	1	25	7	15	51
7	35	HONO	289	487	3	25	10	15	50
8	30	HONO	260	480	3	26	17	11	n.a.

^a H₂O₂ is used for low-NO_x conditions; HONO is used for high-NO_x conditions. ^b Reported value is averaged over the course of the experiment.

injection loop and injected onto a HP5 15 m × 0.53 mm ID × 1 μm thickness column installed on a 6890N Agilent GC. The GC was temperature-programmed as follows; initial temp 60 °C, hold 1 min, ramp 35 °C min⁻¹ to 140 °C, ramp 20 °C min⁻¹ to 200 °C, hold 2 min. The GC response was calibrated by dissolving a known mass of the naphthalene in dichloromethane, and then vaporizing a known volume of that solution into a 38 L Teflon chamber.

2.2.2. Chemical Ionization Mass Spectrometry (CIMS). Monitoring of gas-phase oxidation products was carried out in real time by the use of a CIMS instrument. The details of this instrument are described elsewhere.^{17,56,57} Briefly, a 2.5 standard liters per minute (slm) aliquot of air is drawn from the experimental chamber through a 1.6 m long 0.25 in. Teflon tube. 300 standard cubic centimeters per minute (sccm) of this flow is introduced into the CIMS instrument and ionized by a reagent ion. The resultant ions are filtered using a quadrupole mass spectrometer with unit mass resolution. The instrument can operate in both negative mode, using CF₃O⁻ as a reagent ion, and in positive proton transfer reaction (PTR)-MS mode. Negative mode is found to be more selective toward detection of polar molecules, particularly acids, whereas positive mode detects a broader range of organic compounds. Mass scans were performed covering masses 55–450 amu for negative mode, and 56–350 amu for positive mode, with a total scan time of ~9 min. Mass scans were continuously repeated over the course of each experiment.

2.2.3. Gas Chromatography/Electron Impact Time-of-Flight Mass Spectrometry (GC/EI-TOFMS). The GC/EI-TOFMS instrument (Waters, GCT Premier) is outfitted with a standard 6890N Agilent GC for introduction of volatile samples. The ion source employed here is a traditional 70 eV positive (+)EI source. The ions produced are continuously accelerated across the source to 40 eV and perpendicularly extracted into the TOF mass analyzer at a rate >25 kHz. The ions then pass through a single reflectron with an effective path length of 1.2 m. Ions are subsequently detected by a chevron stack of microchannel plates. The arrival times of the ions are recorded by a time-to-digital converter at a rate of 3.6 GHz, providing high mass accuracy (~7000). All data are acquired and analyzed using MassLynx software version 4.1.

Various components have been added to aid with sample introduction into the GC/EI-TOFMS instrument. A preconcentrator (Entech Instruments, model 7100A) is used to draw, concentrate, and focus gas-phase samples into discrete peaks on the GC column. The preconcentrator extracts air from the environmental chamber and then cryogenically traps and concentrates VOCs in the sample. We have used two different trapping methods with the preconcentrator. The first method, microscale purge and trap (MPT), is a three-stage procedure to efficiently concentrate gas samples. The initial trap, which is

filled with glass beads, is used to remove water vapor from the sample and removes bulk atmospheric gases (e.g., O₂ and N₂). The initial concentration step is then followed by trapping of VOCs with a Tenax adsorbent trap, and the sample is subsequently flushed into the cryofocusing module where the sample is focused and rapidly injected onto the GC column. The second method, cold trap dehydration (CTD), uses only the Tenax trap and cryofocusing modules. Although CTD is less effective at removing moisture from humid samples, it is the preferred method of sample concentration for water-soluble compounds such as aldehydes. This method also provides superior handling of samples with high CO₂ levels. Both the MPT and CTD methods have been found to be effective for sampling volatile and semivolatile compounds, although for the highly oxidized products of interest here, the preconcentrator is believed to be the controlling factor for the ultimate detection limit of these latter products. All modules in the preconcentrator have an upper temperature range of 200 °C. Similarly, the transfer line between the preconcentrator and GC can be heated only to a maximum of 150 °C. The upper temperature limit of the preconcentrator makes detection of low-vapor-pressure oxidized compounds challenging.

The concentrations of naphthalene (<40 ppb) employed in the chamber experiments outlined in Table 2 preclude detection of the gas-phase oxidation products by the GC/EI-TOFMS technique as implemented at Caltech. Thus, additional high-concentration experiments were carried out in a separate 3 m³ Teflon chamber to identify gas-phase products from the photooxidation of naphthalene under high- and low-NO_x conditions using the GC/EI-TOFMS instrument. The initial mixing ratio of the naphthalene in these experiments was ~40 ppm, and the concentration of HONO in high-NO_x experiments was ~10 ppm. For low-NO_x experiments initial mixing ratios of H₂O₂ were ~30–80 ppm. Two methods were used to monitor the formation of gas-phase oxidation products; first, 1000 mL samples were drawn from the 3 m³ Teflon chamber and introduced directly into the three-step preconcentrator. After preconcentration, the sample was injected onto the GC DB-5MS column (30 m × 0.25 mm ID × 0.25 μm thickness) and temperature-programmed as follows: initial temp 40 °C, hold 2 min, ramp 5 °C min⁻¹ to 300 °C. This method has limited time resolution due to the preconcentration and GC steps. In order to improve the time resolution, Tenax tube samples were collected. Air from the 3 m³ Teflon chamber was drawn through Tenax TA glass tubes (Supelco, 6 mm × 11.5 cm) at a rate of 0.455 L min⁻¹ using a critical orifice. Each tube sampled chamber air for 20 min. Subsequently, the tubes were desorbed at 300 °C into the preconcentrator and analyzed as described above. Gas-phase products were identified by NIST library searching the mass spectra,⁵⁸ and authentic standards were used when possible. No

differences were observed between the preconcentrator MPT and CTD methods.

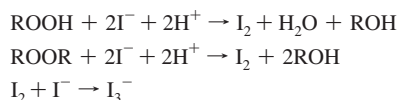
2.3. Particle-Phase Measurements.

2.3.1. Chamber Filter Sample Collection, Extraction, and Off-Line Detailed Chemical Characterization Protocols. A detailed description of the aerosol filter sample collection and extraction protocol has been previously published.⁵⁹ Briefly, aerosol samples are collected on Teflon filters (PALL Life Sciences, 47-mm diameter, 1.0- μm pore size, teflomembrane). Filter samplers employed for aerosol filter sample collection used a front and back-up filter sampling approach, where back-up filters were collected in order to examine if aerosol breakthrough was occurring on the front filter or whether evaporation of semivolatiles from the front filter was occurring during filter sampling. In all experiments outlined in Table 2, no SOA constituents were found on the back-up filters, and as a result, all detailed chemical characterizations are reported only for the front filters. Filter sampling was initiated when the aerosol volume reached its maximum (constant) value, as determined by the DMA. Depending on the total volume concentration of aerosol in the chamber, the duration of filter sampling was 1.8–2.1 h, which resulted in 2.0–2.9 m³ of total chamber air sampled. Teflon filter extraction protocols in high-purity methanol (LC-MS CHROMASOLV-Grade, Sigma-Aldrich) have been described previously.⁵⁹ Additional filter extractions using 5 mL of high-purity acetonitrile (LC-MS CHROMASOLV-Grade, Sigma-Aldrich) were also performed by 45 min of sonication to ensure detection of SOA constituents not soluble in methanol. No additional compounds were recovered using the less-polar acetonitrile solvent. Thus, all results from the off-line ESI-MS measurements are reported only for the methanol filter extractions. The resultant filter extracts were then analyzed by a Waters ACQUITY ultra performance liquid chromatography (UPLC) system, coupled with a Waters LCT Premier TOF mass spectrometer equipped with an ESI source, allowing for accurate mass measurements (i.e., determination of molecular formulas) to be obtained for each observed ion. Operation protocols, including column information and employed chromatographic method, for the UPLC/ESI-TOFMS technique have been described in detail previously.⁵⁹

Selected naphthalene low- and high-NO_x methanol filter extracts were also analyzed by a Thermo Finnigan Surveyor high performance liquid chromatography (HPLC) system (pump and autosampler) coupled to a Thermo Finnigan LCQ ion trap mass spectrometer (ITMS) equipped with an ESI source, allowing for tandem MS measurements (i.e., generation of product ions) to be obtained. The combination of accurate mass and tandem MS measurements significantly aided in detailed structural characterization efforts. Data were acquired and processed using Xcalibur version 1.3 software. A Waters Atlantis T3 column (3 μm particle size; 2.1 \times 150 mm) was employed, which is similar to the Water ACQUITY UPLC HSS column used for the UPLC/ESI-TOFMS analysis. The mobile phases consisted of 0.1% acetic acid in water (A) and 0.1% acetic acid in methanol (B). The applied 45 min gradient elution program was as follows: the concentration of eluent B was kept at 3% for 4 min, then increased to 100% in 21 min, holding at 100% for 10 min, then decreased to 3% in 5 min, and kept at 3% for 5 min. The injection volume and flow rate were 10 μL and 0.2 mL min⁻¹, respectively. The ion trap mass analyzer was operated under the following conditions: sheath gas flow (N₂), 65 arbitrary units; auxiliary gas flow (N₂), 3 arbitrary units; source voltage, -4.5 kV; capillary voltage, -14.5 V; tube lens offset, 7 V; capillary temperature, 200 °C; and maximum ion

injection time, 200 ms. Two scan events were used during each chromatographic run; scan event 1 was the full scan mode in which data were collected from m/z 120 to 600 in the negative ionization mode and scan event 2 was the MS² mode in which product ions were generated from significant base peak ions observed in scan event 1. For MS² experiments, an isolation width of 2.5 m/z units and a normalized collision energy level of 35% were applied. The [M - H]⁻ ion signal optimization was carried out by introducing a 1 mg mL⁻¹ malic acid standard solution. Due to the on-axis ESI source that is characteristic of the LCQ ITMS instrument, a solvent delay time of 3.5 min (which diverted the column effluent from the ESI source to waste) was employed to prevent clogging by nonvolatile salts at the entrance of the capillary.

Measurements of total peroxide content from the extracted filter samples were acquired by the UV-vis iodometric spectroscopy method.¹⁹ Filter samples used for this analysis were extracted and prepared differently from the filter samples used in the UPLC/ESI-TOFMS and HPLC/ESI-ITMS analyses.¹¹ Standard calibration curves were generated using a series of benzoyl peroxide solutions. The structure of the benzoyl peroxide, a peroxy group linking two benzene rings, was judged to be an excellent surrogate for the naphthalene system. Calibrations and measurements were performed on a Hewlett-Packard 8452A diode array spectrophotometer. Peroxides in the form of HOOH, ROOH, and ROOR are quantified by measuring the absorbance at 470 nm of the reaction product I₃⁻ produced under anaerobic, dark, and acidic conditions by the following reaction scheme:



Detection of I₃⁻ at 470 nm is 10 nm to the red from the peak of the characteristic absorbance of I₃⁻ and has been chosen to avoid interferences with other organic compounds absorbing in this region. Extractions from three high-NO_x and three low-NO_x filters were performed to ensure reproducibility across experiments. No contribution of H₂O₂ to this measurement is expected due to the dry conditions employed in the present experiments, as well as owing to previous quality control experiments demonstrating that no H₂O₂ could be measured on filter samples collected from a nonirradiated chamber mixture containing only gaseous H₂O₂, VOC, and ammonium sulfate seed aerosol. These latter quality control filter samples were collected for the same duration as filter samples collected from SOA chamber experiments.

Of particular concern to the UV-vis measurements is the presence of nitronaphthalenes and nitrobenzenes in high-NO_x filter samples, which in solution have a color similar to the I₃⁻ produced from the reaction of I⁻ with the peroxides in solution. 1000 ppm standard solutions of nitronaphthalenes (i.e., 4-nitro-1-naphthol and 2-nitro-1-naphthol), nitrobenzenes (i.e., 2-nitrophenol and 3-hydroxy-4-nitrobenzoic acid), and epoxides (i.e., α -pinene oxide, 2-methyl-2-vinylloxirane, and 2,3-epoxy-1,4-diol) were prepared and tested to confirm that no interferences were present from these compounds in the UV-vis measurement. From the analyses of the 1000 ppm standards, it was found that the nitronaphthalenes and nitrobenzenes were the only classes of compounds to absorb weakly at 470 nm, and as a result, we reanalyzed the nitronaphthalene and nitrobenzene standards at a concentration more relevant to the high-NO_x SOA

Photooxidation of Naphthalene

samples characterized in the current study. Since the highest concentration of the nitronaphthalenes and of the nitrobenzenes was measured at ~ 5 ppm by the UPLC/(–)ESI-TOFMS technique (Tables 2S–4S, Supporting Information), the absorbance of a 5 ppm standard mixture of the nitronaphthalenes (i.e., 4-nitro-1-naphthol and 2-nitro-1-naphthol) and of the nitrobenzenes (i.e., 2-nitrophenol and 3-hydroxy-4-nitrobenzoic acid) was measured by the UV–vis technique. It was found that the absorbance of this standard mixture, which possessed a yellowish color characteristic of nitroaromatics in solution, was insignificant at this SOA-relevant concentration.

Non-nitro containing benzene standards (i.e., phthalic acid and *trans*-cinnamic acid) were also prepared and analyzed. These compounds did not contribute to the absorbance measurement at 470 nm, consistent with the lack of color observed in their respective standard solutions. As a result of these measurements, it was assumed that the absorbance (peroxide) measurements acquired for the high- and low- NO_x SOA samples were not affected by chemical artifacts. Finally, blank Teflon filters were also extracted and prepared in the same manner as the filter samples collected from chamber experiments; these blank filters produced no significant absorbance at 470 nm, indicating that the filter medium did not interfere with the peroxide measurements.

2.3.2. High-Resolution Time-of-Flight Aerosol Mass Spectrometry (HR-ToF-AMS). Real-time aerosol mass spectra were obtained using an Aerodyne HR-ToF-AMS.⁶⁰ The HR-ToF-AMS was operated in both a lower resolution, higher sensitivity “V-mode”, and a high-resolution “W” mode, switching between modes once every minute. The V-mode data were analyzed to extract sulfate, ammonium, and organic spectra.⁶¹ Calculation of the SOA densities were achieved by comparing the particle mass distributions obtained using the particle ToF mode and the volume distributions obtained by the DMA in nucleation (seed-free) experiments.⁶² O/C, N/C, and H/C ratios were determined from W mode data using the APES toolbox and applying the procedures outlined in Aiken et al.^{63,64} The particle-phase signal of CO^+ and the organic contribution to H_xO^+ ions were estimated as described in Aiken et al.⁶⁴

2.3.3. Particle-into-Liquid Sampler/Ion Chromatography (PILS/IC). The PILS/IC instrument is designed to measure aerosol water-soluble ions and is based on the original design of Weber et al.⁶⁵ The current instrument has been modified to utilize syringe pumps to introduce the samples from the impactor into vials for later analysis by IC.⁶⁶ Chamber air, sampled through a 1 mm cut-size impactor, is passed through three denuders (URG and Sunset Laboratories) to remove gas-phase species. The aerosol is mixed with steam in a condensation chamber and grows by condensation of supersaturated water vapor to diameters $>1 \mu\text{m}$. Droplets grow sufficiently large to be collected by impingement on a quartz impactor, are washed to the bottom of the impactor, then collected and stored in airtight vials. Vials are analyzed off-line by IC (ICS-2000 with 25 μL sample loop, Dionex Inc.); columns used in the IC and the chromatographic methods employed have been previously described in detail by Sorooshian et al.⁶⁶ Vials were collected prior to each experiment to establish background levels of individual species, including Na^+ , NH_4^+ , K^+ , Mg^{2+} , Ca^{2+} , SO_4^{2-} , Cl^- , NO_2^- , NO_3^- , oxalate, pyruvate, formate, and phthalate. Chromatographic peaks were identified and quantified using authentic standards; standards used in the current work are: terephthalic acid, benzoic acid, *trans*-cinnamic acid, 5-hydroxy isophthalic acid, 1,2,4-benzene tricarboxylic acid, 4-formylcinnamic acid, 2-hydroxy isophthalic acid, 3-hydroxy benzoic

acid, 4-hydroxybenzoic acid, 3-formyl benzoic acid, 3-hydroxy-4-nitrobenzoic, 2-nitrophenol, 2-nitro-1-naphthol, 4-nitro-1-naphthol, and salicylic acid. Additionally, the presence of dicarboxylic acids of C_2 (oxalic), C_3 (malonic), C_4 (succinic), C_5 (glutaric), and C_6 (adipic) compounds were investigated using authentic standards.

2.4. Ambient Aerosol Samples: Filter Collection Protocols and Off-Line Chemical Analysis. Selected archived quartz fiber filters collected from Birmingham, AL during the Southeastern Aerosol Research and Characterization (SEARCH) 2004 campaign were reanalyzed by the UPLC/(–)ESI-TOFMS technique, as described above for the naphthalene SOA chamber filters. Details of the SEARCH network, which includes descriptions of each site, aerosol filter sample collection protocols, gas- and particle-phase measurements conducted, can be found elsewhere.^{67,68} Birmingham, AL (denoted as BHM in the SEARCH network) is an urban site consisting of both industrial and residential settings. Quartz fiber filter extractions and sample preparation procedures have been described previously.⁶⁹ However, solid-phase extraction (SPE) was not employed in the current study to avoid possible loss of early eluting naphthalene SOA products.

In addition to the ambient aerosol filters samples collected from Birmingham, AL, quartz fiber filters were also collected in Pasadena, CA, during June and July, 2009 using the same high-volume filter sampling approach as used by the SEARCH network. These samples are a part of the Pasadena Aerosol Characterization Observatory (PACO), an ambient sampling study located on the campus of Caltech. Selected PACO filter samples collected on June 3, June 19, and July 14, 2009, were analyzed by the UPLC/(–)ESI-TOFMS technique as described above. These filters represent 4 h integrated morning (7–11 a.m.) and 4 h integrated afternoon (3–7 p.m.) sampling periods. June 19 and July 14 were chosen for this chemical analysis due to the high total organic mass aerosol loadings as measured by a compact time-of-flight AMS instrument (maximum of 21.12 and 11.72 $\mu\text{g m}^{-3}$, respectively, assuming a collection efficiency of 0.5), O_3 mixing ratios (71 and 56 ppb, respectively), and daytime temperature (29 and 34 °C, respectively). June 3 was chosen as a relatively clean day for comparison with June 19 and July 14, and had a maximum total organic mass aerosol loading of 5.66 $\mu\text{g m}^{-3}$ (assuming a collection efficiency of 0.5), O_3 mixing ratio of 19 ppb, and daytime temperature of 20 °C. Further results and details from the PACO 2009 campaign will be presented in a forthcoming publication. Here, the chemical characterization data obtained from the ambient filters were compared to that of the naphthalene SOA chamber experiments to identify potential ambient SOA tracer compounds that can be used in source apportionment studies.

2.5. Chemicals. Most of the reagents used in this study were purchased from Sigma Aldrich and their stated purities are listed in Table 1S (Supporting Information). Additionally, 2-formylcinnamaldehyde was synthesized by ozonolysis of naphthalene using the technique of Larson et al.,⁷⁰ but was not purified. Identification of both *E*- and *Z*-isomers was confirmed by NMR measurements.

3. Results

3.1. High- NO_x Conditions.

3.1.1. Chemical Characterization of High- NO_x Gas-Phase Oxidation Products. Table 3 lists the gas-phase products detected by the CIMS instrument in positive and negative ion modes and structures identified by the GC/EI-TOFMS technique. These data are compared to aerosol measurements made by the UPLC/ESI-TOFMS technique, thus establishing the connection between the gas and particle phases. When the CIMS is operated

TABLE 3: Summary of Chemically Characterized Gas- and Particle-Phase Products Produced from the Photooxidation of Naphthalene

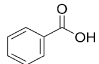
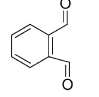
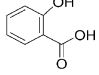
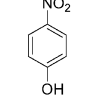
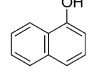
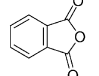
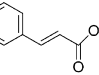
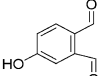
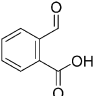
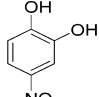
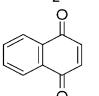
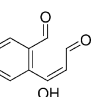
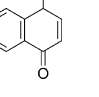
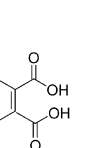
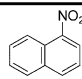
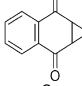
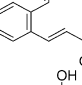
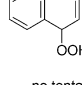
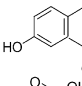
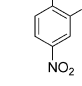
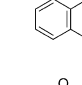
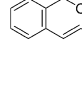
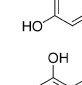
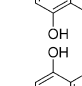
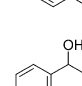
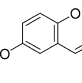
MW	Gas-phase measurements				Particle-phase measurements					proposed structure ^a
	CIMS detection ^a			GC/EI-TOFMS		UPLC/ESI-TOFMS				
	[M + H] ⁺	[M + F] ⁻	[M + CF ₃ O] ⁻	accurate mass	error (mDa)	accurate mass ^b	avg. error (mDa)	% SOA ^c	% SOA ^d	
122	B	B		122.0368	-0.4	121.0301 121.0293 121.0267	0.3	1.57	2.12	
134	B			134.0390	2.4	135.0444	-0.2	n.q.	n.q.	
138		B	B			137.0253 137.0228 137.0255 137.0222	-0.05	1.64	3.63	
139						138.0225 138.0179 138.0198	1.0	1.13	0	
144	B	B	B			143.0531 143.0536	3.7	n.q.	n.q.	
148	B	B	B							
148						147.0432 147.0473 147.0480	1.6	0.25	0.57	
150						151.0401	0.6	n.q.	n.q.	
50	B	B	B			149.0231 149.0241 149.0239 149.0248	-0.1	1.24	2.8	
155						154.013	2.5	0.94	0	
158	B			158.0387	1.9	159.0453	0.7	n.q.	n.q.	
160	B		B	160.0524	0.40					
160						161.0578	-2.5	n.q.	n.q.	
164						165.0539 165.0545 165.0525	-1.6	n.d.	n.q.	
166	B					165.0181 165.0148	2.3	2.71	4.01	

TABLE 3: Continued

MW	Gas-phase measurements				Particle-phase measurements					proposed structure ^e
	CIMS detection ^a			GC/EI-TOFMS		UPLC/ESI-TOFMS				
	[M + H] ⁺	[M + F] [−]	[M + CF ₃ O] [−]	accurate mass	error (mDa)	accurate mass ^b	avg. error (mDa)	% SOA ^c	% SOA ^d	
173				173.0495 173.0477	1.7 1.3					
174	B	B	B	174.0328	1.1					
176	B	B	B			175.0377 175.0375 175.0395 175.0403	0.8	1.46	0.53	
178	B		B			179.069	-1.8	n.q.	n.q.	
180						179.0325 179.0327 179.0341 179.0320	0.6	2.53	4.56	no tentative structure proposed
182						181.0128 181.0146 181.0128	0.3	3.3	9.8	
183						182.0096 182.0072	0.5	0.52	0	
189	H	H		189.0417	-0.9	188.0336 188.0367 188.0310 188.0341 188.0326 188.0357	0.9	0.4	0	
192	B					191.0364 191.0381 191.0345 191.0375	0.0	2.05	1.28	
192						193.0511	1.0	n.q.	n.q.	
198						197.0108	2.2	n.q.	3.5	
205			H			204.0295 204.0281 204.0286	1.0	0.39	0	
207						206.0477 206.0469	2.0	0.07	0	
208	B					207.03020 207.02891 207.02930 207.03070 207.02830	-0.6	2.18	4.54	

^a CIMS does not permit structural identification. All proposed structures are derived from either GC/TOFMS, UPLC/TOFMS, or previously identified structures found in the literature. H denotes products observed only under high-NO_x conditions. B denotes products observed under both NO_x conditions. ^b Accurate masses are determined by [M - H]⁺ or [M + H]⁺ mode. Reported masses are thus 1 H⁺ from the true mass. ^c High-NO_x case (HNO_x). ^d Low-NO_x case (LNO_x). ^e For simplicity only one isomer is shown. Number of observed isomers can be determined by the number of entries in the accurate mass column.

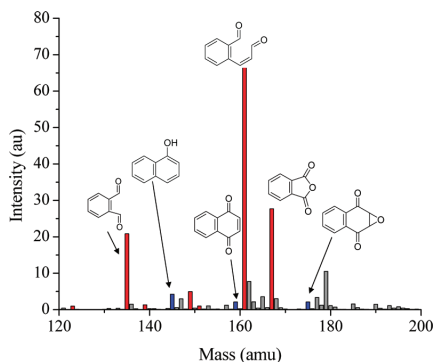


Figure 1. (+)CIMS mass spectrum taken at 70% reacted naphthalene under high- NO_x conditions. Red data indicate ring-opening products. Ring-retaining products are indicated in blue.

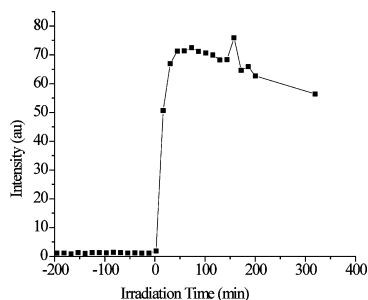


Figure 2. Time trace of 2-formylcinnamaldehyde obtained by the (+)CIMS technique.

in positive mode, compounds with proton affinities higher than that of water extract a proton and are subsequently detected by quadrupole MS; this mode is used for detecting a wide variety of organic compounds. The masses seen in positive mode will generally be detected as $[\text{M} + \text{H}]^+$ ions and are denoted in the CIMS $[\text{M} + \text{H}]^+$ column shown in Table 3. The negative mode of operation is highly selective toward acidic and polar molecules. The analyte clusters with CF_3O^- forming an $[\text{M} + \text{CF}_3\text{O}]^-$ cluster ion, or subsequently loses CF_2O to form the $[\text{M} + \text{F}]^-$ ion. Generally, identification of an $[\text{M} + \text{F}]^-$ ion corresponds with detecting carboxylic acids, while $[\text{M} + \text{CF}_3\text{O}]^-$ ions may also include hydroxy carbonyls. Owing to the unit-mass resolution of the CIMS technique, structural assignments are based on the results from the GC/EI-TOFMS and from previous results on the photooxidation of naphthalene. Products identified, along with suggested structures and accurate mass measurements obtained by the GC/EI-TOFMS technique are presented in Table 3.

The (+)CIMS mass spectrum from a typical high- NO_x experiment is shown in Figure 1. 2-Formylcinnamaldehyde (at m/z 161), phthalaldehyde (at m/z 135), and phthalic anhydride (at m/z 167) represent the largest peaks. We refer to these compounds as “ring-opening” products and indicate their presence in Figure 1 by the red mass spectral peaks. These observed compounds are consistent with those of other studies that report products of naphthalene and will be discussed subsequently. Closed-ring or “ring-retaining” compounds, such as isomeric naphthols (at m/z 145), 1,4-naphthoquinone (at m/z 159), 2,3-epoxy-1,4-naphthoquinone (at m/z 175), and isomeric nitronaphthols (at m/z 190), are also tentatively identified, as indicated by blue mass spectral peaks in Figure 1.

In the CIMS positive mode, the most abundant gas-phase product identified is a compound detected at m/z 161 (Figure 1). This compound is also observed in the GC/EI-TOFMS data and is positively identified as 2-formylcinnamaldehyde based on a mass spectral comparison with a synthesized standard (as shown in Figure 2S, Supporting Information). The present amounts of this compound are significantly less than found in other studies^{71,72} due to losses in the preconcentrator. The time trace for 2-formylcinnamaldehyde under typical high- NO_x conditions in Figure 2 indicates that 2-formylcinnamaldehyde grows rapidly once oxidation is initiated, then decays relatively slowly. From the (–)CIMS measurements, we learn that, after about 2 h of irradiation, all the HONO is consumed; naphthalene concentrations stabilize and generation of 2-formylcinnamaldehyde ends. 2-formylcinnamaldehyde then decays at a rate of 0.06 h^{-1} due to photolysis. After 6 h of irradiation, ~70% of the initially formed 2-formylcinnamaldehyde remains.

Results from the GC/EI-TOFMS technique demonstrate the presence of both the 1- and 2-nitronaphthalene isomers in the gas phase. 1-Nitronaphthalene has been positively identified using an authentic reference standard (Sigma-Aldrich, 99%) in conjunction with NIST library matching. 2-Nitronaphthalene is identified based on NIST library matching, accurate mass measurements, and comparison of the mass spectrum with the 1-nitronaphthalene isomer. Nitronaphthols are also identified based on NIST library matching. The 4-nitro-1-naphthol authentic standard was run for comparison, but did not match the retention time of the assigned peak. We expect that this is another structural isomer of 4-nitro-1-naphthol, most likely either 1-nitro-2-naphthol or 2-nitro-1-naphthol, both of which have been identified in previous studies.^{72,73} Naphthoquinone and 2,3-epoxy-1,4-naphthoquinone are also observed. In addition to these ring-retaining compounds, benzoic acid and phthalaldehyde are also observed by the GC/EI-TOFMS technique. Chromatograms for selected photooxidation products observed by the GC/EI-TOFMS method are shown in Figure 1S (Supporting Information).

The two methods of sample collection described in Section 2.2.3 yield similar results. Directly introducing the sample into the preconcentrator yielded greater intensities for the nitronaphthalene products; however, the gas-phase product of MW 160 (2-formylcinnamaldehyde) was detected with reduced efficiency using this method. Although the second Tenax tube method detected the gas-phase product of MW 160 with greater efficiency, phthalaldehyde was not detected. Detection of all other oxidation products was comparable using these two sampling techniques.

3.1.2. Chemical Characterization of High- NO_x SOA. The chemical composition of naphthalene SOA was probed with the battery of techniques described earlier. HR-ToF-AMS particle-phase data were acquired under a wide range of initial naphthalene mixing ratios. The naphthalene mixing ratios for which aerosol measurements from other instruments were acquired are 20–30 ppb. Hydrocarbon mixing ratios, along with the calculated density and observed aerosol atomic O/C, N/C, and H/C ratios are presented in Table 4. Errors in accuracy associated with AMS compositional ratios are reported as $\pm 30\%$, $\pm 22\%$, and $\pm 10\%$ of the measured O/C, N/C, and H/C ratios, respectively, in accordance with findings from Aiken et al.⁶⁴ Densities of 1.48 g cm^{-3} were found for high- NO_x SOA.

Under high- NO_x conditions, ~53% of the overall SOA mass is chemically characterized by off-line chemical analyses of aerosol filter samples using both the UPLC/(–)ESI-TOFMS and total peroxide content measurement techniques. An UPLC/

TABLE 4: Summary of Experimental Conditions and Results from the HR-ToF-AMS Instrument

[naphthalene] (ppb)	NO _x	seed vol ($\mu\text{m}^3/\text{cm}^3$)	end vol ($\mu\text{m}^3/\text{cm}^3$)	density (g/cm^3)	SOA mass ($\mu\text{g}/\text{m}^3$)	O/C ratio	N/C ratio	H/C ratio
5	low	10.64	18.48	1.55	12.15	0.61 ± 0.18	0	0.97 ± 0.1
20	low	10.48	41.48	1.55	48.06	0.72 ± 0.22	0	0.88 ± 0.09
60	low	13	143	1.55	201.5	0.6 ± 0.18	0	0.82 ± 0.08
5	high	12.25	16.23	1.48	6.18	0.55 ± 0.17	0.01 ± 0.02	1.03 ± 0.1
25	high	12.82	39.18	1.48	40.87	0.55 ± 0.17	0.01 ± 0.02	0.90 ± 0.1
30	high	0	26.3	1.48	40.76	0.45 ± 0.15	0.01 ± 0.02	0.90 ± 0.1
40	high	14.67	63.11	1.48	75.08	0.51 ± 0.15	0.01 ± 0.01	0.81 ± 0.08

(−)ESI-TOFMS base peak ion chromatogram (BPC) obtained for a typical high-NO_x naphthalene SOA experiment is shown in Figure 3. Peaks found under both the high- and low-NO_x conditions are denoted in black, while those SOA constituents found only in the high-NO_x case are denoted in green. Due to the use of (NH₄)SO₄ seed aerosol, bisulfate (detected as *m/z* 97) was found to elute first from the reverse-phase C18 column. A complete listing of the high-NO_x SOA constituents identified and quantified by the UPLC/(−)ESI-TOFMS technique is provided in Tables 2S–4S (Supporting Information). As shown in Tables 2S–4S (Supporting Information) and Table 3, ~24–28% of the high-NO_x naphthalene SOA is chemically characterized at the molecular level by the UPLC/(−)ESI-TOFMS technique. These chemical characterizations are further supported by the tandem MS measurements provided by the HPLC/(−)ESI-ITMS technique; major product ions produced for each of the major characterized high-NO_x SOA constituents are also listed in Tables 2S–4S (Supporting Information). All SOA constituents were quantified by calibration with either an authentic or surrogate standard. Dominant contributions to the high-NO_x SOA mass come from phthalic acid and hydroxy benzoic acids. Standard deviations for each UPLC/(−)ESI-TOFMS identified product were calculated across experiments (experiments 2–5 in Table 2). The fraction of SOA mass assigned to each product has a standard deviation of less than 3%, and the average standard deviation for the entire product range was ~2%, indicating the high level of reproducibility of these experiments.

As shown by the time trace in Figure 4, analysis by the PILS/IC technique confirms that phthalic acid is a significant component of the high-NO_x SOA (Retention Time (RT) = 13.88

min), increasing from 0 to $5.23 \mu\text{g m}^{-3}$ over the course of the experiment (Experiment 7 in Table 2). Figure 5 shows the ion chromatograms for a high-NO_x chamber sample on the bottom panel. The top panel shows a chromatogram from a 2 ppm standard of phthalic acid. The chromatographic peak with RT of 15.27 min also shows trends of increasing concentration with photochemical age and is not present in background vials, suggesting that this peak corresponds to a SOA constituent; however, this compound could not be identified using available standards. No other water-soluble SOA constituents are observed by the PILS/IC technique, indicating that small organic acids do not account for the unidentified fraction of the SOA mass. This is in contrast to data from the photooxidation of single-ringed aromatic compounds, such as benzene, toluene, and *m*-xylene, for which small organic acids comprise a substantial portion of the overall SOA mass (unpublished data). Small organic acids have also been observed in SOA generated from the photooxidation of 1,3,5-trimethylbenzene.⁷⁴

On the basis of results from the UPLC/(−)ESI-TOFMS method, N-containing compounds account for ~3% of the total high-NO_x SOA mass formed. Most of the N-containing compounds were quantified using calibration curves generated by either 2-nitro-1-naphthol or 4-nitro-1-naphthol standards. Using 4-nitro-1-naphthol in the quantification of these products yields concentrations that are an order of magnitude reduced from calibrations utilizing the 2-nitro-1-naphthol isomer. Final quantitative results reported here are determined by use of the more conservative mass concentrations. Quantification of these chemically characterized SOA constituents yields an N/C ratio of 0.04. This ratio should be considered as a lower limit for the N/C ratio, because some of the N-containing compounds that are

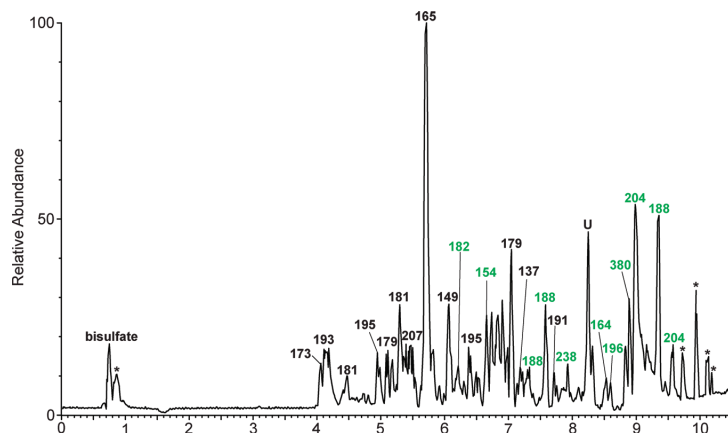


Figure 3. UPLC/(−)ESI-TOFMS base peak ion chromatogram (BPC) of a representative naphthalene high-NO_x SOA sample (Experiment 6). Chromatographic peaks designated with black [M − H][−] ions are also observed in the naphthalene low-NO_x SOA samples. Chromatographic peaks designated with green [M − H][−] ions are only observed in the naphthalene high-NO_x SOA samples. Chromatographic peaks designated with an asterisk, *, were also observed on a blank filter, and they are not considered high-NO_x SOA constituents. Major chromatographic peaks that remain uncharacterized in this study are designated as: U.

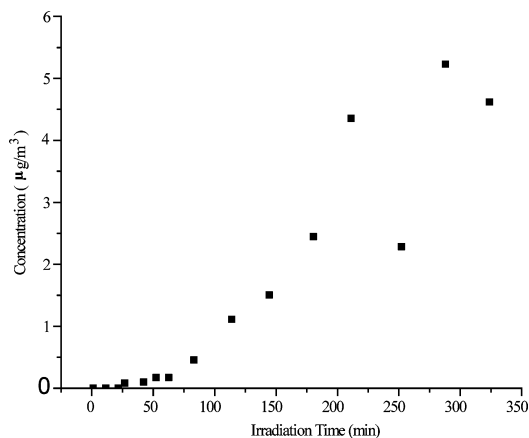


Figure 4. Time trace of phthalic acid acquired from Experiment 6 using the PILS/IC technique.

likely formed are not directly detectable by the UPLC/(−)ESI-TOFMS technique unless the molecule also contains a functional group with an acidic proton that can be abstracted. For example, the UPLC/(−)ESI-TOFMS method detects six isomers of nitronaphthol, as shown in Table 3; however, the 1- and 2-nitronaphthalene compounds identified in the gas phase by the GC/EI-TOFMS technique are not detected, even though the nitronaphthalenes are reported to exist primarily in the particle phase.⁴⁶ Given that the 1- and 2-nitronaphthalene isomers are reported to account for 0.3–7%^{43,45,72} of the gas-phase yield, and may partition into the particle phase,⁴⁶ the detection of these nonacidic nitronaphthalenes in the aerosol phase would likely increase the N/C ratio. We also expect that the formation of PANs, for example from phthalaldehyde, may play a significant role in SOA formation in the atmosphere. However, owing to the large NO to NO₂ ratio employed in these experiments, and to the difficulty in detecting nonacidic N-containing compounds, PANs are not observed in either the gas- or aerosol-phase.

Bulk HR-ToF-AMS measurements yield measurements of N-containing compounds producing N/C ratios ranging from 0.01–0.044. We place upper and lower bounds on the N/C ratio using calculations with and without the addition of compounds that possess NO⁺ and NO₂⁺ mass spectral peaks, respectively. Under high-NO_x conditions, OH and NO₂ can react to form nitric acid. Nitric acid can then react with ammonium from the ammonium sulfate seed to produce inorganic nitrates. This process should be of minimal importance for the experiments performed here owing to the dry experimental conditions; however, for the lower-limit calculations, we exclude compounds that have contributions from NO⁺ and NO₂⁺ mass spectral peaks from the N/C calculation to prevent biasing the chemical composition calculations with the formation of these inorganic nitrates. These lower-limit calculations include only the measurement of organic nitrate (NO₃) functional groups, yielding an atomic N/C ratio of 0.01. Only one organic nitrate is identified by the UPLC/(−)ESI-TOFMS method, supporting the minimal contribution from this class of compounds. However, inclusion of “NO family” ions with mass spectral peaks corresponding to NO⁺ and NO₂⁺ is necessary to account for the NO₂ groups observed in compounds such as nitronaphthalene, but may introduce artifacts from inorganic nitrates. Inclusion of the NO and NO₂ groups increases the atomic N/C ratio to 0.044, thus providing an upper bound of the N/C ratio. Inclusion of these compounds into the composition calculations also shifts the O/C ratios from 0.51 ± 0.17 (Table 4) to 0.57 ± 0.17 . Again, the upper-bound of 0.044 ± 0.01 for the N/C is in good agreement with the lower bound of 0.036 obtained from the UPLC/(−)ESI-TOFMS data as discussed above.

In general, the procedures for compositional analysis determined from high-resolution AMS data are still relatively new, and further studies of the technique are necessary to fully understand the data acquired using this complex instrument. For example, calibrations of compositional ratios performed here are based on AMS data from Aiken et al.,⁶³ which likely possess a different molecular composition than that of the current experiments. To achieve more accurate ratios, the ionization efficiency of each oxidation product by atomizing standards into

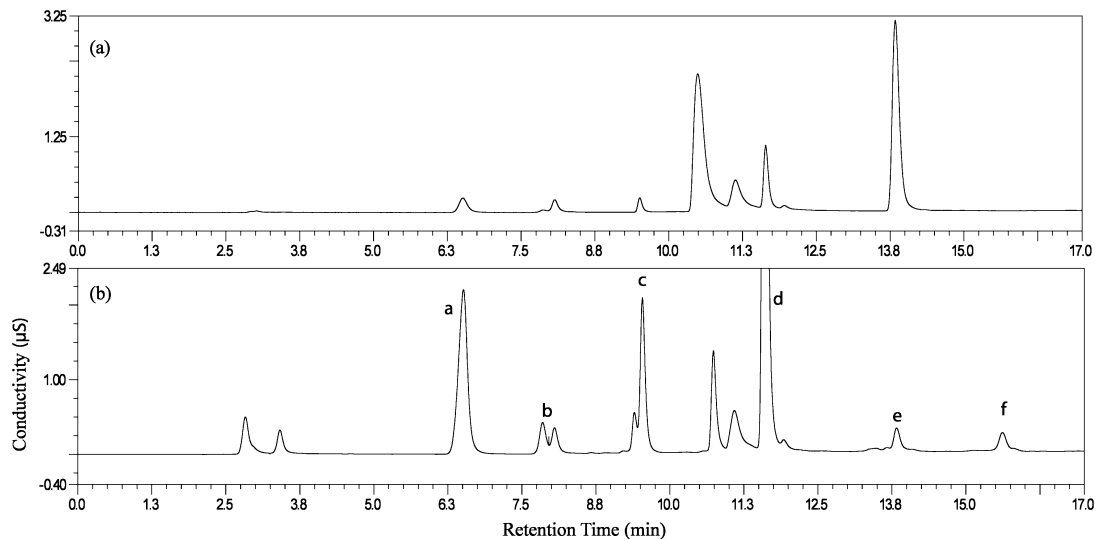


Figure 5. Chromatograms obtained by the PILS/IC technique. The top panel shows a 2 ppm standard of phthalic acid. The bottom panel shows a representative chromatogram of a PILS sample collected under high-NO_x conditions in the presence of ammonium sulfate seed (Experiment 7). Peak assignments are: a-chloride, b-nitrite, c-nitrate, d-sulfate, e-phthalic acid, f-unidentified peak (see text).

Photooxidation of Naphthalene

the AMS instrument need to be investigated or alternatively, a much larger database of structures would need to be assembled. More work needs to be performed to fully characterize the appropriateness of the compositional ratios acquired by this technique, particularly for the N-containing compounds which have received less attention.

The high- NO_x naphthalene SOA chemically characterized through the filter sampling methods exhibits an average atomic O/C ratio of 0.48. This ratio is largely consistent with the measurements from the HR-ToF-AMS technique, from which an overall O/C ratio of 0.51 ± 0.17 is detected. Atomic H/C ratios of 0.83 calculated from the filter data are also in agreement with the HR-ToF-AMS value of 0.9 ± 0.10 , and as stated above, the N/C ratios are also in relative agreement. The implications of the agreement of the O/C, H/C, and N/C ratios between these two analytical techniques is that the 53% of the total SOA mass that has been chemically characterized is an excellent representation of the chemical composition and oxidation level of the entire high- NO_x naphthalene SOA.

The total peroxide measurement based on the iodometric spectroscopic method indicates that under high- NO_x conditions ~28% of the total SOA mass can be attributed to organic peroxides (i.e., ROOH and/or ROOR). Contributions of organic peroxides are calculated by determining the molar concentration of peroxides in the solution. The measured concentration of peroxides obtained by absorption at 470 nm is converted to $\mu\text{g m}^{-3}$ using the known solution volume, molar-weighted average mass, and the volume of chamber air sampled. The molar-weighted average MW is determined by multiplying the MW of each product by the product mole fraction and summing over the individual products. For the high- NO_x system, we have taken a molar-weighted average mass of the chemically characterized SOA constituents listed in Tables 2S–4S (Supporting Information) and assumed this to be the average MW of the unknown organic peroxide structures. The assumption that this average MW would be representative for the unknown organic peroxides is supported by the similar O/C, N/C, and H/C ratios found using both the chemically characterized filter data and the total aerosol HR-ToF-AMS measurements. For the high- NO_x case, the molar-weighted average mass is determined to be 172 amu. As will be discussed subsequently, we believe this is a conservative estimate of the average peroxide mass. If the actual average mass of the peroxides is indeed higher than the assumed mass of 172 amu, then the contribution from peroxides to the total SOA mass would increase. It should be noted that the iodometric spectroscopic method provides no detailed chemical characterization of the quantified organic peroxide content.

3.2. Low- NO_x Conditions.

3.2.1. Chemical Characterization of Low- NO_x Gas-Phase Oxidation Products. A representative (+)CIMS mass spectrum obtained for naphthalene photooxidation under low- NO_x conditions is shown in Figure 6. This mass spectrum was taken at the same fraction of naphthalene reacted as that for the high- NO_x experiment previously shown in Figure 2, and thus the extents of reaction are similar. Whereas the tentatively identified products are the same as those observed under high- NO_x conditions, the relative intensities of the identified compounds are substantially different. In the low- NO_x case, the intensities of the ring-retaining products (e.g., naphthol, naphthoquinone, and epoxyquinone), as denoted by blue mass spectral peaks in Figure 6, are all significantly greater than those found under high- NO_x conditions. Nevertheless, the m/z 161 signal continues to dominate the overall (+)CIMS mass spectrum. When compared with data from both the high- NO_x experiments and

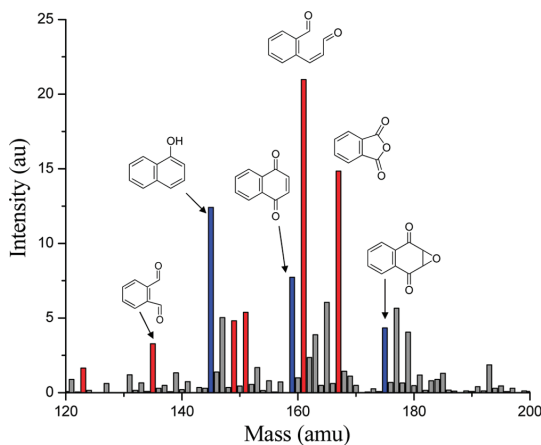


Figure 6. (+)CIMS mass spectrum taken at 70% reacted naphthalene under low- NO_x conditions. Red data indicate ring-opening products. Ring-retaining products are indicated in blue.

from injection of the synthesized standard, it is found that the GC retention times, mass spectra, and exact masses (i.e., chemical formulas) obtained using the GC/EL-TOFMS technique match, thus confirming that the compound observed at m/z 161 in the (+)CIMS mass spectrum under low- NO_x conditions is 2-formylcinnamaldehyde.

3.2.2. Chemical Characterization of Low- NO_x SOA. An UPLC/(−)ESI-TOFMS BPC obtained for a typical low- NO_x naphthalene SOA experiment is shown in Figure 7. Detailed comparison of this chromatogram and the high- NO_x BPC (Figure 3) demonstrates that the aerosol compositions are quite similar. All of the chromatographic peaks are also observed in the naphthalene high- NO_x SOA samples. No N-containing SOA constituents are observed under low- NO_x conditions due to the lack of NO and NO_2 addition reactions. Under low- NO_x conditions, we have been able to chemically characterize ~68% of the SOA mass, as compared to the ~53% identified in the high- NO_x regime. The increase in speciation is the result of a substantial enhancement in the concentration of the acidic species under low- NO_x conditions, with consistent peroxide contributions under both NO_x conditions. As shown in Table 3 and in Supporting Information, the fractions of total SOA mass attributed to phthalic acid and hydroxy phthalic acid, for example, increase by factors of 2 and 3, respectively. Similar increases are observed for benzoic acid, hydroxy benzoic acid, cinnamic acid, and dihydroxy cinnamic acid. The ring-retaining compounds are present in low- NO_x SOA samples, but we cannot remark on their relative abundance compared to the high- NO_x case, owing to the fact that standards are often not available, and these components were not quantified. Detection efficiencies for these nonacidic ring-retaining compounds are lower than those of the acidic ring-opening compounds. Hydroxy cinnamic acid (see Table 3, MW 164) was the only additional compound identified specific to the low- NO_x regime. The atomic O/C compositional ratio from filter sampling methods is 0.50, and the H/C ratio is 0.82. O/C and H/C ratios determined from the HR-ToF-AMS technique are 0.64 ± 0.19 and 0.89 ± 0.1 , respectively.

The total organic peroxide contribution was determined in the same manner as that carried out for the high- NO_x experiments as detailed in Section 3.1.2. The molar-weighted average mass was determined to be slightly higher than that of the high-

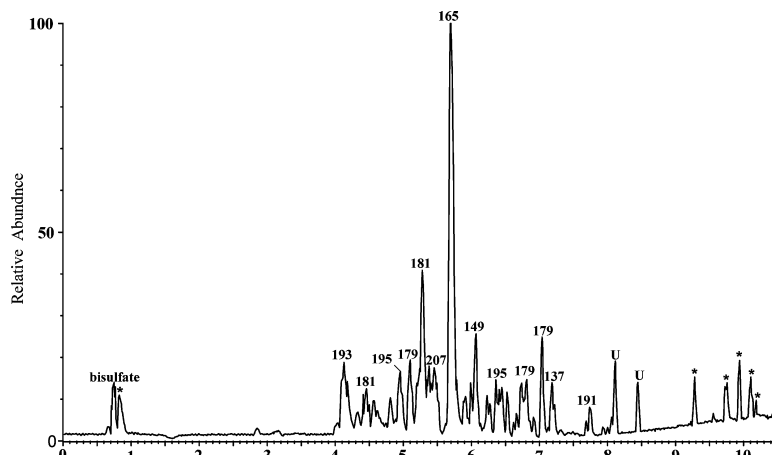


Figure 7. UPLC/(-)ESI-TOFMS base peak ion chromatogram (BPC) of a representative naphthalene low- NO_x SOA sample (Experiment 3). All major chromatographic peaks are marked with their corresponding $[M - H]^-$ base peak ions. Chromatographic peaks designated with an asterisk, *, were also observed on a blank filter, and they are not considered high- NO_x SOA constituents. Major chromatographic peaks that remain uncharacterized in this study are designated as: U.

NO_x SOA at 174 amu due to the increased contribution from larger acids, for example, hydroxy phthalic acid (MW 182 and observed by the UPLC/(-)ESI-TOFMS technique at m/z 181). The total peroxide contribution under low- NO_x conditions is calculated to be $\sim 26.2\%$ of the total SOA mass. This is similar to the 28% contribution found in the high- NO_x case. As in the high- NO_x case, we believe this to be a lower limit of the total peroxide contribution to the SOA mass.

4. Discussion

4.1. High- NO_x Conditions.

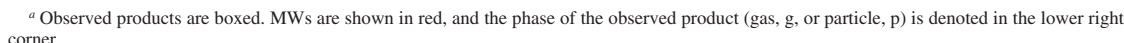
4.1.1. High- NO_x Gas-Phase Chemistry. The gas-phase mechanism of naphthalene photooxidation has been the subject of considerable study. Our present findings can be viewed within the context of this prior work. We concentrate first on the high- NO_x case, an atmospherically interesting situation owing to the coemissions with other anthropogenic sources and the relatively short lifetime of naphthalene in the urban atmosphere.^{43,75–78} Proposed formation mechanisms of the major high- NO_x naphthalene gas-phase products are provided in Scheme 1. The gas-phase photooxidation products detected are boxed, and the MWs of the identified products are highlighted in red. The mechanism presented here does not incorporate all of the chemically characterized products; a complete list of identified products can be found in Tables 2S–4S (Supporting Information). The majority of the gas-phase mechanism has been previously established.^{43,45,47,72,79,80} Qu et al.⁸¹ have performed theoretical calculations exploring the OH oxidation of naphthalene in the presence of O_2 and NO_x , and have detailed much of the gas-phase reaction dynamics. As determined by Wang et al.,⁴⁷ 68% of the OH addition occurs at the C_1 position to form the hydroxycyclohexadienyl radical. The 1-hydroxycyclohexadienyl radical lies 10 kcal mol^{-1} lower in energy than the 2-isomer.⁸¹ The preference for addition at the 1-site is supported by the fact that 2-nitronaphthalene is ~ 2 times more abundant than the 1-nitronaphthalene isomer.⁸⁰ The addition, the 1-site also determines the formation of the epoxide, although 2-formylcinnamaldehyde could be formed from either the 1- or 2-hydroxycyclohexadienyl radical.

The OH-naphthalene adduct reacts with either NO_2 or O_2 . GC/FID data combined with GC/MS-negative ion chemical

ionization (NCI) data from other chamber studies⁸⁰ suggest that the NO_2 and O_2 reactions with the OH-naphthalene adduct may be of equal importance for NO_2 mixing ratios in the range of 60 ppb. The NO_2 mixing ratio used in the present high- NO_x experiments is ~ 80 ppb, so these pathways should be of roughly equal importance in the present experiments. A detailed description of the importance of the NO/NO_2 in these experiments is previously discussed in Section 3.2.1.

The N-containing compounds (i.e., nitronaphthalenes and nitronaphthols) formed through the NO_2 reaction pathway are of particular interest due to their mutagenic properties.^{50,51} In extensive studies of the nitronaphthalene isomers, along with other nitroarene compounds, Arey and co-workers^{43,48,73,80,82} have found that both 1- and 2-nitronaphthalene isomers form during daytime conditions by OH reaction of naphthalene, but actually concentrations of these compounds reach a maximum at night due to N_2O_5 chemistry.⁴⁸ The major loss process for 1- and 2-nitronaphthalene under atmospheric conditions is photolysis, with photolytic lifetimes on the order of 2 h.⁷³ Photolysis is approximately an order of magnitude more important than OH reaction, for which the reaction rate coefficients are 5.4×10^{-12} $\text{cm}^3 \text{ molecule}^{-1} \text{ s}^{-1}$ and 5.6×10^{-12} $\text{cm}^3 \text{ molecule}^{-1} \text{ s}^{-1}$ for the 1- and 2-nitro isomers, respectively. Arey et al.⁷³ also suggest that 1-nitronaphthalene is the precursor to the 1,4-naphthoquinone product, which is formed through a photolysis pathway, denoted in Scheme 1 by an open arrow. These OH rates are consistent with the work of Bunce et al.⁴⁵ for which lifetimes of 20–34 h against OH reaction for the 1-nitronaphthalene and 2-nitronaphthalene isomers, respectively, were calculated using the same OH concentration, but neglecting the photolysis pathway.

Formation of ring-opening compounds is consistent with decomposition of the alkoxy (RO) radicals formed from the $\text{RO}_2 + \text{NO}$ pathway,⁷² which leads to 2-formylcinnamaldehyde (MW 160) and observed by the (+)CIMS technique at m/z 161, the precursor to the majority of the ring-opening products found in Scheme 2. 2-formylcinnamaldehyde is detected as both *E*- and *Z*- isomers and is the major gas-phase product observed under high- NO_x conditions.^{45,71,72} Sasaki et al.⁷² suggested a combined yield for the cinnamaldehyde *E*- and *Z*- isomers of 35%. Although two further compounds with MW 160 are identified,



An alternate route to the formation of 2-formylcinnamaldehyde proposed by Qu et al.⁸¹ involves a hydride shift from the alcohol group on the naphthol peroxy intermediate to form hydroperoxy intermediate. Subsequent loss of OH and breaking of the C₁–C₂ bond yields the 2-formylcinnamaldehyde. The authors calculate that this reaction is exothermic by 24.88 kcal mol⁻¹. The two mechanisms for the formation of 2-formylcinnamaldehyde are shown in Scheme 3. The first mechanism would result in the formation of NO₂ and HO₂, whereas the second mechanism would result in the formation of OH. It is not possible to confirm one mechanism over the other from our data, and both mechanisms remain as plausible routes to the formation of the major 2-formylcinnamaldehyde oxidation product. 2-Formylcinnamaldehyde undergoes further reaction as shown in Scheme 2 to form ring-opening products, including phthalic anhydride, phthalic acid, and phthalaldialdehyde.

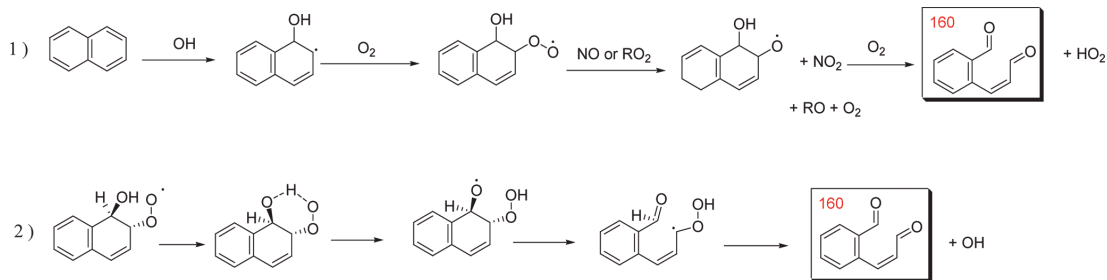
Previous studies present evidence that photolysis plays a significant role in the loss processes for the 2-formylcinnamaldehyde isomers, competing with the various reaction pathways. Wang et al.⁴⁷ have detailed the various loss processes for 2-formylcinnamaldehyde and report a ratio of OH reaction to photolysis of 1.8 under blacklamp photolysis conditions with corrections for wall-loss. A further study by Nishino et al.⁷¹ reexamined the competing pathways of 2-formylcinnamaldehyde OH-reaction versus photolysis. Nishino et al. suggest a yield

Scheme 4

Reaction scheme showing the degradation pathways of 2-oxo-2-phenylacetaldehyde (160) and its intermediates:

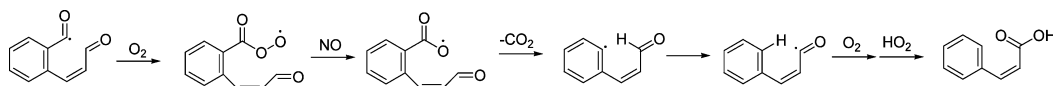
- 160** (2-oxo-2-phenylacetaldehyde, g) reacts with OH to form a radical intermediate, which then reacts with NO to form **134** (2-oxo-2-phenylacetic acid, g, p).
- 160** reacts with O_2 to form **134** and HO_2 and O .
- 160** reacts with O_x to form **148** (2-oxo-2-phenylacetic acid, p) or **176** (2-oxo-2-phenylacetic acid, g, p).
- 148** reacts with O_2 to form **150** (2-oxo-2-phenylacetic acid, p) or **164** (2-oxo-2-phenylacetic acid, p).
- 164** reacts with O_2 to form **180** (2-oxo-2-phenylacetic acid, p).
- 150** reacts with O_2/HO_2 to form **166** (2-oxo-2-phenylacetic acid, p) or **182** (2-oxo-2-phenylacetic acid, p).
- 166** reacts with H_2O to form **182**.

SCHEME 3: Suggested Mechanism for the Formation of 2-Formylcinnamaldehyde^a

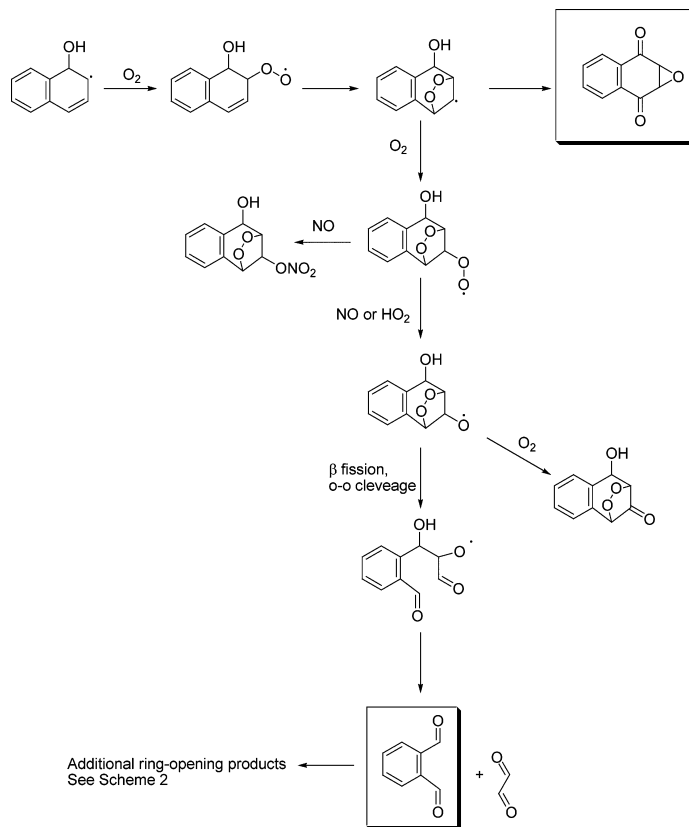


4.1.2. High-NO_x SOA Chemistry. Two previous studies have addressed the chemical composition of SOA formed from the photooxidation of naphthalene.^{46,84} We present here detailed quantitative analysis on the chemical composition and potential reaction pathways relevant to naphthalene high-NO_x SOA formation. The compounds identified from the UPLC/(−)ESI-TOFMS analysis of filter samples yield atomic O/C, N/C, and

SCHEME 4: Possible Mechanism for the Formation of C7 and C9 Compounds



SCHEME 5: Proposed Reaction Mechanisms for Bicyclic Peroxide Structure



H/C ratios that are in agreement with bulk measurements from HR-ToF-AMS samples. This indicates that the chemical nature of the characterized SOA constituents is a good representation of the bulk aerosol formed from the photooxidation of naphthalene under high- NO_x conditions. The chemical mechanisms shown in Schemes 1 and 2 demonstrate how the gas-phase oxidation products are likely to evolve by further oxidation to form the components identified in the aerosol phase. The “g” and “p” superscripts associated with each product denote the phase of the component. A minor fraction of the SOA mass is attributed to the N-containing compounds such as nitronaphthols. The chemically characterized portion of the aerosol, which we assume to be representative of the bulk aerosol based on detailed composition measurements, is primarily composed of single-ring (ring-opening) acids (e.g., formylcinnamic acid and further oxidized compounds from phthalic acid).

We have performed calculations determining the average number of carbonyls/molecule for the SOA in order to compare with previous FTIR measurements. Dekermenjian et al.⁸⁴ reported an average of 3.2 carbonyl/molecule based on the assumption that the average molecule possesses a 10 carbon backbone. As shown in Table 3, many of the compounds with

significant yield possess C8 structures, thus calling into question the appropriateness of assuming a 10-carbon backbone. In order to determine the average number of carbonyls/molecule we have counted the number of carbonyl groups on each identified product, and weighted this number by mole fraction, to establish that the average structure possesses ~ 1.25 carbonyls/molecule. We believe the average we report here is an accurate representation of the degree of molecular oxidation, as it is based on identified structures for which the bulk composition is known. In comparison, the chemical composition determined by FTIR will be strongly dependent on the length of the carbon backbone, the accuracy of the composition calibrations, and the form of the carbonyl group (e.g., acidic, aldehydic, or ketone).⁸⁵

Organic peroxides are found to contribute $\sim 28\%$ of the total high- NO_x SOA mass. We propose that a mechanism for the formation of these compounds may occur through the formation of a bicyclic peroxy radical as shown in Scheme 5. Analogous reaction pathways have been examined in single-ringed aromatic hydrocarbons (SAH). For toluene, benzene, and *m*-xylene it was proposed that isomerization of the primary RO_2 radical to form the bridged bicyclic structure is faster than the competing reaction with NO_2 , and a reaction with NO to form the RO

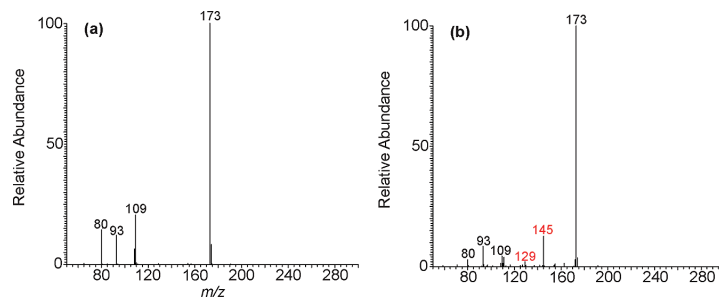


Figure 8. (–)ESI-ITMS MS² of *m/z* 173 collected via direct infusion analysis from (a) a 20 ppm 4-hydroxybenzene sulfonic acid standard and from (b) a naphthalene high-NO_x SOA sample (Experiment 6). Due to the generation of these MS² spectra via direct infusion, isobaric *m/z* 173 ions were analyzed simultaneously from the high-NO_x SOA sample. As a result, red ions highlighted in (b) are not due to the hydroxybenzene sulfonic acid. Product ions observed at *m/z* 93 and 109 are due to neutral losses of SO₂ and SO₃, respectively, which are neutral losses characteristic of aromatic sulfonates. The product ion observed at *m/z* 80 is due to the production of SO₃[–], which is also a characteristic ion of aromatic sulfonates. The hydroxybenzene sulfonic acids lack the presence of a *m/z* 97 ion (i.e., HSO₄[–]) in their MS² spectra, which is a characteristic product ion of organosulfate functional groups (–ROSO₃).

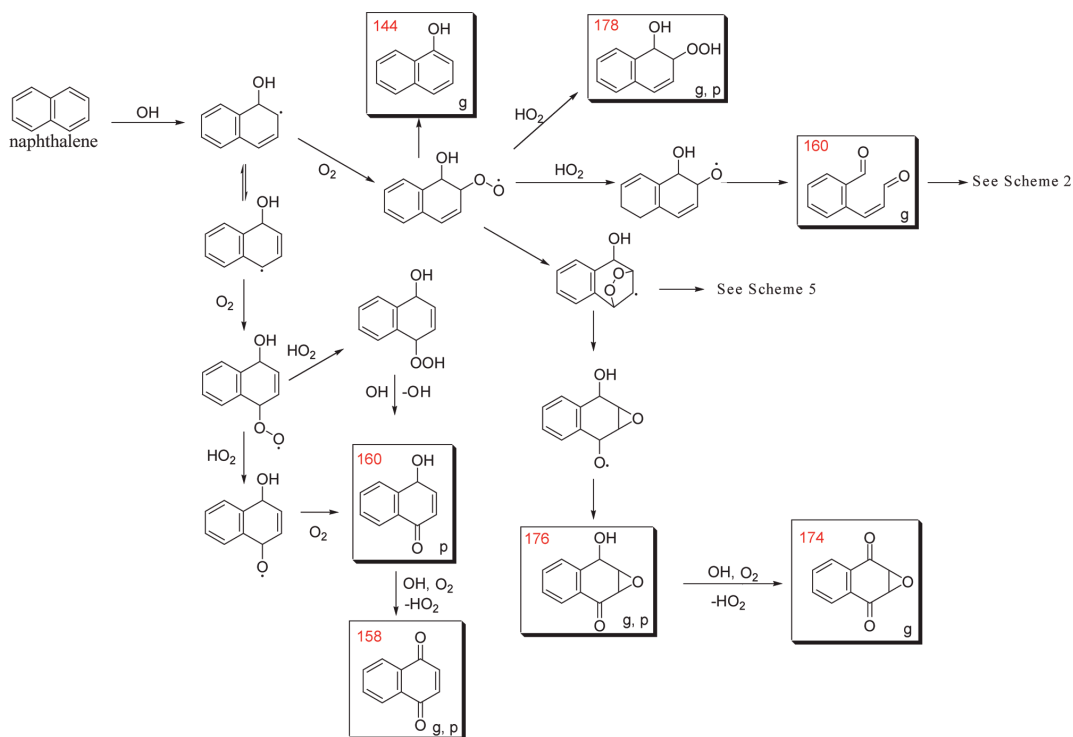
radical may only occur after O₂ addition.⁸⁶ The simplest bicyclic structure from naphthalene, which has molar mass of 192 amu, is shown below in Scheme 5. Thus, structures related to the bicyclic RO₂ radical would yield masses of 192 or higher, and the contributions from peroxides based on the average yield-weighted calculations detailed in Section 3.1.2 would be underestimated. If one uses the single-ringed aromatic compounds as exemplary of the PAH products, then a reasonable mechanism for both peroxides and ring-opening products can be determined as shown in Scheme 5. The initial naphthalene–OH adduct can either undergo hydrogen abstraction through reaction with O₂ to form naphthol or can react with O₂ to form the RO₂ radical. For benzene, master equation calculations suggest that formation of the phenolic compound accounts for 55–65% of the reaction mechanism, and the formation of the bicyclic peroxy radical is the other major pathway.⁸⁷ Resonance fluorescence studies for several aromatic species have also shown that the OH-aromatic adduct reacts preferentially with O₂ over both NO₂ and NO to form either the alcohol or the bicyclic peroxide structure, and reaction with NO can only occur after the initial addition of O₂.⁸⁶ Reactions of the aromatic-peroxy adduct with NO to form the alkoxy radical are found to be of minor importance for the SAH.^{86,88} The bicyclic peroxy radical that forms from the aromatic–OH reaction with O₂ can isomerize to yield an epoxide; however, this route has been suggested based on master equation calculations⁸⁷ for benzene, and based on ab initio calculations⁸⁶ for toluene, to be of minor importance in the atmosphere, although the epoxide formed from this type of mechanism has been detected in the experiments reported here. For benzene, the pathway to the bicyclic RO₂ structure has a 10 kcal mol^{–1} barrier and is exothermic by ~69 kcal mol^{–1}. Comparatively, the barrier to epoxide formation is 74 kcal mol^{–1} and the reaction is exothermic by 59 kcal mol^{–1}.⁸⁷ Once the bicyclic RO₂ radical forms, the radical termination steps can lead to a carbonyl, an organic nitrate, or an RO radical, with the latter undergoing β-fission followed by cleavage of the bridge O–O bond to form ring-opening products. For the SAH, the primary fate of the bicyclic radical is isomerization to form the epoxide or reaction with O₂ to lead to ring-opening products. We include the route through reaction of the alkoxy radical with O₂ to form the carbonyl merely for completeness, but this should be a very minor channel.

Both the mechanism through the bicyclic structure (Scheme 5) and the mechanism shown for the formation of phthalaldehyde in Scheme 2 are supported by the observed concur-

rent growth of glyoxal.⁴⁷ However, reaction through the bicyclic mechanism generates phthalaldehyde and glyoxal as first generation products, while further reaction through 2-formylcinnamaldehyde (Scheme 2) leads to second-generation glyoxal and phthalaldehyde. The bicyclic structure to form ring-opened products has been extensively studied for the single-ringed aromatics,⁸⁹ but to the best of our knowledge, has only been suggested in the pathway to epoxide formation for the PAH compounds. Given that about 70% of the 2-formylcinnamaldehyde was found to remain at the completion of the chamber experiments, formation of the ring-opening products through an alternate pathway may be of significance. Further mechanistic studies on the reaction pathways of bicyclic structures related to PAHs could yield important insights into the further gas-phase reactions of this class of compounds.

In addition to the ring-opening and ring-retaining structures previously outlined, an organic sulfonic acid (R–SO₃), which was characterized as hydroxylbenzene sulfonic acid using an authentic standard, is observed here in naphthalene SOA produced under both high- and low-NO_x conditions in the presence of neutral ammonium sulfate seed aerosol. Comparisons of these mass spectra are displayed in Figure 8. Product ions observed at *m/z* 93 and 109 are due to neutral losses of SO₂ and SO₃, respectively. These neutral losses are characteristic of aromatic sulfonates.⁹⁰ The product ion observed at *m/z* 80 is due to the production of SO₃[–], which is also a characteristic ion of aromatic sulfonates.^{91,92} The hydroxylbenzene sulfonic acids lack the presence of a *m/z* 97 ion (i.e., HSO₄[–]) in their MS² spectra, which is a characteristic product ion of organosulfate functional groups (–ROSO₃).^{29,32,59} The absence of this peak clearly suggests that the product identified cannot be an organosulfate. In combination with the accurate mass measurements and similar retention times, the comparison of these MS² spectra further supports the identification of hydroxylbenzene sulfonic acids in naphthalene low- and high-NO_x SOA formed in the presence of ammonium sulfate seed. The formation of this product requires reaction with the ammonium sulfate seed, as the seed is the only source of sulfur in the system; however, the mechanism by which an organic sulfonic acid would be produced remains unclear. Methyl sulfonate has been reported in marine layer aerosol due to the oxidation of dimethyl sulfide.^{93–95} The presence of sulfonate compounds known as of linear alkylbenzene sulfonates (LAS) has been observed in river and seawater⁹⁶ as well. LAS compounds, which are used as surfactants in the manufacturing of cleaning products,⁹⁷ are

SCHEME 6: Proposed Low- NO_x Mechanism for the Formation of Ring-Retaining Products and 2-Formylcinnamaldehyde (MW 160) under Low- NO_x Conditions^a



^a Observed products are boxed. MWs are shown in red, and the phase of the observed product (gas, g, or particle, p) is denoted in the lower right corner.

found in these aquatic systems due to incomplete removal from wastewaters. Most recently, Altieri et al.⁹⁸ have observed the presence of sulfonates in precipitation samples. The presence of sulfonates in the environment due to pollution sources does not yield insights into the generation of these compounds in our chamber studies. Nevertheless, the photooxidation of PAHs (e.g., naphthalene) in the presence of sulfur-containing aerosols might yield an additional source of sulfonates found in the environment.

4.2. Low- NO_x Conditions.

4.2.1. Low- NO_x Gas-Phase Chemistry. Although the major gas-phase products observed under low- NO_x conditions are similar to those under high- NO_x conditions, the intensities of the resultant compounds differ dramatically. Scheme 6 shows the proposed mechanism for the formation of the identified products under low- NO_x conditions. Under low- NO_x conditions, the ring-opening products can be formed mechanistically through $\text{RO}_2 + \text{RO}_2$ or $\text{RO}_2 + \text{HO}_2$ pathways. Given the high concentrations of HO_2 prevalent in these chamber studies, the $\text{RO}_2 + \text{RO}_2$ route is calculated to be of minor importance compared to $\text{RO}_2 + \text{HO}_2$ reactions. A simple kinetic simulation similar to those performed for SAH,¹³ indicates that in order for $\text{RO}_2 + \text{RO}_2$ mechanisms to be competitive with $\text{RO}_2 + \text{HO}_2$ reactions, $\text{RO}_2 + \text{RO}_2$ rate constants would need to be at least a factor of 10 larger than $\text{RO}_2 + \text{HO}_2$ rate constants based on relative concentrations of RO_2 and HO_2 found in the chamber. From the master chemical mechanism (MCM) version 3.1 it is found that $k_{(\text{RO}_2+\text{HO}_2)}$ are generally on the order of $2.0 \times 10^{-11} \text{ cm}^3 \text{ molecule}^{-1} \text{ s}^{-1}$, whereas $k_{(\text{RO}_2+\text{RO}_2)}$ are no more than $1.0 \times$

$10^{-12} \text{ cm}^3 \text{ molecule}^{-1} \text{ s}^{-1}$, indicating that $\text{RO}_2 + \text{HO}_2$ pathways should dominate over $\text{RO}_2 + \text{RO}_2$ reactions under our experimental conditions.

We also acknowledge that a different pathway for the 1,4-naphthoquinone product under low- NO_x conditions may be possible. In their study of the OH-initiated photooxidation of naphthalene, Qu et al.⁸¹ predict that the quinone is formed by addition of HO_2 to 1-naphthol followed by reaction with O_2 to form the 1,4-carbonyl peroxy naphthalene intermediate. Two subsequent reactions with HO_2 yield 1,4-naphthoquinone and OH radical. The overall reaction is exothermic by -58.49 kcal/mol . This type of HO_2 mechanism has not been well established, and reaction rates have not been reported, thus determining the atmospheric importance of such a mechanism is not possible, although it is energetically plausible.

4.2.2. Low- NO_x SOA Composition Chemistry. Under low- NO_x conditions $\sim 68\%$ of the SOA mass has been identified, of which 26.2% is associated with organic peroxide compounds, and the remaining 42% is chemically characterized at the molecular level in Table 3 (and Tables 5S–7S) with dominant contributions coming from acids. Under low- NO_x conditions a significant enhancement in the formation of acids is observed. As shown in Table 3, the contribution of hydroxyphthalic acid to the overall SOA mass increases from 3% in high- NO_x condition to 9% for the low- NO_x case. The increase in the concentration of acidic species is expected in the low- NO_x case as $\text{RO}_2 + \text{HO}_2$ chemistry dominates over the formation of alkoxy radicals in the absence of NO. However, the formation of alkoxy radicals through an $\text{RO}_2 + \text{HO}_2$ route still leads to

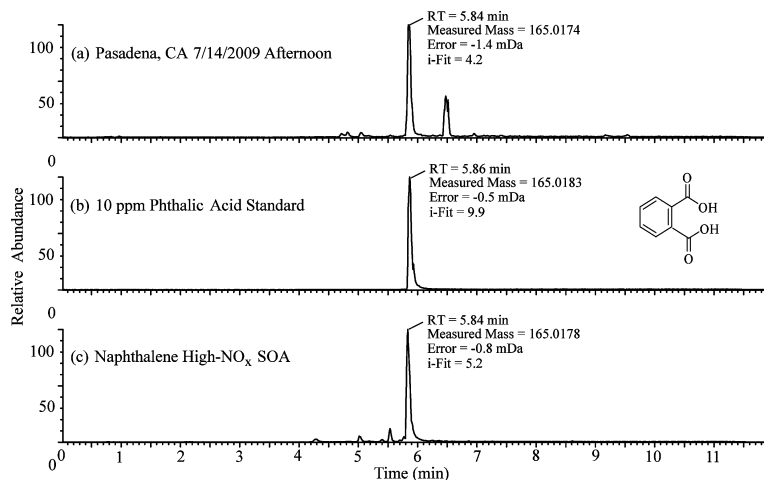


Figure 9. UPLC/(-)ESI-TOFMS EICs of m/z 165 from (a) ambient samples collected in Pasadena, CA, (b) a 10 ppm phthalic acid standard, and (c) naphthalene high- NO_x experiments (Experiment 6).

the presence of ring-opening species, as does the bicyclic mechanism shown in Scheme 5. The 28% of SOA mass attributed to organic peroxides, along with the enhancement of acidic species, indicates the importance of $\text{RO}_2 + \text{HO}_2$ reactions. The further reaction of bicyclic RO_2 radicals may contribute significantly to the generation of ring-opening products, the epoxide, and organic peroxide species. O/C ratios from the filter sampling method are slightly higher than in the high- NO_x data (0.50 vs 0.48, respectively), as is expected given the enhancement of acidic species. AMS data shows that the O/C ratios and H/C ratios are also slightly higher in the low- NO_x experiments, though still within error bars when compared to the high- NO_x experiments. These higher compositional ratios obtained from the AMS technique appear to not only be an effect of increasing acid concentration, but also of aging. Owing to the lower OH concentration achieved in the low- NO_x experiments, longer reaction times are required to reach a constant aerosol volume, thus more oxidation may occur in the aerosol, though the observed effect is small.

4.3. Atmospheric Significance of Naphthalene SOA: Identification of Potential Ambient SOA Tracers in Urban Atmospheres. Urban aerosol filter samples collected in Birmingham, AL and in Pasadena, CA, were examined for the presence of naphthalene SOA constituents chemically characterized in the present study (Table 3). The UPLC/(-)ESI-TOFMS data obtained from the urban aerosol samples are compared to the laboratory-generated high- NO_x naphthalene SOA. Upon detailed comparison of the UPLC/(-)ESI-TOFMS BPCs obtained from both the laboratory-generated and ambient organic aerosol samples, it becomes evident that several of naphthalene high- NO_x SOA constituents characterized in the present study are observed in the urban aerosol samples. Figure 9 shows the UPLC/(-)ESI-TOFMS extracted ion chromatograms (EICs) of m/z 165 obtained from an urban aerosol sample collected from Pasadena, CA, a 10 ppm phthalic acid authentic standard, and a typical naphthalene high- NO_x photooxidation experiment, respectively. The comparison of these 3 EICs suggests that phthalic acid may be a potential ambient naphthalene SOA tracer

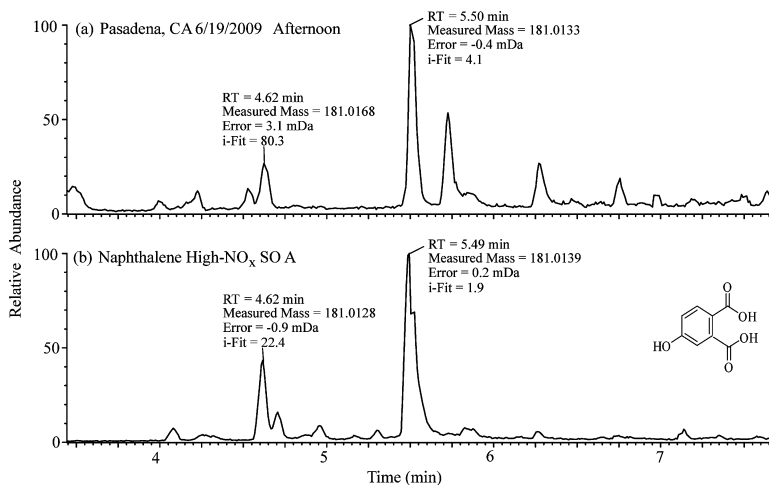


Figure 10. UPLC/(-)ESI-TOFMS EICs of m/z 181 from (a) ambient samples collected in Pasadena, CA and (b) naphthalene high- NO_x experiments (Experiment 6).

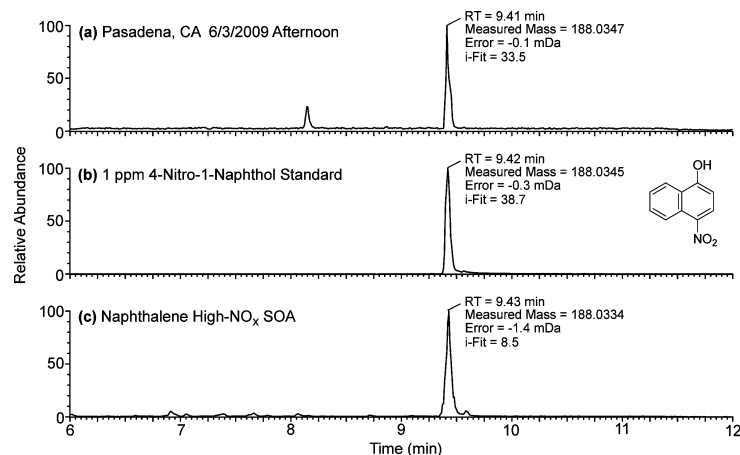


Figure 11. UPLC/(-)ESI-TOFMS EICs of m/z 188 from (a) ambient samples collected in Pasadena, CA, (b) a 1 ppm standard of 4-nitro-1-naphthol, and (c) naphthalene high- NO_x experiments (Experiment 6).

that could be used in a SOA source apportionment methods.^{99,100} Additionally, Figure 3S (Supporting Information) shows the UPLC/(-)ESI-TOFMS EICs of m/z 165 obtained for a typical naphthalene high- NO_x SOA sample, a 10 ppm phthalic acid standard, and an urban aerosol sample collected from Birmingham, AL. The use of phthalic acid as a potential tracer compound for naphthalene photooxidation is tempting due to the large quantities ($\sim 14 \text{ ng m}^{-3}$) found in the ambient aerosol sample collected from Birmingham, AL. In comparison, 2-methyltetrols, which are ambient tracer compounds for isoprene SOA, have been measured between 200 pg m^{-3} and 365 ng m^{-3} during the summer in aerosol samples collected from many forested locations.¹⁰¹ Since isoprene is the most abundant nonmethane hydrocarbon emitted into the atmosphere annually, the mass concentrations of phthalic acid found in urban aerosol samples analyzed in the present study are of some significance. In fact, phthalic acid and other dicarboxylic acids have been previously proposed as tracers.^{102,103} However, because phthalic acid/anhydride is known to be formed from a wide variety of sources including sewage sludge^{104,105} and plastic processing,¹⁰⁶ its use as a tracer is of questionable value.

Figure 10 shows the UPLC/(-)ESI-TOFMS EICs of m/z 181 obtained in a typical naphthalene high- NO_x SOA sample and in an urban aerosol sample collected from Pasadena, CA. The chromatographic peaks eluting at 5.45 min have the same elemental compositions (i.e., molecular formulas) as determined by the accurate mass measurements. This strongly indicates that the hydroxy phthalic acid product characterized in Table 3 can be used as an ambient tracer compound for naphthalene SOA; however, it cannot be ruled out that, as with phthalic acid, other sources may contribute to the formation of hydroxy phthalic acid in ambient aerosol. As a result, we cannot suggest that hydroxy phthalic acid be used solely as an ambient tracer compound for naphthalene SOA.

Another naphthalene high- NO_x SOA constituent found in the urban aerosol samples is 4-nitro-1-naphthol (MW 189). Figure 11 shows the UPLC/(-)ESI-TOFMS EICs of m/z 188 obtained for an urban aerosol sample collected from Pasadena, CA, a 1 ppm 4-nitro-1-naphthol authentic standard, and a typical naphthalene high- NO_x SOA sample. The comparison of these EICs clearly demonstrates the presence of this naphthalene high- NO_x SOA compound in ambient aerosol. Additionally, Figure 4S

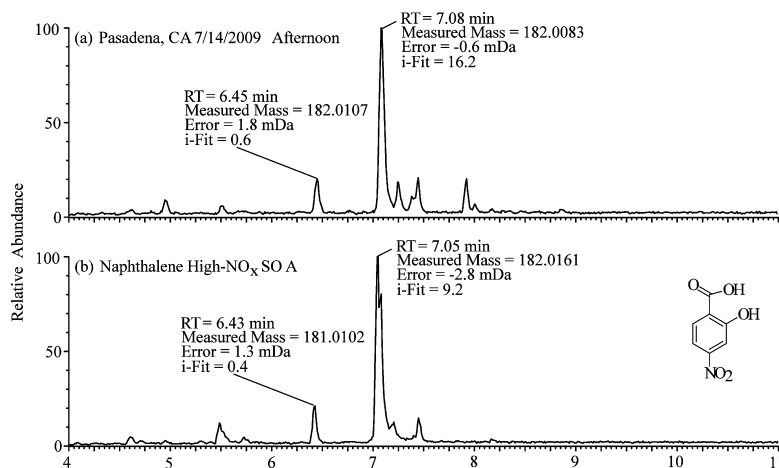


Figure 12. UPLC/(-)ESI-TOFMS EICs of m/z 182 from (a) ambient samples collected in Pasadena, CA and (b) naphthalene high- NO_x experiments (Experiment 6).

(Supporting Information) shows the UPLC/(−)ESI-TOFMS EICs of *m/z* 188 obtained for a typical naphthalene high-NO_x SOA sample, a 1 ppm 4-nitro-1-naphthol authentic standard, and an urban aerosol sample collected from Birmingham, AL, respectively. Concentrations of 4-nitro-1-naphthol from the Birmingham, AL site were found to be 1.6 ng m^{−3}, and the concentration of 4-nitro-1-naphthol collected from Pasadena, CA during summertime polluted conditions was 228 pg m^{−3}. This compound could prove to be an excellent ambient tracer for anthropogenic PAH chemistry. Apparent from the chamber studies, and Birmingham, AL and Pasadena, CA ambient aerosol samples, this compound, found at concentrations comparable to those of other common tracers (i.e., 2-methyltetrol), appears not to have been reported from alternate biogenic or anthropogenic sources. The added concern of N-containing naphthalene compounds, such as the 4-nitro-1-naphthol found in these ambient aerosol samples, as possible carcinogens makes these compounds of particular interest.

Comparison of the UPLC/(−)ESI-TOFMS EICs of *m/z* 182 found in Figure 12 demonstrate that the hydroxy nitrobenzoic acid with MW 183 characterized in the naphthalene high-NO_x SOA (Table 3) is also present in aerosol samples collected from Pasadena, CA. We note that this single-ring aromatic SOA constituent may also form in the atmosphere due to the photooxidation of SAHs (e.g., toluene). However, we have verified that naphthalene is a valid precursor to the presence of this compound in SOA. Since other SAHs and PAHs likely contribute to the formation of this compound in urban aerosol, it is likely not reasonable to use this compound solely as a naphthalene SOA tracer.

As a result of our detailed comparison of the laboratory-generated naphthalene high-NO_x SOA and the urban aerosol samples, we recommend that 4-nitro-1-naphthol might serve as a suitable ambient tracer for naphthalene SOA. It is worth mentioning that other compounds not highlighted here in this discussion were also observed in both the laboratory-generated and ambient aerosol, but these were concluded to be unsuitable ambient tracer compounds for naphthalene SOA; these include the following [M − H][−] ions identified in Table 3: *m/z* 137, 149, 154, 179, 193, and 209.

5. Conclusions

We report extensive studies on the gas- and particle-phase constituents produced from the OH-initiated photooxidation of naphthalene under both high- and low-NO_x conditions. These studies provide significant insights into the chemical mechanisms that lead to SOA formation. For the high-NO_x case, 53% of the SOA mass is chemically identified, of which organic peroxides constitute 28%. The comparison of O/C and H/C ratios between the off-line molecularly characterized analyses are in agreement with measurements from online bulk measurements suggesting that the chemically characterized portion of the aerosol is representative of bulk aerosol components. Additionally, hydroxybenzene sulfonic acid is observed in the aerosol phase for both the low- and high-NO_x cases, although a mechanism for the generation of this product is not established. Under low-NO_x conditions, ~68% of the SOA mass has been chemically identified, of which 26.2% is associated with organic peroxides. A significant enhancement in the formation of acids is observed relative to the high-NO_x case.

Naphthalene high-NO_x SOA constituents characterized in the present study are compared with urban aerosol samples collected from Birmingham, AL and Pasadena, CA, confirming the presence of SOA from naphthalene photooxidation in the urban

atmosphere. In particular, phthalic acid, hydroxy phthalic acid, 4-nitro-1-naphthol and hydroxy nitrobenzoic acid are observed in both the laboratory-generated high-NO_x SOA and the urban organic aerosols. Of these compounds, 4-nitro-1-naphthol appears to be a valid ambient organic tracer for naphthalene high-NO_x SOA.

Acknowledgment. This research was funded by the Office of Science (BER), US Department of Energy Grant No. DE-FG02-05ER63983, US Environmental Protection Agency STAR Research Assistance Agreement No. RD-83374901 and US National Science Foundation grant ATM-0432377. The Electronic Power Research Institute provided support for the SEARCH network field samples. The GC/TOF and CIMS instruments used in this study were purchased as part of a major research instrumentation grant from the National Science Foundation (ATM-0619783). Assembly and testing of the CIMS instrument was supported by the Davidow Discovery Fund. The Waters UPLC/(−)ESI-TOFMS (LCT Premier XT TOFMS) was purchased in 2006 with a grant from the National Science Foundation, Chemistry Research Instrumentation and Facilities Program (CHE-0541745). We thank J. Stockdill for synthesis of 2-formylcinnamaldehyde. We would also like to thank E. S. Edgerton of Atmospheric Research & Analysis (ARA), Inc., for providing the high-volume filter sampler, as well as providing detailed information on its operation procedures, used in the sampling of fine aerosols during PACO. This publication has not been formally reviewed by the EPA. The views expressed in this document are solely those of the authors and EPA does not endorse any products mentioned in this publication.

Note Added in Proof. We proposed the formation of ring-opening products by a bicyclic peroxy intermediate in the text and in Scheme 5. After this work was submitted the following paper came to our attention: Nishino, N.; Arey, J.; Atkinson R. *Environ. Sci. Technol.* **2009**, in press. Nishino et al. also suggest the formation of phthalaldehyde and glyoxal by the route in Scheme 5.

Supporting Information Available: Table 1S lists the chemicals employed in this study along with their purities. Tables 2S–7S display identification, quantification and (−)ESI-ITMS MS² information for experiments 2–8. EICs for selected photooxidation products observed using the GC/ESI-TOFMS technique are shown in Figure 1S. Figure 2S compares mass spectra for 2-formylcinnamaldehyde (MW 160) from injection of the standard and from chamber studies. Figures 3S and 4S compare ambient data collected in Birmingham, AL and samples collected in Pasadena, CA, with authentic standards. This material is available free of charge via the Internet at <http://pubs.acs.org>.

References and Notes

- (1) Kroll, J. H.; Seinfeld, J. H. *Atmos. Environ.* **2008**, *42*.
- (2) Volkamer, R.; Jimenez, J. L.; Martini, F. S.; Dzepina, K.; Zhang, Q.; Salcedo, D.; Molina, L. T.; Worsnop, D. R.; Molina, M. J. *Geophys. Res. Lett.* **2006**, *33*, 4.
- (3) Heald, C. L.; Jacob, D. J.; Park, R. J.; Russell, L. M.; Huebert, B. J.; Seinfeld, J. H.; Liao, H.; Weber, R. J. *Geophys. Res. Lett.* **2005**, *32*, 4.
- (4) de Gouw, J. A.; Middlebrook, A. M.; Warneke, C.; Goldan, P. D.; Kuster, W. C.; Roberts, J. M.; Fehsenfeld, F. C.; Worsnop, D. R.; Canagaratna, M. R.; Pszenny, A. A. P.; Keene, W. C.; Marchewka, M.; Bertman, S. B.; Bates, T. S. *J. Geophys. Res.* **2005**, *110*.
- (5) Claeys, M.; Graham, B.; Vas, G.; Wang, W.; Vermeylen, R.; Pashynska, V.; Cafmeyer, J.; Guyon, P.; Andreae, M. O.; Artaxo, P.; Maenhaut, W. *Science* **2004**, *303*, 1173.

- (6) Claeys, M.; Wang, W.; Ion, A. C.; Kourtchev, I.; Gelencsér, A.; Maenhaut, W. *Atmos. Environ.* **2004**, *38*, 4093.
- (7) Dommen, J.; Metzger, A.; Duplissy, J.; Kalberer, M.; Alfarra, M. R.; Gascho, A.; Weingartner, E.; Prévôt, A. S. H.; Verheggen, B.; Baltensperger, U. *Geophys. Res. Lett.* **2006**, *33*.
- (8) Edney, E. O.; Kleindienst, T. E.; Jaoui, M.; Lewandowski, M.; Offenberg, J. H.; Wang, W.; Claeys, M. *Atmos. Environ.* **2005**, *39*, 5281.
- (9) Kroll, J. H.; Ng, N. L.; Murphy, S. M.; Flagan, R. C.; Seinfeld, J. H. *Geophys. Res. Lett.* **2005**, *32*, L18808.
- (10) Kroll, J. H.; Ng, N. L.; Murphy, S. M.; Flagan, R. C.; Seinfeld, J. H. *Environ. Sci. Technol.* **2006**, *40*, 1869.
- (11) Surratt, J. D.; Murphy, S. M.; Kroll, J. H.; Ng, N. L.; Hildebrandt, L.; Sorooshian, A.; Szmigielski, R.; Vermeylen, R.; Maenhaut, W.; Claeys, M.; Flagan, R. C.; Seinfeld, J. H. *J. Phys. Chem. A* **2006**, *110*, 9665.
- (12) Szmigielski, R.; Surratt, J. D.; Vermeylen, R.; Szmigielska, K.; Kroll, J. H.; Ng, N. L.; Murphy, S. M.; Sorooshian, A.; Seinfeld, J. H.; Claeys, M. *J. Mass Spectrom.* **2007**, *42*, 101.
- (13) Ng, N. L.; Kroll, J. H.; Chan, A. W. H.; Chhabra, P. S. *Atmos. Chem. Phys.* **2007**, *7*.
- (14) Song, C.; Na, K. S.; Cocker, D. R. *Environ. Sci. Technol.* **2005**, *39*, 3143.
- (15) Chan, A. W. H.; Kautzman, K. E.; Chhabra, P. S.; Surratt, J. D.; Chan, M. N.; Crounse, J. D.; Kürten, A.; Wennberg, P. O.; Flagan, R. C.; Seinfeld, J. H. *Atmos. Chem. Phys.* **2009**, *9*, 3049.
- (16) Hatakeyama, S.; Izumi, K.; Fukuyama, T.; Akimoto, H.; Washida, N. *J. Geophys. Res.* **1991**, *96*, 947.
- (17) Ng, N. L.; Chhabra, P. S.; Chan, A. W. H.; Surratt, J. D.; Kroll, J. H.; Kwan, A. J.; McCabe, D. C.; Wennberg, P. O.; Sorooshian, A.; Murphy, S. M.; Dalleska, N. F.; Flagan, R. C.; Seinfeld, J. H. *Atmos. Chem. Phys.* **2007**, *7*, 3909.
- (18) Presto, A. A.; Huff Hartz, K. E.; Donahue, N. M. *Environ. Sci. Technol.* **2005**, *39*.
- (19) Docherty, K. S.; Wu, W.; Lim, Y. B.; Ziemann, P. J. *Environ. Sci. Technol.* **2005**, *39*, 4049.
- (20) Gao, S.; Keywood, M.; Ng, N. L.; Surratt, J.; Varutbangkul, V.; Bahreini, R.; Flagan, R. C.; Seinfeld, J. H. *J. Phys. Chem. A* **2004**, *108*, 10147.
- (21) Iinuma, Y.; Böge, O.; Gnauk, T.; Herrmann, H. *Atmos. Environ.* **2004**, *38*, 761.
- (22) Jang, M. S.; Czoschke, N. M.; Lee, S.; Kamens, R. M. *Science* **2002**, *298*, 814.
- (23) Kalberer, M.; Paulsen, D.; Sax, M.; Steinbacher, M.; Dommen, J.; Prevot, A. S. H.; Fisseha, R.; Weingartner, E.; Frankevich, V.; Zenobi, R.; Baltensperger, U. *Science* **2004**, *303*, 1659.
- (24) Liggitto, J.; Li, S. M.; McLaren, R. *J. Geophys. Res.* **2005**, *110*.
- (25) Liggitto, J.; Li, S. M.; McLaren, R. *Environ. Sci. Technol.* **2005**, *39*, 1532.
- (26) Tobias, H. J.; Ziemann, P. J. *Environ. Sci. Technol.* **2000**, *34*, 2105.
- (27) Tolocka, M. P.; Jang, M.; Ginter, J. M.; Cox, F. J.; Kamens, R. M.; Johnston, M. V. *Environ. Sci. Technol.* **2004**, *38*, 1428.
- (28) Gómez-González, Y.; Surratt, J. D.; Cuyckens, F.; Szmigielski, R.; Vermeylen, R.; Jaoui, M.; Lewandowski, M.; Offenberg, J. H.; Kleindienst, T. E.; Edney, E. O.; Blockhuys, F.; Van Alsenoy, C.; Maenhaut, W.; Claeys, M. *J. Mass Spectrom.* **2008**, *43*, 371.
- (29) Iinuma, Y.; Müller, C.; Berndt, T.; Böge, O.; Claeys, M.; Herrmann, H. *Environ. Sci. Technol.* **2007**, *41*, 6678.
- (30) Iinuma, Y.; Müller, C.; Böge, O.; Gnauk, T.; Herrmann, H. *Atmos. Environ.* **2007**, *41*, 5571.
- (31) Surratt, J. D.; Gómez-González, Y.; Chan, A. W. H.; Vermeylen, R.; Shahgholi, M.; Kleindienst, T. E.; Edney, E. O.; Offenberg, J. H.; Lewandowski, M.; Jaoui, M.; Maenhaut, W.; Claeys, M.; Flagan, R. C.; Seinfeld, J. H. *J. Phys. Chem. A* **2008**, *112*, 8345.
- (32) Surratt, J. D.; Kroll, J. H.; Kleindienst, T. E.; Edney, E. O.; Claeys, M.; Sorooshian, A.; Ng, N. L.; Offenberg, J. H.; Lewandowski, M.; Jaoui, M.; Flagan, R. C.; Seinfeld, J. H. *Environ. Sci. Technol.* **2007**, *41*, 517.
- (33) Galloway, M. M.; Chhabra, P. S.; Chan, A. W. H.; Surratt, J. D.; Flagan, R. C.; Seinfeld, J. H.; Keutsch, F. N. *Atmos. Chem. Phys.* **2009**, *9*, 3331.
- (34) Kroll, J. H.; Ng, N. L.; Murphy, S. M.; Varutbangkul, V.; Flagan, R. C.; Seinfeld, J. H. *J. Geophys. Res.* **2005**, *110*, 10.
- (35) Volkamer, R.; Martini, F. S.; Molina, L. T.; Salcedo, D.; Jimenez, J. L.; Molina, M. J. *Geophys. Res. Lett.* **2007**, *34*.
- (36) Robinson, A. L.; Donahue, N. M.; Shrivastava, M. K.; Weitkamp, E. A.; Sage, A. M.; Grieshop, A. P.; Lane, T. E.; Pierce, J. R.; Pandis, S. N. *Science* **2007**, *315*, 1259.
- (37) Schauer, J. J.; Kleeman, M. J.; Cass, G. R.; Simoneit, B. R. T. *Environ. Sci. Technol.* **1999**, *33*, 1578.
- (38) Schauer, J. J.; Kleeman, M. J.; Cass, G. R.; Simoneit, B. R. T. *Environ. Sci. Technol.* **2002**, *36*, 1169.
- (39) Ravindra, K.; Sokhi, R.; Van Grieken, R. *Atmos. Environ.* **2008**, *42*, 2895.
- (40) Schauer, J. J.; Kleeman, M. J.; Cass, G. R.; Simoneit, B. R. T. *Environ. Sci. Technol.* **2001**, *35*, 1716.
- (41) Schauer, J. J.; Kleeman, M. J.; Cass, G. R.; Simoneit, B. R. T. *Environ. Sci. Technol.* **1999**, *33*, 1566.
- (42) Schauer, J. J.; Kleeman, M. J.; Cass, G. R.; Simoneit, B. R. T. *Environ. Sci. Technol.* **2002**, *36*, 567.
- (43) Atkinson, R.; Arey, J. *Polycycl. Aromatic Compd.* **2007**, *27*, 15.
- (44) Atkinson, R.; Aschmann, S. M.; Arey, J.; Carter, W. P. L. *Int. J. Chem. Kinetics* **1989**, *21*, 801.
- (45) Bunce, N. J.; Liu, L.; Zhu, J.; Lane, D. A. *Environ. Sci. Technol.* **1997**, *31*, 2252.
- (46) Mihele, C. M.; Wiebe, H. A.; Lane, D. A. *Polycycl. Aromatic Compd.* **2002**, *22*, 729.
- (47) Wang, L.; Atkinson, R.; Arey, J. *Environ. Sci. Technol.* **2007**, *41*, 2803.
- (48) Arey, J.; Atkinson, R.; Zielinska, B.; McElroy, P. A. *Environ. Sci. Technol.* **1989**, *23*, 321.
- (49) Gupta, P.; Harger, W. P.; Arey, J. *Atmos. Environ.* **1996**, *30*, 3157.
- (50) Helmig, D.; Arey, J.; Harger, W. P.; Atkinson, R.; Lopezcancio, J. *Environ. Sci. Technol.* **1992**, *26*, 622.
- (51) Helmig, D.; Lopezcancio, J.; Arey, J.; Harger, W. P.; Atkinson, R. *Environ. Sci. Technol.* **1992**, *26*, 2207.
- (52) Groszovsky, A. J.; Sasaki, J. C.; Arey, J.; Eastmond, D. A.; Parks, K. K.; Atkinson, R. *Res. Rep. Health Eff. Inst.* **1999**, *i*.
- (53) Cocker, D. R.; Flagan, R. C.; Seinfeld, J. H. *Environ. Sci. Technol.* **2001**, *35*, 2594.
- (54) Keywood, M. D.; Varutbangkul, V.; Bahreini, R.; Flagan, R. C.; Seinfeld, J. H. *Environ. Sci. Technol.* **2004**, *38*, 4157.
- (55) Burkhardt, M. R.; Maniga, N. I.; Stedman, D. H.; Paur, R. J. *Anal. Chem.* **1988**, *60*, 816.
- (56) Paulot, F.; Crounse, J. D.; Kjaergaard, H. G.; Kroll, J. H.; Seinfeld, J. H.; Wennberg, P. O. *Atmos. Chem. Phys.* **2009**, *9*, 1479.
- (57) Crounse, J. D.; McKinney, K. A.; Kwan, A. J.; Wennberg, P. O. *Anal. Chem.* **2006**, *78*, 6726.
- (58) Stein, S. M. Y.; Tchekhovskii, D.; Mallard, G.; Miksaia, A.; Zaikin, V.; Zhu, J.; Clifton, C.; Sparkman, D. *The NIST Mass Spectral Search Program for the NIST/EPA/NIH Mass Spectral Library*, 2005 ed.; 2005.
- (59) Surratt, J. D.; Gómez-González, Y.; Chan, A. W. H.; Vermeylen, R.; Shahgholi, M.; Kleindienst, T. E.; Edney, E. O.; Offenberg, J. H.; Lewandowski, M.; Jaoui, M.; Maenhaut, W.; Claeys, M.; Flagan, R. C.; Seinfeld, J. H. *J. Phys. Chem. A* **2008**, *112*, 8345.
- (60) DeCarlo, P. F.; Kimmel, J. R.; Trimborn, A.; Northway, M. J.; Jayne, J. T.; Aiken, A. C.; Gonin, M.; Fuhrer, K.; Horvath, T.; Docherty, K. S.; Worsnop, D. R.; Jimenez, J. L. *Anal. Chem.* **2006**, *78*, 8281.
- (61) Allan, J. D.; Delia, A. E.; Coe, H.; Bower, K. N.; Alfarra, M. R.; Jimenez, J. L.; Middlebrook, A. M.; Drewnick, F.; Onasch, T. B.; Canagaratna, M. R.; Jayne, J. T.; Worsnop, D. R. *J. Aerosol Sci.* **2004**, *35*, 909.
- (62) Bahreini, R.; Keywood, M. D.; Ng, N. L.; Varutbangkul, V.; Gao, S.; Flagan, R. C.; Seinfeld, J. H.; Worsnop, D. R.; Jimenez, J. L. *Environ. Sci. Technol.* **2005**, *39*, 5674.
- (63) Aiken, A. C.; DeCarlo, P. F.; Jimenez, J. L. *Anal. Chem.* **2007**, *79*, 8350.
- (64) Aiken, A. C.; Decarlo, P. F.; Kroll, J. H.; Worsnop, D. R.; Huffman, J. A.; Docherty, K. S.; Ulbrich, I. M.; Mohr, C.; Kimmel, J. R.; Sueper, D.; Sun, Y.; Zhang, Q.; Trimborn, A.; Northway, M.; Ziemann, P. J.; Canagaratna, M. R.; Onasch, T. B.; Alfarra, M. R.; Prevot, A. S. H.; Dommen, J.; Duplissy, J.; Metzger, A.; Baltensperger, U.; Jimenez, J. L. *Environ. Sci. Technol.* **2008**, *42*, 4478.
- (65) Weber, R. J.; Orsini, D.; Daun, Y.; Lee, Y. N.; Klotz, P. J.; Brechtel, F. *Aerosol Sci. Technol.* **2001**, *35*, 718.
- (66) Sorooshian, A.; Brechtel, F. J.; Ma, Y. L.; Weber, R. J.; Corless, A.; Flagan, R. C.; Seinfeld, J. H. *Aerosol Sci. Technol.* **2006**, *40*, 396.
- (67) Edgerton, E. S.; Hartsell, B. E.; Saylor, R. D.; Jansen, J. J.; Hansen, D. A.; Hidy, G. M. *J. Air Waste Manage. Assoc.* **2005**, *55*, 1527.
- (68) Hansen, D. A.; Edgerton, E. S.; Hartsell, B. E.; Jansen, J. J.; Kandasamy, N.; Hidy, G. M.; Blanchard, C. L. *J. Air Waste Manage. Assoc.* **2003**, *53*, 1460.
- (69) Gao, S.; Surratt, J. D.; Knipping, E. M.; Edgerton, E. S.; Shahgholi, M.; Seinfeld, J. H. *J. Geophys. Res.* **2006**, *111*, D14314.
- (70) Larson, R. A.; Garrison, W. J.; Marley, K. A. *Tetrahedron Lett.* **1986**, *27*, 3987.
- (71) Nishino, N.; Arey, J.; Atkinson, R. *Environ. Sci. Technol.* **2009**.
- (72) Sasaki, J.; Aschmann, S. M.; Kwok, E. S. C.; Atkinson, R.; Arey, J. *Environ. Sci. Technol.* **1997**, *31*, 3173.
- (73) Atkinson, R.; Aschmann, S. M.; Arey, J.; Zielinska, B.; Schuetzle, D. *Atmos. Environ.* **1989**, *23*, 2679.
- (74) Fisseha, R.; Dommen, J.; Sax, M.; Paulsen, D.; Kalberer, M.; Maurer, R.; Hoffer, F.; Weingartner, E.; Baltensperger, U. *Anal. Chem.* **2004**, *76*, 6535.
- (75) Lu, R.; Wu, J.; Turco, R. P.; Winer, A. M.; Atkinson, R.; Arey, J.; Paulson, S. E.; Lurmann, F. W.; Miguel, A. H.; Eiguren-Fernandez, A. *Atmos. Environ.* **2005**, *39*, 489.

- (76) Fraser, M. P.; Cass, G. R.; Simoneit, B. R. T. *Environ. Sci. Technol.* **1998**, *32*, 2051.
- (77) Marr, L. C.; Kirchstetter, T. W.; Harley, R. A.; Miguel, A. H.; Hering, S. V.; Hammond, S. K. *Environ. Sci. Technol.* **1999**, *33*, 3091.
- (78) Bunce, N. J. D.; H. G. *Can. J. Chem.* **1992**, *70*, 1966.
- (79) Lane, D. A.; Fielder, S. S.; Townsend, S. J.; Bunce, N. J.; Zhu, J.; Liu, L.; Wiens, B.; Pond, P. *Polycycl. Aromatic Compd.* **1996**, *9*, 53.
- (80) Nishino, N.; Atkinson, R.; Arey, J. *Environ. Sci. Technol.* **2008**, *42*, 9203.
- (81) Qu, X. H.; Zhang, Q. Z.; Wang, W. X. *Chem. Phys. Lett.* **2006**, *429*, 77.
- (82) Atkinson, R.; Arey, J. *Polycycl. Aromatic Compd.* **2007**, *27*, 15.
- (83) Nishino, N. A. J.; Atkinson, R. *Environ. Sci. Technol.* **2009**.
- (84) Dekermenjian, M.; Allen, D. T.; Atkinson, R.; Arey, J. *Aerosol Sci. Technol.* **1999**, *30*, 273.
- (85) Palen, E. J.; Allen, D. T.; Pandis, S. N.; Paulson, S. E.; Seinfeld, J. H.; Flagan, R. C. *Atmos. Environ., Part A* **1992**, *26*, 1239.
- (86) Koch, R.; Knispel, R.; Elend, M.; Siese, M.; Zetzsch, C. *Atmos. Chem. Phys.* **2007**, *7*, 2057.
- (87) Glowacki, D. R.; Wang, L. M.; Pilling, M. J. *J. Phys. Chem. A* **2009**, *113*, 5385.
- (88) Suh, I.; Zhang, R. Y.; Molina, L. T.; Molina, M. J. *J. Am. Chem. Soc.* **2003**, *125*, 12655.
- (89) Calvert, J. G.; Atkinson, R.; Becker, K. H.; Kamens, R. M.; Seinfeld, J. H.; Wallington, T. J.; Yarwood, G. *The Mechanisms of Atmospheric Oxidation of Aromatic Hydrocarbons*; Oxford University Press, Inc.: New York, 2002.
- (90) Reemtsma, T. J. *Chromatogr. A* **2003**, *1000*, 477.
- (91) Rodil, R.; Quintana, J. B.; Lopez-Mahia, P.; Muniategui-Lorenzo, S.; Prada-Rodriguez, D. *Anal. Chem.* **2008**, *80*, 1307.
- (92) Frömel, T.; Peschka, M.; Fichtner, N.; Hierse, W.; Ignatiev, N. V.; Bauer, K. H.; Knepper, T. P. *Rapid Commun. Mass Spectrom.* **2008**, *22*, 3957.
- (93) Barnes, I.; Hjorth, J.; Mihalopoulos, N. *Chem. Rev.* **2006**, *106*, 940.
- (94) Johnson, M. T.; Bell, T. G. *Environ. Chem.* **2008**, *5*, 259.
- (95) Tang, M. J.; Zhu, T. *Sci. China Ser. B-Chem.* **2009**, *52*, 93.
- (96) Lara-Martin, P. A.; Gomez-Parra, A.; Gonzalez-Mazo, E. *Environ. Pollut.* **2008**, *156*, 36.
- (97) Lara-Martin, P. A.; Gomez-Parra, A.; Gonzalez-Mazo, E. *J. Chromatogr. A* **2006**, *1137*, 188.
- (98) Altieri, K. E.; Turpin, B. J.; Seitzinger, S. P. *Atmos. Chem. Phys.* **2009**, *9*, 2533.
- (99) Kleindienst, T. E.; Jaoui, M.; Lewandowski, M.; Offenberg, J. H.; Lewis, C. W.; Bhawe, P. V.; Edney, E. O. *Atmos. Environ.* **2007**, *41*, 8288.
- (100) Offenberg, J. H.; Lewis, C. W.; Lewandowski, M.; Jaoui, M.; Kleindienst, T. E.; Edney, E. O. *Environ. Sci. Technol.* **2007**, *41*, 3972.
- (101) Hallquist, M.; Wenger, J. C.; Baltensperger, U.; Rudich, Y.; Simpson, D.; Claeys, M.; Dommen, J.; Donahue, N. M.; George, C.; Goldstein, A. H.; Hamilton, J. F.; Herrmann, H.; Hoffmann, T.; Iinuma, Y.; Jang, M.; Jenkin, M. E.; Jimenez, J. L.; Kiendler-Scharr, A.; Maenhaut, W.; McFiggans, G.; Mentel, T. F.; Monod, A.; Prevot, A. S. H.; Seinfeld, J. H.; Surratt, J. D.; Szmigielski, R.; Wildt, J. *Atmos. Chem. Phys.* **2009**, *9*, 5155.
- (102) Schuetzle, D.; Cronn, D.; Crittenden, A. L.; Charlson, R. J. *Environ. Sci. Technol.* **1975**, *9*, 838.
- (103) Chebbi, A.; Carlier, P. *Atmos. Environ.* **1996**, *30*, 4233.
- (104) Mougin, C.; Dappozze, F.; Brault, A.; Malosse, C.; Schmidt, J. E.; Amellal-Nassr, N.; Patureau, D. *Environ. Chem. Lett.* **2006**, *4*, 201.
- (105) Thiruvankatachari, R.; Kwon, T. O.; Moon, I. S. *J. Environ. Sci. Health, Part A* **2006**, *41*, 1685.
- (106) Butte, W.; Hostrup, O.; Walker, G. *Gefahrstoffe Reinhaltung Der Luft* **2008**, *68*, 79.

JP908530S